NAM

Special Report on the Zeerijp Earthquake Swarm starting 4th October 2021

Datum November 2021

Editors Jan van Elk and Jeroen Uilenreef

Contents

Summary and Conclusions 5
Half yearly monitoring report and special report 5
Analysis of Ground Movement of the two Zeerijp Events 5
Empirical Green's Function Approach 5
1 Introduction 6
1.1 Reason for this Special Report 6
1.2 Content of this Special Report 7
2 Analysis of the Surface Ground-Motions Recorded During the Zeerijp ML 2.5 Earthquake of 4th October 2021 9
2.1 Introduction 9
2.2 Peak Ground Accelerations and Velocities 11
2.3 Ground-Motion Durations 15
2.4 Spectral Accelerations and Comparison with Ground-Motion Models 19
2.5 Concluding remarks Zeerijp Earthquake 4th October 2021 (2.5) 22
3 Analysis of the Surface Ground-Motions Recorded During the Appingedam M_L 1.8 Earthquake of 4th October 2021 24
3.1 Introduction 24
3.2 Peak Ground Accelerations and Velocities 26
3.3 Ground-Motion Durations 30
3.4 Spectral Accelerations and Comparison with Ground-Motion Models 32
3.5 Concluding remarks Appingedam Earthquake 4th October 2021 (1.8) 34
4 Analysis of the Surface Ground-Motions Recorded During the Zeerijp M_L 2.2 Earthquake of 4th October 2021 36
4.1 Introduction 36
4.2 Peak Ground Accelerations and Velocities 38
4.3 Ground-Motion Durations 42
4.4 Spectral Accelerations and Comparison with Ground-Motion Models 46
4.5 Concluding remarks Zeerijp earthquake 4th October 2021 (2.2) 47
5 Comparison of the Surface Ground-Motions Recorded During the Zeerijp M_L 2.5 and M_L 2.2 Earthquakes of 4th October 2021 49
5.1 Introduction 49
5.2 Fit to the empirical PGV GMPEs 50
5.3 Trends of PGA, PGV and Spectral Acceleration with distance 53
5.4 Spatial distribution and ratios of ground-motion amplitudes 57

5.5 Time-histories and response spectra 63
5.6 Concluding remarks 70
6 Empirical Green's functions methodology 71
6.1 The earthquake swarm commencing on 4th October 71
6.2 Empirical Green's Function Approach 76
7 Damage Notifications 82
7.1 Damage Claims received by IMG 82
8 References 84
Appendix A – Overview of results analysis using the automated FWI methodology for the induced earthquakes in the Groningen gas field 85
Appendix B – Time-histories of acceleration and velocity and accumulation of Arias Intensity 91
Appendix C – Time-histories of acceleration and velocity and accumulation of Arias Intensity 180
Appendix D – Evaluation of the hypocentre and source mechanism of the earthquake with a magnitude of 1.7 near Westeremden on 8th November 2021 269

Summary and Conclusions

Half yearly monitoring report and special report

This report was prepared in response to the exceedance of monitoring level 2 for earthquake density, as a result of the earthquake near Westeremden on 8th November 2021. At that time, NAM was also preparing the half yearly monitoring report. Both these reports focus on the analysis of the earthquake swarm in Groningen that commenced on the 4th October with the earthquake near Zeerijp with a magnitude of M_L=2.5. To avoid duplication the analysis of the swarm has been reported as follows. The analysis of the swarm and the estimation of the hypocentre and source mechanism of these earthquakes using the automated full wave form inversion was reported in the half yearly monitoring report. This special report contains the analysis of ground movements (PGV and PGA) of the three main earthquake events of this swarm (all on 4th October) and a comparison of the ground movement of the two earthquake events near Zeerijp.

Analysis of Ground Movement of the two Zeerijp Events

Two earthquakes occurred within a small epicentral distance on 4th October 2021 near the village of Zeerijp, one of M_L2.5 and one of M_L2.2. The patterns of recorded PGA, PGV and Spectral Accelerations with distance are similar for both events, including their outliers such as station G480. The PGA and PGV values recorded are different by a factor of approximately 2, which matches the value of the magnitude scaling predicted by the empirical PGV GMPEs between the magnitudes of the events. The time-histories, response spectra and Arias Intensity accumulation of the recordings of the two events at each station are visually very similar, as are the values of 5-75% significant duration calculated for each record.

This report contains a preliminary comparison of the recorded ground-motions; the strong similarities observed between the data recorded during the two events, as well as the information that appears to suggest that the difference between many recordings of the events can be approximated by a simple scaling factor, warrants more thorough investigation and analyses, which can yield important conclusions about the variation and scaling of ground-motions in Groningen and elsewhere.

Empirical Green's Function Approach (preliminary)

In the half-yearly seismic monitoring report for 1st November 2021 an analysis of the hypocentre and source mechanism for the earthquakes near Zeerijp using the automated full wave-form inversion was presented.

Additionally, the Empirical Green's Function method has been applied to earthquake pairs in the swarm of events with subsequent analysis of the azimuthal variation of the source time function to reveal details of the rupture propagation. For the largest event pair we obtain estimates of the rupture propagation direction and distance. An interpretation of this result as the projection onto the horizontal plane of down-dip propagation is consistent with the event locations and focal mechanisms as well as the detailed underlying fault map.

Building Damage Notification

The reporting on building damage resulting from these earthquakes is based on the news releases from the IMG (Instituut Mijnbouwschade Groningen).

1 Introduction

1.1 Reason for this Special Report

When larger earthquakes have occurred or other remarkable events have happened (like a swarm of smaller earthquakes), NAM published a report within two weeks after the event. To date eleven of these reports have been published. These reports are listed in table 1.1.

Title	Date
Rapportage recente aardbevingen Wirdum en Garsthuizen 2016/2017	Mar 2017
Ground Motions from the ML 2.6 Slochteren Earthquake of 27th May 2017	June 2017
Special Report on the earthquake density and activity rate following the earthquakes in Appingedam (ML=1.8) and Scharmer (ML=1.5) in August 2017	Sept 2017
Special Report on the Loppersum earthquakes – December 2017	Dec 2017
Special Report on the Zeerijp Earthquake	Jan 2018
Short special report Exceedance Activity Rate - February 2018	Feb 2018
Special Report - Westerwijtwerd Earthquake - 22nd May 2019	May 2019
Analyse overschrijding MRP-grenswaarde Aardbevingsdichtheid 9 september 2019	Sept 2019
Analyse overschrijding aardbevingsdichtheid - 3 december 2019	Dec 2019
Special Report on the Zijldijk M_L = 2.5 Earthquake of 2nd May 2020	May 2020
Special Report on the Loppersum M_L=2.7 earthquake of 14th June 2020	August 2020

Table 1.1 Reports analysing remarkable events in the earthquake record, like larger events or earthquake swarms.

The earthquake swarm near Zeerijp, which commenced on the 4th October 2021 raised the located earthquake density to above monitoring level 1. The earthquake near Westeremden on the 8th November 2021, with a magnitude 1.7, raised the local earthquake density 0.42 earthquakes per km^2 per year, which is above monitoring level 2 (Fig. 1.1).

This recent exceedance of the local earthquake density near Loppersum requires NAM to submit a Special Report. The epicentral locations of the earthquakes near Zeerijp and Westeremden were all located very close together and had therefore a large impact on the earthquake density. The development of the earthquake activity rate is shown in figure 1.2.

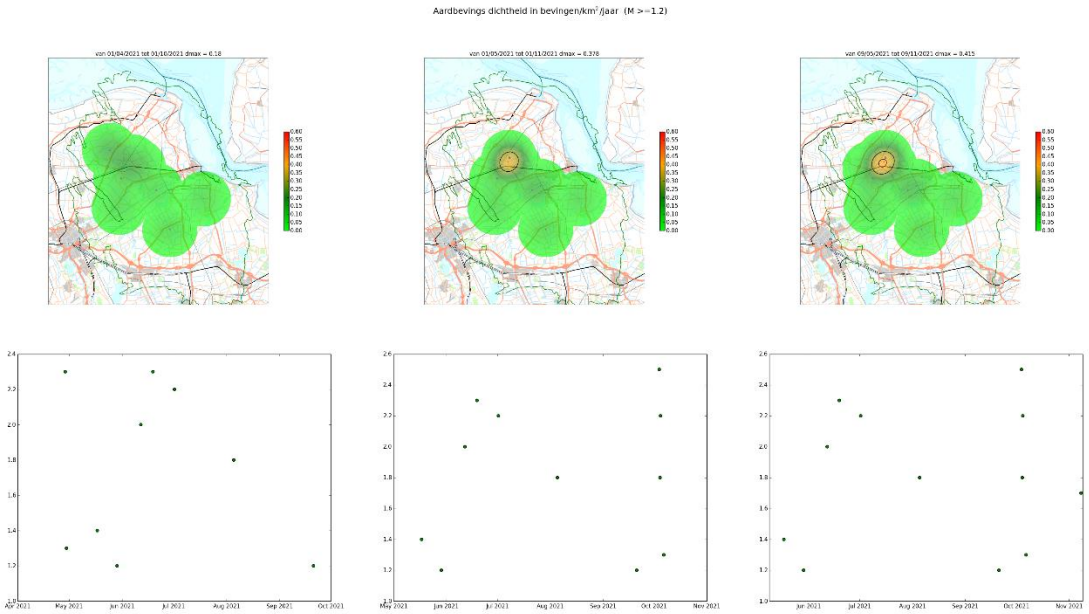

Fig. 1.1 Development of the earthquake density. The density is shown for 1st October (before the earthquake swarm), 1st November (after the earthquake swarm) and 9th November (after the second monitoring level was exceeded)

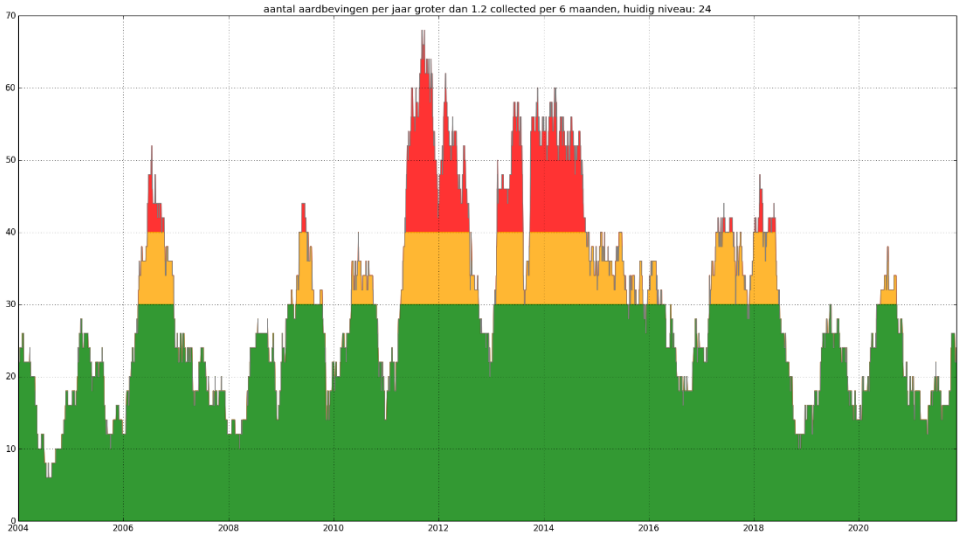

Fig. 1.2 Development of the earthquake activity rate. The activity rate is currently below monitoring level 1.

1.2 Content of this Special Report

Focus of this special report will be the Zeerijp earthquake swarm commencing on the 4th October 2021, as this made the largest contribution to the increase of the earthquake density near Zeerijp. The first of these earthquakes occurred on 4th October 2021 near Zeerijp and had a magnitude of M_L = 2.5. In this report the earthquake records obtained during this earthquake (chapter 2) and two earthquakes on the same day are discussed. These are an earthquake near Appingedam with magnitude 1.8 (chapter 3) and near Zeerijp with magnitude 2.2 (chapter 4). A comparison of the ground motions recorded for the two earthquakes on the 4th October near Zeerijp is included in chapter 5.

An analysis of the earthquake record is prepared at 6-month intervals since submitting Winningsplan 2016 (table 1.2).

Title	Date
Analyse seismiciteit	Nov 2016
Rapportage Seismiciteit Groningen - November 2017	Nov 2017
Rapportage Seismiciteit Groningen - Juni 2018	July 2018
Rapportage Seismiciteit Groningen - November 2018	Nov 2018
Rapportage Seismiciteit Groningen - Mei 2019	May 2019
Rapportage seismiciteit Groningen - November 2019	Nov 2019
Rapportage Seismiciteit Groningen - Mei 2020	Apr 2020
Rapportage seismiciteit Groningen - November 2020	Nov 2021
Rapportage Seismiciteit Groningen - Mei 2021	June 2021
Rapportage seismiciteit Groningen - November 2021	Nov 2021

Table 1.2 Half-yearly surveillance reports issued by NAM to SodM and published on the NAM onderzoeksrapporten-webpage.

This special report is issued simultaneously with the half-yearly seismic monitoring report for 1st November 2021. The analysis of hypocentre and source mechanism using the automated full wave form analysis for earthquakes in this swarm before 1st November have been discussed and included in this half-yearly monitoring report. Analysis of the earthquakes of this earthquake swarm as contained in the monitoring report have not been repeated in this Special Report. An overview table of the hypocentre and source mechanism evaluated using the for automated full wave form analysis for the earthquakes that occurred between 1st January 2020 and 8th November 2021 is included as Appendix A.

The automated FWI analysis of the Westeremden earthquake of 8th November 2021 with a magnitude of 1.7 has been included in this report as Appendix D.

A discussion of the hypocentre and source mechanism of the earthquakes in the swarm is contained in chapter 6. This also contains a preliminary discussion of the rupture mechanism of the earthquakes near Zeerijp based on a preliminary analysis using the empirical Green's functions approach. A review of the damage to buildings these earthquakes have caused is presented in chapter 7.

2 Analysis of the Surface Ground-Motions Recorded During the Zeerijp ML 2.5 Earthquake of 4th October 2021

2.1 Introduction

On Monday 4 October 2021 at 02:59 UTC (04:59 am local time), an earthquake of local magnitude (M_L) of 2.5 occurred near the village of Zeerijp, in the northern part of the Groningen field (Figure 2.1). The epicentral coordinates (245553 X, 596700 Y) depicted in Figure 2.1, as well as a focal depth of 3 km, were calculated by Dr Jesper Spetzler of KNMI using the 3D EDT method (Spetzler & Dost, 2017).

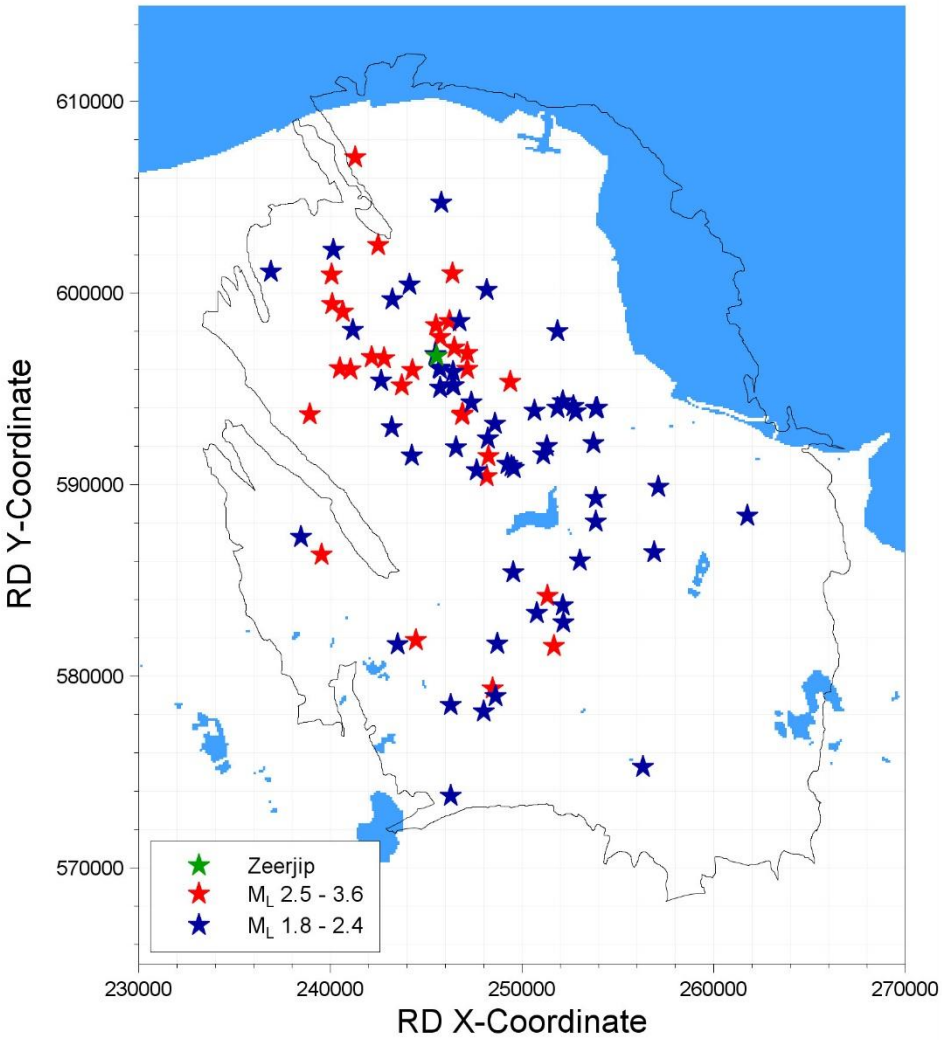

Figure 2.1. Epicentre of Zeerijp earthquake (green star) together with epicentres of previous earthquakes of $M_L \geq 2.5$ (red stars) and of M_L 1.8-2.4 (blue stars)

Two more events occurred on the same day, one with a local magnitude of 1.8 in Appingedam at 15:33 pm local time and another one with a magnitude of 2.2 also in Zeerijp at 22:47 local time. The last event with a magnitude equal or larger to M_L2.5–the smallest magnitude considered in the Groningen Hazard & Risk Assessment- was the M_L2.7 Loppersum earthquake of 14 July 2020. In keeping with trend during more recent earthquakes (Figure 2.2), the latest earthquake has triggered a large number

of accelerograms, as a direct result of the expansion of the strong-motion recording networks in the Groningen field (Dost *et al*., 2017; Ntinalexis *et al*., 2019).

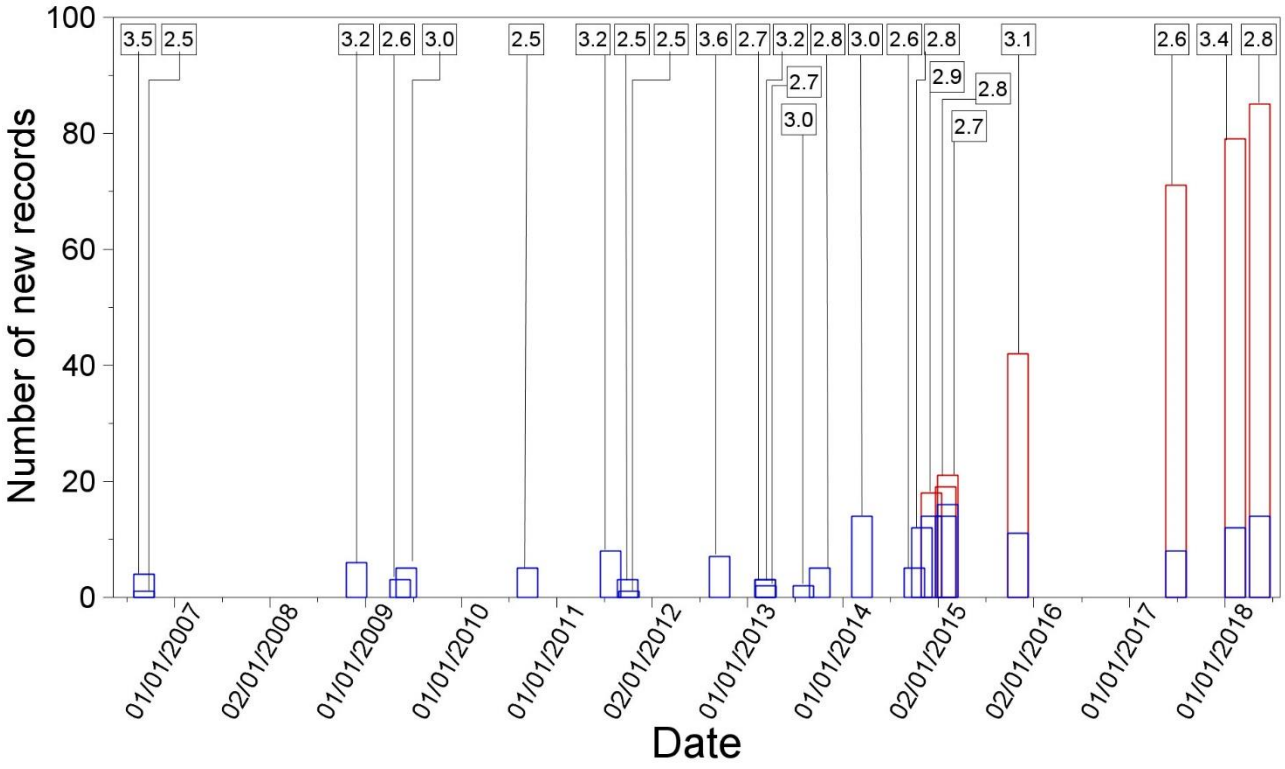

Figure 2.2. Diagram illustrating the timing of earthquakes of $M_L \geq 2.5$ in the Groningen field until the end of 2018 and the number of records yielded by the permanent KNMI network (B-stations, blue) and by the expanded borehole geophone network (G-stations, red).

The KNMI portal (http://rdsa.knmi.nl/dataportal/) made accelerograms from the earthquake available within an hour of the event and 82 three-component recordings were downloaded and processed for this preliminary assessment of the motions. The records were processed as described by Edwards & Ntinalexis (2021) and a total of 53 records were deemed usable. Figure 2.3 shows the usable recordings in the magnitude-distance occupied by the database used to derive the current empirical Ground-Motion Prediction Equations (GMPEs) used to estimate values of peak ground velocity (PGV) occurring during earthquakes in the Groningen field (Bommer *et al*., 2021b). This chapter presents an overview of the recorded motions from the Zeerijp event in terms of their amplitudes and durations, and discusses how the recorded amplitudes of motion compare with predictions from the empirical PGV GMPE and the V7 Ground-Motion Model (GMM; Bommer *et al*., 2021a) The discussions focus primarily on peak ground acceleration (PGA), which is assumed equal to the spectral acceleration at a period of 0.01 seconds, and PGV, which has been shown to correlate very well with the spectral acceleration at a period of 0.3 seconds for the Groningen data (Figure 2.4).

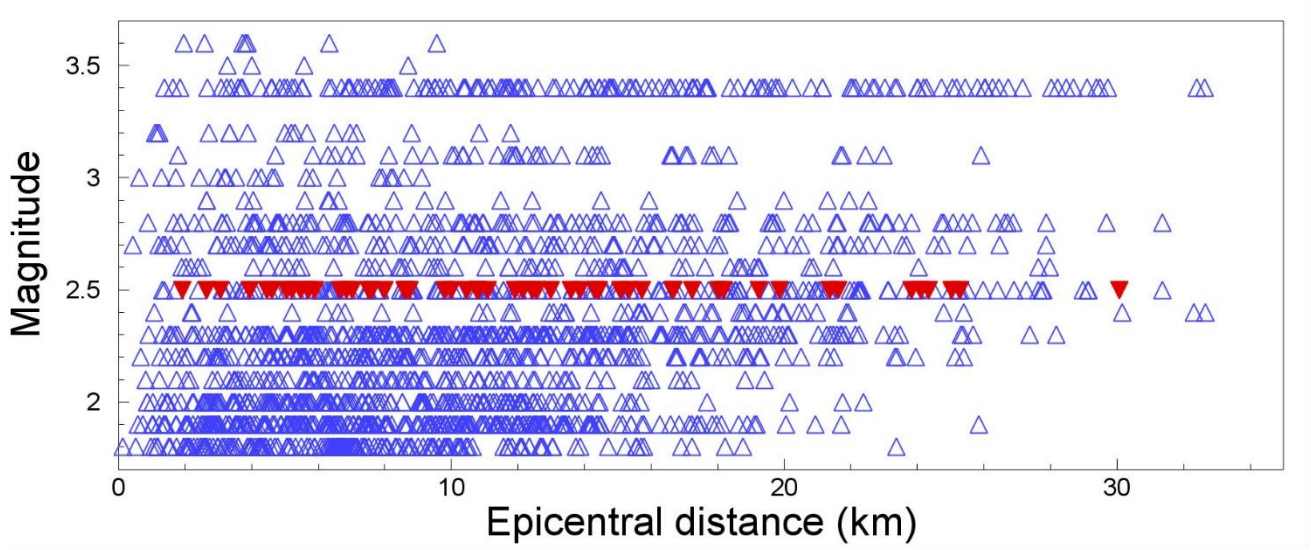

Figure 2.3. Magnitude-distance distribution of the Groningen strong-motion database including the recordings of the 4 October 2021 Zeerijp earthquake

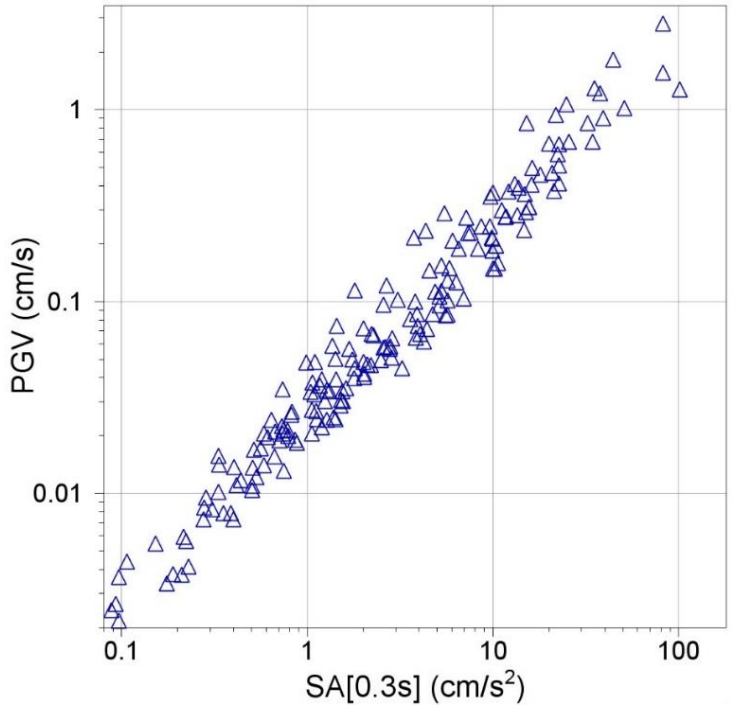

Figure 2.4. Correlation between values of PGV and spectral accelerations at 0.3 seconds for the Groningen strong-motion database (Bommer et al., 2018)

2.2 Peak Ground Accelerations and Velocities

Figures 2.5 and 2.6 show the horizontal values of PGA and PGV of three component definitions from each recording obtained during the Zeerijp earthquake plotted against the distance of the recording site from the epicentre. The largest and third largest amplitude was obtained at the G140 station located 1.9 km from the epicentre: the PGAs recorded at the horizontal components of this station are 12.26 cm/s^2 on the H2 (EW) component and 5.08 cm/s^2 on the H1 (NS) component. The second largest PGA values was recorded at station G180 and 2.65 km from the epicentre: 6.02 cm/s^2 on the H1 (NS) component. The largest PGV value was also at station G140 and is 0.36 cm/s (H2/EW), while the second largest PGV value was recorded at the H1/NS component of G140: 0.16 cm/s.

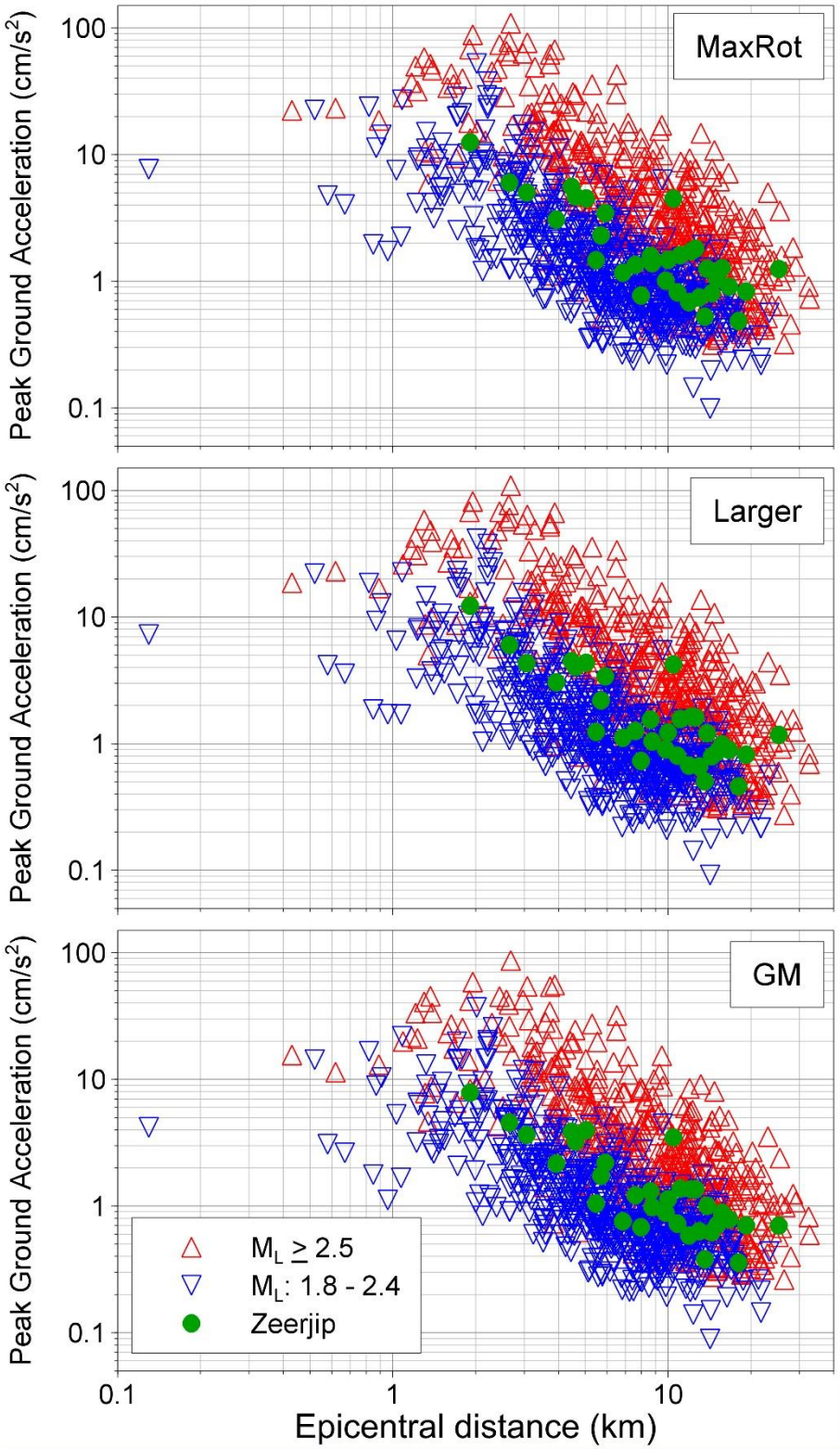

Figure 2.5. Horizontal components of PGA recorded during the Zeerijp earthquake and previous earthquakes plotted against epicentral distance

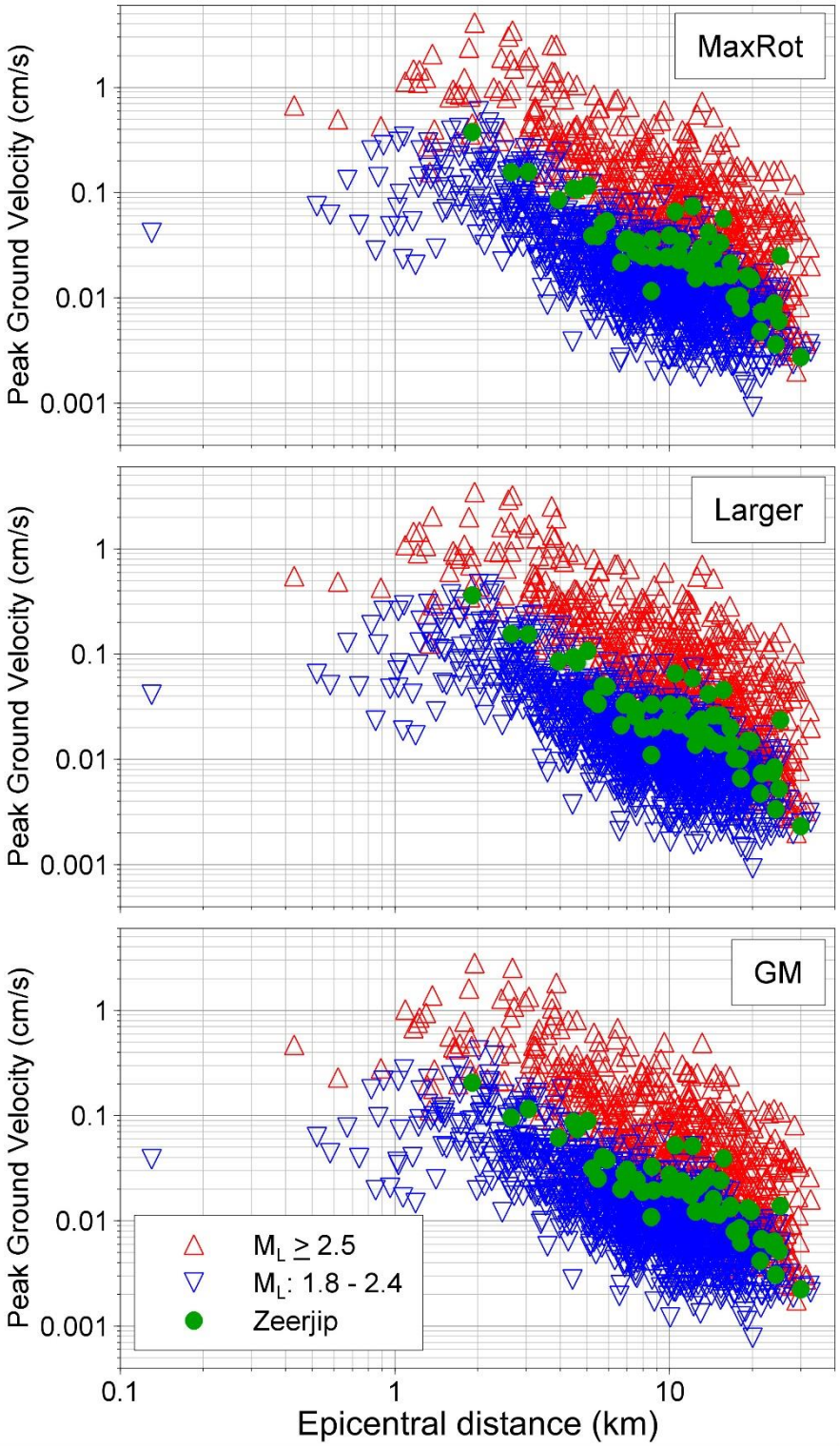

Figure 2.6. Horizontal components of PGV recorded during the Zeerijp earthquake and previous earthquakes plotted against epicentral distance

From Figures 2.5 and 2.6 it is immediately apparent that the amplitudes of motion are consistent with previous earthquakes of comparable size. Figure 2.7 shows the horizontal components of PGA and PGV obtained within 6 km of the epicentre, from which it can be appreciated that the very strong polarisation often observed in Groningen recordings (*e.g.*, Bommer *et al.*, 2017) is also apparent in records of this event.

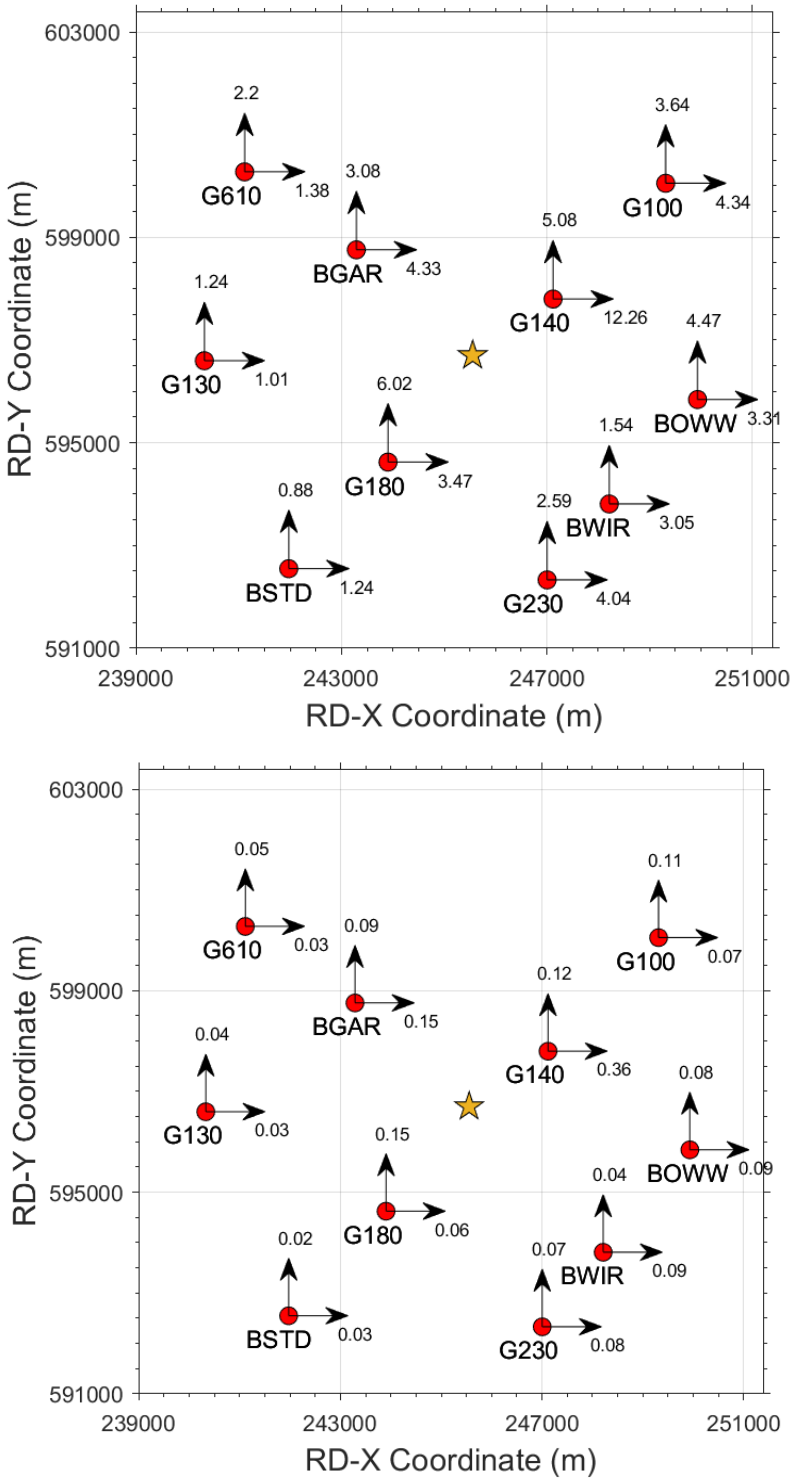

Figure 2.7. Horizontal components of PGA (upper) and PGV (lower) recorded during the Zeerijp earthquake at epicentral distances of less than 6 km; units are cm/s² and cm/s, respectively.

As already shown in Figures 2.5 and 2.6, the amplitudes decay rapidly with distance although the effect of simultaneous arrivals of direct and critically refracted/reflected waves leads to an increase in amplitudes at some locations between 12 and 20 km from the epicentre. However, these effects do not lead to significant absolute amplitudes at those distances and it is clear from Figure 2.7 that, outside the epicentral area, the motions are of very low amplitude: < 0.01*g* for PGA and < 0.1 cm/s for PGV.

Overall, the motions appear similar to those observed in previous earthquakes. Figure 2.8 shows the geometric mean horizontal components of PGA and PGV plotted against magnitude together with the corresponding values from the complete database.

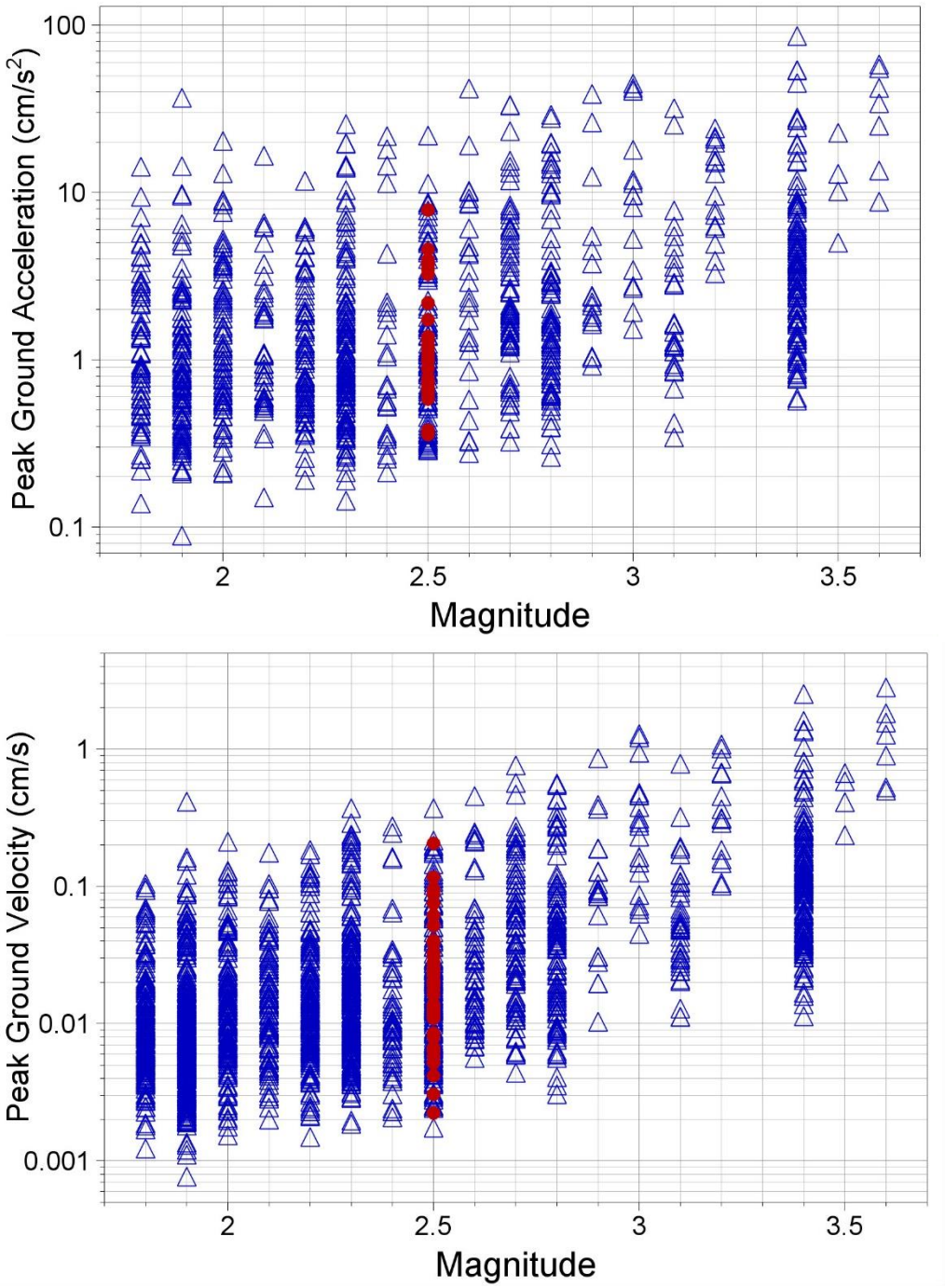

Figure 2.8. Geometric mean horizontal components of PGA (upper) and PGV (lower) recorded during the Zeerijp earthquake (red) and in previous earthquakes (blue) plotted against local magnitude

2.3 Ground-Motion Durations

The maximum amplitude of ground shaking, whether represented by PGA or PGV, provides a simple indication of the strength of the motion but the potential for adverse effects—such as damage to masonry buildings or triggering liquefaction—also depends on the duration or number of cycles of the motion.

A feature that has been consistently observed in the Groningen ground motions is a very pronounced negative correlation between PGA and duration, with high amplitude motions consistently associated with shaking of very short duration (Bommer *et al.*, 2016). The same pattern is observed in the recordings of the Zeerijp earthquake, as shown in Figure 2.9. The largest value of PGA, recorded on the H2 (EW) component at the G140 station, is associated with a duration of two seconds (2.035 s). The horizontal components of both acceleration and velocity from this station are shown in Figure 2.10, which also shows the build-up of Arias intensity (which is a measure of the energy in the motion) over time. The strong concentration of the energy in a single pulse of motion in the H2 component is immediately apparent. The larger amplitude component of the G180 recording—the second closest station to the epicentre and source of the second and third largest PGA values—is associated with a significant duration of 2.67 s (Figure 2.11). The durations typically observed in short-distance earthquake recordings in Groningen are usually even smaller (often less than one second). In both recordings in this case, the duration is elongated by a strong P-wave arrival approximately two seconds before the time of the S-wave peak.

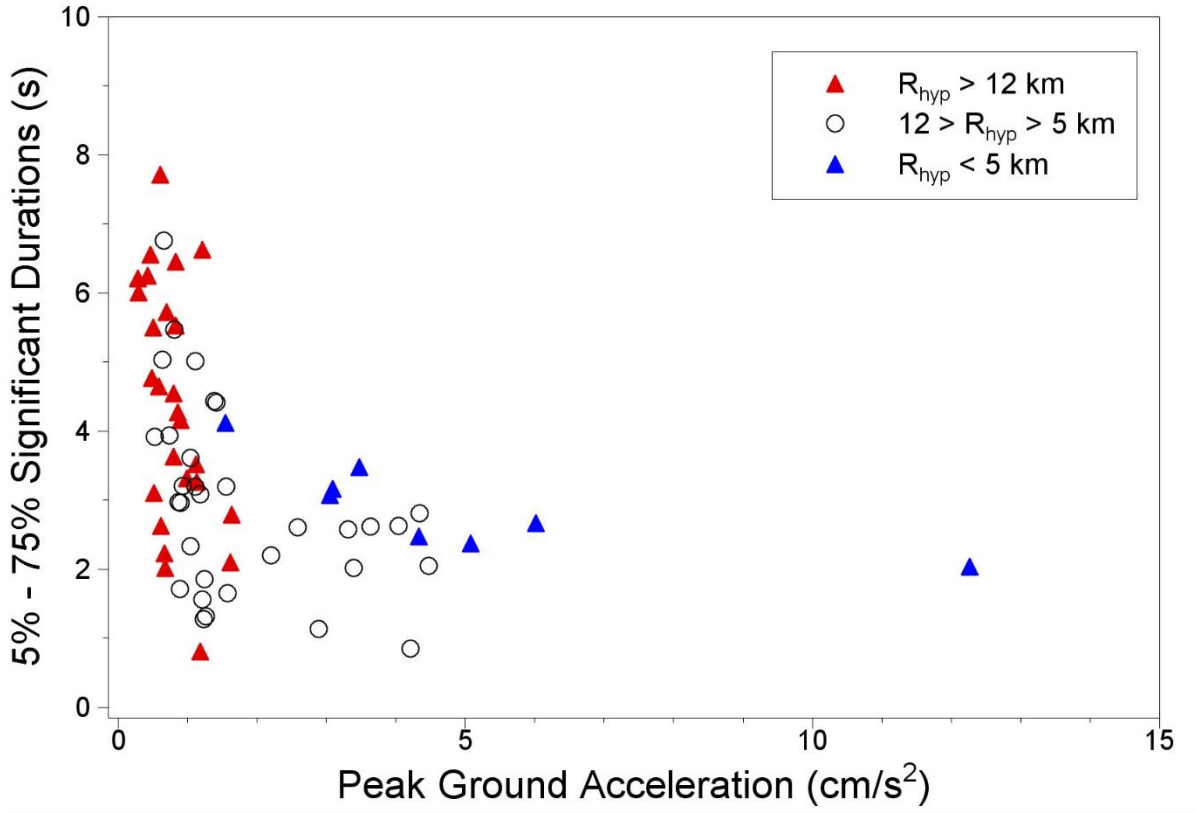

Figure 2.9. Pairs of PGA and significant duration for individual components of the Loppersum records, with symbols indicating the rupture distance of the recording.

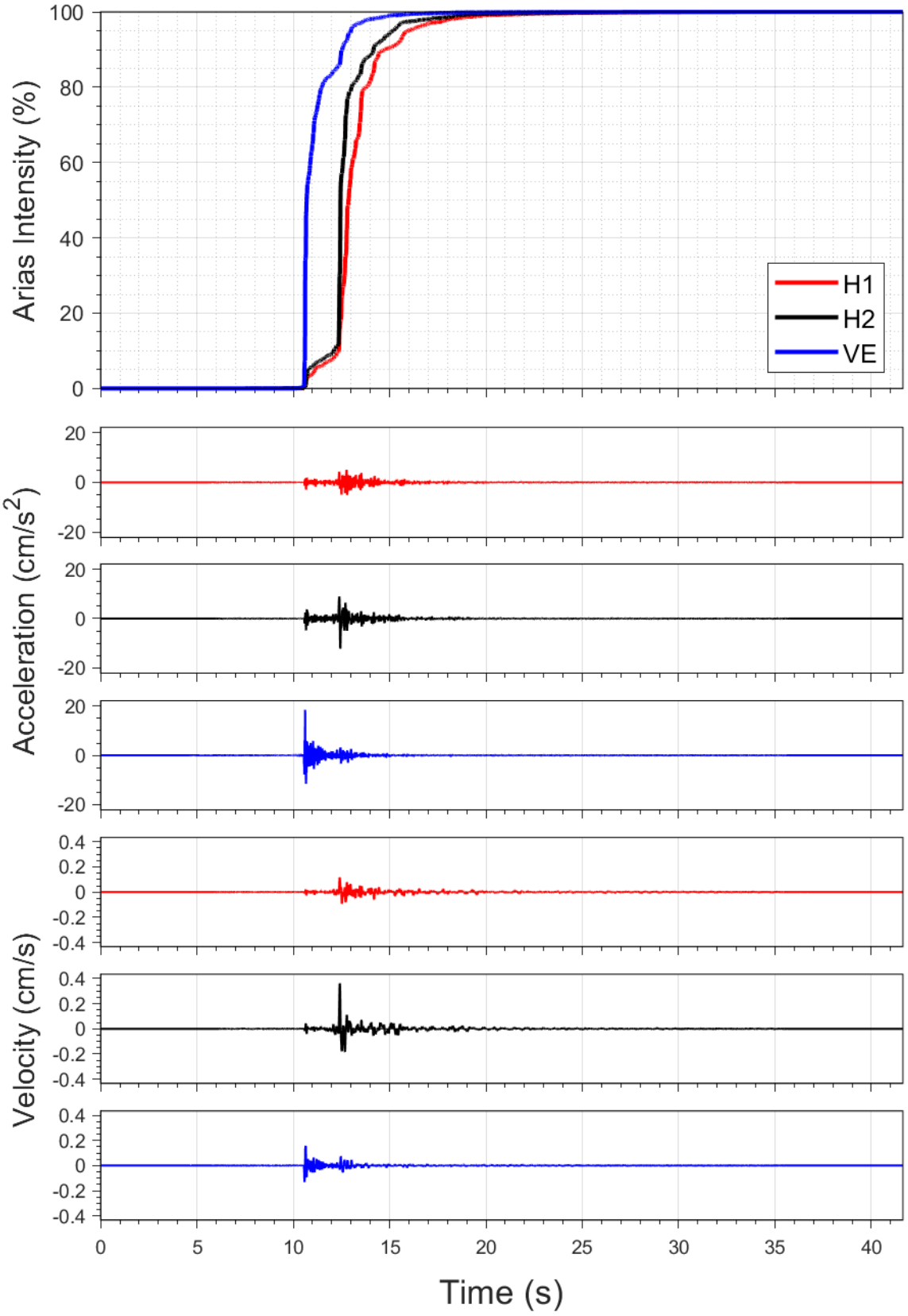

Figure 2.10. Horizontal components of acceleration and velocity from the G140 station; the upper frame shows the accumulation of Arias intensity (energy) over time.

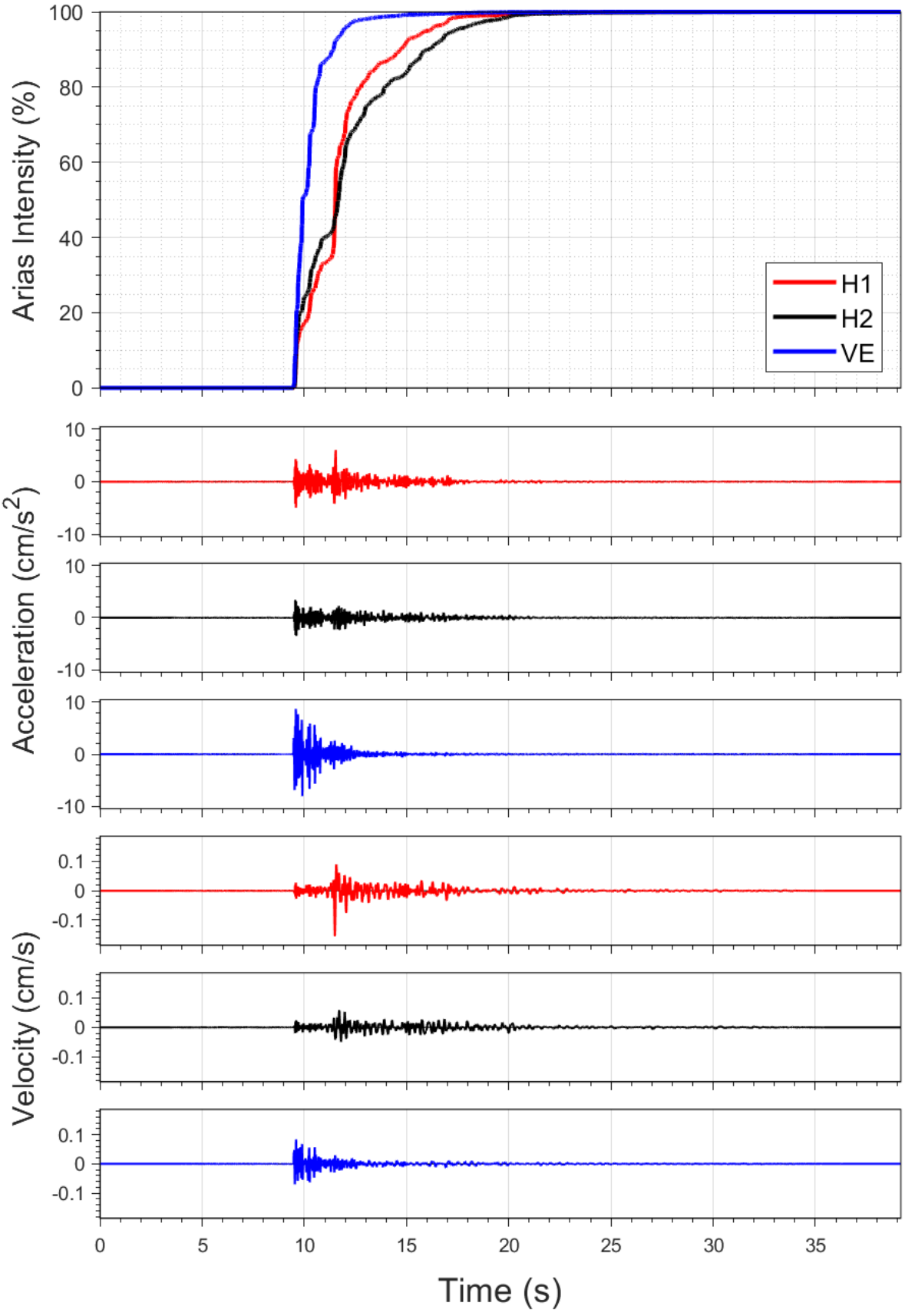

Figure 2.11. Horizontal components of acceleration and velocity from the G180 station; the upper frame shows the accumulation of Arias intensity (energy) over time.

2.4 Spectral Accelerations and Comparison with Ground-Motion Models

Additional insight into the nature of the ground motions can be obtained from the 5%-damped acceleration response spectra. The horizontal acceleration response spectra from the G140 and G180 recordings of the Zeerijp earthquake are shown in Figure 2.12.

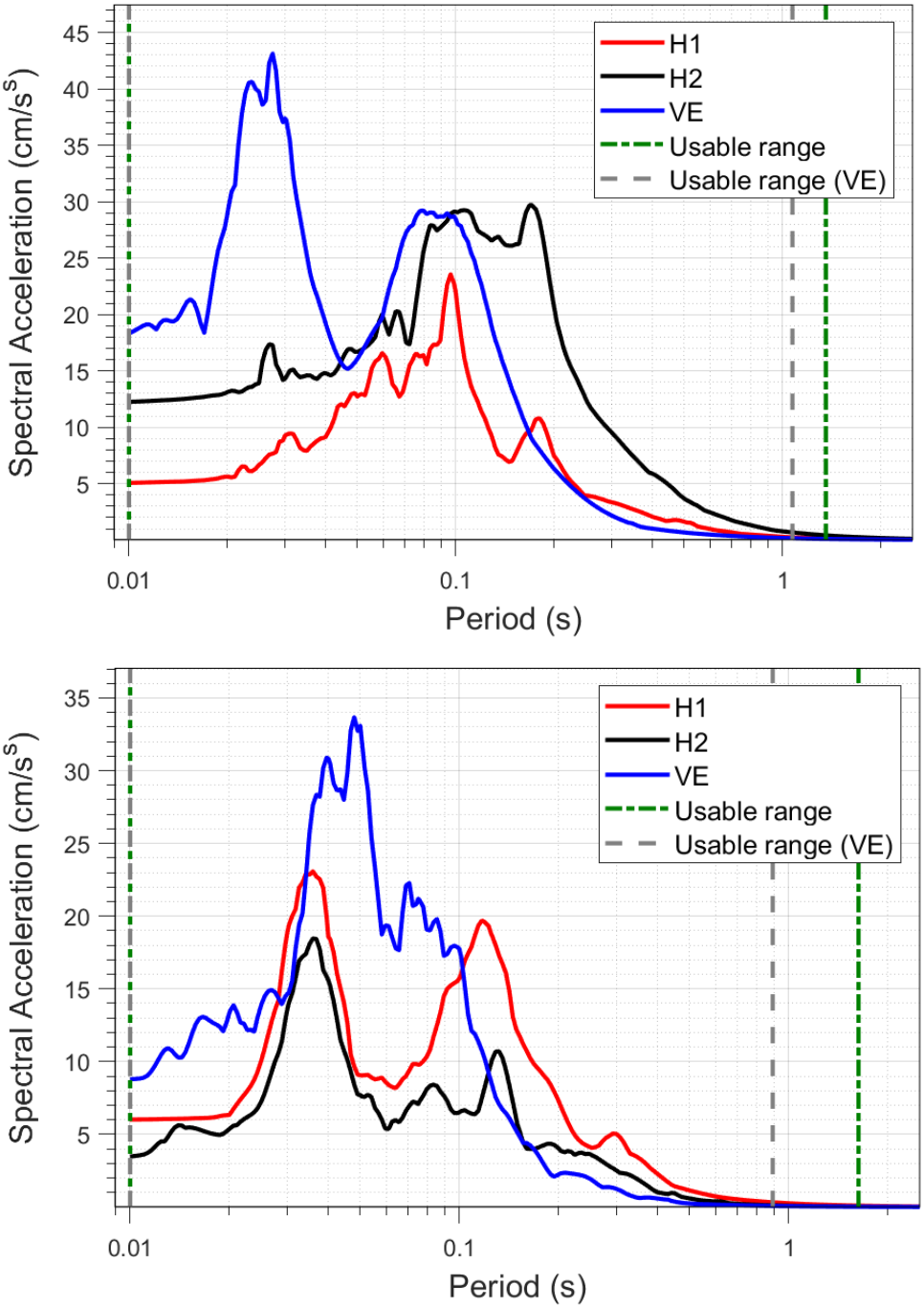

Figure 2.12. Horizontal response spectra from the G140 (upper) and G180 (lower) stations; vertical spectra plotted as dashed lines beyond maximum usable period.

The spectral shapes are consistent with previous observations in the field. The divergence between the red and black curves in both frames shows that the horizontal polarisation of both recordings seen for PGA and PGV (Figure 2.7) persists across the entire range of usable response periods.

For this preliminary analysis, the key question of interest is whether the motions recorded in this earthquake are consistent with the current GMM and empirical PGV GMPEs being used in the Groningen field. The current GMM is the V7 GMM, published a few days before the earthquake occurred (Bommer *et al.*, 2021a), and we have simply calculated the total residuals at the surface for different ground-motion parameters. In each case, the residual is the natural logarithm of the ratio of the observed (recorded) to the median predicted value, so a residual of 0.7 indicates that the recorded value was underestimated by a factor of 2 by the model and a residual of -0.7 would indicate over-prediction by a factor of 2. Figure 2.13 shows the residuals of spectral accelerations at 0.01 seconds with respect to the V7 GMM plotted against rupture distance. The scatter is very considerable but similar to the scatter of the data used in the V7 GMM development, while the residuals are centred fractionally above the zero line, which suggests a slight under-prediction by the model. At longer periods (Figures 2.14-2.17), the scatter is smaller however the residuals are better centred on the zero line, indicating that the median predictions of the model provide an overall good fit to the data. A weak trend of the residuals with distance can be observed, with a larger residuals observed at longer distances.

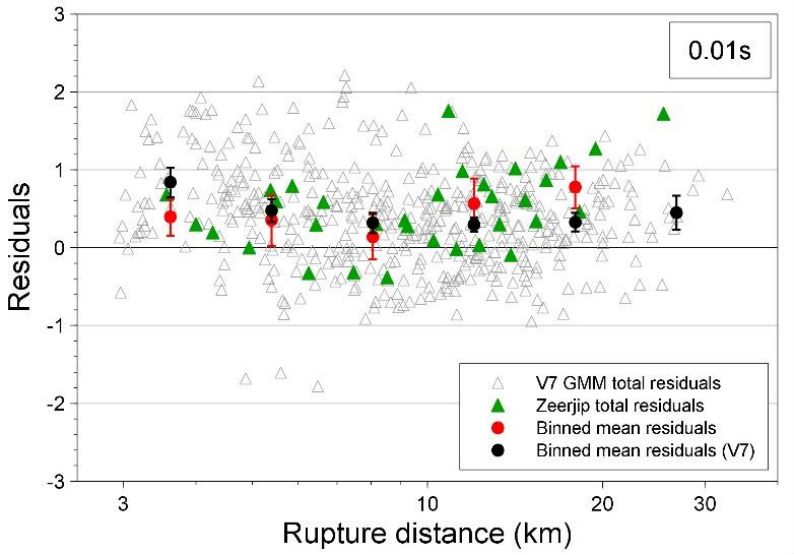

Figure 2.13. Residuals of Sa(T) with respect to the central branch of the V7 GMM at 0.01 seconds

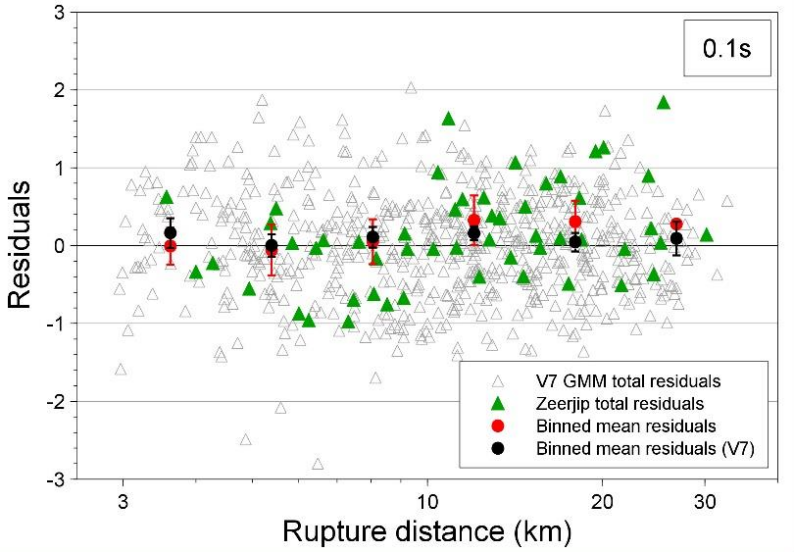

Figure 2.14. Residuals of Sa(T) with respect to the central branch of the V7 GMM at 0.1 seconds

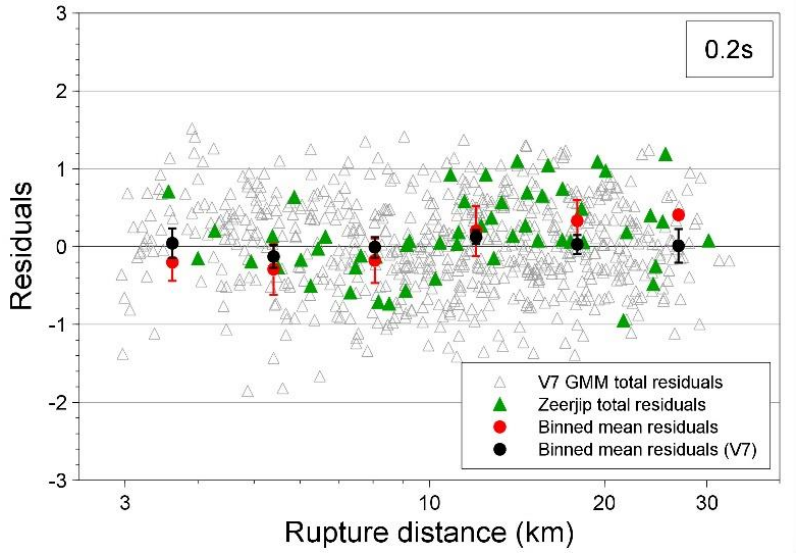

Figure 2.15. Residuals of Sa(T) with respect to the central branch of the V7 GMM at 0.2 seconds

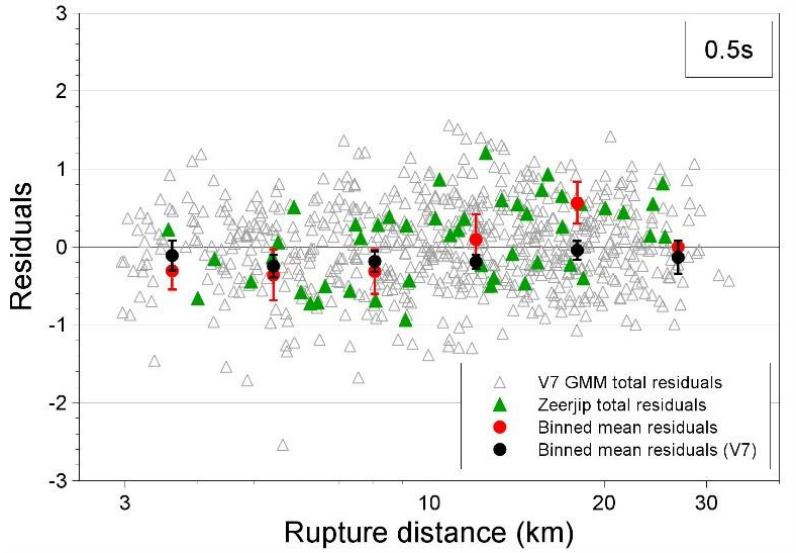

Figure 2.16. Residuals of Sa(T) with respect to the central branch of the V7 GMM at 0.5 seconds

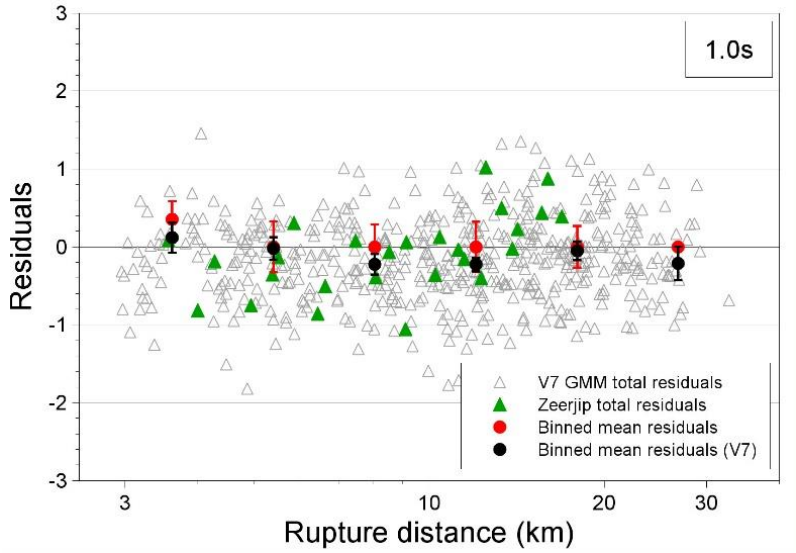

Figure 2.17. Residuals of Sa(T) with respect to the central branch of the V7 GMM at 1 second

The current empirical PGV model was also developed in 2021 (Bommer *et al*., 2021b) and we have calculated the total, inter- and intra- event residuals. Figure 2.15 shows the intra-event residuals of three component definitions of PGV with respect to the empirical GMPE plotted against hypocentral distance. With one exception, nearly all residuals of the Zeerijp earthquake recordings are within two within-event standard deviations of the zero line, which suggests that the model captures well the variability of the data. Similarly, to the residuals of the V7 GMM, a trend of the residuals with distance can be observed; in this case, it is clear that this trend arises from a group of positive residuals at about 15 km of hypocentral distance and one large positive residual at 25 km. In both cases however, the residuals are within the scatter of the data of the full database.

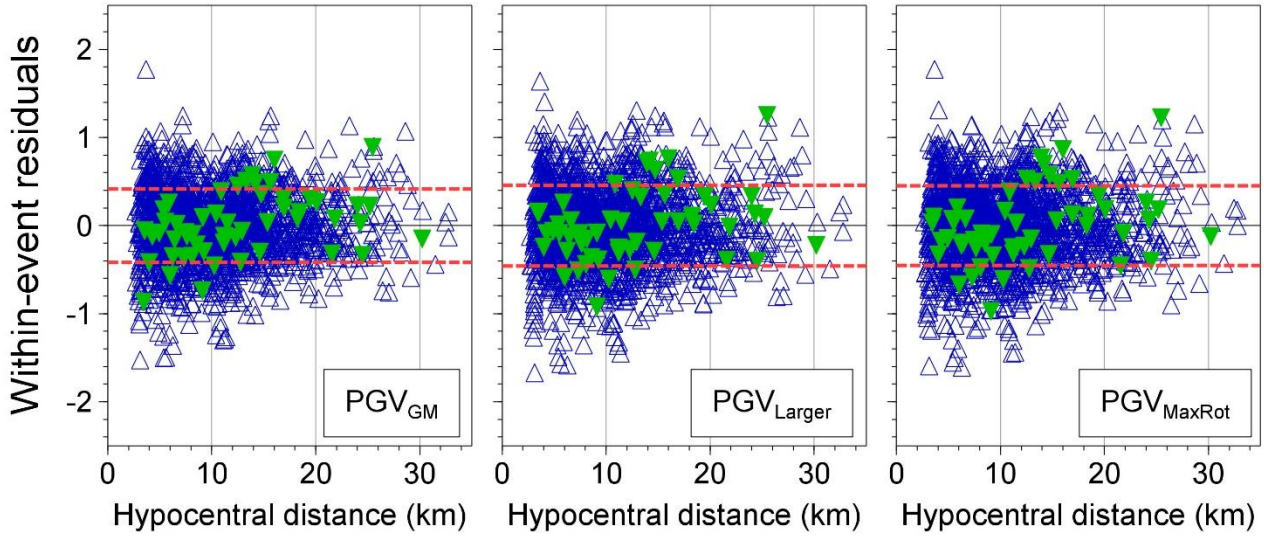

Figure 2.18. Event- and station-corrected within-event residuals of three component definitions of PGV with respect to the equations of the empirical PGV GMPE (Bommer et al., 2021b). Residuals of the Zeerijp earthquake recordings are shown in green and of other events in blue. The within-event standard deviation (φ_{SS}) is shown in red dashed lines.

Figure 2.16 compares the inter-event residuals (event-terms) of the Zeerijp earthquake to those of the previous events of the database. These event terms effectively represent the average offset of the recorded motions from each earthquake compared to the median prediction from the empirical model for the event magnitude, with a positive event-term indicating a stronger-than-average earthquake, a negative value a somewhat weaker-than-average earthquake. The event-term of the Zeerijp earthquake has a value very close to zero, confirming that the PGV values recorded are consistent with the model predictions and with PGV values recorded in previous events.

2.5 Concluding remarks Zeerijp Earthquake 4th October 2021 (2.5)

The M_L 2.5 Zeerijp earthquake of 4 October 2021 has generated a large number of ground-motion recordings. The largest component of PGA recorded in this earthquake is 0.01*g* and the largest value of PGV—which is generally considered a better indicator of the damage potential of the motion—recorded in this latest event is just 0.36 cm/s, which is significantly smaller than the largest value of the Groningen ground-motion database, a 3.46 cm/s recorded in the Huizinge earthquake.

An important observation is that the motions recorded in the Zeerijp earthquake are consistent with the predictions from the ground-motion model currently deployed in the seismic hazard and risk modelling for Groningen (NAM HRA and TNO SDRA) and the empirical PGV GMPEs used to assess damage claims.

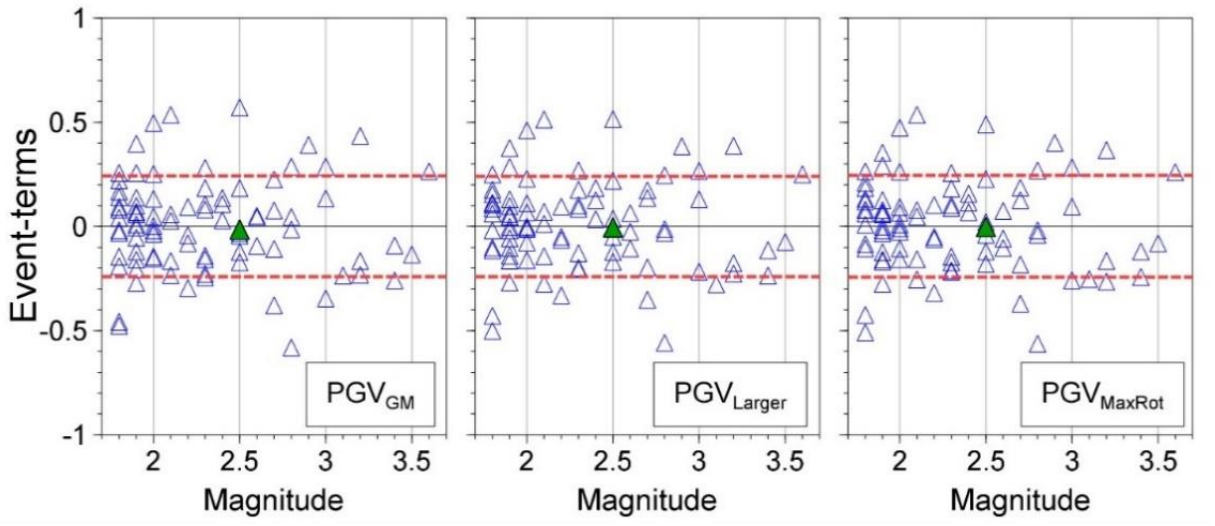

Figure 2.19. Inter-event residuals of three component definitions of PGV with respect to the equations of the empirical PGV GMPE (Bommer et al., 2021b). Residuals of the Zeerijp earthquake recordings are shown in green and of older events in blue. The inter-event standard deviation is shown in red dashed lines.

3 Analysis of the Surface Ground-Motions Recorded During the Appingedam M_L 1.8 Earthquake of 4th October 2021

3.1 Introduction

On Monday 4 October 2021 at 13:33 UTC (15:33 pm local time), an earthquake of local magnitude (M_L) of 1.8 occurred near the village of Appingedam, in the eastern part of the Groningen field (Figure 3.1). The epicentral coordinates (251118 X, 591576Y) depicted in Figure 3.1, as well as a focal depth of 3.1km, were calculated by Dr Jesper Spetzler of KNMI using the 3D EDT method (Spetzler & Dost, 2017).

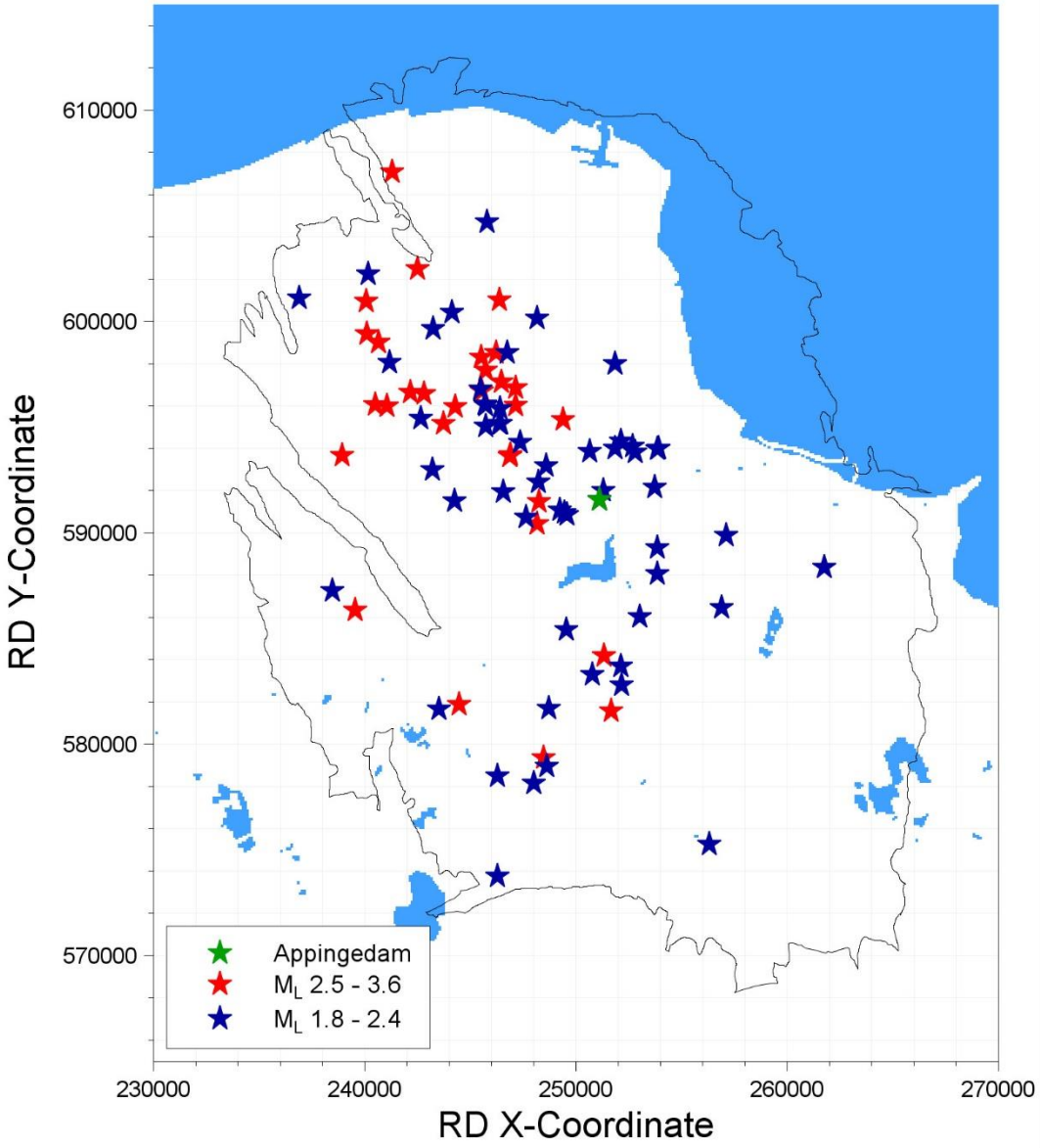

Figure 3.1. Epicentre of Appingedam earthquake (green star) together with epicentres of previous earthquakes of $M_L \geq 2.5$ (red stars) and of M_L 1.8-2.4 (blue stars)

Two more events occurred on the same day, both near the village of Zeerijp in the north-west, one with a local magnitude of 2.5 at 04:59 pm local time and another one with a magnitude of 2.2 at 20:47. The last event with a magnitude equal or larger to M_L1.8–the smallest magnitude considered in the development of the empirical PGV GMPEs for Groningen (Bommer *et al*., 2021b)- was the M_L1.8 Hellum earthquake of 5 August 2021.

The KNMI portal (http://rdsa.knmi.nl/dataportal/) made accelerograms from the earthquake available within an hour of the event and 83 three-component recordings were downloaded and processed for this preliminary assessment of the motions. The records were processed as described by Edwards & Ntinalexis (2021) and only 6 records were deemed usable. This very small number is a result of generally very low recorded amplitudes with small signal-to-noise ratios, which were influenced by the small magnitude of the event as well as the location of its epicentre, at the eastern edge of the field and a distance to many recording stations that is significant for an event of this magnitude.

Figure 3.2 shows the usable recordings in the magnitude-distance occupied by the database used to derive the current empirical Ground-Motion Prediction Equations (GMPEs) used to estimate values of peak ground velocity (PGV) occurring during earthquakes in the Groningen field (Bommer *et al*., 2021b). This chapter presents an overview of the recorded motions from the Appingedam event in terms of their amplitudes and durations, and discusses how the recorded amplitudes of motion compare with predictions from the empirical PGV GMPE and the V7 Ground-Motion Model (GMM; Bommer *et al*., 2021a) The discussions focus primarily on peak ground acceleration (PGA), which is assumed equal to the spectral acceleration at a period of 0.01 seconds, and PGV, which has been shown to correlate very well with the spectral acceleration at a period of 0.3 seconds for the Groningen data (Figure 3.3).

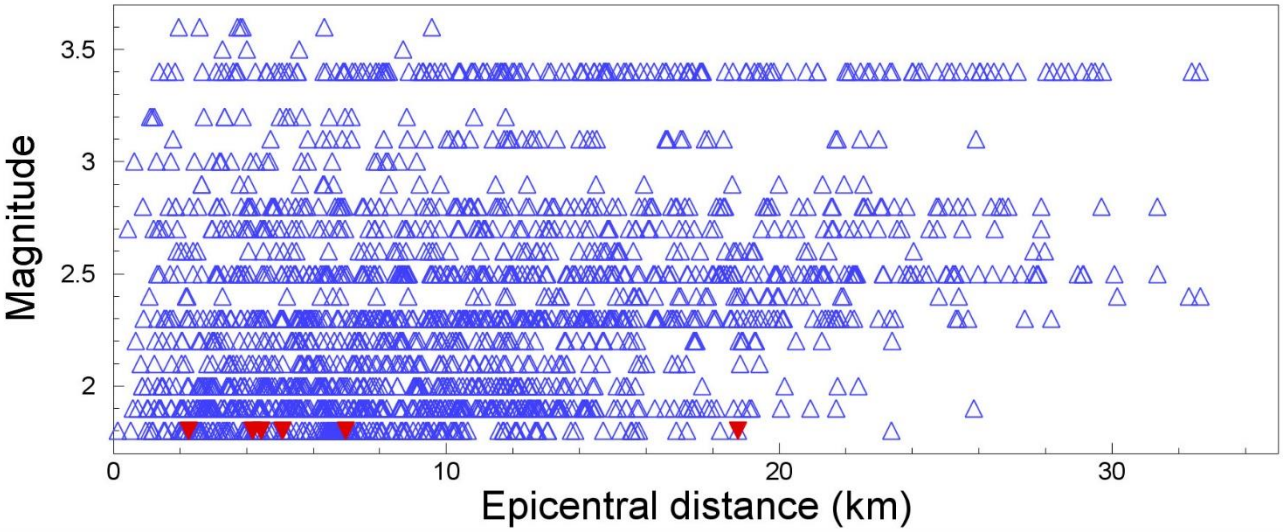

Figure 3.2. Magnitude-distance distribution of the Groningen strong-motion database including the recordings of the 4 October 2021 Appingedam earthquake

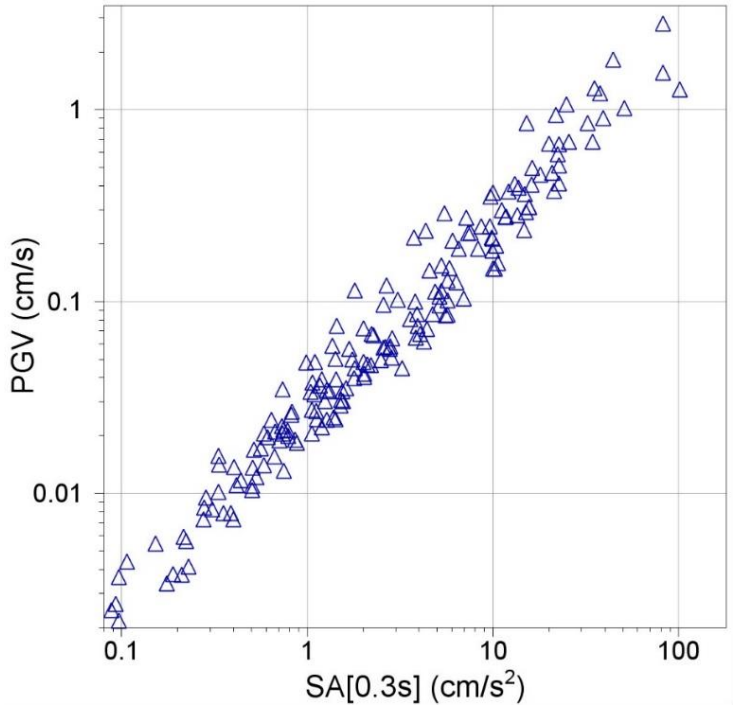

Figure 3.3. Correlation between values of PGV and spectral accelerations at 0.3 seconds for the Groningen strong-motion database (Bommer et al., 2018)

3.2 Peak Ground Accelerations and Velocities

Figures 3.4 and 3.5 show the horizontal values of PGV and PGA of three component definitions from each recording obtained during the Zeerijp earthquake plotted against the distance of the recording site from the epicentre. The largest amplitude was obtained at the H2 (EW) component of station G240 located 2.25 km from the epicentre: the PGA recorded is 1.75 cm/s^2. The second and third largest PGA values were recorded at station G300, 5.09 km from the epicentre: 1.40 cm/s^2 on the H2 (EW) component and 1.30 on the H1 (NS) component. The three largest PGV values were recorded at the same stations and are 0.043 cm/s (H2 component of G240), 0.020 cm/s (H1 component of G300) and 0.017 (H2 component of G300).

From Figures 3.4 and 3.5 it is immediately apparent that the amplitudes of motion are lower than previous earthquakes of comparable size. Figure 3.5 shows the horizontal components of PGA and PGV obtained within 6 km of the epicentre, from which it can be appreciated that the very strong polarisation often observed in near-source Groningen recordings (*e.g.*, Bommer *et al.*, 2017) is also apparent in records of this event.

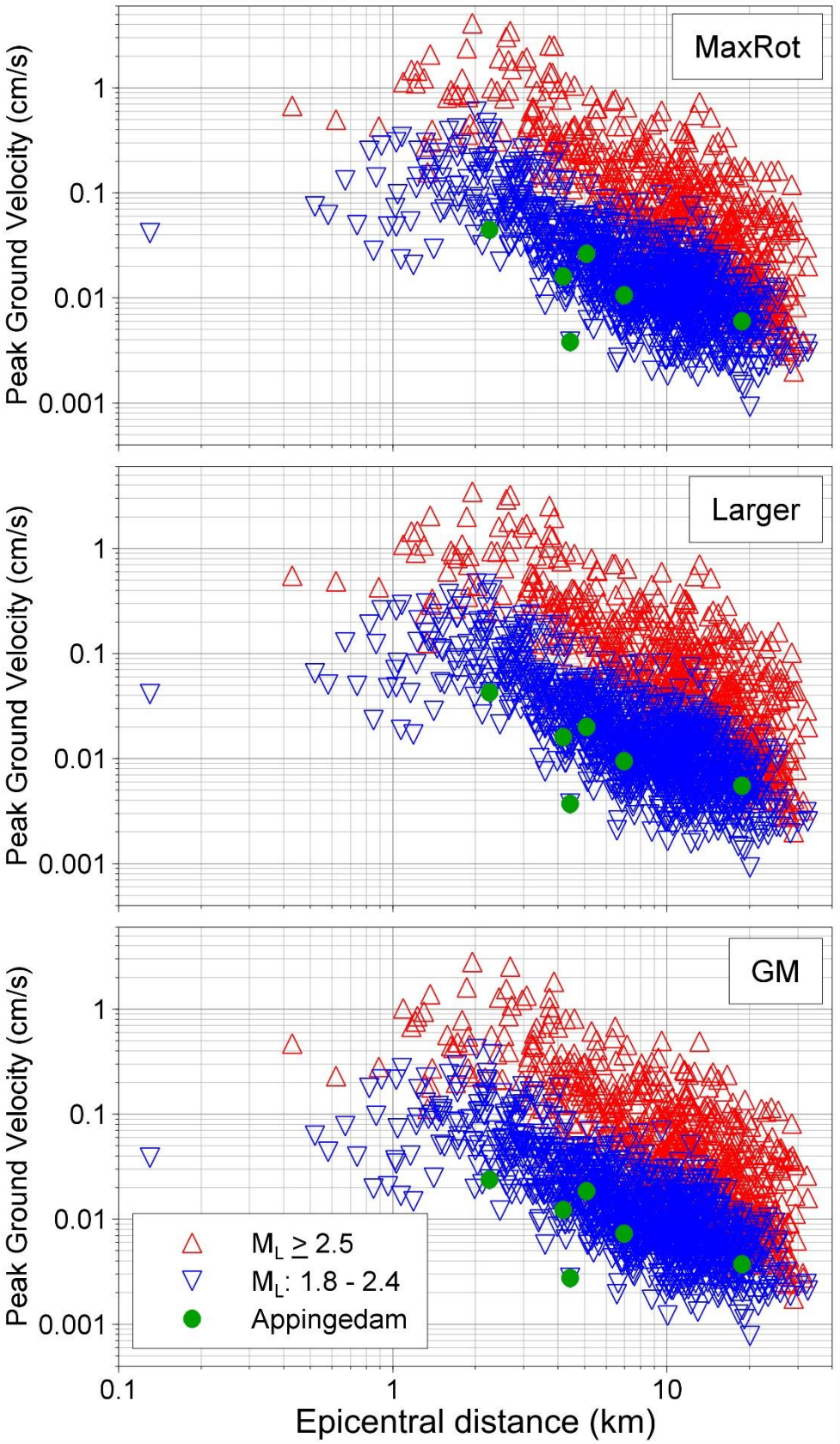

Figure 3.4. Horizontal components of PGV recorded during the Appingedam earthquake and previous earthquakes plotted against epicentral distance

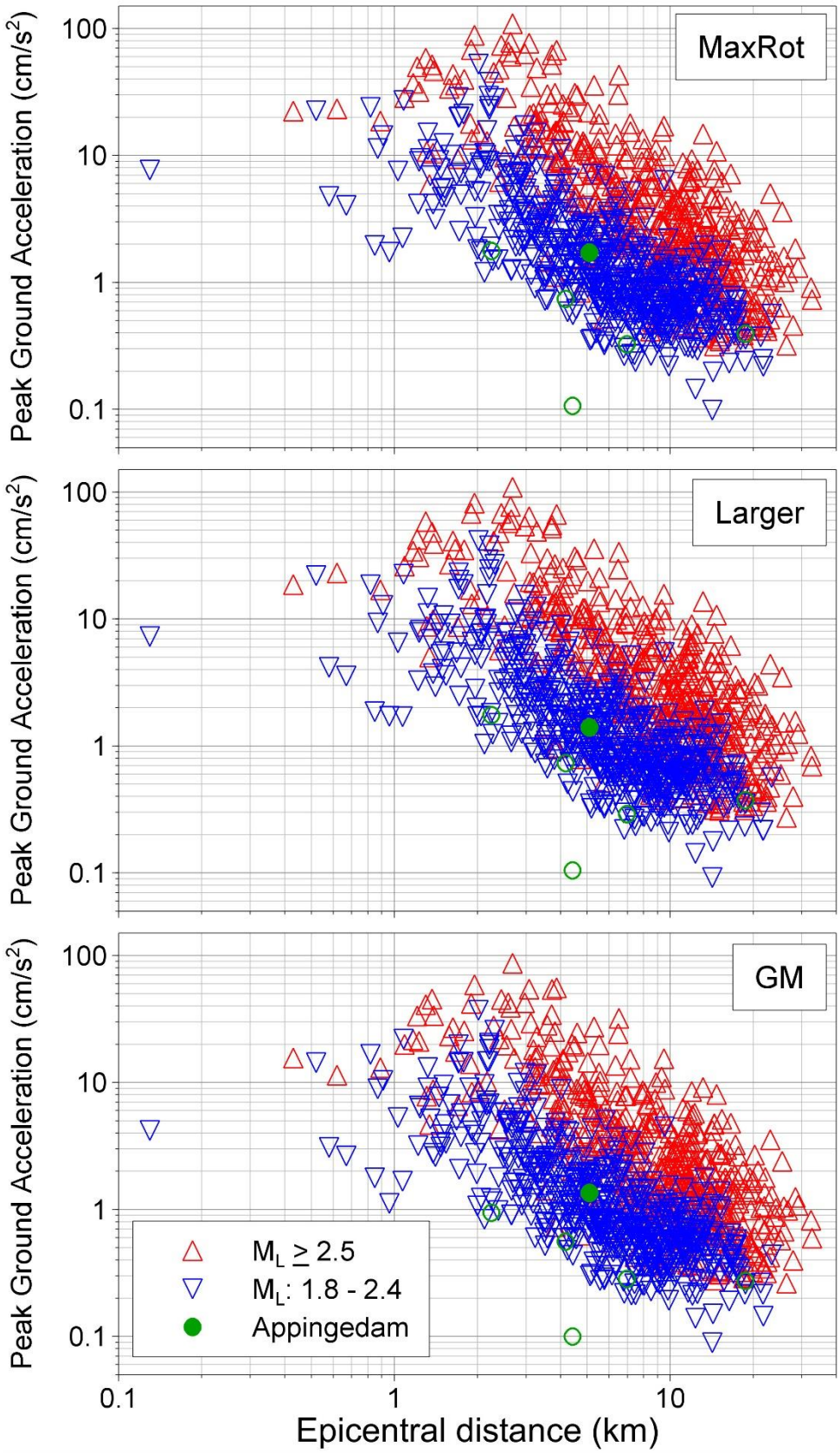

Figure 3.5. Horizontal components of PGV recorded during the Appingedam earthquake and previous earthquakes plotted against epicentral distance. PGA values recorded during the earthquake but considered unusable following processing are also included in open circles

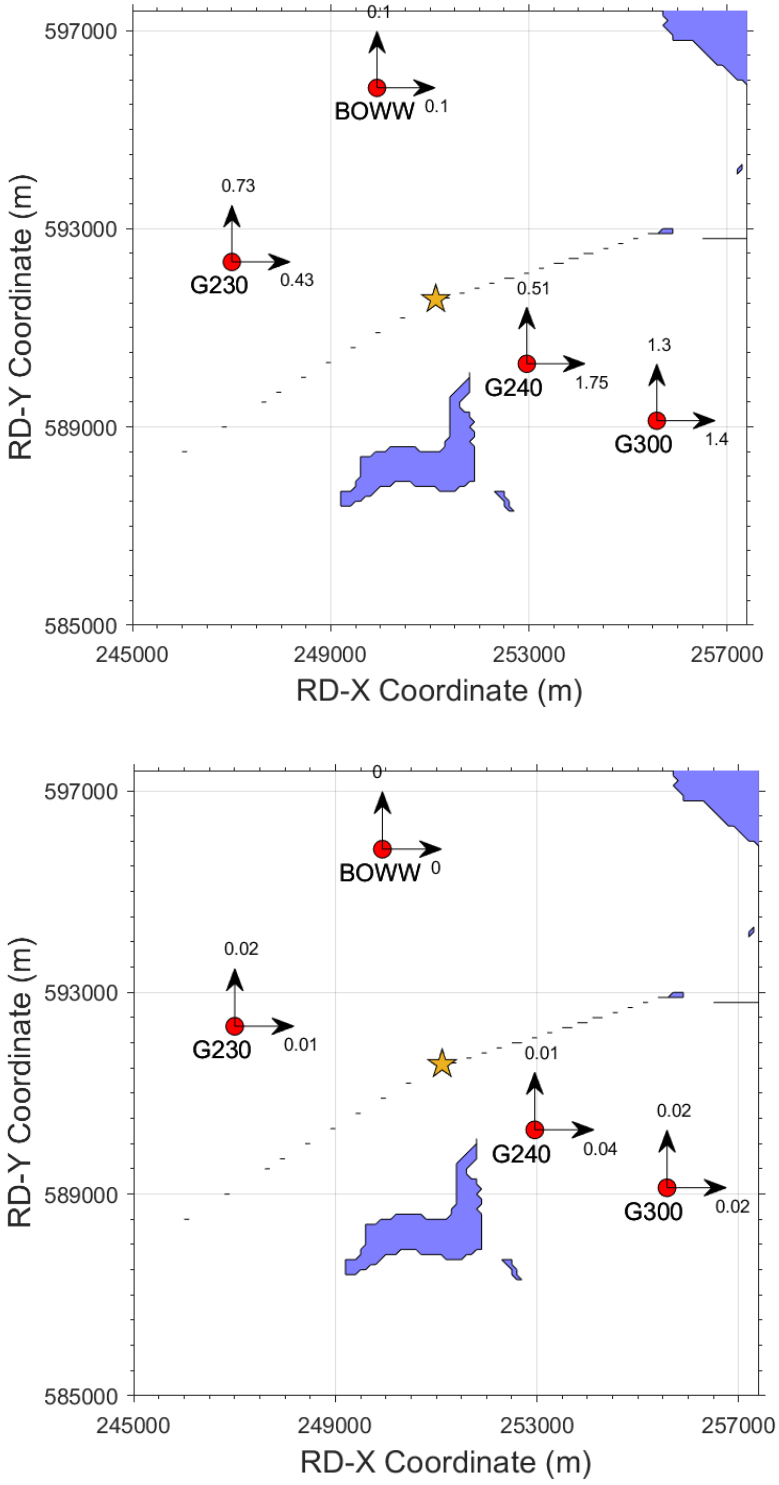

Figure 3.6. Horizontal components of PGA (upper) and PGV (lower) recorded during the Appingedam earthquake at epicentral distances of less than 6 km; units are cm/s² and cm/s, respectively.

As already shown in Figures 3.4 and 3.5, the amplitudes decay rapidly with distance although the effect of simultaneous arrivals of direct and critically refracted/reflected waves leads to an increase in amplitudes at some locations between 12 and 20 km from the epicentre. However, these effects do not lead to significant absolute amplitudes at those distances and it is clear from Figure 3.6 that, outside the epicentral area, the motions are of very low amplitude: < 0.001*g* for PGA and < 0.05 cm/s for PGV.

Overall, the motions appear lower on average than those observed in previous earthquakes. Figure 3.7 shows the geometric mean horizontal components of PGA and PGV plotted against magnitude together with the corresponding values from the complete database.

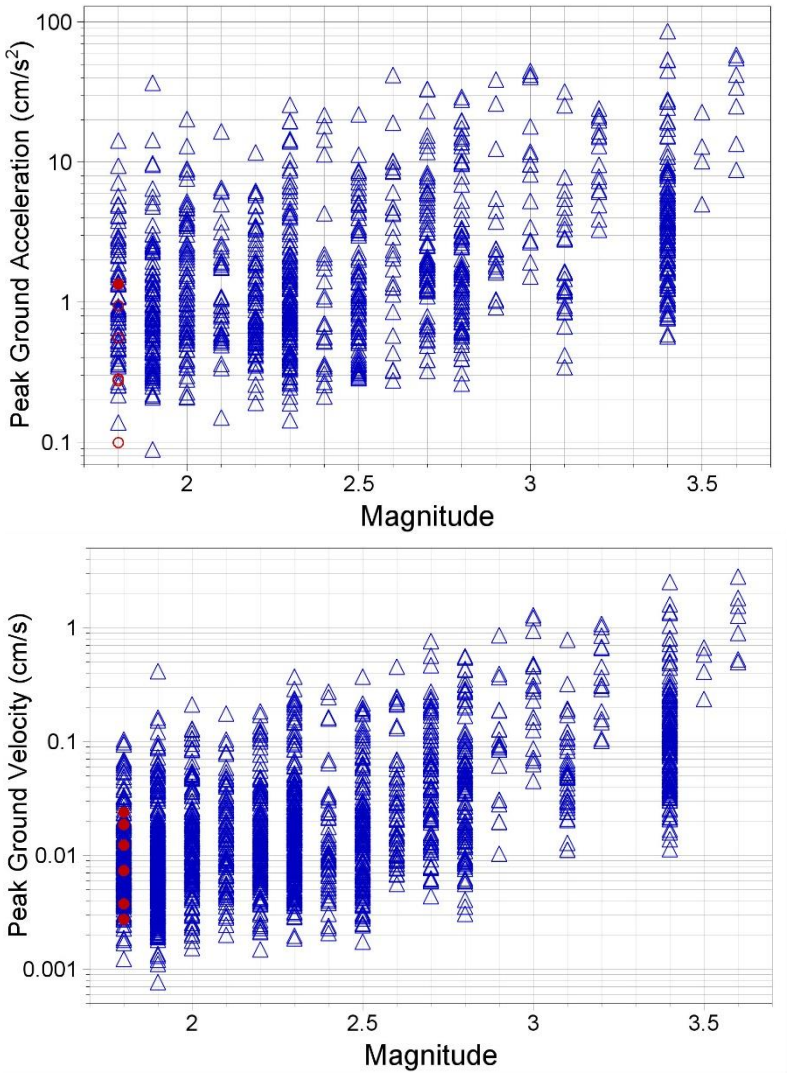

Figure 3.7. Geometric mean horizontal components of PGA (upper) and PGV (lower) recorded during the Appingedam earthquake (red) and in previous earthquakes (blue) plotted against local magnitude. PGA values recorded during the earthquake but considered unusable following processing are also included in open circles

3.3 Ground-Motion Durations

The maximum amplitude of ground shaking, whether represented by PGA or PGV, provides a simple indication of the strength of the motion but the potential for adverse effects—such as damage to masonry buildings or triggering liquefaction—also depends on the duration or number of cycles of the motion.

A feature that has been consistently observed in the Groningen ground motions is a very pronounced negative correlation between PGA and duration, with high amplitude motions consistently associated with shaking of very short duration (Bommer *et al.*, 2016). The same pattern is observed in the recordings of the Appingedam earthquake. The largest value of PGA, recorded on the H2 (EW) component at the G240 station, is associated with a duration smaller than one second (0.67 s). The horizontal components of both acceleration and velocity from this station are shown in Figure 3.8, which also shows the build-up of Arias intensity (which is a measure of the energy in the motion) over

time. The strong concentration of the energy in a single pulse of motion in the H2 component is immediately apparent. The larger amplitude component of the G300 recording—the source of the second largest PGA value—is associated with a significant duration of 2.355 s (Figure 3.9).

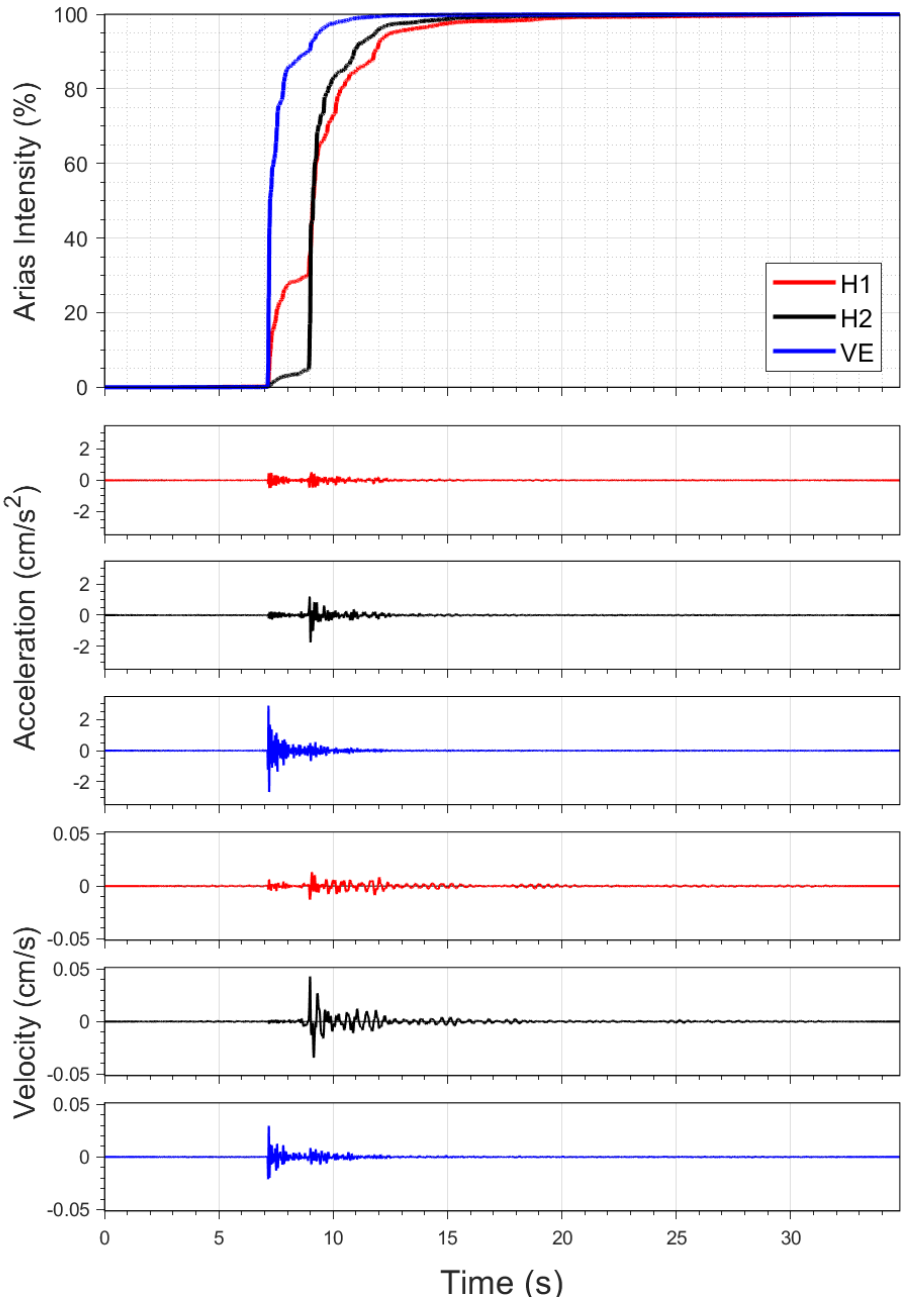

Figure 3.8. Horizontal components of acceleration and velocity from the G240 station; the upper frame shows the accumulation of Arias intensity (energy) over time.

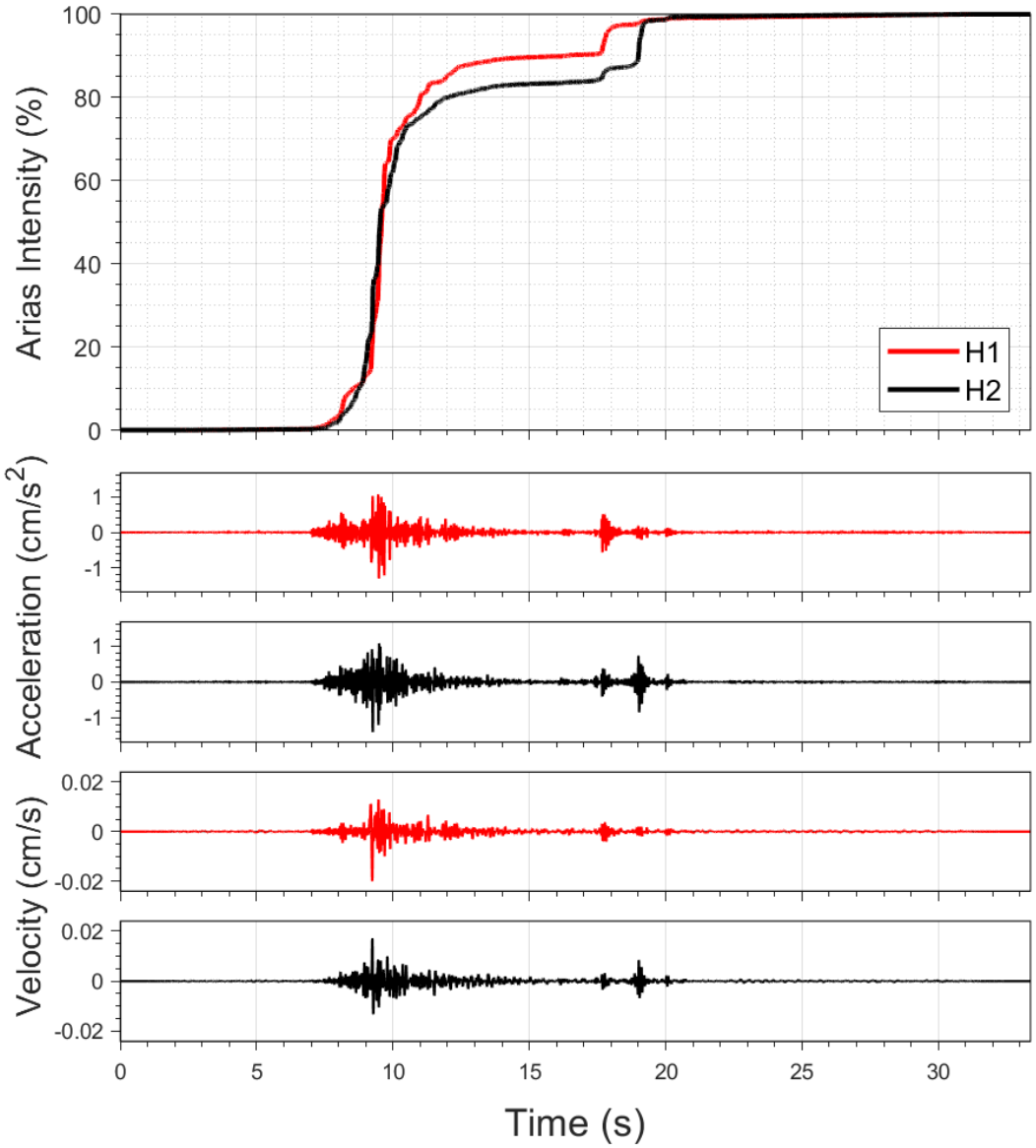

Figure 3.9. Horizontal components of acceleration and velocity from the G300 station; the upper frame shows the accumulation of Arias intensity (energy) over time.

3.4 Spectral Accelerations and Comparison with Ground-Motion Models

Additional insight into the nature of the ground motions can be obtained from the 5%-damped acceleration response spectra. The horizontal acceleration response spectra from the G240 and G300 recordings of the Appingedam earthquake are shown in Figure 3.10. The spectral shapes are consistent with previous observations in the field. The divergence between the red and black curves in the upper frame shows that the horizontal polarisation of the G240 recording seen for PGA and PGV (Figure 3.6) persists across the entire range of usable response periods.

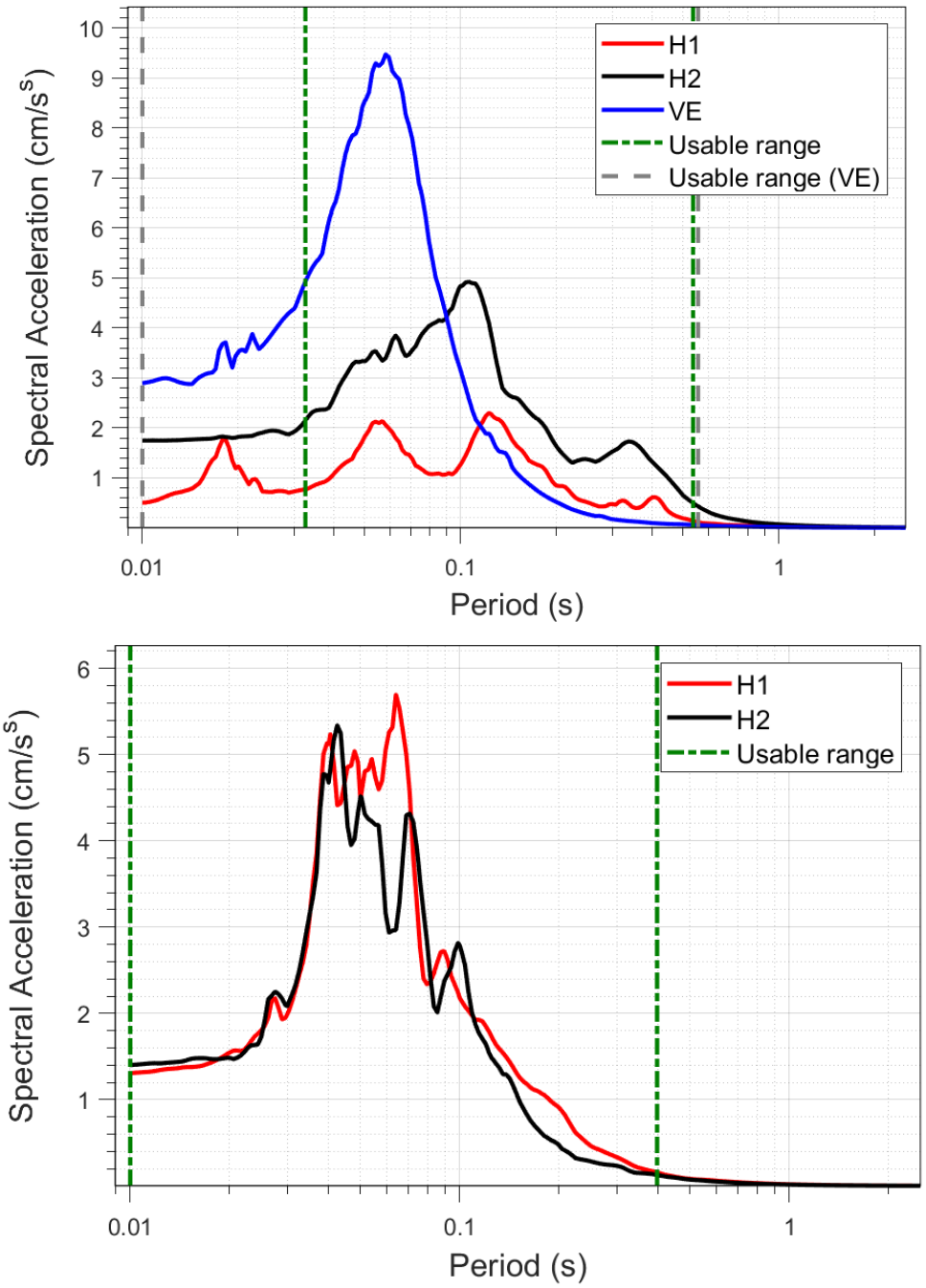

Figure 3.10. Horizontal response spectra from the G240 (upper) and G300 (lower) stations; vertical spectra plotted as dashed lines beyond maximum usable period.

For this preliminary analysis, the key question of interest is whether the motions recorded in this earthquake are consistent with the empirical PGV GMPEs being used in the Groningen field. The current empirical PGV model was developed in 2021 and published shortly before the event (Bommer *et al*., 2021b) and we have calculated the total, inter- and intra- event residuals. Figure 3.10 shows the intra-event residuals of three component definitions of PGV with respect to the empirical GMPE plotted against hypocentral distance. With one exception, nearly all residuals of the Appingedam earthquake recordings are within two within-event standard deviations of the zero line, which suggests that the model captures well the variability of the data.

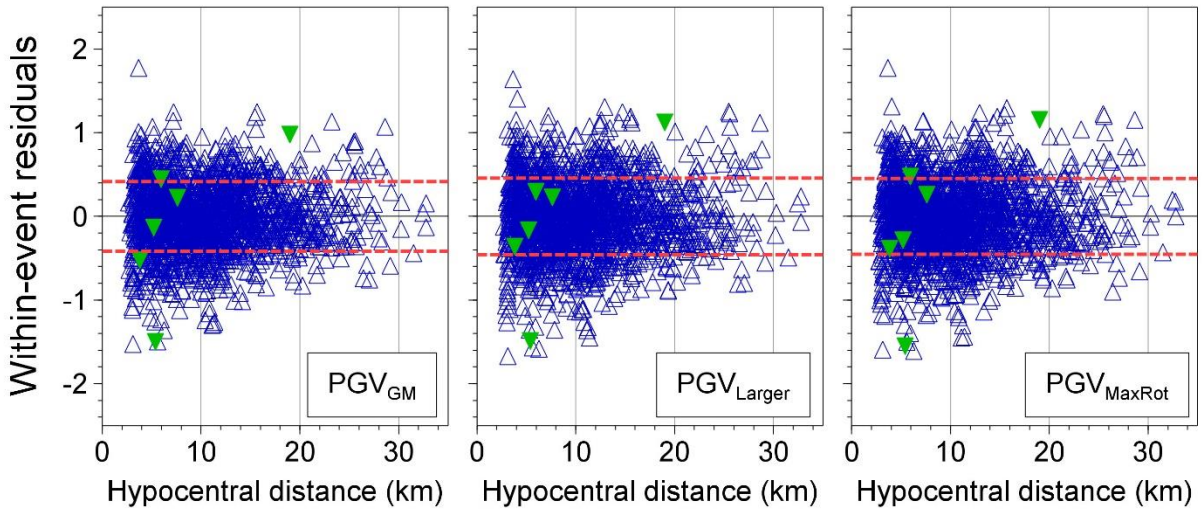

Figure 3.11. Event- and station-corrected within-event residuals of three component definitions of PGV with respect to the equations of the empirical PGV GMPE (Bommer et al., 2021b). Residuals of the Zeerijp earthquake recordings are shown in green and of other events in blue. The within-event standard deviation (φ_{SS}) is shown in red dashed lines.

Figure 3.12 compares the inter-event residuals (event-terms) of the Zeerijp earthquake to those of the previous events of the database. These event terms effectively represent the average offset of the recorded motions from each earthquake compared to the median prediction from the empirical model for the event magnitude, with a positive event-term indicating a stronger-than-average earthquake, a negative value a somewhat weaker-than-average earthquake. The event-term of the Appingedam earthquake is strongly negative, almost one inter-event standard deviation below zero for the geometric-component, indicating an over-prediction by the model medians and smaller PGV values recorded than in previous events.

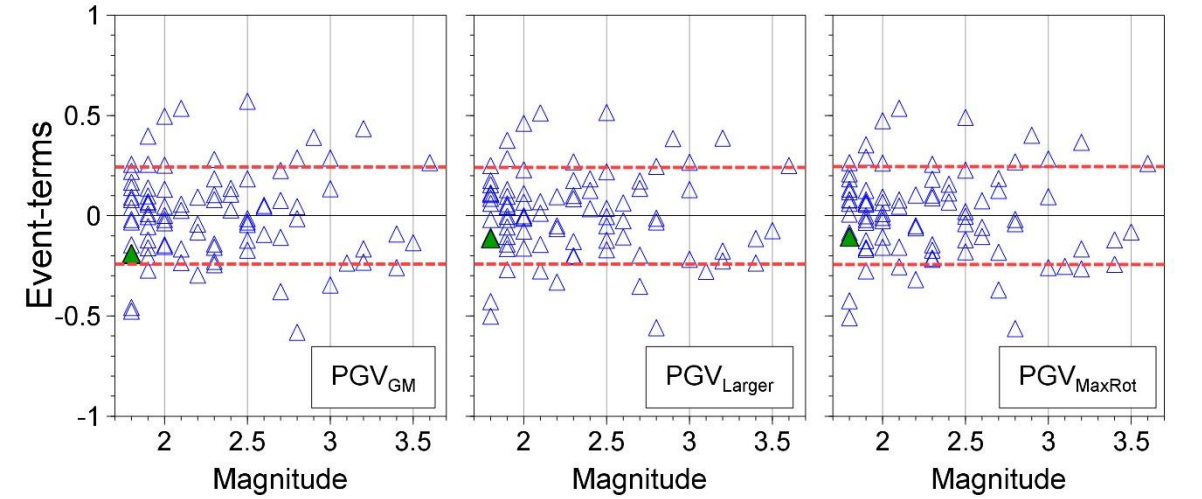

Figure 3.12. Inter-event residuals of three component definitions of PGV with respect to the equations of the empirical PGV GMPE (Bommer et al., 2021b). Residuals of the Appingedam earthquake recordings are shown in green and of older events in blue. The inter-event standard deviation is shown in red dashed lines.

3.5 Concluding remarks Appingedam Earthquake 4th October 2021 (1.8)

The M_L 1.8 Appingedam earthquake of 4 October 2021 has generated a small number of ground-motion recordings of relatively small amplitudes. The largest component of PGA recorded in this earthquake is 0.002*g* and the largest value of PGV—which is generally considered a better indicator

of the damage potential of the motion—recorded in this latest event is just 0.04 cm/s, which is significantly smaller than the largest value of the Groningen ground-motion database, a 3.46 cm/s recorded in the Huizinge earthquake.

An important observation is that the motions recorded in the Appingedam earthquake are consistent but lower than the median predictions of the empirical PGV GMPEs used to assess damage claims.

4 Analysis of the Surface Ground-Motions Recorded During the Zeerijp M_L 2.2 Earthquake of 4th October 2021

4.1 Introduction

On Monday 4 October 2021 at 18:47 UTC (20:47 pm local time), an earthquake of local magnitude (M_L) of 2.5 occurred near the village of Zeerijp, in the northern part of the Groningen field (Figure 4.1). The epicentral coordinates (245484 X, 596810Y) depicted in Figure 4.1, as well as a focal depth of 2.7km, were calculated by Dr Jesper Spetzler of KNMI using the 3D EDT method (Spetzler & Dost, 2017).

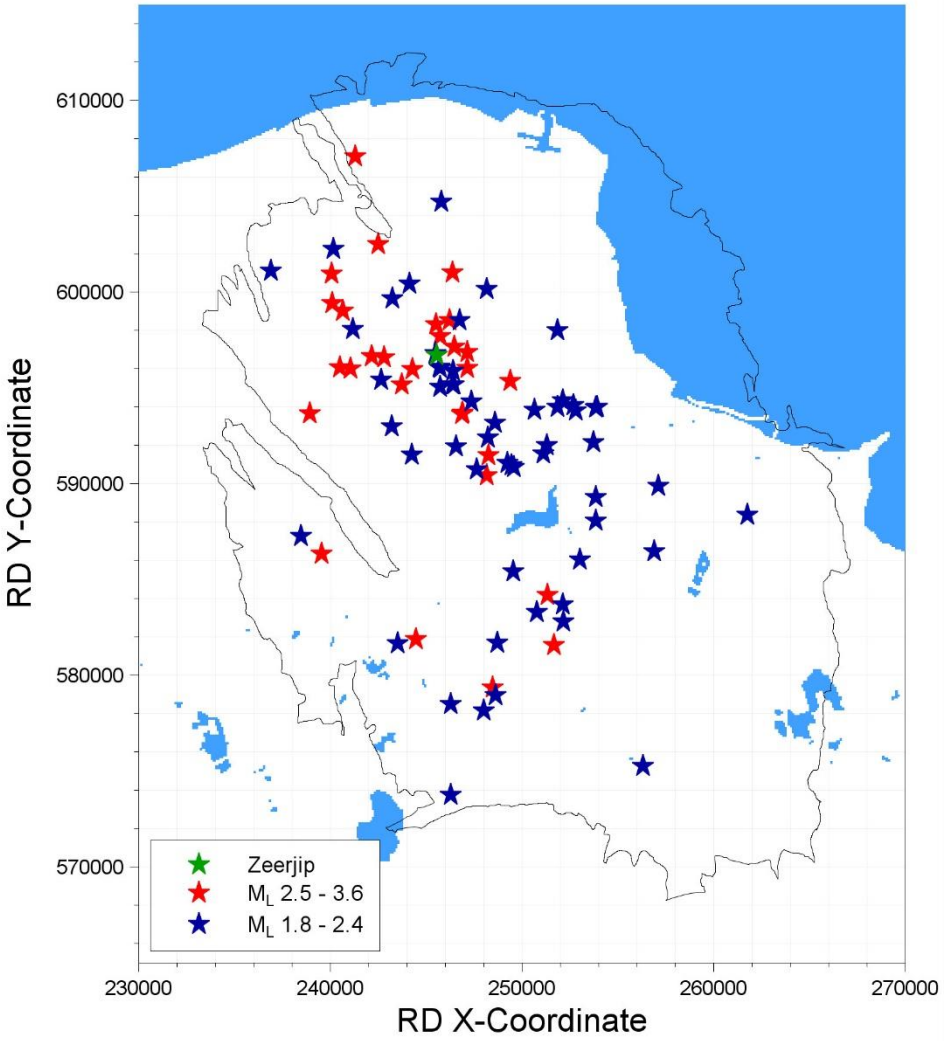

Figure 4.1. Epicentre of Zeerijp earthquake (green star) together with epicentres of previous earthquakes of $M_L \geq 2.5$ (red stars) and of M_L 1.8-2.4 (blue stars)

Two more events occurred on the same day, one with a local magnitude of 1.8 in Appingedam at 15:33 pm local time and another one with a magnitude of 2.5 also in Zeerijp earlier at 04:59. The last event with a magnitude equal or larger to M_L1.8–the smallest magnitude considered in the development of the empirical PGV GMPEs for Groningen (Bommer *et al.*, 2021b) was the M_L1.8 Hellum earthquake of

5 August 2021. In keeping with trend during more recent earthquakes (Figure 4.2), the latest earthquake has triggered a large number of accelerograms, as a direct result of the expansion of the strong-motion recording networks in the Groningen field (Dost *et al*., 2017; Ntinalexis *et al*., 2019).

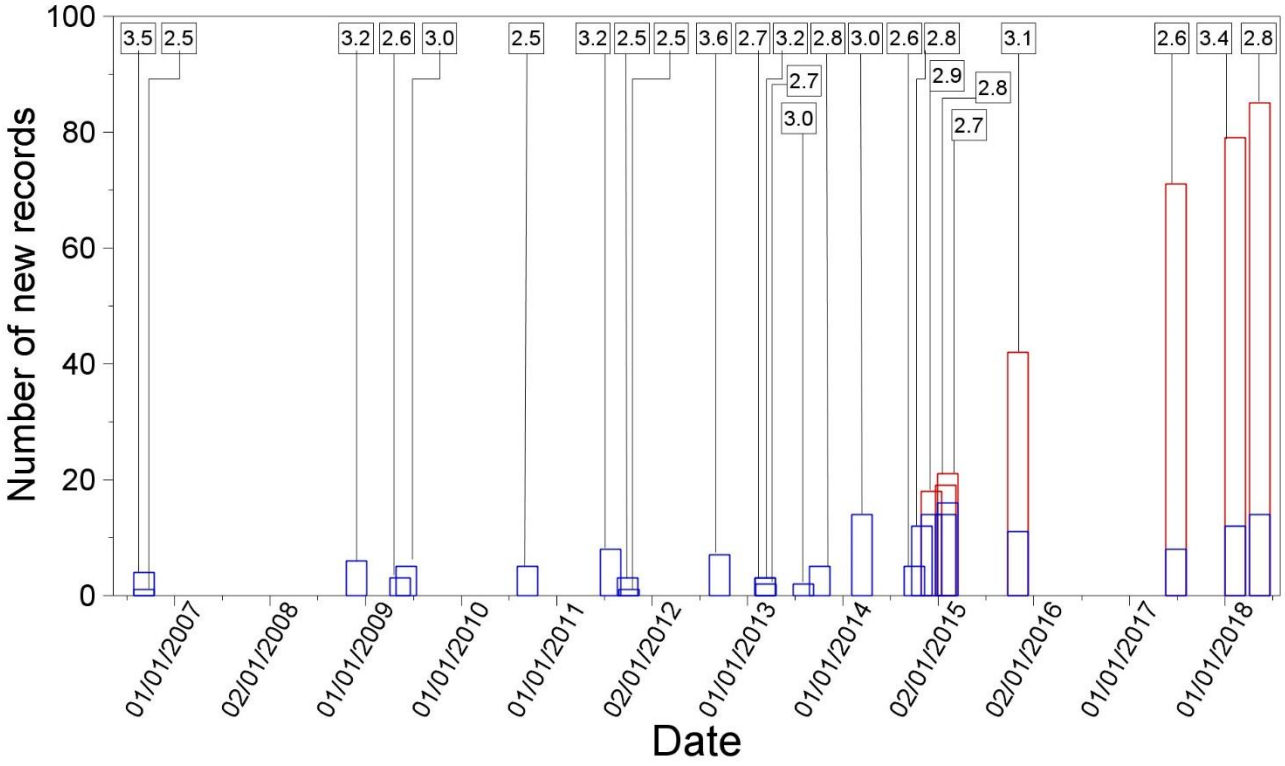

Figure 4.2. Diagram illustrating the timing of earthquakes of $M_L \geq 2.5$ in the Groningen field until the end of 2018 and the number of records yielded by the permanent KNMI network (B-stations, blue) and by the expanded borehole geophone network (G-stations, red).

The KNMI portal (http://rdsa.knmi.nl/dataportal/) made accelerograms from the earthquake available within an hour of the event and 82 three-component recordings were downloaded and processed for this preliminary assessment of the motions. The records were processed as described by Edwards & Ntinalexis (2021) and a total of 50 records were deemed usable. Figure 4.3 shows the usable recordings in the magnitude-distance occupied by the database used to derive the current empirical Ground-Motion Prediction Equations (GMPEs) used to estimate values of peak ground velocity (PGV) occurring during earthquakes in the Groningen field (Bommer *et al*., 2021b). This chapter presents an overview of the recorded motions from the Zeerijp event in terms of their amplitudes and durations, and discusses how the recorded amplitudes of motion compare with predictions from the empirical PGV GMPE and the V7 Ground-Motion Model (GMM; Bommer *et al*., 2021a) The discussions focus primarily on peak ground acceleration (PGA), which is assumed equal to the spectral acceleration at a period of 0.01 seconds, and PGV, which has been shown to correlate very well with the spectral acceleration at a period of 0.3 seconds for the Groningen data (Figure 4.4).

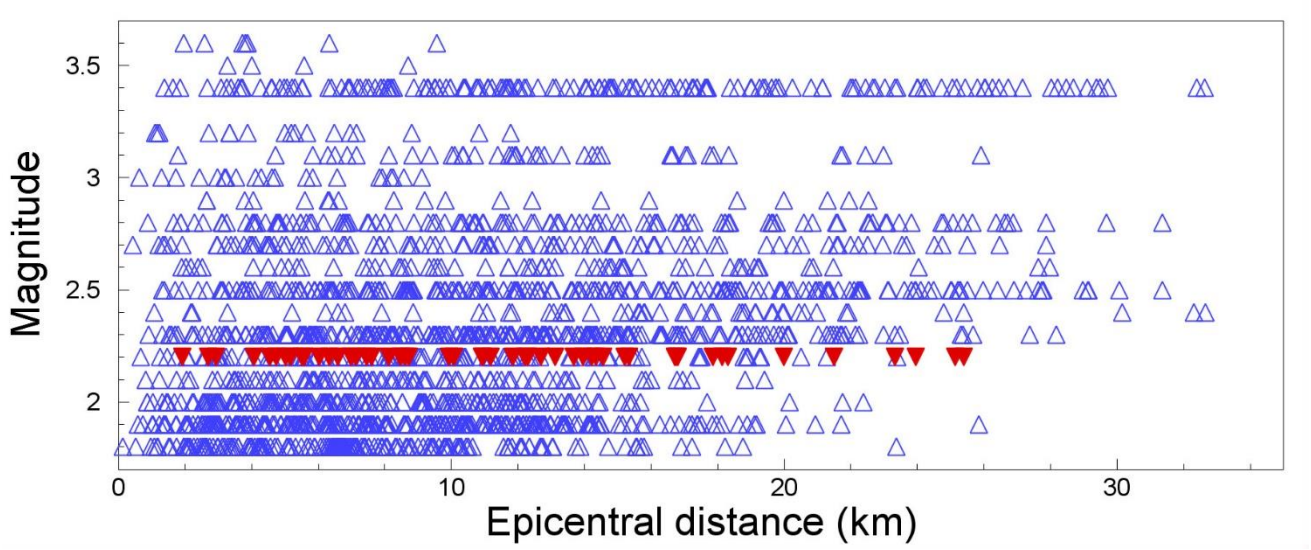

Figure 4.3. Magnitude-distance distribution of the Groningen strong-motion database including the recordings of the 4 October 2021 Zeerijp earthquake

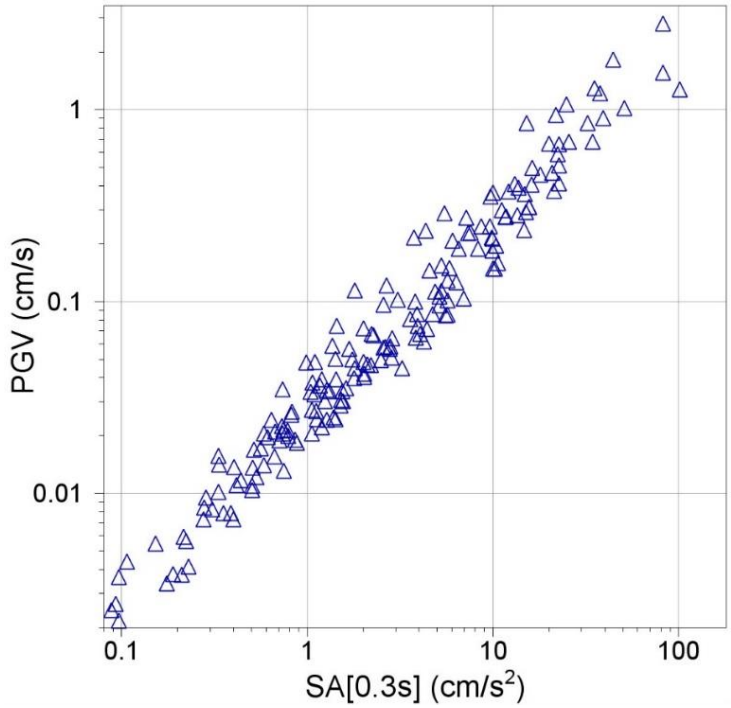

Figure 4.4. Correlation between values of PGV and spectral accelerations at 0.3 seconds for the Groningen strong-motion database (Bommer et al., 2018)

4.2 Peak Ground Accelerations and Velocities

Figures 4.5 and 4.6 show the horizontal values of PGA and PGV of three component definitions from each recording obtained during the Zeerijp earthquake plotted against the distance of the recording site from the epicentre. The largest amplitude was obtained at the H2 (EW) component of station G140 located 1.9 km from the epicentre: the PGA recorded is 6.53 cm/s^2. The second largest PGA value was recorded at station BGAR, 2.93 km from the epicentre: 4.00 cm/s^2 on the EW component. The largest PGV and second largest PGV values were recorded at the same components of the two stations and are 0.19 cm/s and 0.09 cm/s, respectively.

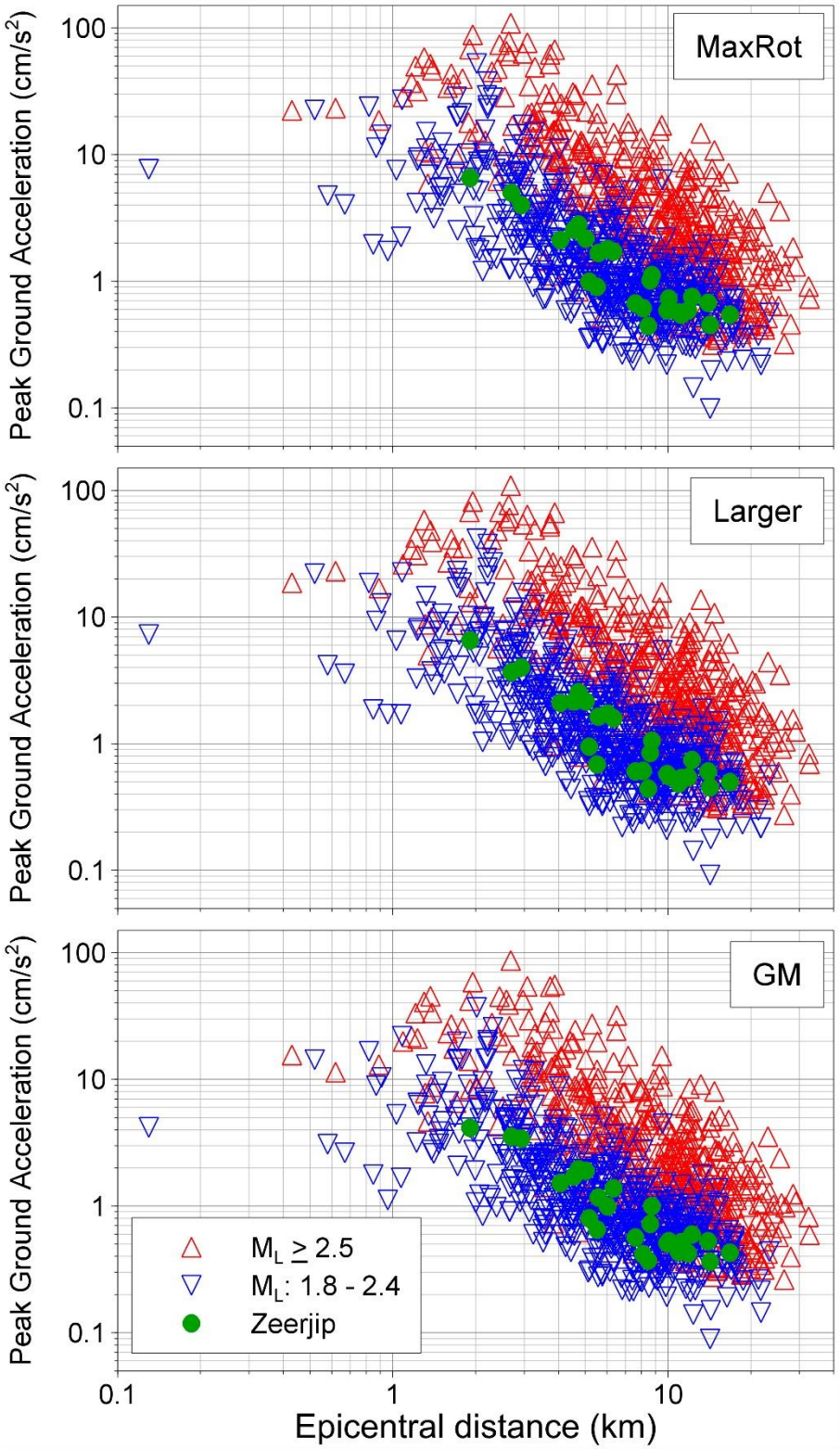

Figure 4.5. Horizontal components of PGA recorded during the Zeerijp earthquake and previous earthquakes plotted against epicentral distance

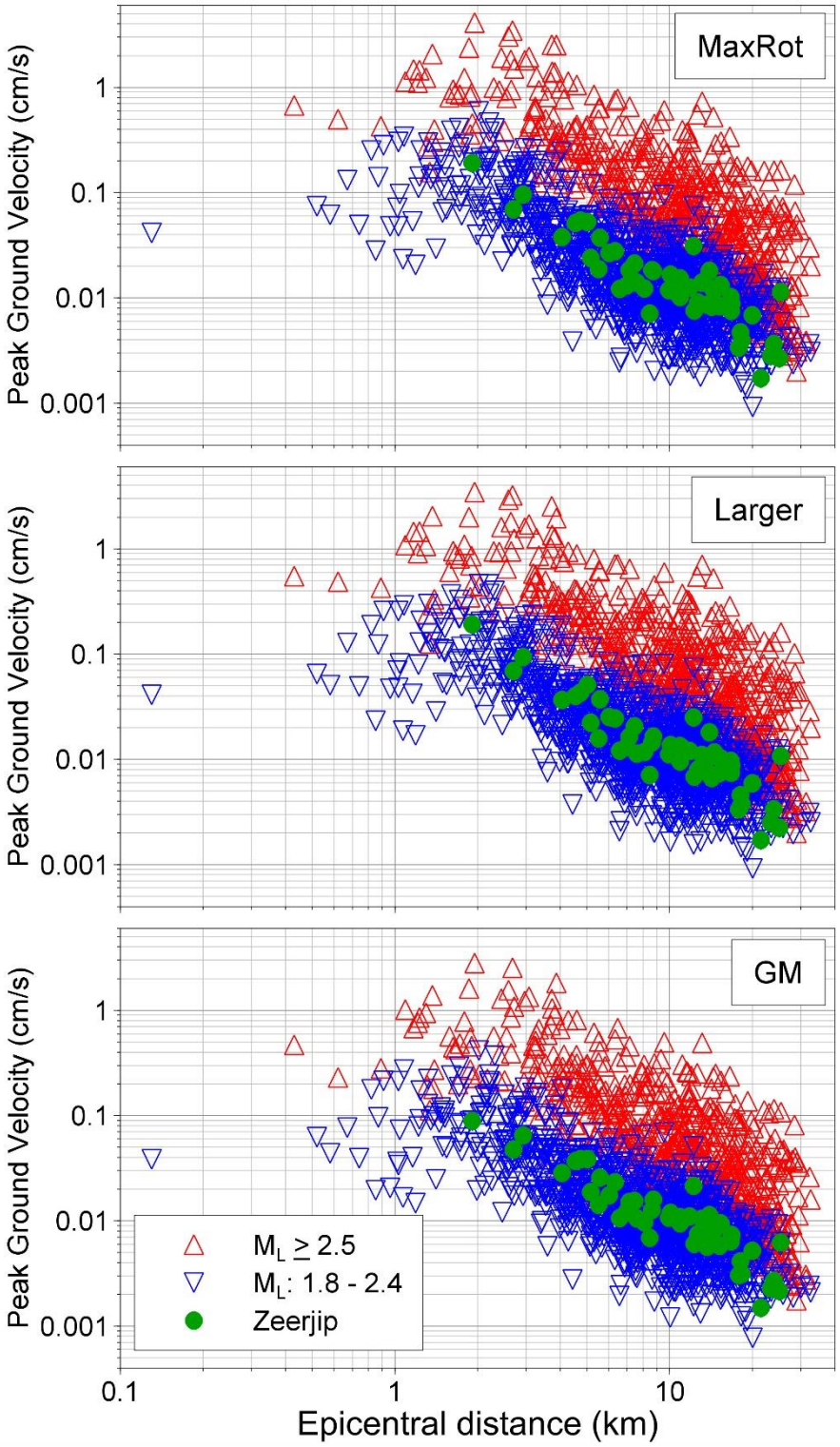

Figure 4.6. Horizontal components of PGV recorded during the Zeerijp earthquake and previous earthquakes plotted against epicentral distance

From Figures 4.5 and 4.6 it is immediately apparent that the amplitudes of motion are consistent with previous earthquakes of comparable size. Figure 4.7 shows the horizontal components of PGA and PGV obtained within 6 km of the epicentre, from which it can be appreciated that the very strong polarisation often observed in Groningen recordings (*e.g.*, Bommer *et al.*, 2017) is also apparent in records of this event.

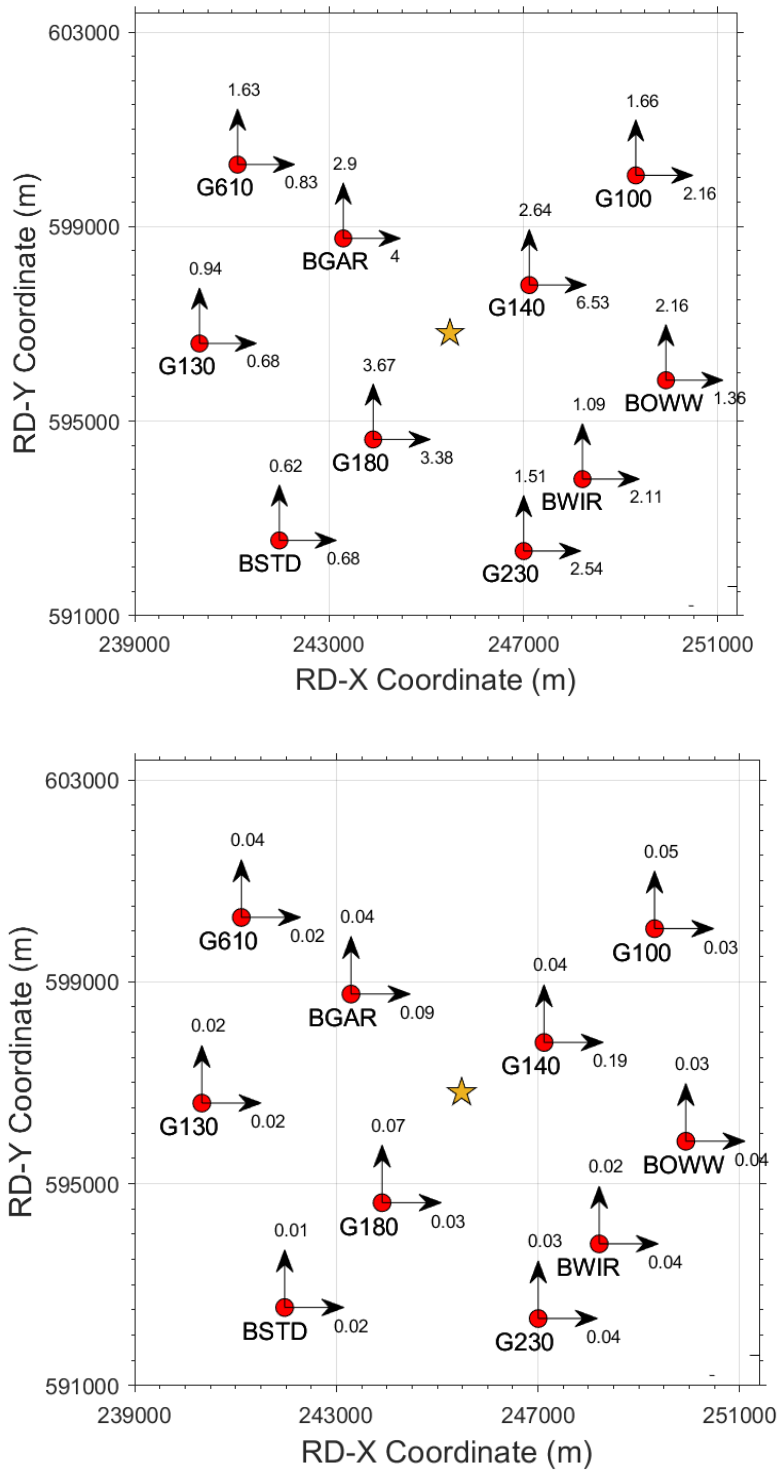

Figure 4.7. Horizontal components of PGA (upper) and PGV (lower) recorded during the Zeerijp earthquake at epicentral distances of less than 6 km; units are cm/s² and cm/s, respectively.

As already shown in Figures 4.5 and 4.6, the amplitudes decay rapidly with distance although the effect of simultaneous arrivals of direct and critically refracted/reflected waves leads to an increase in amplitudes at some locations between 12 and 20 km from the epicentre. However, these effects do not lead to significant absolute amplitudes at those distances and it is clear from Figure 4.7 that, outside the epicentral area, the motions are of very low amplitude: < 0.01*g* for PGA and < 0.1 cm/s for PGV.

Overall, the motions appear similar to those observed in previous earthquakes. Figure 4.8 shows the geometric mean horizontal components of PGA and PGV plotted against magnitude together with the corresponding values from the complete database.

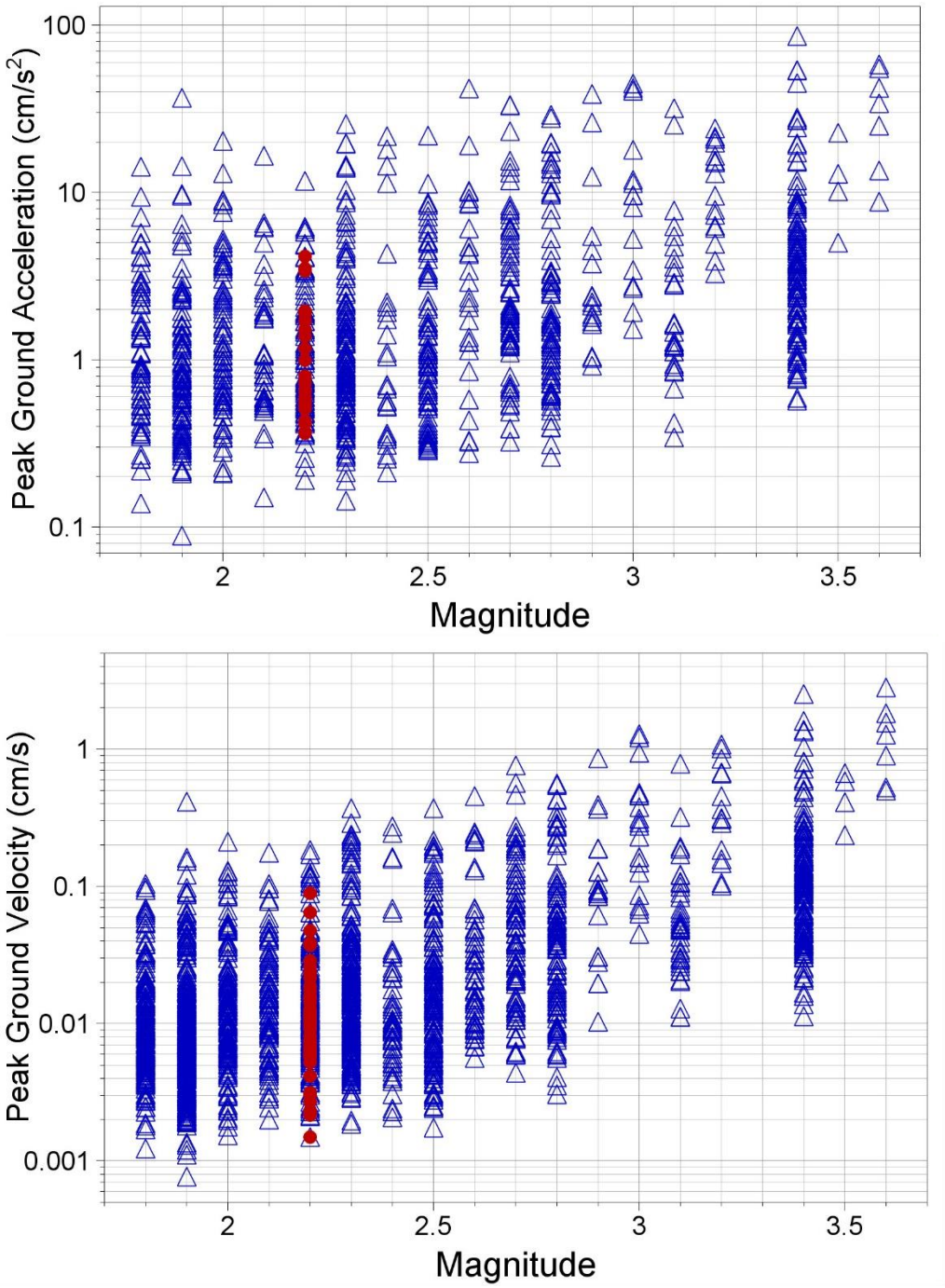

Figure 4.8. Geometric mean horizontal components of PGA (upper) and PGV (lower) recorded during the Zeerijp earthquake (red) and in previous earthquakes (blue) plotted against local magnitude

4.3 Ground-Motion Durations

The maximum amplitude of ground shaking, whether represented by PGA or PGV, provides a simple indication of the strength of the motion but the potential for adverse effects—such as damage to masonry buildings or triggering liquefaction—also depends on the duration or number of cycles of the motion.

A feature that has been consistently observed in the Groningen ground motions is a very pronounced negative correlation between PGA and duration, with high amplitude motions consistently associated with shaking of very short duration (Bommer *et al.*, 2016). The same pattern is observed in the recordings of the Zeerijp earthquake, as shown in Figure 4.9. The largest value of PGA, recorded on the H2 (EW) component at the G140 station, is associated with a duration of two seconds (2.14 s). The horizontal components of both acceleration and velocity from this station are shown in Figure 4.10, which also shows the build-up of Arias intensity (which is a measure of the energy in the motion) over time. The strong concentration of the energy in a single pulse of motion in the H2 component is immediately apparent. The larger amplitude component of the BGAR recording—the source of the second largest PGA value—is associated with a significant duration of 2.5 s (Figure 4.11). The durations typically observed in short-distance earthquake recordings in Groningen are usually even smaller (often less than one second). In the G140 recording, the duration is elongated by a strong P-wave arrival approximately two seconds before the time of the S-wave peak.

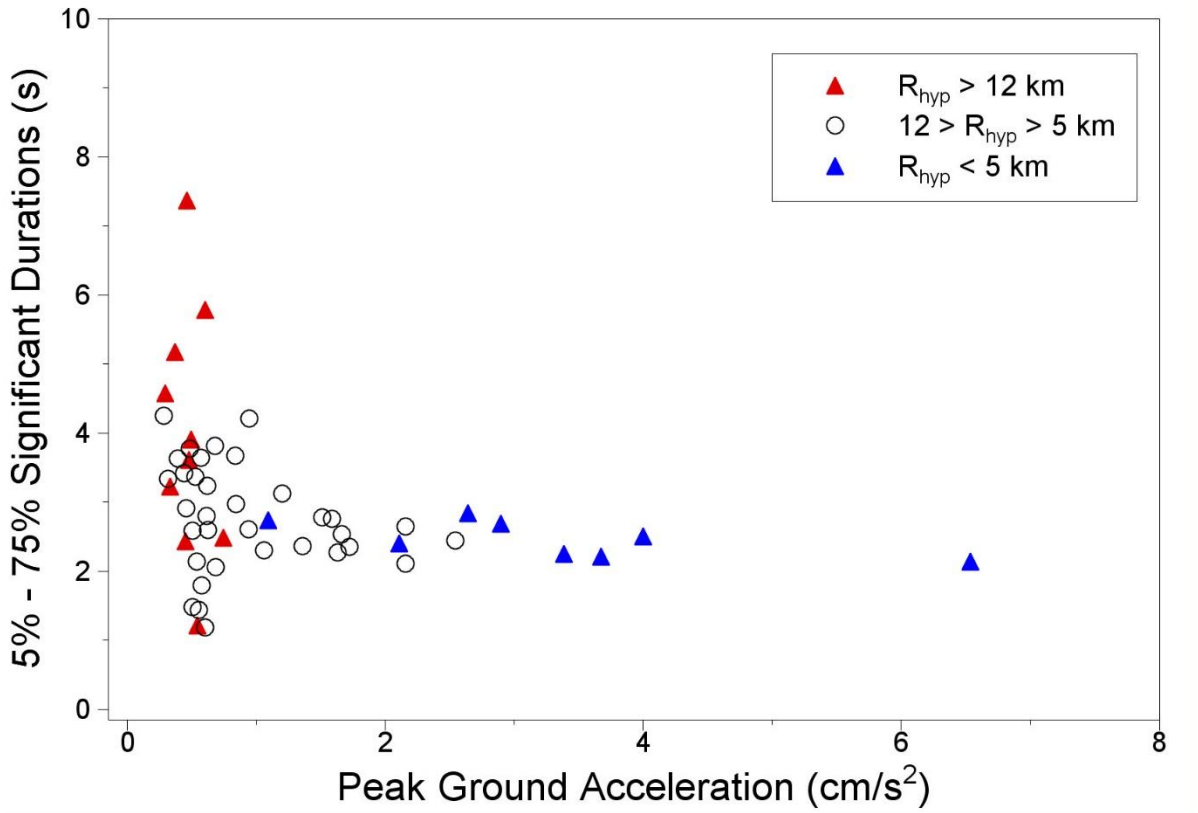

Figure 4.9. Pairs of PGA and significant duration for individual components of the Loppersum records, with symbols indicating the rupture distance of the recording.

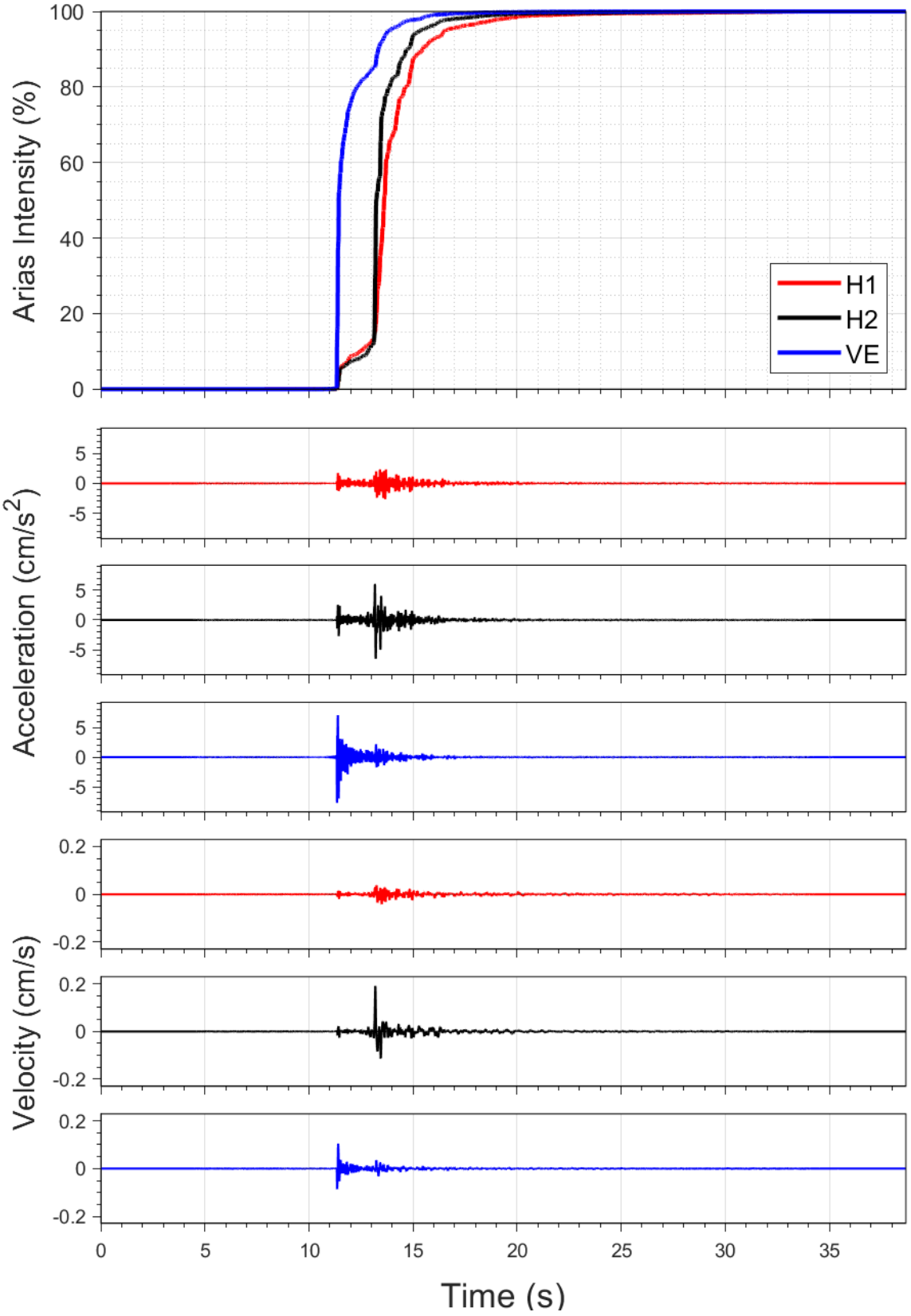

Figure 4.10. Horizontal components of acceleration and velocity from the G140 station; the upper frame shows the accumulation of Arias intensity (energy) over time.

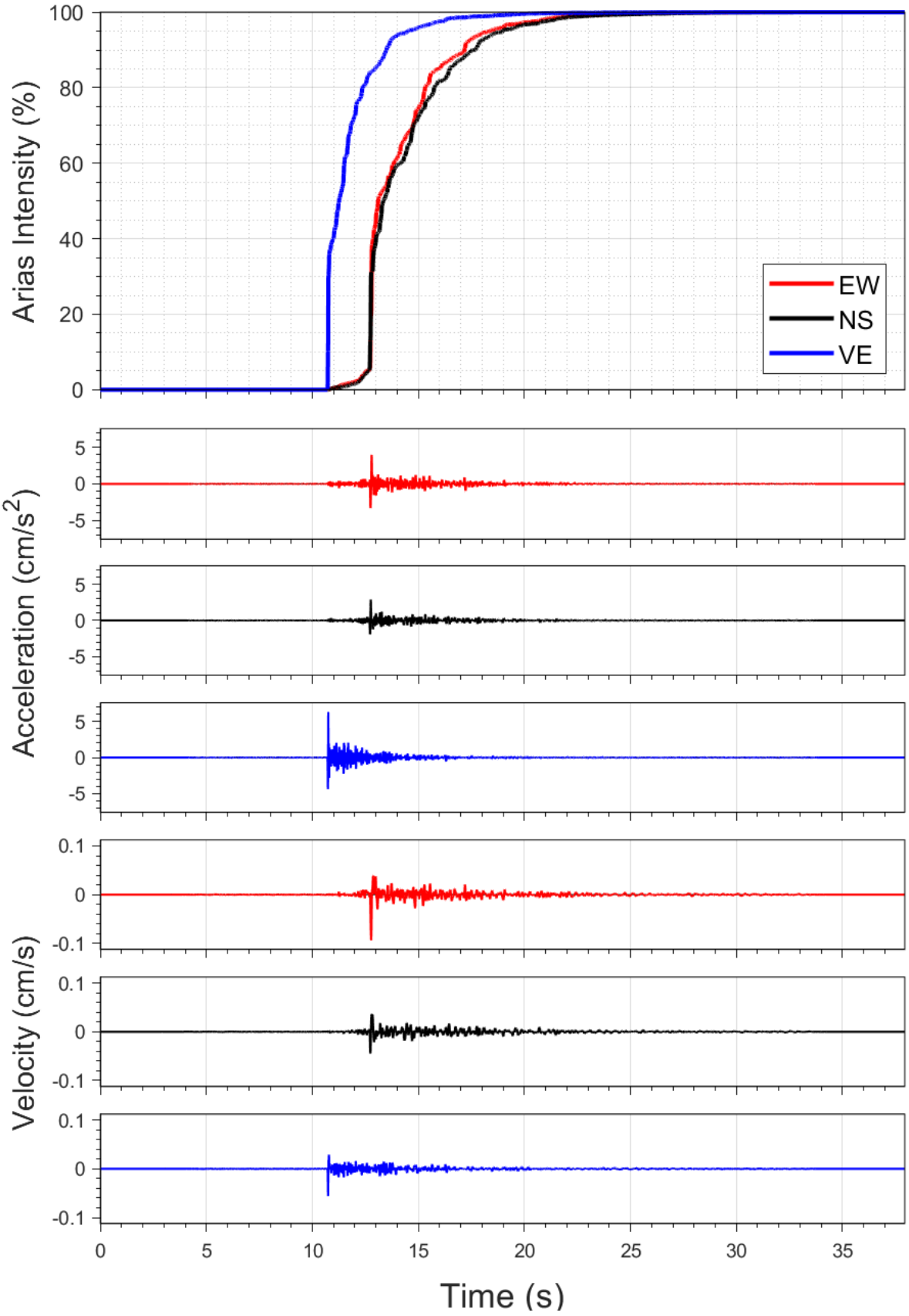

Figure 4.11. Horizontal components of acceleration and velocity from the BGAR station; the upper frame shows the accumulation of Arias intensity (energy) over time.

4.4 Spectral Accelerations and Comparison with Ground-Motion Models

Additional insight into the nature of the ground motions can be obtained from the 5%-damped acceleration response spectra. The horizontal acceleration response spectra from the G140 and BGAR recordings of the Zeerijp earthquake are shown in Figure 4.12. The spectral shapes are consistent with previous observations in the field. The divergence between the red and black curves in both frames shows that the horizontal polarisation of both recordings seen for PGA and PGV (Figure 4.7) persists across the entire range of usable response periods, although, for BGAR, the spectra converge between 0.05 and 0.06 seconds as well as at about 0.2 seconds.

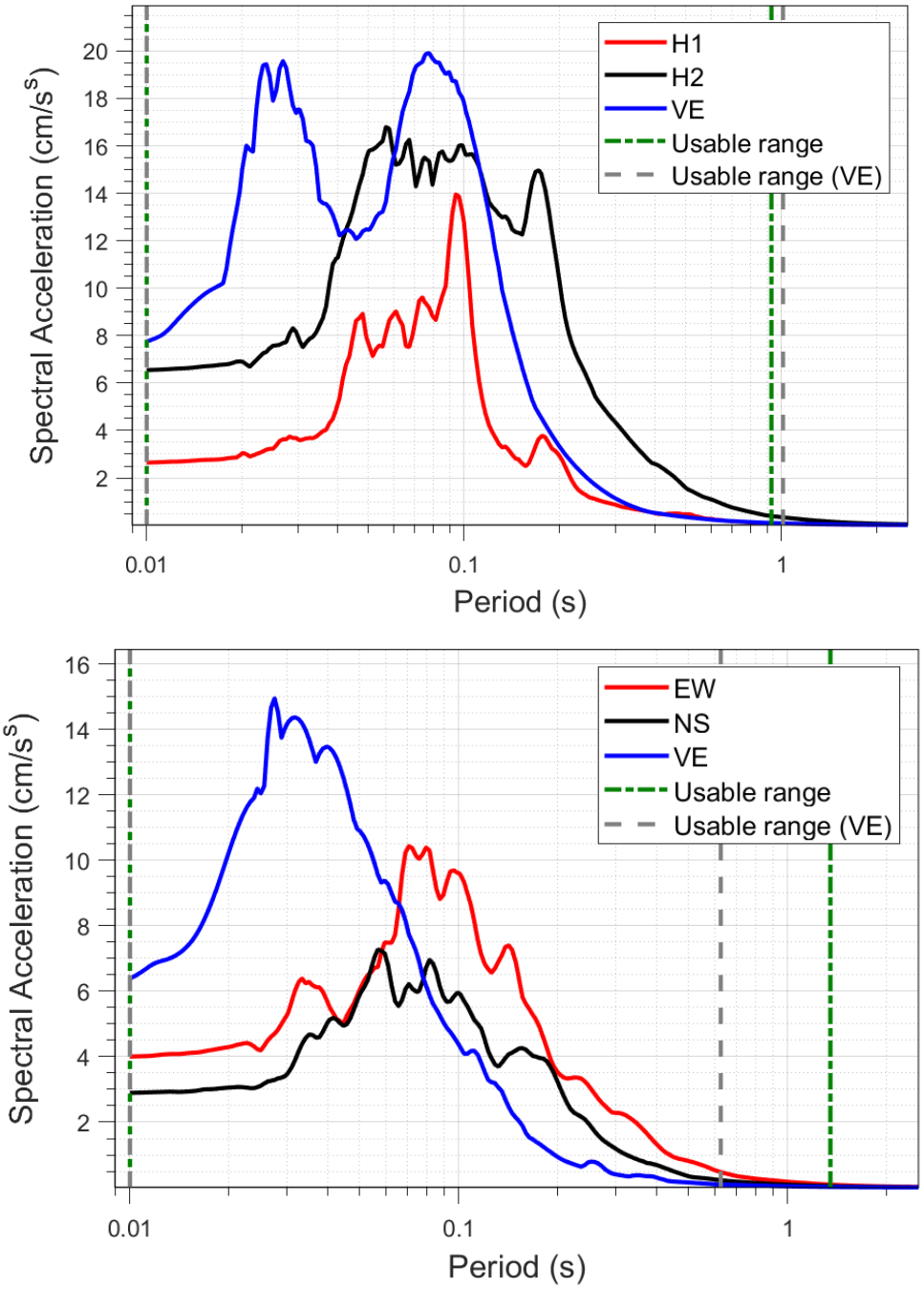

Figure 4.12. Horizontal response spectra from the G140 (upper) and BGAR (lower) stations; vertical spectra plotted as dashed lines beyond maximum usable period.

For this preliminary analysis, the key question of interest is whether the motions recorded in this earthquake are consistent with the empirical PGV GMPEs being used in the Groningen field. The current empirical PGV model was developed in 2021 and published shortly before the event (Bommer *et al*., 2021b) and we have calculated the total, inter- and intra- event residuals. Figure 4.13 shows the intra-event residuals of three component definitions of PGV with respect to the empirical GMPE plotted against hypocentral distance. With one exception, nearly all residuals of the Zeerijp earthquake recordings are within two within-event standard deviations of the zero line, which suggests that the model captures well the variability of the data. A weak trend of the residuals with distance can be observed and it is clear that this trend is a visual result of a group of positive residuals at about 15 km of hypocentral distance and one large positive residual at 25 km. In both cases however, the residuals are within the scatter of the data of the full database.

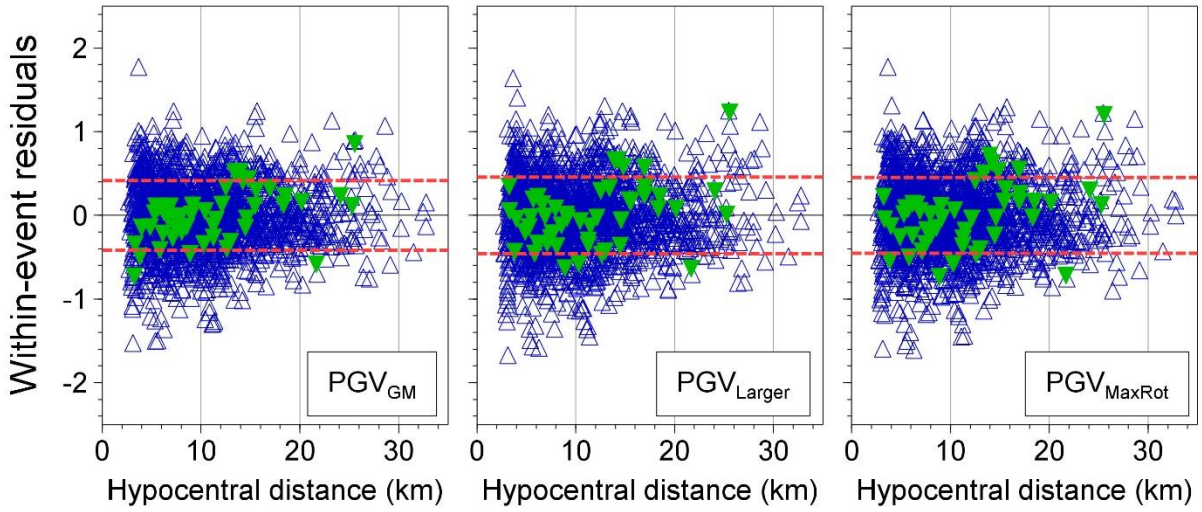

Figure 4.13. Event- and station-corrected within-event residuals of three component definitions of PGV with respect to the equations of the empirical PGV GMPE (Bommer et al., 2021b). Residuals of the Zeerijp earthquake recordings are shown in green and of other events in blue. The within-event standard deviation (φ_{SS}) is shown in red dashed lines.

Figure 4.14 compares the inter-event residuals (event-terms) of the Zeerijp earthquake to those of the previous events of the database. These event terms effectively represent the average offset of the recorded motions from each earthquake compared to the median prediction from the empirical model for the event magnitude, with a positive event-term indicating a stronger-than-average earthquake, a negative value a somewhat weaker-than-average earthquake. The event-term of the Zeerijp earthquake has a value slightly smaller than zero, indicating a small over-prediction by the model and relatively smaller PGV values recorded than in previous events.

4.5 Concluding remarks Zeerijp earthquake 4th October 2021 (2.2)

The M_L 2.2 Zeerijp earthquake of 4 October 2021 has generated a large number of ground-motion recordings. The largest component of PGA recorded in this earthquake is 0.007*g* and the largest value of PGV—which is generally considered a better indicator of the damage potential of the motion—recorded in this latest event is just 0.19 cm/s, which is significantly smaller than the largest value of the Groningen ground-motion database, a 3.46 cm/s recorded in the Huizinge earthquake.

An important observation is that the motions recorded in the Zeerijp earthquake are consistent with the predictions from the ground-motion model currently deployed in the seismic hazard and risk

modelling for Groningen (NAM HRA and TNO SDRA) and the empirical PGV GMPEs used to assess damage claims.

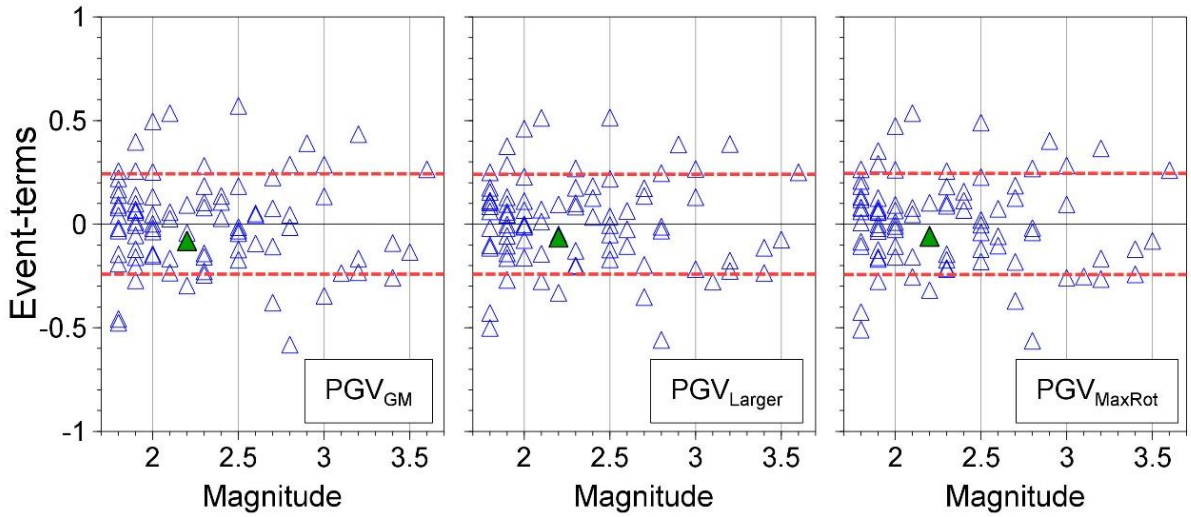

Figure 4.14. Inter-event residuals of three component definitions of PGV with respect to the equations of the empirical PGV GMPE (Bommer et al., 2021b). Residuals of the Zeerijp earthquake recordings are shown in green and of older events in blue. The inter-event standard deviation is shown in red dashed lines.

5 Comparison of the Surface Ground-Motions Recorded During the Zeerijp M_L 2.5 and M_L 2.2 Earthquakes of 4th October 2021

5.1 Introduction

On Monday 4 October 2021 at 02:59 and 20:47 UTC (04:59 am and 22:47 pm local time), two earthquakes of local magnitude (M_L) of 2.5 and 2.2, respectively, occurred near the village of Zeerijp, in the northern part of the Groningen field (Figure 5.1). The hypocentral coordinates determined by Dr Jesper Spetzler of the KNMI using the 3D EDT method (Spetzler & Dost, 2017) are 245553 X, 596700 Y and 3 km depth for the first event and 245553 X, 596700 Y and 2.7 km depth for the second. This places the distance of the two epicentres at only 112 metres and their hypocentral distance at 320 metres.

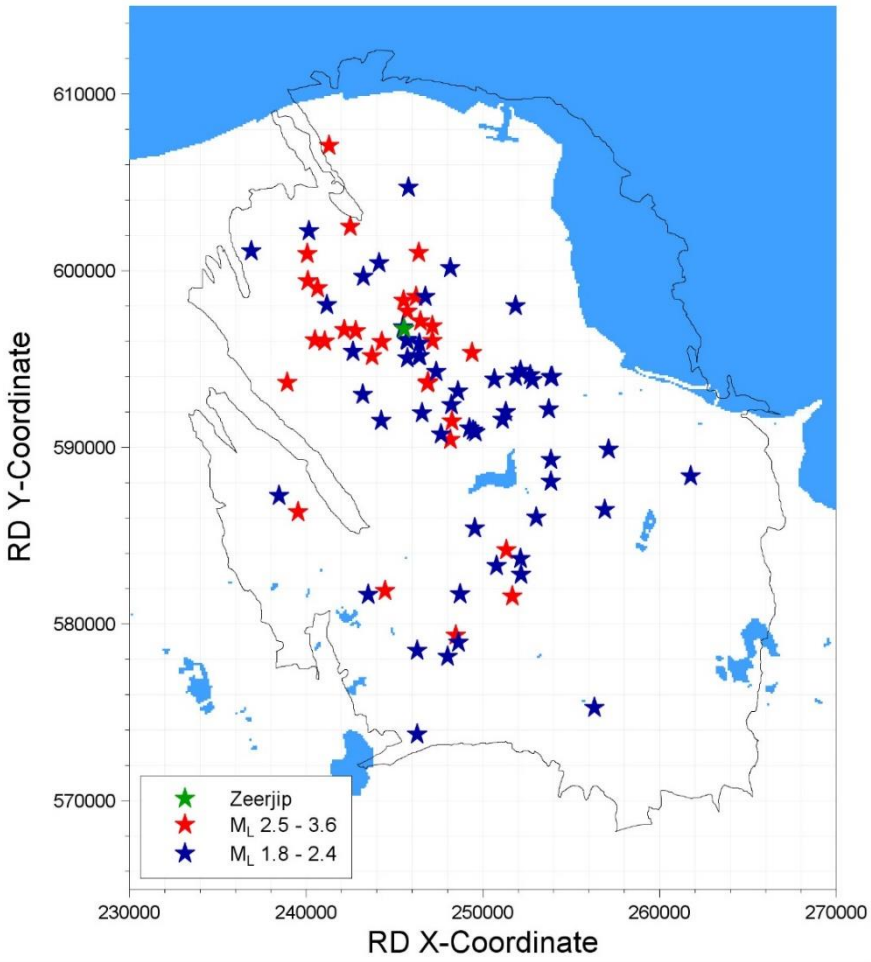

Figure 5.1. Epicentres of the Zeerijp earthquakes (green stars) together with epicentres of previous earthquakes of $M_L \geq 2.5$ (red stars) and of M_L 1.8-2.4 (blue stars)

For each of the two events, 82 three-component recordings were downloaded and processed as described by Edwards & Ntinalexis (2021), with a total of 53 records deemed usable from the larger event and 50 from the smaller and a total of 44 stations generating useable records for both events. Figure 5.2 shows the usable recordings of both events in the magnitude range of applicability of the

current empirical Ground-Motion Prediction Equations (GMPEs) used to estimate values of peak ground velocity (PGV) occurring during earthquakes in the Groningen field (Bommer *et al*., 2021).

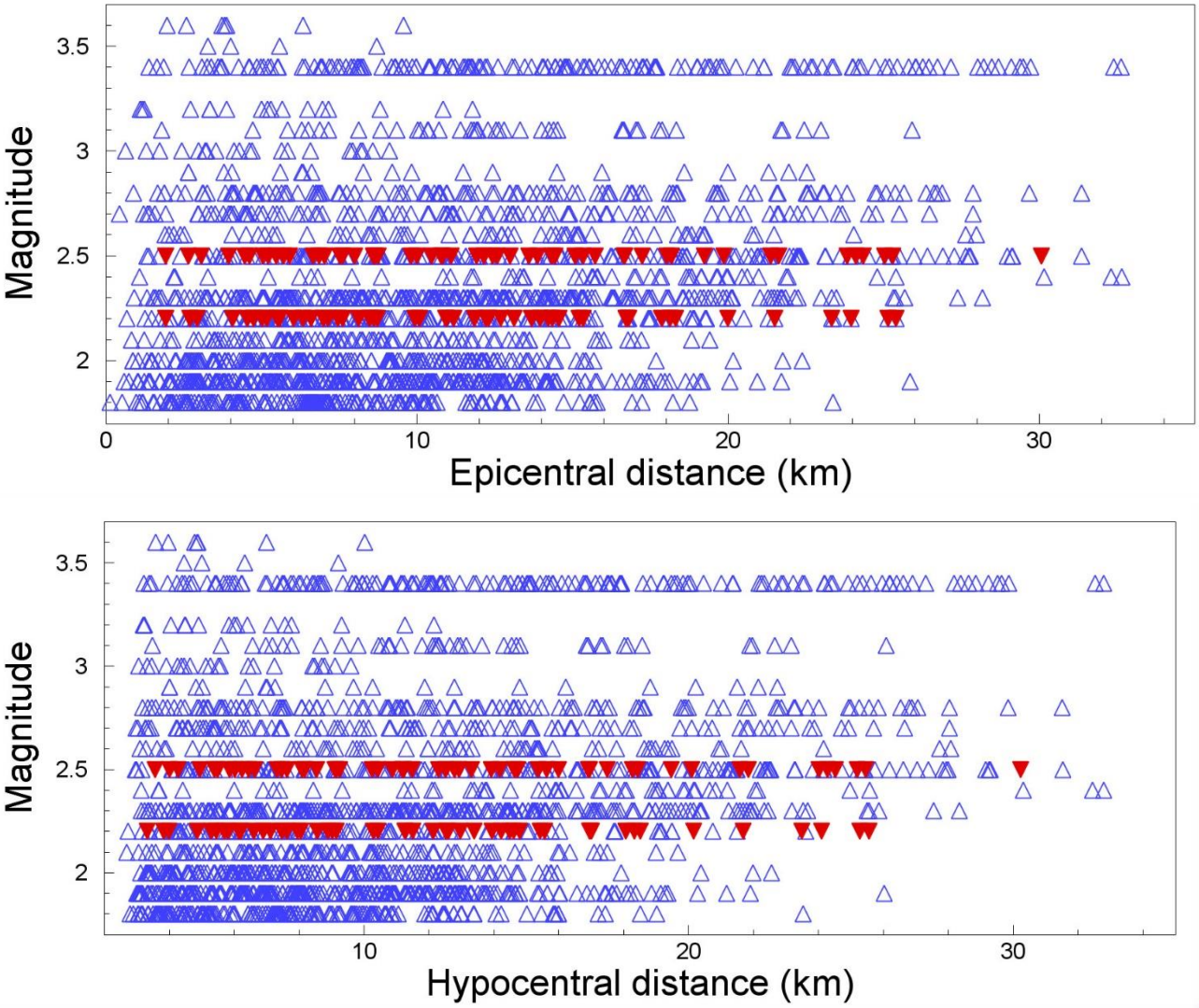

Figure 5.2. Magnitude-distance distribution of the Groningen strong-motion database including the recordings of the 4 October 2021 Zeerijp earthquakes

As shown in Figure 5.2, the epicentral and hypocentral distances of the recording stations are nearly virtual identical for the stations that recorded both events. Since the two epicentres are in close proximity, this also applied to the source-to-site paths. This, combined by the large number of usable recordings available from both events, presents the unique opportunity to compare the ground-motions recorded and examine the influence of magnitude on ground-motion scaling.

This report presents these comparisons and discusses the differences and similarities of the recorded ground-motions. The discussions focus primarily on peak ground velocity (PGV), although they extend to pseudo-spectral acceleration (PSA) and duration.

5.2 Fit to the empirical PGV GMPEs

Figure 5.3 presents the event-terms of the two earthquakes with respect to the empirical PGV GMPEs and compares them to the event-terms of the earthquakes used in the derivation of the model. The event-terms of the two Zeerijp events are similar; both are close to but fractionally smaller than zero, indicating that the median predictions of the model, approximate the recorded motions well on

average while being larger by a small degree. The event-term of the M_L2.2 event is smaller, which suggests that the ground-motions generated by that event remain comparatively weaker than those of the M_L2.5 event even when their magnitude difference is taken into account. It must be noted, however, that, as seen clearly in Figure 5.3, this is a small difference

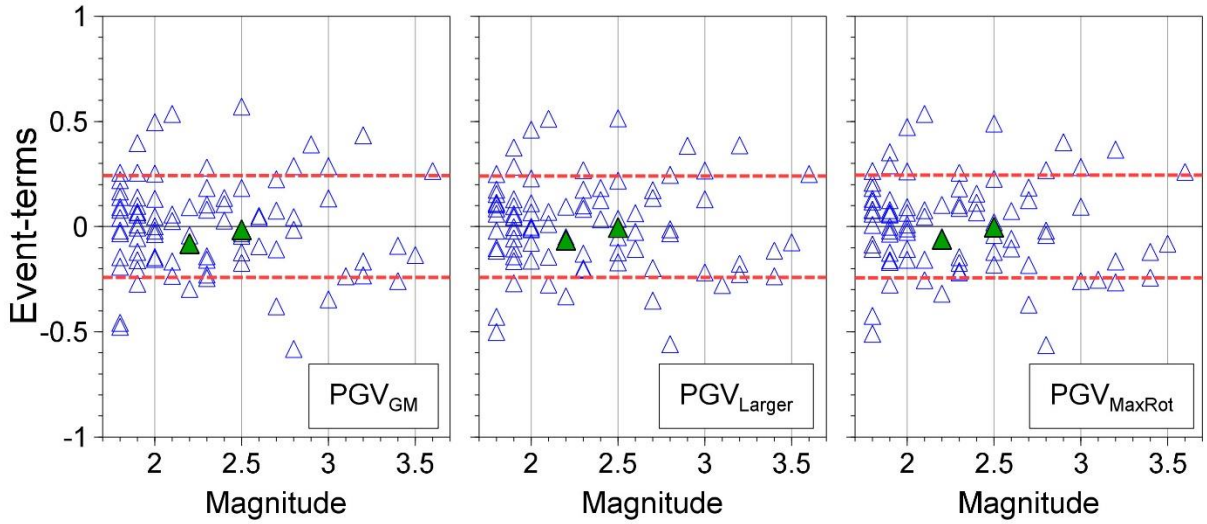

Figure 5.3. Inter-event residuals of three component definitions of PGV with respect to the equations of the empirical PGV GMPE (Bommer et al., 2021). Residuals of the Zeerijp earthquakes are shown in green and of other events in blue. The inter-event standard deviation is shown in red dashed lines.

While event-terms (or inter-event residuals) describe the average difference of recorded motions to model predictions, within-event residuals compare predictions and observations at each recording station. Figure 5.4 shows the event- and station-corrected within-event residuals of the PGV values recorded during the two events with respect to the empirical PGV GMPEs, as well as the residuals of the database used to develop the GMPEs. The patterns observed for both events are remarkably similar. Most of the points plotted are within the bounds of the within-event standard deviation and all points except one are within two standard deviations. Residuals below a hypocentral distance of about 12 km are centred slightly below zero, while the residuals at longer distances are centred slightly above, indicating a weak trend of the residuals with distance. The greatest visual similarity can be observed in the MaxRot component (more often referred to as GMRotD100), which is the only component definition among the three that is independent of the orientation of the recording stations (Boore *et al.*, 2006) and is always at the direction of the greatest shaking.

A striking feature of both sets of residuals is their outlier at 25 km, which belongs to station G480. A station-term has been calculated for each station used in the development of the PGV GMPEs, which, similarly to an event-term, describes the average behaviour of the residuals of the station and captures unique site characteristics which are not fully described by the simple site response term of the equations. The station-terms for this station are positive: 0.25 (GM), 0.27 (Larger) and 0.26 (MaxRot). This indicates that ground-motions at this station tend to be under-predicted by the PGV GMPEs, with local site amplification being larger than predicted by the model. This is consistent with the observation of the large positive residual in Figure 5.4.

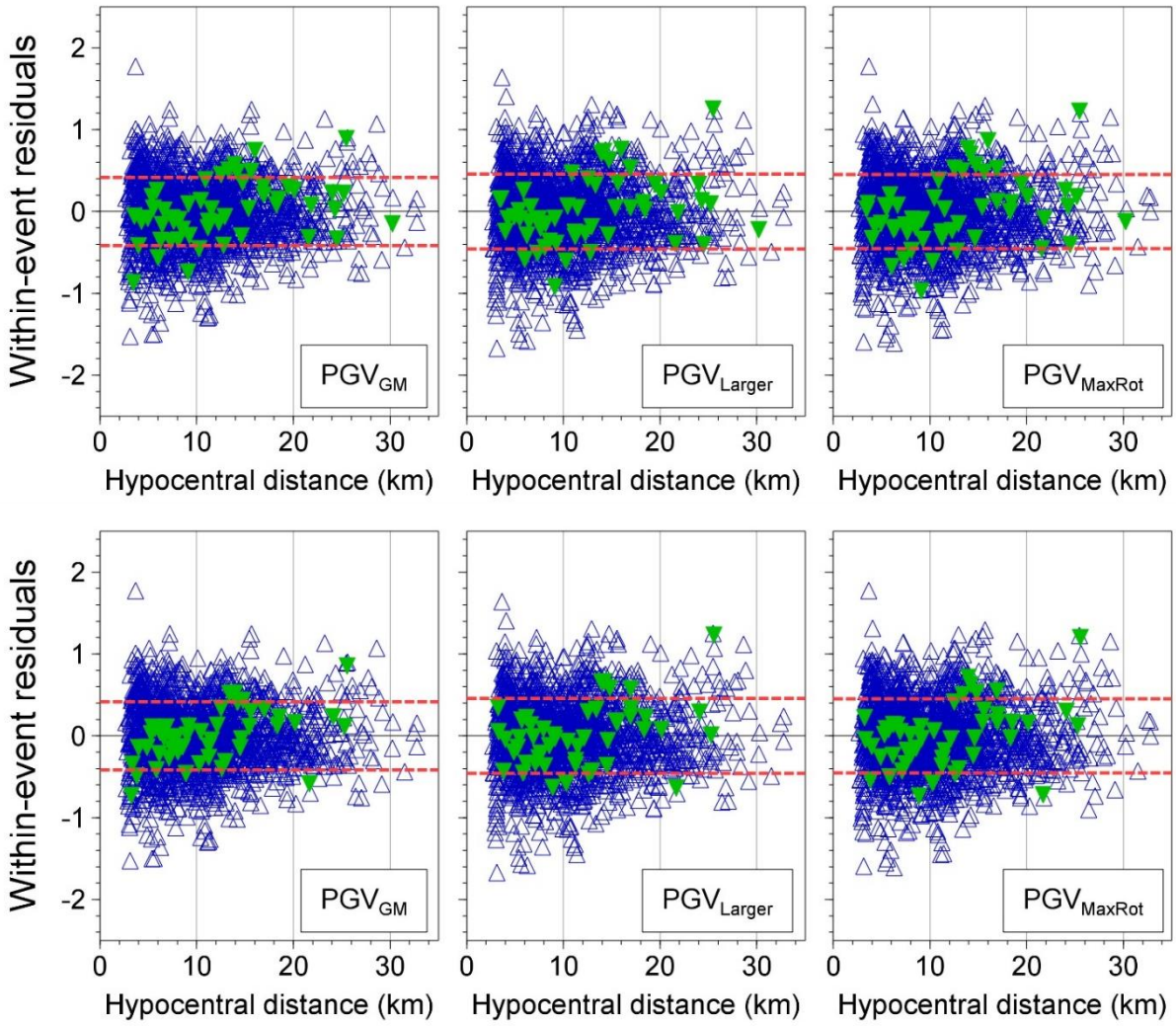

Figure 5.4. Event- and station-corrected within-event residuals of three component definitions of PGV with respect to the equations of the empirical PGV GMPE (Bommer et al., 2021b). Residuals of the Zeerijp earthquakes recordings are shown in green and of other events in blue. The within-event standard deviation (φ_{SS}) is shown in red dashed lines. The residuals of the M_L 2.5 event are shown in the upper, while those of the M_L 2.2 event are shown in the lower row of frames.

The station-corrected residuals of G480 are plotted again separately in Figure 5.5. It can be observed that the residuals of the two Zeerijp events are consistent between them but unusually larger than the other residuals of that station. With magnitude, distance, the site V_{S30} as well as the event-terms and station-terms already taken into account when predicting the PGV values at that station, the only unique effect that is common in both recordings, not shared with the other recordings of that station and not taken into account in the predictions is the source-to-site path. The consistency of the residuals between the G480 recordings of the two events highlights the importance of the path effects in the ground-motion amplitude. Whether this observation extends beyond PGV and holds for Spectral Acceleration is examined in the following pages.

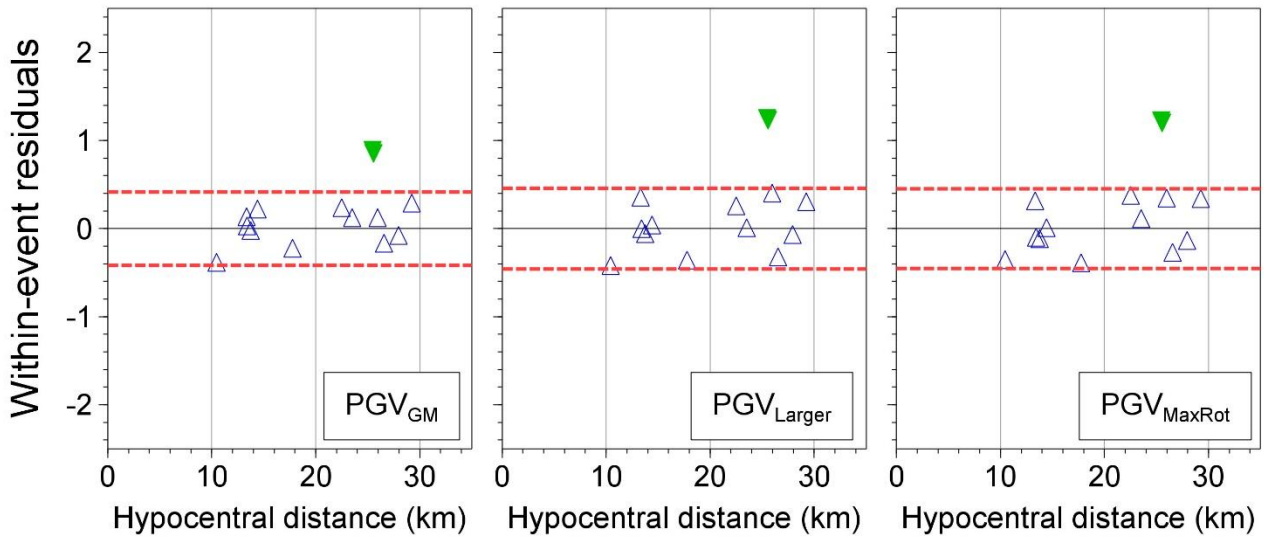

Figure 5.5 Event- and station-corrected within-event residuals of recordings from station G480 with respect to the equations of the empirical PGV GMPE (Bommer et al., 2021b). The within-event standard deviation (φ_{SS}) is shown in red dashed lines. The residuals Zeerijp earthquakes are shown in green.

5.3 Trends of PGA, PGV and Spectral Acceleration with distance

Figure 5.6 shows the PGV values recorded during both events, plotted against the hypocentral distance of each recording station, for the three component definitions predicted by the empirical GMPEs. The median and event-corrected predictions of the GMPEs for events of the same magnitude and a V_{S30} of 200 cm/s (the approximate field average) are also shown.

The observed trends are very similar for both events, especially at the shorter distances, below 10 km. The small adjustment of the GMPE medians by the event-terms shows how well the model median predictions fit the data. In the case of the larger event, the adjustment is so small that the median and event-corrected medians cannot be visually distinguished.

Similar trends with respect to distance are also visible when plotting the recorded horizontal PGA values for the same three component definitions (Figure 5.7), although fewer datapoints are available for this comparison, as many of the recorded PGA values, especially of the smaller event, were deemed unusable during processing. Comparing the recorded spectral accelerations at the periods of 0.1, 0.2 and 0.5 (Figure 5.8) leads to the same observations.

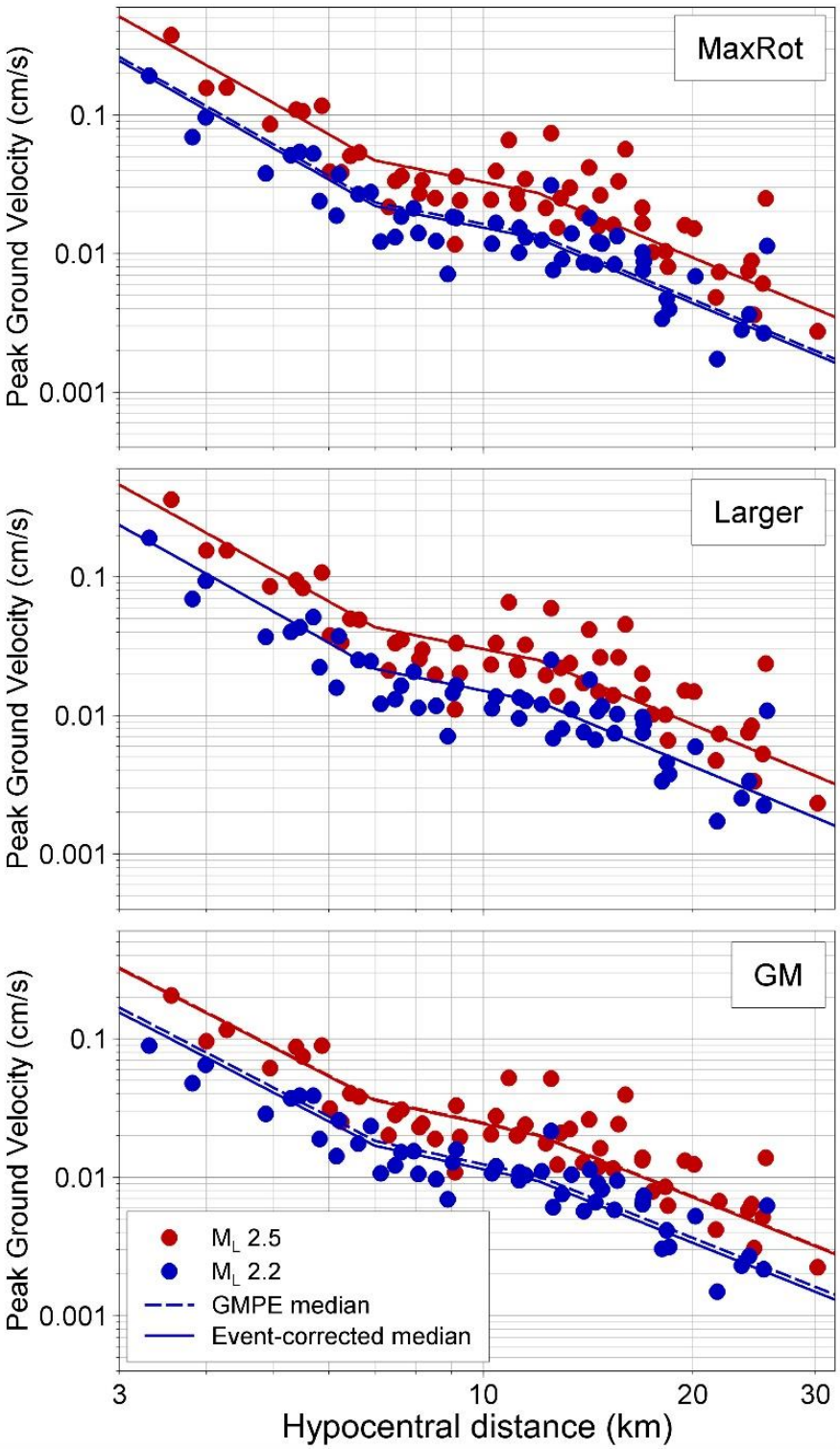

Figure 5.6 Horizontal components of PGV recorded during the Zeerijp earthquakes plotted against hypocentral distance

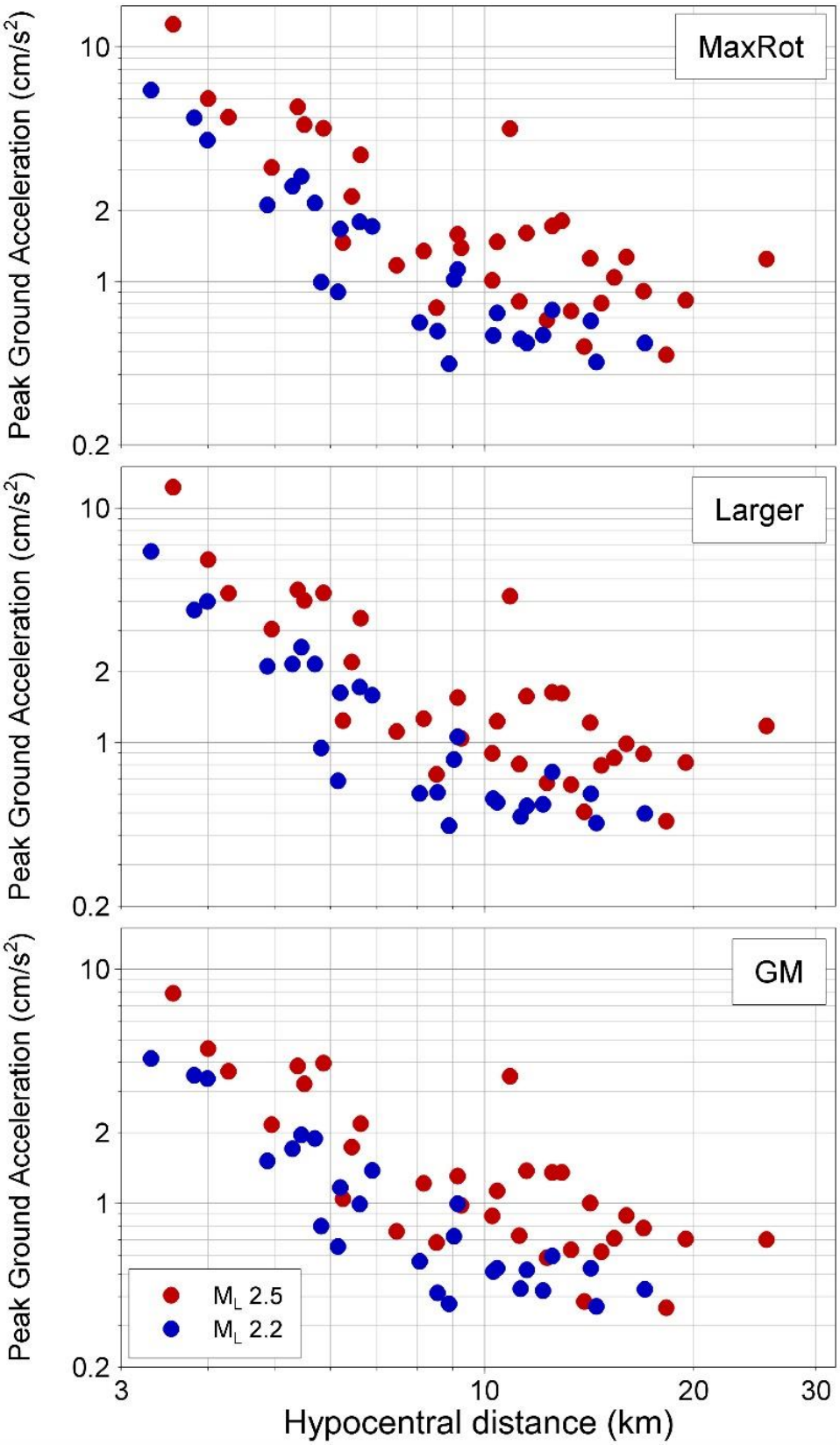

Figure 5.7 Horizontal components of PGA recorded during the Zeerijp earthquakes plotted against epicentral distance.

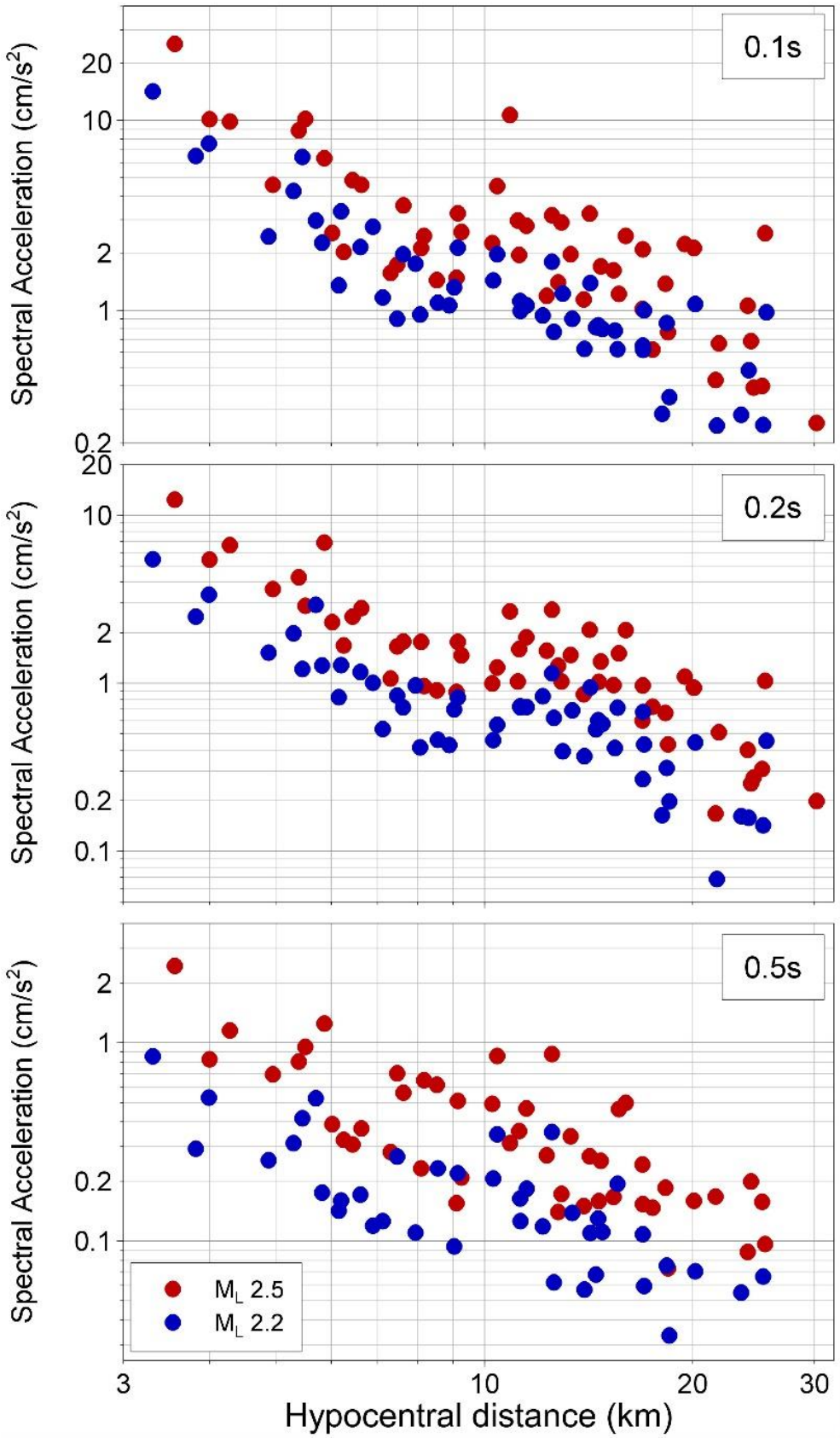

Figure 5.8 Geometric-mean horizontal component Spectral Accelerations recorded during the Zeerijp earthquakes plotted against epicentral distance

5.4 Spatial distribution and ratios of ground-motion amplitudes

Figure 5.9 presents contour lines generated using the recorded PGV MaxRot values on the map of the Groningen area, for each of the two Zeerijp events. The same comparison is made in Figure 5.10 for PGA MaxRot, while Figure 5.11 shows ratios of the recorded PGV and PGA values shown in Figures 5.9 and 5.10. Please note that these contours aim to demonstrate the variation of the recorded values instead of being approximations or predictions of the ground-motion outside of the recording stations. The locations of the recording stations are not shown in Figures 5.9 and 5.10 to avoid very busy plots but are shown in Figure 5.11.

The patterns observed for both PGA and PGV MaxRot are similar, with larger amplitudes recorded towards the north-east of the epicentres and smaller amplitudes recorded towards its south. Small variation in the ratios of the PGA and PGV values recorded in the two events can be observed in Figure 5.11, however it is clear that the average ratio, which appears to cover most of the field, is approximately 2 for both PGA and PGV. Moreover, it can be seen that the ratio is approximately 2 in all of the locations of the recording stations, which also indicates that the higher values shown in some locations towards the edges of the map are a result of the simple extrapolation that was used to generate the contours and do not genuinely represent the difference of the ground-motions. Indeed, the ratio of the exponents of the magnitude scaling term of the empirical PGV GMPEs (see Eq.3.1 of Bommer et al., 2021) for magnitudes of 2.5 and 2.2 is approximately 2 for all three component definitions.

These patterns are confirmed in Figures 5.12 and 5.13, which show the as-recorded horizontal components of PGA and PGV at the recording stations that are located within 6 km of the two epicentres. The stations immediately to the north and east of the epicentres have recorded larger values of PGA and PGV. As shown in Figures 5.14 and 5.15, the ratios that can be observed vary from 1 to 3, with ratios of the PGA components displaying larger scatter and appearing centred slightly below 2, while the ratios of the as-recorded PGV components are approximately centred to the line of 2.

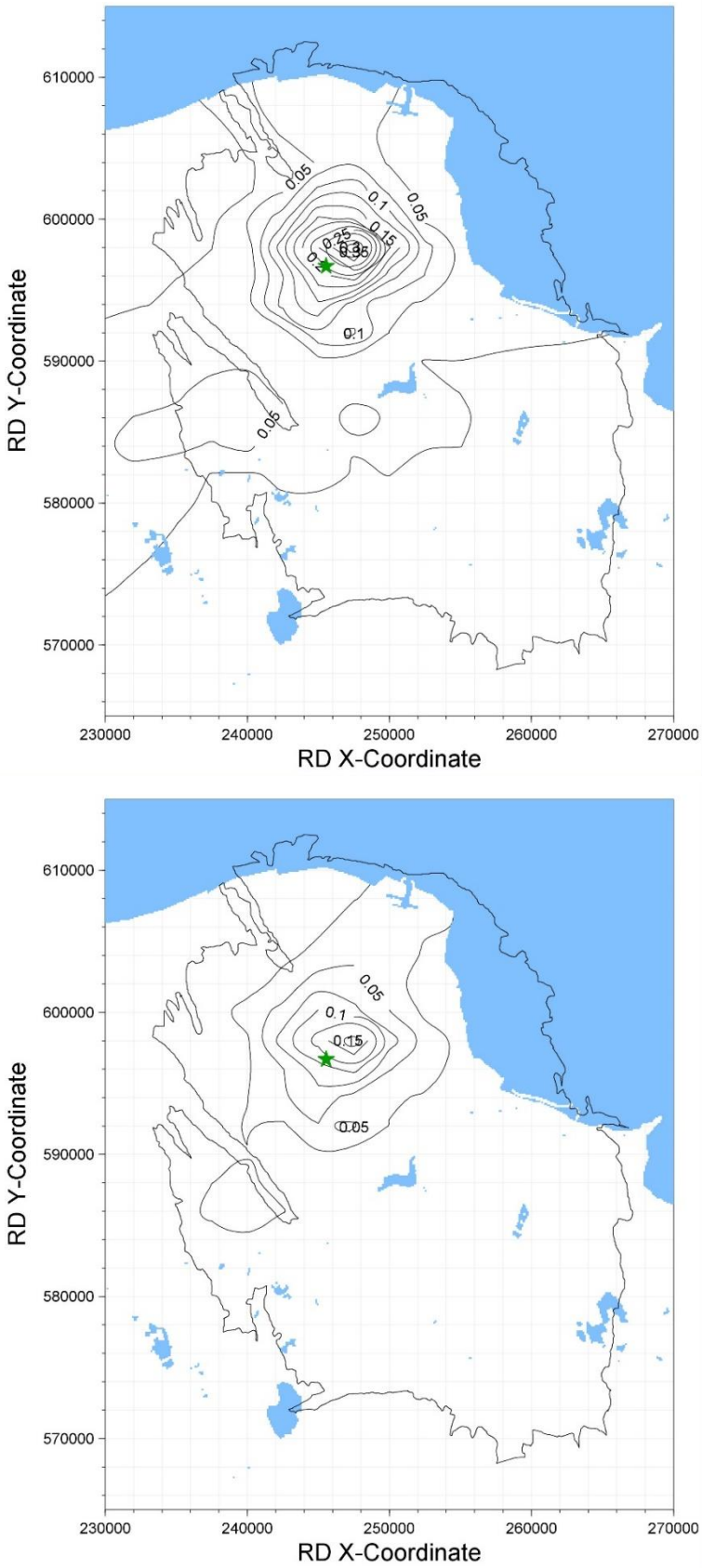

Figure 5.9 Contours of MaxRot PGV recorded during the M_L2.5 (upper) and M_L2.2 (lower) Zeerijp events. Units are cm/s; unnumbered lines represent increments of 0.025 cm/s

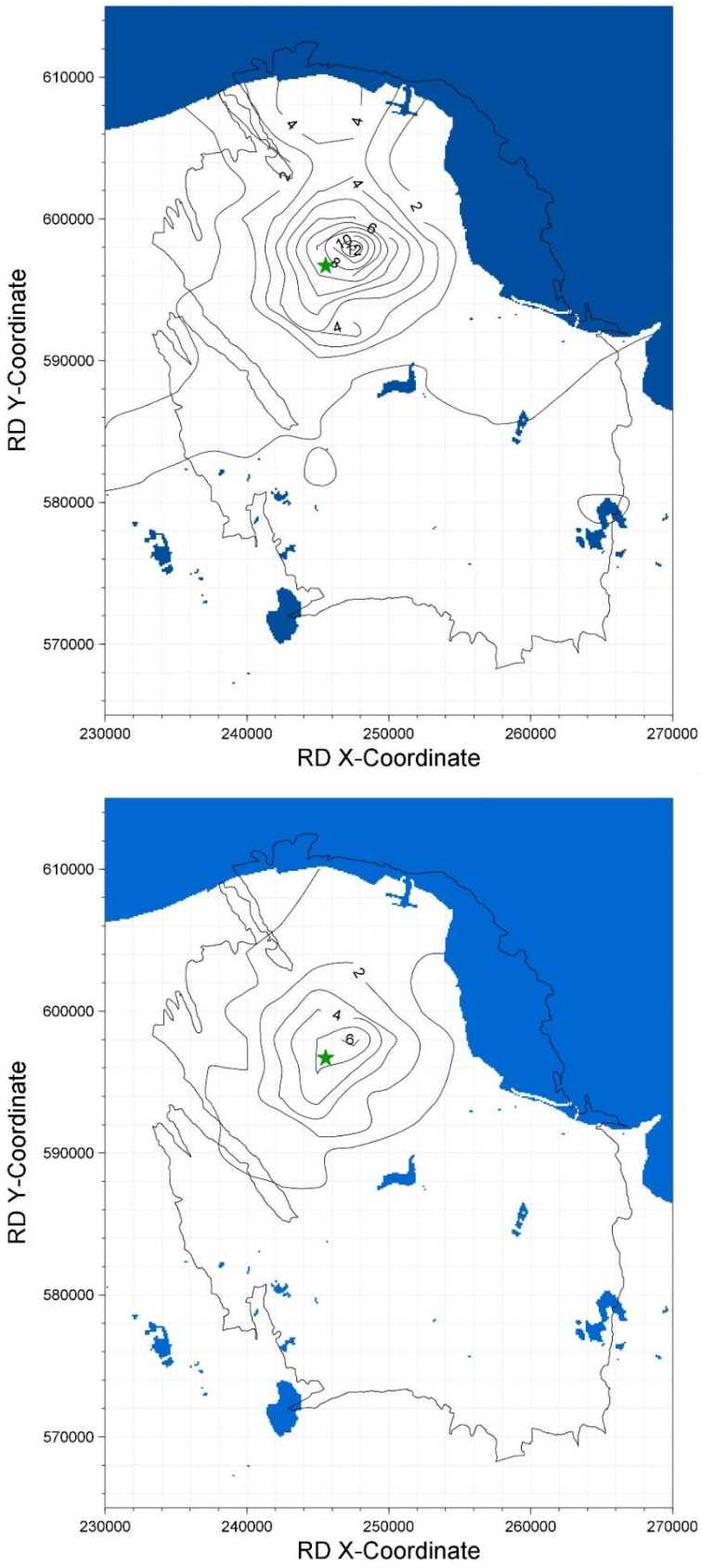

Figure 5.10 Contours of MaxRot PGA recorded during the M_L2.5 (upper) and M_L2.2 (lower) Zeerijp events. Units are cm/s²; unnumbered lines represent increments of 1 cm/s²

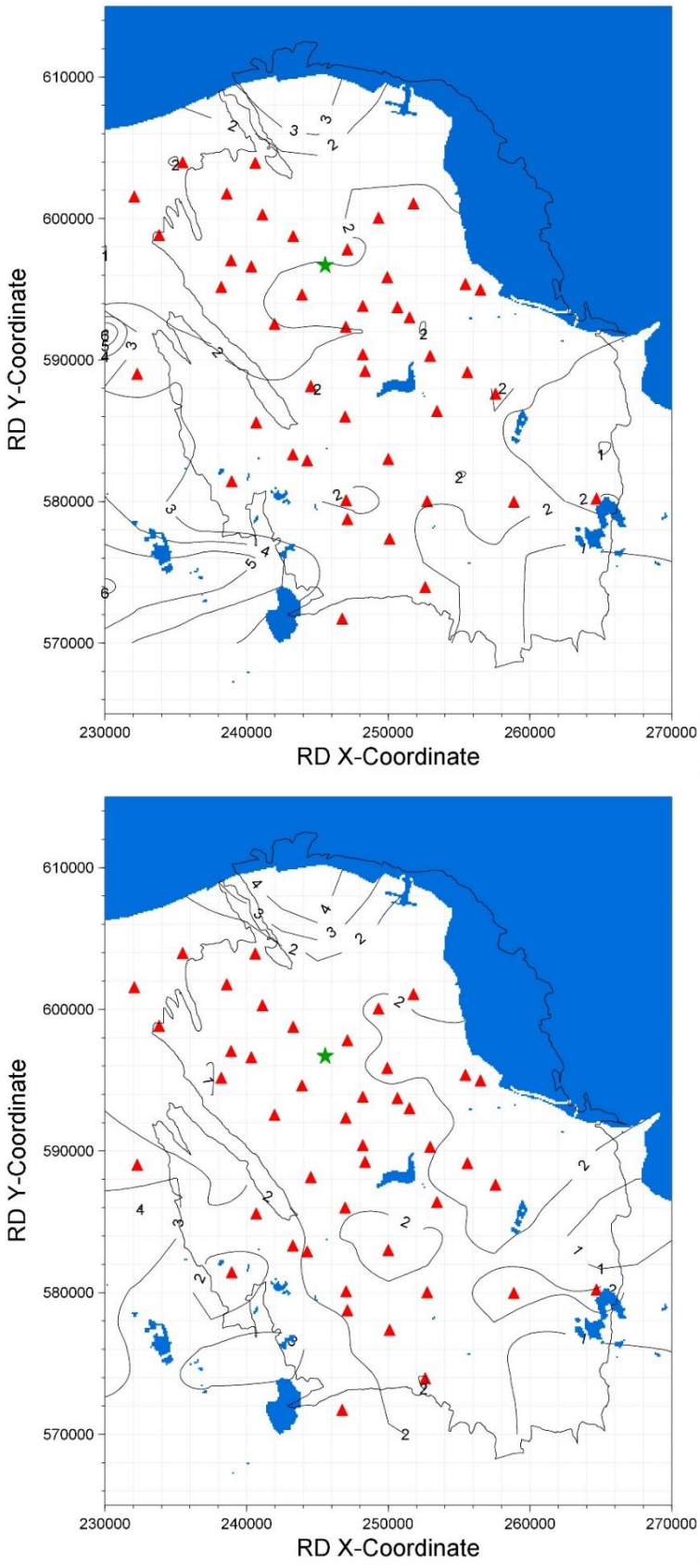

Figure 5.11. Contours of ratios of MaxRot PGV (upper) and PGA (lower) values recorded during the M_L2.5 event to those recorded during the M_L2.2 event.

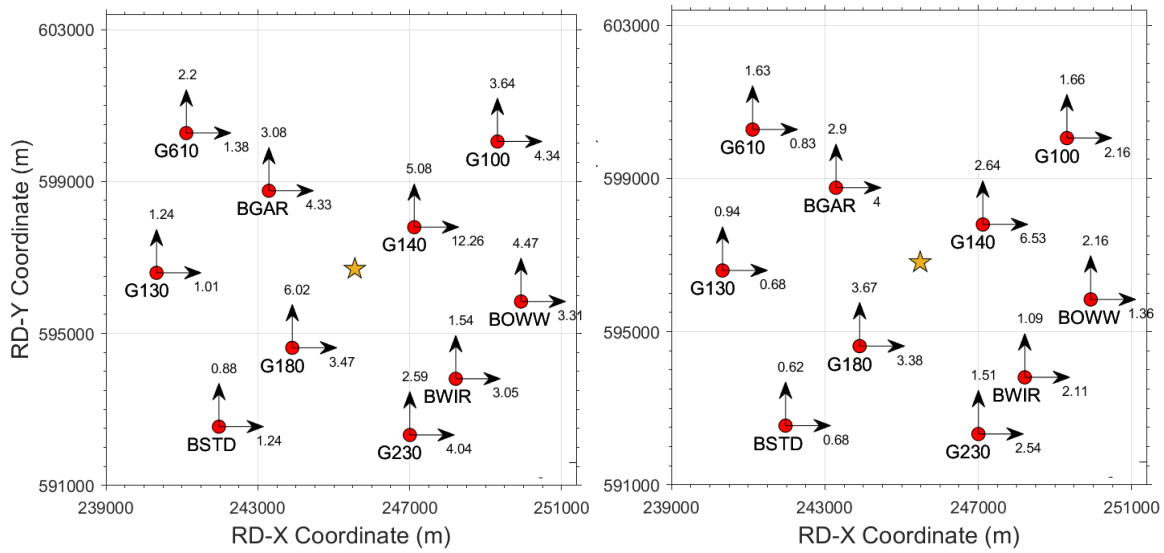

Figure 5.12. Horizontal components of PGA recorded during the Zeerijp earthquakes at epicentral distances of less than 6 km; units are cm/s².

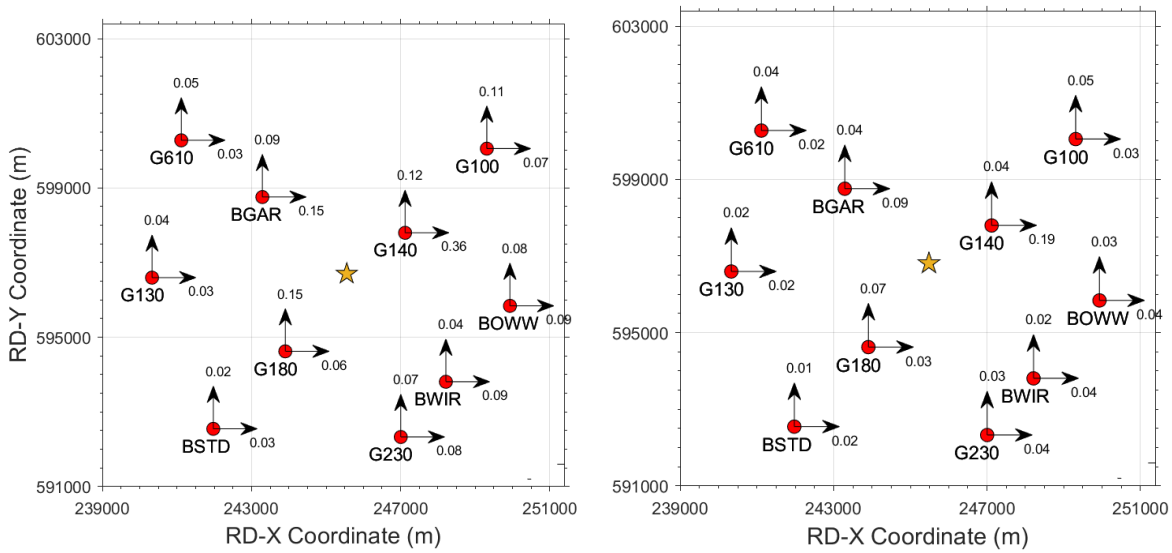

Figure 5.13. Horizontal components of PGV recorded during the Zeerijp earthquakes at epicentral distances of less than 6 km; units are cm/s.

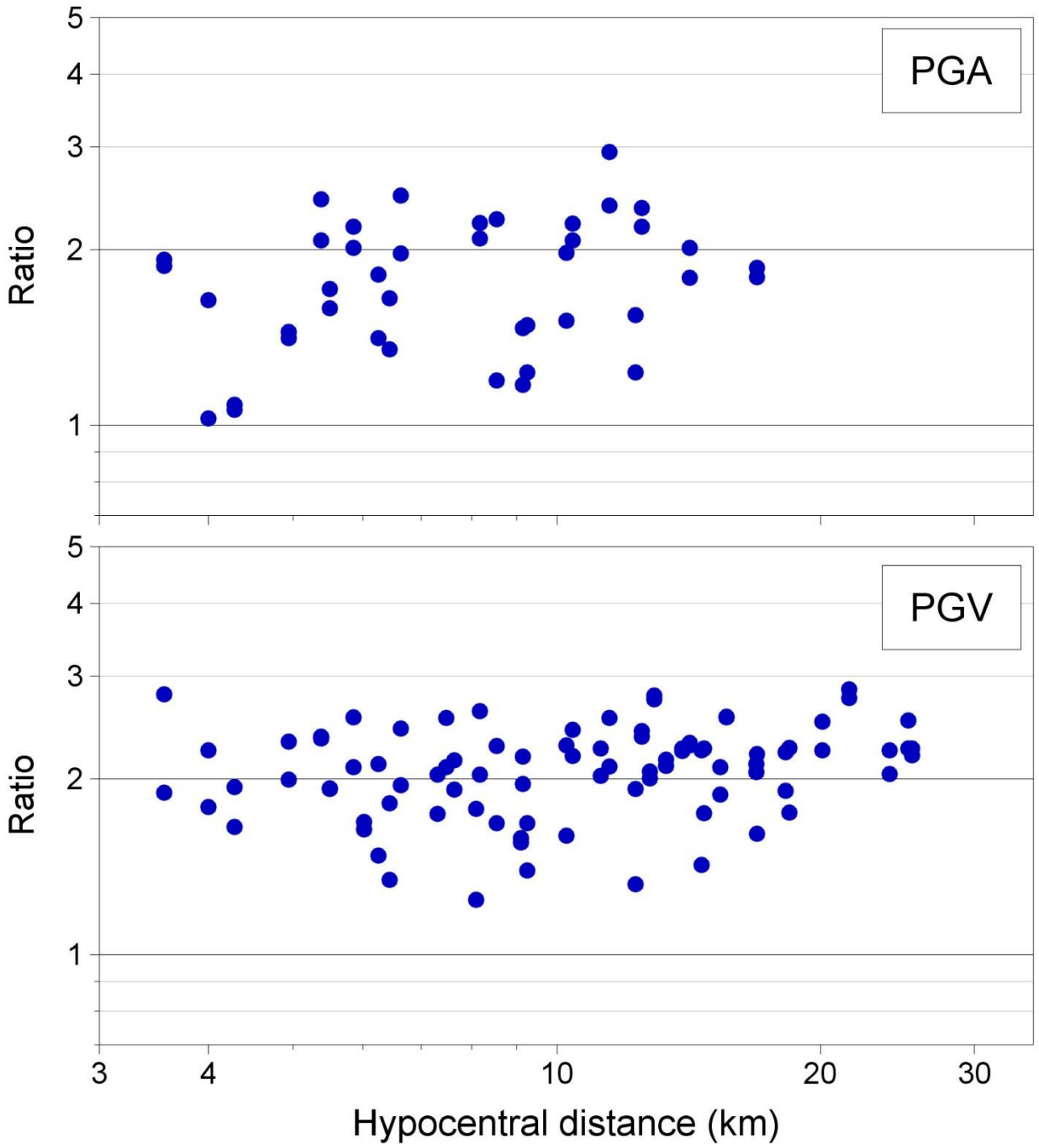

Figure 5.14 *Ratios of as-recorded horizontal PGA and PGV values recorded during the M_L2.5 event to those recorded during the M_L2.2 event.*

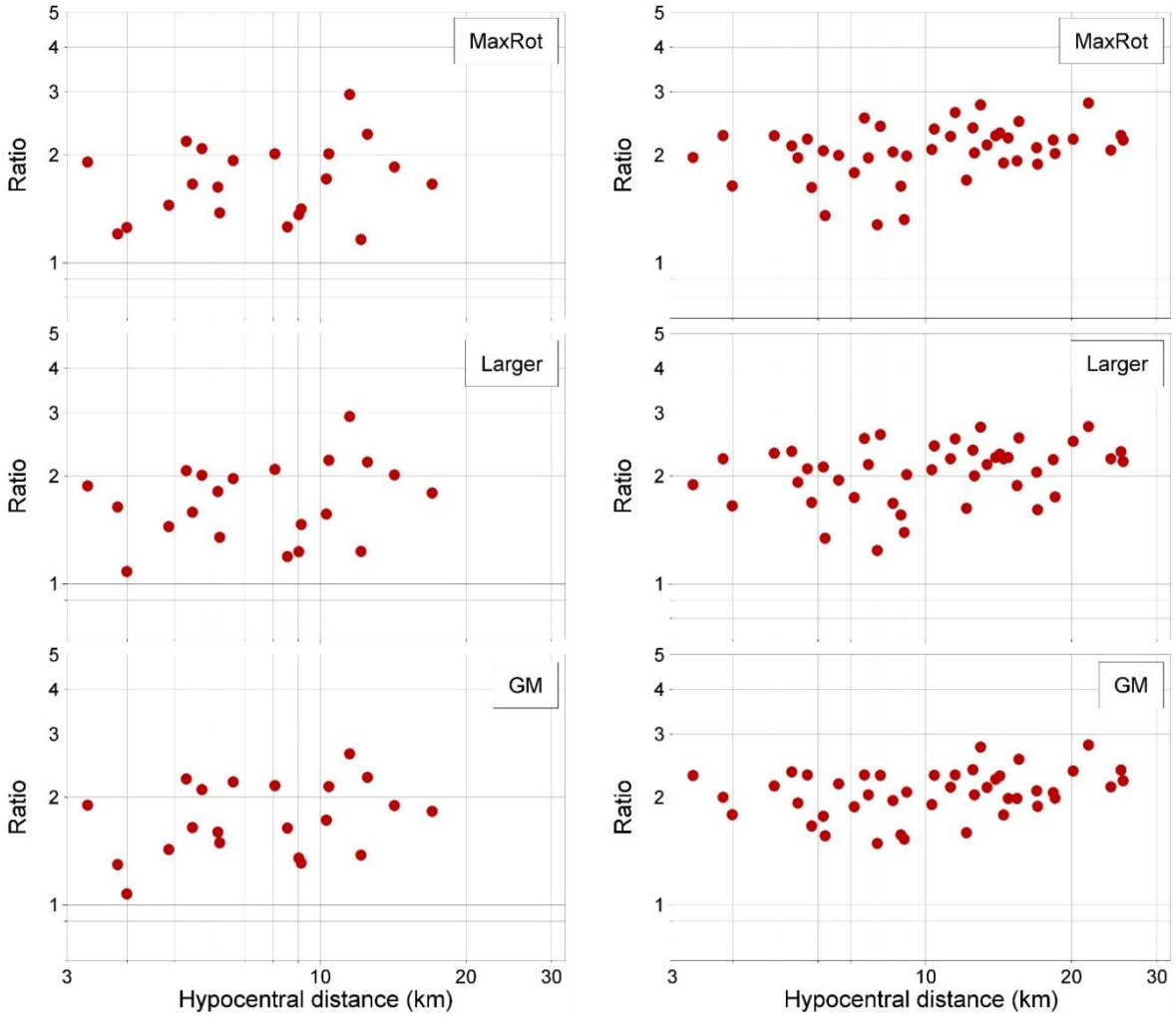

Figure 5.15 *Ratios of horizontal components of PGA (left) and PGV (right) recorded during the Zeerijp earthquakes plotted against hypocentral distance*

5.5 Time-histories and response spectra

A direct comparison of the recorded time-histories is carried out in Figures 5.16 to 5.19 below, for the three closest stations as well as station G480, which has been discussed above as an outlier.

The visual similarities of the time-histories of each station are remarkable and suggest that the only difference between the time-histories is a simple scaling factor. Some differences do exist, associated primarily with the peak of the time-histories (*e.g.* component H1 of station G180 in Figure 5.17), but they are small. Moreover, the Arias Intensity accumulation (shown in the upper frames of the plots) is similar, which is another confirmation of the similarity of the time-histories and indicates that their durations are similar as well. The ratios of the 5-75% significant durations are shown in Figure 5.20. The full suite of time-histories of acceleration and velocity and the accumulation of Arias Intensity, for all stations that recorded both events, is included in Appendix B.

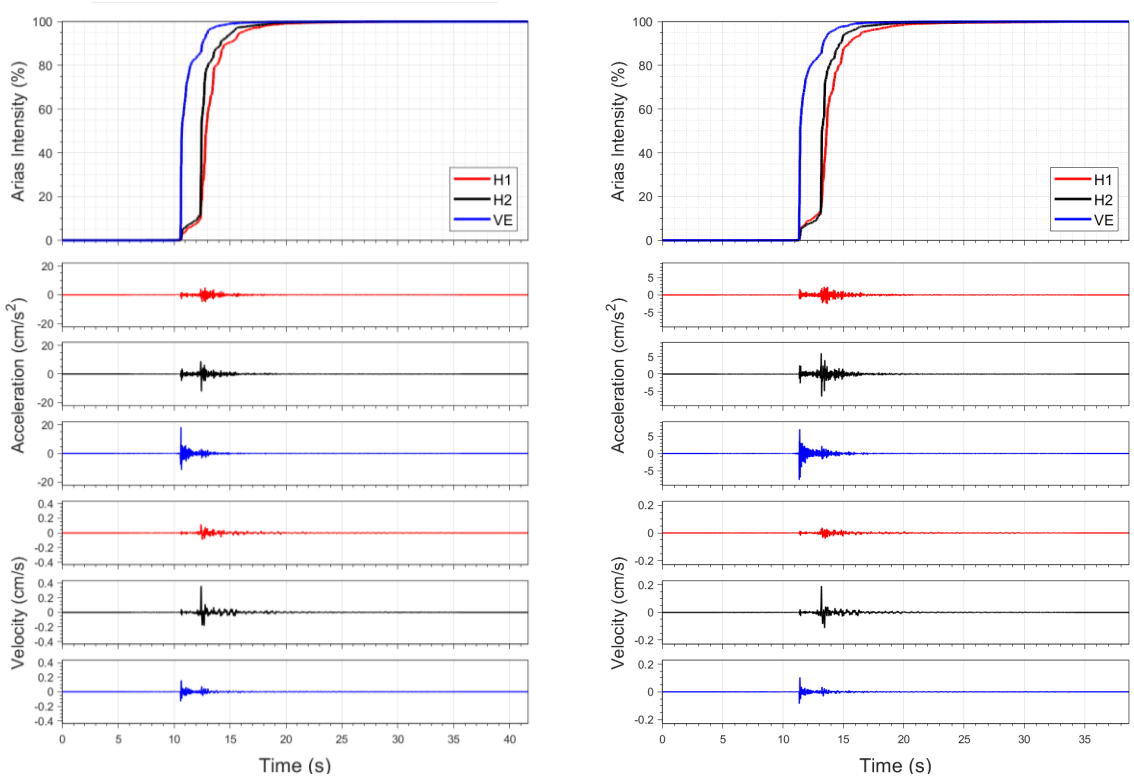

Figure 5.16 *Horizontal components of acceleration and velocity from the G140 station; the upper frame shows the accumulation of Arias intensity (energy) over time. The M_L 2.5 record is shown on the left and the M_L2.2 record is shown in the right*

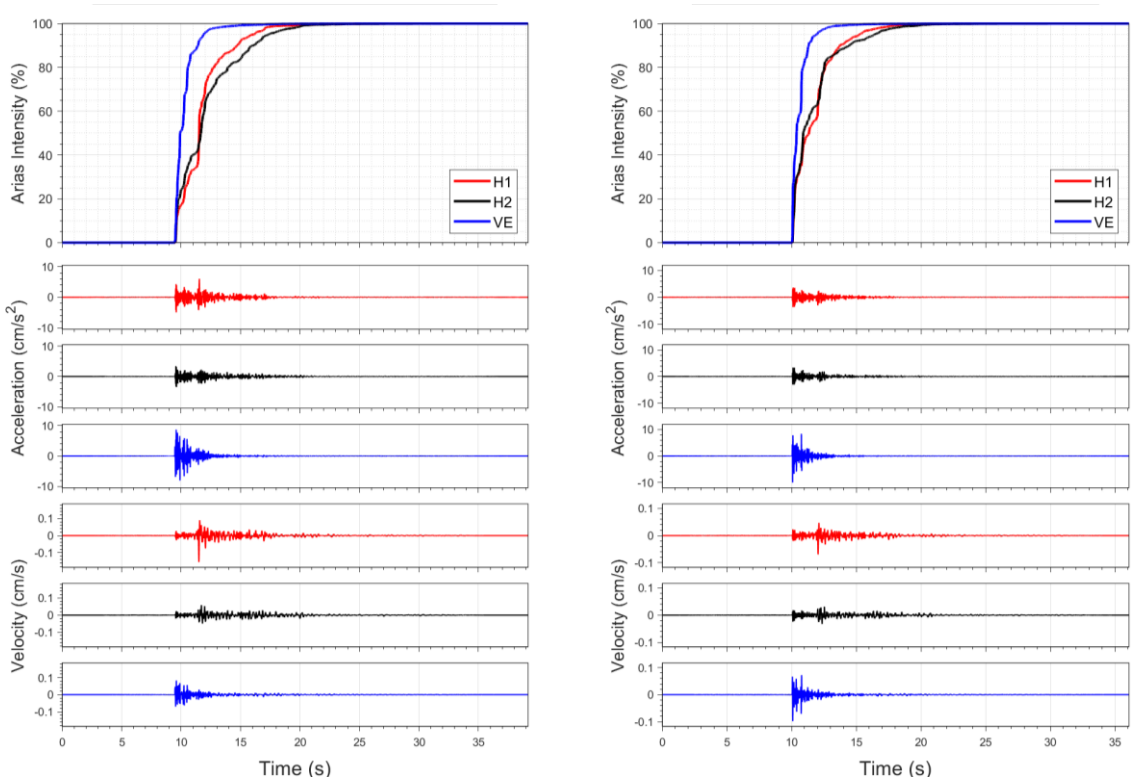

Figure 5.17 *Horizontal components of acceleration and velocity from the G180 station; the upper frame shows the accumulation of Arias intensity (energy) over time. The M_L 2.5 record is shown on the left and the M_L2.2 record is shown in the right*

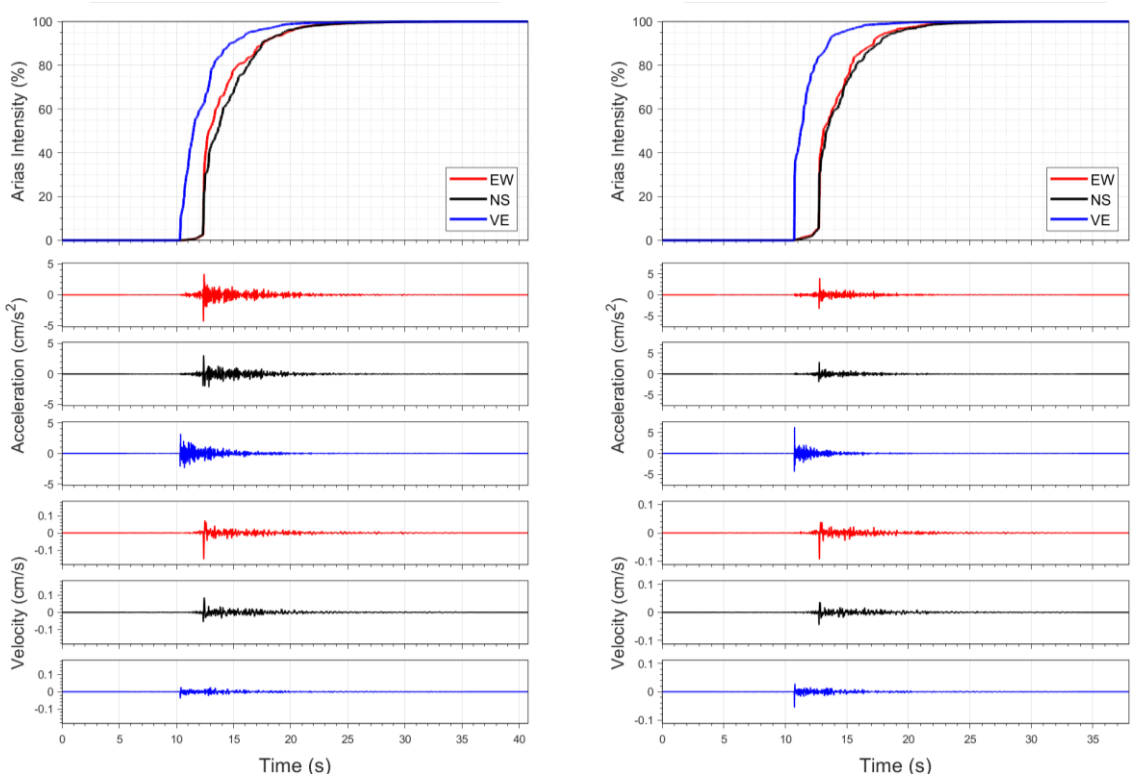

Figure 5.18 *Horizontal components of acceleration and velocity from the BGAR station; the upper frame shows the accumulation of Arias intensity (energy) over time. The M_L 2.5 record is shown on the left and the M_L2.2 record is shown in the right*

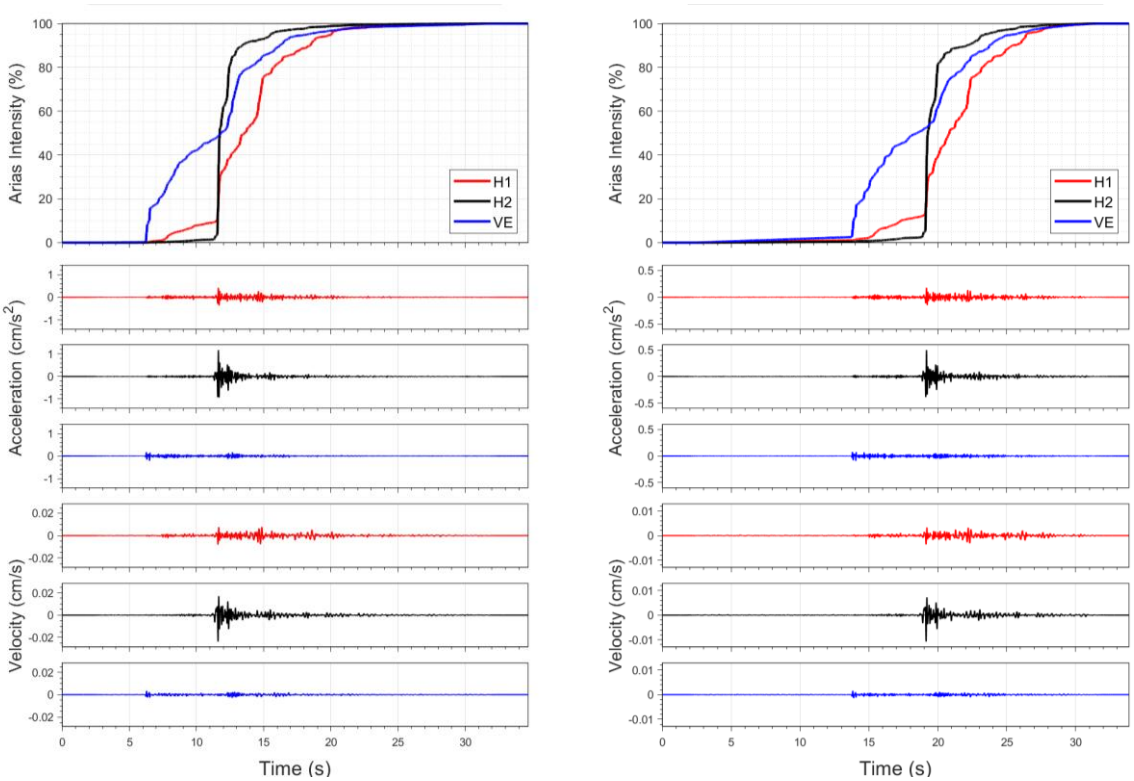

Figure 5.19 *Horizontal components of acceleration and velocity from the G480 station; the upper frame shows the accumulation of Arias intensity (energy) over time. The M_L 2.5 record is shown on the left and the M_L2.2 record is shown in the right*

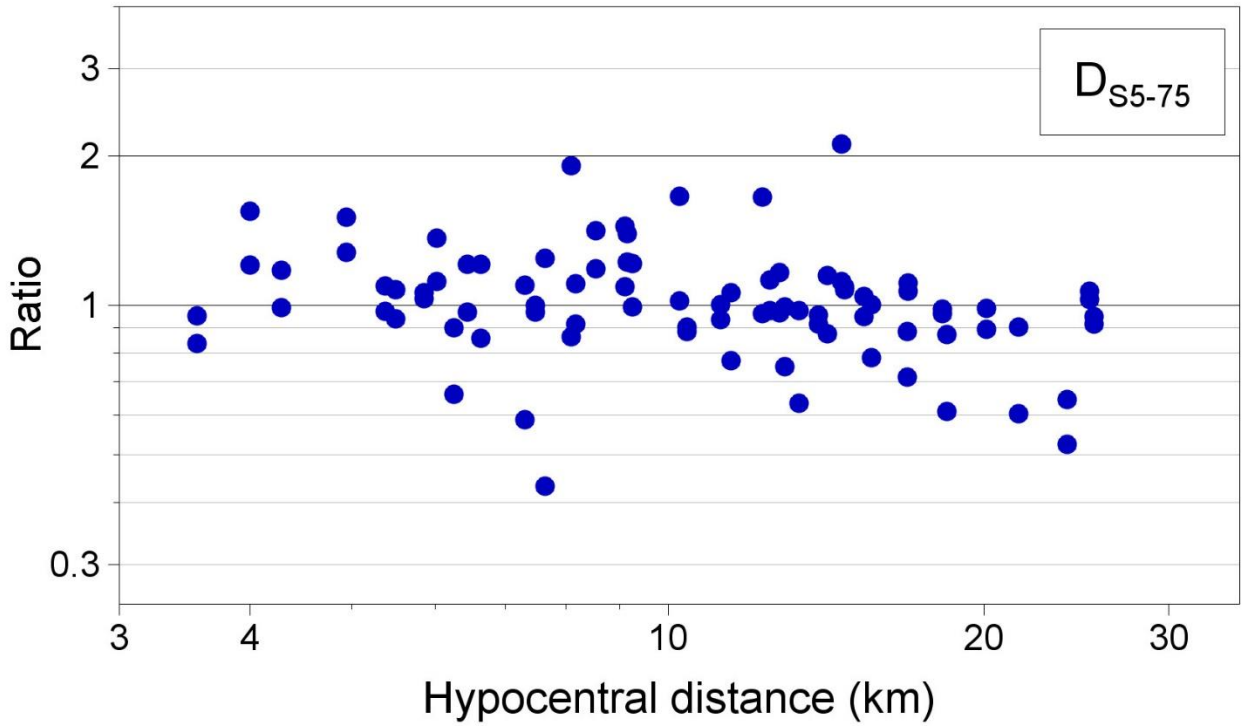

Figure 5.20 *Ratios of as-recorded horizontal PGA and PGV values recorded during the M_L2.5 event to those recorded during the M_L2.2 event.*

As expected from observing Figures 5.16 – 5.19, the ratios durations of the as-recorded horizontal components are well centred on the value of one and hence were very similar during both events. This is consistent with the latest model for durations developed for the Groningen field by Bommer *et al*. (2018), whereby durations do not scale with magnitude below the magnitude of 3.25.

The pseudo-acceleration response spectra and Fourier spectra of the same stations are compared in Figures 5.21 – 5.24; the full suite of spectra from the recordings of all 44 stations that recorded both events are included in Appendix C. As observed, with a few exceptions (such as the response spectra of station BGAR), the shapes of the spectra for each station remain similar for both recorded events.

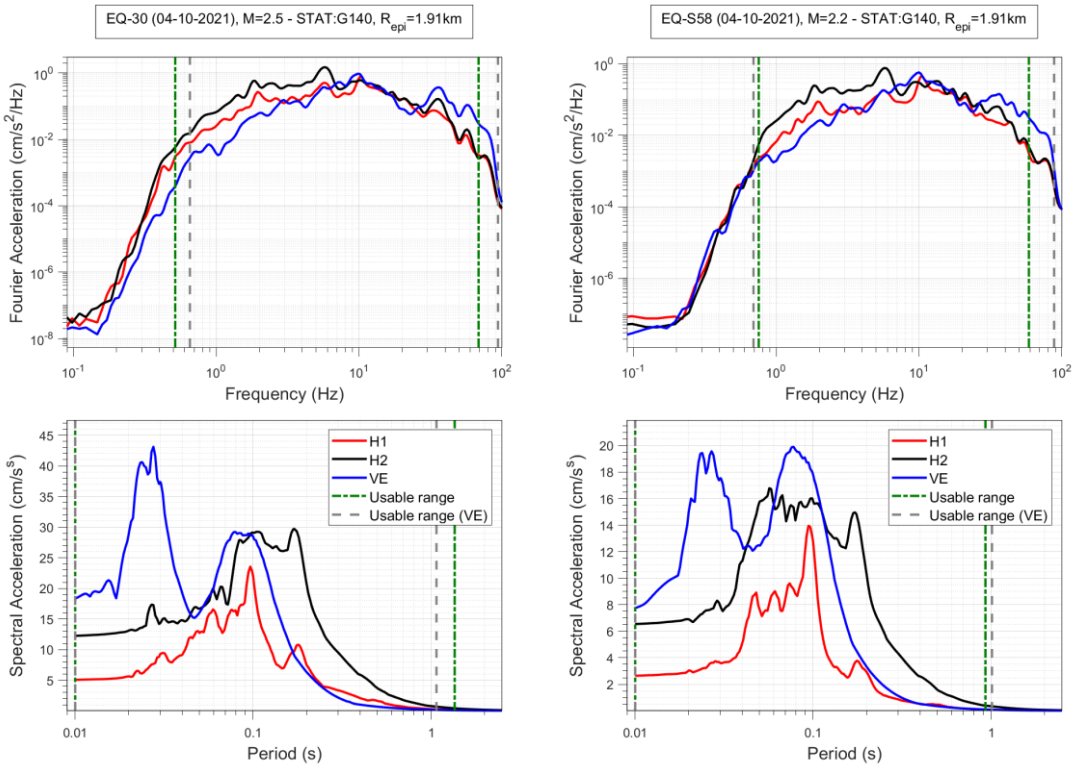

Figure 5.21 *Pseudo-acceleration response spectra and Fourier spectra from the G140 station. Spectra corresponding to the M_L 2.5 events are shown on the left and those corresponding to the M_L2.2 are shown in the right*

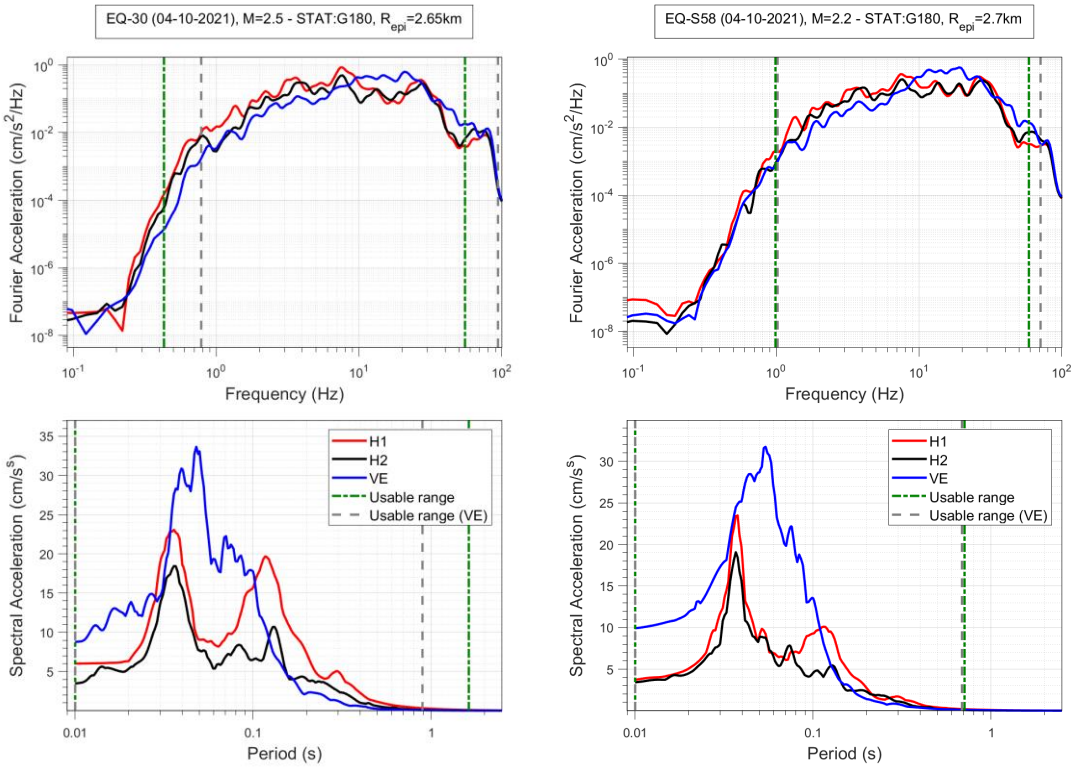

Figure 5.22 Pseudo-acceleration response spectra and Fourier spectra from the G180 station. *Spectra corresponding to the M_L 2.5 events are shown on the left and those corresponding to the M_L2.2 are shown in the right*

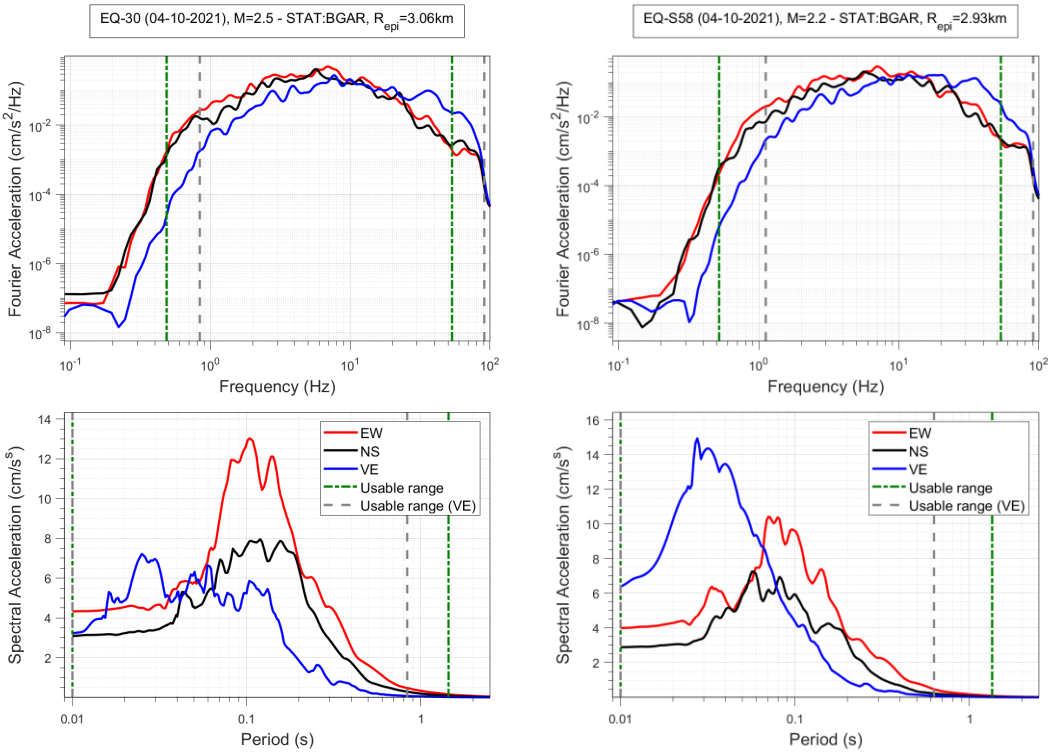

Figure 5.23 Pseudo-acceleration response spectra and Fourier spectra from the BGAR station. Spectra corresponding to the M_L 2.5 events are shown on the left and those corresponding to the M_L2.2 are shown in the right.

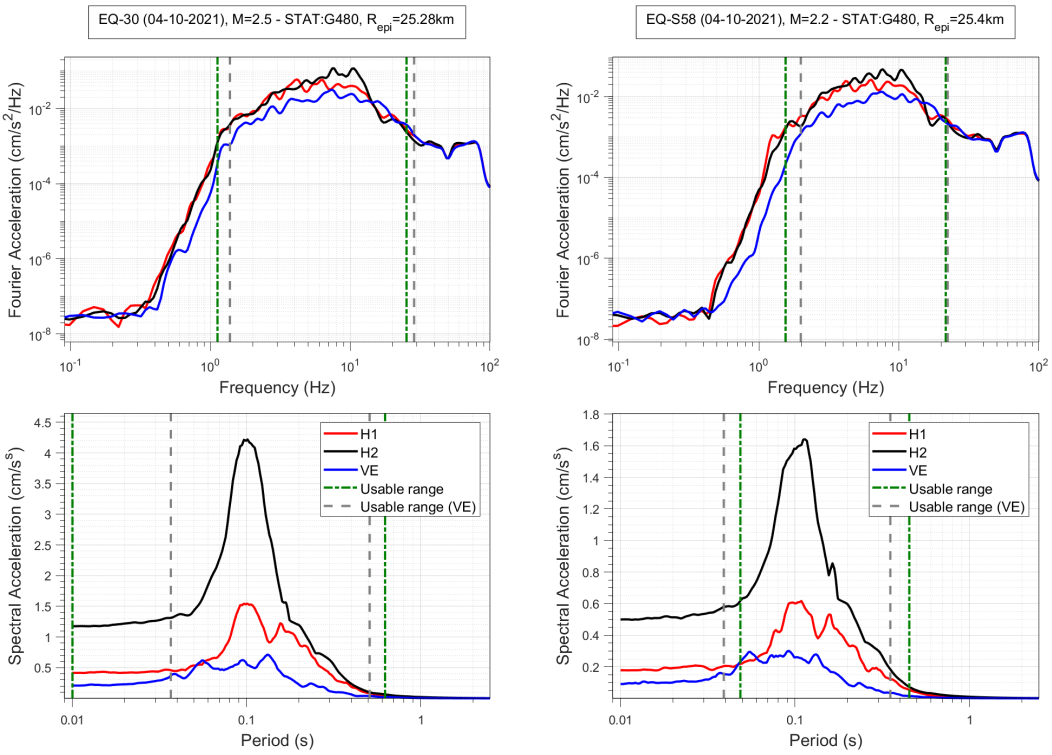

Figure 5.24 Pseudo-acceleration response spectra and Fourier spectra from the G480 station. Spectra corresponding to the M_L 2.5 events are shown on the left and those corresponding to the M_L2.2 are shown in the right

Figure 5.25 presents ratios of the pseudo-acceleration response spectra of the as-recorded horizontal components of the records obtained during the M_L2.5 event to those obtained during the M_L2.2 event. Each curve is shown only within the usable period range of the records it represents. Large variations

can be observed in the ratios, with their arithmetic and geometric means fluctuating around the value of 2. The scatter is reduced at periods longer than 0.2 seconds, where the average ratios are slightly above 2. A similar image is produced when plotting ratios of the geometric-mean components (Figure 5.26) although with smaller variation in the observed ratios.

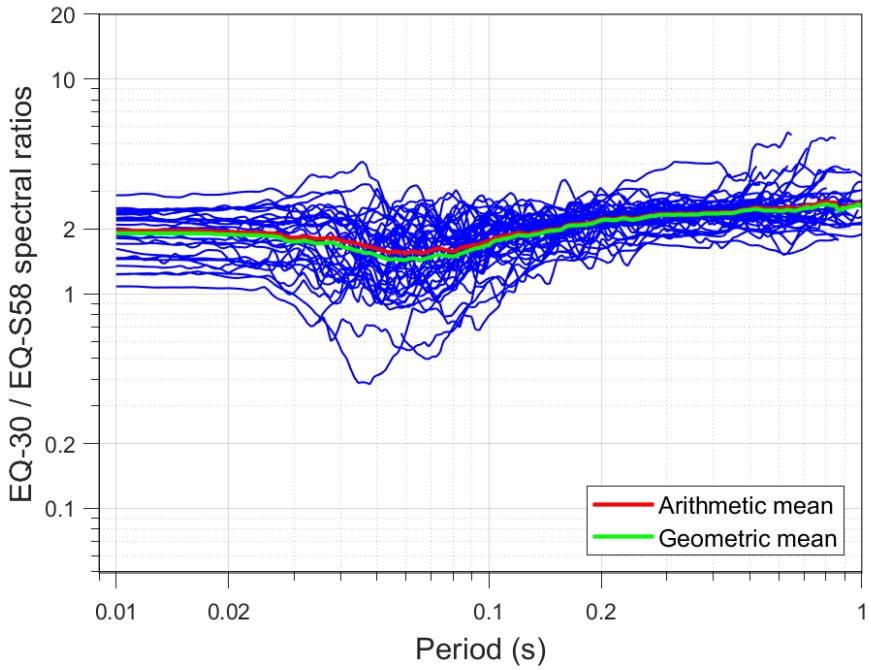

Figure 5.25 *Ratios of pseudo-acceleration response spectra of the as-recorded horizontal components of acceleration recorded in the M_L2.5 event to those recorded during the M_L2.2 Zeerijp event.*

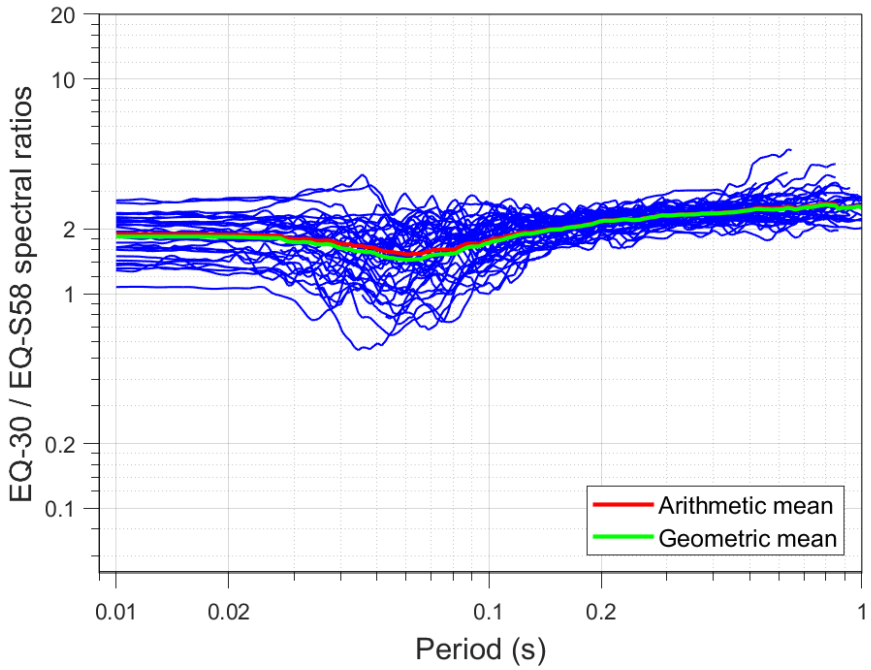

Figure 5.25 Ratios of pseudo-acceleration response spectra of the Geometric-Mean horizontal components of acceleration recorded in the M_L2.5 event to those recorded during the M_L2.2 Zeerijp event

5.6 Concluding remarks

Two earthquakes occurred within a small epicentral distance on 4th October 2021 near the village of Zeerijp, one of M_L2.5 and one of M_L2.2. The patterns of recorded PGA, PGV and Spectral Accelerations with distance are similar for both events, including their outliers such as station G480. The PGA and PGV values recorded are different by a factor of approximately 2, which matches the value of the magnitude scaling predicted by the empirical PGV GMPEs between the magnitudes of the events. The time-histories, response spectra and Arias Intensity accumulation of the recordings of the two events at each station are visually very similar, as are the values of 5-75% significant duration calculated for each record.

This report contains a preliminary comparison of the recorded ground-motions; the strong similarities observed between the data recorded during the two events, as well as the information that appears to suggest that the difference between many recordings of the events can be approximated by a simple scaling factor, warrants more thorough investigation and analyses, which can yield important conclusions about the variation and scaling of ground-motions in Groningen and elsewhere.

6 Empirical Green's functions methodology

6.1 The earthquake swarm commencing on 4th October

On 4th October three earthquakes have been registered in the Groningen area. Two of these occurred close to Zeerijp and had a magnitude of M_L=2.5 and M_L=2.2 on the Richter scale, respectively. The third earthquake on that day occurred near Appingedam and had a magnitude of 1.8. In de following two weeks more earthquakes were recorded. Table 6.1 provides an overview of these earthquakes.

Date (UTC)	Time (UTC)	Time (CEST)	Location	Magnitude
4 okt 2021	02:59:08	04:59	Zeerijp	2,5
4 okt 2021	13:33:45	15:33	Appingedam	1,8
4 okt 2021	20:47:42	22:47	Zeerijp	2,2
6 okt 2021	18:57:56	20:57	Zeerijp	1,3
7 okt 2021	11:53:20	13:53	Zeerijp	0,6
15 okt 2021	15:04:21	17:04	Zeerijp	1,1
5 nov 2021	22:38:26	00:38	Scharmer	1.1
8 nov 2021	01:52:16	03:52	Westeremden	1.7

Table 6.1 Overview of the earthquake swarm, which commenced on 4th October 2021.

Because most of these earthquakes occurred in the vicinity of Zeerijp the local earthquake density was strongly affected by the earthquake swarm. Figures 6.1 to 6.3 show the development of the earthquake density during October and early November 2021. The figures show the earthquake density for the Groningen gas field on 1st September 2021, 1st October 2021, 5th October 2021, 1st November, 2021 and 8th November 2021. Figure 6.4 shows the development of the trend parameter for the number of earthquakes up to 8th November 2021.

Using the automated Full-Waveform Inversion (FWI) method both the hypocentre and the source mechanism were determined. The results for the hypocentre of these earthquakes have been summarised in table 6.2. The detailed analysis of these earthquakes using the FWI-method are included in the half-yearly monitoring report for 1st November 2021.

File	Date	Location	Northing (m)	Easting (m)	Depth (m)
39	4 October 2021	Zeerijp	596750	245550	3000
40	4 October 2021	Appingedam	591500	251150	2850
41	4 October 2021	Zeerijp	596700	245550	3050
42	6 October 2021	Zeerijp	596600	245450	2850
43	7 October 2021	Zeerijp	596650	245550	3000
46	22 October 2021	Zeerijp	596400	245550	2850
51	8 November 2021	Westeremden	583700	244250	2700

Table 6.2 Overview of the hypocentre for the earthquake swarm that commenced on 4th October 2021.

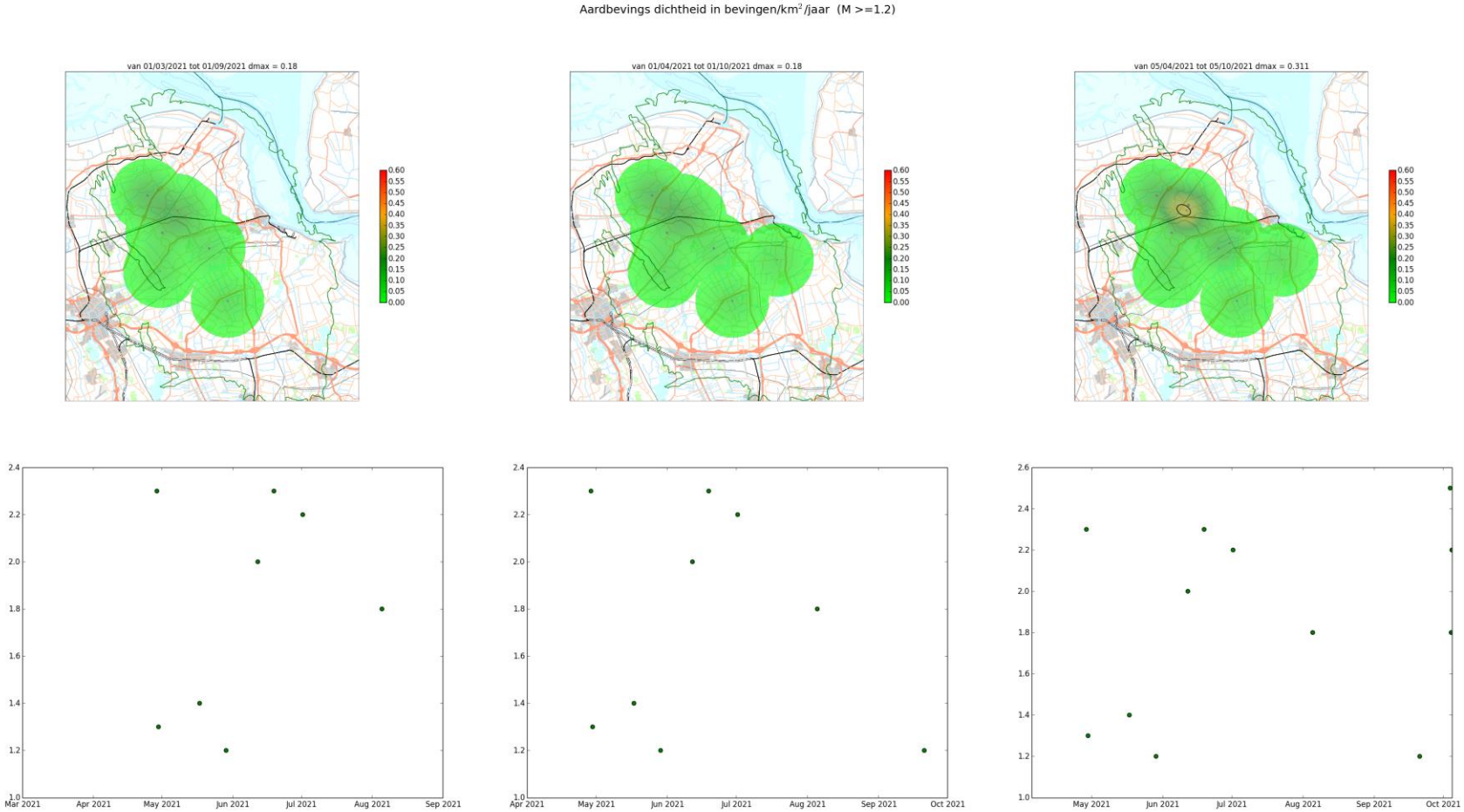

Figure 6.1 This panel shows the earthquake density (above) en the magnitude of the earthquakes versus time (below) for three different time periods. Left this is shown for the 6 months preceding 1st September 2021, in the centre for the 6 months preceding 1st October 2021 and to the right the period preceding 5th October 2021.

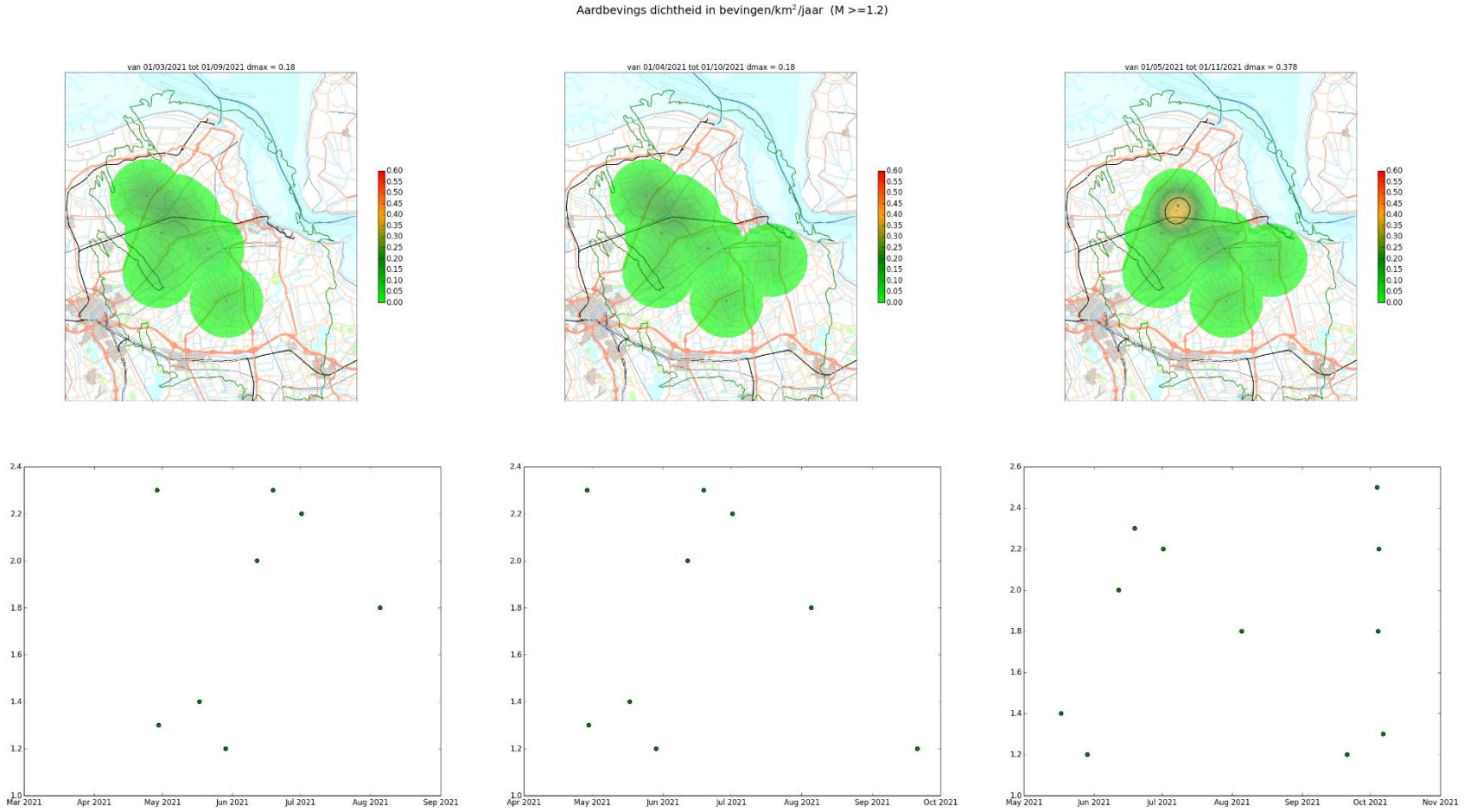

Figure 6.2 This panel shows the earthquake density (above) en the magnitude of the earthquakes versus time (below) for three different time periods. Left this is shown for the 6 months preceding 1st September 2021, in the centre for the 6 months preceding 1st October 2021 and to the right the period preceding 1st November 2021.

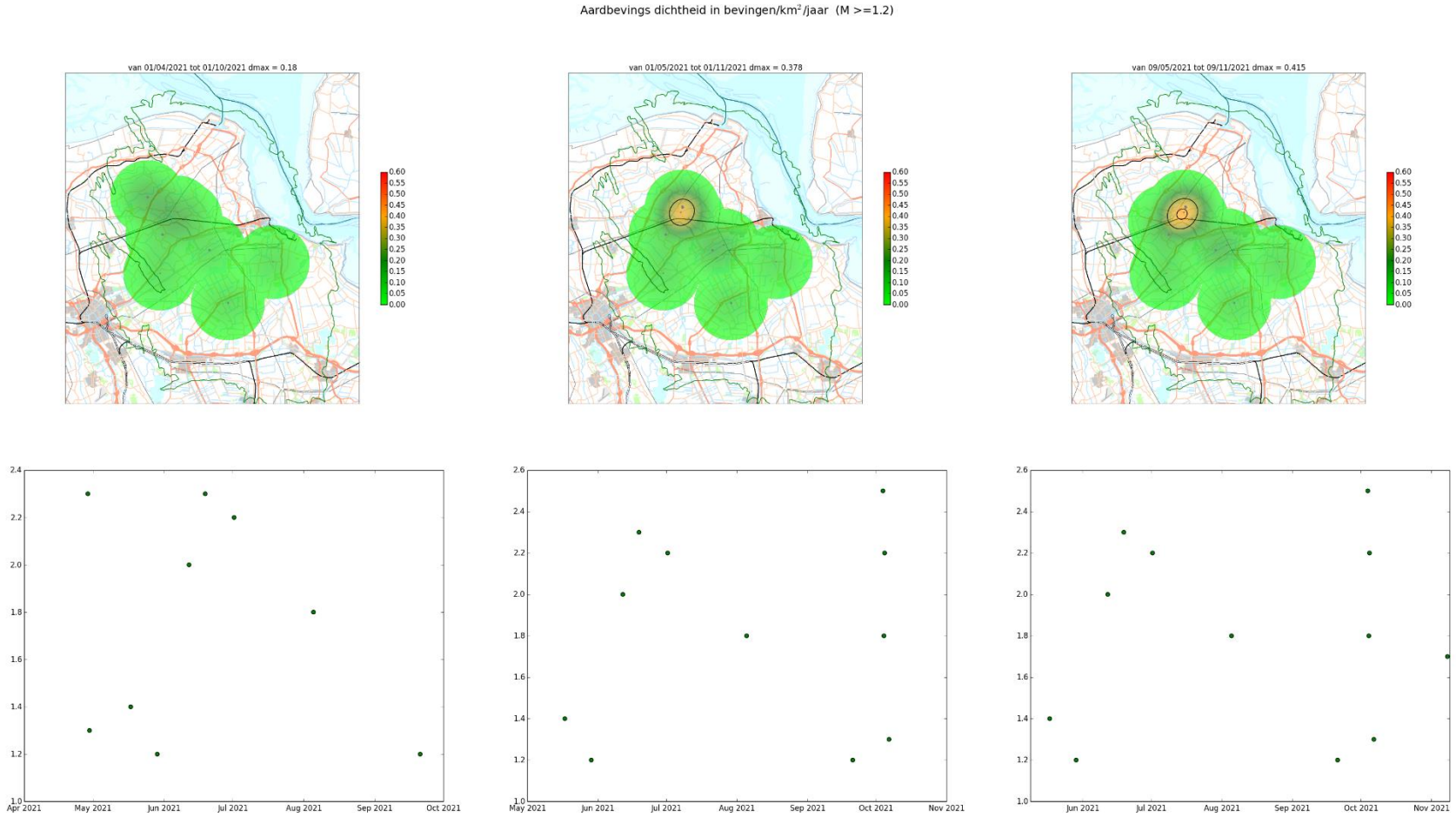

Figure 6.3 This panel shows the earthquake density (above) en the magnitude of the earthquakes versus time (below) for three different time periods. Left this is shown for the 6 months preceding 1st October 2021, in the centre for the 6 months preceding 1st November 2021 and to the right the period preceding 9th November 2021.

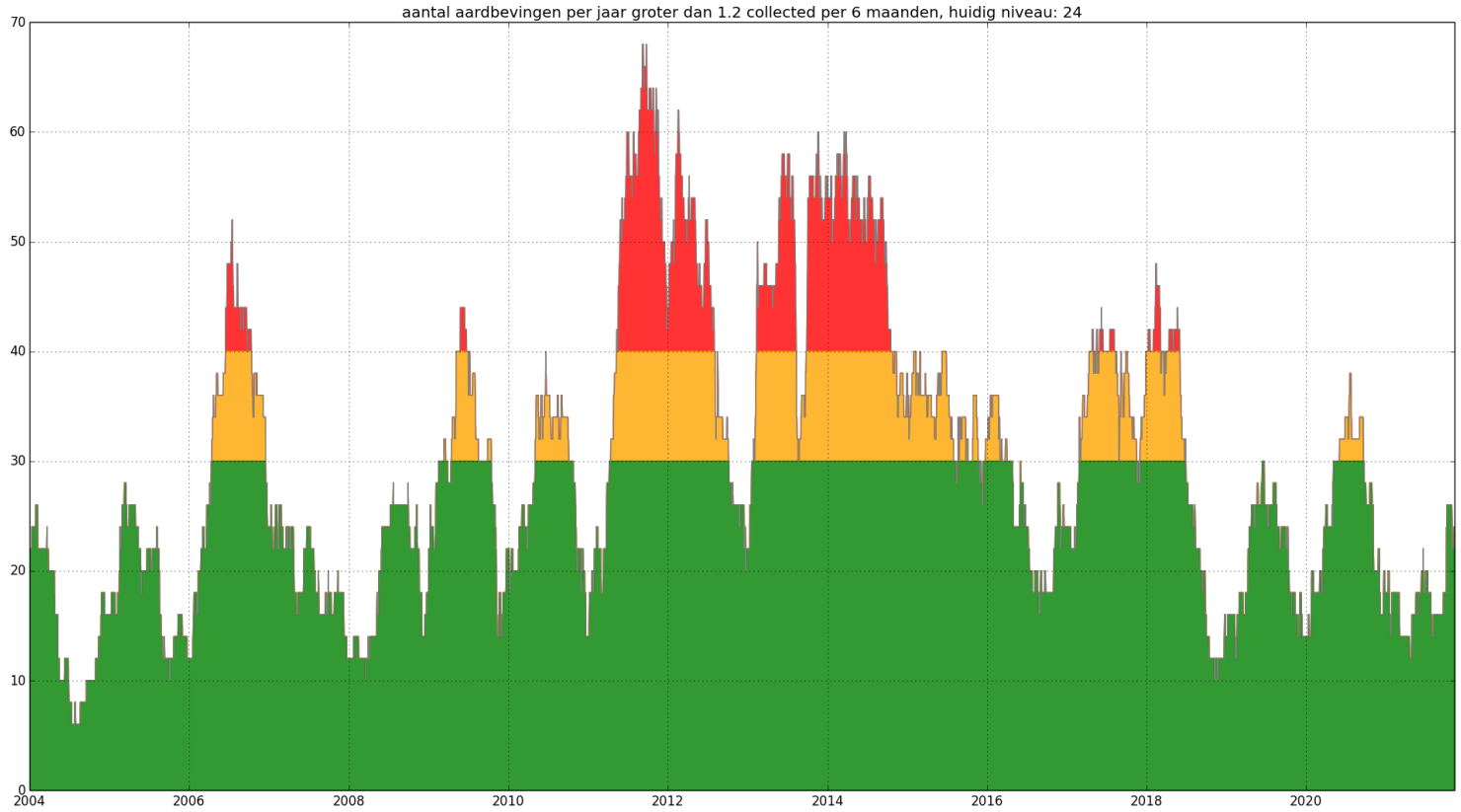

Figure 6.4 The trend parameter for the number of earthquakes for the period ending on 9th November 2021.

The automated FWI-analysis shows that the epicentre of the earthquakes near Zeerijp are located very close together. The hypocentres of these earthquakes are all at around 3 km depth. The orientation of the source mechanisms also aligns closely with local faults. The earthquakes most likely took place on the same fault of nearby faults. More on this in the next section. The epicentra of four of the earthquakes of the swarm are located in a circle with the radius of 150 m (table 6.3).

File	Datum	Locatie	Horizontal distance to the central location	Total distance to the central location
39	4-Oct-21	Zeerijp	132	141
41	4-Oct-21	Zeerijp	82	130
42	6-Oct-21	Zeerijp	82	130
43	7-Oct-21	Zeerijp	36	62
46	22-Oct-21	Zeerijp	221	242

Table 6.3 Overview of the distance of the hypocentre of the earthquake swarm commencing on 4th October 2021 to the central location (N: 596620, E: 245530, D: 2950).

6.2 Empirical Green's Function Approach (preliminary)

The earthquake swarm can also be analysed using the empirical Green's functions approach (Oates et al, 2020). We have applied the Empirical Green's Function (EGF) method to pairs of these earthquakes with strongly correlated seismograms with the aim of estimating the horizontal rupture propagation direction and distance for comparison with mapped reservoir-level faulting.

The EGF method takes pairs of nearby events with similar mechanisms but usually significantly different magnitudes and, by deconvolution of the larger event with the smaller, removes the effects of propagation through the subsurface from the larger event's seismogram. The aim is to give a clean representation of the earthquake source time function, which is suitable for further quantitative analysis. If the smaller event in the EGF data analysis – the so-called empirical Green's Function – is small enough to be considered a point source, then the output from the deconvolution is an approximation of the larger event's source time function.

It can be shown that the horizontal component of rupture propagation leads to a sinusoidal azimuthal variation of the duration of the source time function, with amplitude proportional to the rupture propagation distance. This variation of the source duration due to rupture propagation can be understood as an example of Doppler broadening of a signal, exactly analogous to the shift in pitch as a source of sound, such as a car siren, approaches and then recedes.

The EGF process can also be applied to pairs of events which are both large enough to be considered as propagating ruptures. If the rupture propagation directions of the two events are parallel or opposite to each other, the azimuthal variation of the duration is proportional to respectively the sum or difference of the rupture propagation distances of the two events. Our EGF workflow involves deconvolution, trace scaling and then picking of the zero crossings at the start and end of the source time function traces. This gives a dataset of measurements of the duration as a function of the source-receiver azimuth angle which is then fitted with a sinusoidal Doppler broadening expression to generate estimates of the rupture propagation direction and distance. A quality measure, ξ, for the parameter inversion is calculated from the residuals for the best fit Doppler model: this quality measure varies between 0 (the Doppler model fit is no better than the azimuth-independent average) and 1 (the data points fall exactly on the sinusoidal model curve).

Further explanation of the technical details of the EGF method and its application to the Groningen earthquake data up to mid-2019 can be found in the NAM report by Oates et al (2020).

Cross-correlation of all earthquake pairs in the Groningen catalogue, found the following strongly correlated pairs from the period of interest in October 2021: 21039/21041, 21039/21043, 21041/21043, 21036/21046, 21042/21036, and 21042/21046. The six individual events have nearby locations and can be divided into two obvious clusters with contrasting focal mechanisms (see figure 6.6 and table 6.4). The EGF deconvolution workflow has been applied to the six event pairs which can be formed by pairing events with a common focal mechanism. Although the two largest events have significant magnitudes, the EGF results obtained for all but one of the pairs have low values of the fit quality metric indicating a small horizontal rupture propagation distance and/or high levels of noise on the EGF output due to either one or both of the events having low signal amplitude. Where low signal levels lead to particularly variable picking results, the maximum source-receiver offset has been limited to 20km to reduce the number of mis-picks.

In the earlier EGF analysis of event pairs up to mid-2019, it was found that rupture propagation directions for the best quality results ($\xi \geq 0.5$) correlated very well with the mapped fault traces at Top Rotliegend level; with declining quality this visual correlation degrades. The highest quality result from the current analysis is for event pair 21039/21041 which has $\xi = 0.42$. Plotting all results with $\xi \geq 0.4$ from the current and previous EGF analyses gives the plot of rupture propagation vectors shown in figure 6.7 In figures 6.8 and 6.9 the azimuthally varying EGF output and picked duration are shown for the same event pair.

Note how in figure 6.7 the rupture propagation direction coincides very well with a faint underlying fault lineament. Note however that the focal mechanisms of the cluster of events 21039-21041-21043 (figure 6.6) align with the adjoining fault trace, that is they are at an angle of about 60° to the observed rupture propagation direction. The clustered events are located very close to the junction of these two fault lineaments (tail of the red vector in figure 6.7) so mechanisms and rupture propagation vectors could be expected to align with one or other of these. The most straightforward candidate explanation for this observation would be that the horizontal rupture propagation observed is the projection of predominantly down-dip rupture propagation. If this is the case then the EGF result, focal mechanisms and fault map are all consistent with a simple conceptual model of a rupture propagating along the fault plane on which the failure occurs. Otherwise a more complex conceptual model of composite failure around the junction of the two faults would be needed.

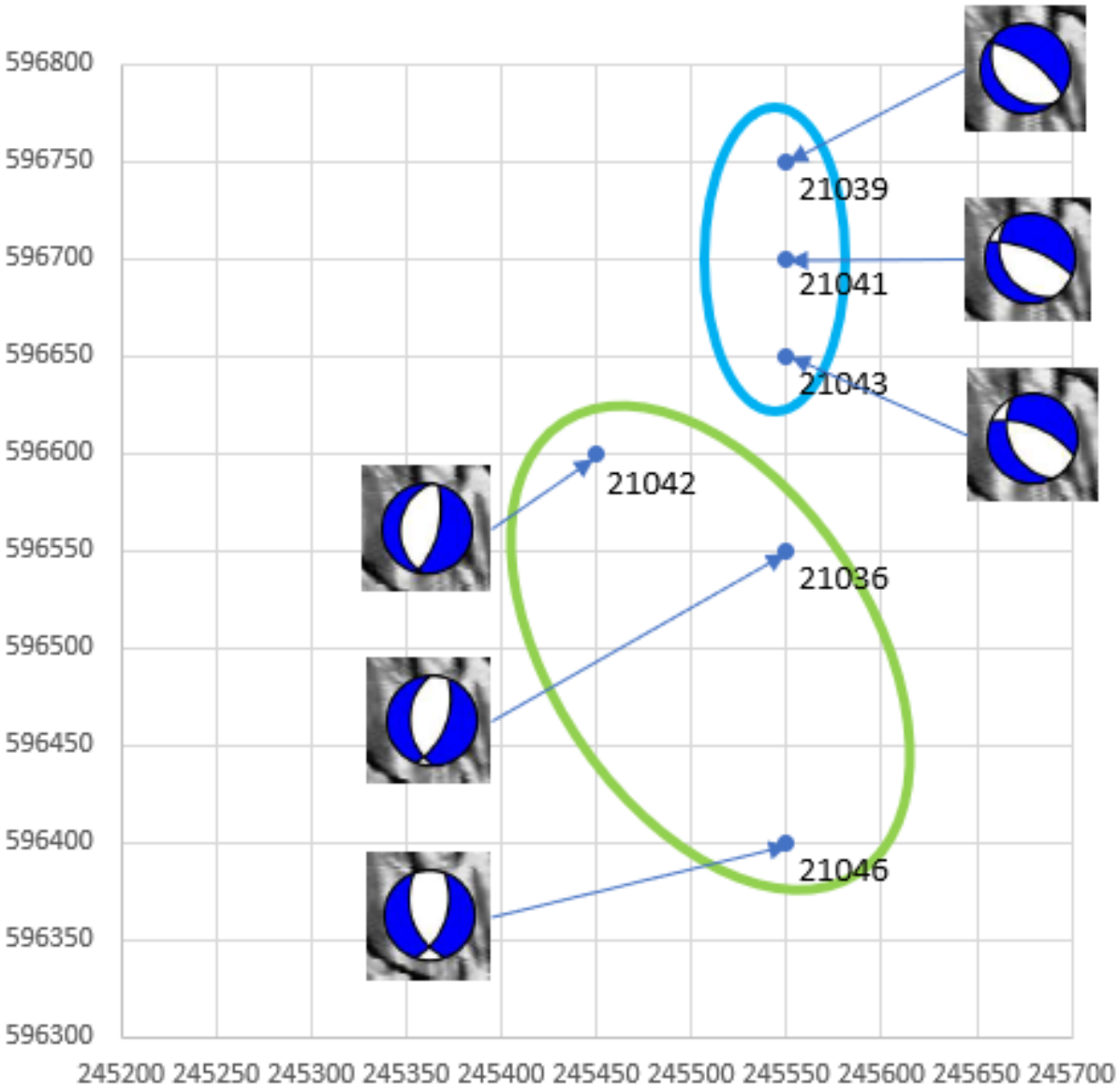

Figure 6.6 Locations and focal mechanism plots for events analysed with EGF workflow. Note how events 21039-21041-21043 and 21036-21042-21046 form two clusters with distinct focal mechanisms.

Child Event ID	Parent Event ID	Child Magnitude	Parent Magnitude	Child Easting	Child Northing	Child Depth	Parent Easting	Parent Northing	Parent Depth	Azimuth (° from N)	L (m)	ξ
21041	21039	2.2	2.5	596700	245550	3050	596750	245550	3000	74.88	25.85	0.42
21043	21039	0.6	2.5	596650	245550	3000	596750	245550	3000	74.81	15.82	0.08
21043	21041	0.6	2.2	596650	245550	3000	596700	245550	3050	29.00	3.37	0.02
21046	21042	0.8	1.3	596400	245550	2850	596600	245450	2850			
21036	21042	0.9	1.3	596550	245550	2900	596600	245450	2850	16.16	18.34	0.09
21046	21036	0.8	0.9	596400	245550	2850	596550	245550	2900			

Table 6.4 Summary of EGF results for the event clusters shown in figure 6.6.

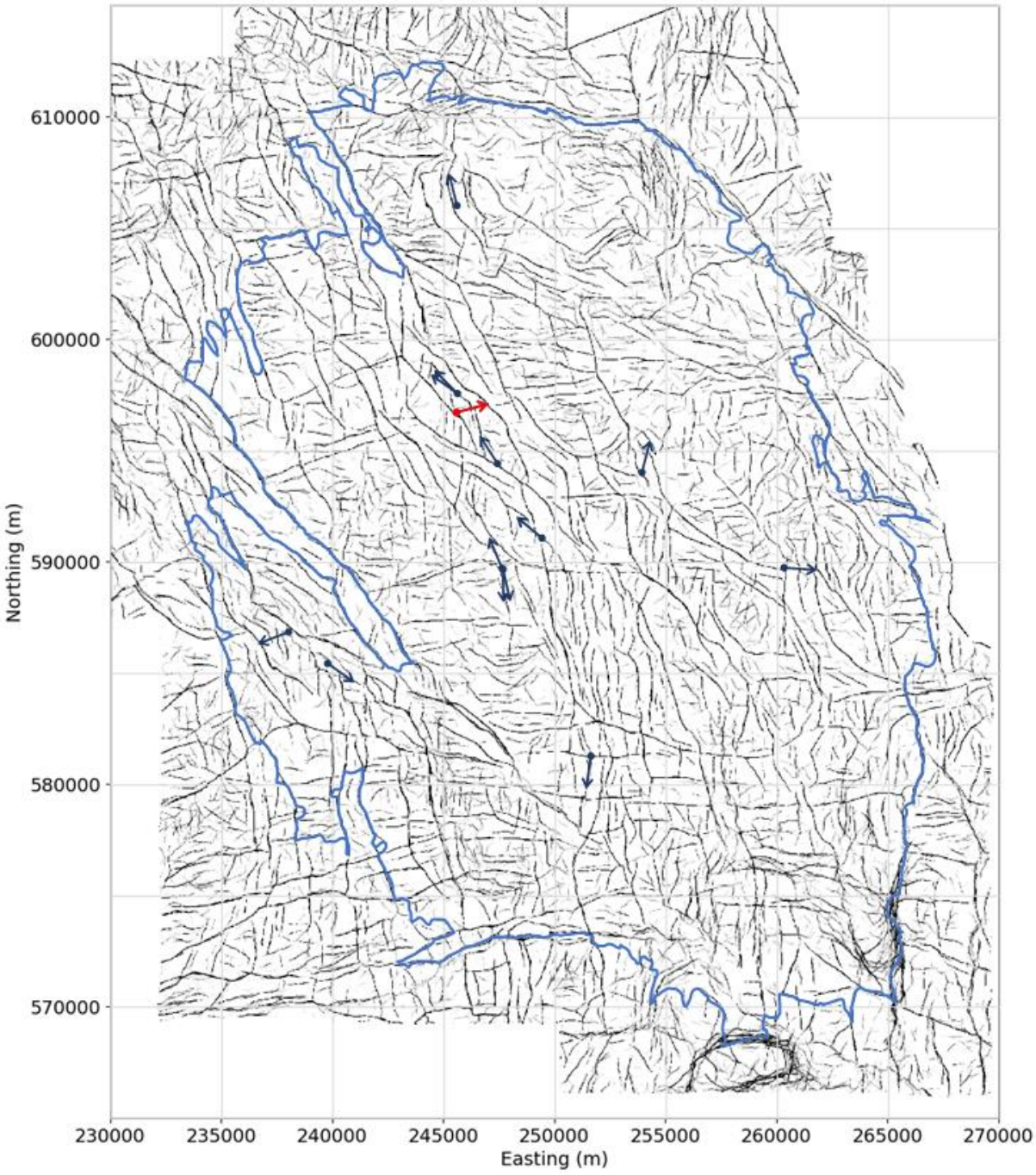
610000
600000
590000
580000
570000
Northing (m)
230000
235000
240000
245000
250000
255000
260000
265000
270000
Easting (m)

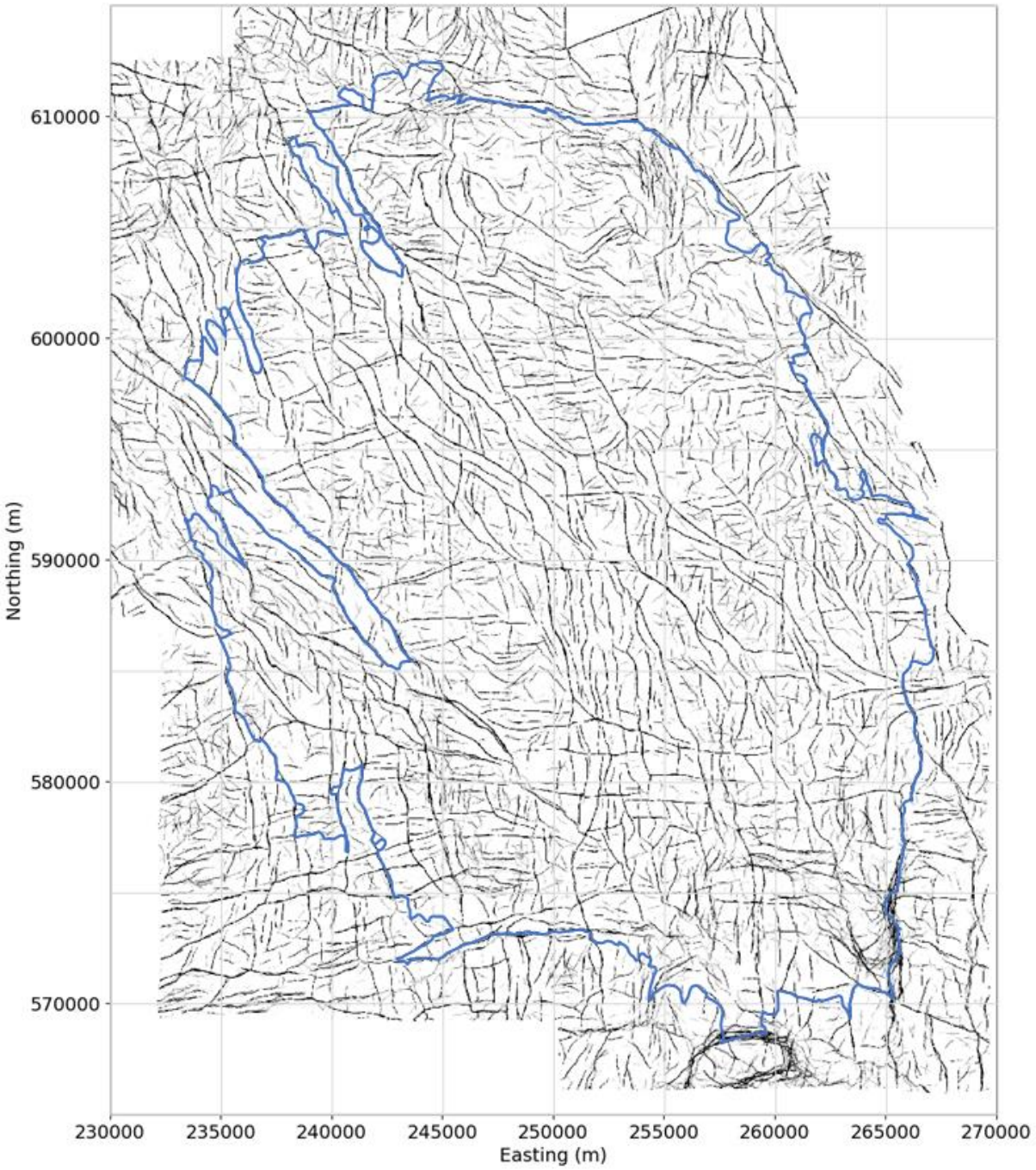

Figure 6.7 Scaled horizontal rupture vectors overlain on the fault map. In each of these plots the base map shows the detailed fault interpretation generated by Kortekaas & Jaarsma (2017). The outline of the gas field is shown as a blue contour. The vectors give only the horizontal rupture propagation direction (vectors are drawn with a constant length), obtained from the inversion of the picked durations. The upper plot shows the highest quality event pairs for which $\xi \geq 0.4$; the red vector is the result for event pair 21039/21041; the blue vectors are for event pairs from the previous EGF analysis. The lower plot is the base fault map and field outline without events.

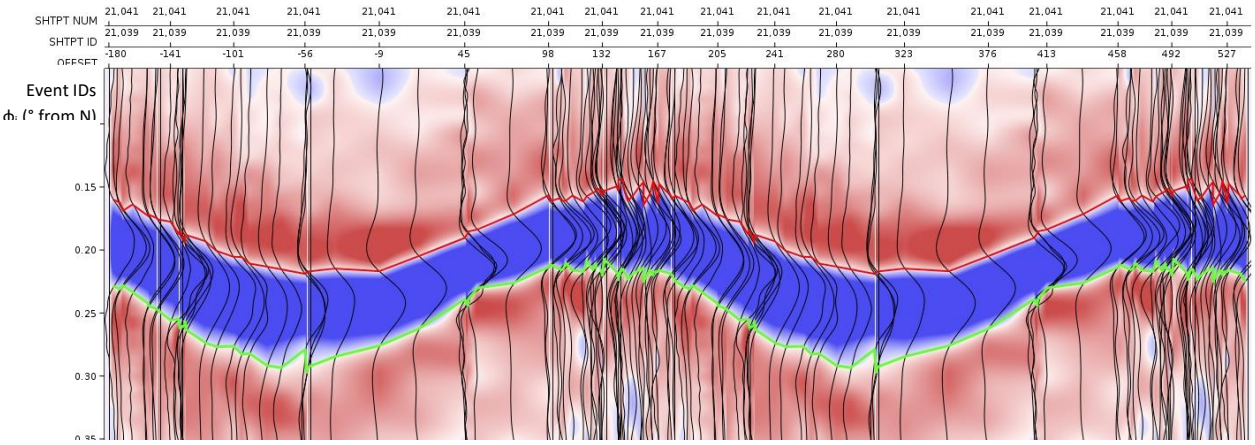

Figure 6.8 EGF trace output for event pair 21039/21041 as a function of azimuth with respect to North. The traces have been duplicated and displayed on the interval $[-180°, 540°]$ to ensure that periodic effects are not obscured. Duration is the difference between picked start and end times of the source time function as shown.

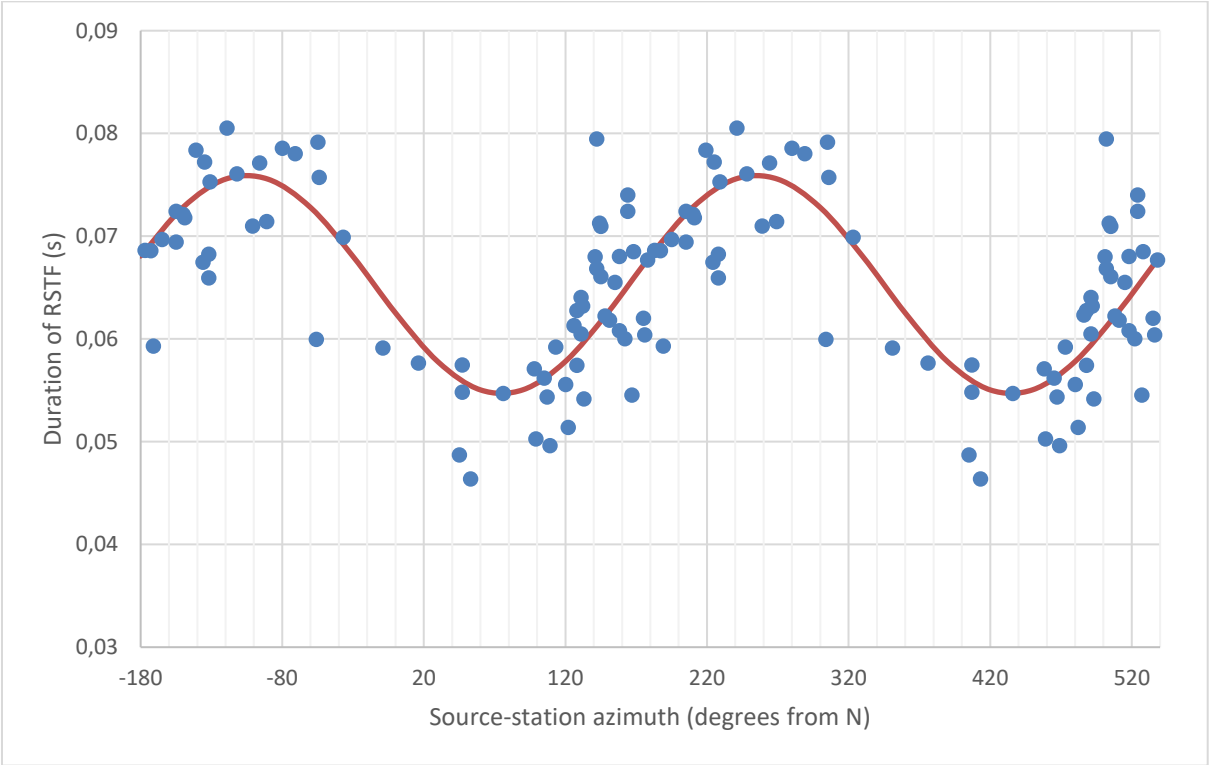

Figure 6.9 Picked duration between the zero crossings of the RSTF traces for event pair 21039/21041 (blue data points) with Doppler model fit (orange curve). Results are shown on the interval $[-180°, 540°]$ as for the seismogram display.

7 Damage Notifications

7.1 Building Damage Claims received by IMG

The IMG (Instituut Mijnbouwschade Groningen) tasked with the damage claim handling and repair of damage resulting from the gas production from the Groningen field has reported on the damage due to the Zeerijp and Appingedam earthquakes on the website in the weekly update on damage claims received and settled.

The day after the earthquakes, on the 5th October 2021, the IMG reported that:

> *In the immediate vicinity of the earthquakes of Zeerijp and Appingedam, eight new damage reports have been made since yesterday morning until 12:00 today. In addition, seven reports have been made of a potentially acutely unsafe situation.*

IMG do acknowledge in the same news article that a potentially acutely unsafe situation (AOS) does not mean there is a relation to gas production. In the case of an AOS report, it is not assessed whether the damage is the result of gas extraction or gas storage.

https://www.schadedoormijnbouw.nl/nieuws/schademeldingen-bevingen-zeerijp-en-appingedam

The following week on 12th October the IMG reported that (Ref. 26):

> *Last week, 544 new reports of physical damage (cracks in walls, among others) were received. That is an increase of 164 reports compared to the previous week. The increase is probably the result of the earthquakes at Zeerijp and Appingedam last week.*

https://www.schadedoormijnbouw.nl/nieuws/weekcijfers-544-meldingen-fysieke-schade-171-meldingen-waardedaling

As NAM is not involved in the damage claims process, it does not have additional information to that made public by IMG.

In chapter 2 the ground motions resulting from the Zeerijp swarm of earthquakes were presented. At a distance from the epicentre of 20 km the PGV is 0.1 $^{mm}/_{s}$ from largest of the swarm (M_L = 2.5). For reference these vibration levels correspond to the normal vibration levels occurring in buildings from everyday use.

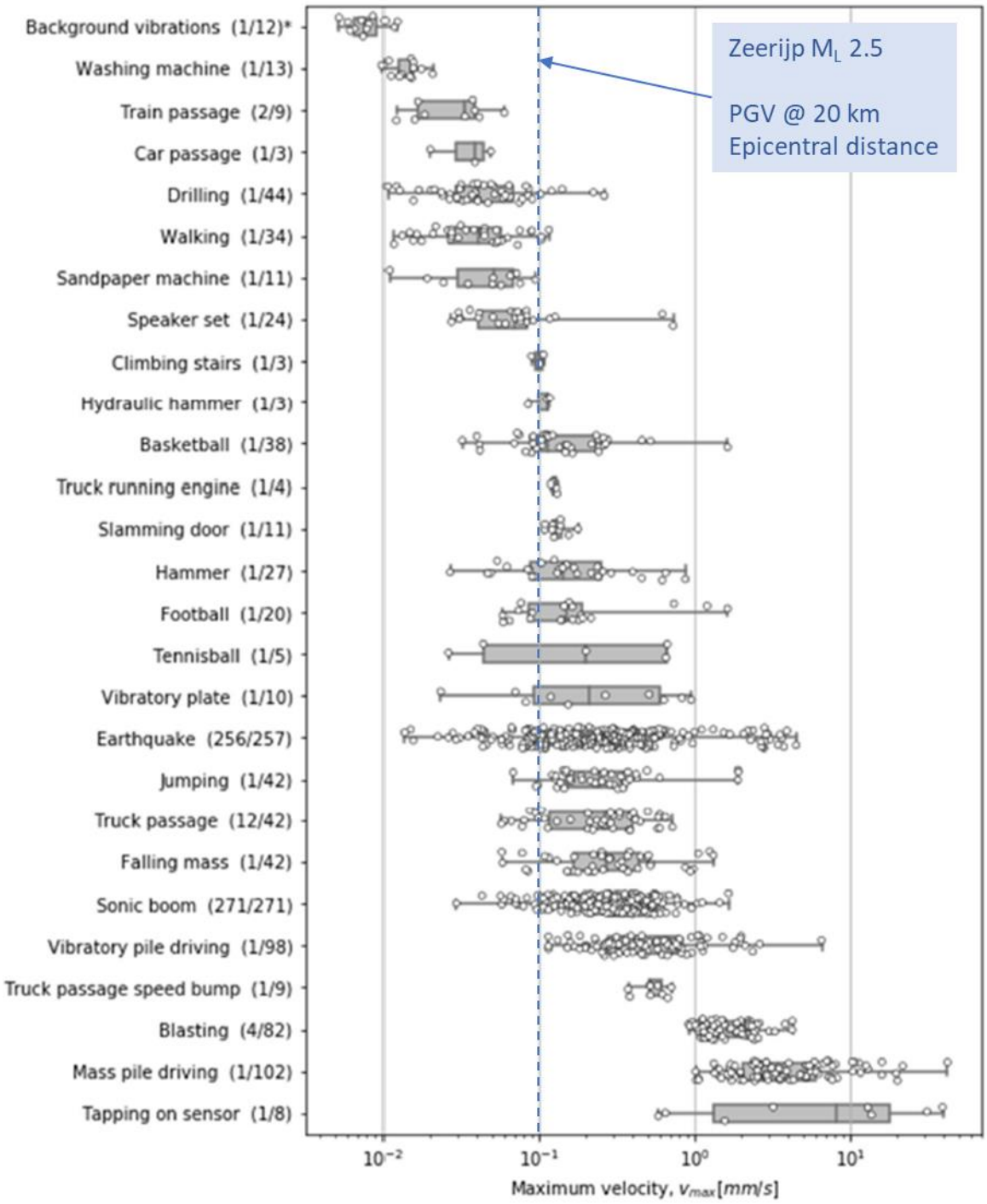

*Figure 7.1 Boxplots and samples for the absolute maximum velocity v_{max} obtained in all tests. *(number of buildings/number of measured signals) taken from a vibration characterization study by TNO Ref. 41. The blue lines were added to indicate the vibration level at 20 km distance from the Zeerijp M_L 2.5 earthquake of 4th October 2021.*

At these vibration levels there is only a neglectable chance of aesthetic damage to masonry and damage to a structurally sound building, that brings it to a state of near collapse can be excluded. The level of ground motions seen for the Zeerijp earthquake could not have caused a state of near collapse for structurally sound buildings near the epicentre, let alone at 20 km from the epicentre. Also damage to infrastructure is not expected as a result of the Zeerijp and Appingedam earthquakes.

8 References

Bommer, J.J., B. Dost, B. Edwards, P.P. Kruiver, P. Meijer, M. Ntinalexis, A. Rodriguez-Marek, E. Ruigrok, J. Spetzler & P.J. Stafford (2018). V5 Ground-Motion Model for the Groningen Field. Revision 1, 14 March 2018, 299 pp.

Bommer, J.J., B. Dost, B. Edwards, P.J. Stafford, J. van Elk, D. Doornhof & M. Ntinalexis (2016). Developing an application-specific ground-motion model for induced seismicity. *Bulletin of the Seismological Society of America* **106**(1), 158-173.

Bommer, J.J., B. Edwards, P.P. Kruiver, A. Rodriguez-Marek, P.J. Stafford, M. Ntinalexis, E. Ruigrok & B. Dost (2021). *V7 Ground-Motion Model for Induced Seismicity in the Groningen Gas Field*. Revision 1, 29 September 2021, 273 pp.

Bommer, J.J., P.J. Stafford, B. Edwards, B. Dost, E. van Dedem, A. Rodriguez-Marek, P. Kruiver, J. van Elk, D. Doornhof & M. Ntinalexis (2017). Framework for a ground-motion model for induced seismic hazard and risk analysis in the Groningen gas field, The Netherlands. *Earthquake Spectra* **33**(2), 481-498.

Bommer, J. J., P. J. Stafford, and M. Ntinalexis (2019). Empirical Equations for the Prediction of Peak Ground Velocity due to Induced Earthquakes in the Groningen Gas Field, 10 March 2019

Bommer, J. J., P. J. Stafford, and M. Ntinalexis (2021). Empirical Equations for the Prediction of Peak Ground Velocity due to Induced Earthquakes in the Groningen Gas Field, 1 October 2021

Dost, B., E. Ruigrok & J. Spetzler (2017). Development of probabilistic seismic hazard assessment for the Groningen gas field. Netherlands Journal of Geoscience 96, s235–s245.

Boore, D.M., J. Watson-Lamprey and N. A. Abrahamson (2006). Orientation-Independent Measures of Ground Motion. Bulletin of the Seismological Society of America, doi: 10.1785/0120050209

Edwards, B. & M. Ntinalexis (2021). Usable bandwidth of weak-motion data: application to induced seismicity in the Groningen Gas Field, the Netherlands. Journal of Seismology, doi: 10.1007/s10950-021-10010-7.

Ntinalexis, M., J.J. Bommer, E. Ruigrok, B. Edwards, R. Pinho, B. Dost, A.A. Correia, J. Uilenreef, P.J. Stafford & J. van Elk (2019). Ground-motion networks in the Groningen field: usability and consistency of surface recordings. Journal of Seismology 23(6), 1233-1253.

Oates, S., Tomic, J., Zurek, B., Piesold, T., and van Dedem, E., Empirical Green's Function analysis of some induced earthquake pairs from the Groningen gas field, August 2020

Spetzler J., J. & B. Dost (2017). Hypocentre estimation of induced earthquakes in Groningen. Geophysical Journal International **209**(1), 453–465.

Appendix A – Overview of results analysis using the automated FWI methodology for the induced earthquakes in the Groningen gas field

#	Date	Time	Name	Northing	Easting	Depth	Strike_1	Dip_1	Rake_1	Strike_2	Dip_2	Rake_2	Isotropic	CLVD	Double-Coupled	KNMI Magn
1	03/01/2020	10:36:29.410	Zuidbroek	578650	252900	2800	191.92	23.85	-83.27	4.37	62.82	-93.05	-40.078	-4.788	55.133	0.6
2	07/01/2020	9:15:31.430	Harkstede	581900	242450	2900	3.24	70.41	-63.78	121.87	30.16	-145.95	24.225	-6.247	69.529	0.8
3	10/01/2020	23:10:21.080	Schildwolde	581900	252300	2950	188.87	45.50	-63.00	343.15	72.82	-109.81	-24.141	36.234	39.626	1.3
5	23/01/2020	10:12:12.620	Lageland	584100	244800	3050	299.99	61.11	-128.69	166.11	57.16	-49.35	14.578	26.082	59.340	1.3
6	24/01/2020	21:35:02.655	Nieuwolda	587300	261700	3000	139.55	44.76	-95.72	325.62	63.63	-85.51	-23.748	28.729	47.523	1.6
7	26/01/2020	8:03:16.440	Kolham	577600	245100	2800	201.58	51.80	81.06	37.21	35.14	102.25	55.295	4.084	40.620	1.4
9	28/02/2020	2:46:06.515	Scheemda	577100	260000	2650	106.93	64.57	-104.82	307.88	43.53	-70.41	-34.002	21.764	44.234	0.3
10	02/03/2020	13:41:18.915	Wagenborgen	586500	256800	2950	154.65	38.53	-54.31	295.50	66.39	-113.37	-39.821	9.944	50.235	2.1
11	05/03/2020	20:08:52.075	Wagenborgen	586450	256900	2900	136.53	26.60	-141.46	11.07	73.79	-68.61	-22.796	-0.023	77.181	0.3
12	17/03/2020	7:18:33.705	Appingedam	592100	251150	2900	196.33	78.05	-68.89	315.40	24.33	-148.77	-22.509	0.744	76.748	0.8
13	17/03/2020	8:54:55.135	Garsthuizen	599700	243800	3000	155.12	10.82	122.89	296.94	45.59	81.79	51.488	31.525	16.987	1.4
14	17/03/2020	12:44:06.690	Sappemeer	579100	248750	2800	195.78	52.02	-93.43	19.27	63.00	-86.97	-27.287	35.838	36.875	1.8
15	22/03/2020	19:33:12.540	Krewerd	598100	251800	2800	145.97	23.06	-63.77	294.72	55.81	-102.08	-30.326	-20.652	49.022	2.3
16	23/03/2020	0:15:13.845	Thesinge	589400	237750	3100	316.55	71.94	-93.55	224.49	3.38	-3.16	23.808	-28.338	47.855	1.1
17	23/03/2020	1:06:01.195	Krewerd	597850	251900	2900	109.29	20.66	-108.02	307.28	80.44	-83.65	-18.373	18.055	63.572	1.1
18	30/03/2020	4:49:40.330	Tjuchem	588300	253700	2900	164.87	77.48	-74.47	320.02	36.59	-116.01	-13.471	36.536	49.993	1.0
19	30/03/2020	23:53:23.195	Zuidbroek	576500	255450	2600	145.51	47.92	-45.91	285.10	77.92	-121.88	-29.026	34.305	36.669	1.3
20	04/04/2020	4:37:23.610	Oosterwijtwerd	594450	250000	2800	134.62	21.98	-76.94	299.60	59.32	-95.64	-25.628	-15.262	59.110	0.6
21	23/04/2020	19:54:31.435	Appingedam	593550	253750	2950	16.66	47.25	-86.87	193.24	60.57	-92.64	21.704	28.888	49.408	0.3
22	26/04/2020	0:14:06.170	Zuidbroek	578400	252950	2750	208.23	36.78	-81.32	18.63	63.20	-95.81	-42.017	12.144	45.838	0.8
23	27/04/2020	14:14:57.850	Froombosch	578850	249200	2850	213.12	67.70	-71.41	10.45	49.31	-112.90	-41.685	27.432	30.883	0.6
24	28/04/2020	1:51:19.500	Bedum	591650	233500	2850	314.24	62.65	-91.70	136.49	45.75	-87.89	22.117	29.613	48.270	0.4
25	28/04/2020	10:20:14.735	Zeerijp	598150	245900	2850	143.84	25.17	-120.52	14.79	29.66	-64.12	-38.075	-44.331	17.594	1.6

#	Date	Time	Name	Northing	Easting	Depth	Strike_1	Dip_1	Rake_1	Strike_2	Dip_2	Rake_2	Isotropic	CLVD	Double-Coupled	KNMI Magn
26	01/05/2020	16:13:57.145	Haren	575450	236750	3200	182.03	25.09	-54.52	306.05	32.87	-116.97	-24.240	-52.732	23.028	0.6
27	02/05/2020	3:13:15.925	Zijldijk	600950	246300	2850	348.14	31.24	-79.54	156.72	65.62	-95.93	0.995	14.026	84.979	2.5
28	02/05/2020	21:04:22.690	Scharmer	584400	244750	3000	15.78	39.22	-40.57	136.91	62.26	-122.87	-22.218	-7.226	70.557	1.2
29	03/05/2020	22:28:52.845	Oosterwijtwerd	594450	250050	2900	153.70	34.23	-67.80	308.93	63.88	-103.70	-36.745	7.736	55.520	0.9
30	04/05/2020	11:11:11.770	Siddeburen	586050	252900	2900	134.62	43.14	-96.08	320.12	75.74	-85.72	-35.682	35.485	28.833	1.8
31	05/05/2020	21:59:55.795	Peize	577000	231000	3400	271.00	76.91	-104.34	122.51	27.75	-58.80	-32.698	15.738	51.564	0.9
32	08/05/2020	5:54:28.235	Eems-Dollard (nabij Emden)	595600	259250	2950	320.42	77.50	98.61	120.23	25.17	69.91	-31.282	-16.681	52.037	0.7
33	10/05/2020	4:15:56.705	Noordbroek	581350	252200	2850	159.10	51.46	-94.42	346.86	34.70	-83.92	-34.351	-6.075	59.574	0.1
34	11/05/2020	19:07:28.940	Garrelsweer	590400	248250	2850	127.61	55.12	-87.14	301.36	26.98	-95.18	-36.534	-11.293	52.174	0.3
35	31/05/2020	11:33:57.505	Garsthuizen	599100	244850	3150	87.89	72.42	-97.19	304.70	11.94	-54.78	18.761	-14.254	66.985	0.6
37	01/06/2020	17:55:04.010	Wirdum	592450	248150	3050	155.85	19.72	-66.85	310.27	64.53	-98.45	-33.501	-11.048	55.452	1.9
38	04/06/2020	23:04:15.940	Overschild	588750	250500	2900	192.52	44.58	-79.07	358.56	51.49	-99.79	-25.655	8.609	65.737	1.3
39	10/06/2020	7:19:12.920	Wirdum	592300	248900	3000	96.84	70.11	-99.06	328.82	11.24	-40.57	-16.682	-22.840	60.478	1.0
40	13/06/2020	20:28:45.345	Harkstede	582600	240950	3100	166.53	35.68	-128.30	30.67	62.86	-66.03	-13.494	0.230	86.276	0.8
41	21/06/2020	23:26:19.035	Overschild	587750	246200	3000	189.74	52.55	-77.34	323.22	15.76	-129.82	-24.780	-38.244	36.976	0.8
42	21/06/2020	23:26:19.035	Overschild	587750	246200	3000	189.74	52.55	-77.34	323.22	15.76	-129.82	-24.780	-38.244	36.976	0.8
43	24/06/2020	18:54:16.010	Groningen	586150	235050	3050	129.38	80.25	-105.77	349.35	24.68	-50.10	-35.397	13.208	51.395	0.7
44	26/06/2020	14:56:20.700	Woldendorp	588700	262650	2950	167.06	31.48	-72.83	328.34	66.12	-99.70	-22.710	10.647	66.643	1.3
45	29/06/2020	20:10:50.475	Tjuchem	590200	254200	3000	188.21	56.53	-89.96	8.14	38.03	-90.05	-37.050	6.499	56.451	0.7
46	03/07/2020	6:49:21.880	Loppersum	595150	245650	3100	111.28	53.37	-138.57	357.05	55.09	-42.80	-43.475	-5.255	51.270	0.7
47	14/07/2020	15:18:47.290	Loppersum	596150	244300	3050	4.27	24.01	-27.69	109.58	56.92	-115.46	-42.293	-27.670	30.037	2.7
48	15/07/2020	6:15:38.655	Loppersum	596050	244300	3050	342.73	49.77	-63.67	94.60	25.04	-143.15	-47.191	-28.336	24.472	0.6
49	16/07/2020	0:45:21.030	Hellum	586000	252950	2850	127.67	42.68	-98.55	315.56	74.83	-84.00	-16.792	43.896	39.312	1.8
50	19/07/2020	2:07:52.650	Startenhuizen	599600	243200	3050	38.71	83.49	-41.53	169.07	58.81	-150.39	-21.317	44.321	34.362	2.3

#	Date	Time	Name	Northing	Easting	Depth	Strike_1	Dip_1	Rake_1	Strike_2	Dip_2	Rake_2	Isotropic	CLVD	Double-Coupled	KNMI Magn
52	21/07/2020	6:07:03.440	Scharmer	584150	243350	2700	193.43	35.28	-94.43	20.14	39.68	-85.99	-16.743	-26.745	56.512	1.1
55	01/09/2020	4:31:15.825	Uithuizermeeden	604300	245600	3050	172.85	79.26	-17.37	318.13	88.54	-159.72	-47.505	44.317	8.178	1.9
56	03/09/2020	5:29:00.985	Westeremden	595400	242650	3000	133.99	40.64	-106.73	337.74	45.27	-74.70	-28.032	-10.232	61.735	2.0
57	07/09/2020	16:52:27.200	Groningen	581600	233950	3250	311.42	42.48	-92.97	135.94	40.81	-86.93	22.044	-11.822	66.134	0.9
58	08/09/2020	23:34:24.340	Harkstede	583450	241350	2750	334.37	36.58	-111.01	178.89	59.57	-75.65	42.453	4.577	52.969	0.4
63	07/10/2020	2:07:16.155	Siddeburen	585850	253000	2800	94.46	24.40	-103.16	289.01	64.97	-84.04	-18.023	-2.486	79.491	0.5
64	16/10/2020	21:52:21.035	Loppersum	594450	246850	3000	169.45	32.55	-79.15	334.00	43.00	-98.54	-29.006	-22.865	48.129	1.0
65	18/10/2020	12:23:08.940	Zandeweer	601700	240900	2950	84.98	28.22	-35.48	199.63	59.33	-116.60	-9.143	-31.000	59.856	1.7
67	05/11/2020	22:27:58.500	Garrelsweer	593750	246850	2950	165.14	37.54	-79.99	332.34	51.69	-97.76	-23.562	-2.567	73.872	0.5
68	16/11/2020	4:53:59.405	Garsthuizen	598900	244650	3050	77.51	72.20	-96.57	275.31	21.95	-73.05	23.287	5.551	71.161	1.1
70	28/11/2020	19:44:41.720	Loppersum	594650	244200	2900	306.79	79.74	-91.13	129.80	21.62	-86.99	-1.364	24.234	74.403	0.7
72	15/12/2020	2:57:19.030	Rottum	600350	236300	3150	6.12	8.51	-37.63	314.35	87.45	96.73	-12.277	15.156	72.566	1.0
73	16/12/2020	1:03:48.850	Rottum	600300	236350	3100	315.79	4.01	-72.47	118.27	88.08	-91.21	4.971	4.180	90.849	0.5
74	19/12/2020	6:24:09.920	Rottum	600250	236350	3200	118.85	67.28	-103.87	321.23	37.91	-68.91	-33.367	18.160	48.474	1.3
75	21/12/2020	9:29:31.285	Loppersum	595650	243500	3100	357.00	84.18	-45.68	122.70	52.17	-151.64	-16.661	38.900	44.439	1.9
1	10/01/2021	22:39:07.750	Sappemeer	577700	248200	2850	25.17	71.83	-69.18	162.30	31.34	-130.49	-2.865	12.023	85.112	1.3
2	24/01/2021	9:35:04.685	Tjuchem	588250	253800	2900	154.88	71.53	-104.67	2.10	32.92	-63.77	-17.265	19.949	62.786	1.9
3	27/01/2021	13:26:49.465	Loppersum	595150	246350	2950	154.24	29.72	-114.37	2.71	59.74	-76.30	-20.777	-6.340	72.883	1.9
4	28/01/2021	2:40:49.785	Leermens	597050	248150	2800	138.89	69.74	-94.85	326.24	38.86	-82.74	-13.558	32.775	53.666	0.2
5	31/01/2021	18:47:51.205	Stedum	593000	244100	3050	132.81	23.35	-104.38	334.42	34.21	-79.92	-42.487	-35.754	21.760	1.0
9	13/03/2021	6:00:49.960	Loppersum	594850	244950	3100	137.89	20.39	-113.92	342.10	78.71	-81.72	-37.800	10.178	52.022	0.6
11	31/03/2021	1:24:59.285	Wirdum	590900	249550	3000	142.77	48.11	-133.04	11.87	63.43	-55.38	-21.655	13.715	64.630	1.0
13	28/04/2021	19:46:26.625	Huizinge	598400	241100	2850	170.49	29.44	-73.40	326.21	40.02	-102.61	-43.157	-25.493	31.350	2.3
16	17/05/2021	12:28:58.505	Loppersum	596200	245300	2850	192.37	46.31	-86.50	1.62	16.98	-98.70	-17.460	-43.322	39.218	1.5
17	26/05/2021	15:57:42.040	Wirdum	592750	248650	2950	357.39	36.12	-101.49	196.99	33.51	-77.72	-29.512	-30.735	39.753	0.6

#	Date	Time	Name	Northing	Easting	Depth	Strike_1	Dip_1	Rake_1	Strike_2	Dip_2	Rake_2	Isotropic	CLVD	Double-Coupled	KNMI Magn
18	29/05/2021	2:55:20.665	Ten Boer	587900	242950	2900	358.29	58.36	-92.60	181.79	46.14	-86.93	20.261	24.478	55.261	1.2
19	29/05/2021	7:34:51.585	Westeremden	596000	241950	2850	28.48	66.18	40.46	269.83	58.77	144.49	26.456	-15.393	58.151	0.6
21	11/06/2021	23:29:27.790	Loppersum	595400	246400	2950	161.64	35.80	-92.76	345.29	48.74	-87.85	-22.883	-9.577	67.540	2.0
22	19/06/2021	0:14:29.805	Stedum	592900	243300	2900	127.69	24.83	-127.15	354.51	50.89	-70.92	-23.939	-31.755	44.306	0.9
23	19/06/2021	1:03:55.450	Stedum	592950	243250	2950	99.12	26.40	-116.82	320.43	35.09	-69.58	-27.632	-44.228	28.140	2.3
24	01/07/2021	15:38:14.085	Wirdum	591000	249550	2800	152.83	40.68	-96.87	341.48	52.59	-84.37	-29.409	4.732	65.859	2.2
25	01/07/2021	20:07:30.655	Wirdum	591000	249550	2800	163.62	50.88	-99.31	1.96	30.45	-75.65	-34.990	-14.000	51.010	0.4
26	14/07/2021	4:10:36.780	Winneweer	592250	245550	2800	356.48	41.22	-68.85	146.87	46.61	-109.10	-21.553	-10.153	68.294	0.2
27	18/07/2021	6:58:32.890	Muntendam	575900	256000	2750	33.14	41.99	-69.56	195.79	82.26	-103.64	1.555	59.376	39.069	0.3
28	05/08/2021	6:33:40.510	Garsthuizen	598050	243200	2900	113.89	64.41	-81.11	230.93	9.32	-149.42	-17.673	-35.276	47.051	0.6
29	05/08/2021	7:14:45.975	Hellum	583850	252150	2850	195.43	54.97	-53.82	329.66	54.71	-126.31	-26.726	12.585	60.689	1.8
31	09/08/2021	19:35:29.975	Meedhuizen	589450	258000	2800	176.43	36.69	-80.46	344.57	53.74	-97.06	-6.634	-0.351	93.016	0.9
32	19/08/2021	22:25:23.435	Stedum	593000	244150	3050	143.46	42.76	-57.55	285.29	59.83	-114.92	-51.190	5.839	42.971	0.3
33	26/08/2021	21:19:42.400	Wirdum	592400	249600	2850	149.95	55.24	-105.50	359.48	32.67	-66.01	-30.083	-8.506	61.412	0.9
34	05/09/2021	11:44:13.465	Loppersum	595050	246100	2950	8.92	31.72	-53.20	139.87	49.30	-114.54	-39.806	-21.449	38.744	0.3
36	18/09/2021	19:07:38.565	Zeerijp	596550	245550	2900	178.19	37.80	-108.34	22.83	48.62	-75.11	-32.204	-9.105	58.691	0.9
37	20/09/2021	20:51:07.955	Meedhuizen	589400	258250	2900	165.72	32.78	-93.16	349.20	64.51	-88.10	-27.118	11.743	61.138	1.2
38	29/09/2021	22:20:33.830	Overschild	590900	249600	3000	328.44	26.96	-36.52	93.22	77.60	-111.90	-21.268	6.299	72.433	0.8
39	04/10/2021	2:59:08.525	Zeerijp	596750	245550	3000	137.91	24.93	-79.07	306.16	68.43	-94.93	-28.762	4.706	66.532	2.5
40	04/10/2021	13:33:45.495	Appingedam	591500	251150	2850	162.11	37.27	-93.09	346.25	48.00	-87.48	-16.578	-9.040	74.382	1.8
41	04/10/2021	20:47:42.910	Zeerijp	596700	245550	3050	148.97	26.92	-56.03	295.00	78.77	-104.95	-27.633	17.636	54.731	2.2
42	06/10/2021	18:57:56.725	Zeerijp	596600	245450	2850	185.36	28.32	-97.65	14.02	62.12	-85.91	-18.671	0.304	81.025	1.3
43	07/10/2021	11:53:20.265	Zeerijp	596650	245550	3000	153.51	36.41	-55.27	292.43	60.11	-112.96	-35.987	-1.113	62.900	0.6
45	18/10/2021	16:56:55.145	Sint Annen	589600	241100	2850	178.85	53.71	-99.02	21.49	23.22	-71.31	-3.931	-29.637	66.432	1.1
46	22/10/2021	21:11:20.640	Zeerijp	596400	245550	2850	160.37	47.04	-118.52	13.80	58.69	-65.86	-39.339	12.853	47.808	0.8

#	Date	Time	Name	Northing	Easting	Depth	Strike_1	Dip_1	Rake_1	Strike_2	Dip_2	Rake_2	Isotropic	CLVD	Double-Coupled	KNMI Magn
47	27/10/2021	0:27:59.915	Eppenhuizen	600600	241950	3000	125.93	69.87	-104.01	326.69	40.49	-69.52	-38.970	22.754	38.276	0.5
48	27/10/2021	9:13:39.365	Zeerijp	596800	244900	2850	10.37	52.23	-76.72	170.64	42.77	-105.51	-35.232	4.718	60.050	0.4
49	31/10/2021	21:36:42.755	Garrelsweer	591900	245900	3050	178.04	47.59	-103.94	12.15	66.03	-78.78	-44.701	24.892	30.408	0.7
51	05/11/2021	22:38:27.000	Scharmer	583700	244250	2700	202.54	48.05	-93.98	26.64	63.96	-86.71	-22.580	34.246	43.174	1.1
52	08/11/2021	1:52:16.370	Westeremden	594850	242850	2850	130.45	26.85	-125.69	351.10	63.02	-72.80	-7.049	-11.935	81.017	1.7

Appendix B – Time-histories of acceleration and velocity and accumulation of Arias Intensity

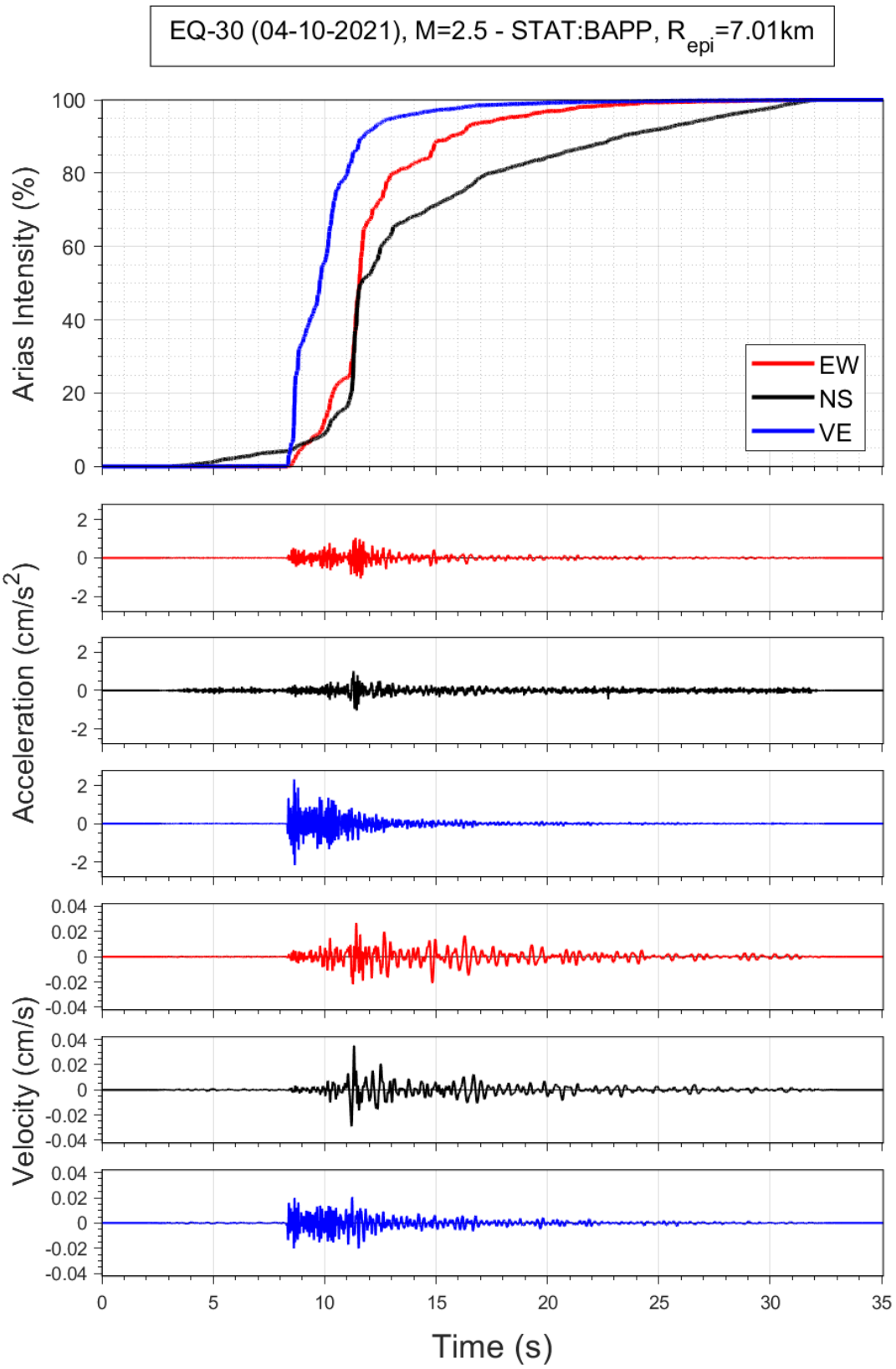
EQ-30 (04-10-2021), M=2.5 - STAT:BAPP, R epi =7.01km
Arias Intensity (%)
EW
NS
VE
Acceleration (cm/s2)
Velocity (cm/s)
Time (s)

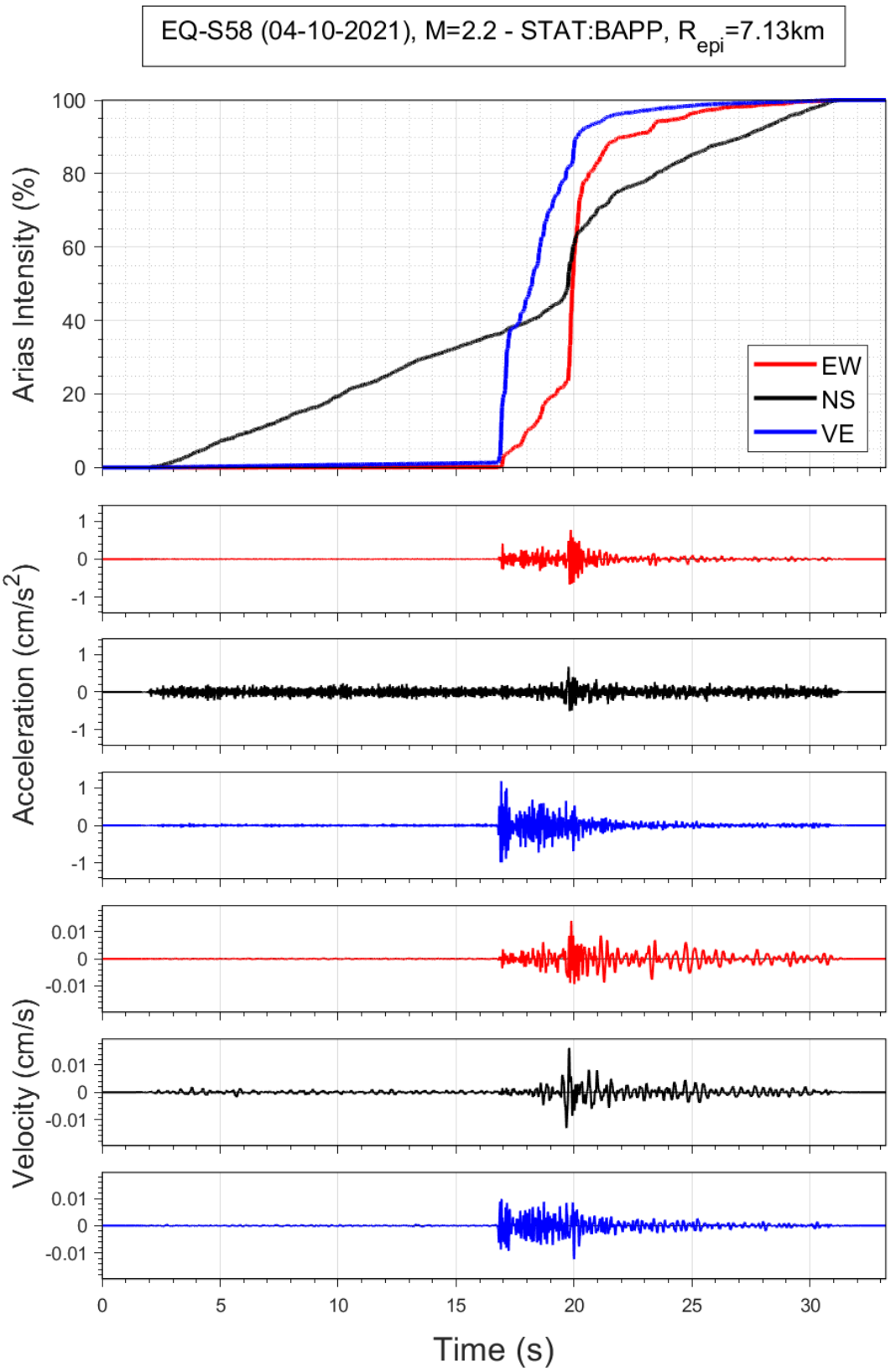
EQ-S58 (04-10-2021), M=2.2 - STAT:BAPP, R epi =7.13km
Arias Intensity (%)
EW
NS
VE
Acceleration (cm/s2)
Velocity (cm/s)
Time (s)

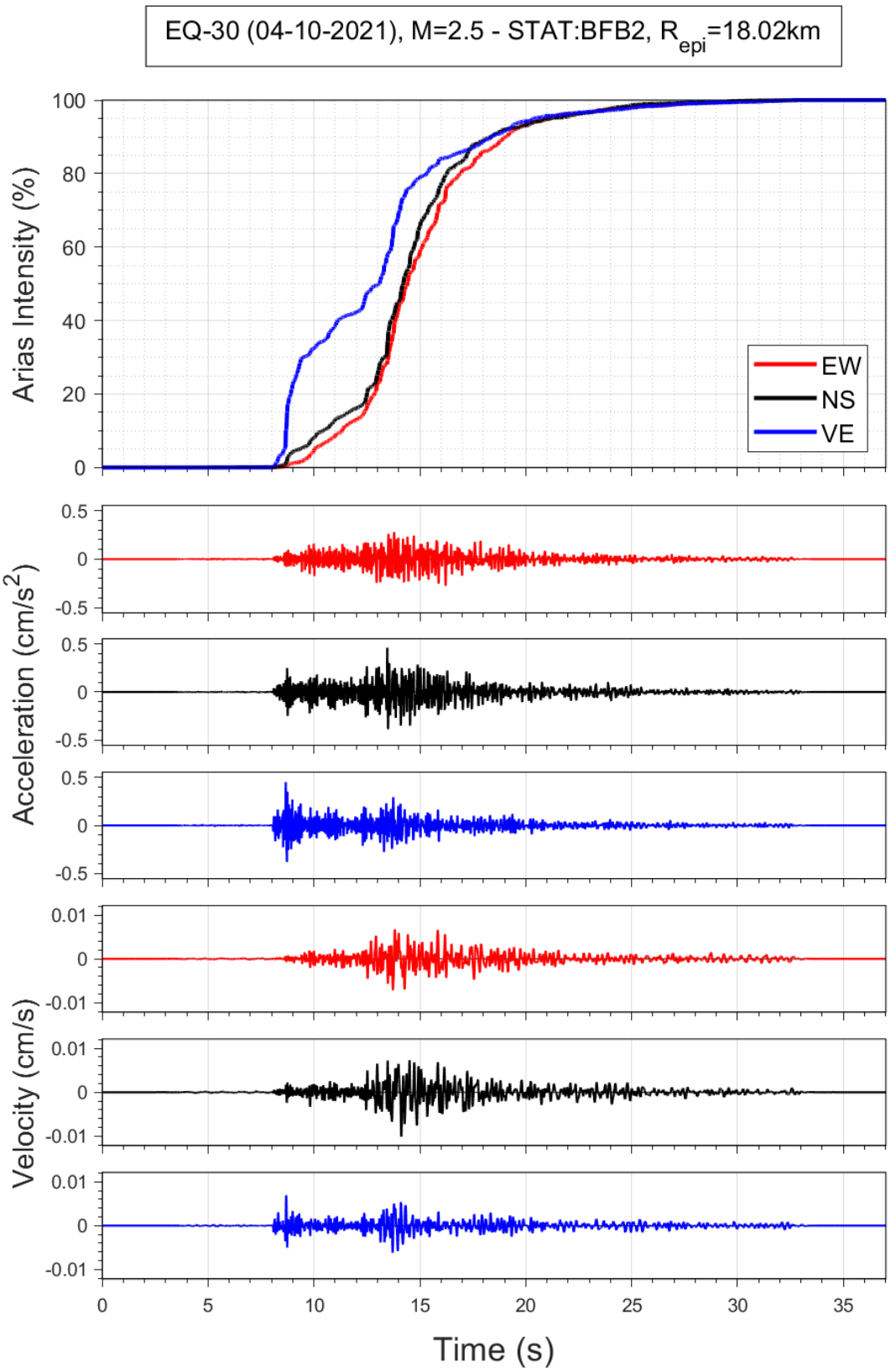
EQ-30 (04-10-2021), M=2.5 - STAT:BFB2, R_epi=18.02km
Arias Intensity (%)
EW
NS
VE
Acceleration (cm/s2)
Velocity (cm/s)
Time (s)

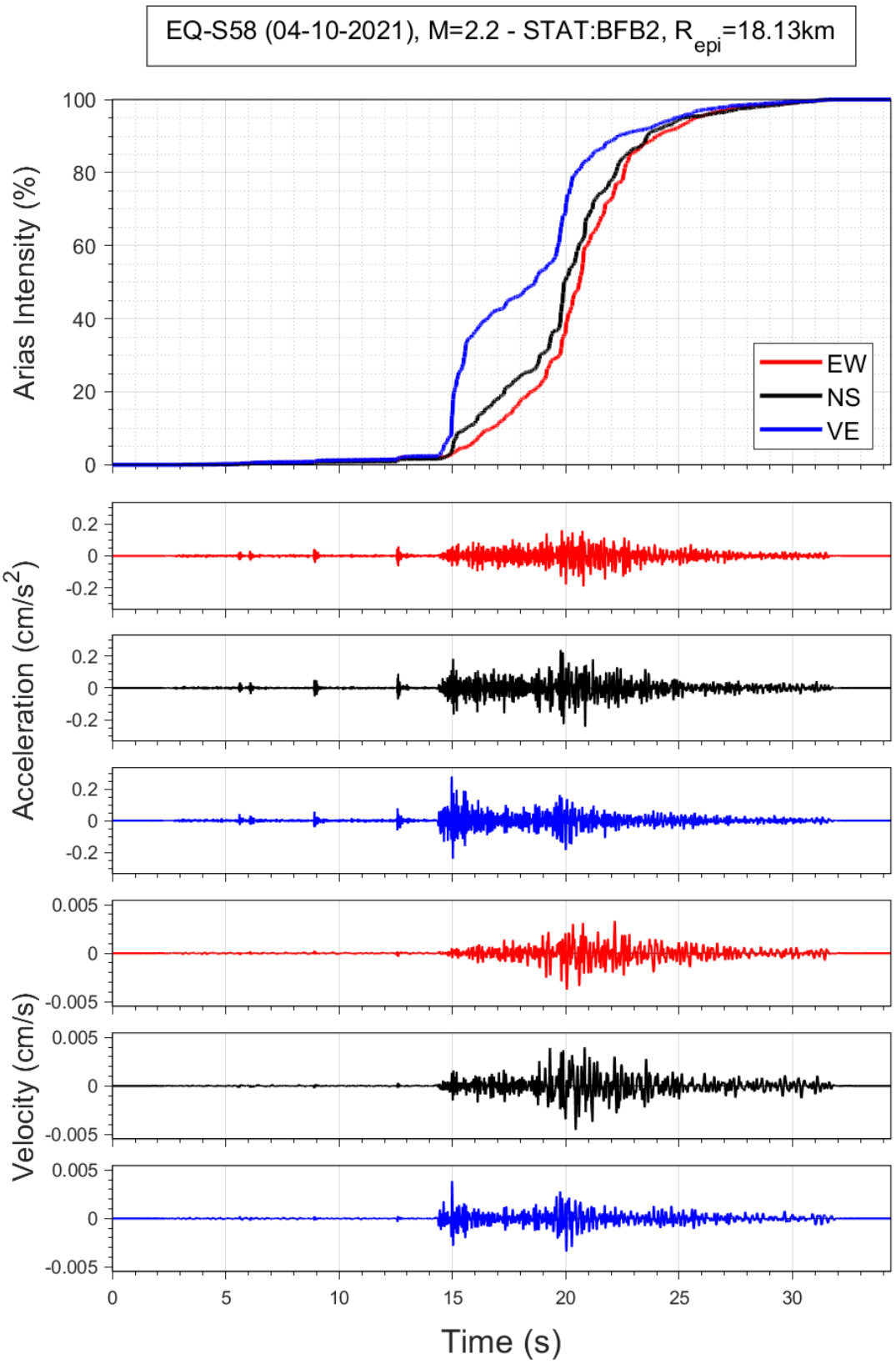
EQ-S58 (04-10-2021), M=2.2 - STAT:BFB2, R epi =18.13km
Arias Intensity (%)
EW
NS
VE
Acceleration (cm/s2)
Velocity (cm/s)
Time (s)

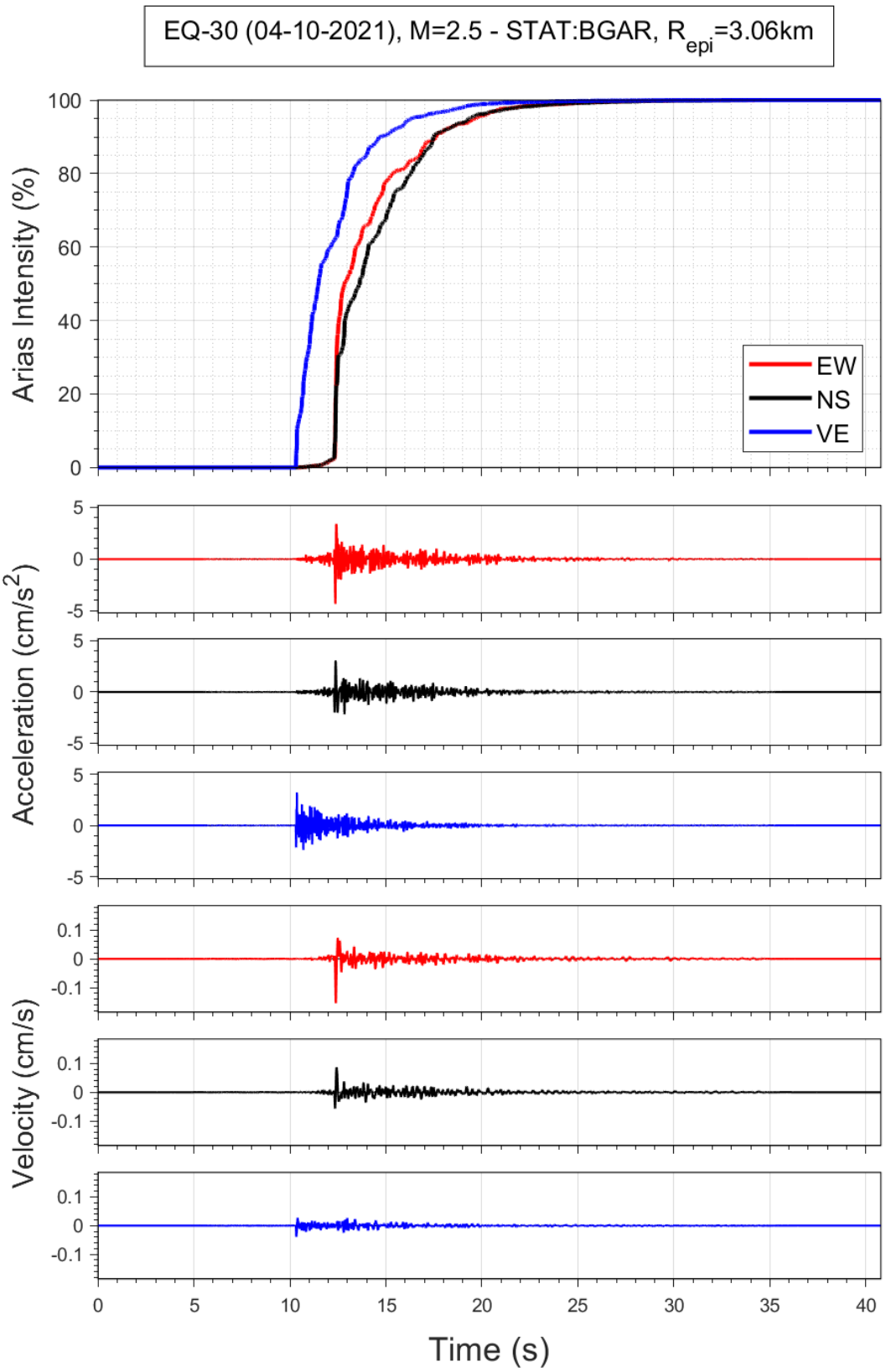
EQ-30 (04-10-2021), M=2.5 - STAT:BGAR, R epi =3.06km
Arias Intensity (%)
EW
NS
VE
Acceleration (cm/s2)
Velocity (cm/s)
Time (s)

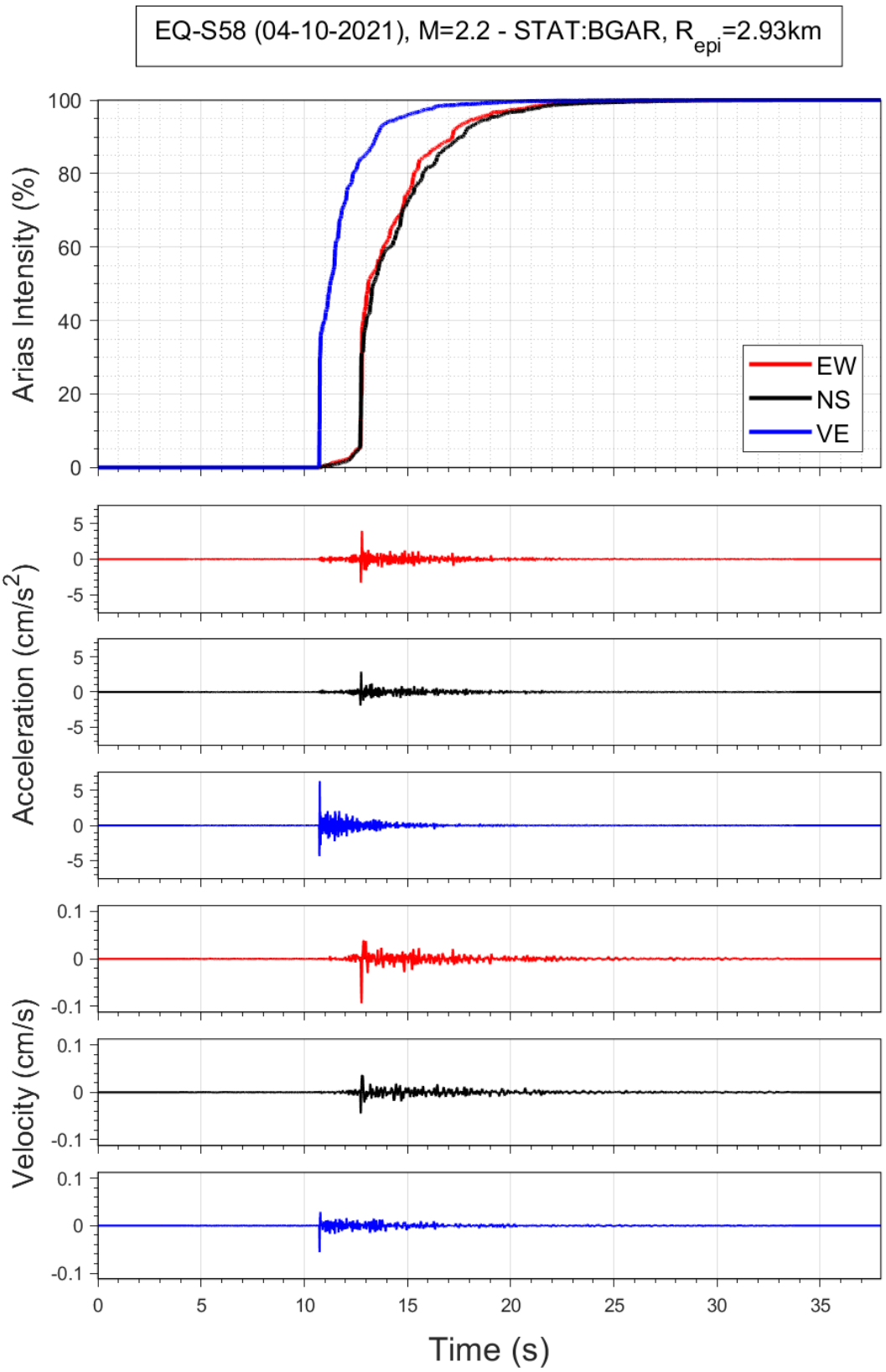
EQ-S58 (04-10-2021), M=2.2 - STAT:BGAR, R epi =2.93km
Arias Intensity (%)
EW
NS
VE
Acceleration (cm/s2)
Velocity (cm/s)
Time (s)

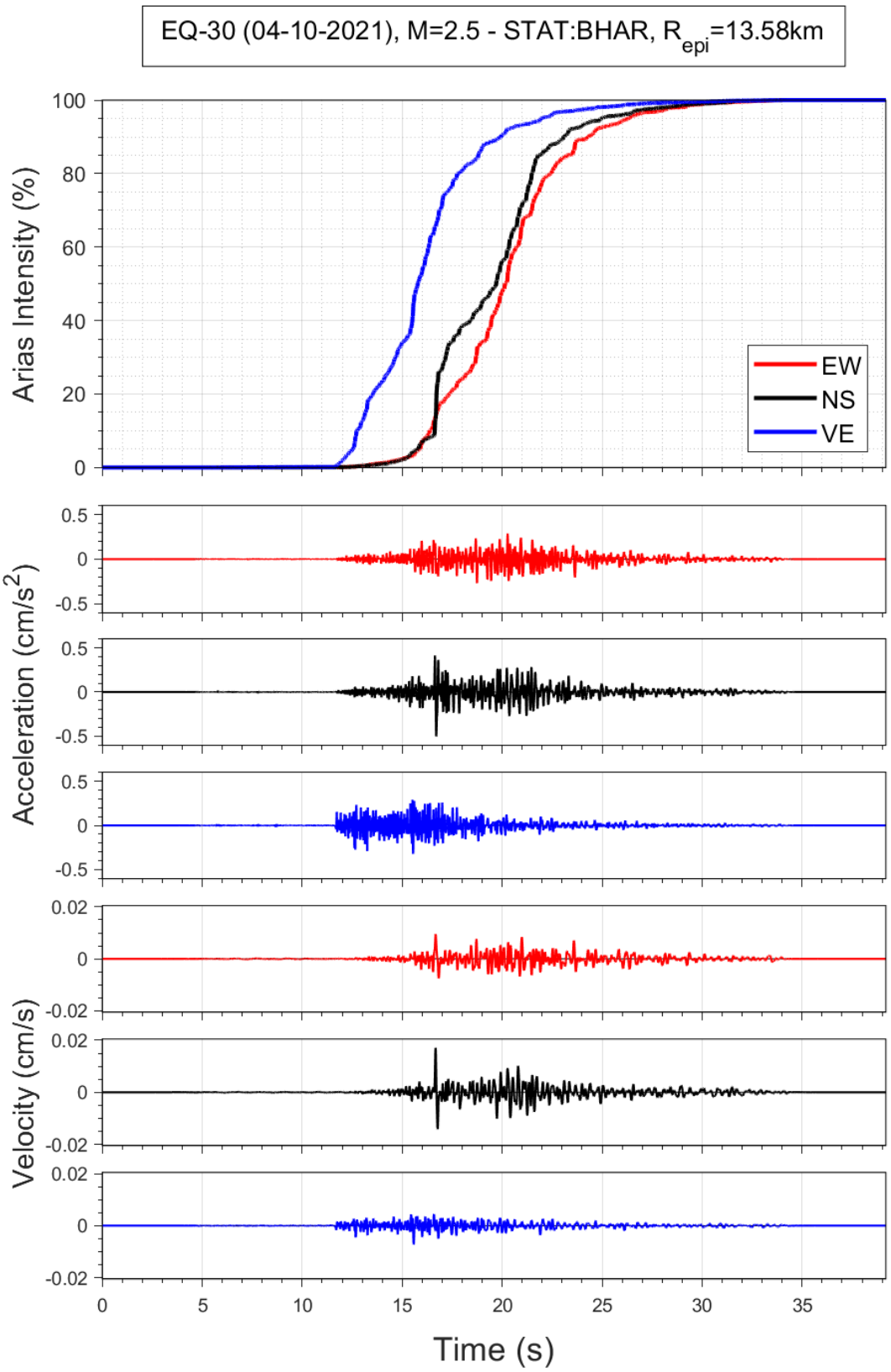
EQ-30 (04-10-2021), M=2.5 - STAT:BHAR, R epi =13.58km
Arias Intensity (%)
Acceleration (cm/s2)
Velocity (cm/s)
Time (s)
EW
NS
VE

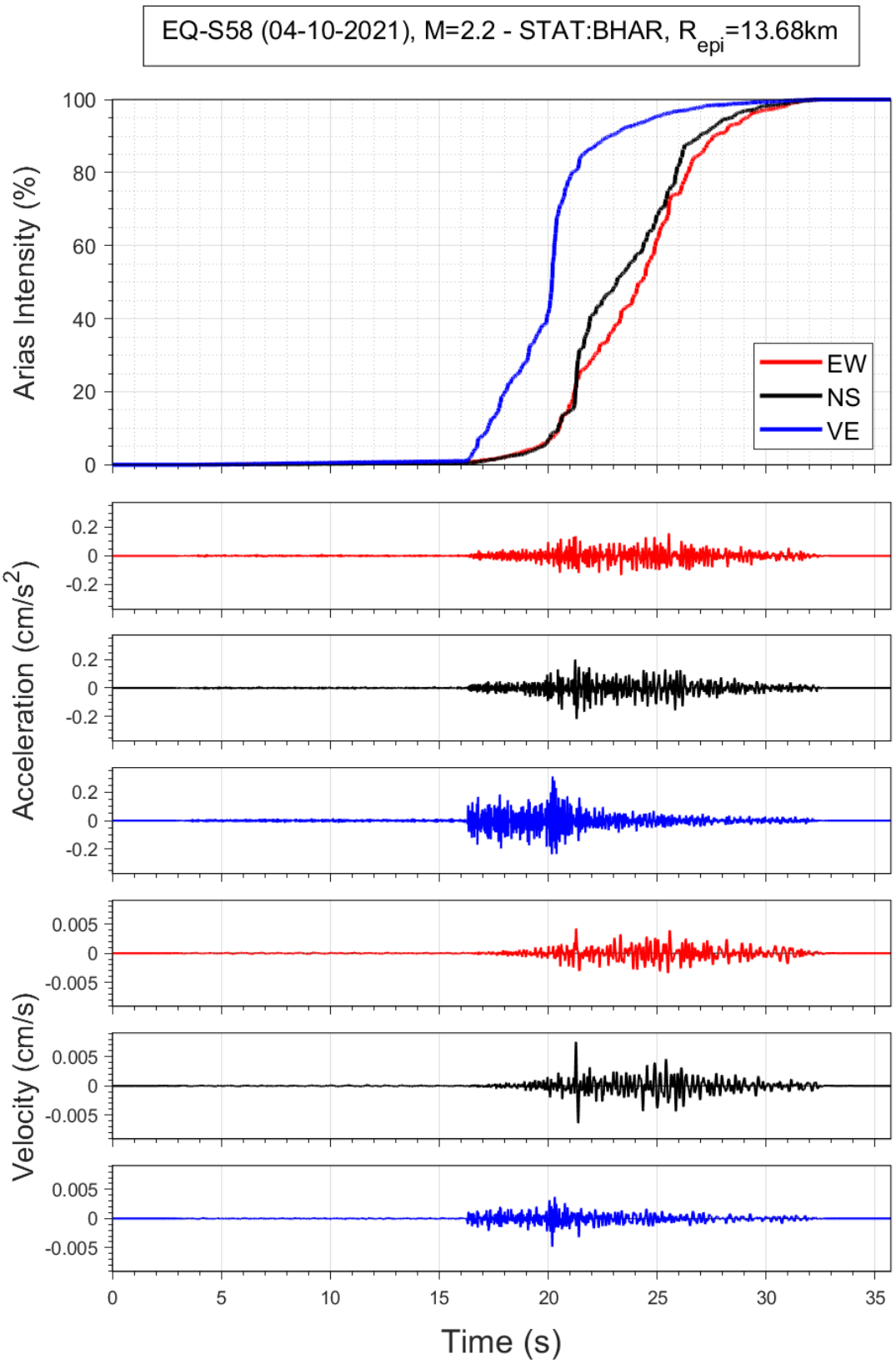
EQ-S58 (04-10-2021), M=2.2 - STAT:BHAR, R epi =13.68km
Arias Intensity (%)
EW
NS
VE
Acceleration (cm/s2)
Velocity (cm/s)
Time (s)

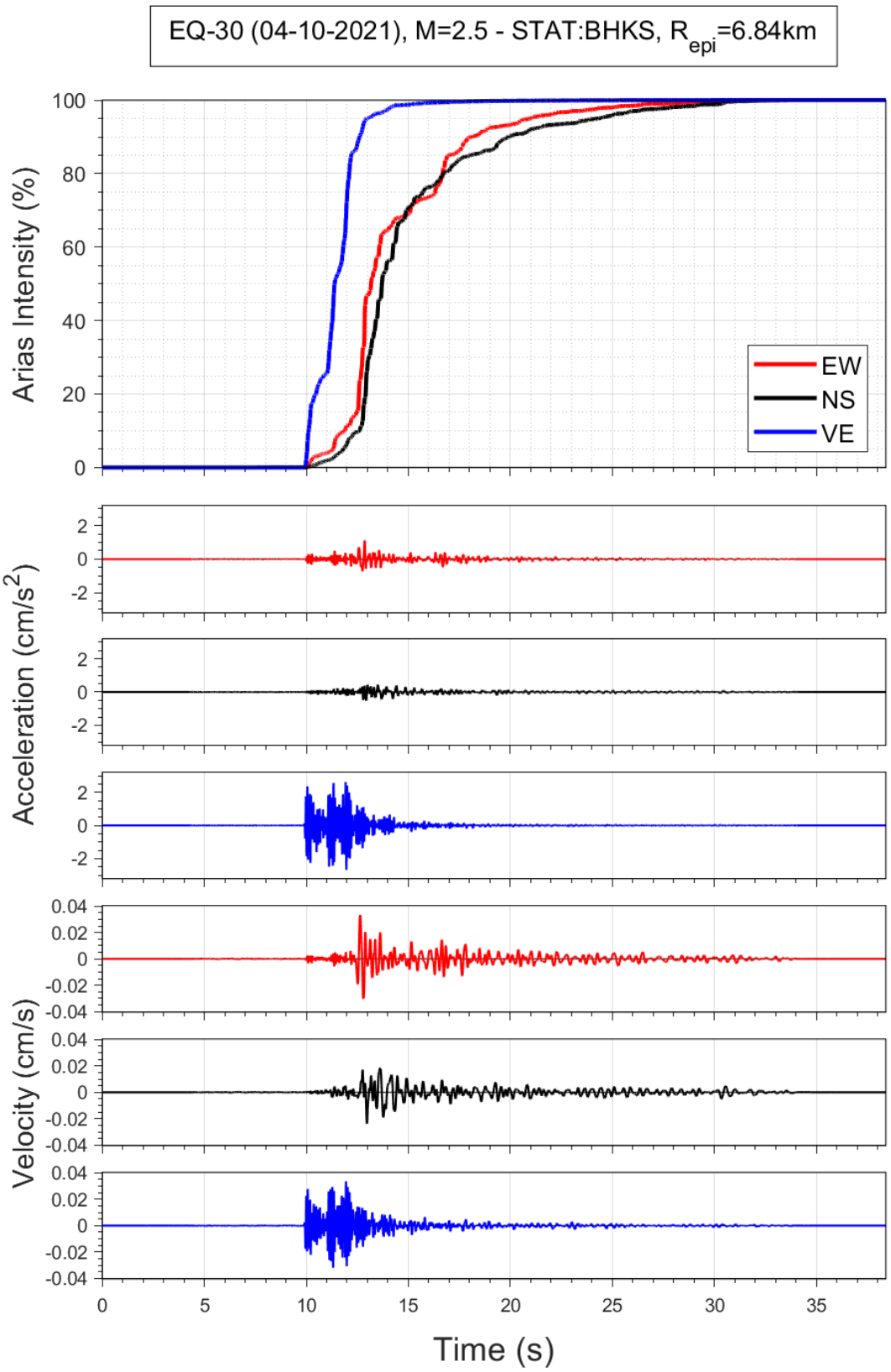
EQ-30 (04-10-2021), M=2.5 - STAT:BHKS, R epi =6.84km
Arias Intensity (%)
EW
NS
VE
Acceleration (cm/s2)
Velocity (cm/s)
Time (s)

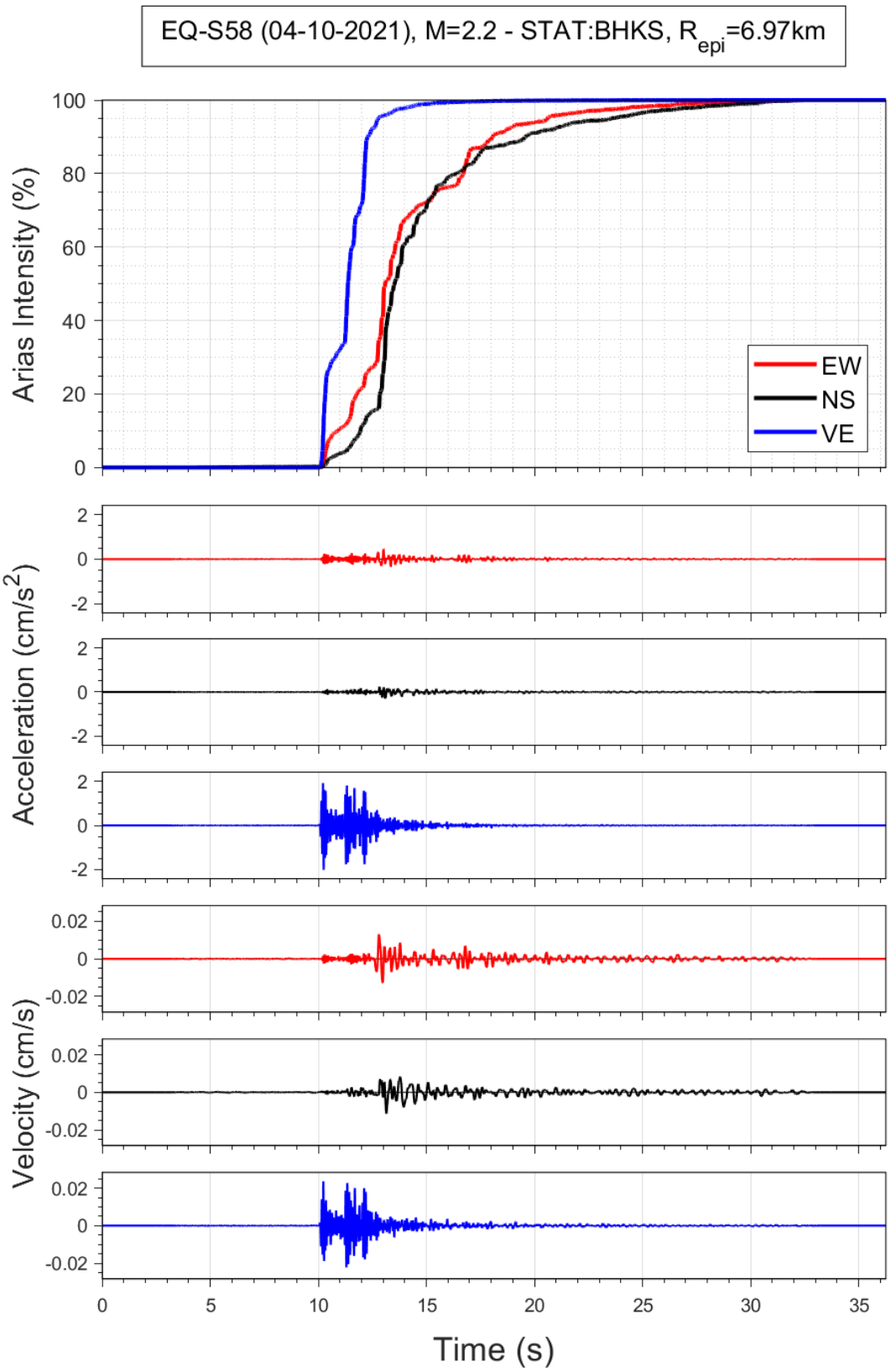
EQ-S58 (04-10-2021), M=2.2 - STAT:BHKS, R epi =6.97km
Arias Intensity (%)
EW
NS
VE
Acceleration (cm/s2)
Velocity (cm/s)
Time (s)

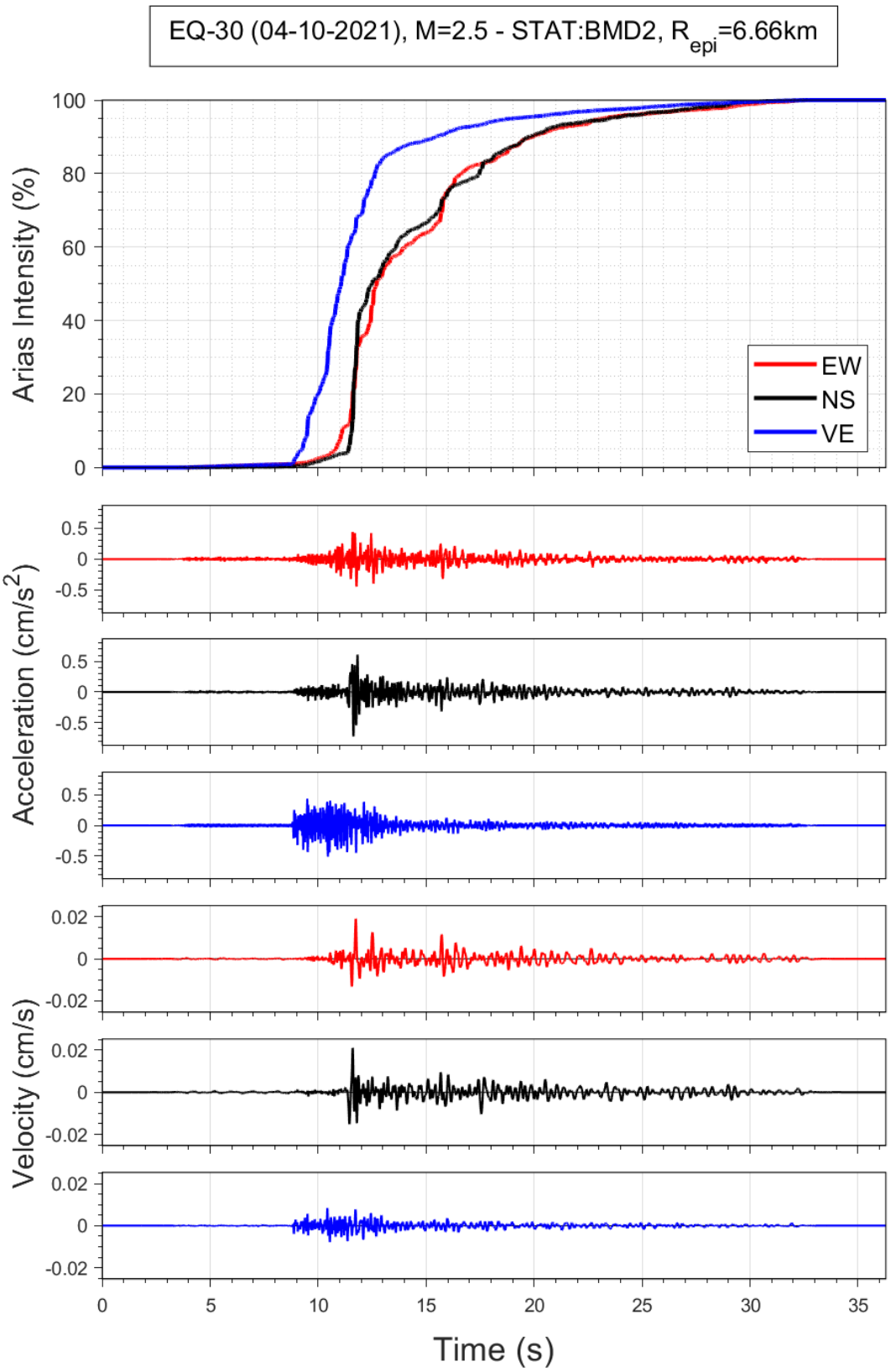
EQ-30 (04-10-2021), M=2.5 - STAT:BMD2, R epi =6.66km
Arias Intensity (%)
EW
NS
VE
Acceleration (cm/s2)
Velocity (cm/s)
Time (s)

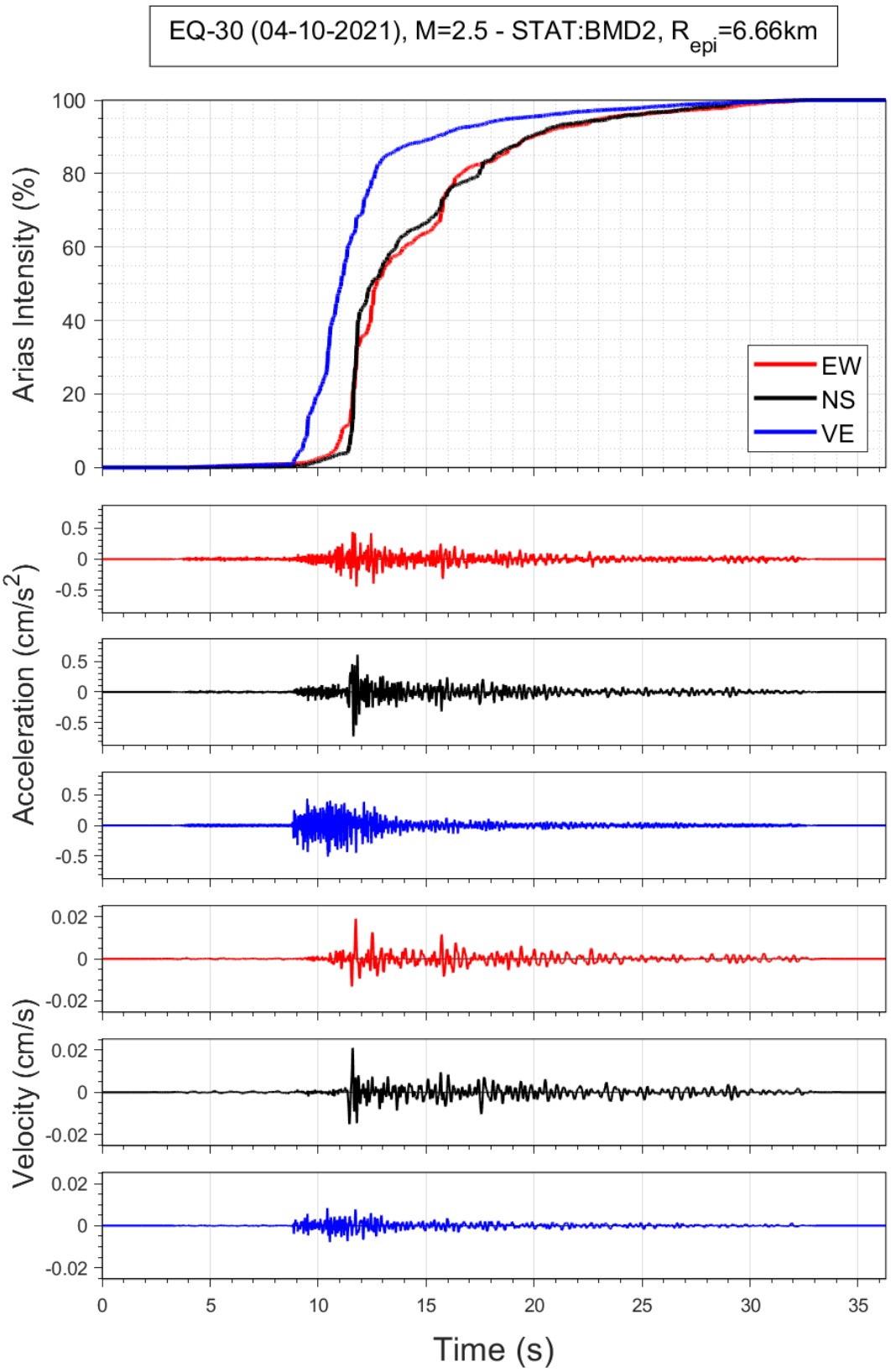
EQ-30 (04-10-2021), M=2.5 - STAT:BMD2, R epi =6.66km
Arias Intensity (%)
EW
NS
VE
Acceleration (cm/s2)
Velocity (cm/s)
Time (s)

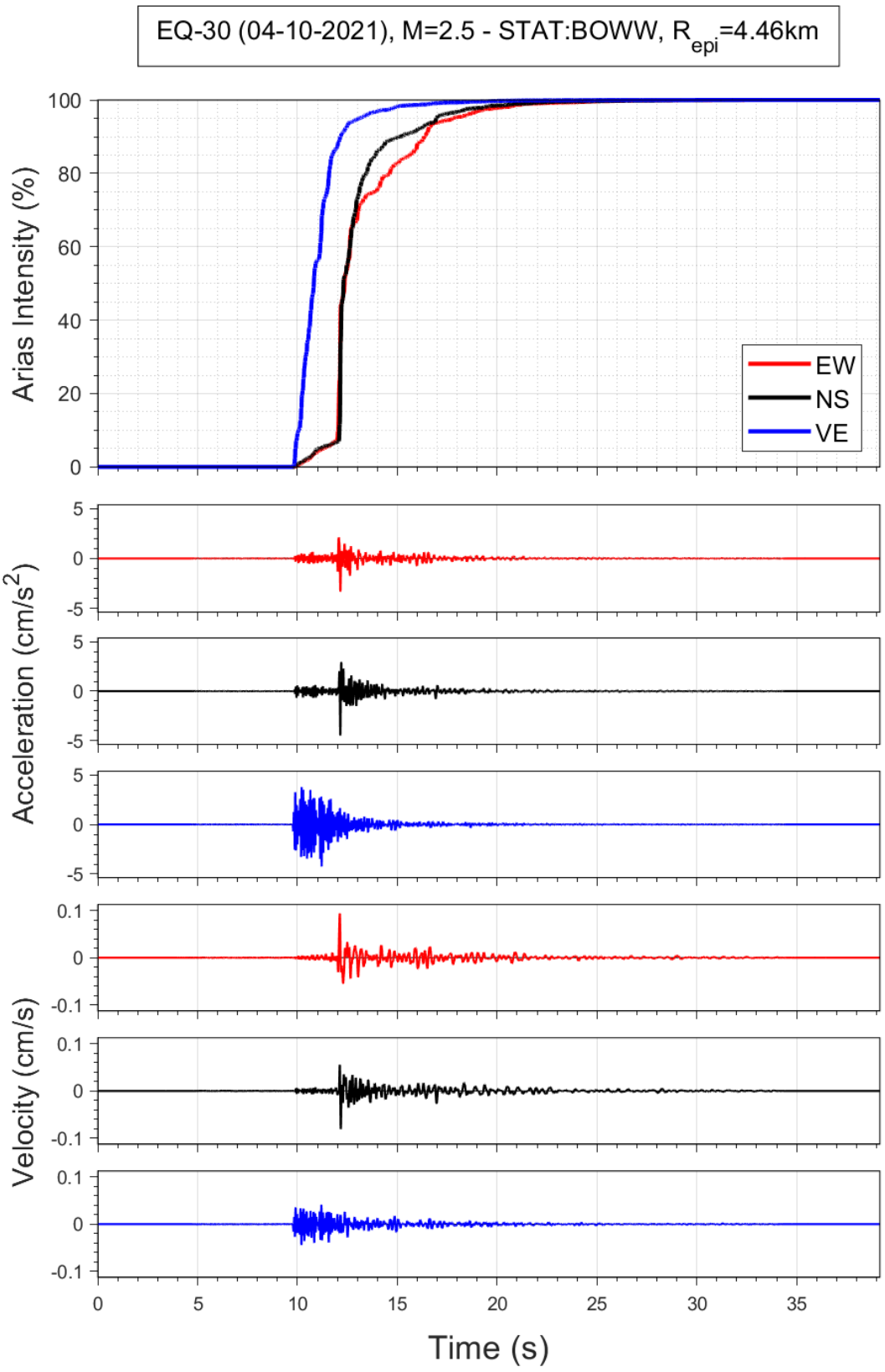
EQ-30 (04-10-2021), M=2.5 - STAT:BOWW, R_epi=4.46km
Arias Intensity (%)
EW
NS
VE
Acceleration (cm/s2)
Velocity (cm/s)
Time (s)

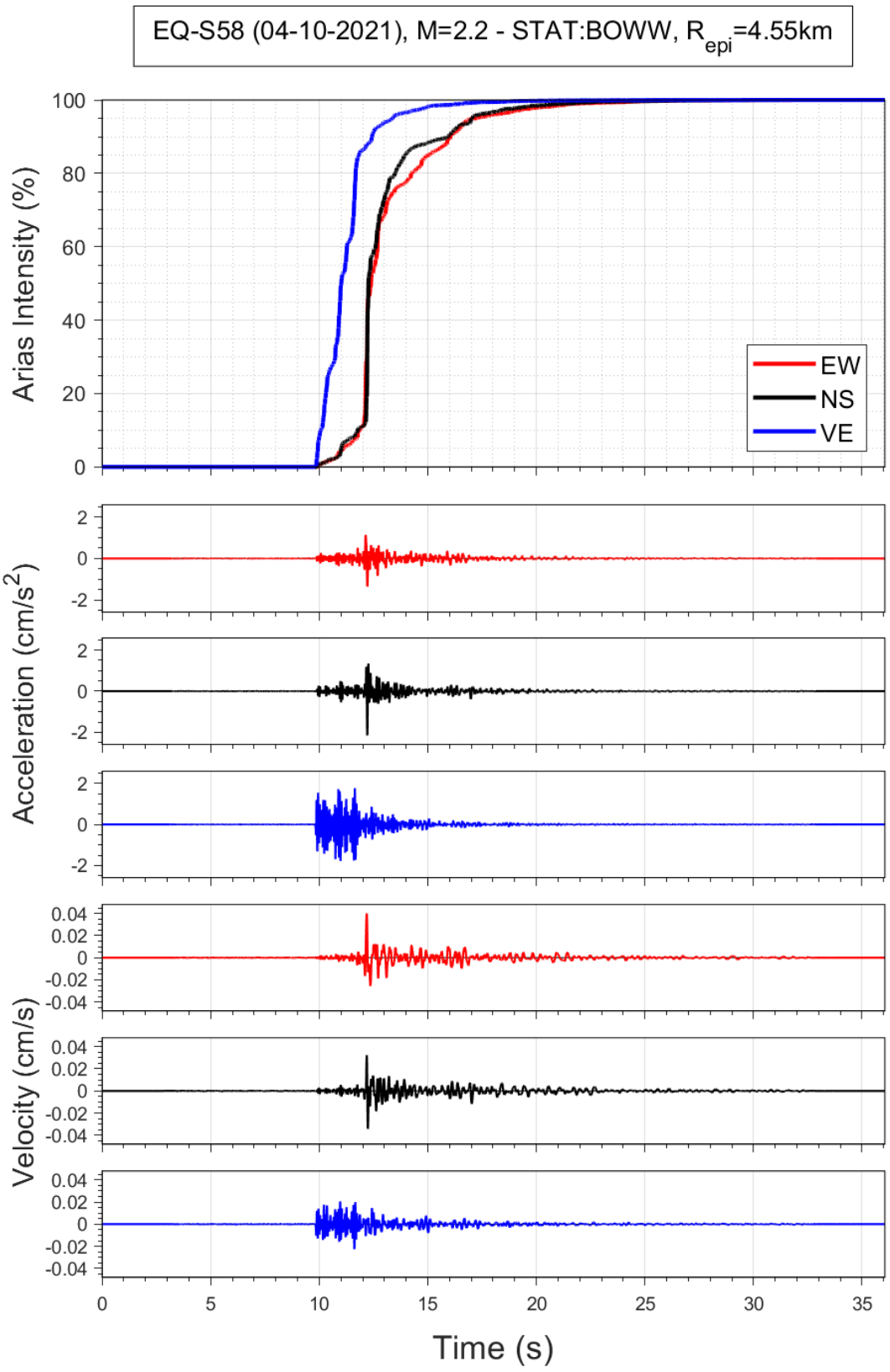
EQ-S58 (04-10-2021), M=2.2 - STAT:BOWW, R$_{epi}$=4.55km
Arias Intensity (%)
EW
NS
VE
Acceleration (cm/s^2)
Velocity (cm/s)
Time (s)

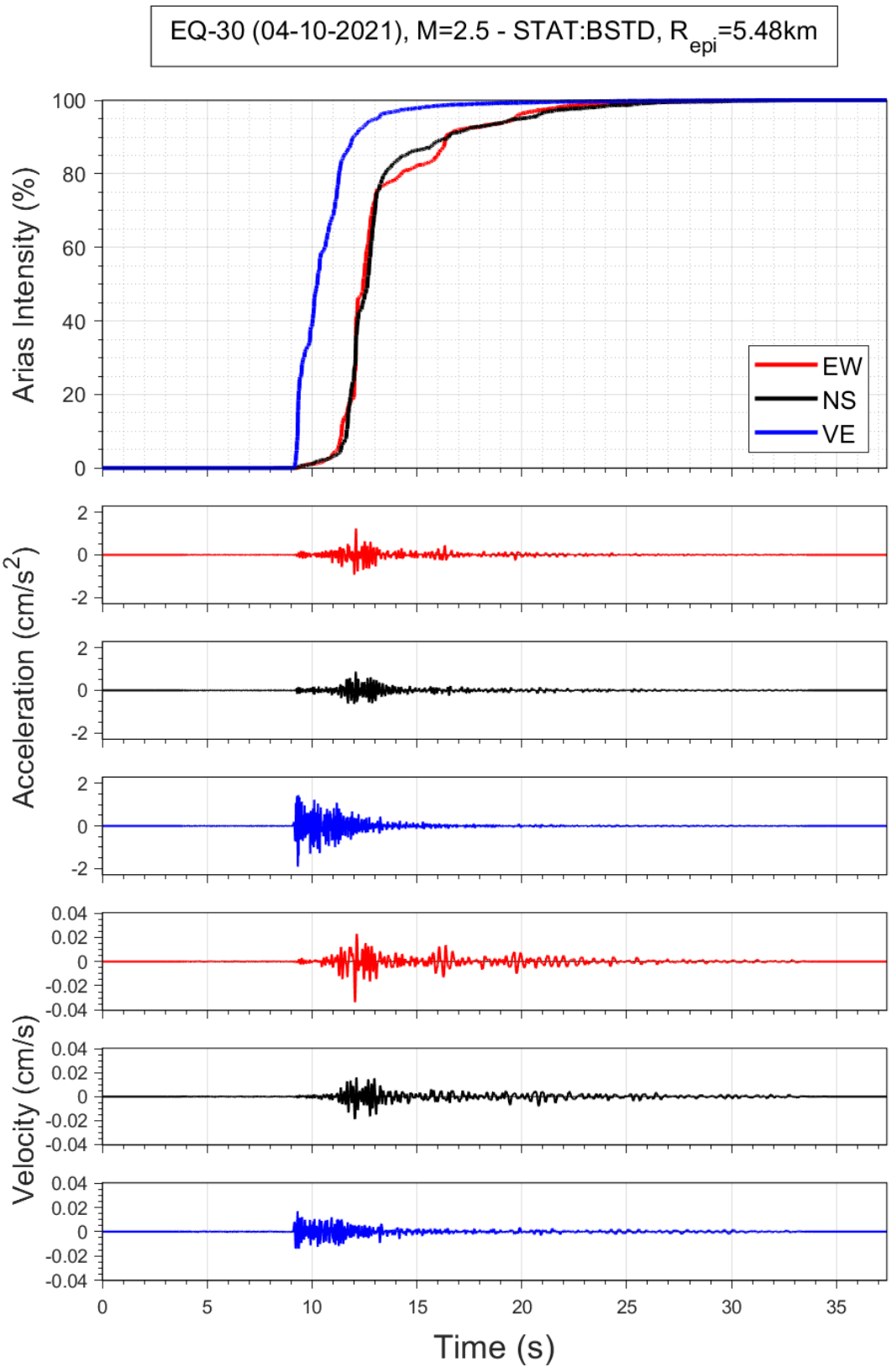
EQ-30 (04-10-2021), M=2.5 - STAT:BSTD, R epi =5.48km
Arias Intensity (%)
EW
NS
VE
Acceleration (cm/s2)
Velocity (cm/s)
Time (s)

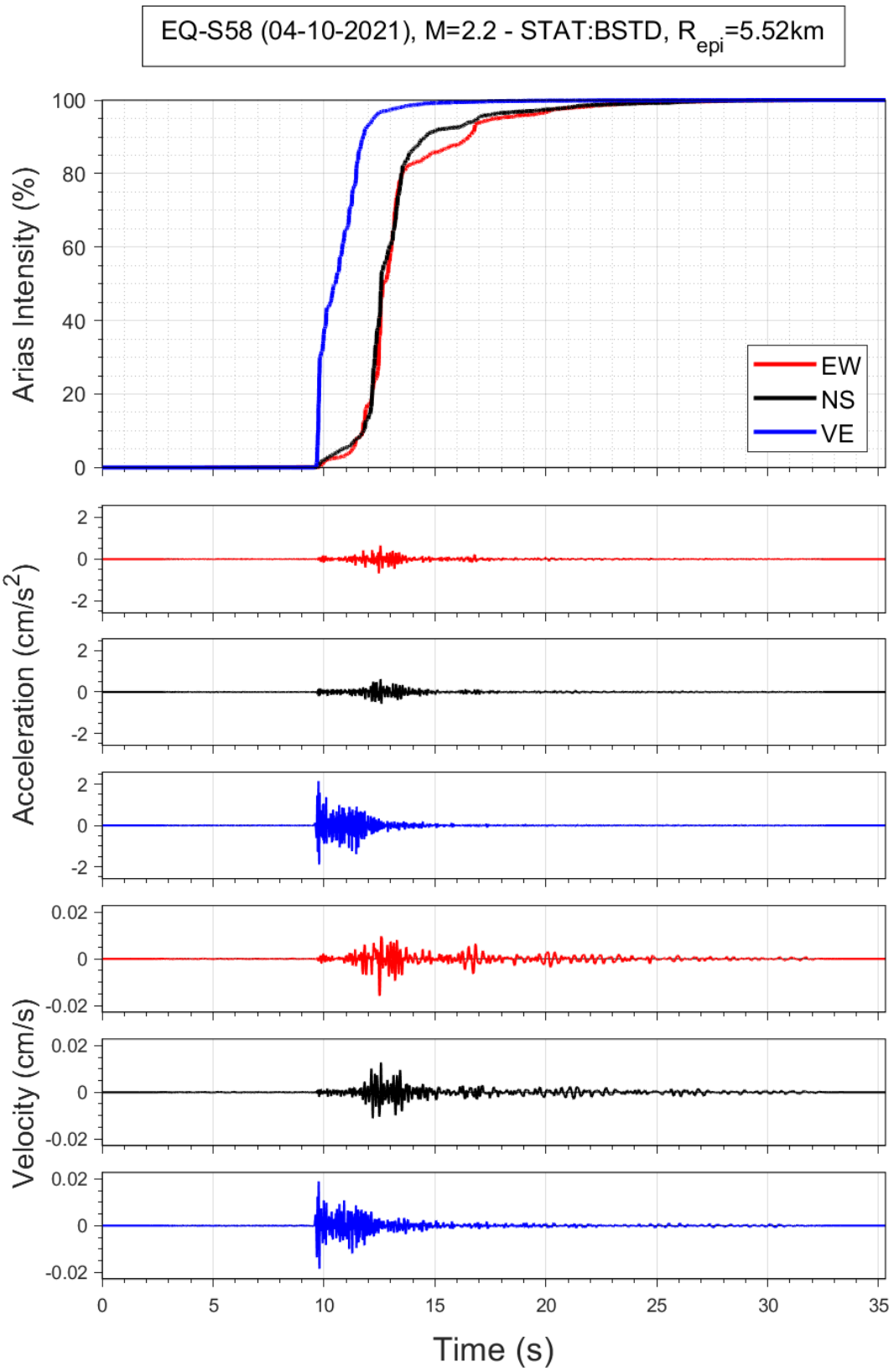
EQ-S58 (04-10-2021), M=2.2 - STAT:BSTD, R epi =5.52km
Arias Intensity (%)
EW
NS
VE
Acceleration (cm/s2)
Velocity (cm/s)
Time (s)

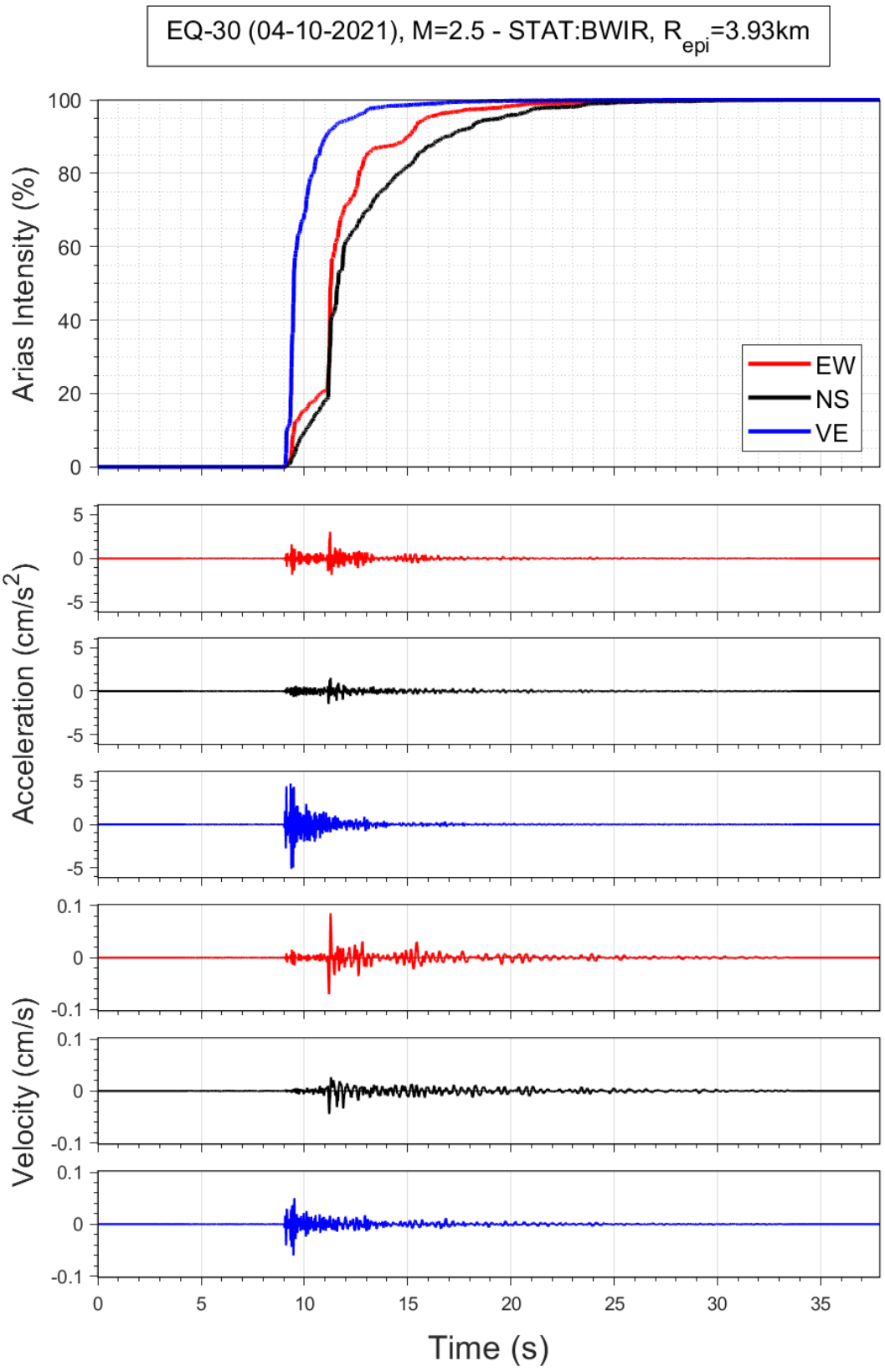
EQ-30 (04-10-2021), M=2.5 - STAT:BWIR, R_epi=3.93km
Arias Intensity (%)
EW
NS
VE
Acceleration (cm/s2)
Velocity (cm/s)
Time (s)

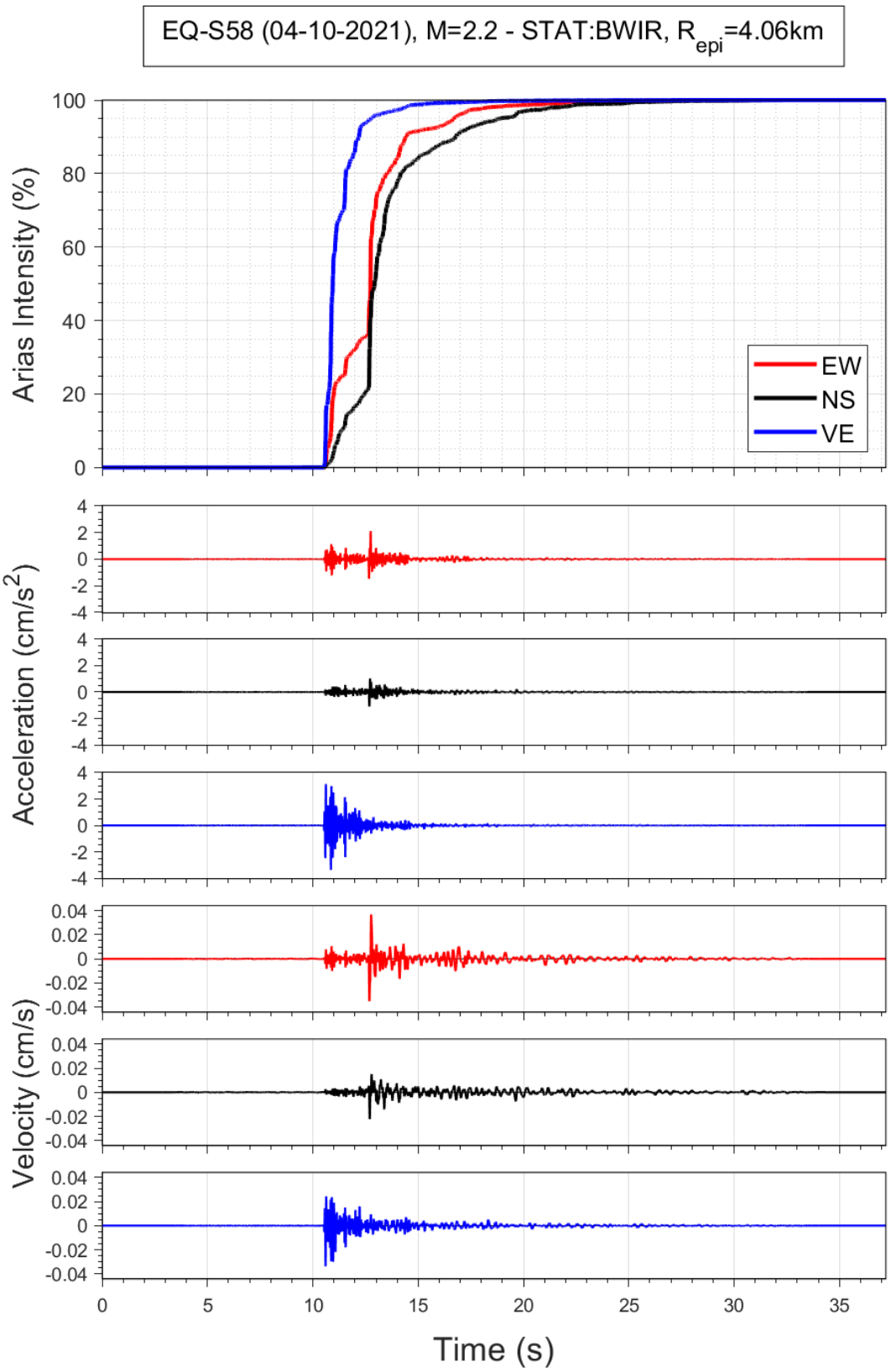
EQ-S58 (04-10-2021), M=2.2 - STAT:BWIR, R_epi=4.06km
Arias Intensity (%)
EW
NS
VE
Acceleration (cm/s2)
Velocity (cm/s)
Time (s)

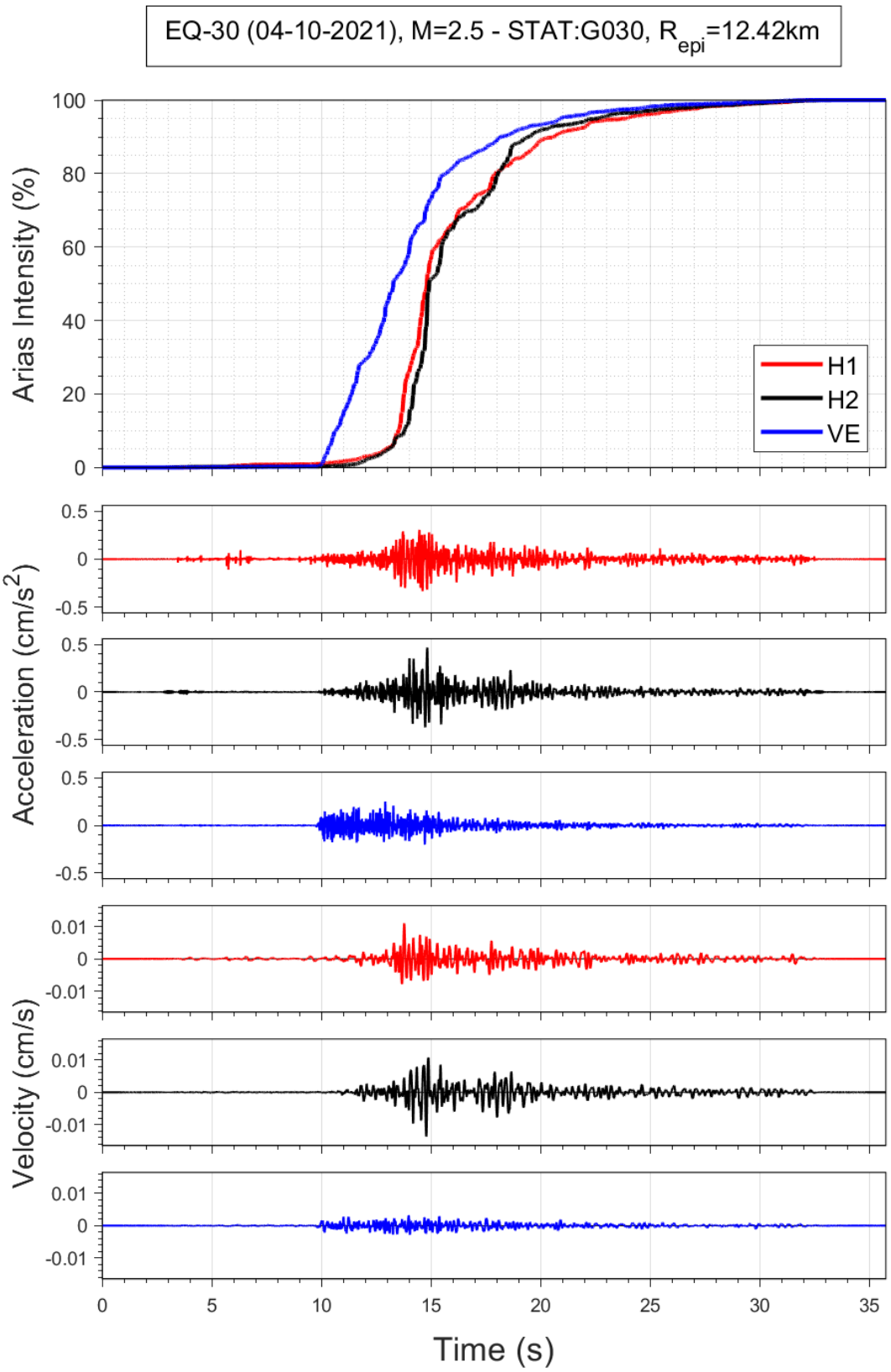
EQ-30 (04-10-2021), M=2.5 - STAT:G030, R_epi=12.42km
Arias Intensity (%)
H1
H2
VE
Acceleration (cm/s2)
Velocity (cm/s)
Time (s)

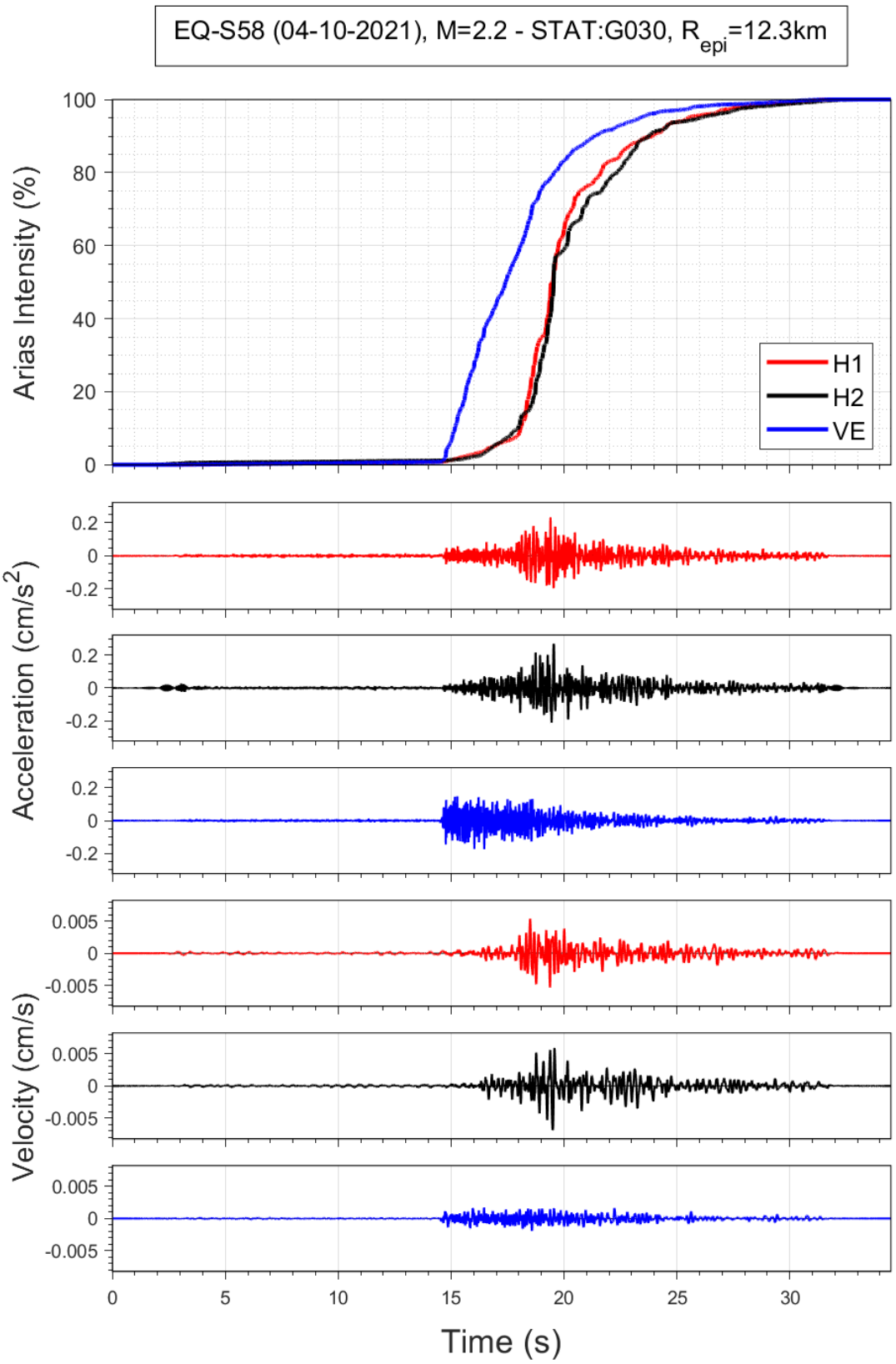
EQ-S58 (04-10-2021), M=2.2 - STAT:G030, R_epi=12.3km
Arias Intensity (%)
100
80
60
40
20
0
H1
H2
VE
Acceleration (cm/s²)
0.2
0
-0.2
Velocity (cm/s)
0.005
0
-0.005
0
5
10
15
20
25
30
Time (s)

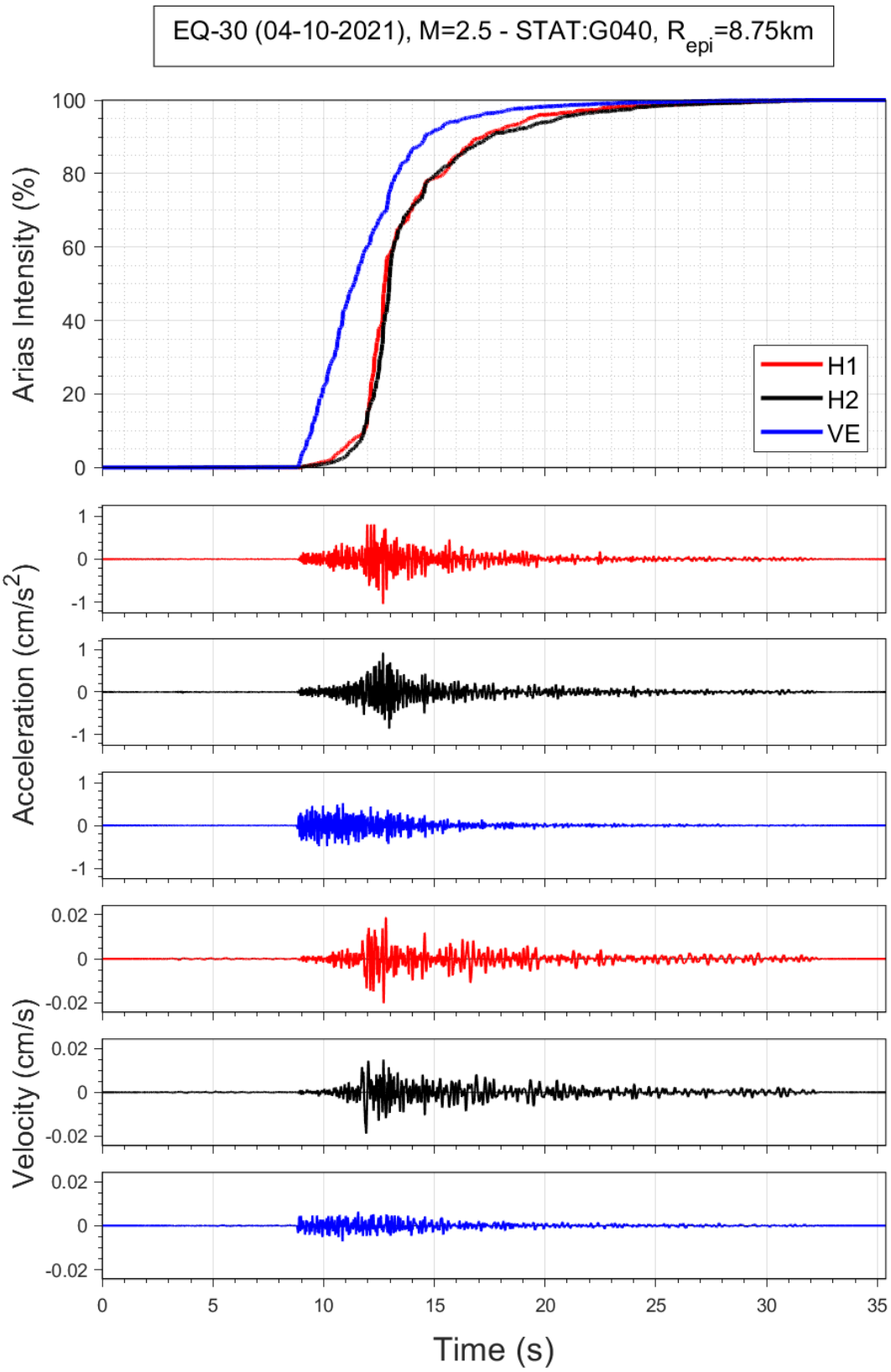
EQ-30 (04-10-2021), M=2.5 - STAT:G040, R epi =8.75km
Arias Intensity (%)
H1
H2
VE
Acceleration (cm/s2)
Velocity (cm/s)
Time (s)

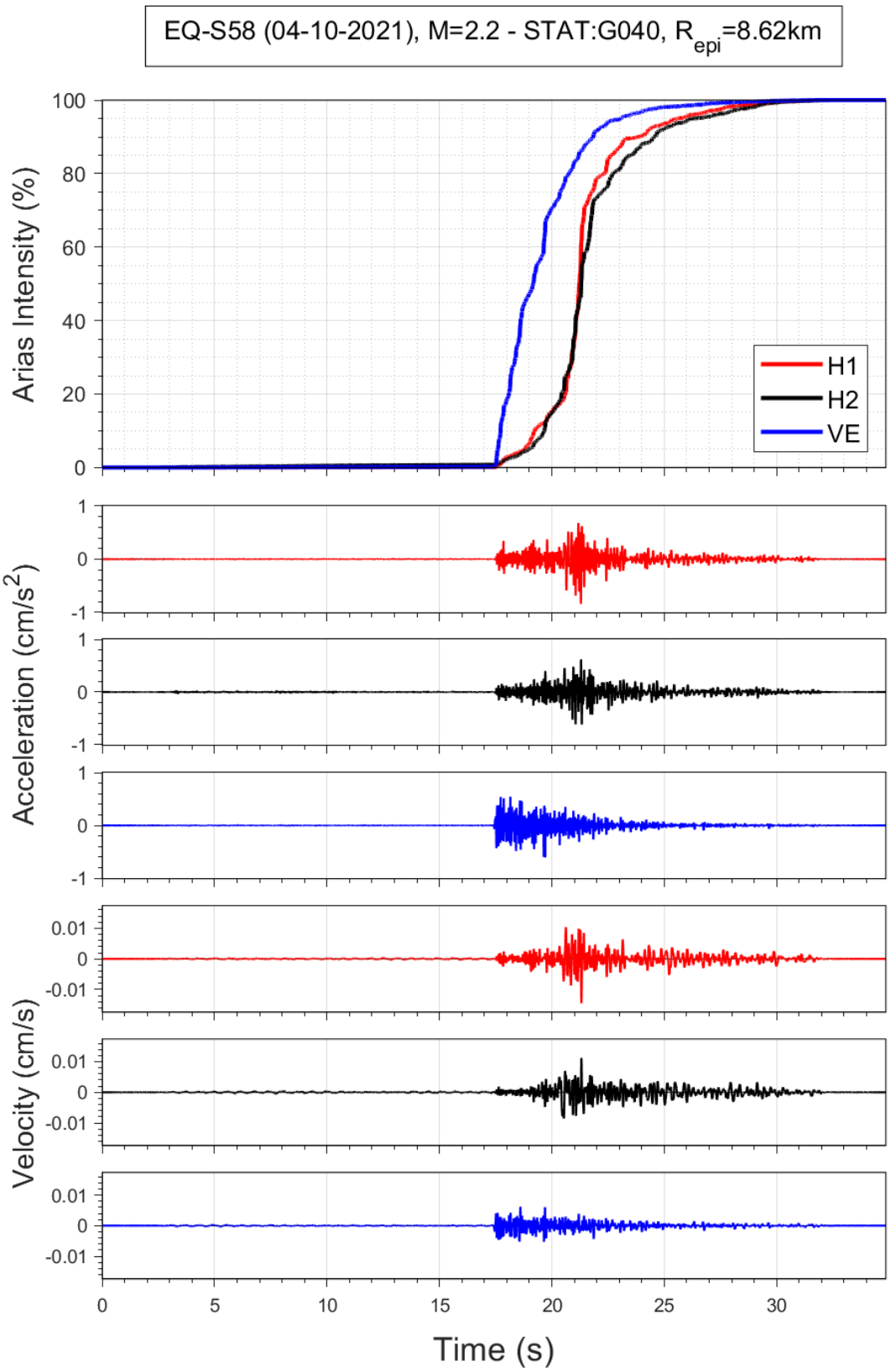
EQ-S58 (04-10-2021), M=2.2 - STAT:G040, R epi =8.62km
Arias Intensity (%)
H1
H2
VE
Acceleration (cm/s2)
Velocity (cm/s)
Time (s)

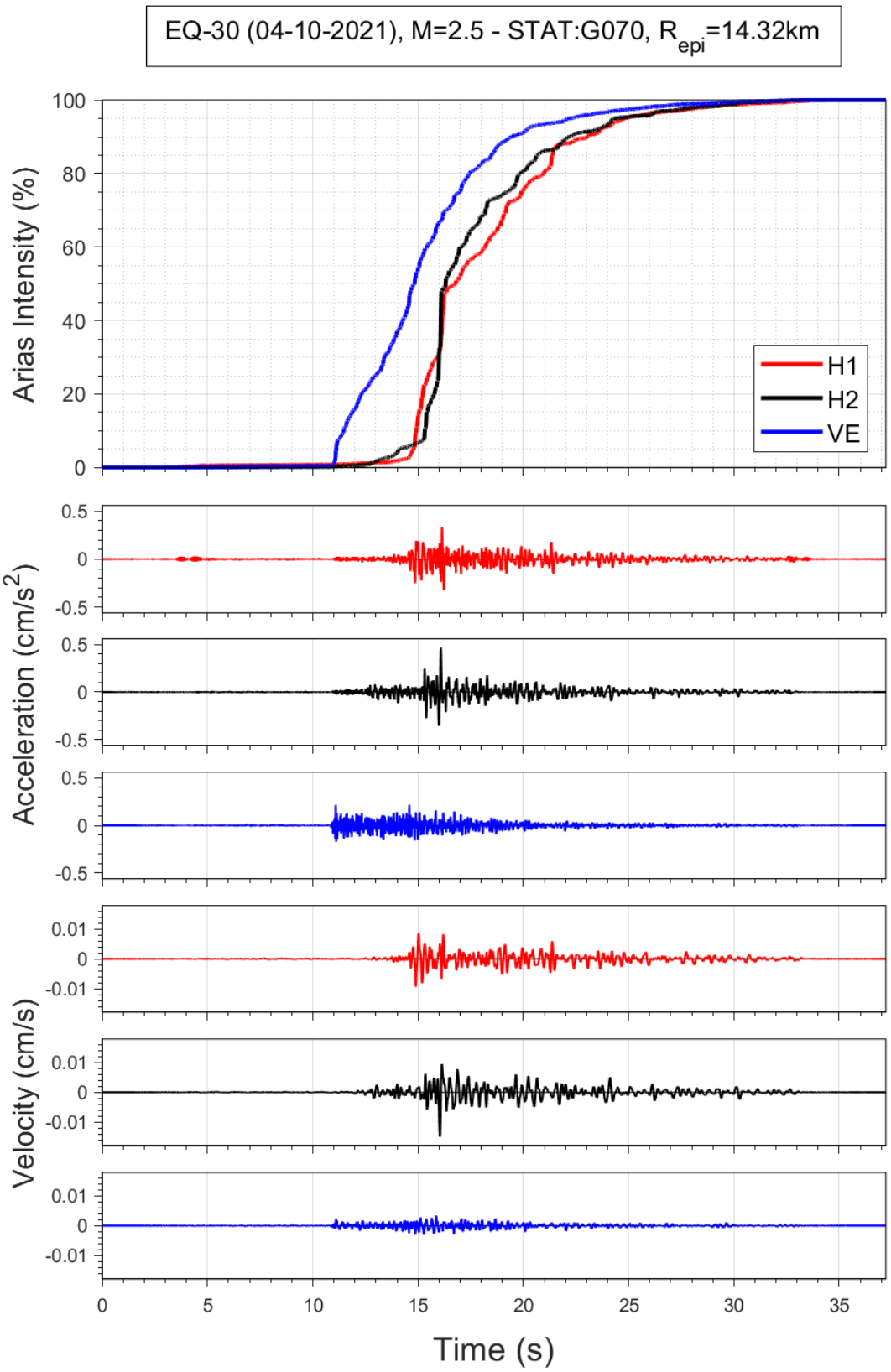
EQ-30 (04-10-2021), M=2.5 - STAT:G070, R epi =14.32km
Arias Intensity (%)
H1
H2
VE
Acceleration (cm/s2)
Velocity (cm/s)
Time (s)

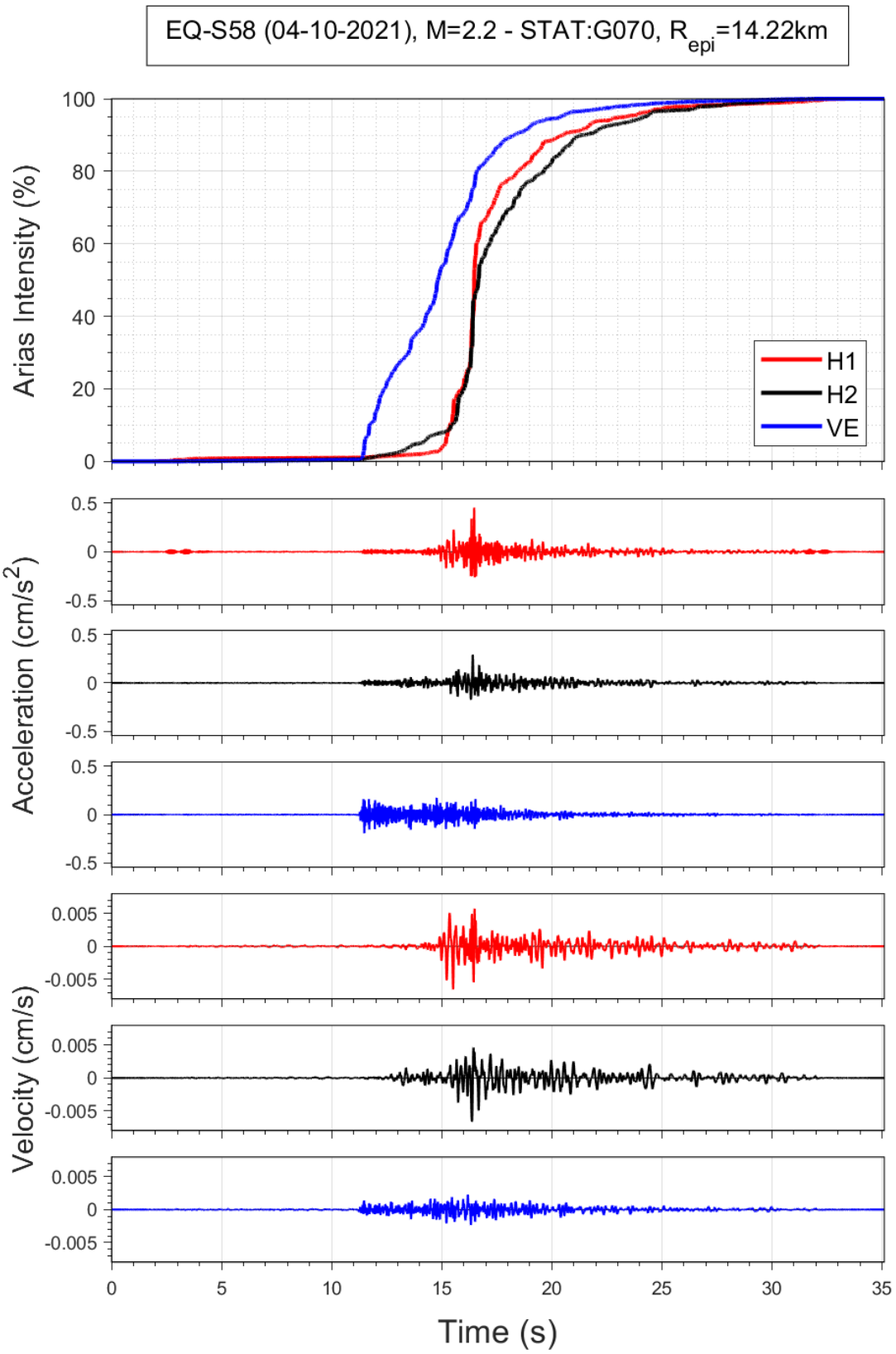
EQ-S58 (04-10-2021), M=2.2 - STAT:G070, R epi =14.22km
Arias Intensity (%)
Acceleration (cm/s2)
Velocity (cm/s)
H1
H2
VE
Time (s)

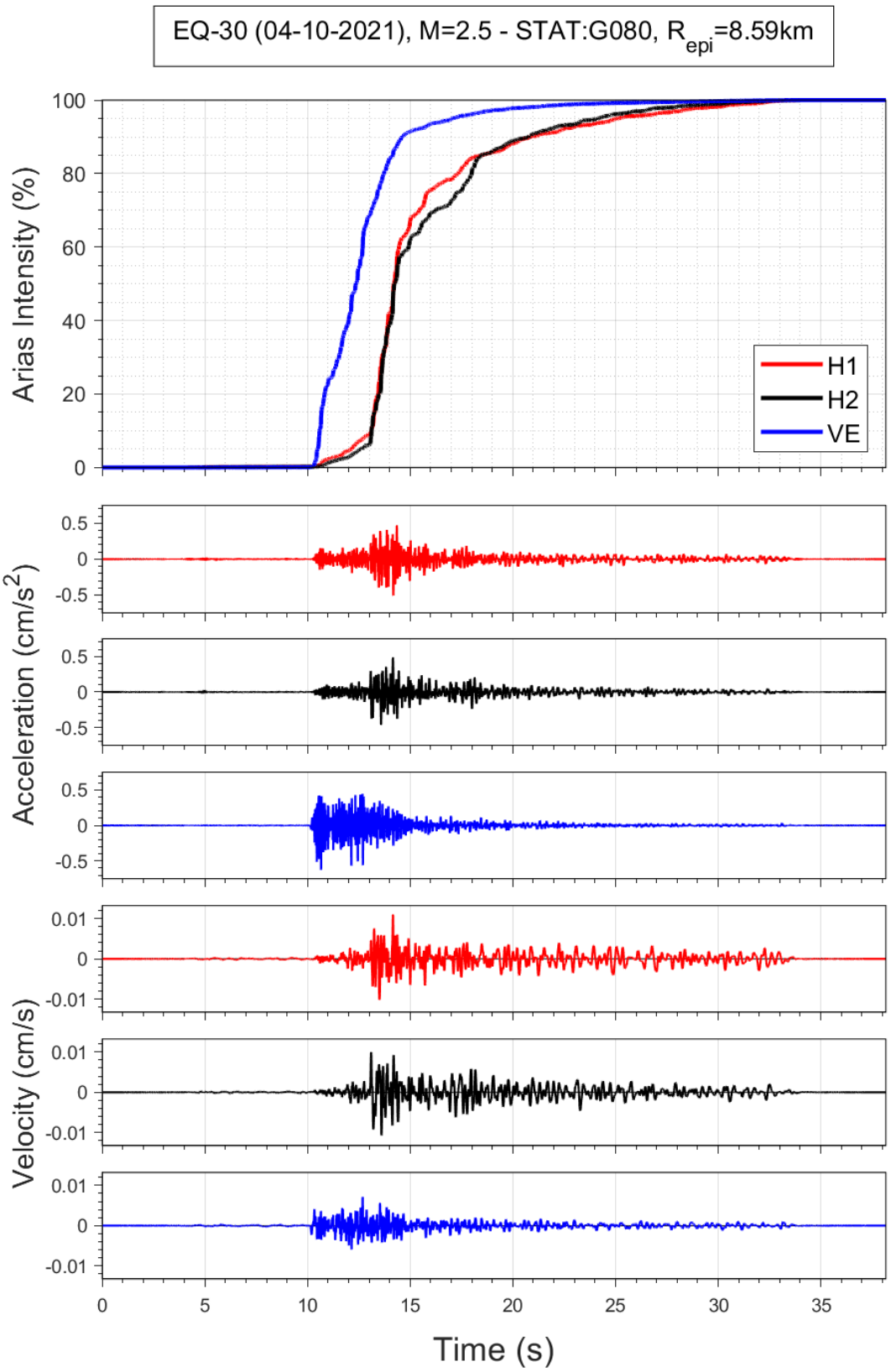
EQ-30 (04-10-2021), M=2.5 - STAT:G080, R epi =8.59km
Arias Intensity (%)
H1
H2
VE
Acceleration (cm/s2)
Velocity (cm/s)
Time (s)

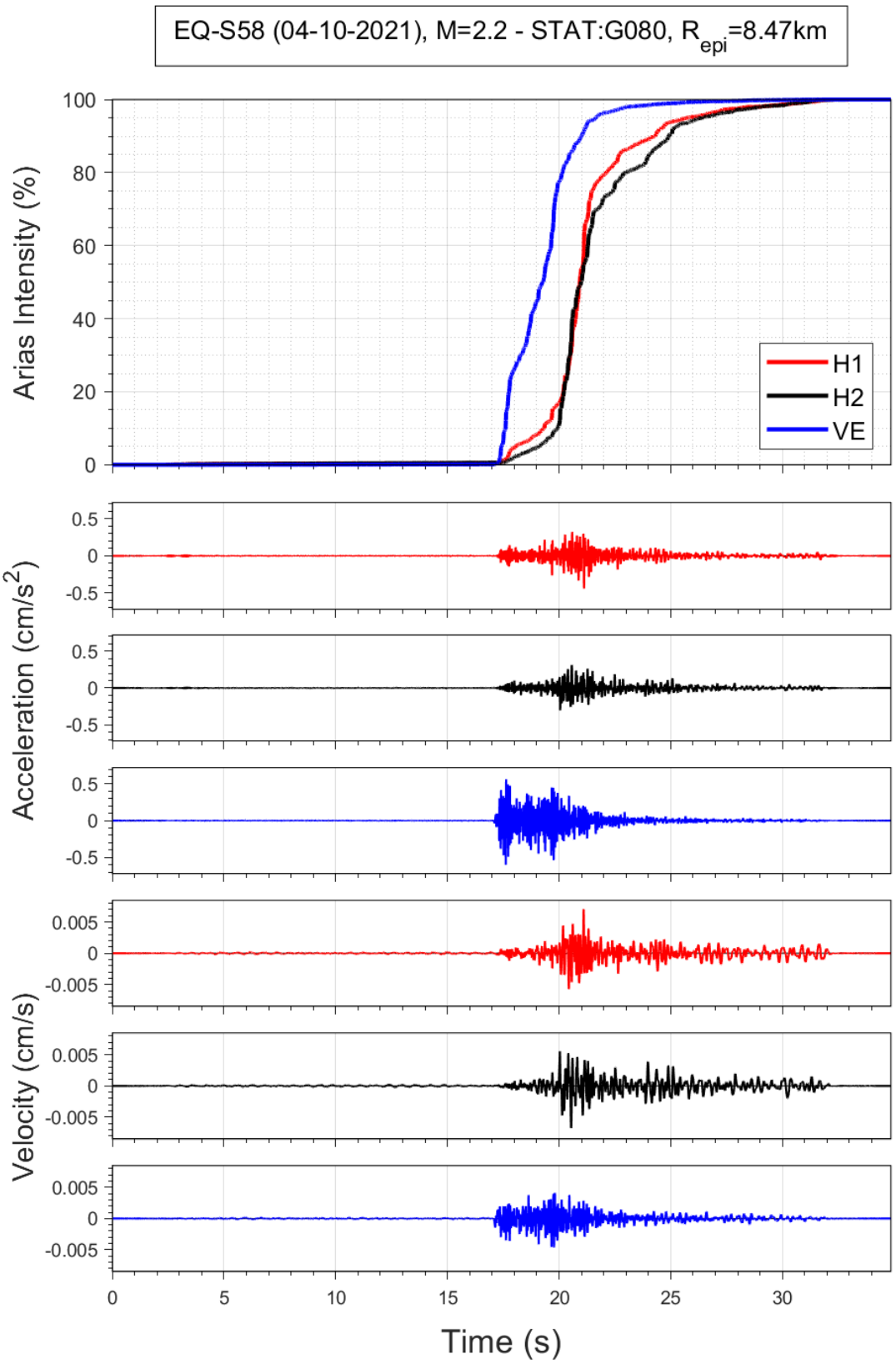
EQ-S58 (04-10-2021), M=2.2 - STAT:G080, R epi =8.47km
Arias Intensity (%)
H1
H2
VE
Acceleration (cm/s2)
Velocity (cm/s)
Time (s)

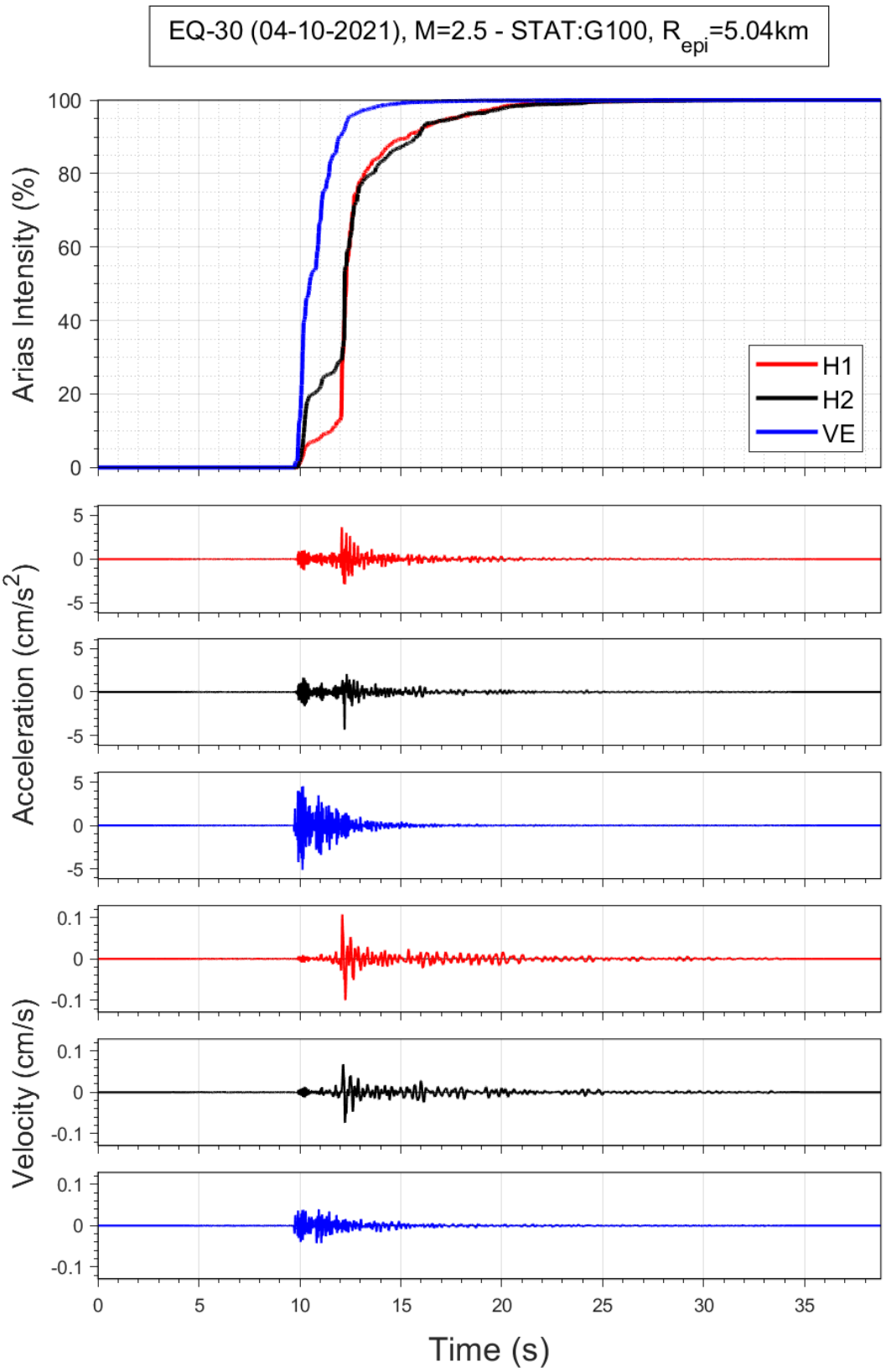
EQ-30 (04-10-2021), M=2.5 - STAT:G100, R epi =5.04km
Arias Intensity (%)
H1
H2
VE
Acceleration (cm/s2)
Velocity (cm/s)
Time (s)

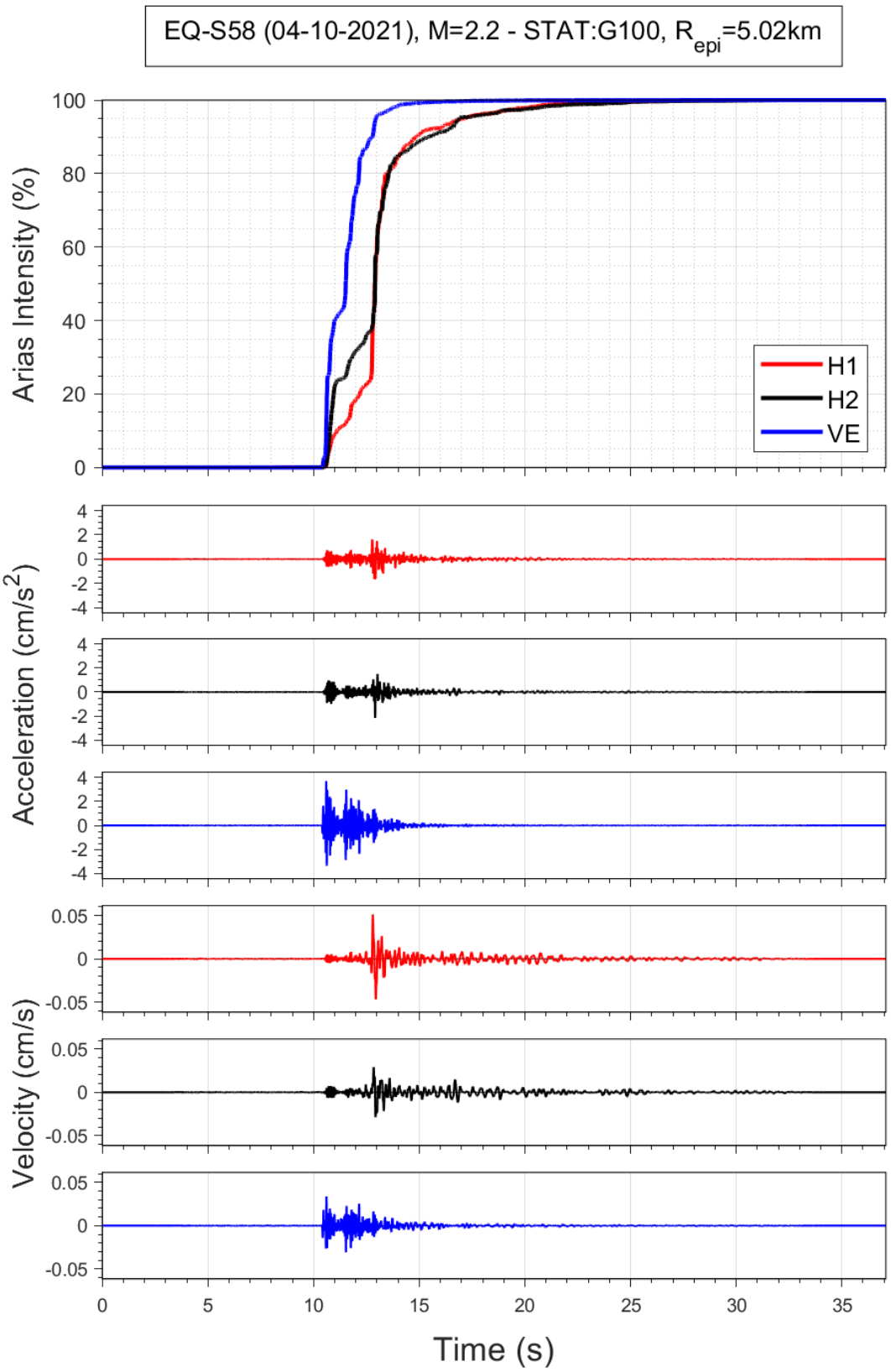
EQ-S58 (04-10-2021), M=2.2 - STAT:G100, R epi =5.02km
Arias Intensity (%)
H1
H2
VE
Acceleration (cm/s2)
Velocity (cm/s)
Time (s)

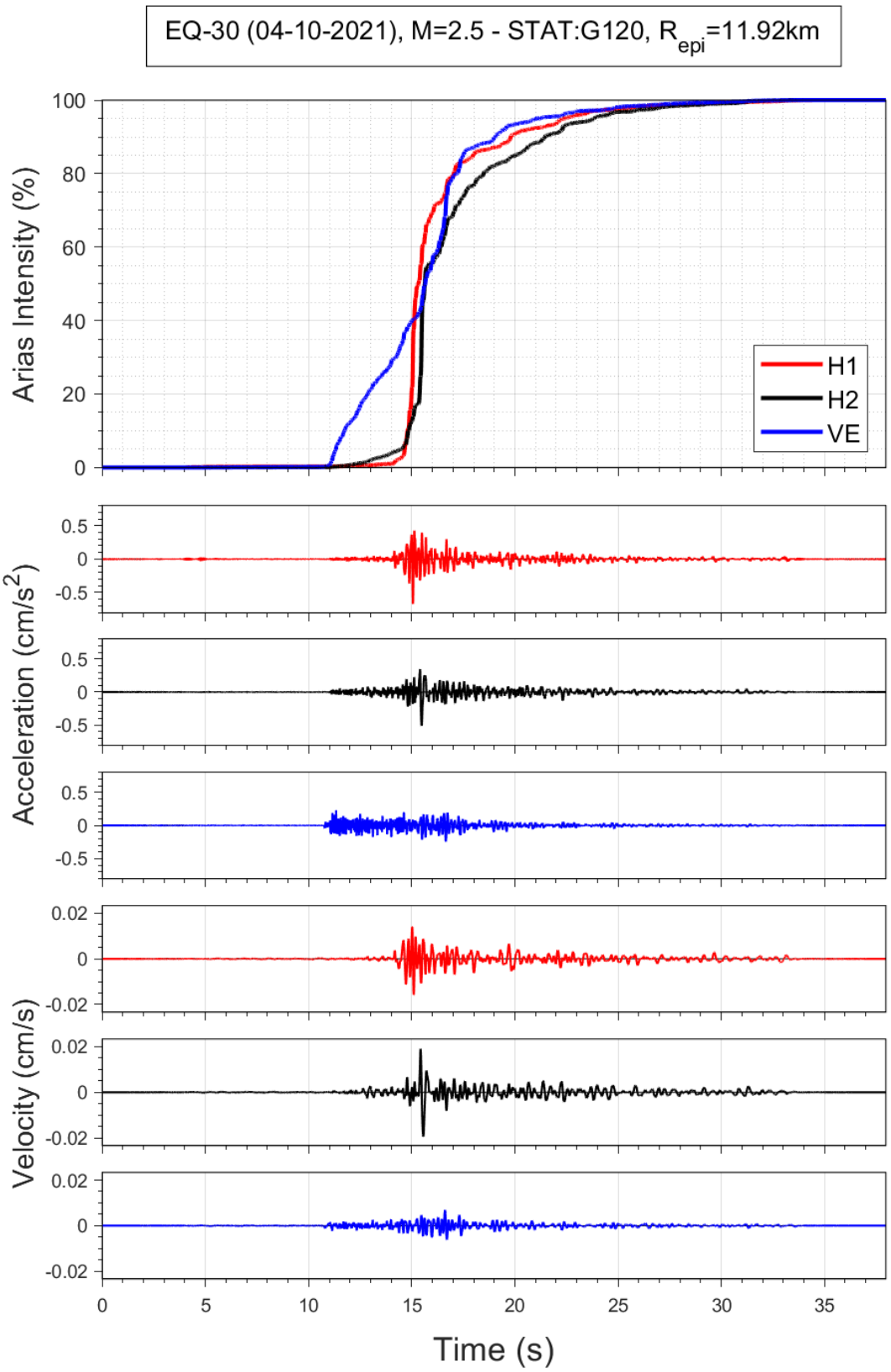
EQ-30 (04-10-2021), M=2.5 - STAT:G120, R_epi=11.92km
Arias Intensity (%)
Acceleration (cm/s²)
Velocity (cm/s)
Time (s)
H1
H2
VE

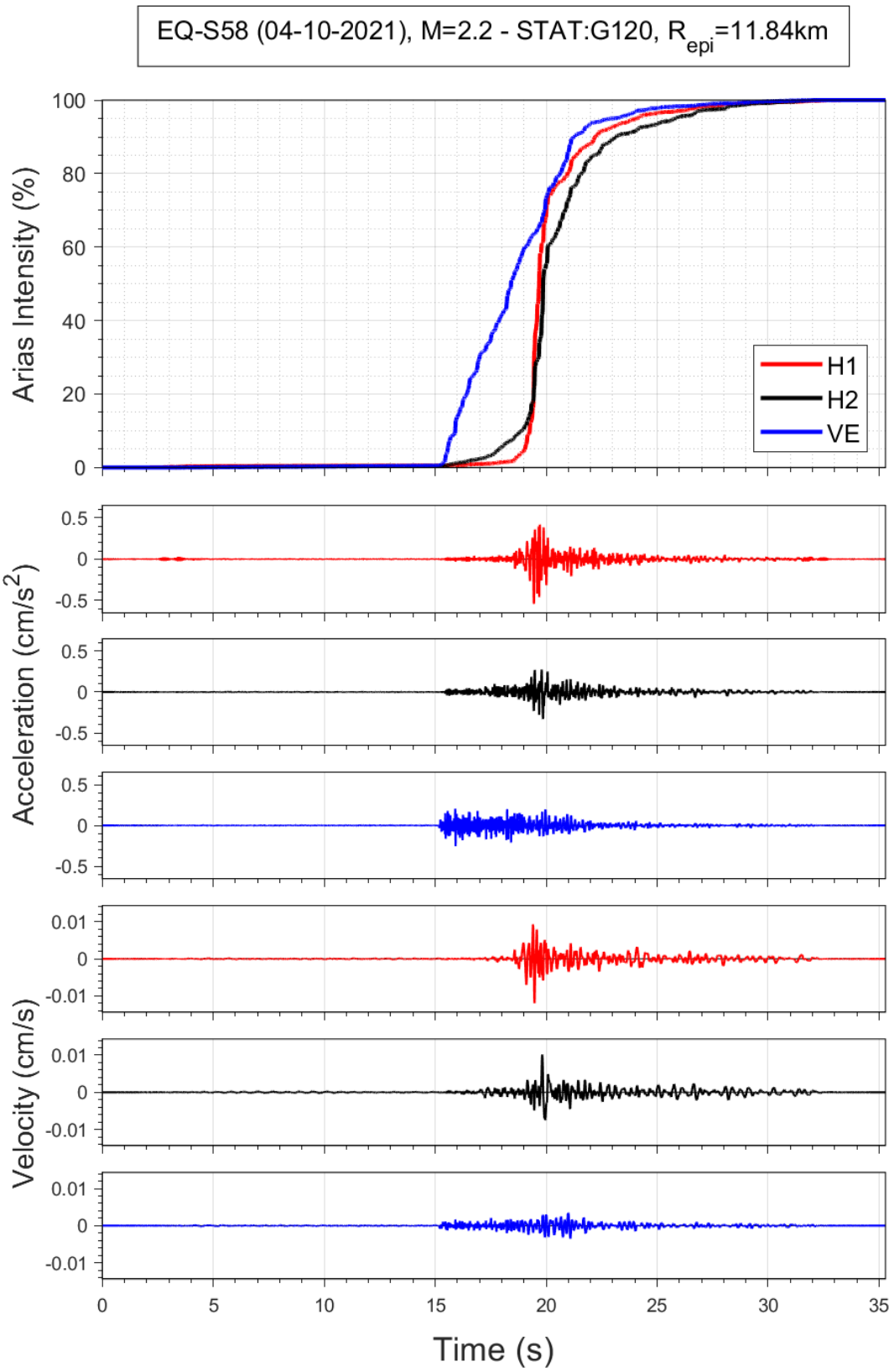
EQ-S58 (04-10-2021), M=2.2 - STAT:G120, R epi =11.84km
Arias Intensity (%)
H1
H2
VE
Acceleration (cm/s2)
Velocity (cm/s)
Time (s)

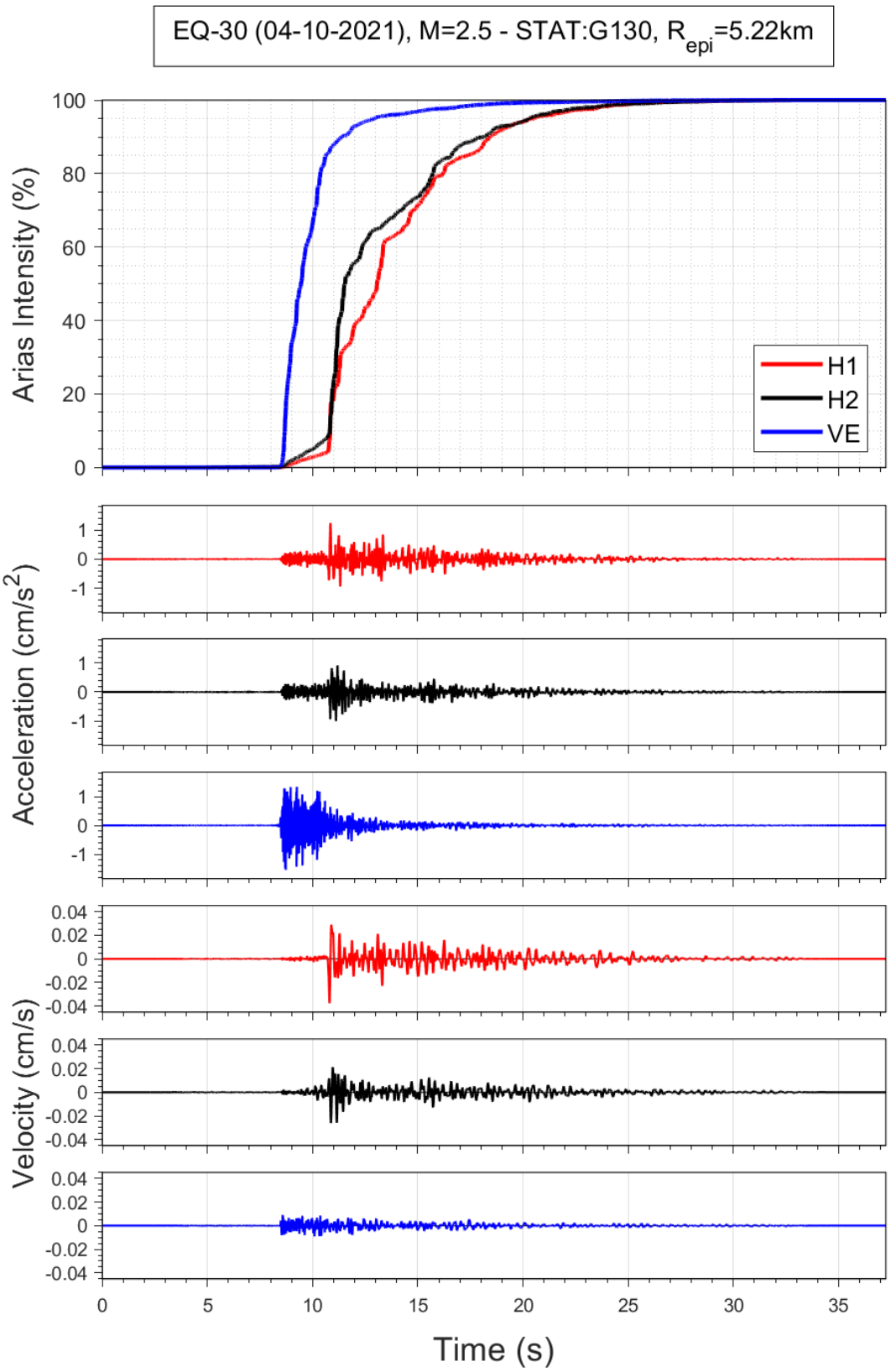
EQ-30 (04-10-2021), M=2.5 - STAT:G130, R epi =5.22km
Arias Intensity (%)
H1
H2
VE
Acceleration (cm/s2)
Velocity (cm/s)
Time (s)

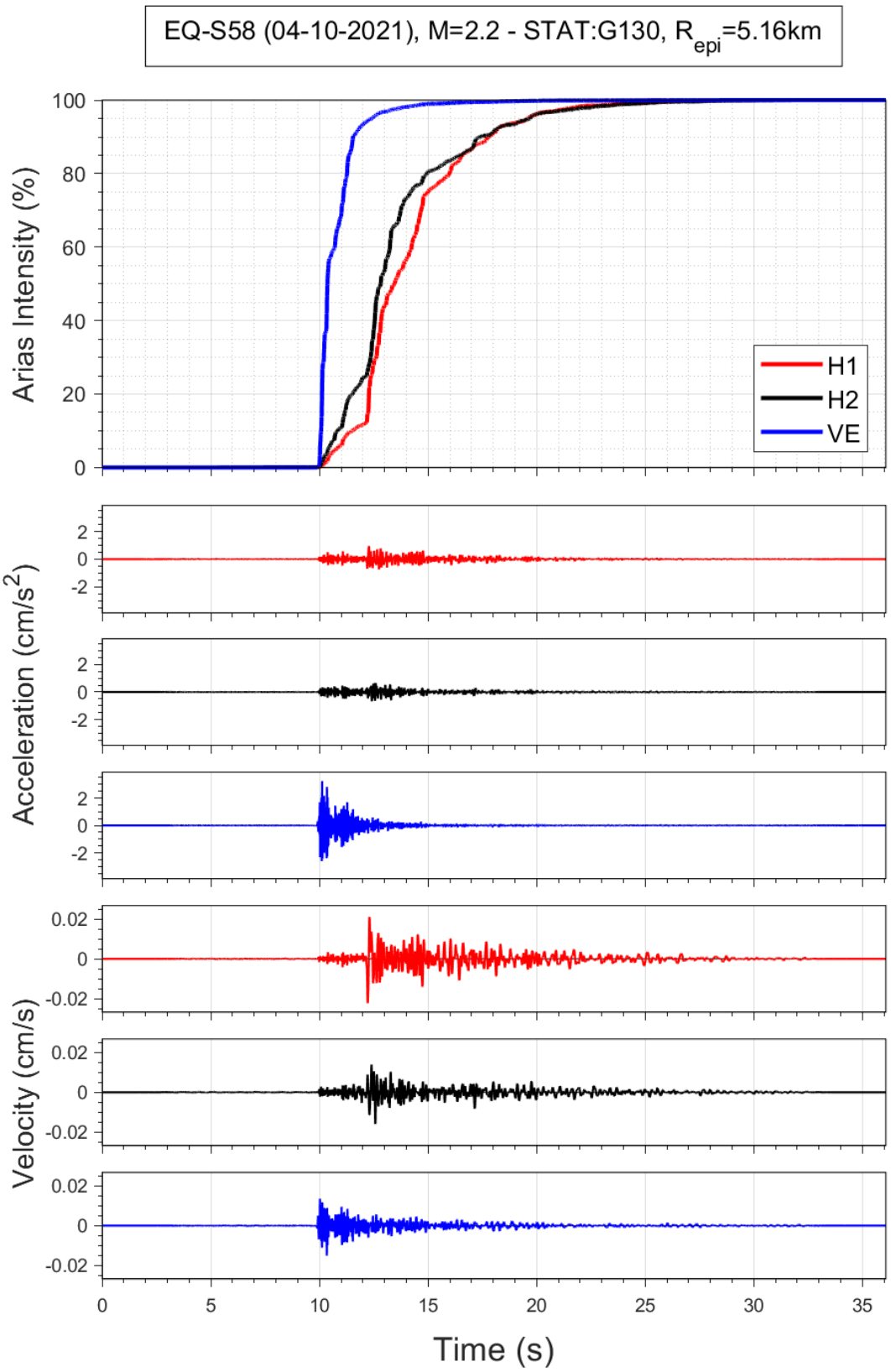
EQ-S58 (04-10-2021), M=2.2 - STAT:G130, R epi =5.16km
Arias Intensity (%)
H1
H2
VE
Acceleration (cm/s2)
Velocity (cm/s)
Time (s)

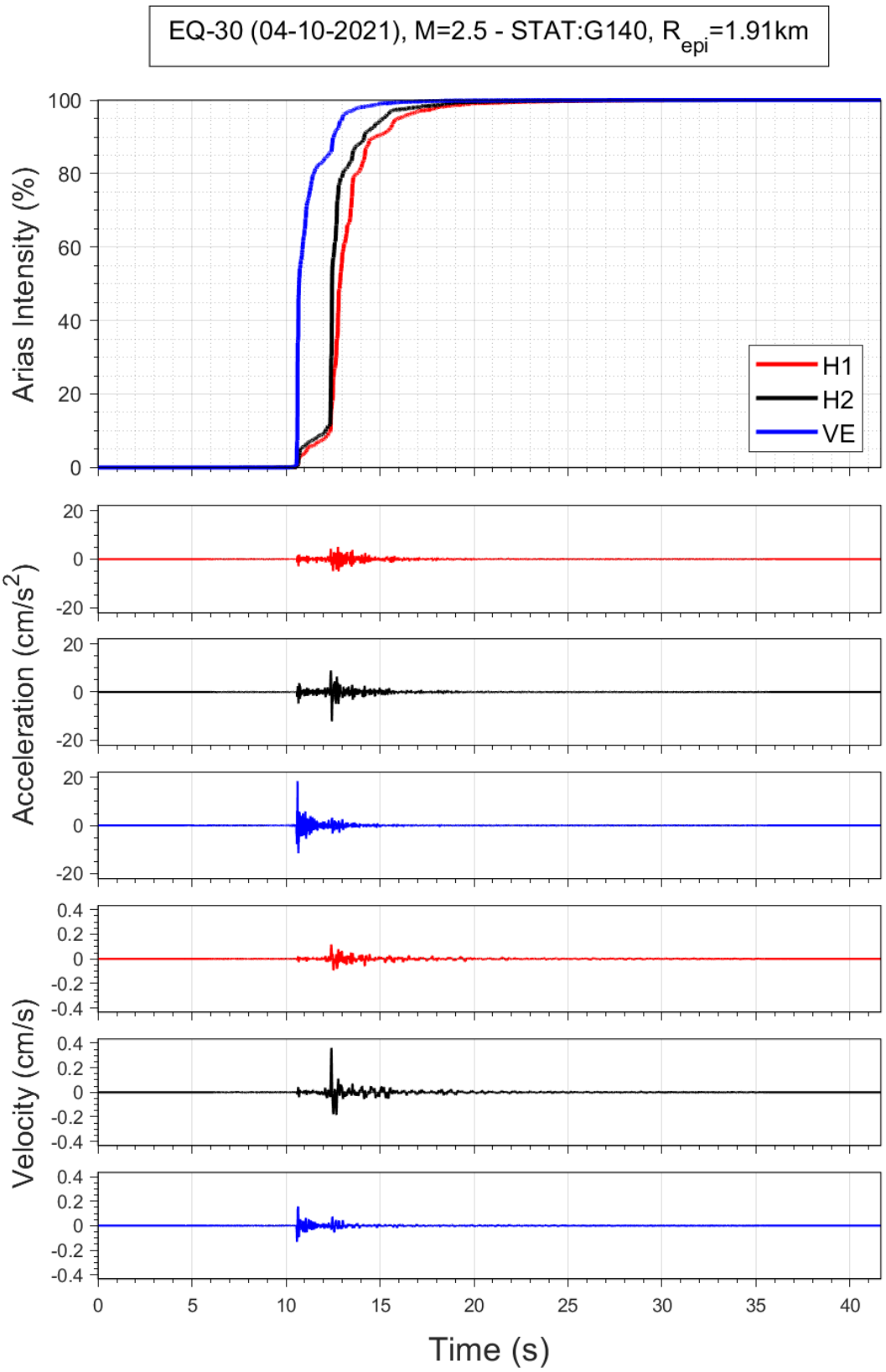
EQ-30 (04-10-2021), M=2.5 - STAT:G140, R epi =1.91km
Arias Intensity (%)
H1
H2
VE
Acceleration (cm/s2)
Velocity (cm/s)
Time (s)

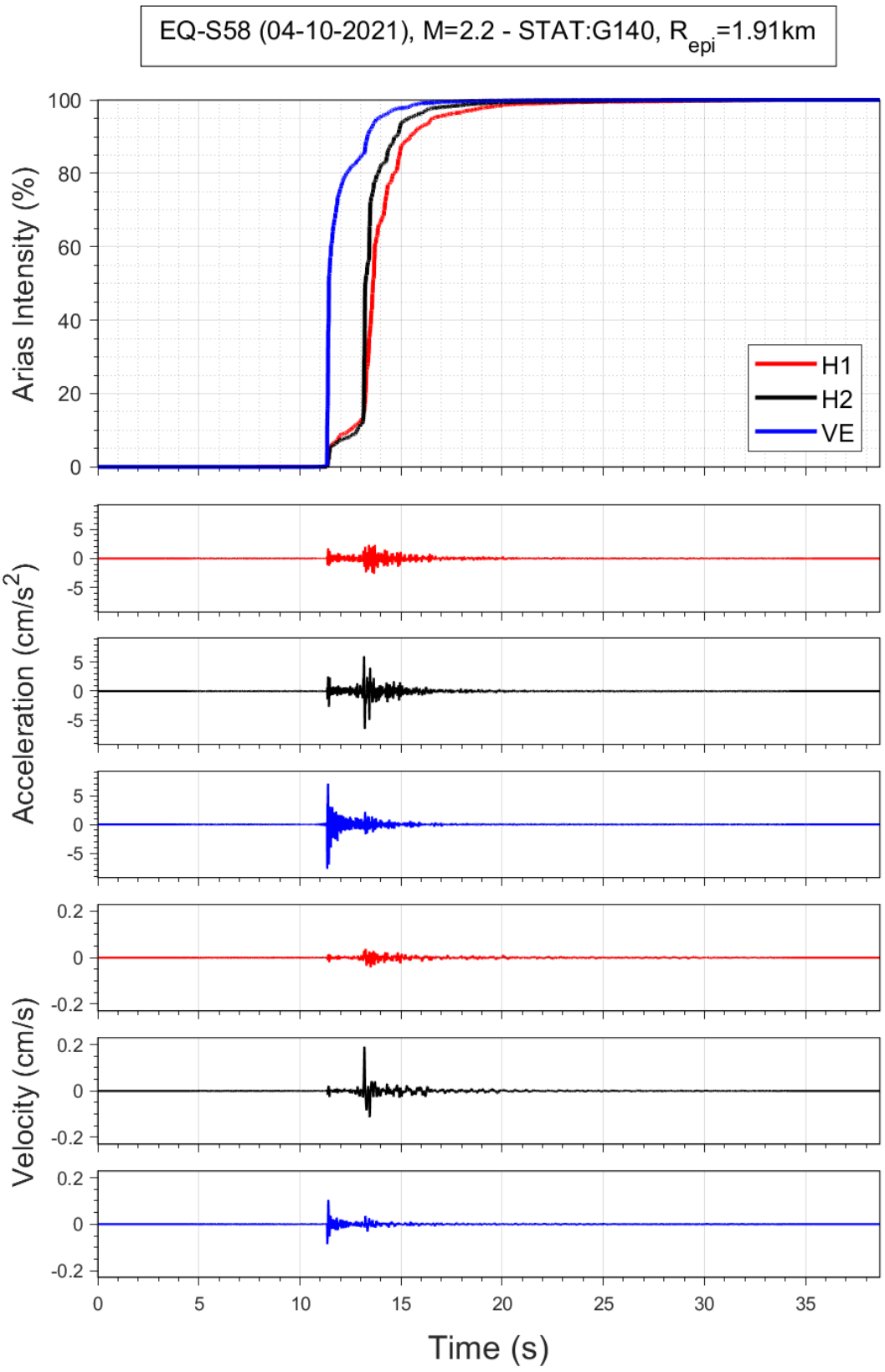
EQ-S58 (04-10-2021), M=2.2 - STAT:G140, R epi =1.91km
Arias Intensity (%)
H1
H2
VE
Acceleration (cm/s2)
Velocity (cm/s)
Time (s)

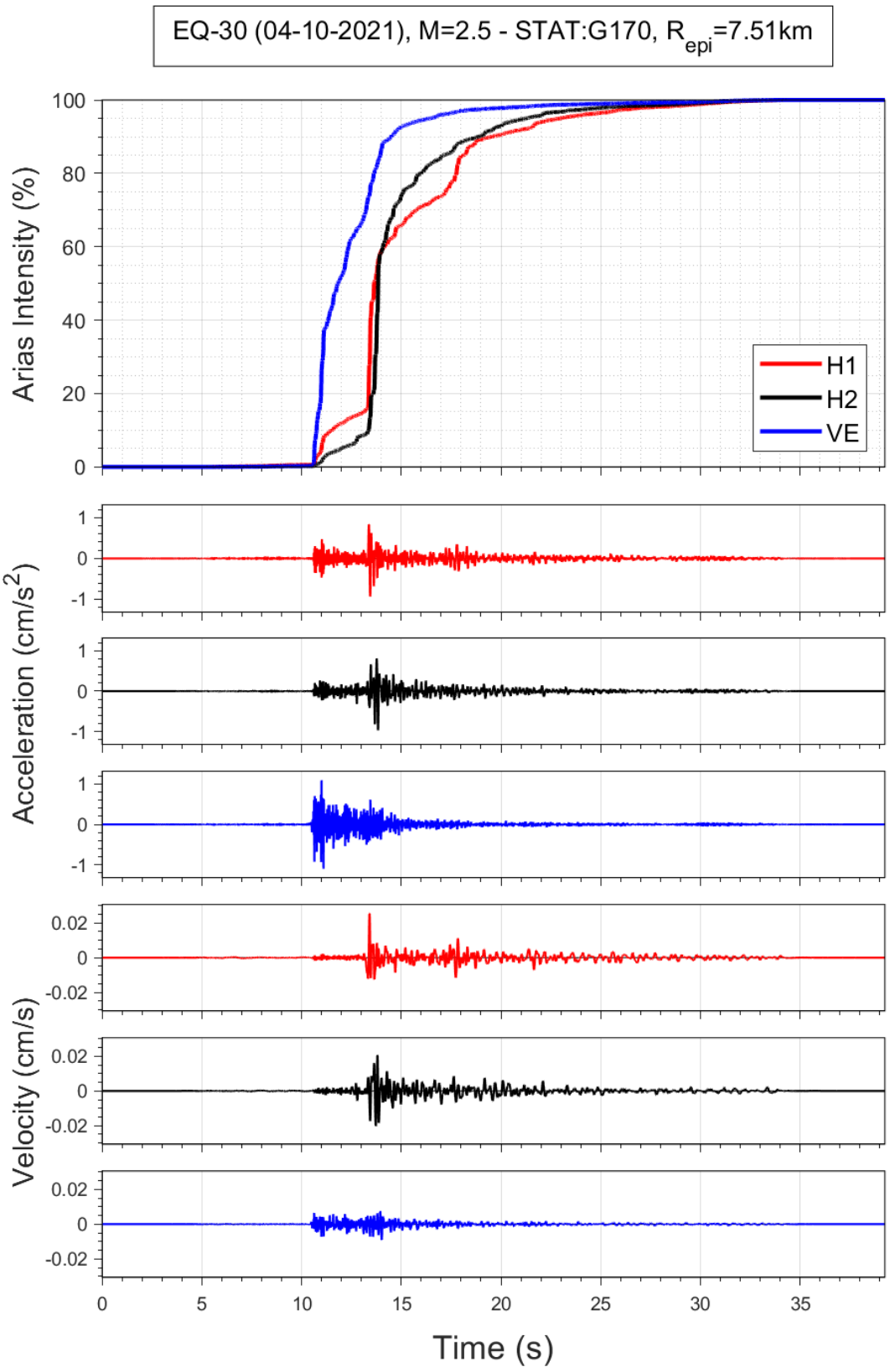
EQ-30 (04-10-2021), M=2.5 - STAT:G170, R epi =7.51km
Arias Intensity (%)
H1
H2
VE
Acceleration (cm/s2)
Velocity (cm/s)
Time (s)

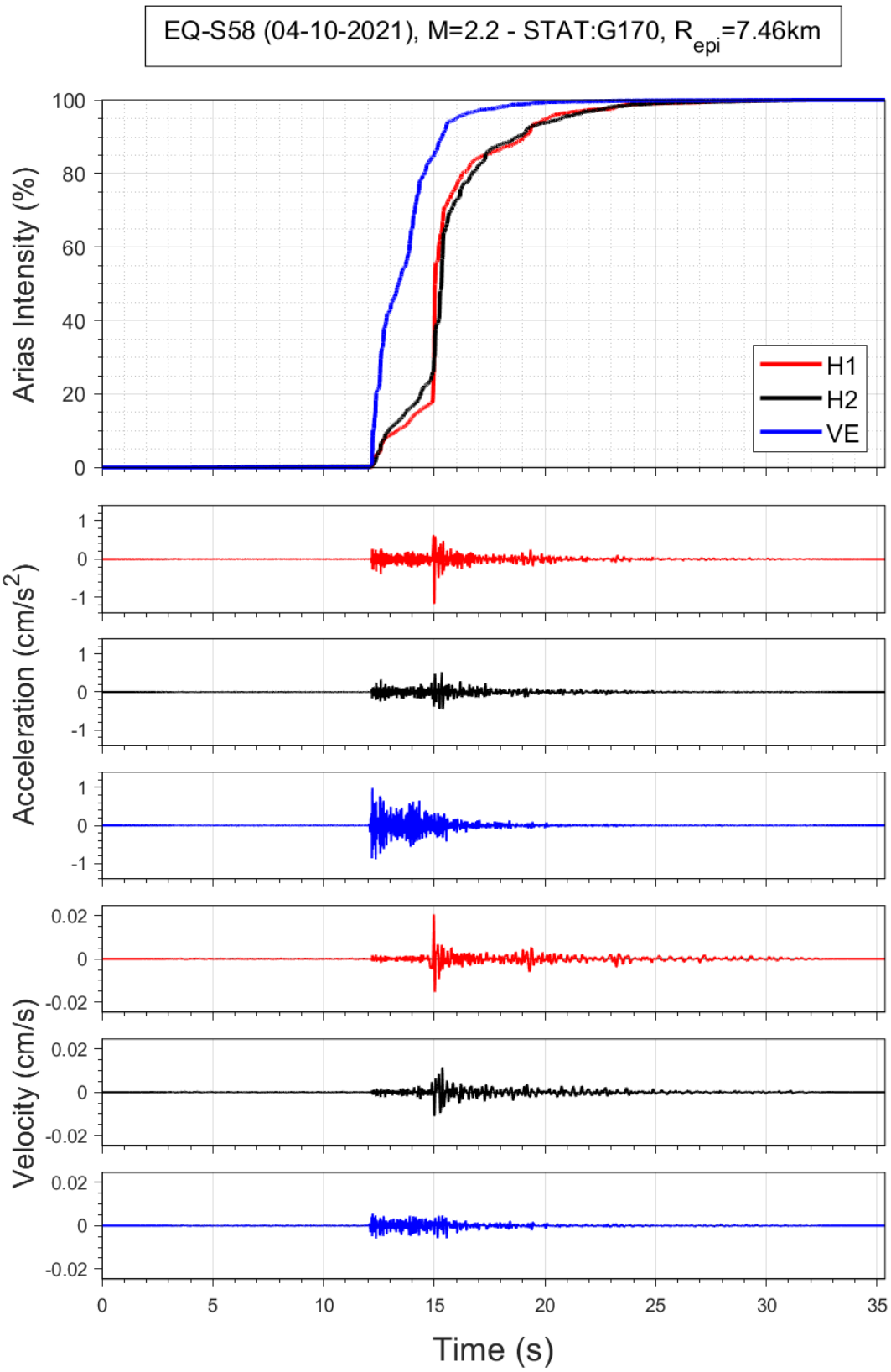
EQ-S58 (04-10-2021), M=2.2 - STAT:G170, R_epi=7.46km
Arias Intensity (%)
H1
H2
VE
Acceleration (cm/s²)
Velocity (cm/s)
Time (s)

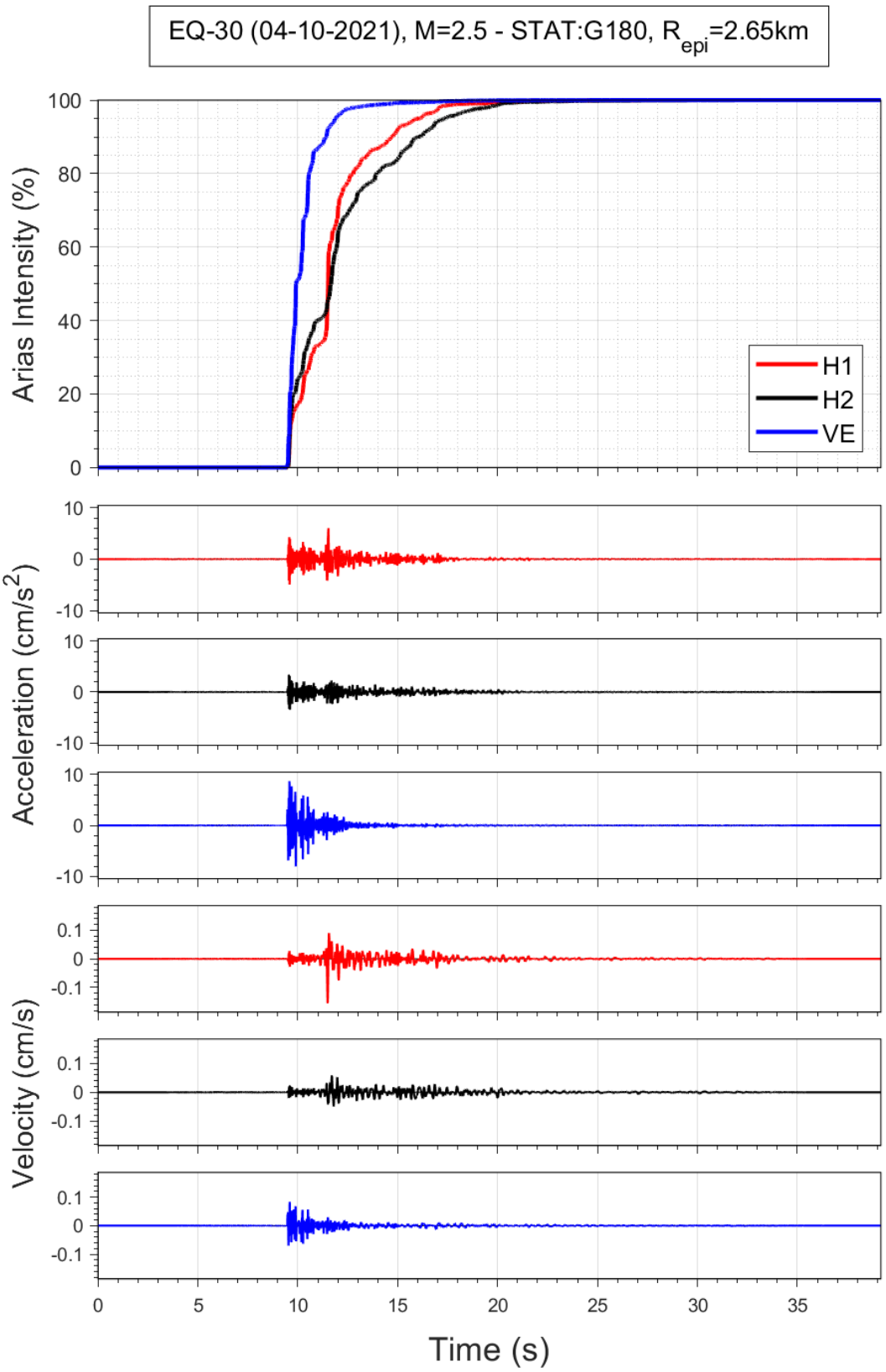
EQ-30 (04-10-2021), M=2.5 - STAT:G180, R epi =2.65km
Arias Intensity (%)
H1
H2
VE
Acceleration (cm/s2)
Velocity (cm/s)
Time (s)

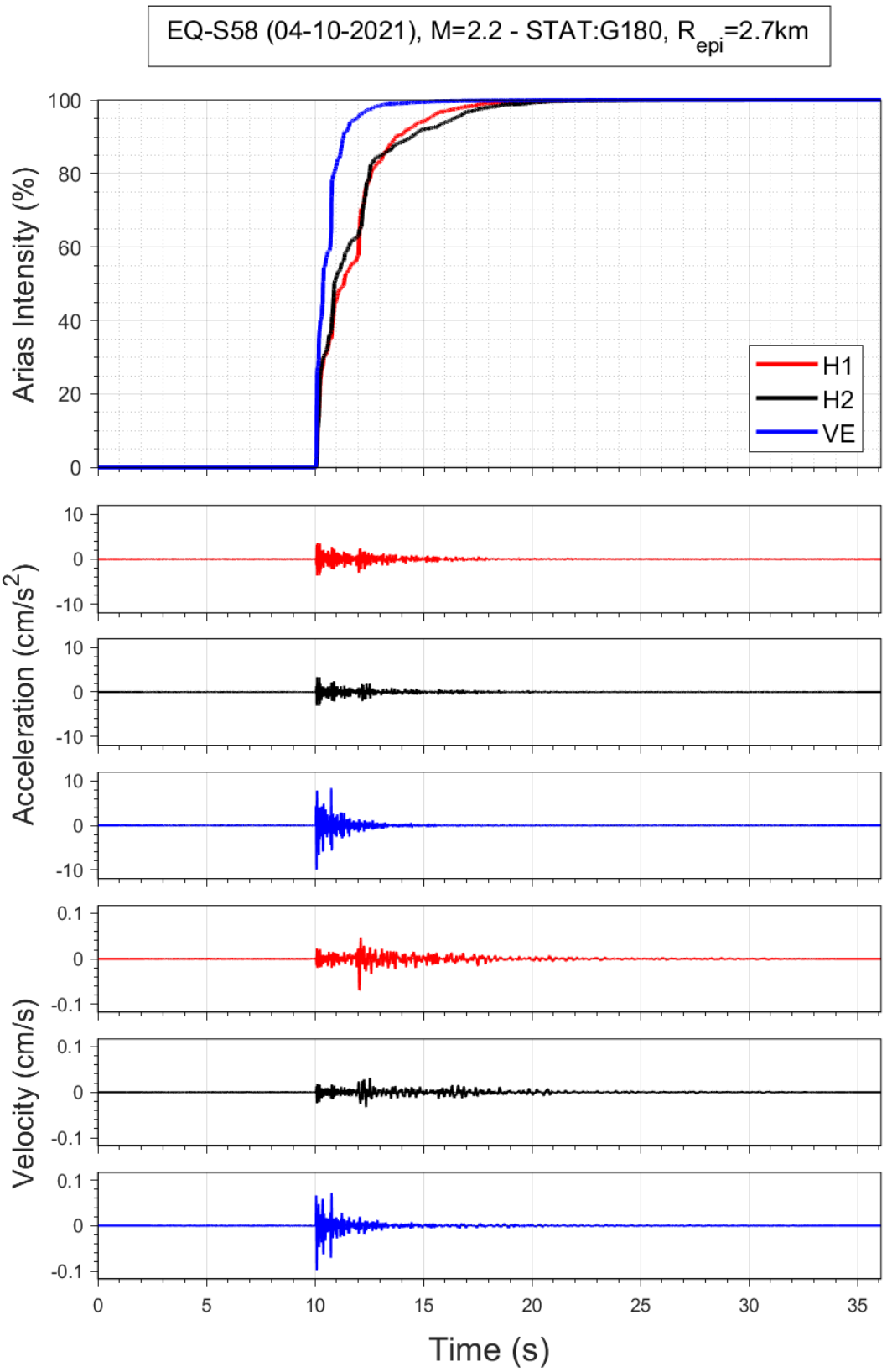
EQ-S58 (04-10-2021), M=2.2 - STAT:G180, R epi =2.7km
Arias Intensity (%)
H1
H2
VE
Acceleration (cm/s2)
Velocity (cm/s)
Time (s)

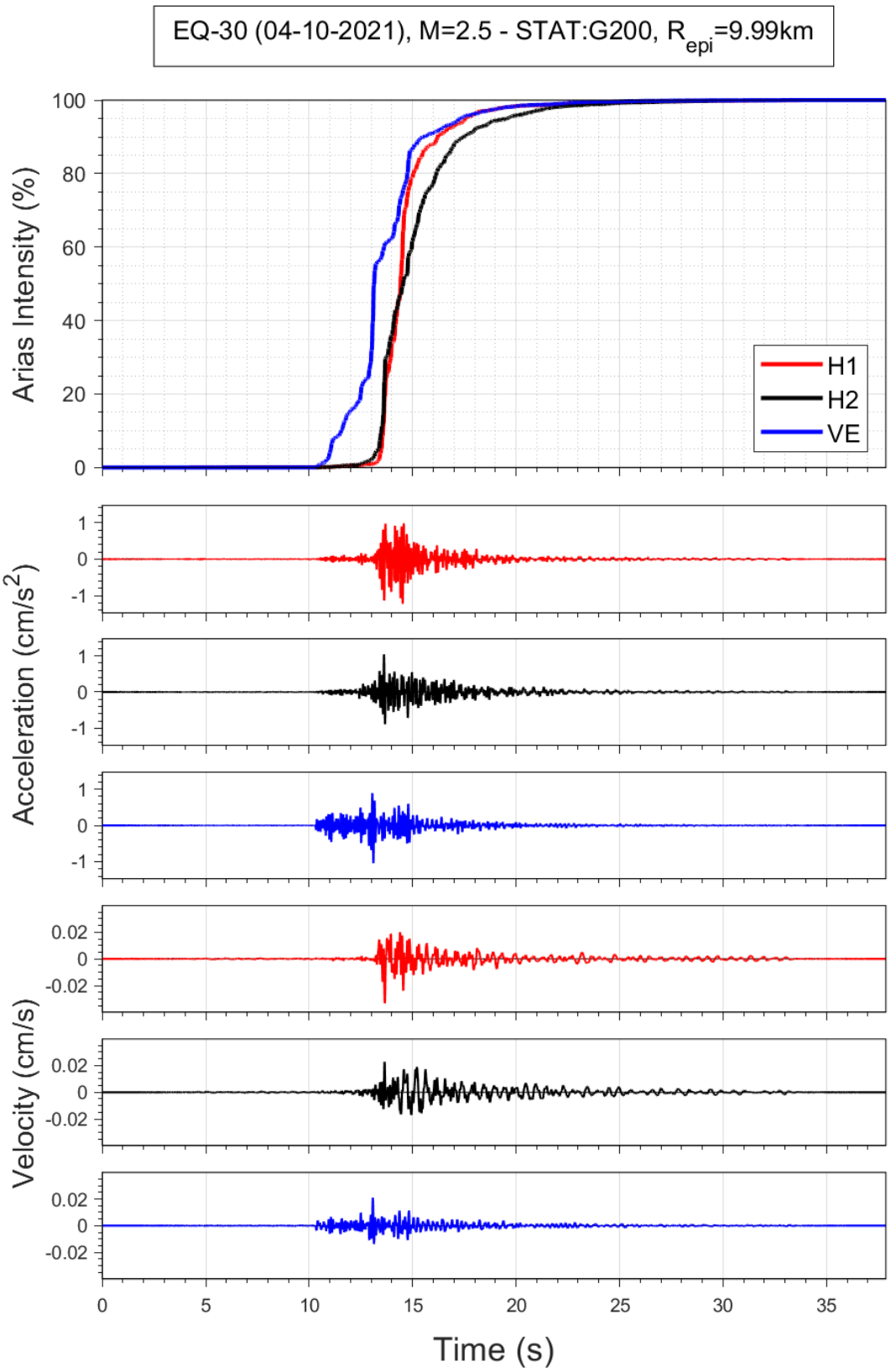
EQ-30 (04-10-2021), M=2.5 - STAT:G200, R epi =9.99km
Arias Intensity (%)
H1
H2
VE
Acceleration (cm/s2)
Velocity (cm/s)
Time (s)

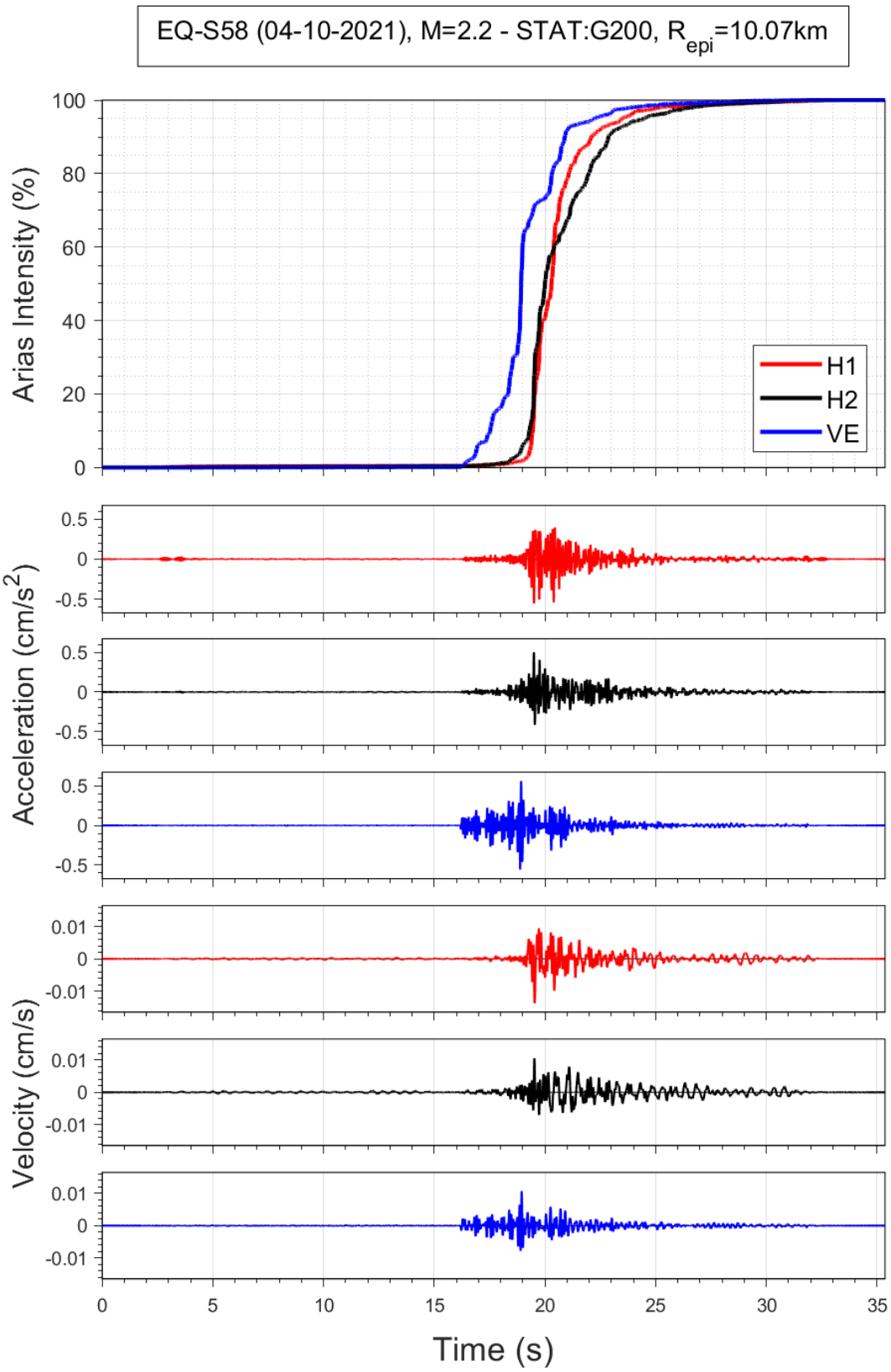
EQ-S58 (04-10-2021), M=2.2 - STAT:G200, R epi =10.07km
Arias Intensity (%)
H1
H2
VE
Acceleration (cm/s2)
Velocity (cm/s)
Time (s)

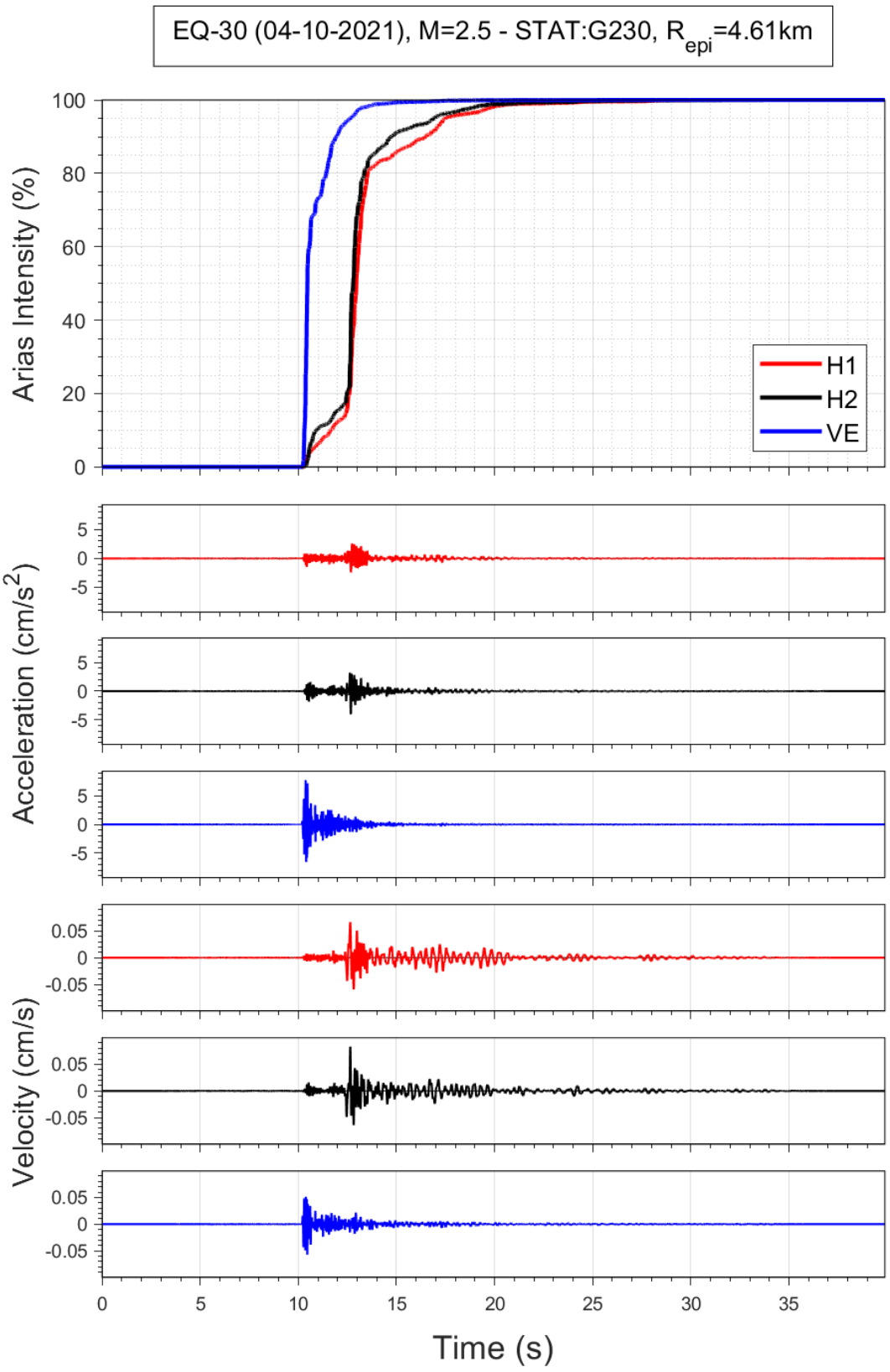
EQ-30 (04-10-2021), M=2.5 - STAT:G230, R epi =4.61km
Arias Intensity (%)
H1
H2
VE
Acceleration (cm/s2)
Velocity (cm/s)
Time (s)

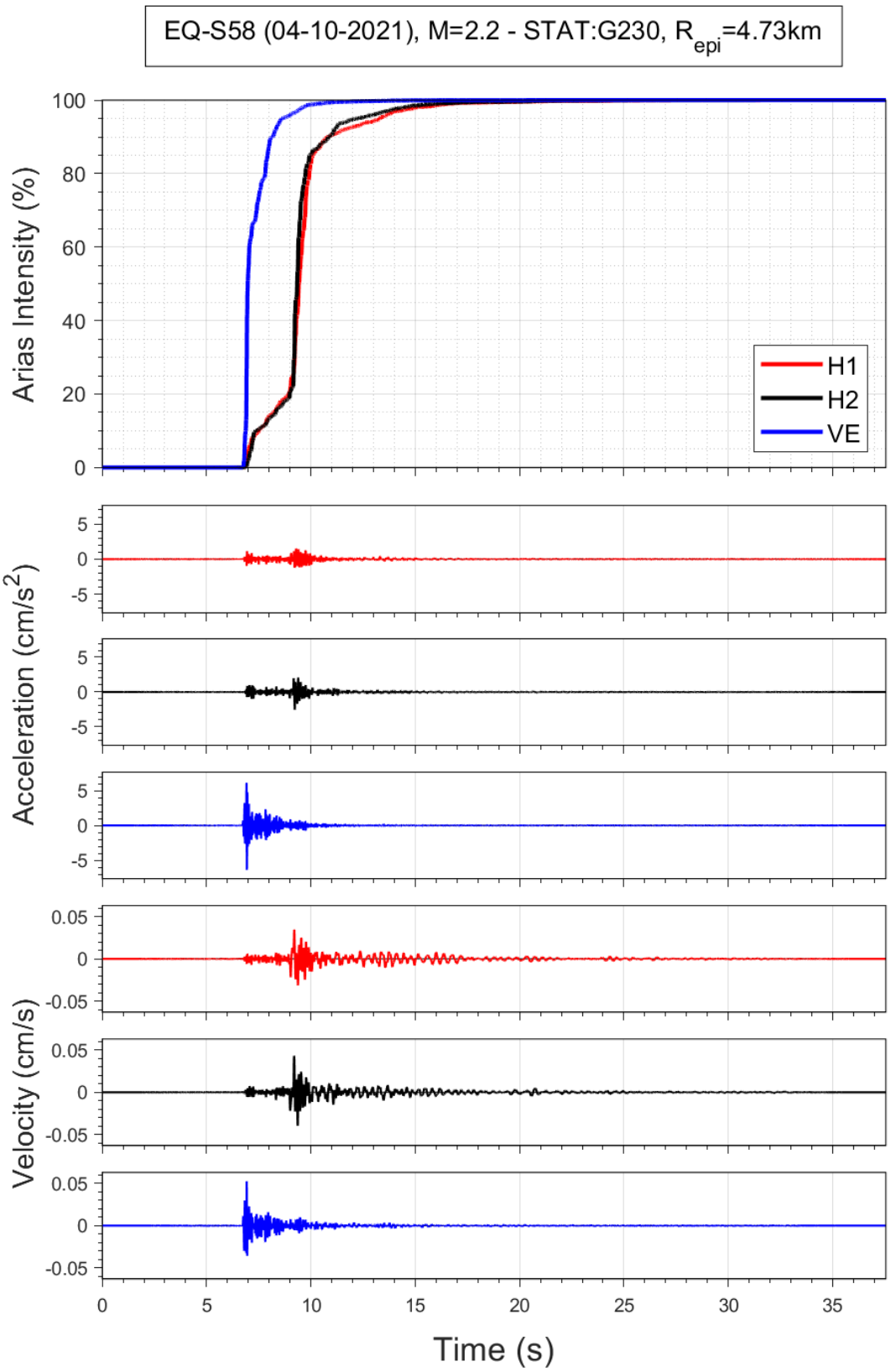
EQ-S58 (04-10-2021), M=2.2 - STAT:G230, R_epi=4.73km
Arias Intensity (%)
H1
H2
VE
Acceleration (cm/s2)
Velocity (cm/s)
Time (s)

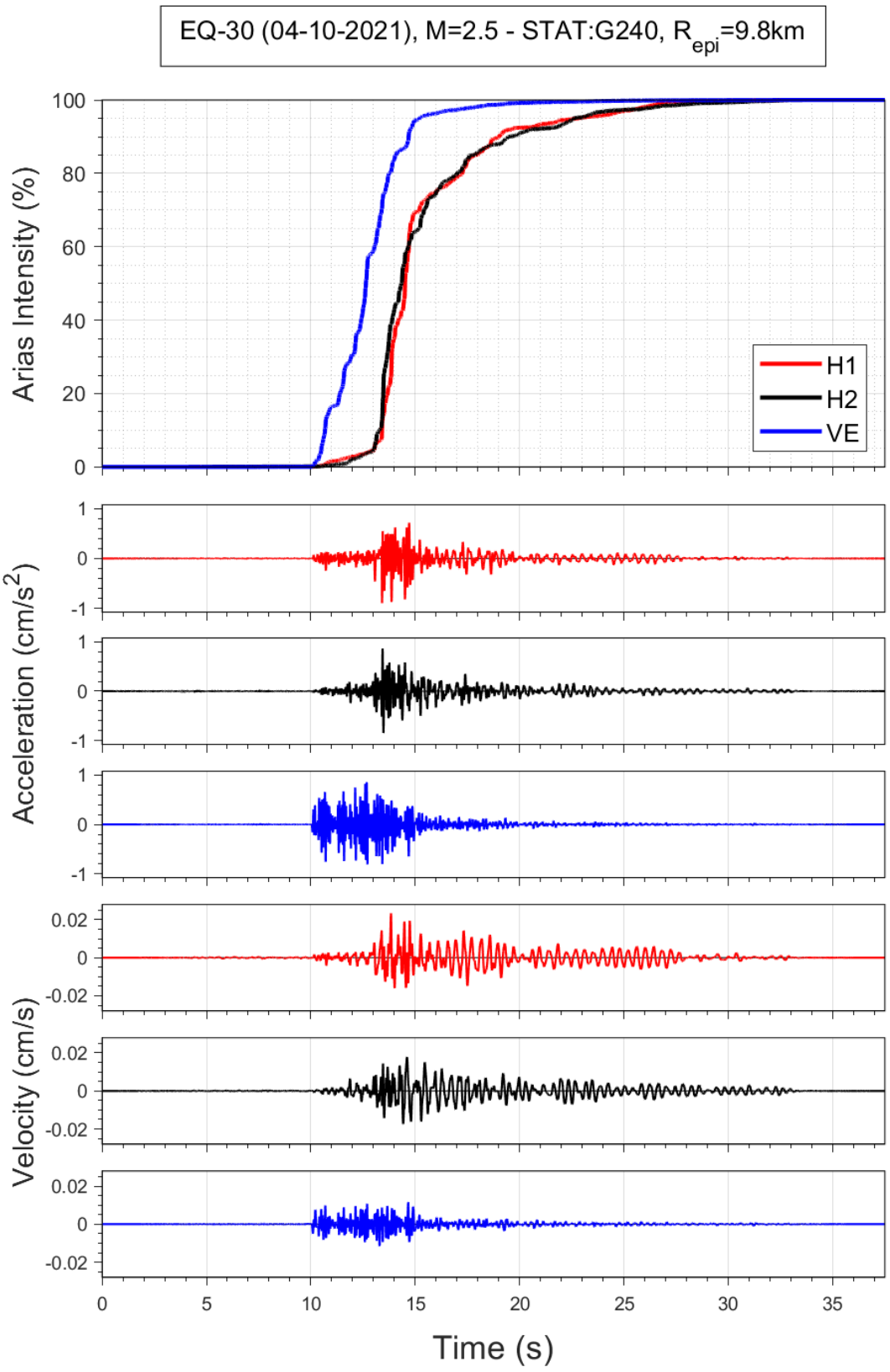
EQ-30 (04-10-2021), M=2.5 - STAT:G240, R_epi=9.8km
Arias Intensity (%)
Acceleration (cm/s²)
Velocity (cm/s)
Time (s)
H1
H2
VE

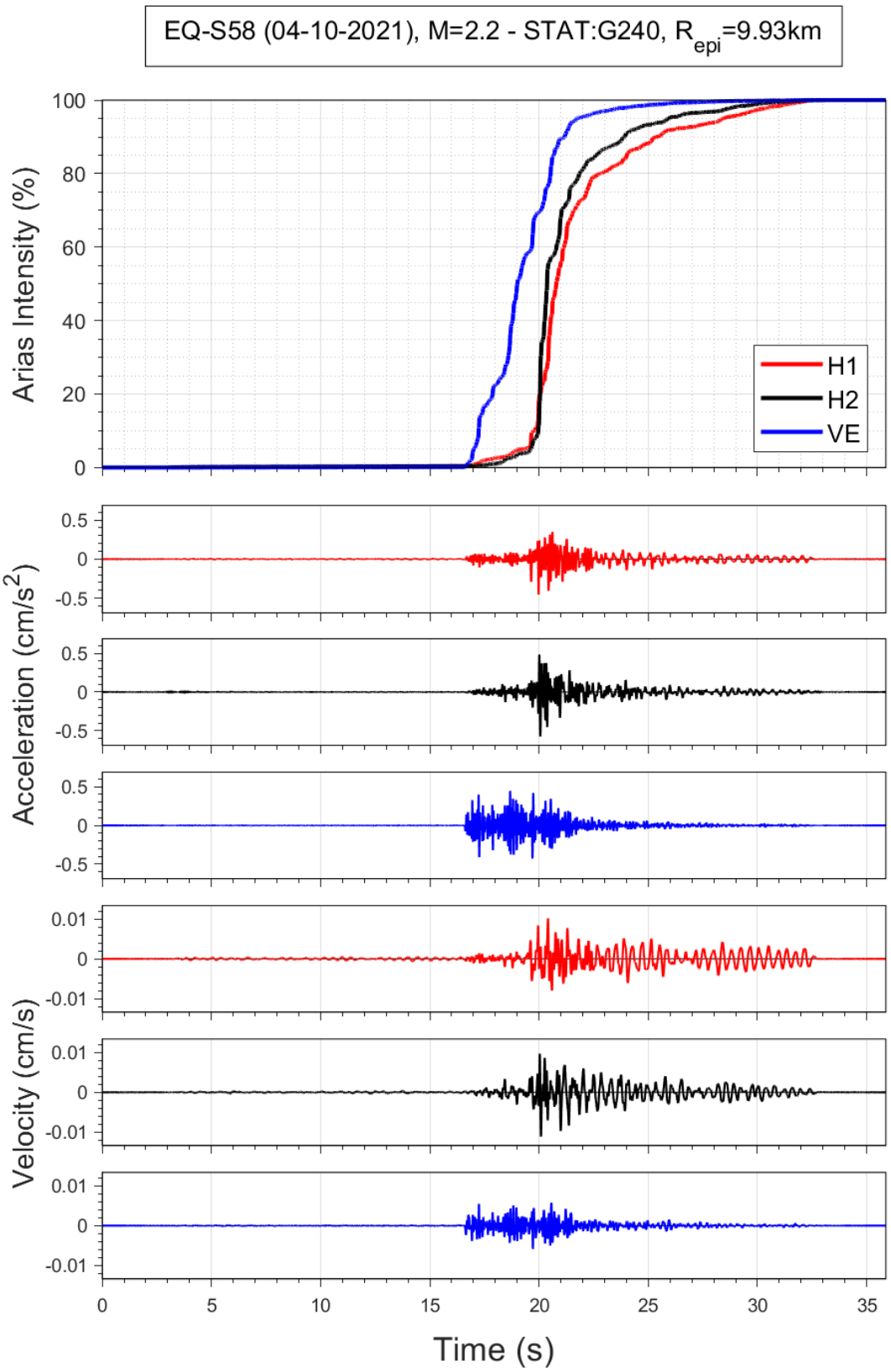
EQ-S58 (04-10-2021), M=2.2 - STAT:G240, R epi =9.93km
Arias Intensity (%)
H1
H2
VE
Acceleration (cm/s2)
Velocity (cm/s)
Time (s)

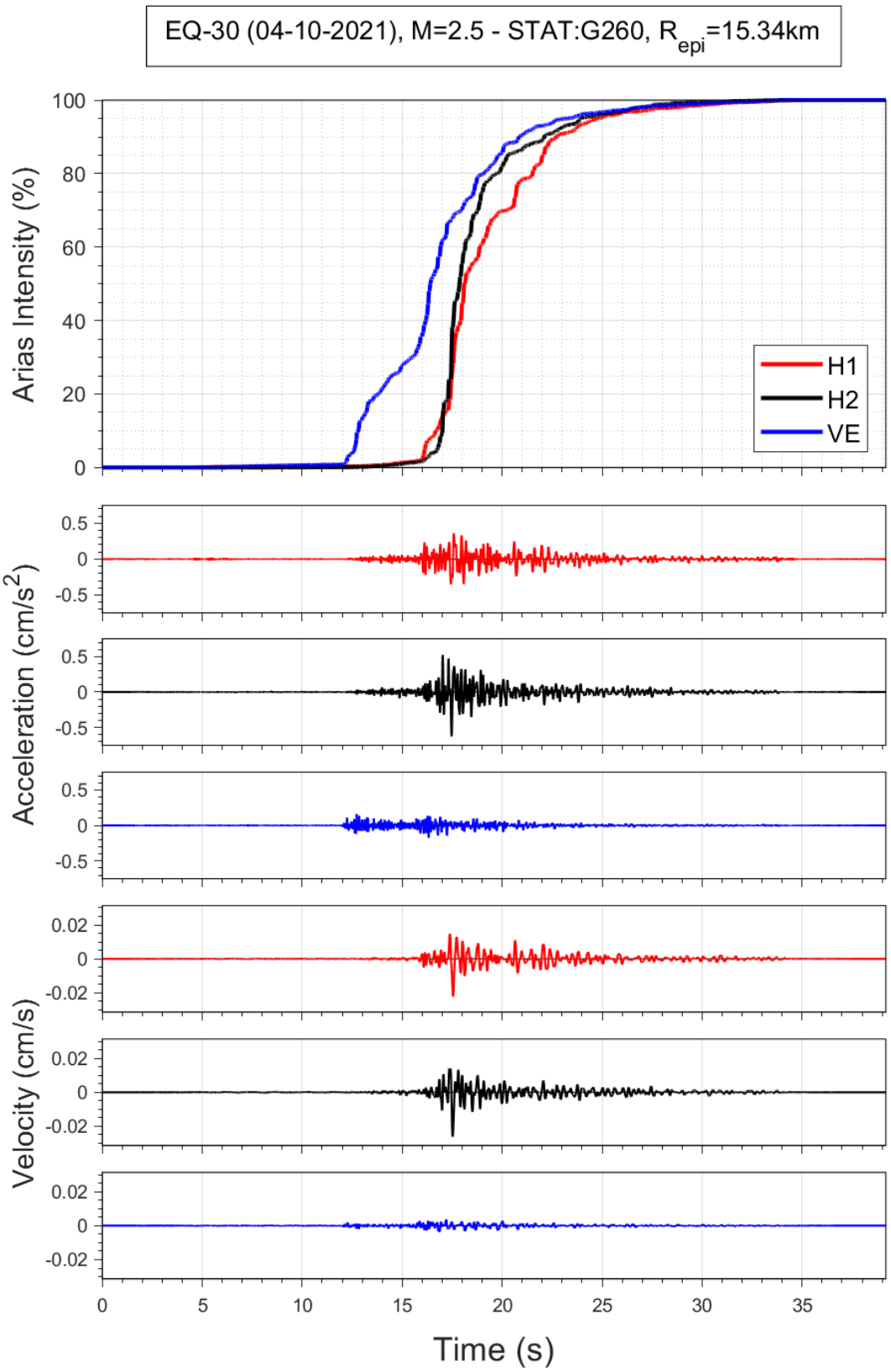
EQ-30 (04-10-2021), M=2.5 - STAT:G260, R epi =15.34km
Arias Intensity (%)
H1
H2
VE
Acceleration (cm/s2)
Velocity (cm/s)
Time (s)

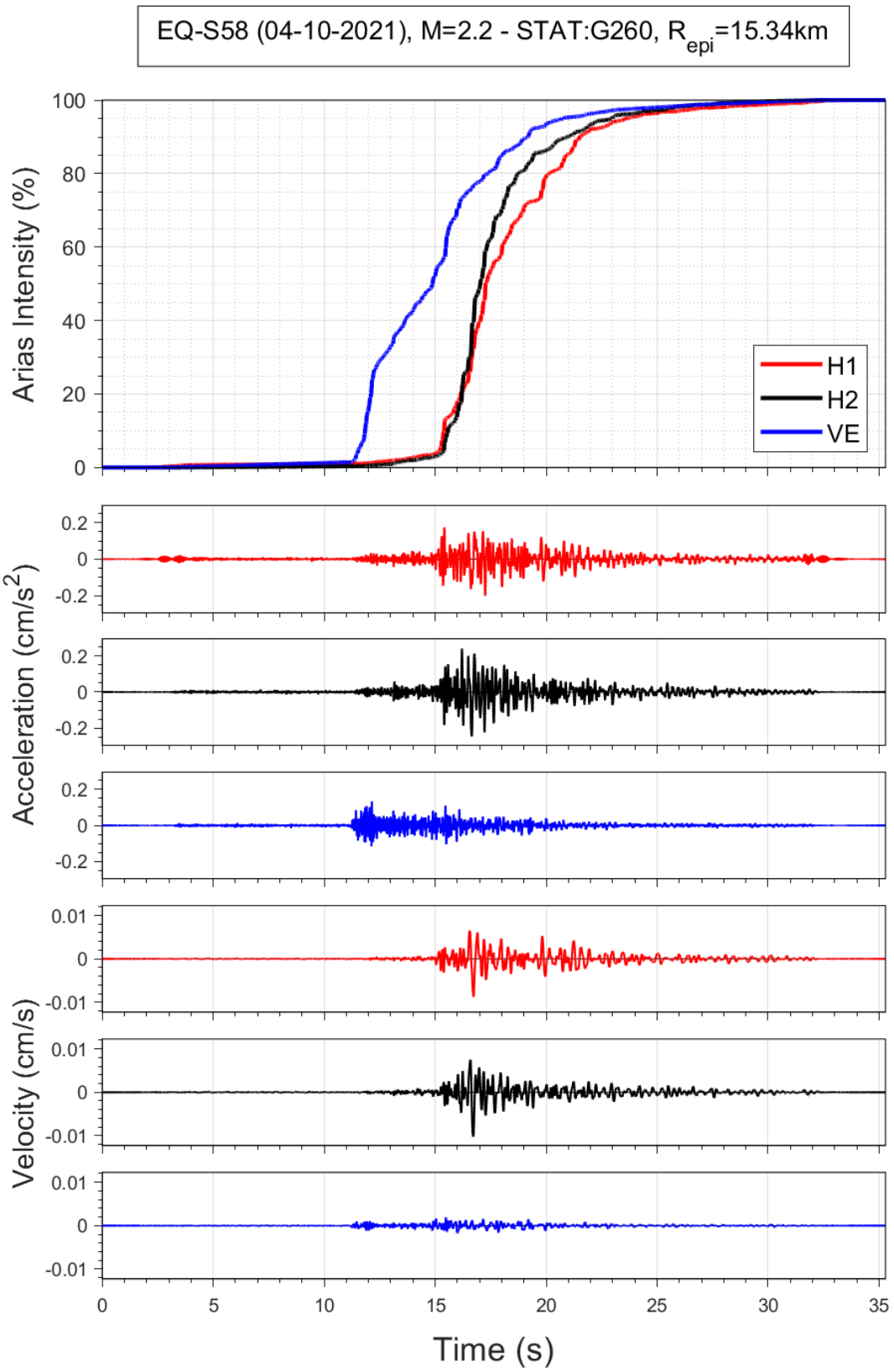
EQ-S58 (04-10-2021), M=2.2 - STAT:G260, R epi =15.34km
Arias Intensity (%)
H1
H2
VE
Acceleration (cm/s2)
Velocity (cm/s)
Time (s)

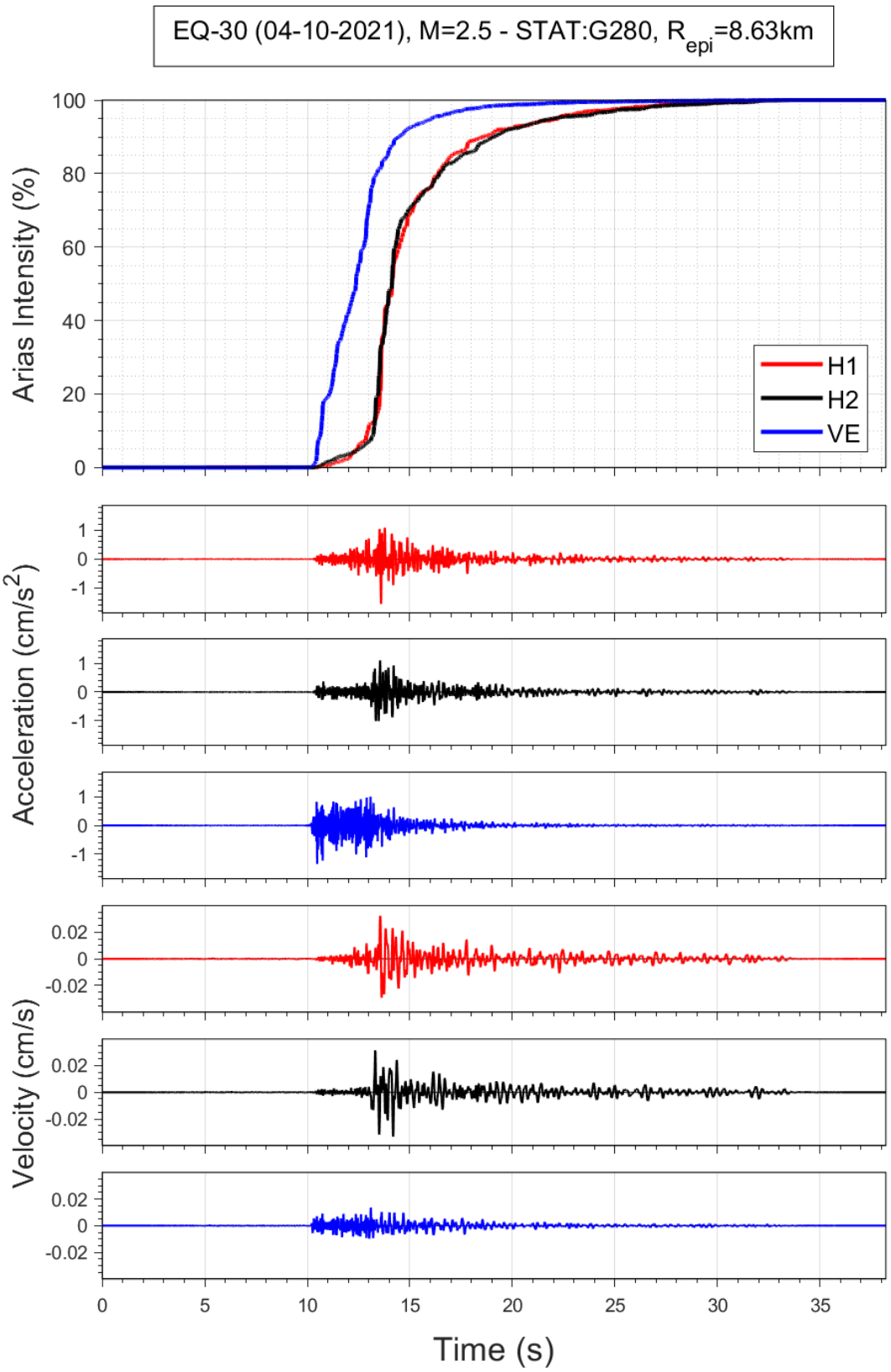
EQ-30 (04-10-2021), M=2.5 - STAT:G280, R epi =8.63km
Arias Intensity (%)
H1
H2
VE
Acceleration (cm/s2)
Velocity (cm/s)
Time (s)

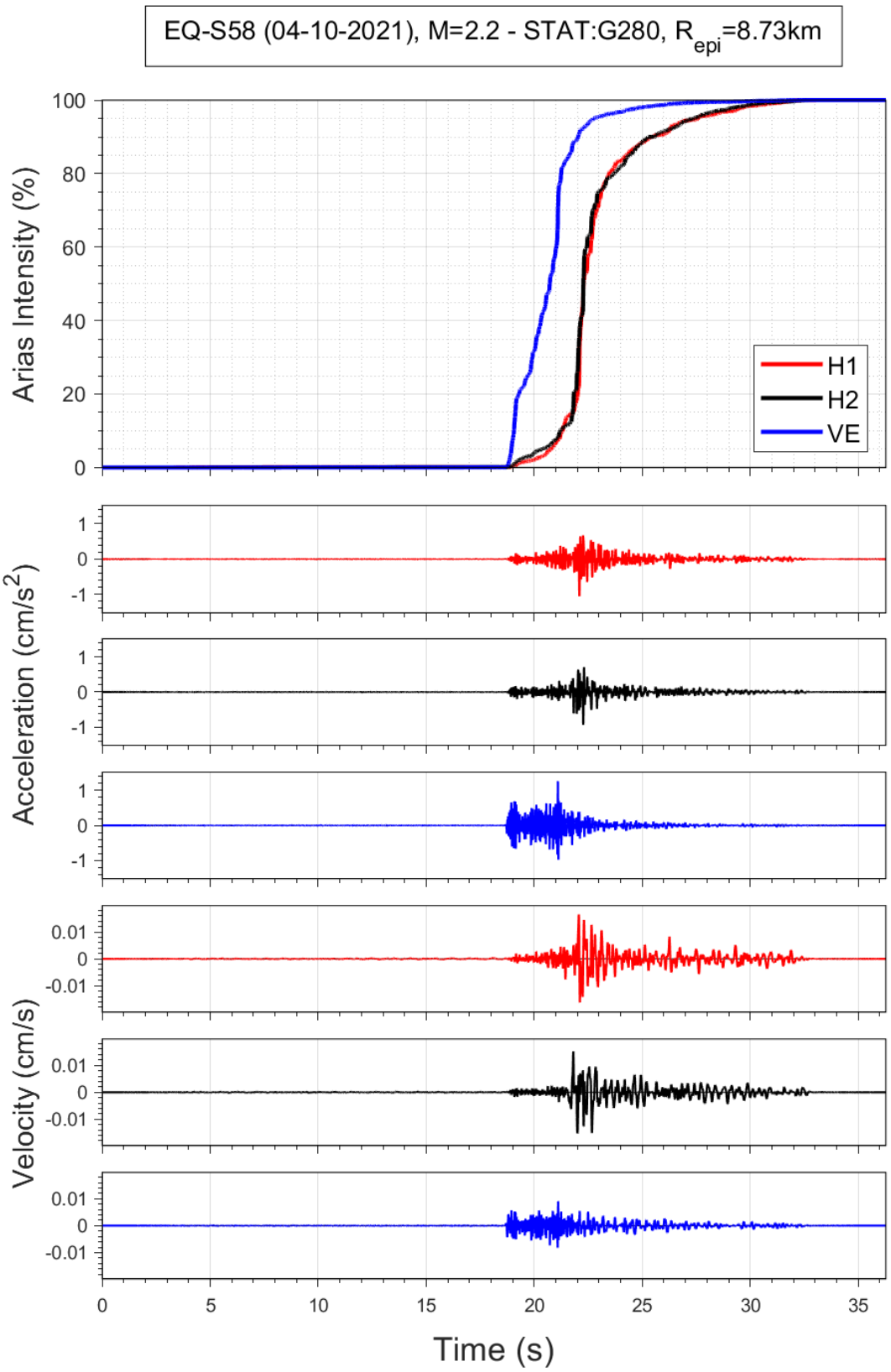
EQ-S58 (04-10-2021), M=2.2 - STAT:G280, R epi =8.73km
Arias Intensity (%)
H1
H2
VE
Acceleration (cm/s2)
Velocity (cm/s)
Time (s)

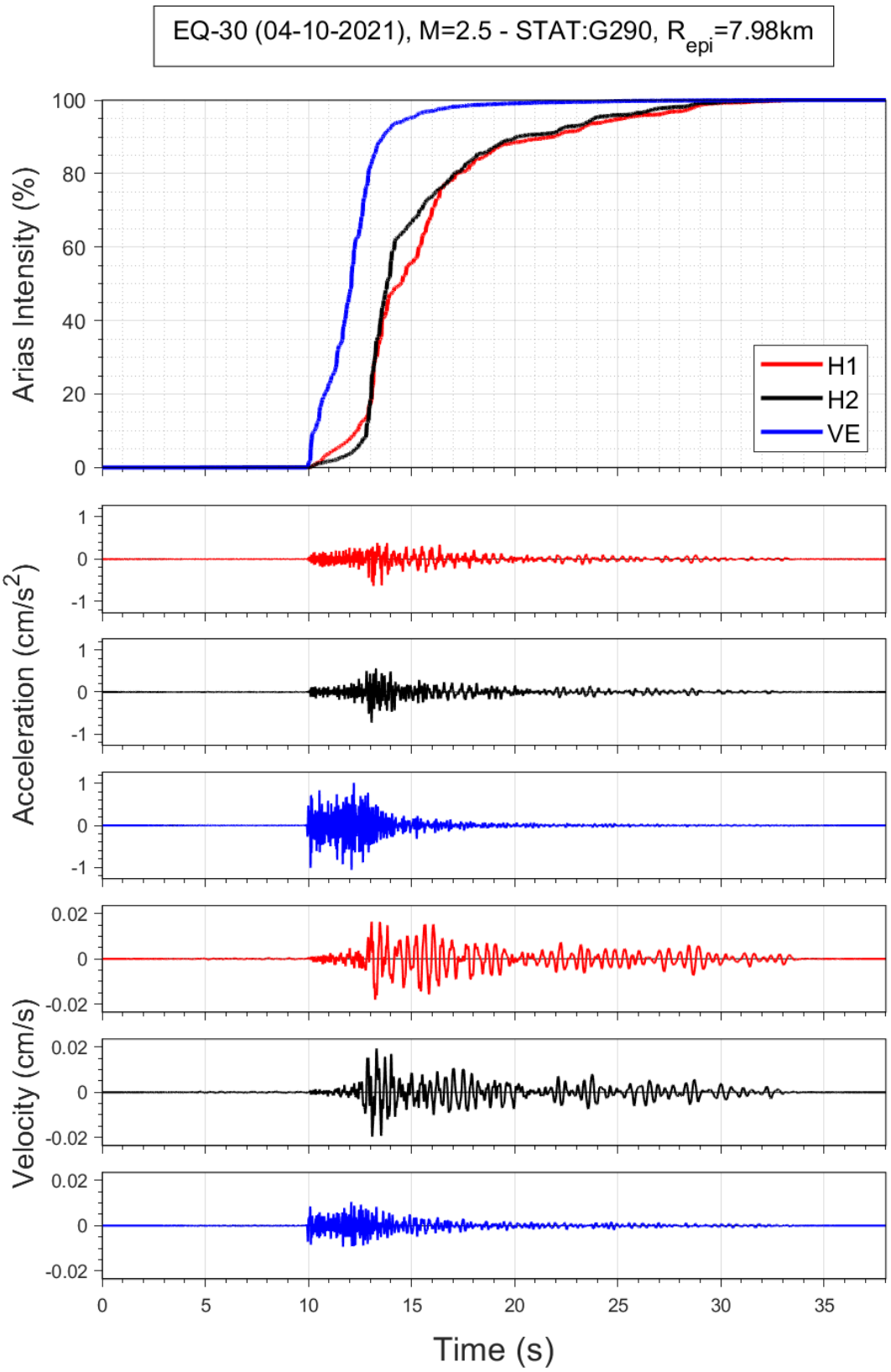
EQ-30 (04-10-2021), M=2.5 - STAT:G290, R epi =7.98km
Arias Intensity (%)
H1
H2
VE
Acceleration (cm/s2)
Velocity (cm/s)
Time (s)

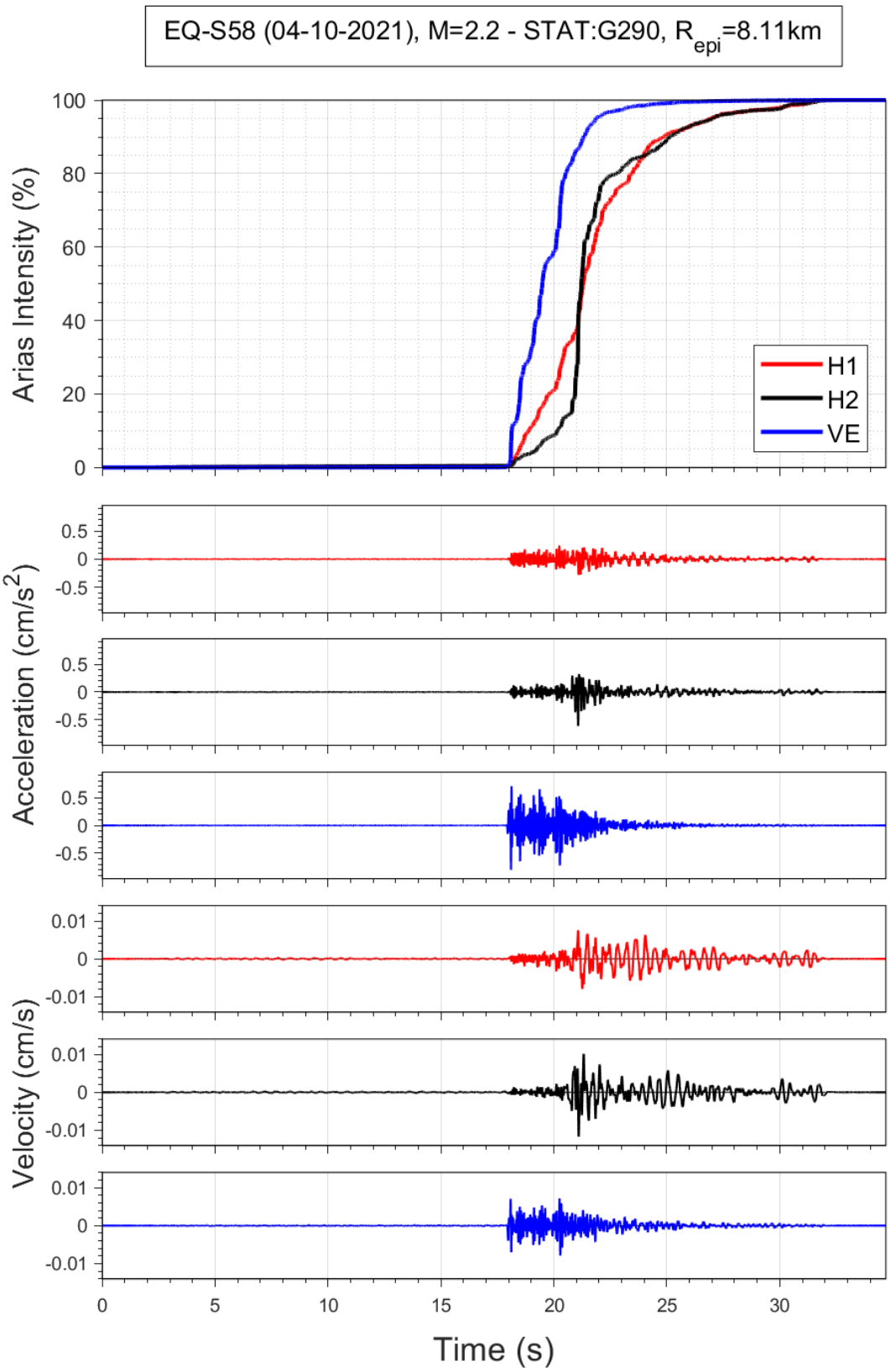
EQ-S58 (04-10-2021), M=2.2 - STAT:G290, R epi =8.11km
Arias Intensity (%)
100
80
60
40
20
0
H1
H2
VE
Acceleration (cm/s2)
0.5
0
-0.5
Velocity (cm/s)
0.01
0
-0.01
0
5
10
15
20
25
30
Time (s)

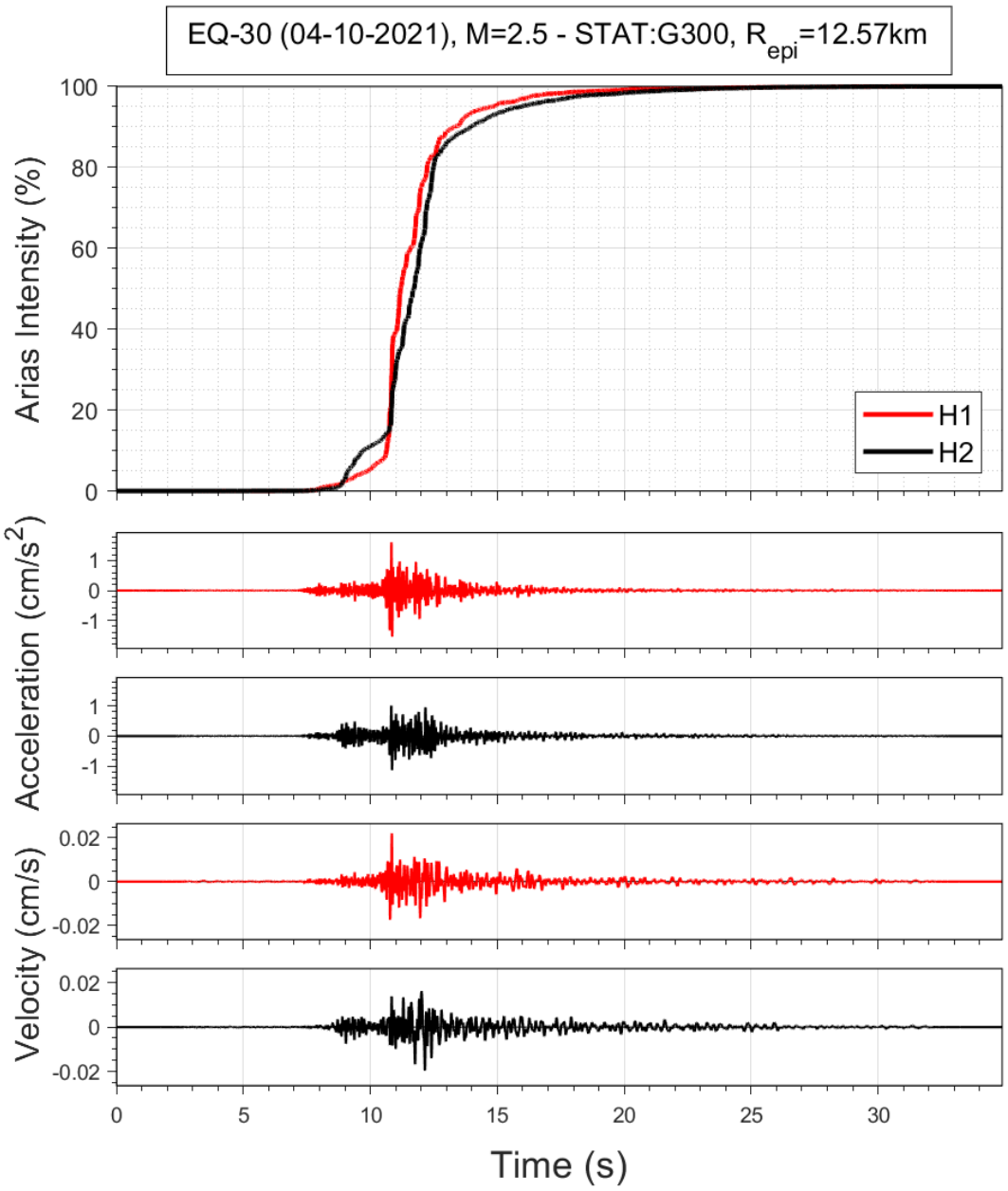
EQ-30 (04-10-2021), M=2.5 - STAT:G300, R epi =12.57km
Arias Intensity (%)
100
80
60
40
20
0
H1
H2
Acceleration (cm/s2)
1
0
-1
1
0
-1
Velocity (cm/s)
0.02
0
-0.02
0.02
0
-0.02
0
5
10
15
20
25
30
Time (s)

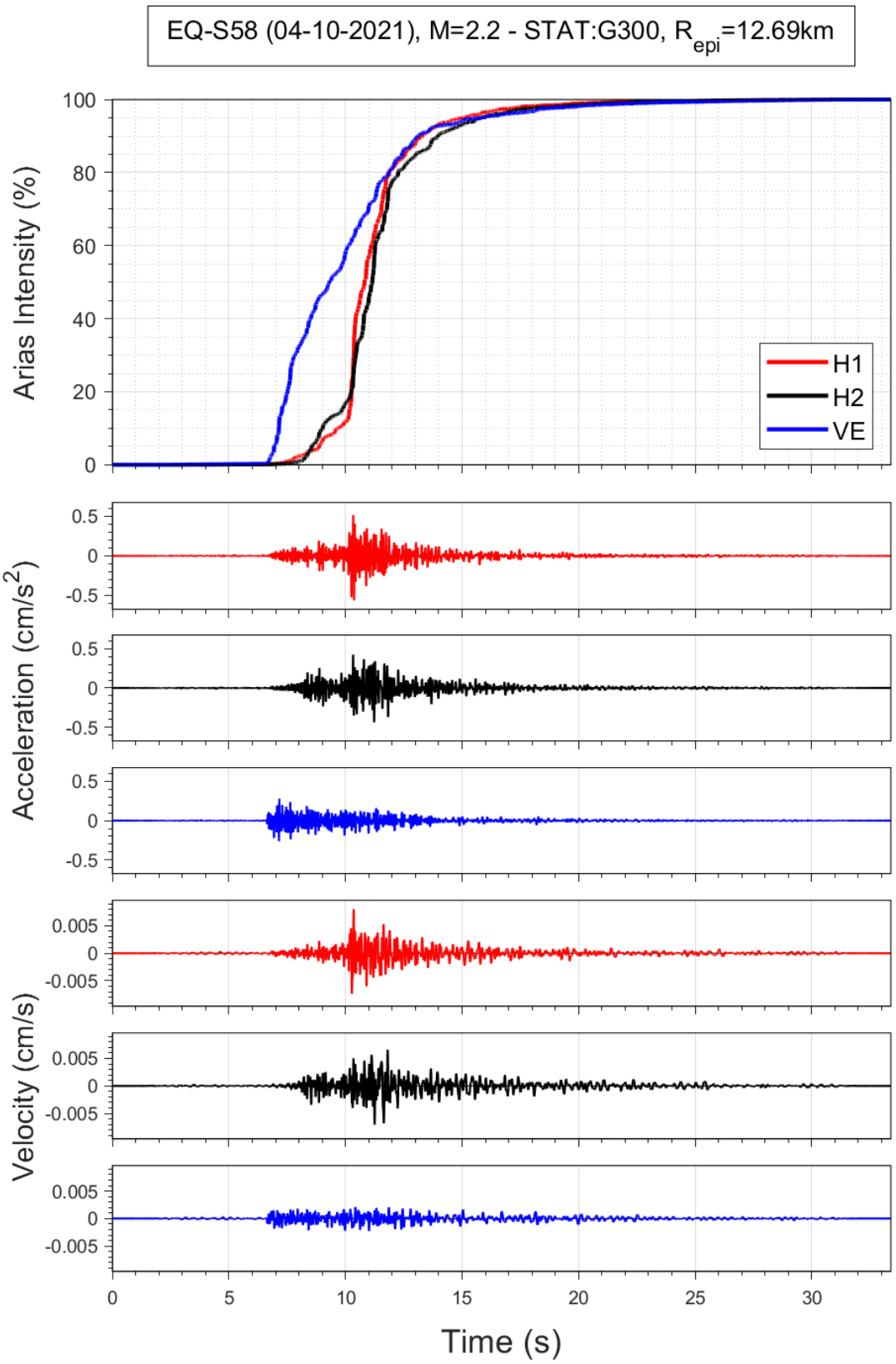
EQ-S58 (04-10-2021), M=2.2 - STAT:G300, R epi =12.69km
Arias Intensity (%)
100
80
60
40
20
0
H1
H2
VE
Acceleration (cm/s2)
0.5
0
-0.5
Velocity (cm/s)
0.005
0
-0.005
0
5
10
15
20
25
30
Time (s)

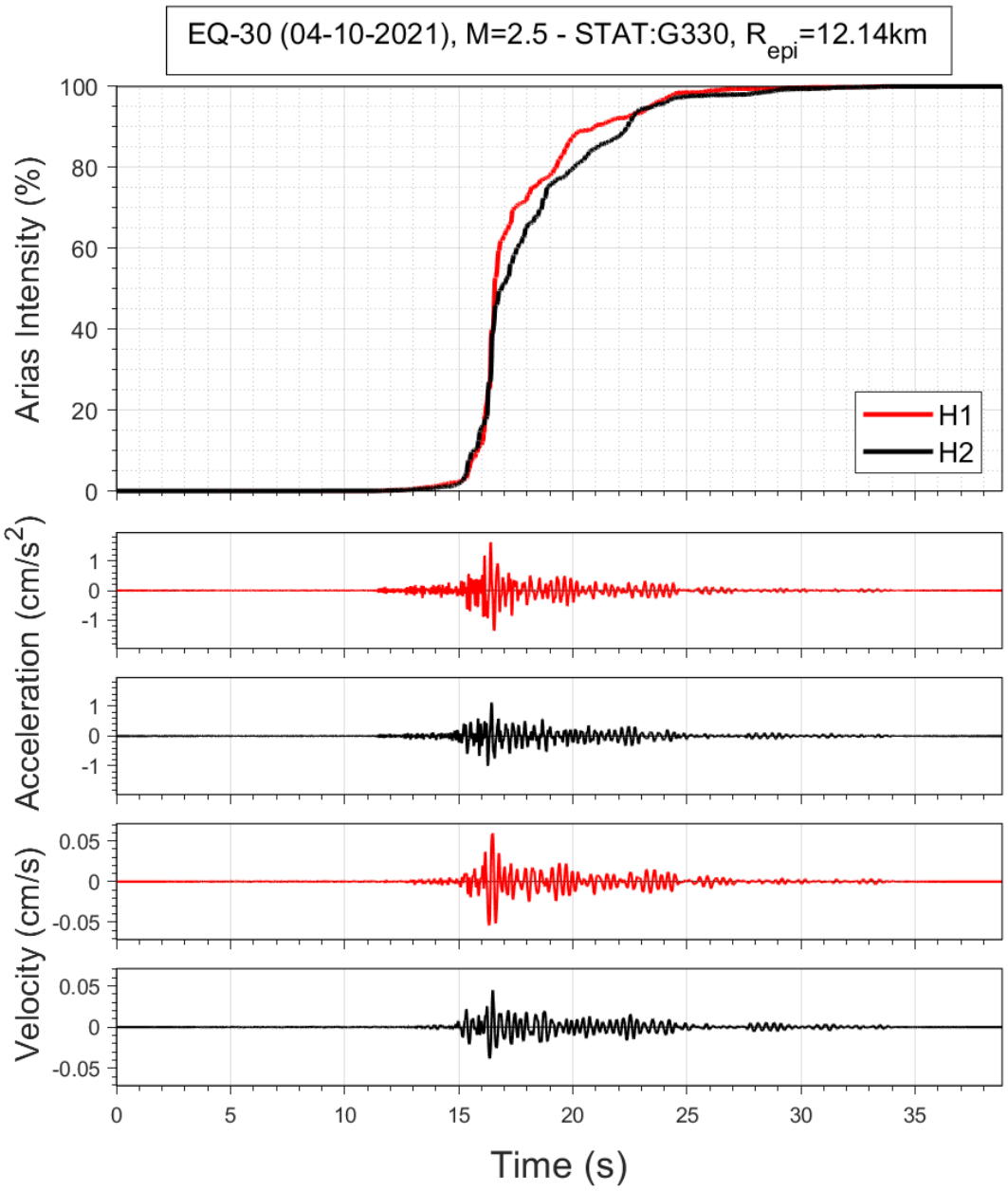
EQ-30 (04-10-2021), M=2.5 - STAT:G330, R epi =12.14km
Arias Intensity (%)
100
80
60
40
20
0
H1
H2
Acceleration (cm/s2)
1
0
-1
1
0
-1
Velocity (cm/s)
0.05
0
-0.05
0.05
0
-0.05
0
5
10
15
20
25
30
35
Time (s)

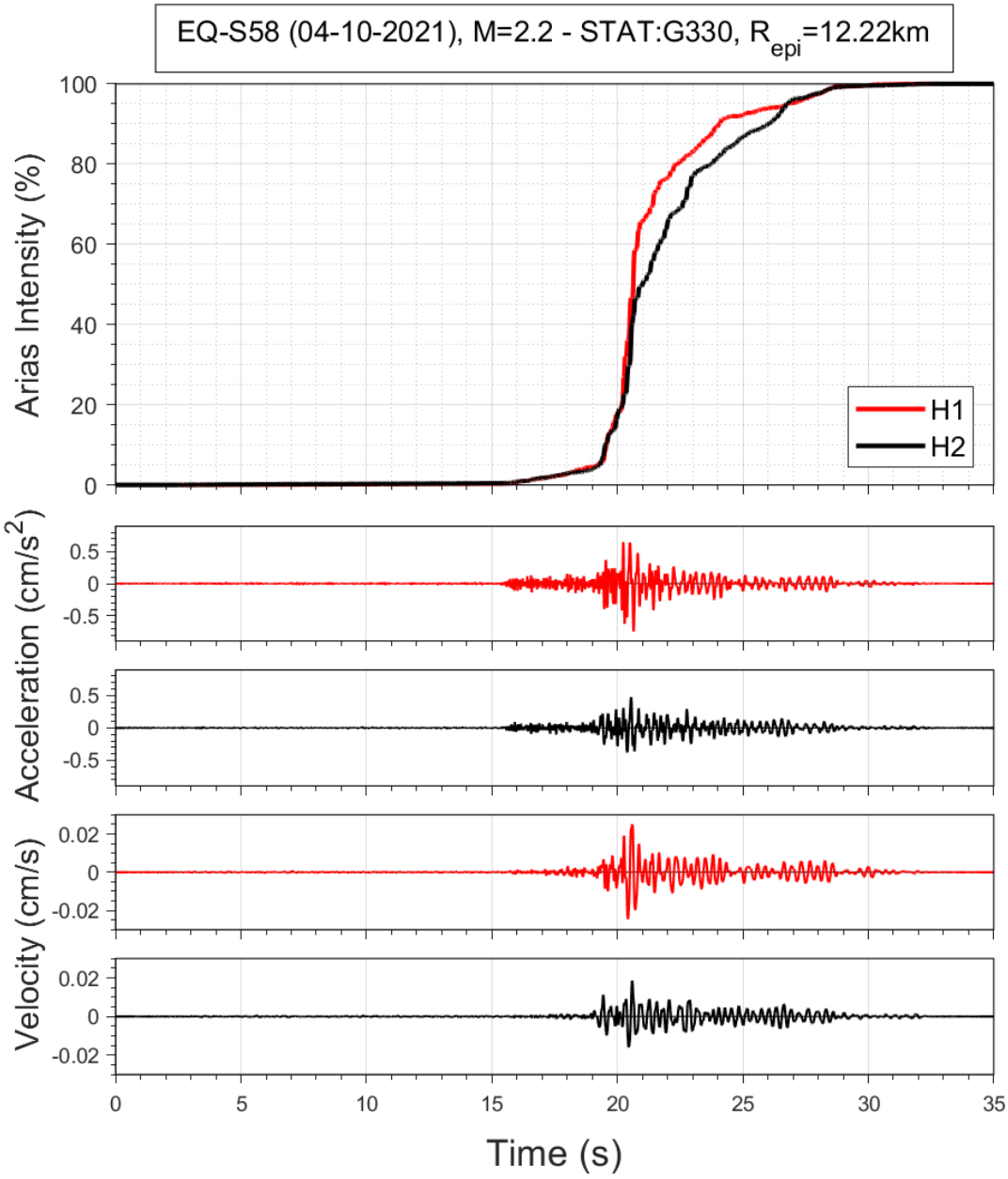
EQ-S58 (04-10-2021), M=2.2 - STAT:G330, R epi =12.22km
Arias Intensity (%)
100
80
60
40
20
0
H1
H2
Acceleration (cm/s2)
0.5
0
-0.5
0.5
0
-0.5
Velocity (cm/s)
0.02
0
-0.02
0.02
0
-0.02
0
5
10
15
20
25
30
35
Time (s)

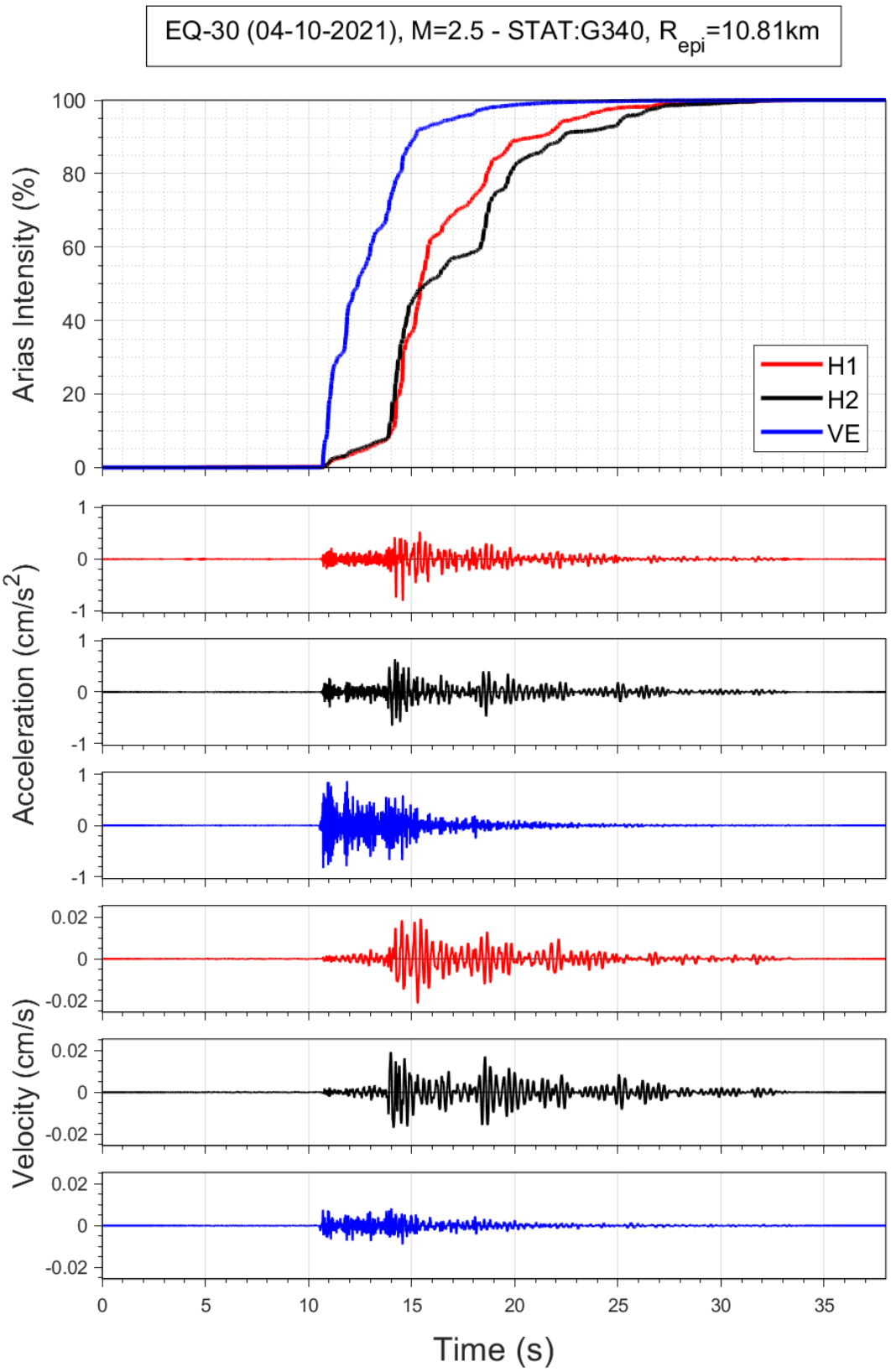
EQ-30 (04-10-2021), M=2.5 - STAT:G340, R epi =10.81km
Arias Intensity (%)
H1
H2
VE
Acceleration (cm/s2)
Velocity (cm/s)
Time (s)

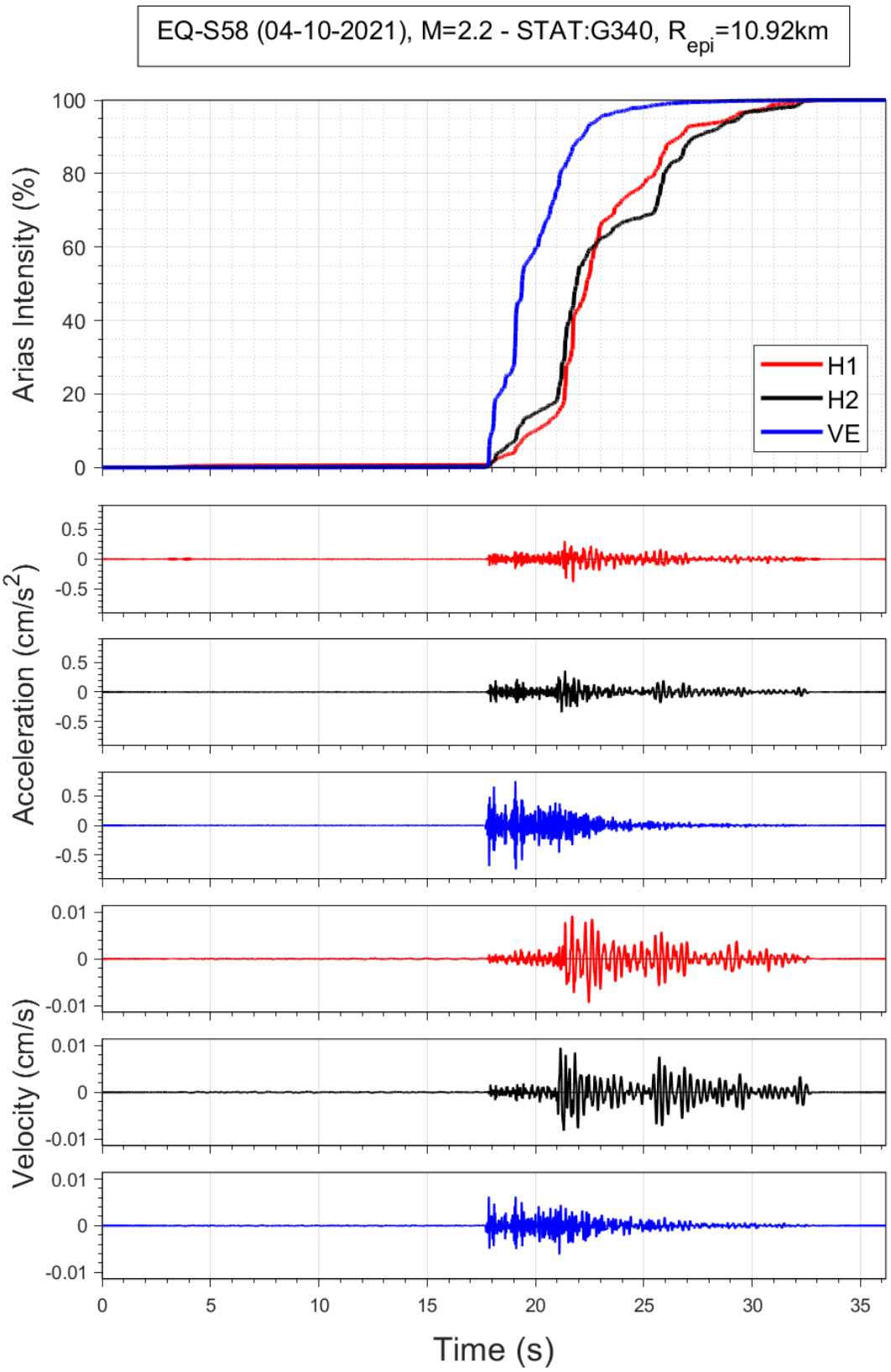
EQ-S58 (04-10-2021), M=2.2 - STAT:G340, R epi =10.92km
Arias Intensity (%)
H1
H2
VE
Acceleration (cm/s2)
Velocity (cm/s)
Time (s)

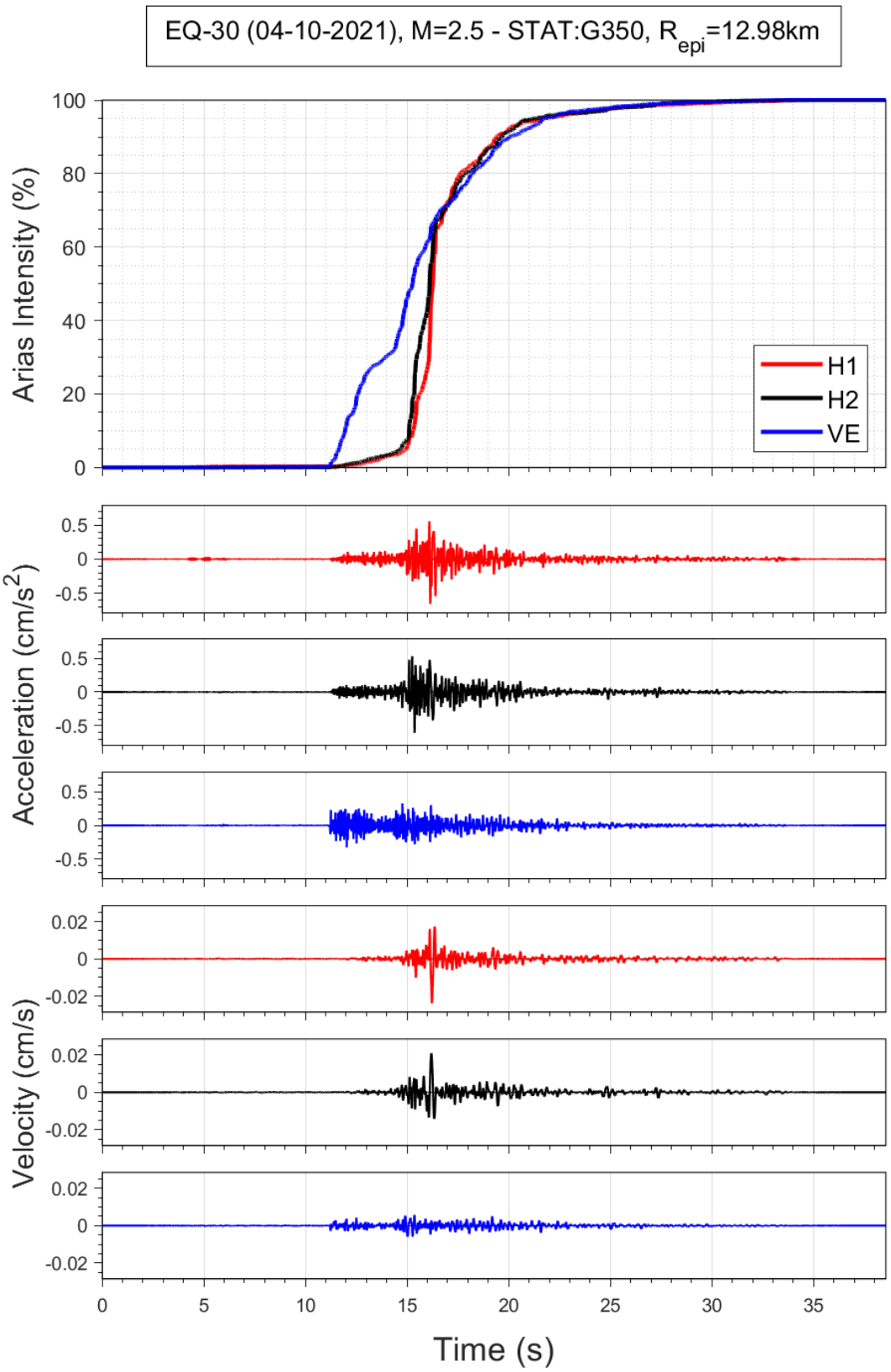
EQ-30 (04-10-2021), M=2.5 - STAT:G350, R epi =12.98km
Arias Intensity (%)
H1
H2
VE
Acceleration (cm/s2)
Velocity (cm/s)
Time (s)

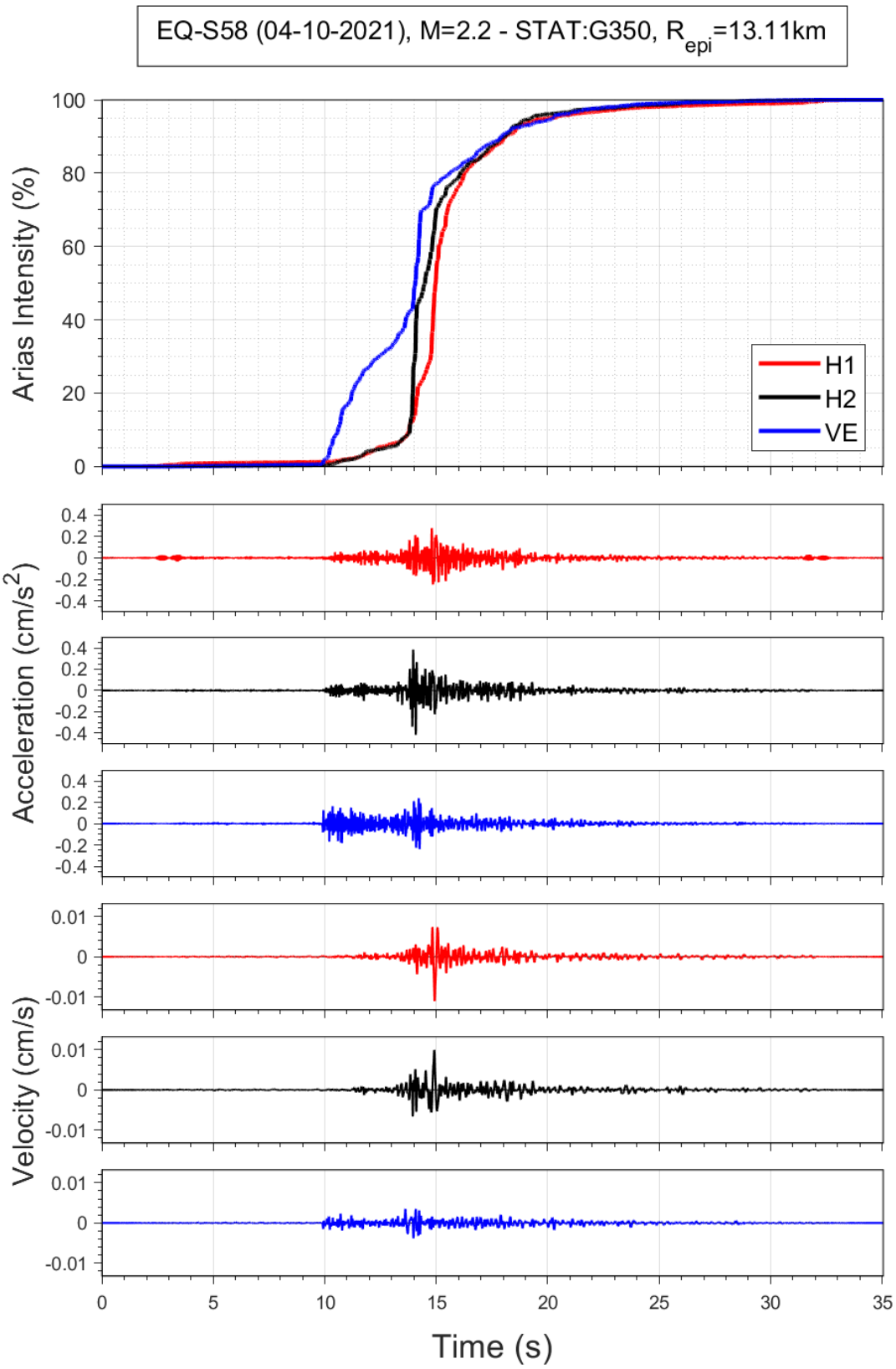
EQ-S58 (04-10-2021), M=2.2 - STAT:G350, R epi =13.11km
Arias Intensity (%)
H1
H2
VE
Acceleration (cm/s2)
Velocity (cm/s)
Time (s)

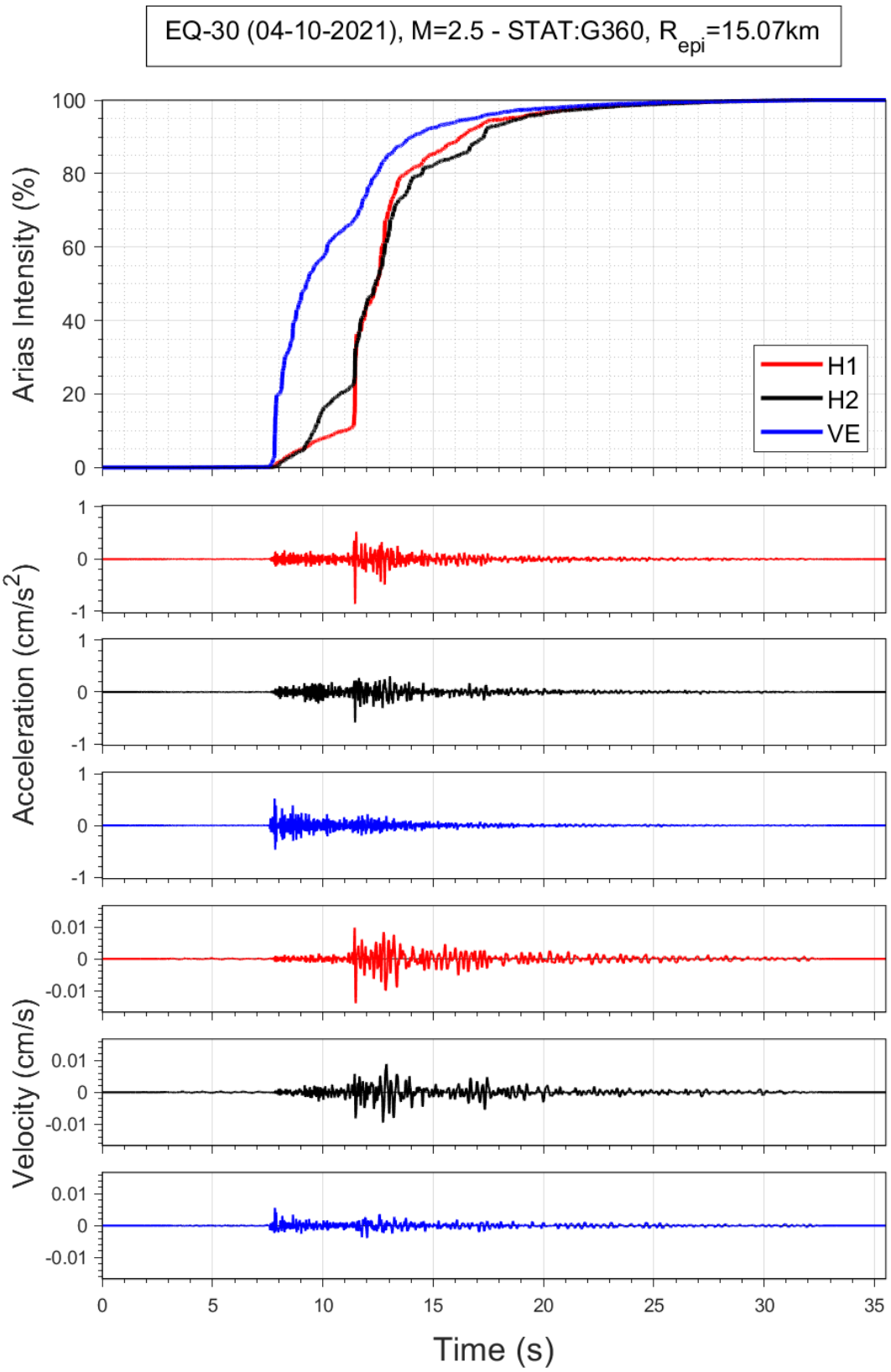
EQ-30 (04-10-2021), M=2.5 - STAT:G360, R_epi=15.07km
Arias Intensity (%)
H1
H2
VE
Acceleration (cm/s²)
Velocity (cm/s)
Time (s)

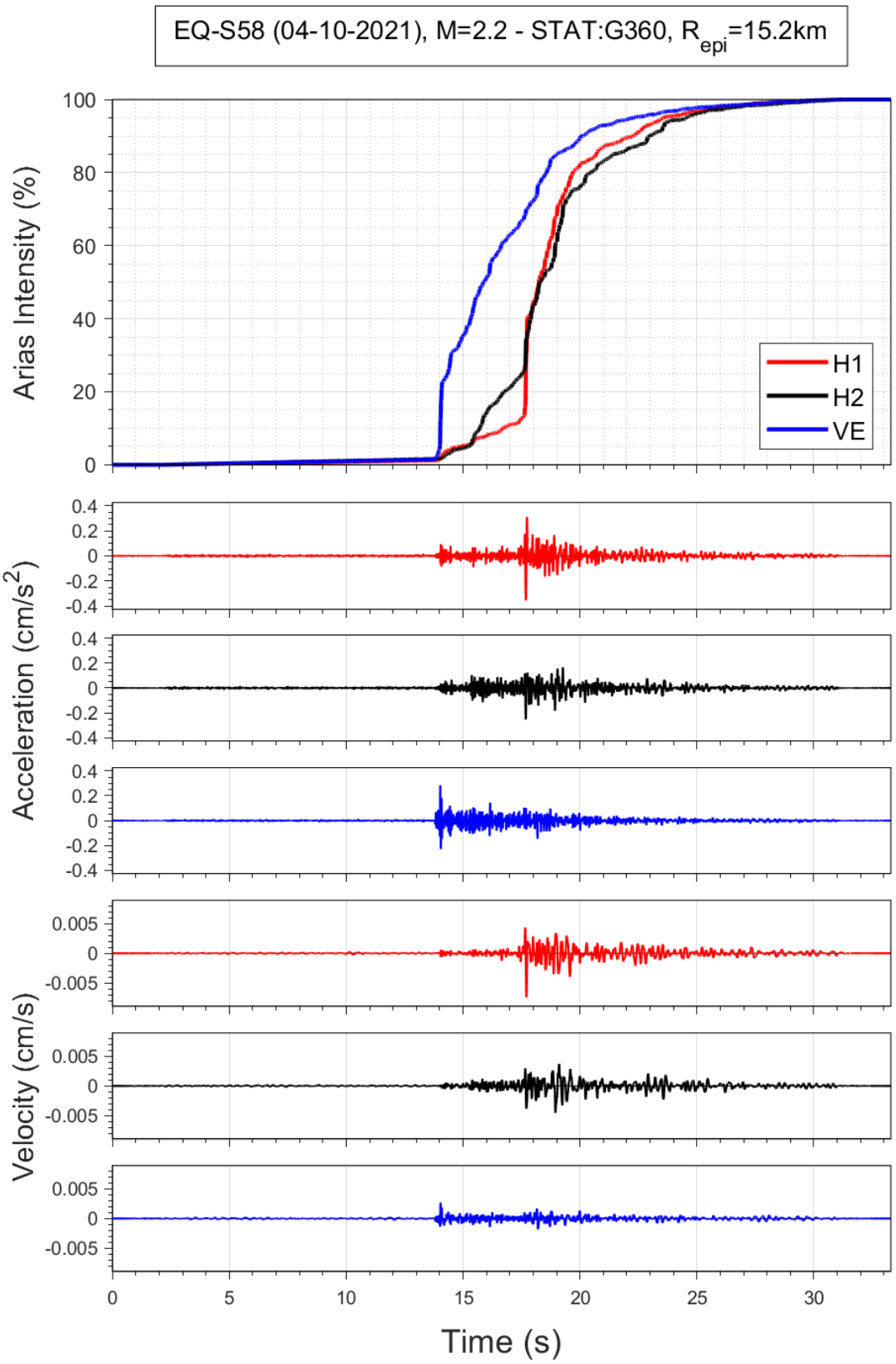
EQ-S58 (04-10-2021), M=2.2 - STAT:G360, R epi =15.2km
Arias Intensity (%)
H1
H2
VE
Acceleration (cm/s2)
Velocity (cm/s)
Time (s)

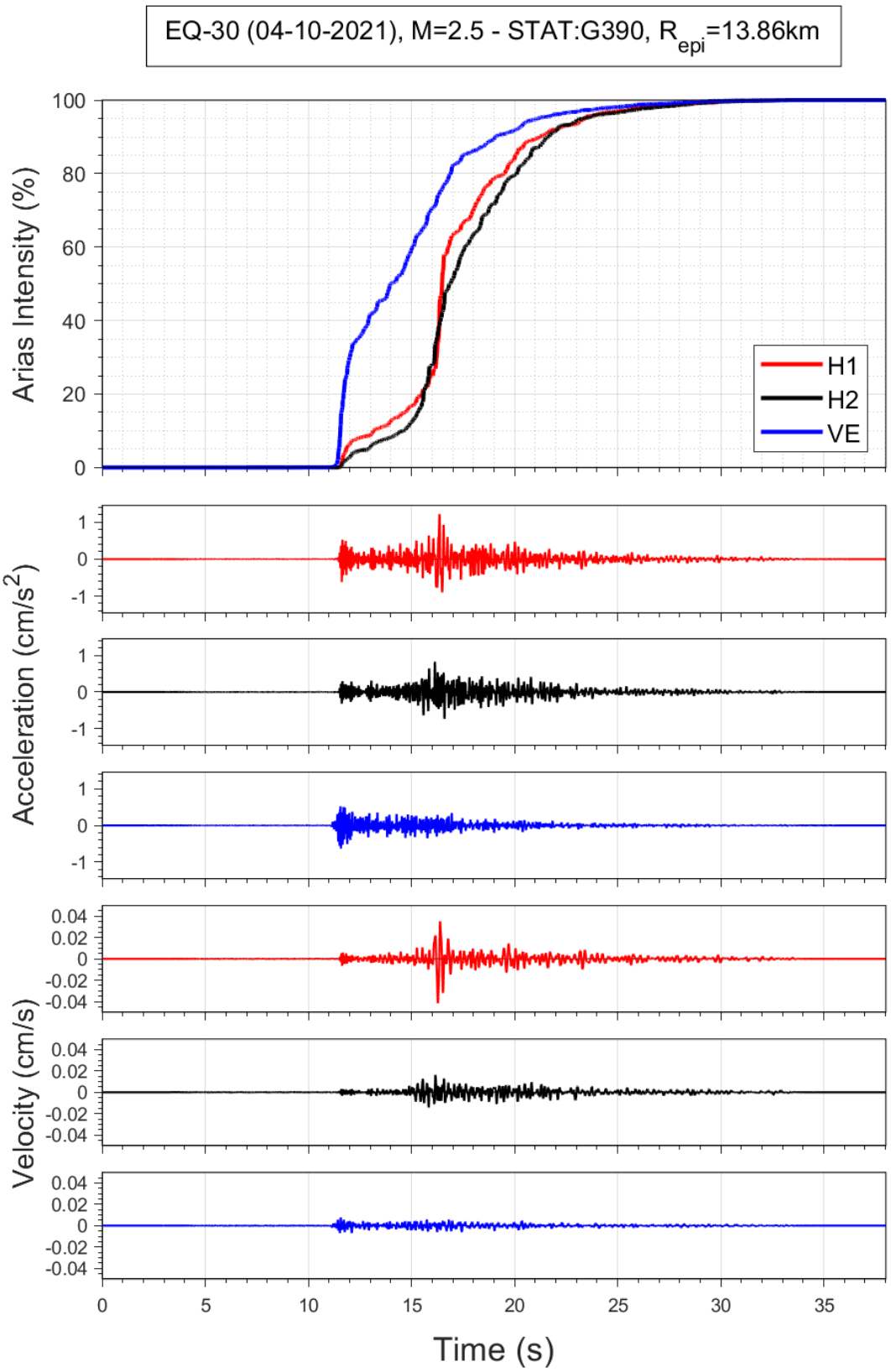
EQ-30 (04-10-2021), M=2.5 - STAT:G390, R epi =13.86km
Arias Intensity (%)
H1
H2
VE
Acceleration (cm/s2)
Velocity (cm/s)
Time (s)

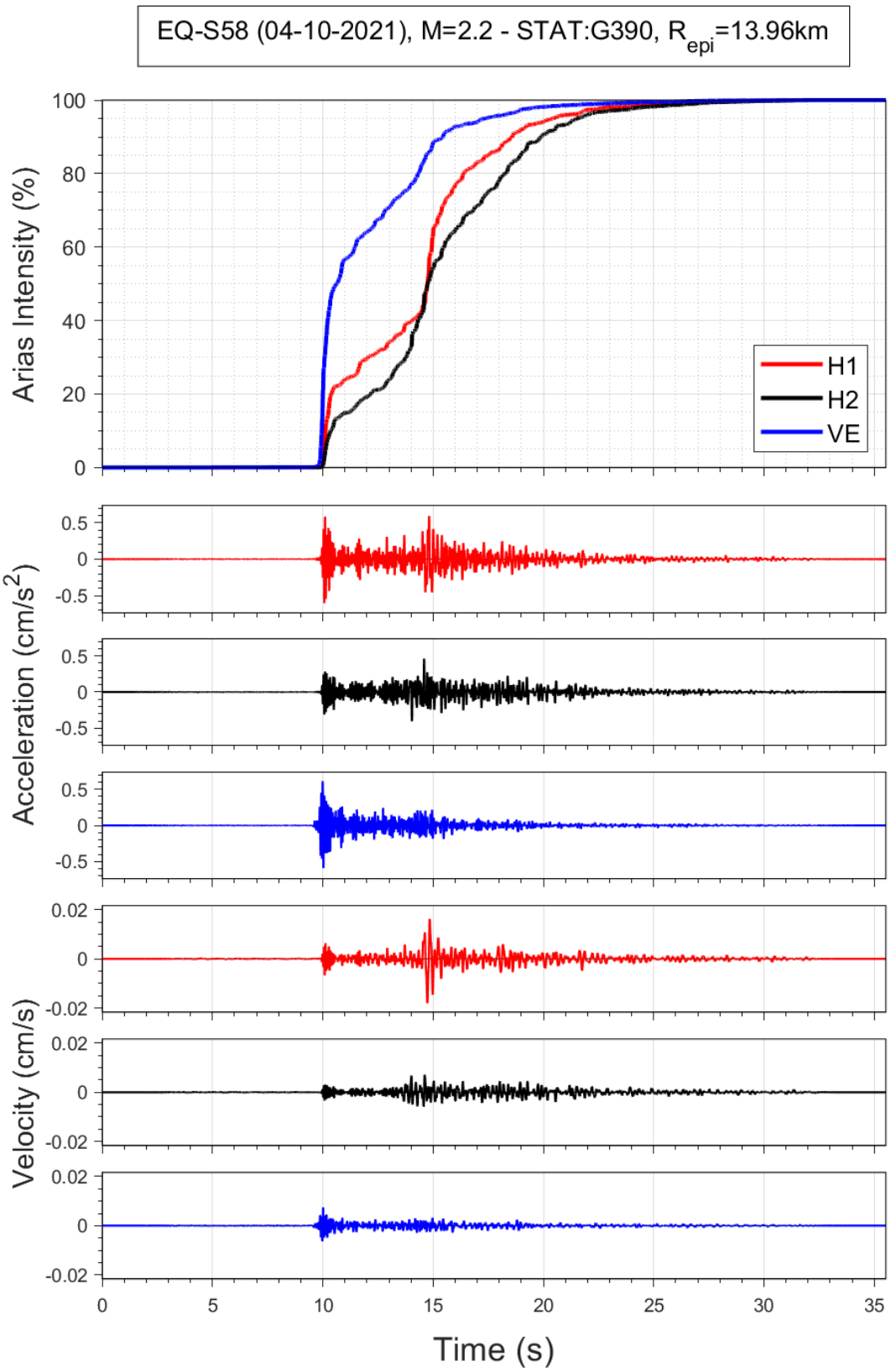
EQ-S58 (04-10-2021), M=2.2 - STAT:G390, R epi =13.96km
Arias Intensity (%)
H1
H2
VE
Acceleration (cm/s2)
Velocity (cm/s)
Time (s)

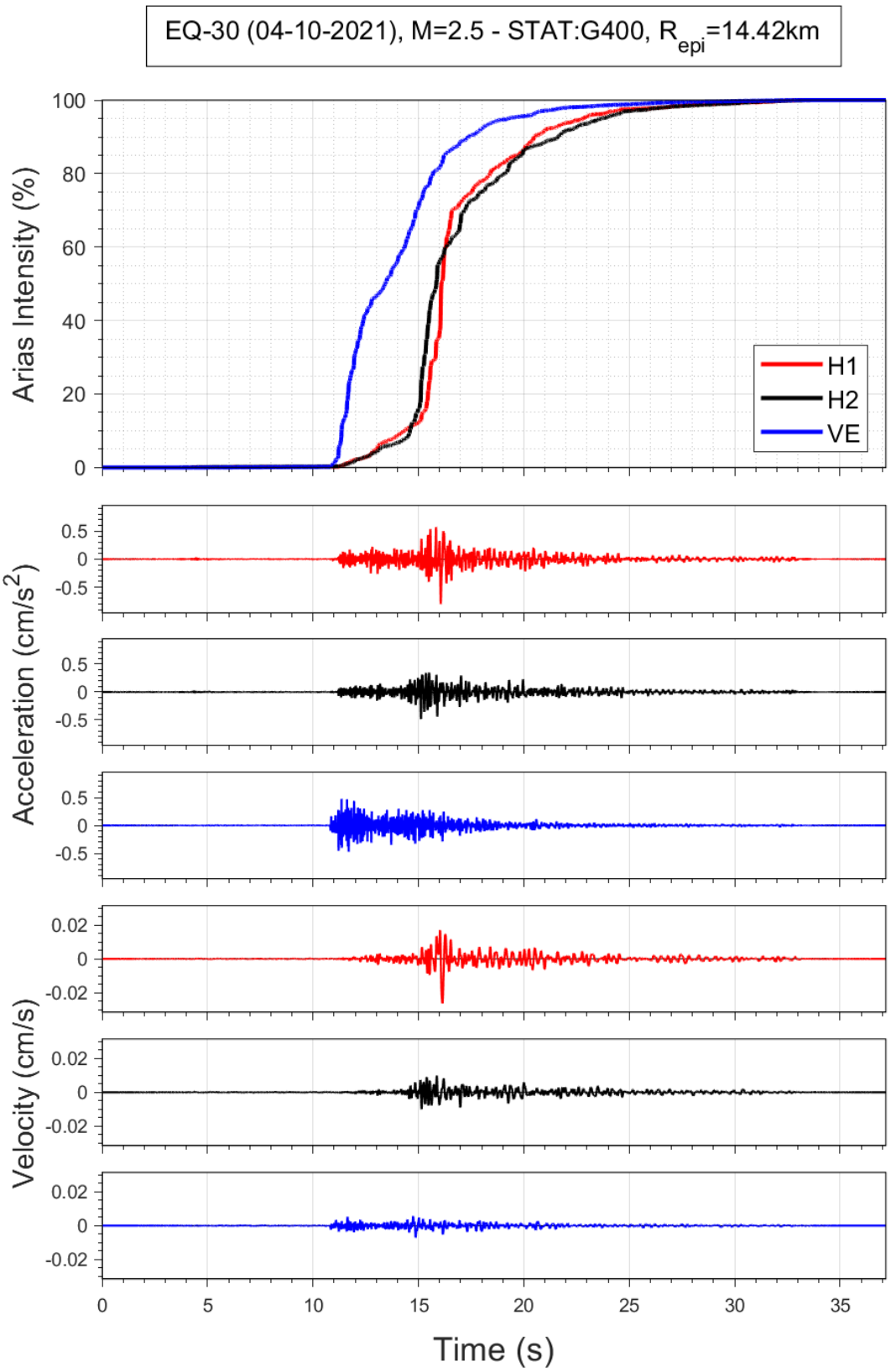
EQ-30 (04-10-2021), M=2.5 - STAT:G400, R epi =14.42km
Arias Intensity (%)
H1
H2
VE
Acceleration (cm/s2)
Velocity (cm/s)
Time (s)

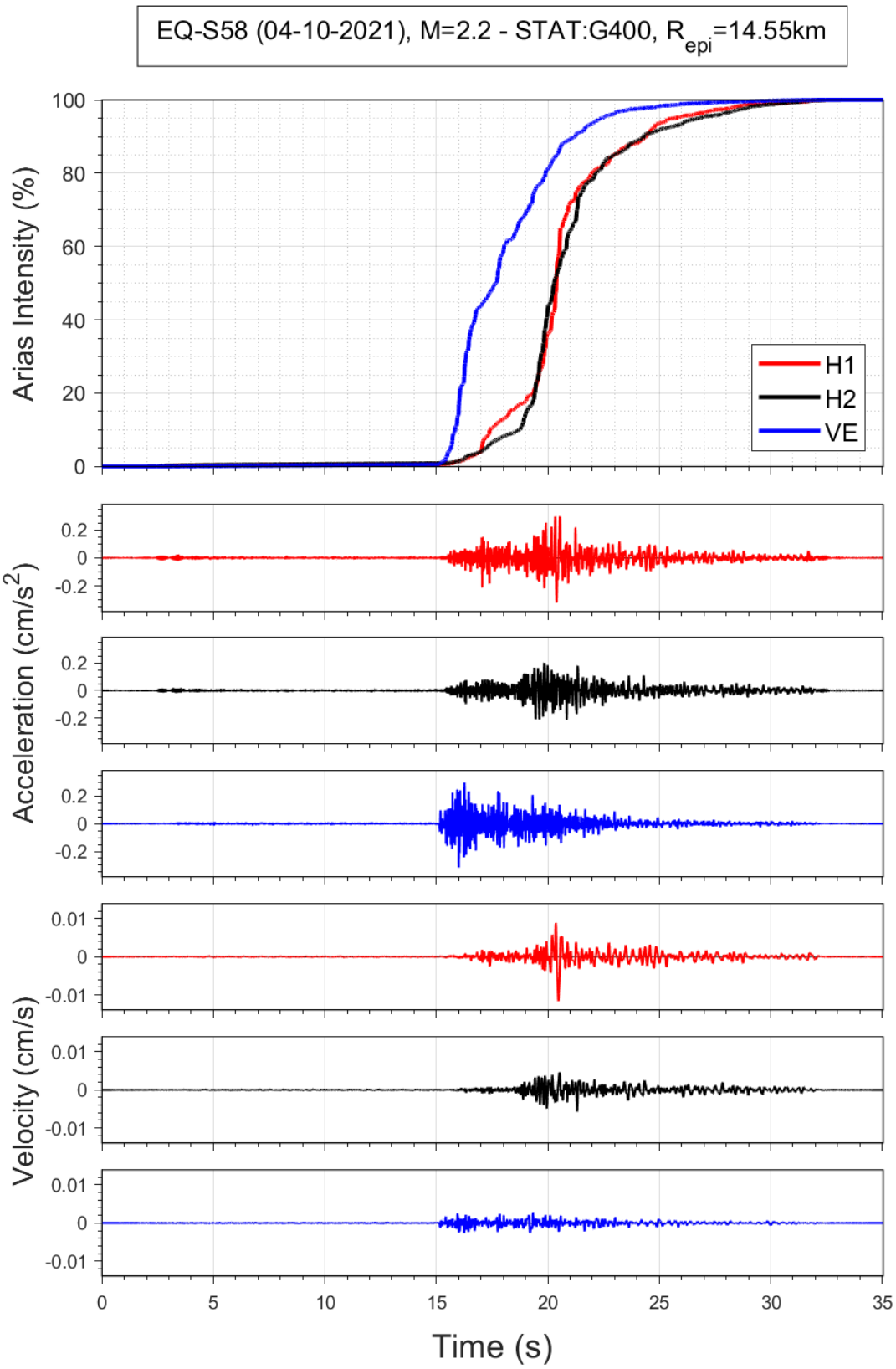
EQ-S58 (04-10-2021), M=2.2 - STAT:G400, R epi =14.55km
Arias Intensity (%)
H1
H2
VE
Acceleration (cm/s2)
Velocity (cm/s)
Time (s)

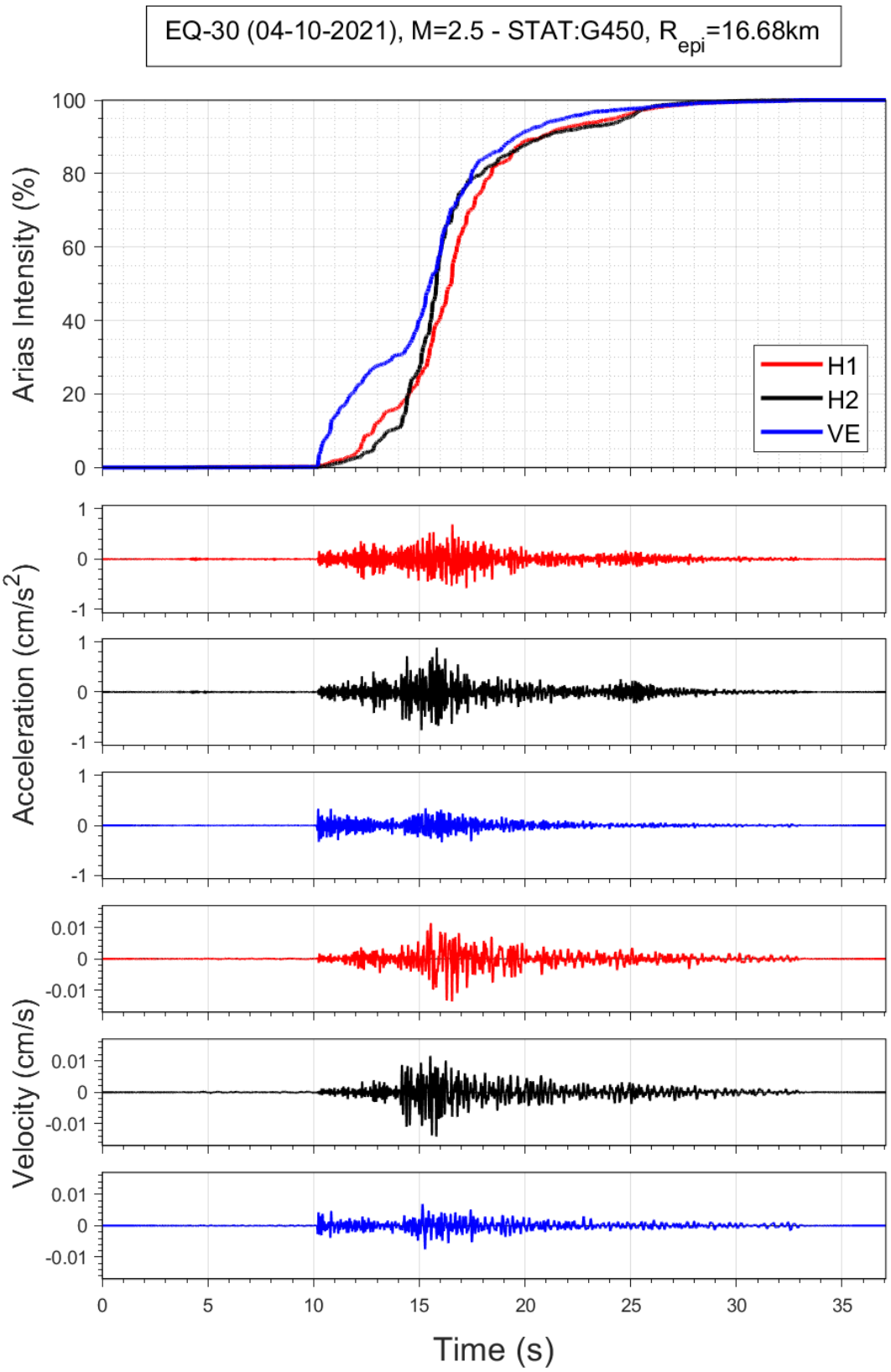
EQ-30 (04-10-2021), M=2.5 - STAT:G450, R epi =16.68km
Arias Intensity (%)
H1
H2
VE
Acceleration (cm/s2)
Velocity (cm/s)
Time (s)

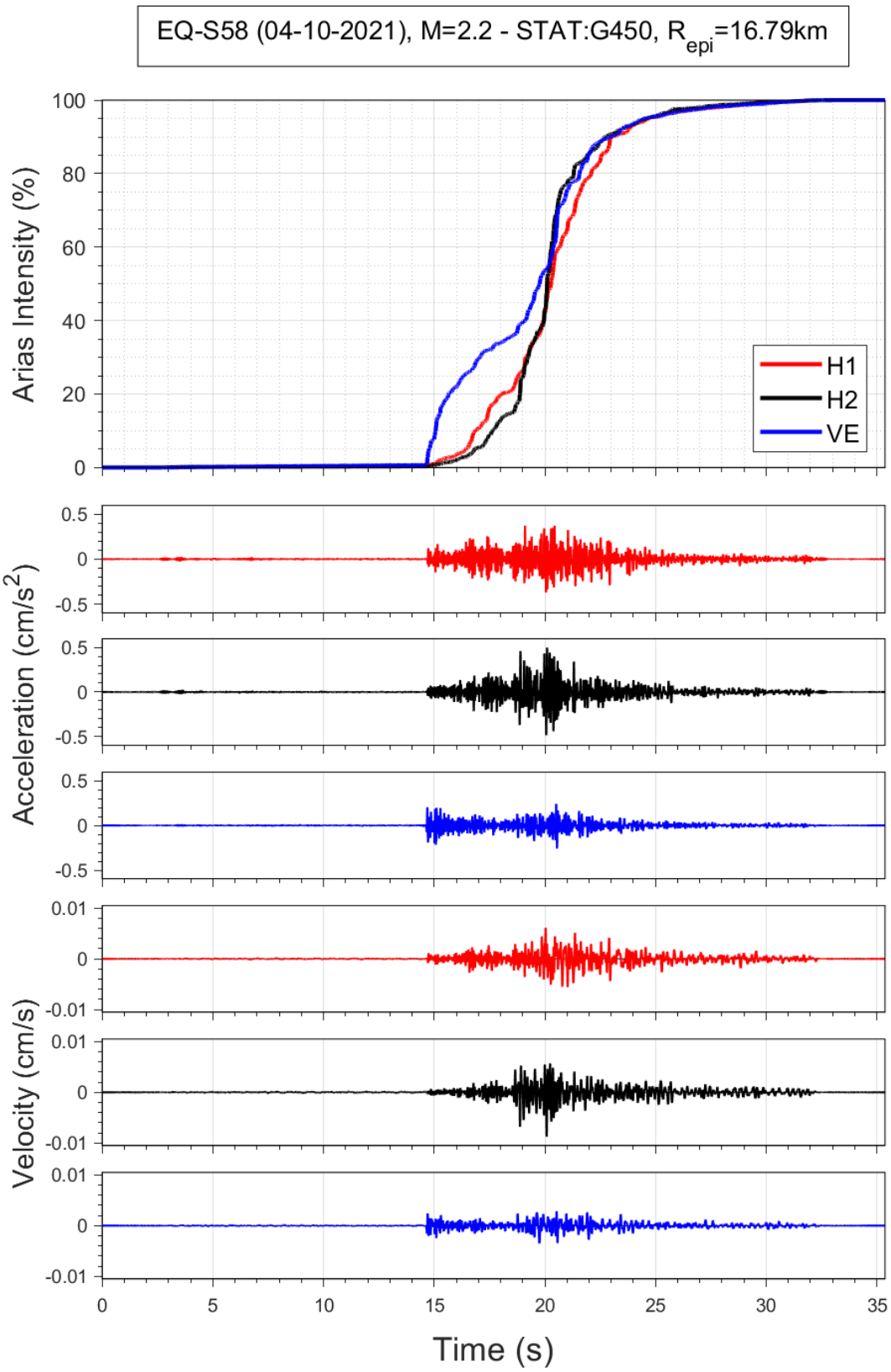
EQ-S58 (04-10-2021), M=2.2 - STAT:G450, R epi =16.79km
Arias Intensity (%)
H1
H2
VE
Acceleration (cm/s2)
Velocity (cm/s)
Time (s)

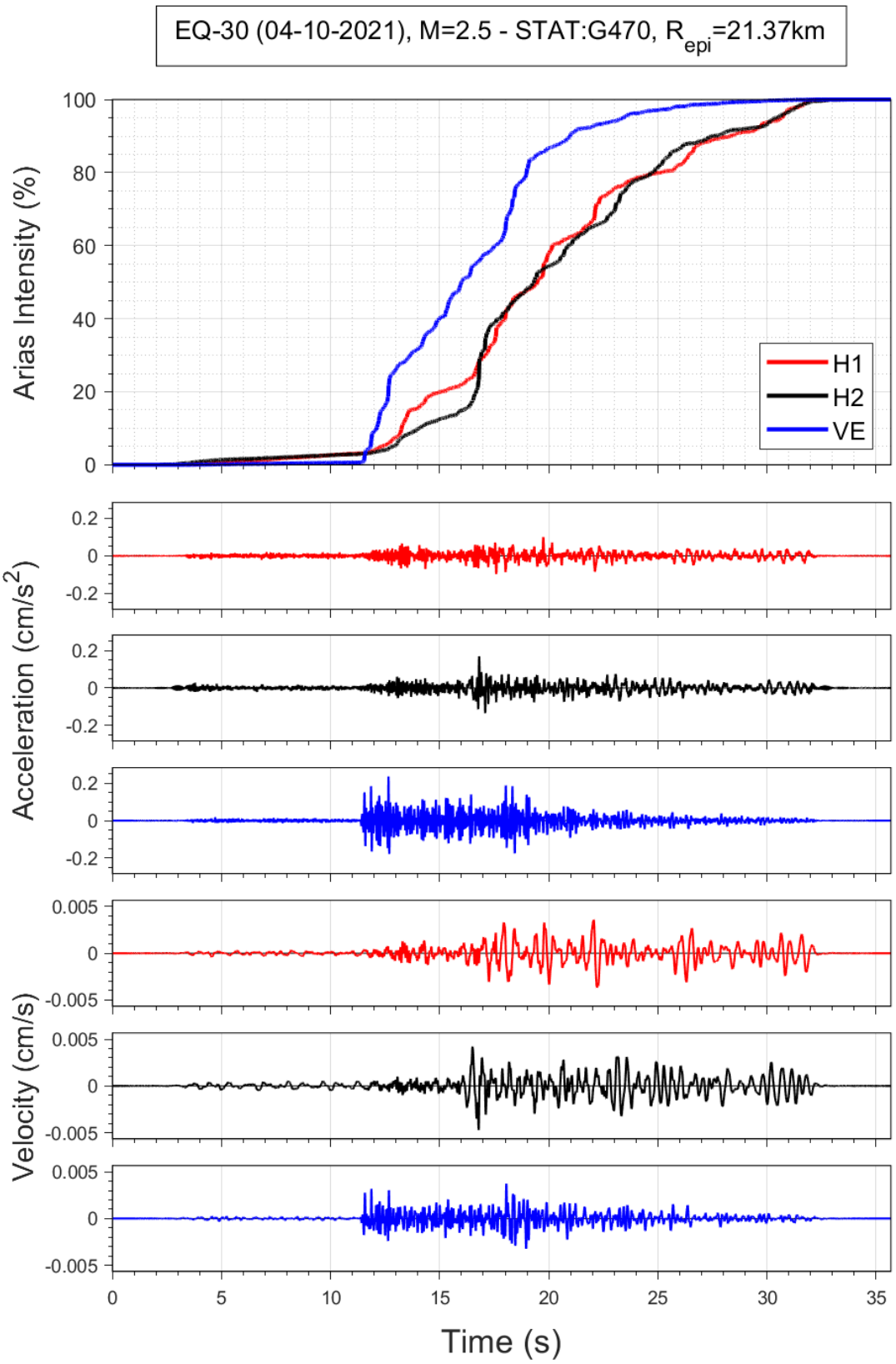
EQ-30 (04-10-2021), M=2.5 - STAT:G470, R_epi=21.37km
Arias Intensity (%)
Acceleration (cm/s²)
Velocity (cm/s)
Time (s)
H1
H2
VE

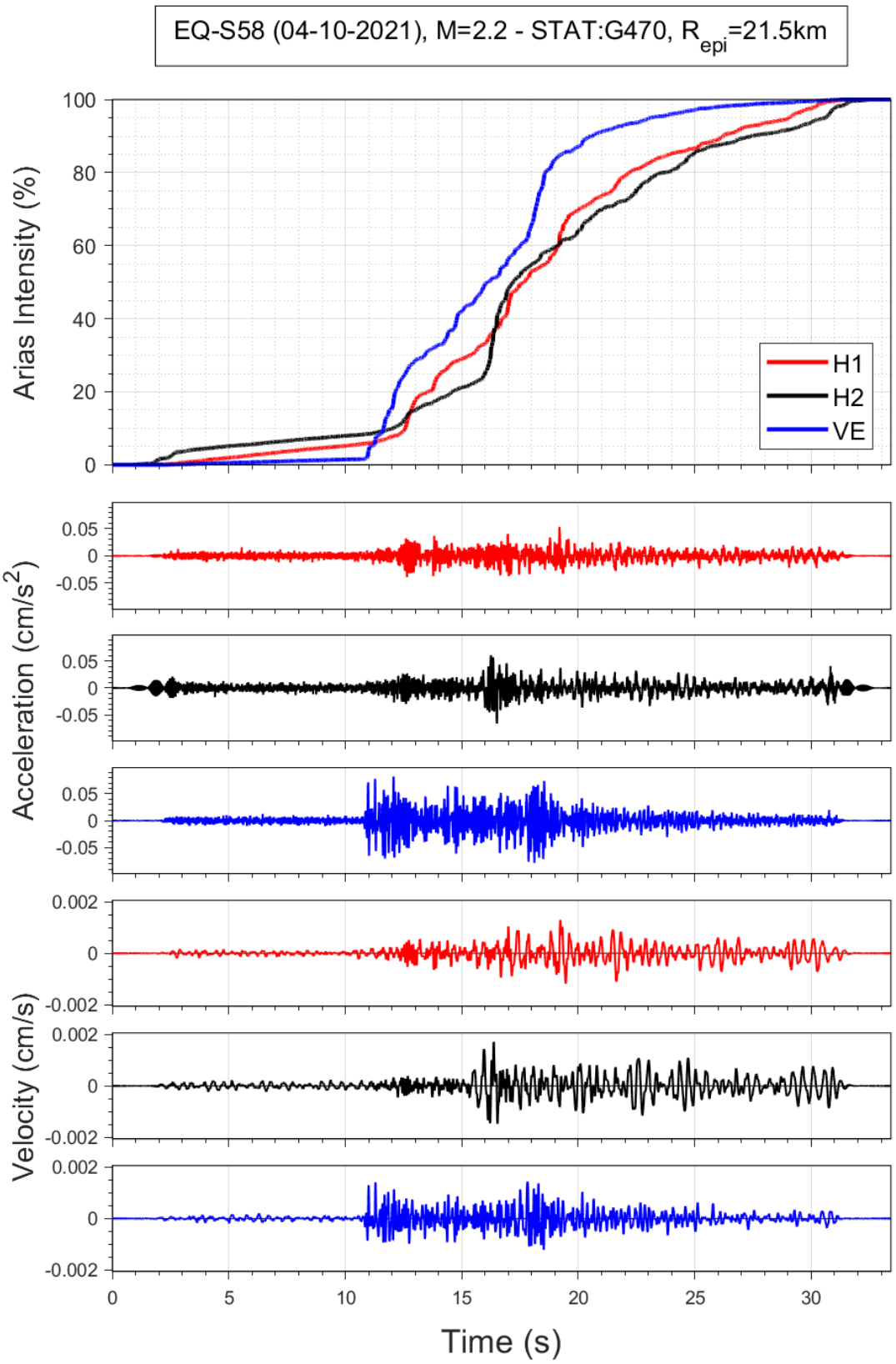
EQ-S58 (04-10-2021), M=2.2 - STAT:G470, R epi =21.5km
Arias Intensity (%)
100
80
60
40
20
0
H1
H2
VE
Acceleration (cm/s2)
0.05
0
-0.05
Velocity (cm/s)
0.002
0
-0.002
0
5
10
15
20
25
30
Time (s)

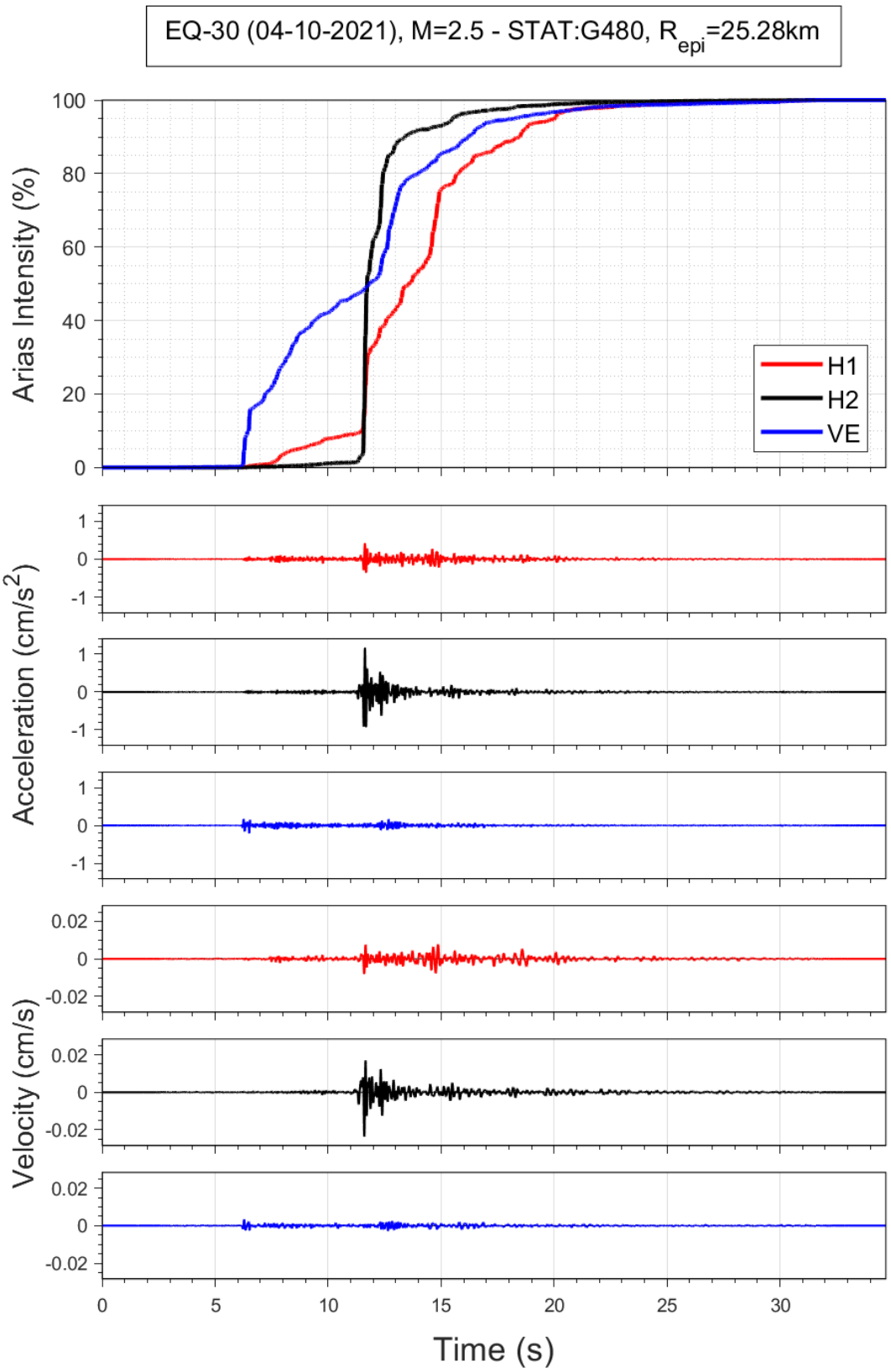
EQ-30 (04-10-2021), M=2.5 - STAT:G480, R_epi=25.28km
Arias Intensity (%)
Acceleration (cm/s²)
Velocity (cm/s)
H1
H2
VE
Time (s)

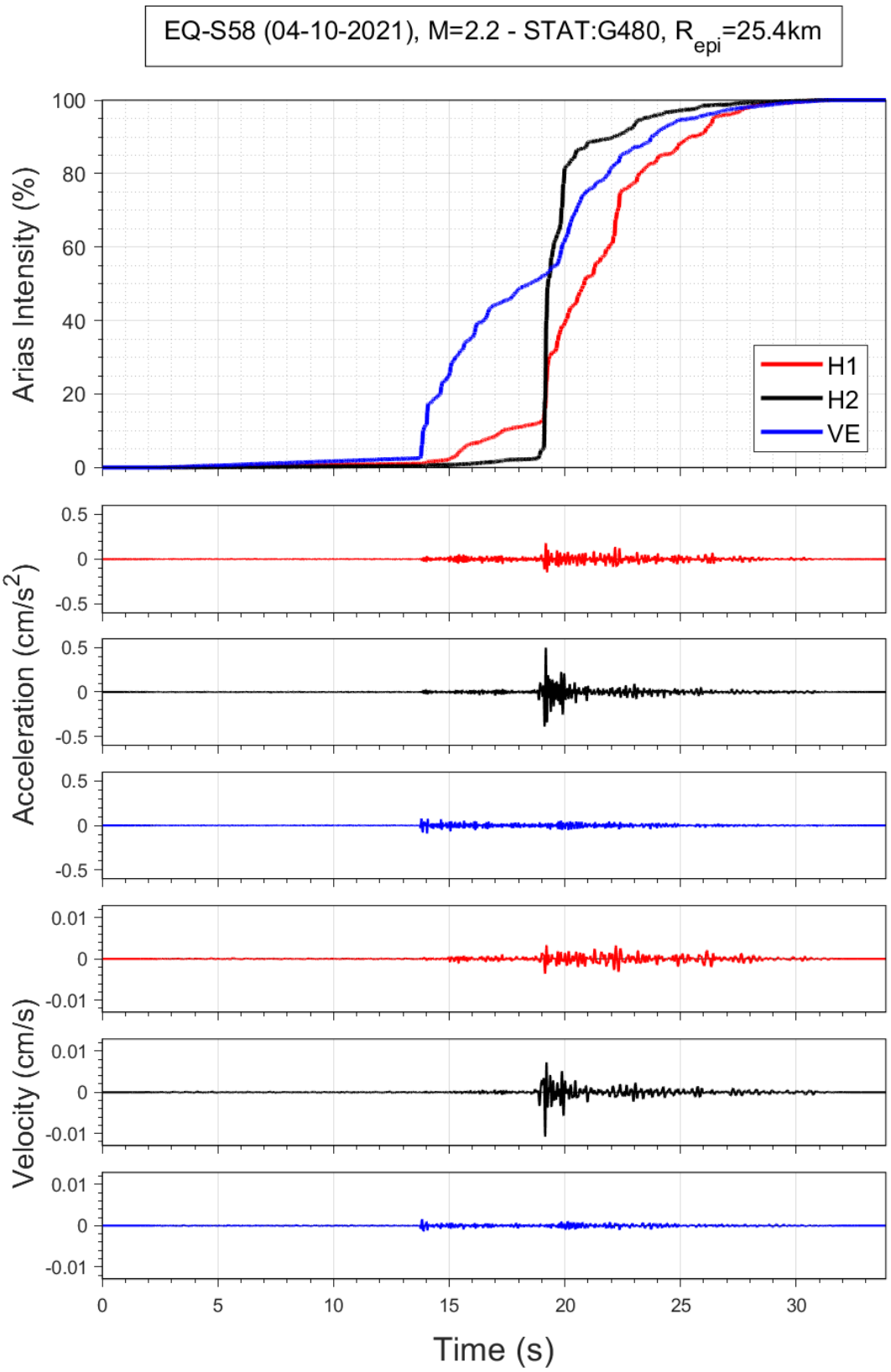
EQ-S58 (04-10-2021), M=2.2 - STAT:G480, R epi =25.4km
Arias Intensity (%)
H1
H2
VE
Acceleration (cm/s2)
Velocity (cm/s)
Time (s)

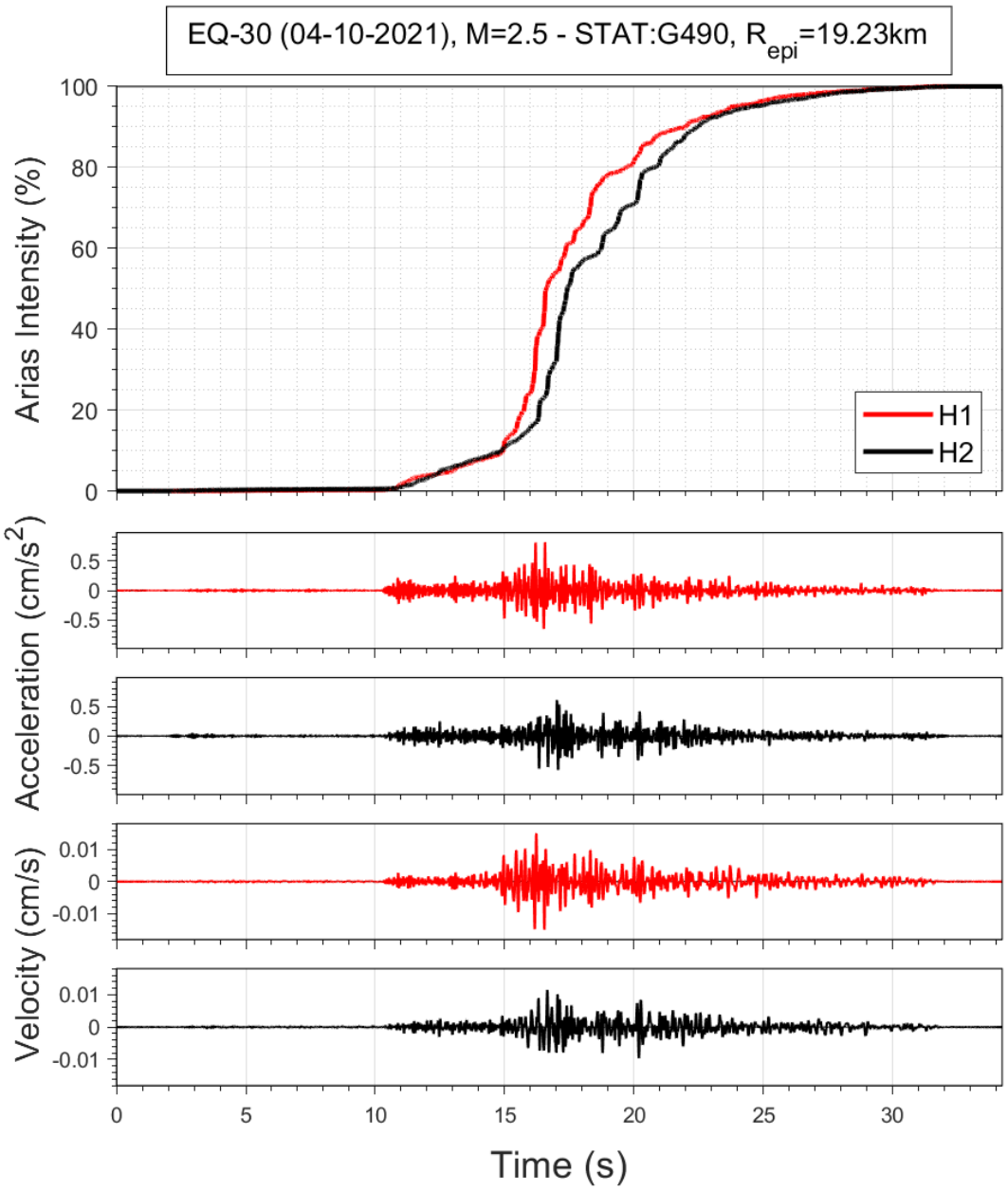
EQ-30 (04-10-2021), M=2.5 - STAT:G490, R epi =19.23km
Arias Intensity (%)
100
80
60
40
20
0
H1
H2
Acceleration (cm/s2)
0.5
0
-0.5
0.5
0
-0.5
Velocity (cm/s)
0.01
0
-0.01
0.01
0
-0.01
0
5
10
15
20
25
30
Time (s)

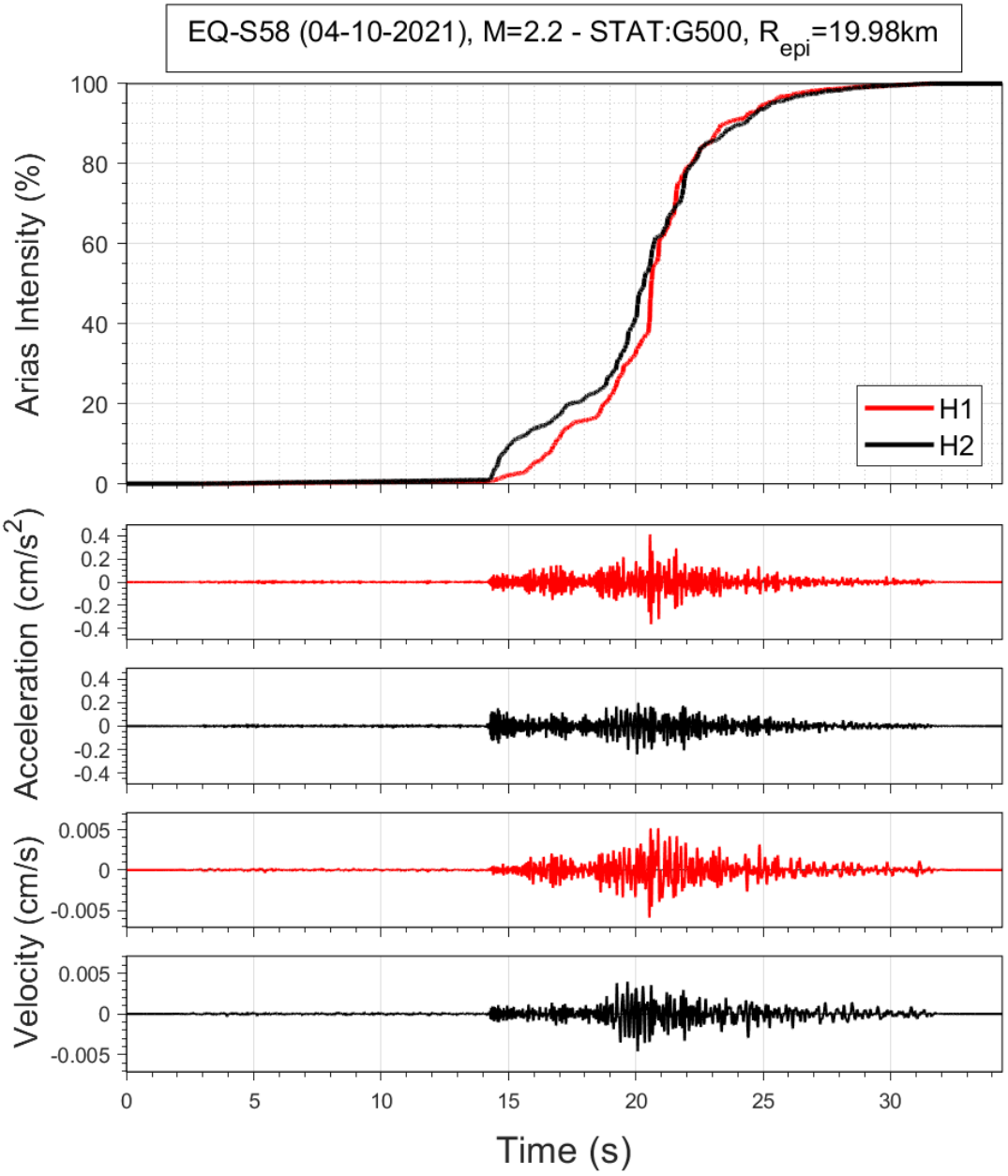
EQ-S58 (04-10-2021), M=2.2 - STAT:G500, R epi =19.98km
Arias Intensity (%)
H1
H2
Acceleration (cm/s2)
Velocity (cm/s)
Time (s)

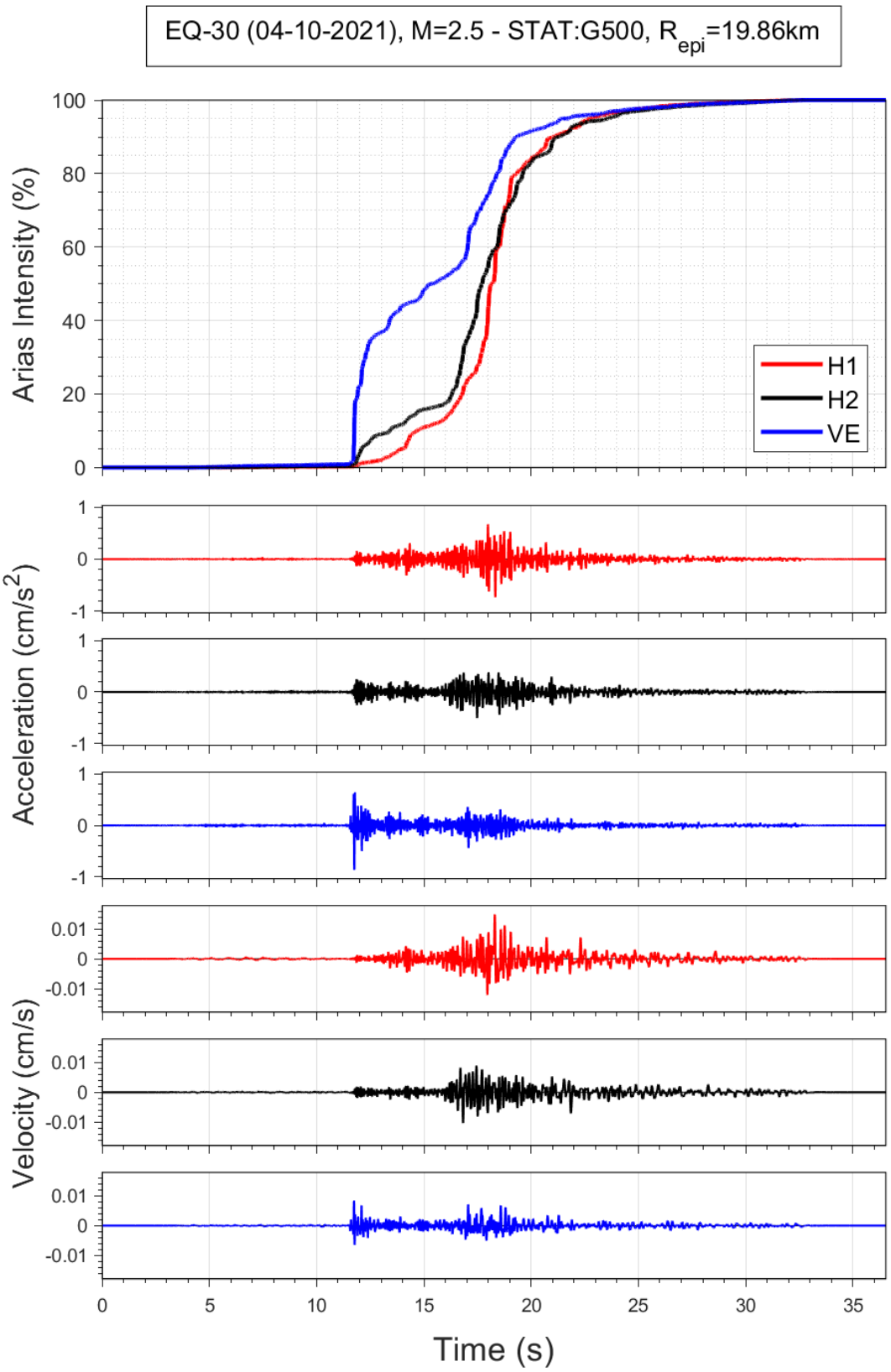
EQ-30 (04-10-2021), M=2.5 - STAT:G500, R epi =19.86km
Arias Intensity (%)
H1
H2
VE
Acceleration (cm/s2)
Velocity (cm/s)
Time (s)

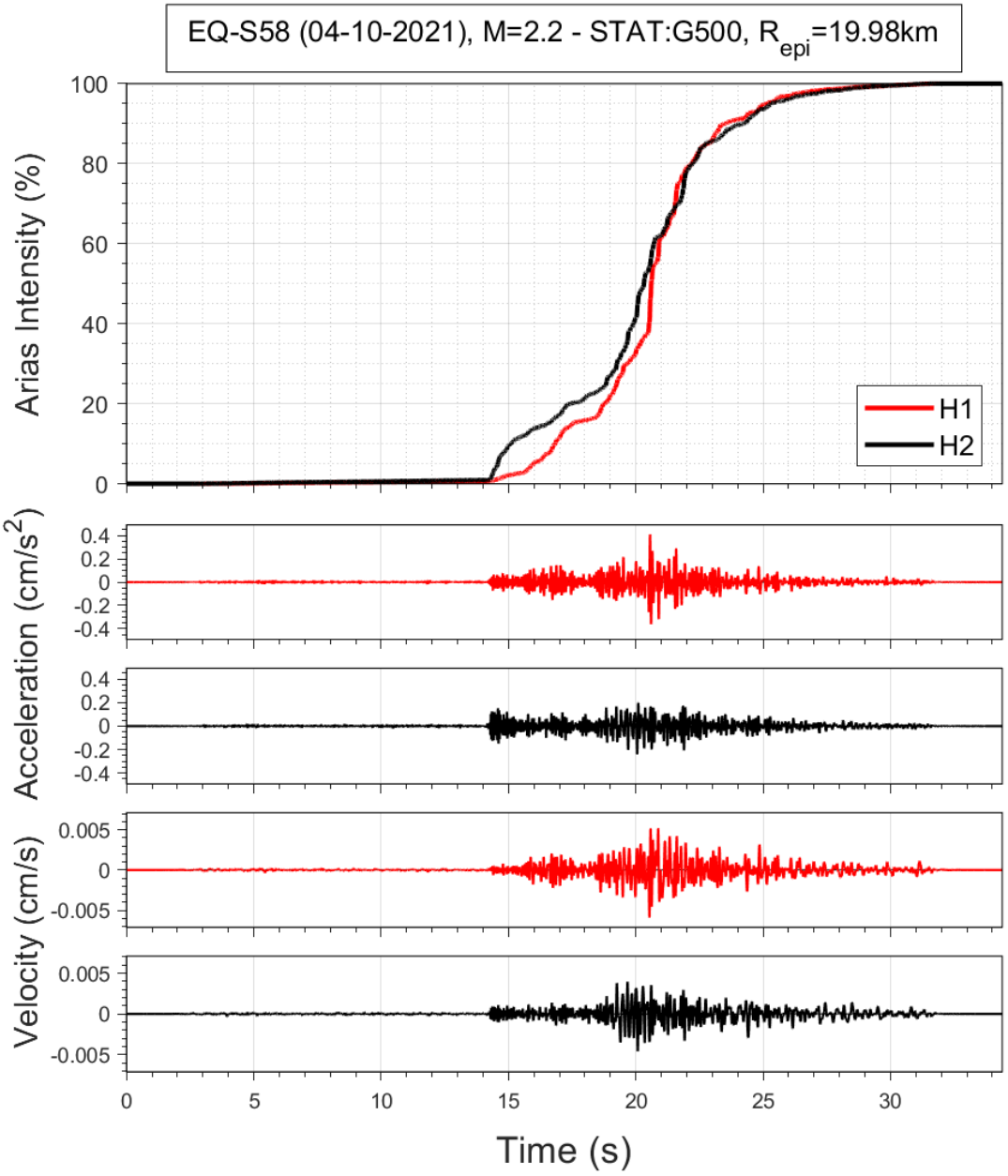
EQ-S58 (04-10-2021), M=2.2 - STAT:G500, R epi =19.98km
Arias Intensity (%)
H1
H2
Acceleration (cm/s2)
Velocity (cm/s)
Time (s)

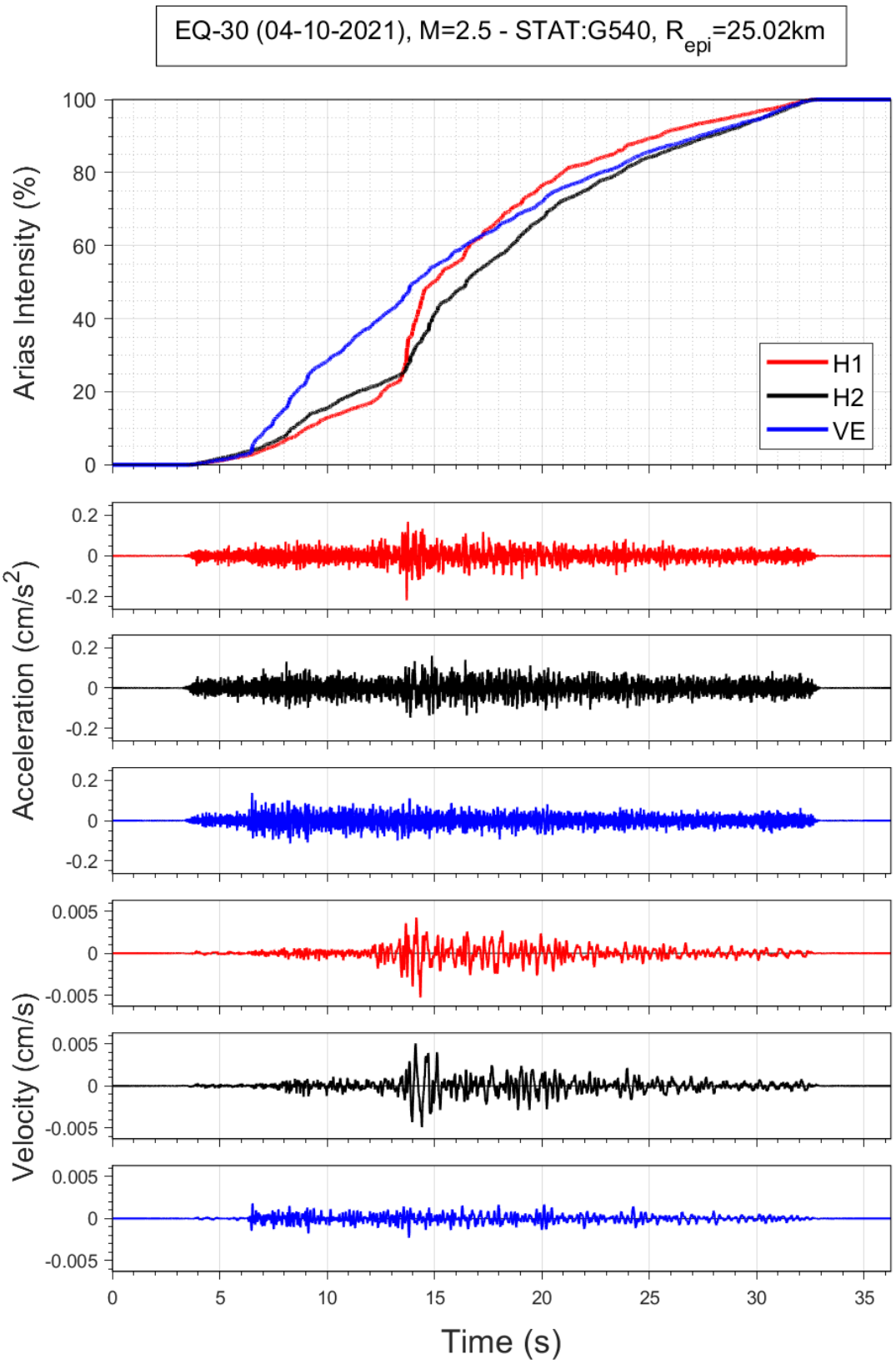
EQ-30 (04-10-2021), M=2.5 - STAT:G540, R epi =25.02km
Arias Intensity (%)
H1
H2
VE
Acceleration (cm/s2)
Velocity (cm/s)
Time (s)

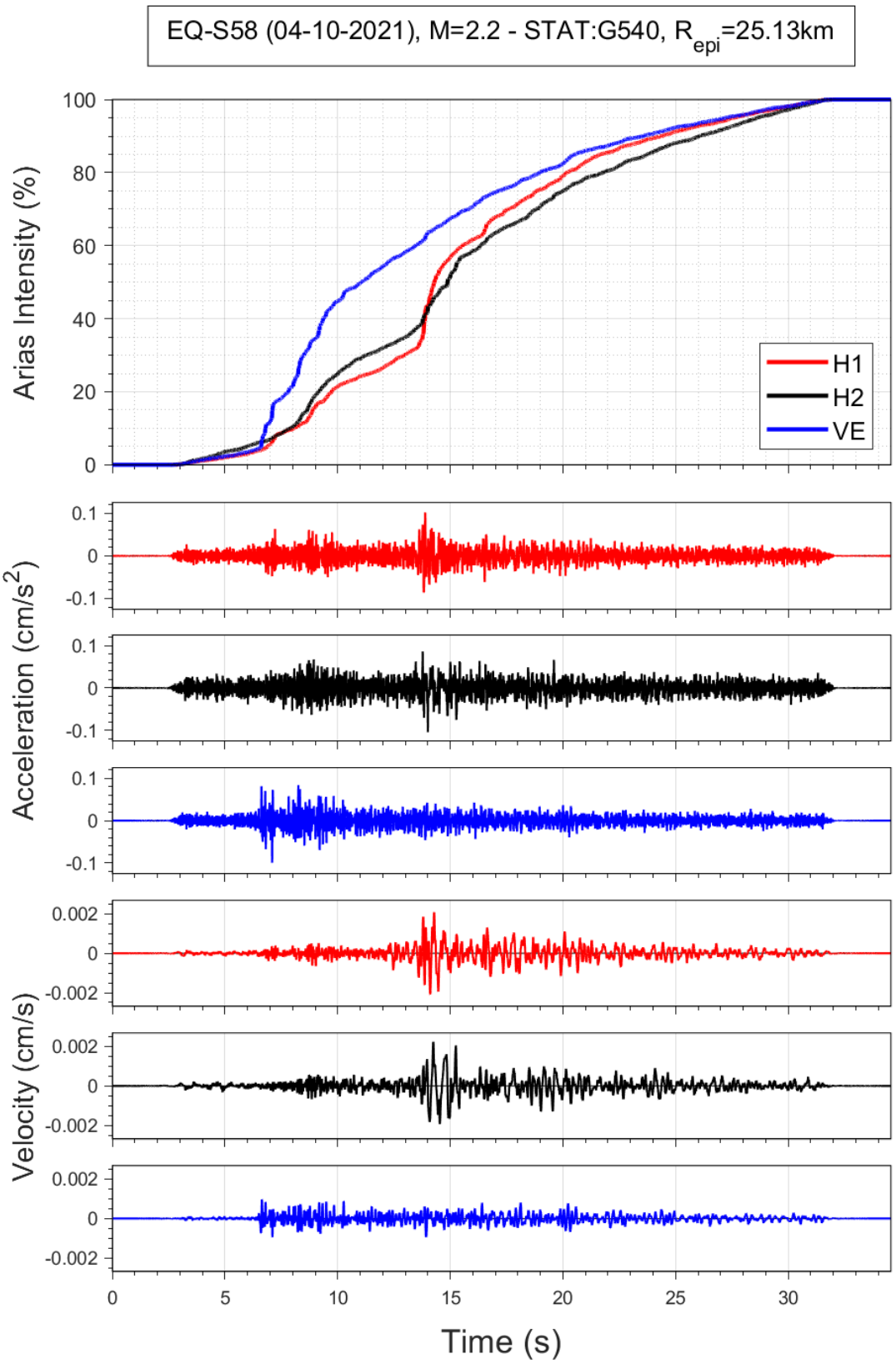
EQ-S58 (04-10-2021), M=2.2 - STAT:G540, R epi =25.13km
Arias Intensity (%)
H1
H2
VE
Acceleration (cm/s2)
Velocity (cm/s)
Time (s)

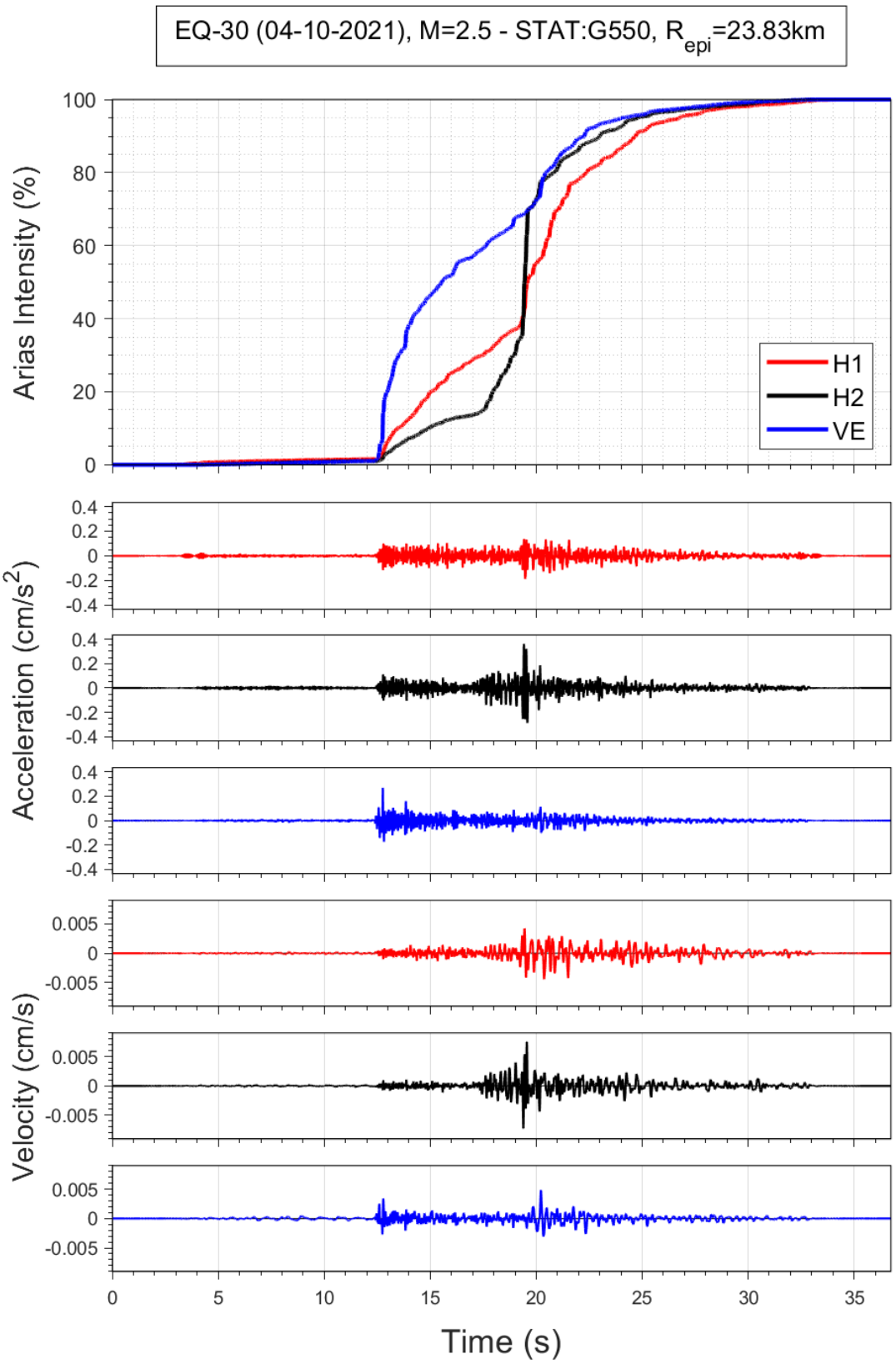
EQ-30 (04-10-2021), M=2.5 - STAT:G550, R epi =23.83km
Arias Intensity (%)
H1
H2
VE
Acceleration (cm/s2)
Velocity (cm/s)
Time (s)

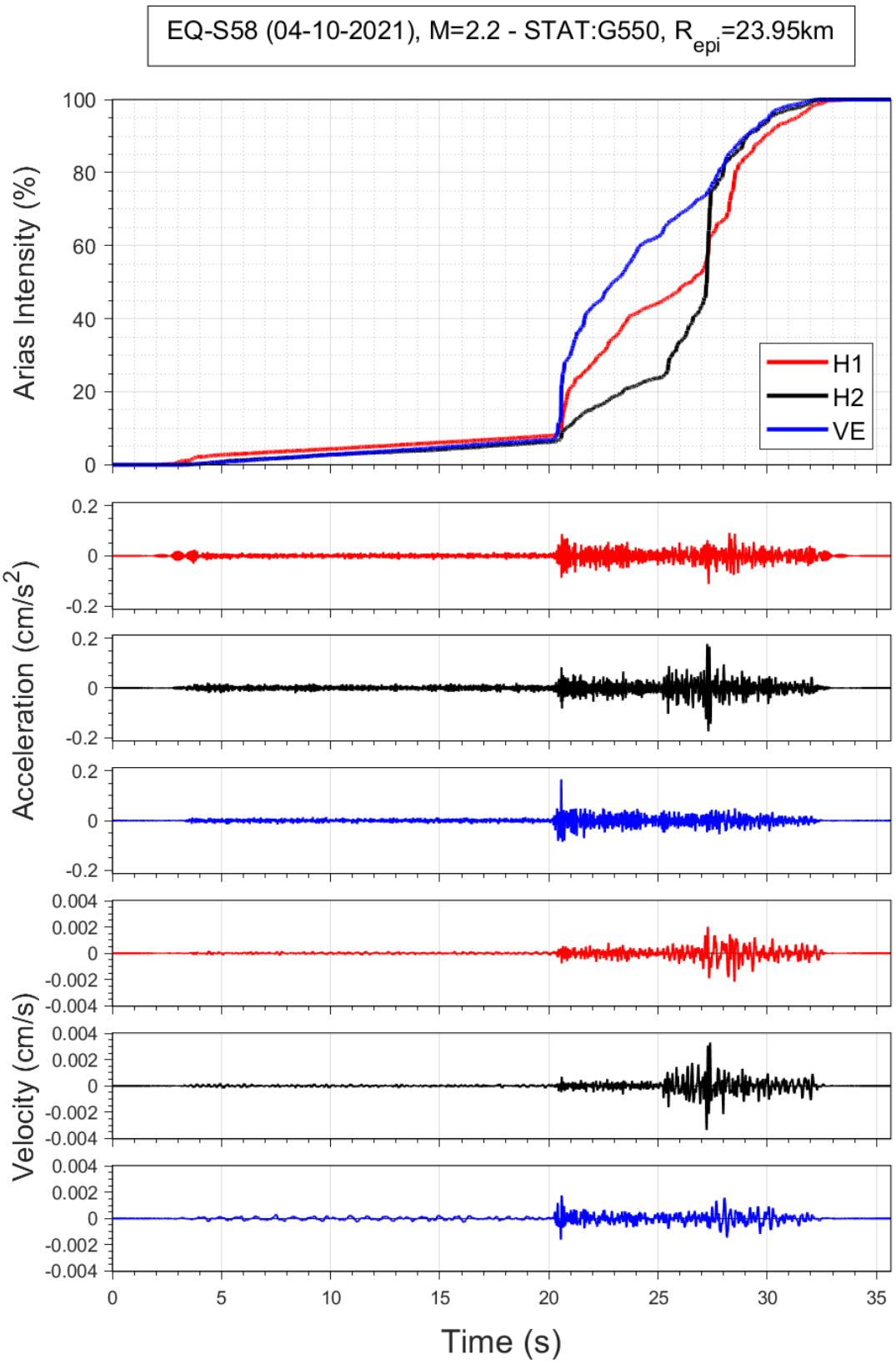
EQ-S58 (04-10-2021), M=2.2 - STAT:G550, R epi =23.95km
Arias Intensity (%)
H1
H2
VE
Acceleration (cm/s2)
Velocity (cm/s)
Time (s)

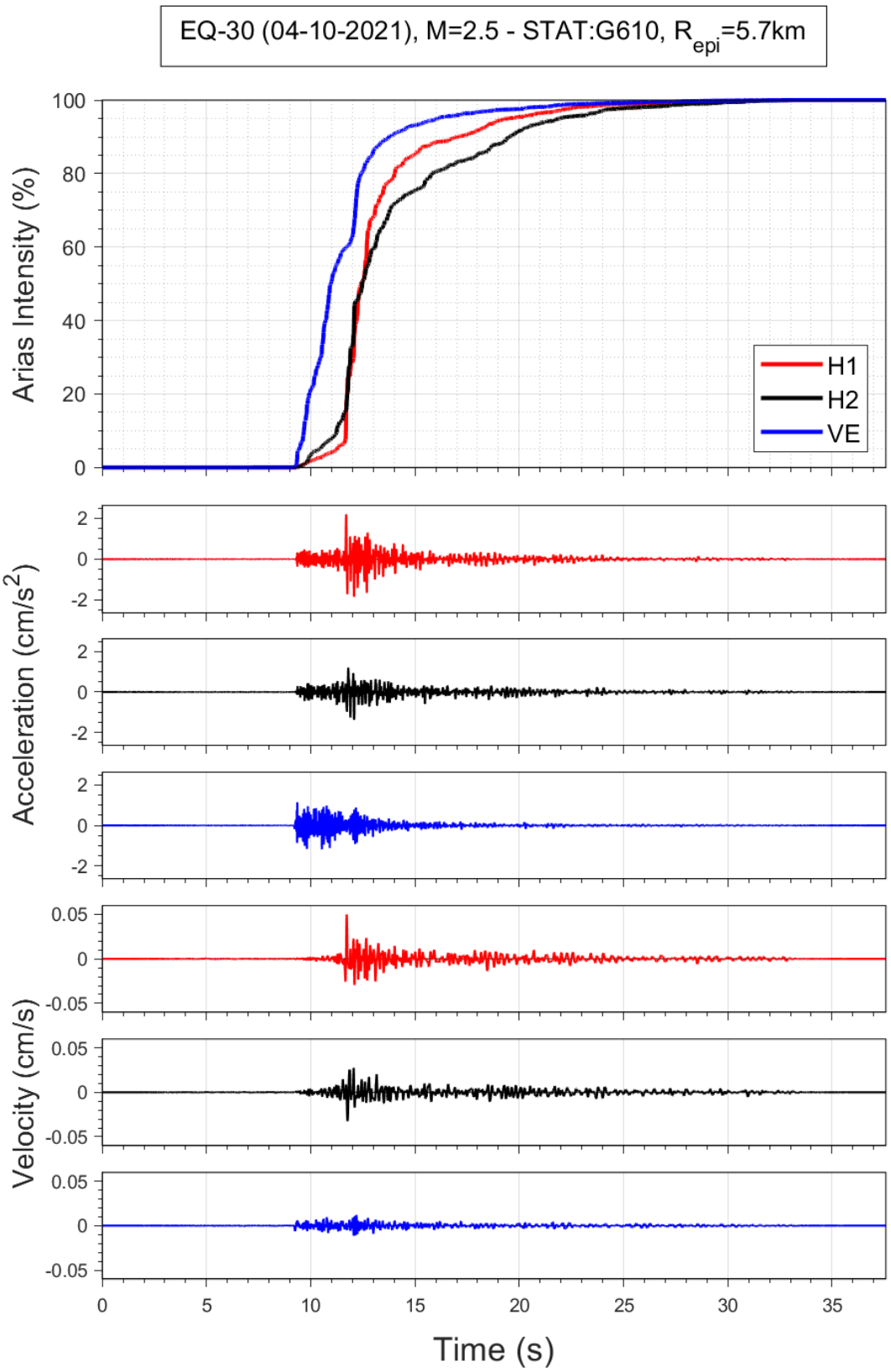
EQ-30 (04-10-2021), M=2.5 - STAT:G610, R_epi=5.7km
Arias Intensity (%)
100
80
60
40
20
0
H1
H2
VE
Acceleration (cm/s2)
2
0
-2
Velocity (cm/s)
0.05
0
-0.05
0
5
10
15
20
25
30
35
Time (s)

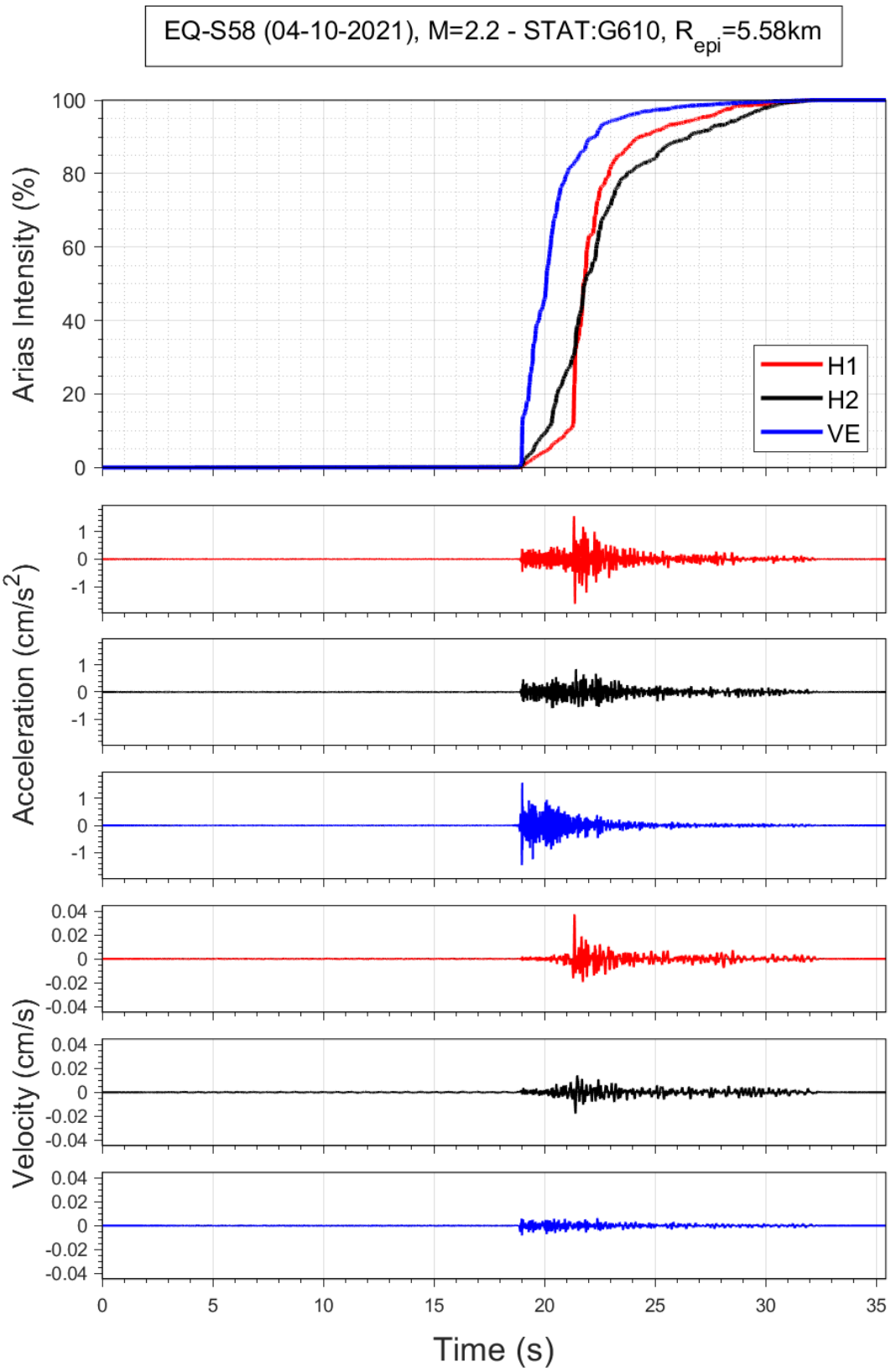
EQ-S58 (04-10-2021), M=2.2 - STAT:G610, R epi =5.58km
Arias Intensity (%)
H1
H2
VE
Acceleration (cm/s2)
Velocity (cm/s)
Time (s)

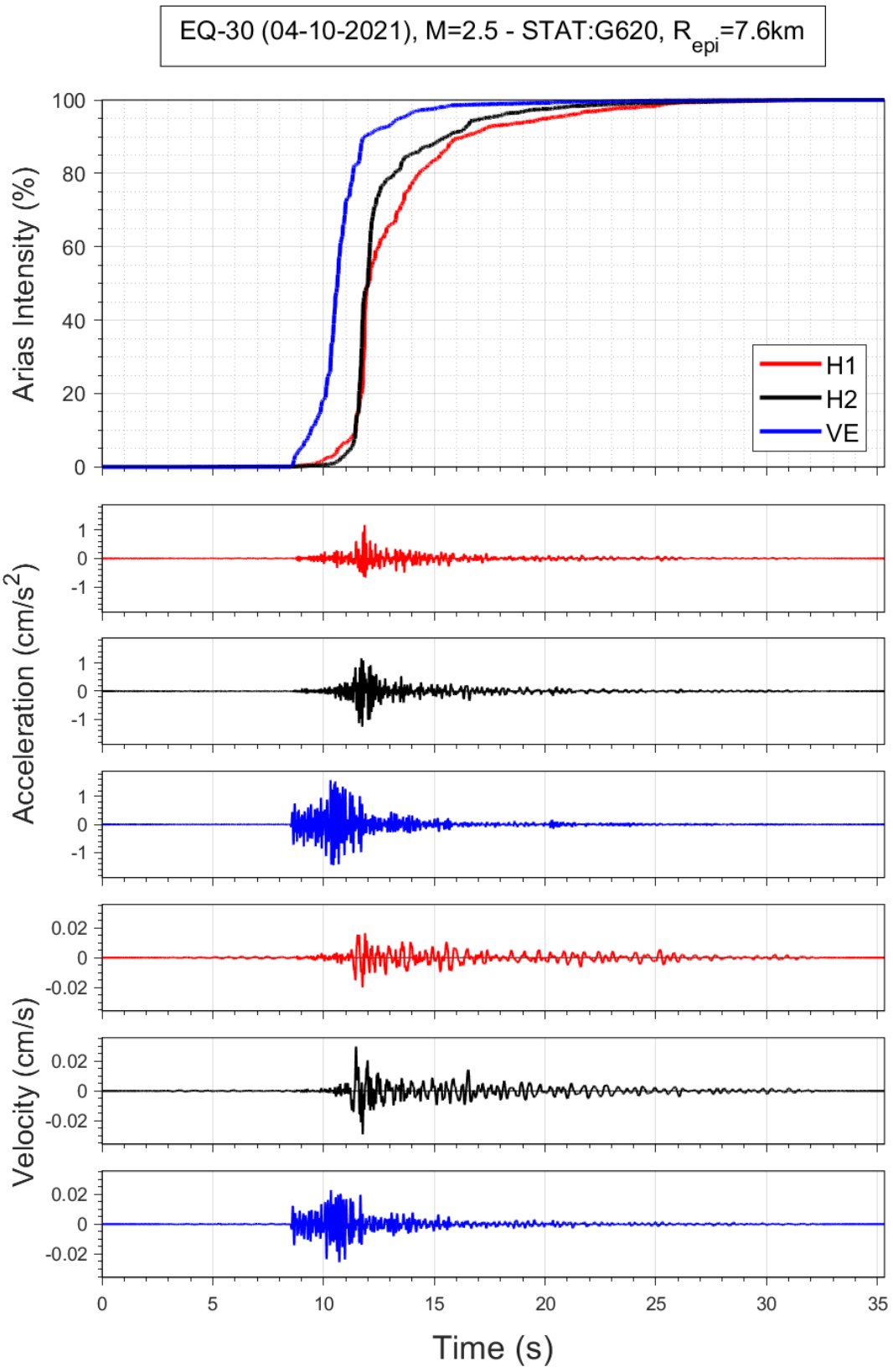
EQ-30 (04-10-2021), M=2.5 - STAT:G620, R epi =7.6km
Arias Intensity (%)
H1
H2
VE
Acceleration (cm/s2)
Velocity (cm/s)
Time (s)

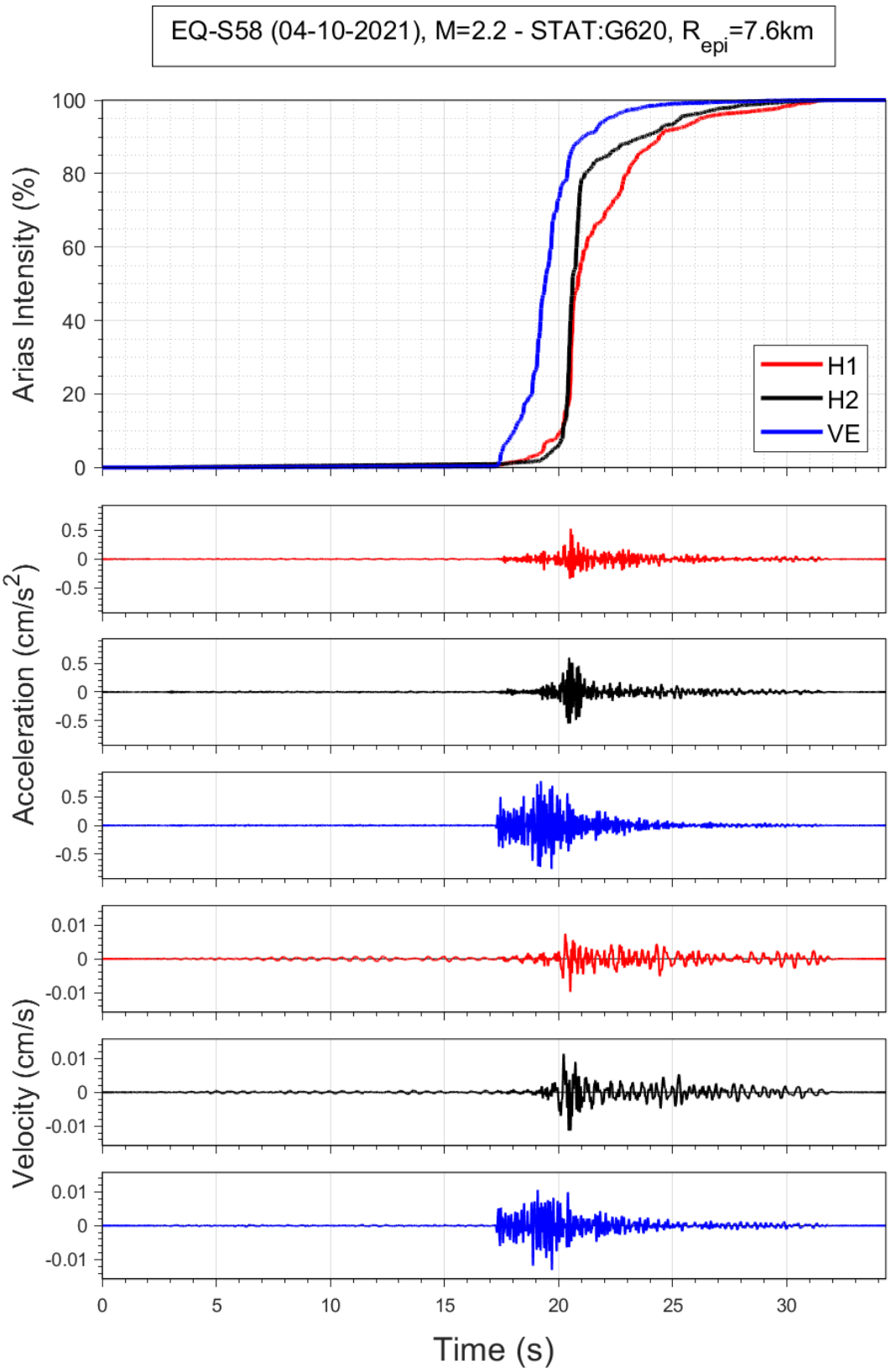
EQ-S58 (04-10-2021), M=2.2 - STAT:G620, R epi =7.6km
Arias Intensity (%)
H1
H2
VE
Acceleration (cm/s2)
Velocity (cm/s)
Time (s)

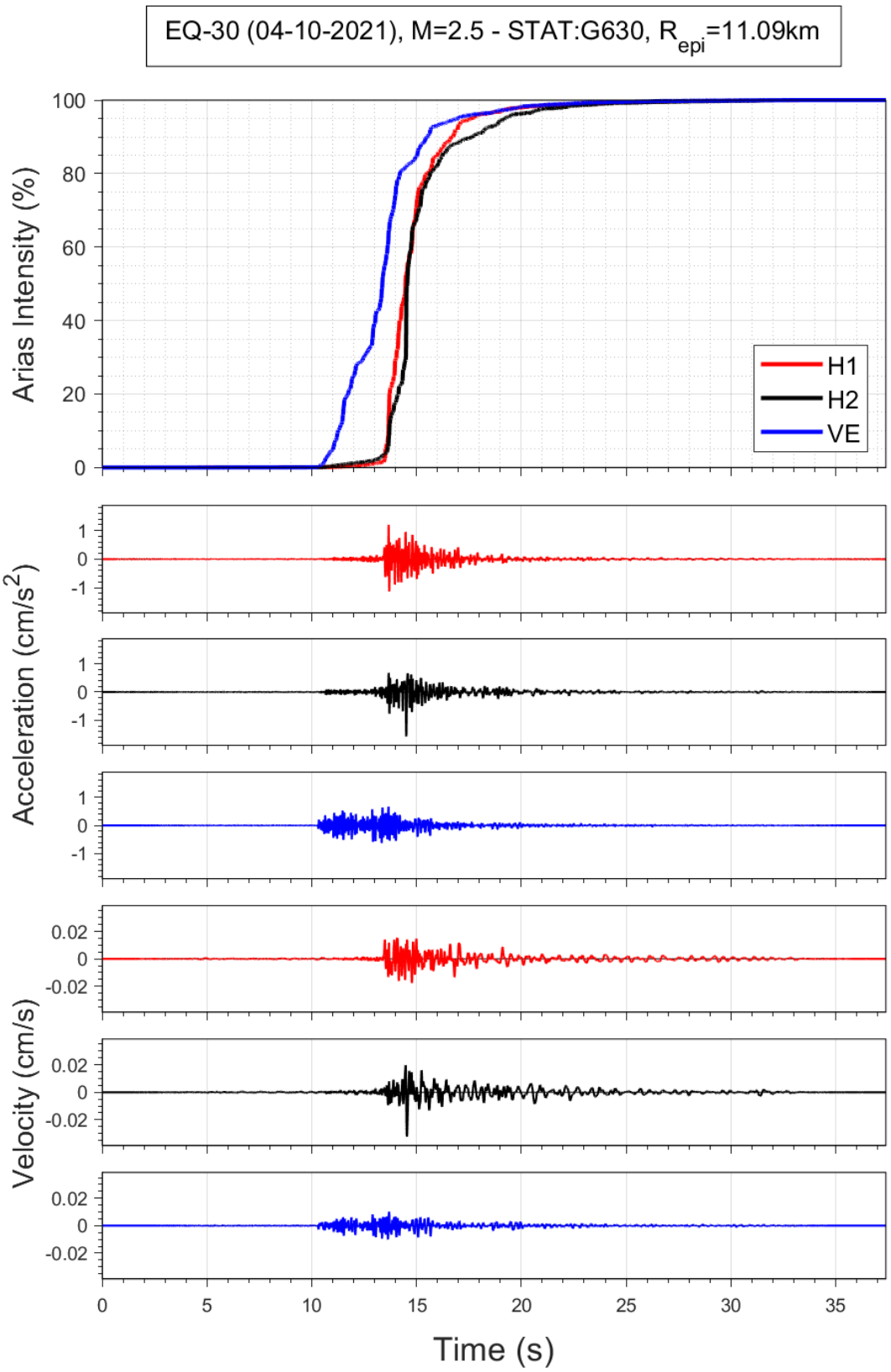
EQ-30 (04-10-2021), M=2.5 - STAT:G630, R epi =11.09km
Arias Intensity (%)
H1
H2
VE
Acceleration (cm/s2)
Velocity (cm/s)
Time (s)

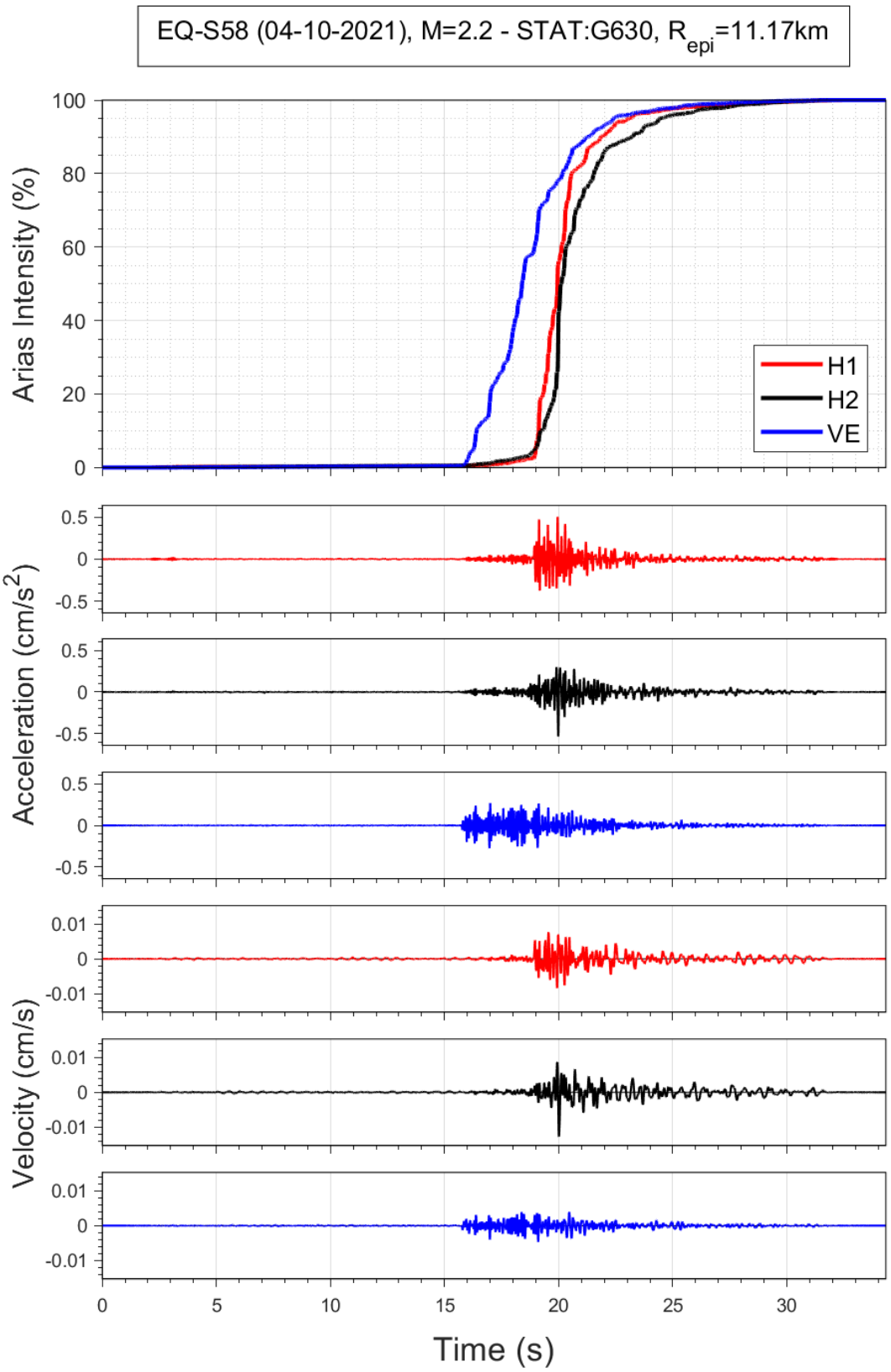
EQ-S58 (04-10-2021), M=2.2 - STAT:G630, R epi =11.17km
Arias Intensity (%)
100
80
60
40
20
0
H1
H2
VE
Acceleration (cm/s2)
0.5
0
-0.5
Velocity (cm/s)
0.01
0
-0.01
0
5
10
15
20
25
30
Time (s)

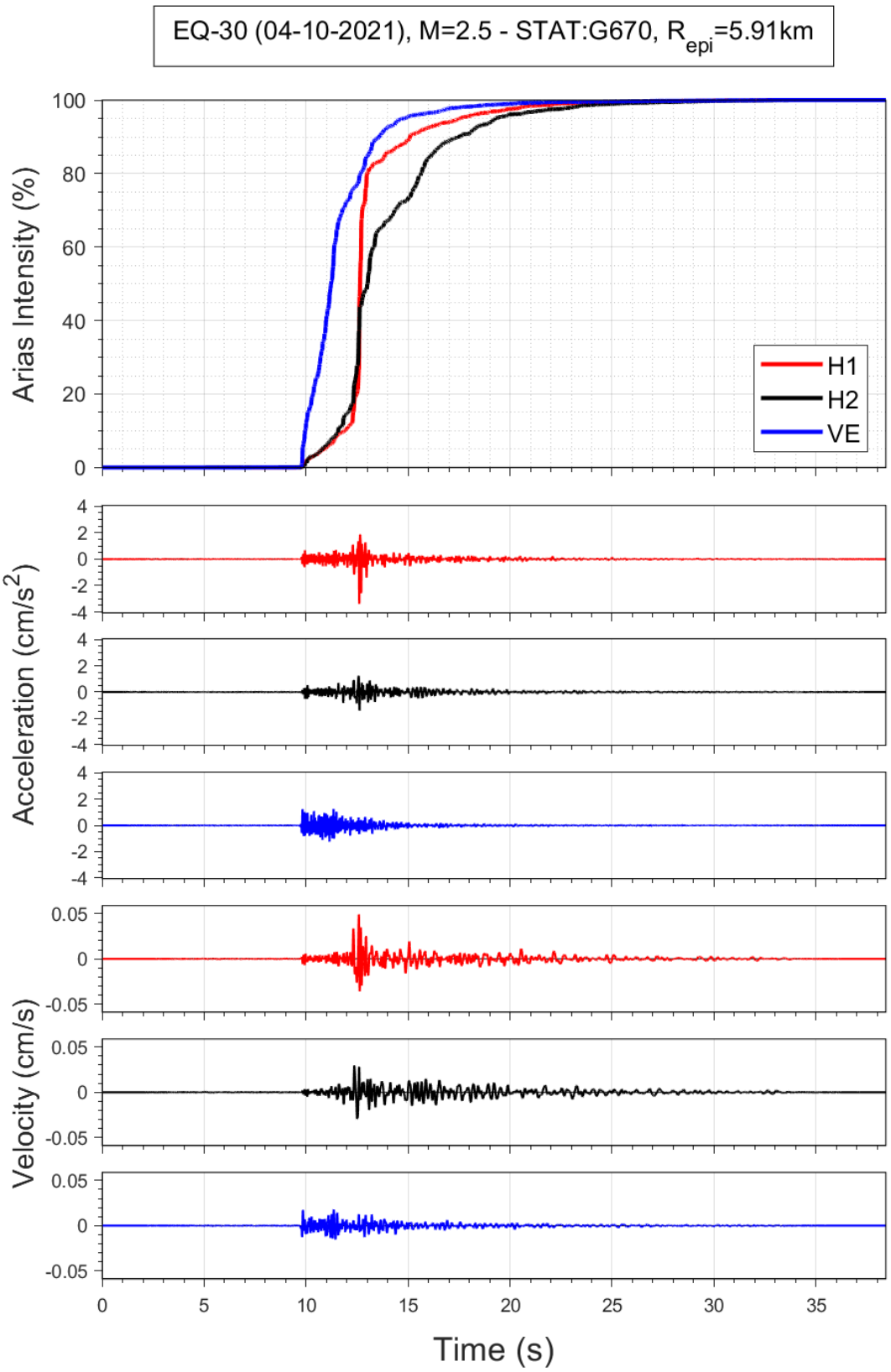
EQ-30 (04-10-2021), M=2.5 - STAT:G670, R epi =5.91km
Arias Intensity (%)
H1
H2
VE
Acceleration (cm/s2)
Velocity (cm/s)
Time (s)

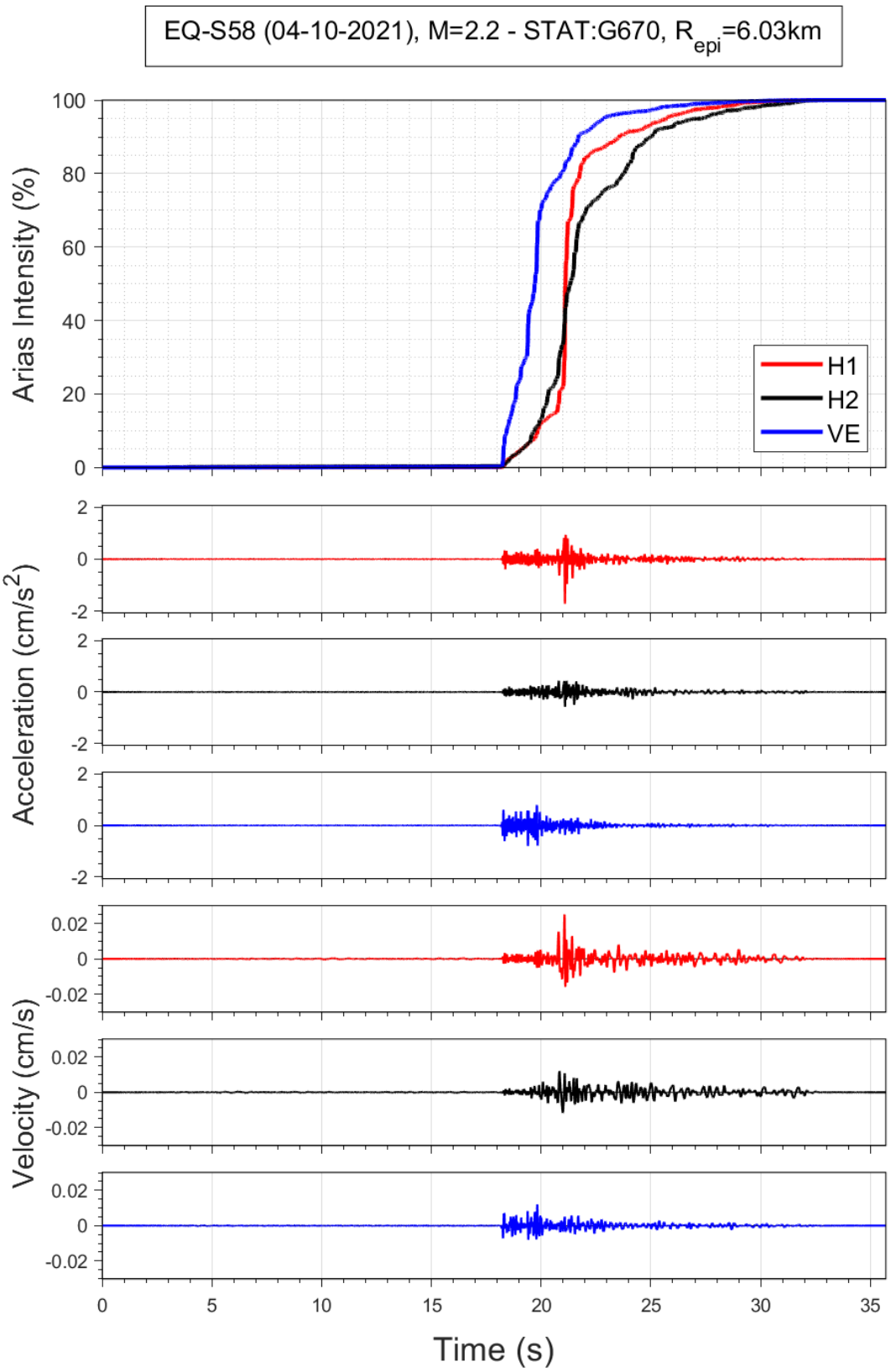
EQ-S58 (04-10-2021), M=2.2 - STAT:G670, R epi =6.03km
Arias Intensity (%)
H1
H2
VE
Acceleration (cm/s2)
Velocity (cm/s)
Time (s)

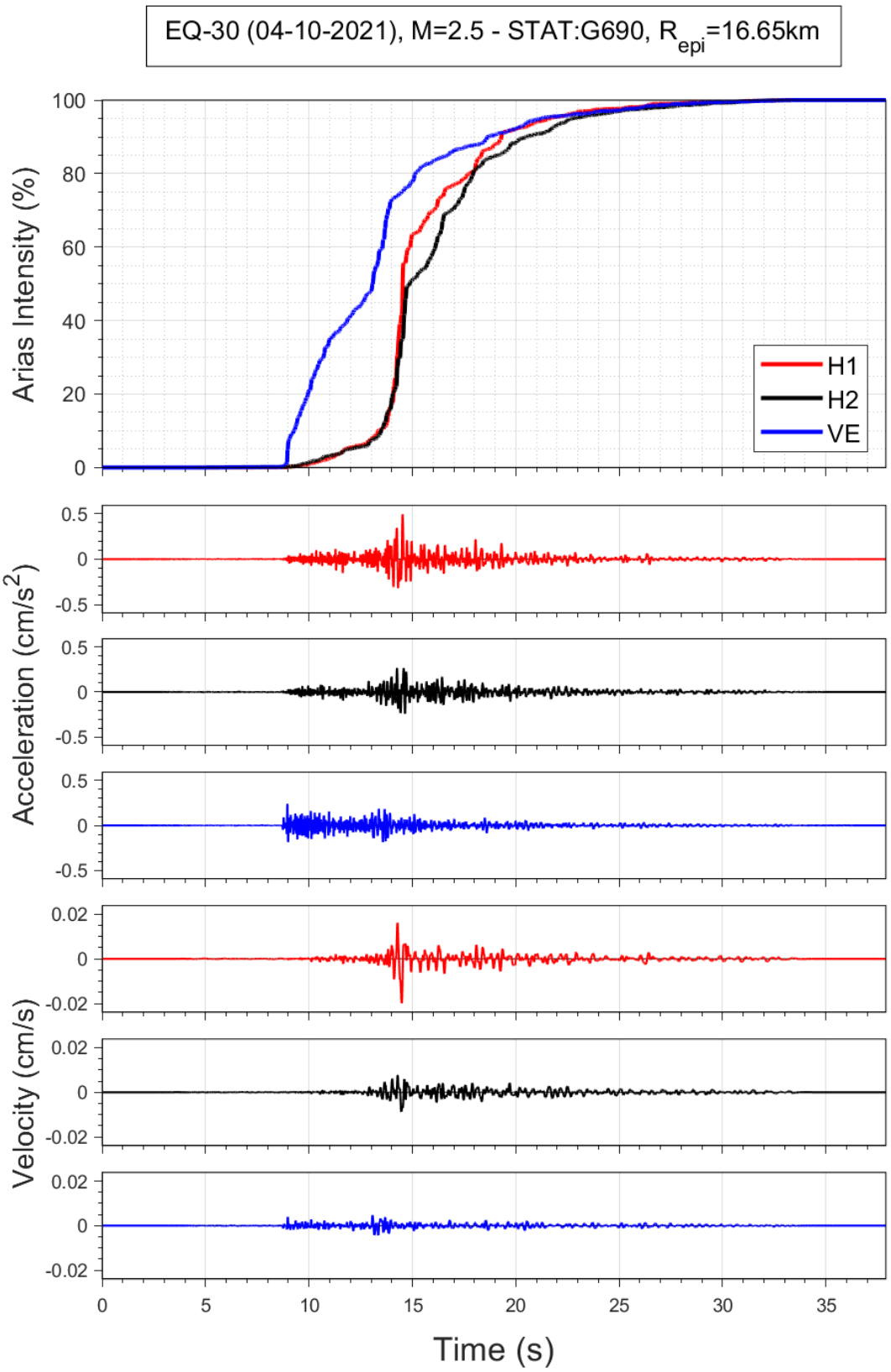
EQ-30 (04-10-2021), M=2.5 - STAT:G690, R epi =16.65km
Arias Intensity (%)
H1
H2
VE
Acceleration (cm/s2)
Velocity (cm/s)
Time (s)

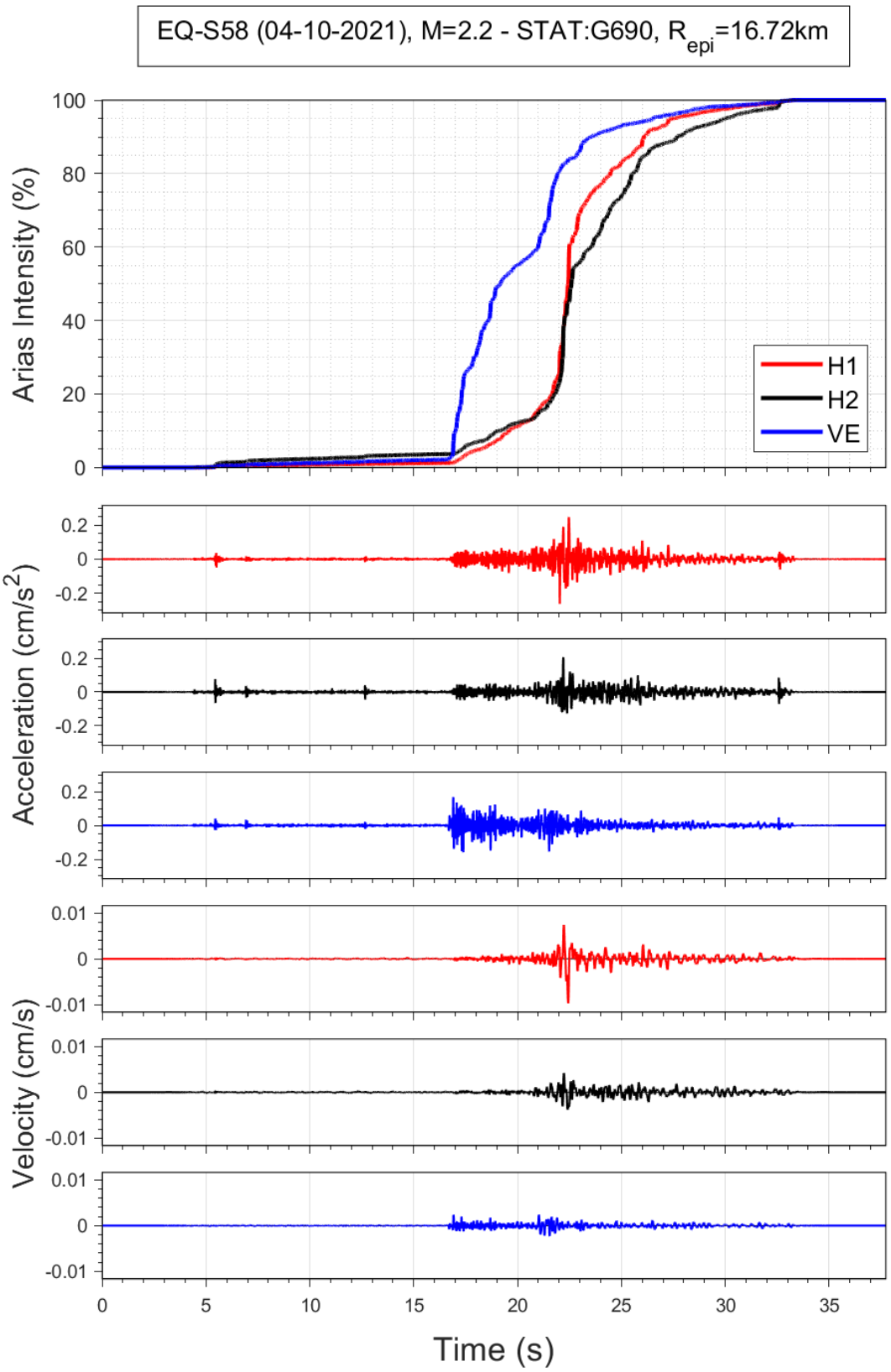
EQ-S58 (04-10-2021), M=2.2 - STAT:G690, R epi =16.72km
Arias Intensity (%)
H1
H2
VE
Acceleration (cm/s2)
Velocity (cm/s)
Time (s)

Appendix C – Time-histories of acceleration and velocity and accumulation of Arias Intensity

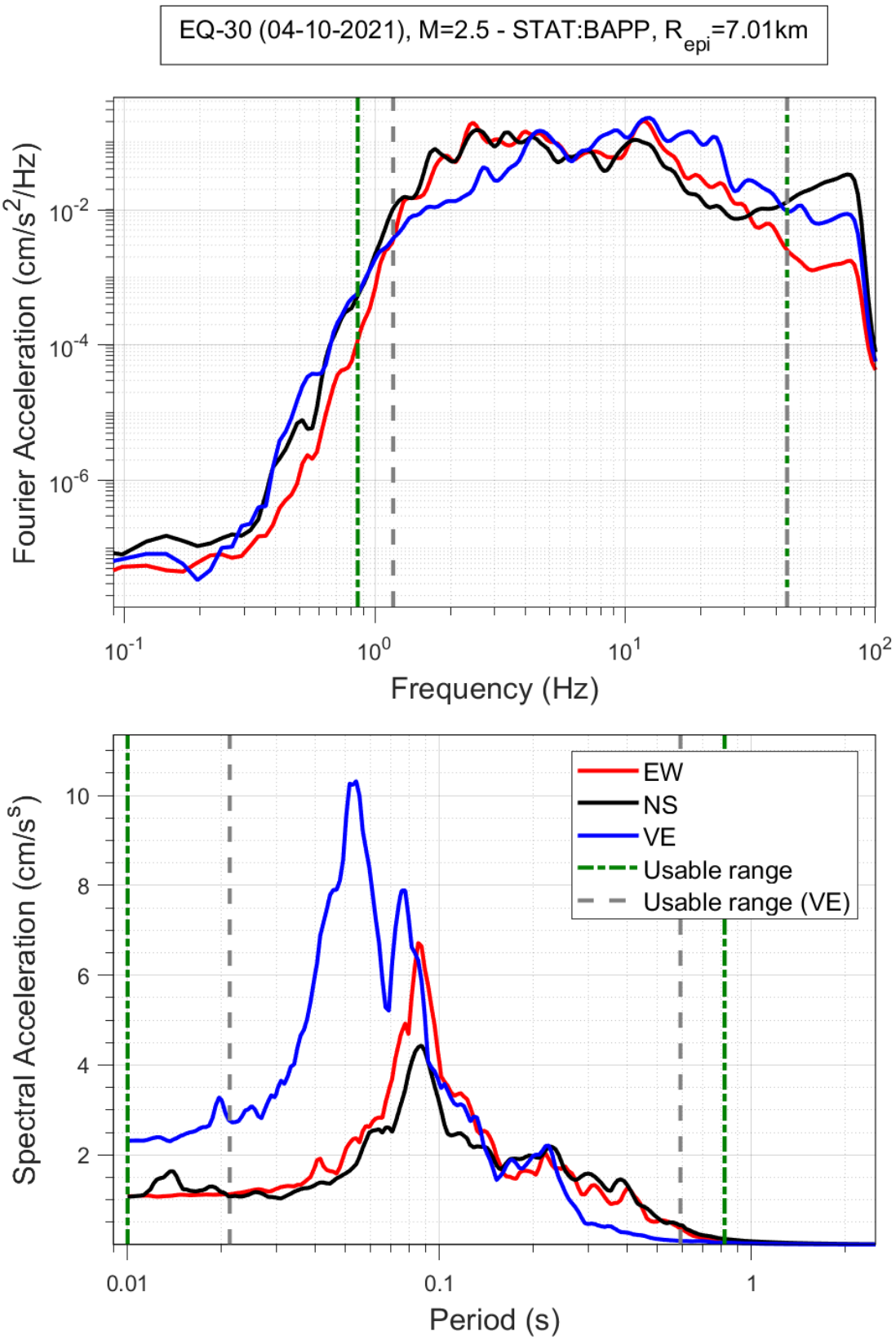
EQ-30 (04-10-2021), M=2.5 - STAT:BAPP, R epi =7.01km
Fourier Acceleration (cm/s2/Hz)
10-2
10-4
10-6
10-1
100
101
102
Frequency (Hz)
Spectral Acceleration (cm/s2)
10
8
6
4
2
0.01
0.1
1
Period (s)
EW
NS
VE
Usable range
Usable range (VE)

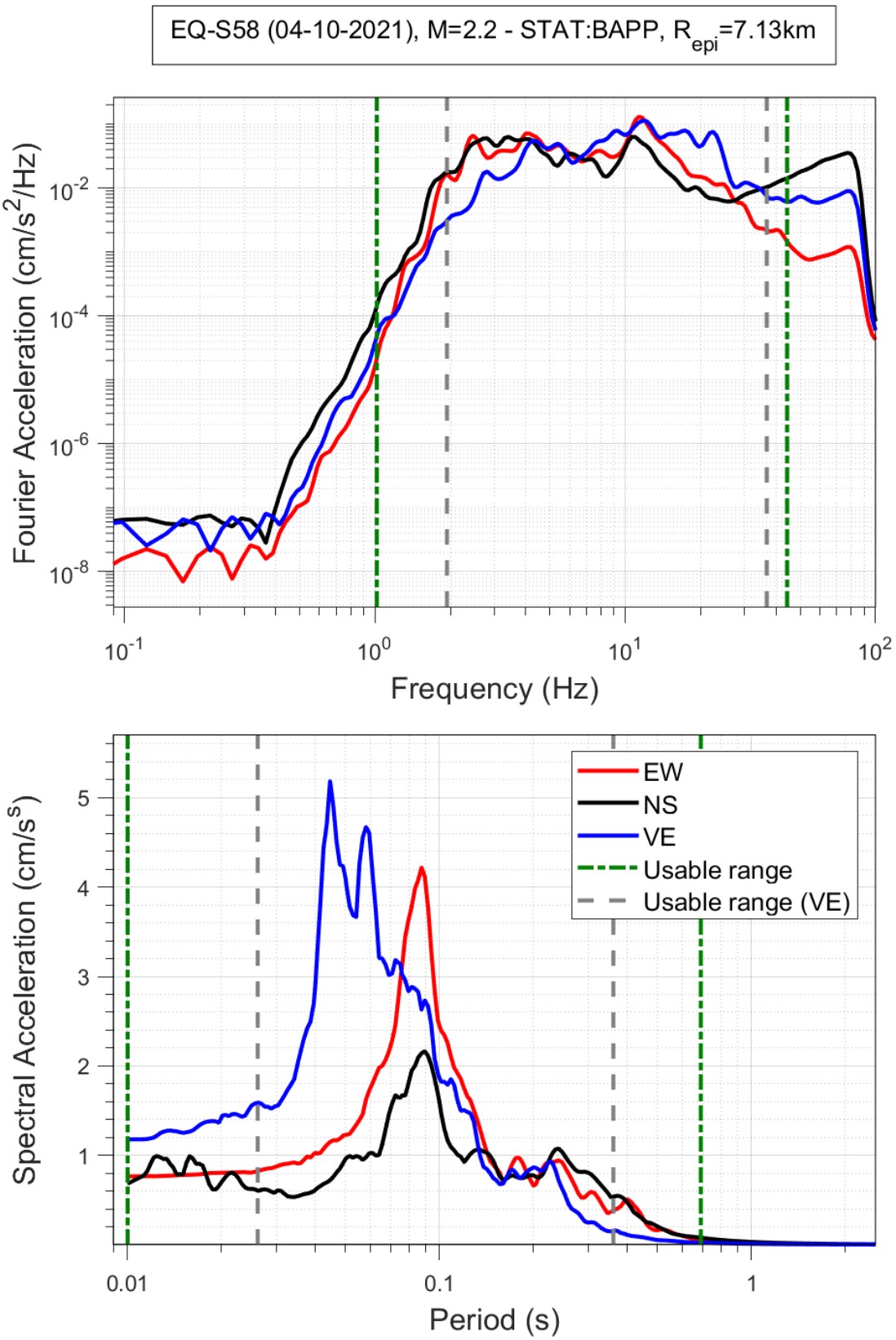
EQ-S58 (04-10-2021), M=2.2 - STAT:BAPP, R_epi=7.13km
Fourier Acceleration (cm/s²/Hz)
10^-2
10^-4
10^-6
10^-8
10^-1
10^0
10^1
10^2
Frequency (Hz)
Spectral Acceleration (cm/s^s)
5
4
3
2
1
0.01
0.1
1
Period (s)
EW
NS
VE
Usable range
Usable range (VE)

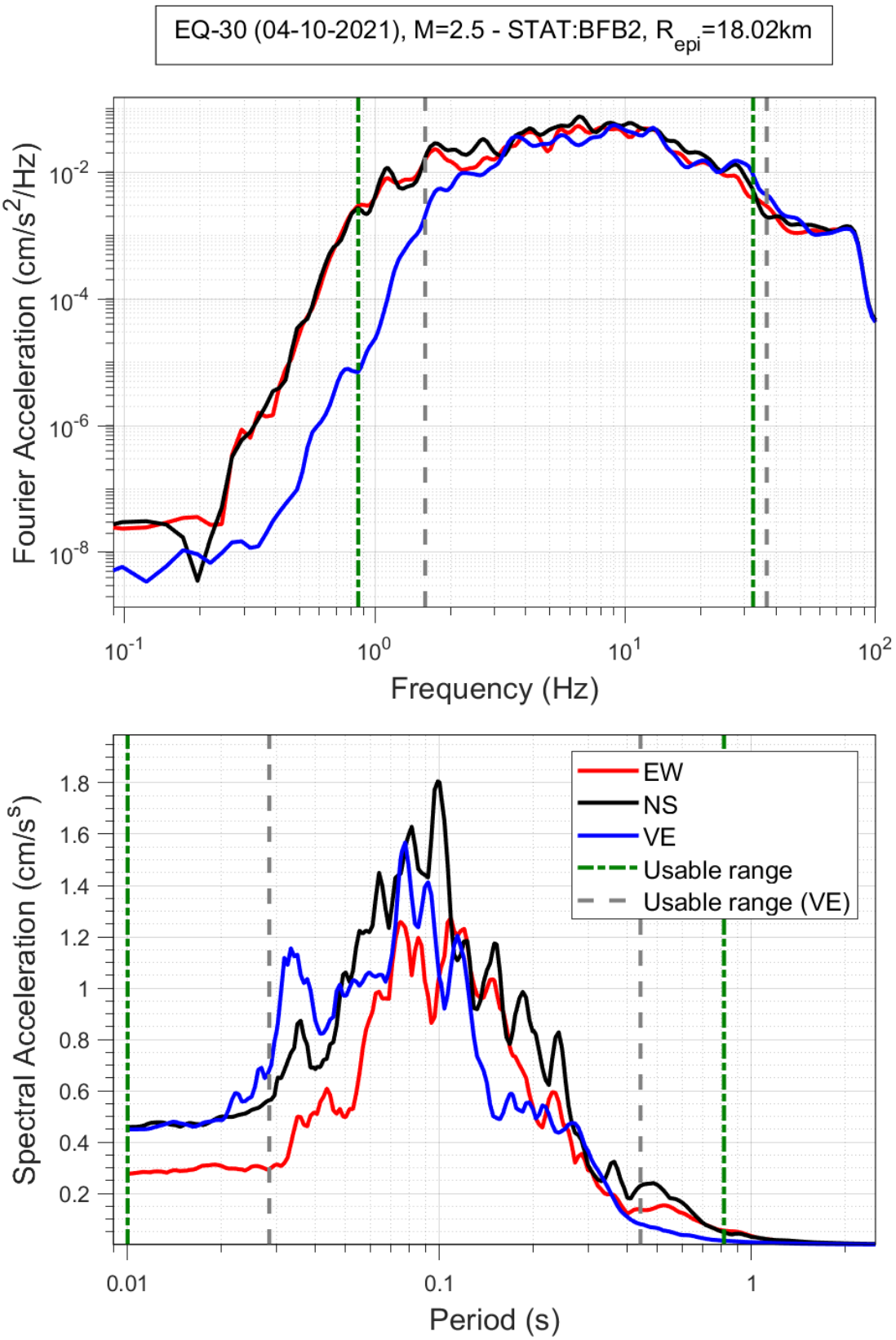
EQ-30 (04-10-2021), M=2.5 - STAT:BFB2, R_epi=18.02km
Fourier Acceleration (cm/s²/Hz)
10^-2
10^-4
10^-6
10^-8
10^-1
10^0
10^1
10^2
Frequency (Hz)
Spectral Acceleration (cm/s^s)
1.8
1.6
1.4
1.2
1
0.8
0.6
0.4
0.2
0.01
0.1
1
Period (s)
EW
NS
VE
Usable range
Usable range (VE)

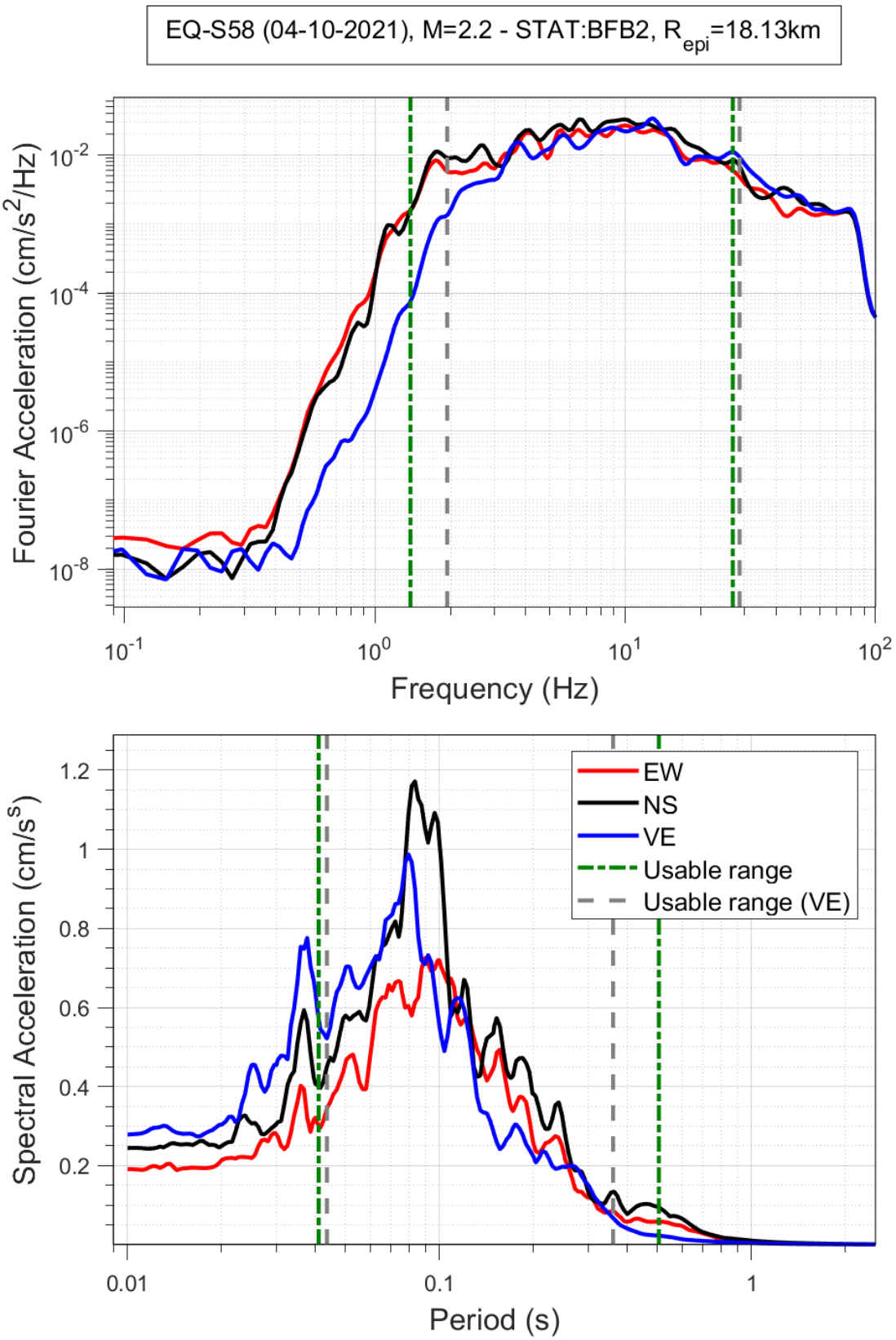
EQ-S58 (04-10-2021), M=2.2 - STAT:BFB2, R epi =18.13km
Fourier Acceleration (cm/s2/Hz)
10-2
10-4
10-6
10-8
10-1
100
101
102
Frequency (Hz)
Spectral Acceleration (cm/s2)
1.2
1
0.8
0.6
0.4
0.2
0.01
0.1
1
Period (s)
EW
NS
VE
Usable range
Usable range (VE)

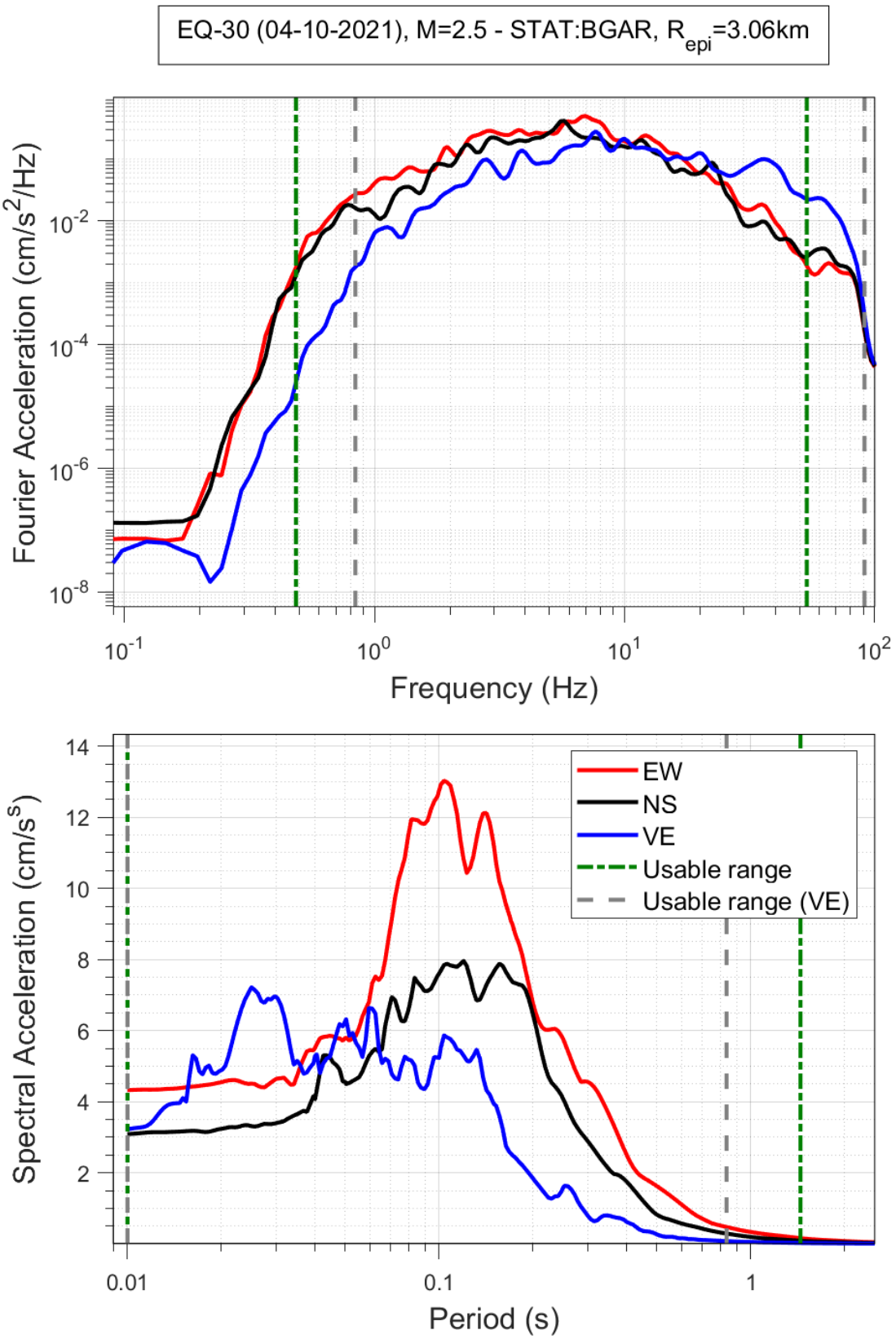
EQ-30 (04-10-2021), M=2.5 - STAT:BGAR, R_epi=3.06km
Fourier Acceleration (cm/s²/Hz)
10^-2
10^-4
10^-6
10^-8
10^-1
10^0
10^1
10^2
Frequency (Hz)
Spectral Acceleration (cm/s^s)
14
12
10
8
6
4
2
0.01
0.1
1
Period (s)
EW
NS
VE
Usable range
Usable range (VE)

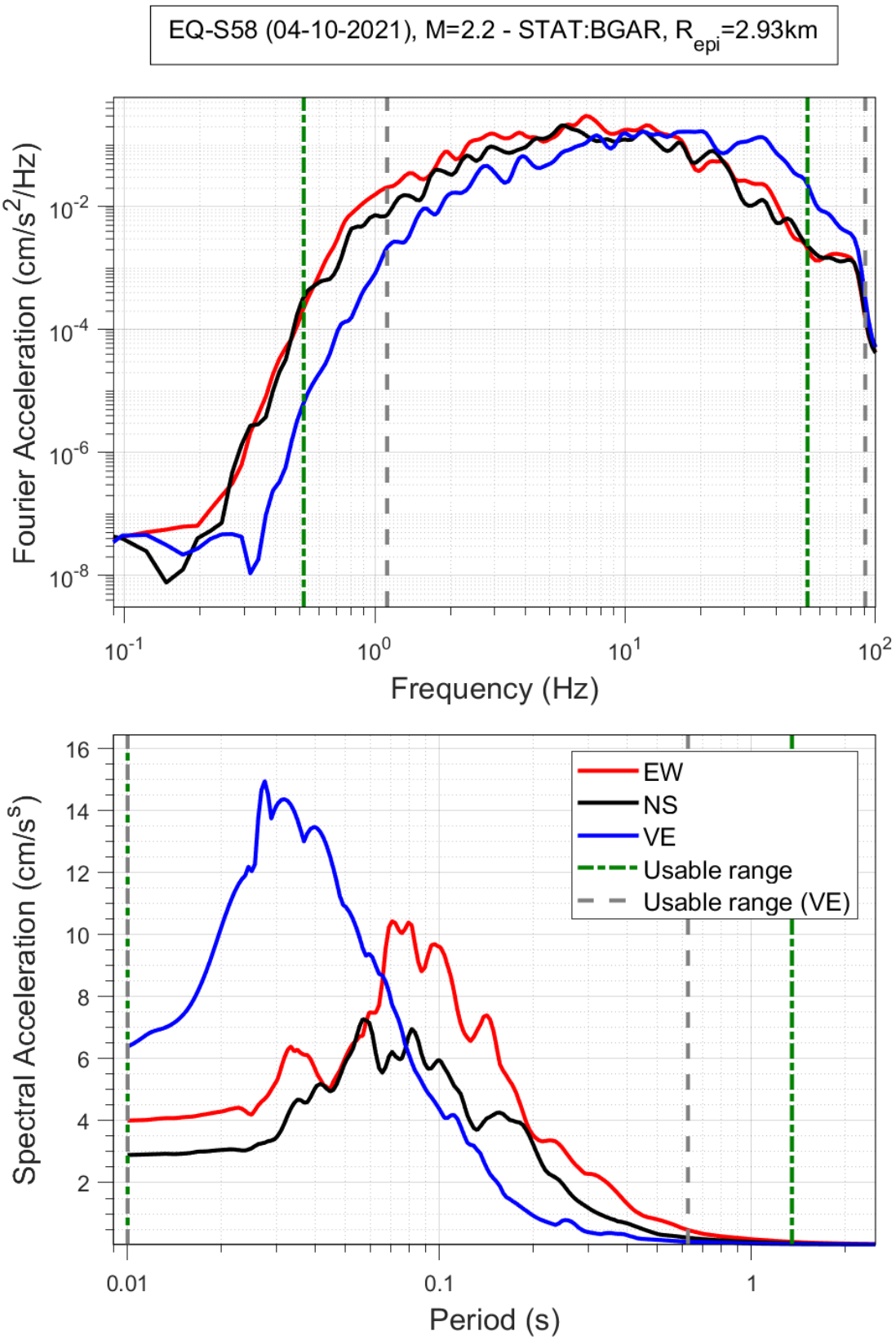
EQ-S58 (04-10-2021), M=2.2 - STAT:BGAR, R_epi=2.93km
Fourier Acceleration (cm/s²/Hz)
10^-2
10^-4
10^-6
10^-8
10^-1
10^0
10^1
10^2
Frequency (Hz)
Spectral Acceleration (cm/s²)
16
14
12
10
8
6
4
2
0.01
0.1
1
Period (s)
EW
NS
VE
Usable range
Usable range (VE)

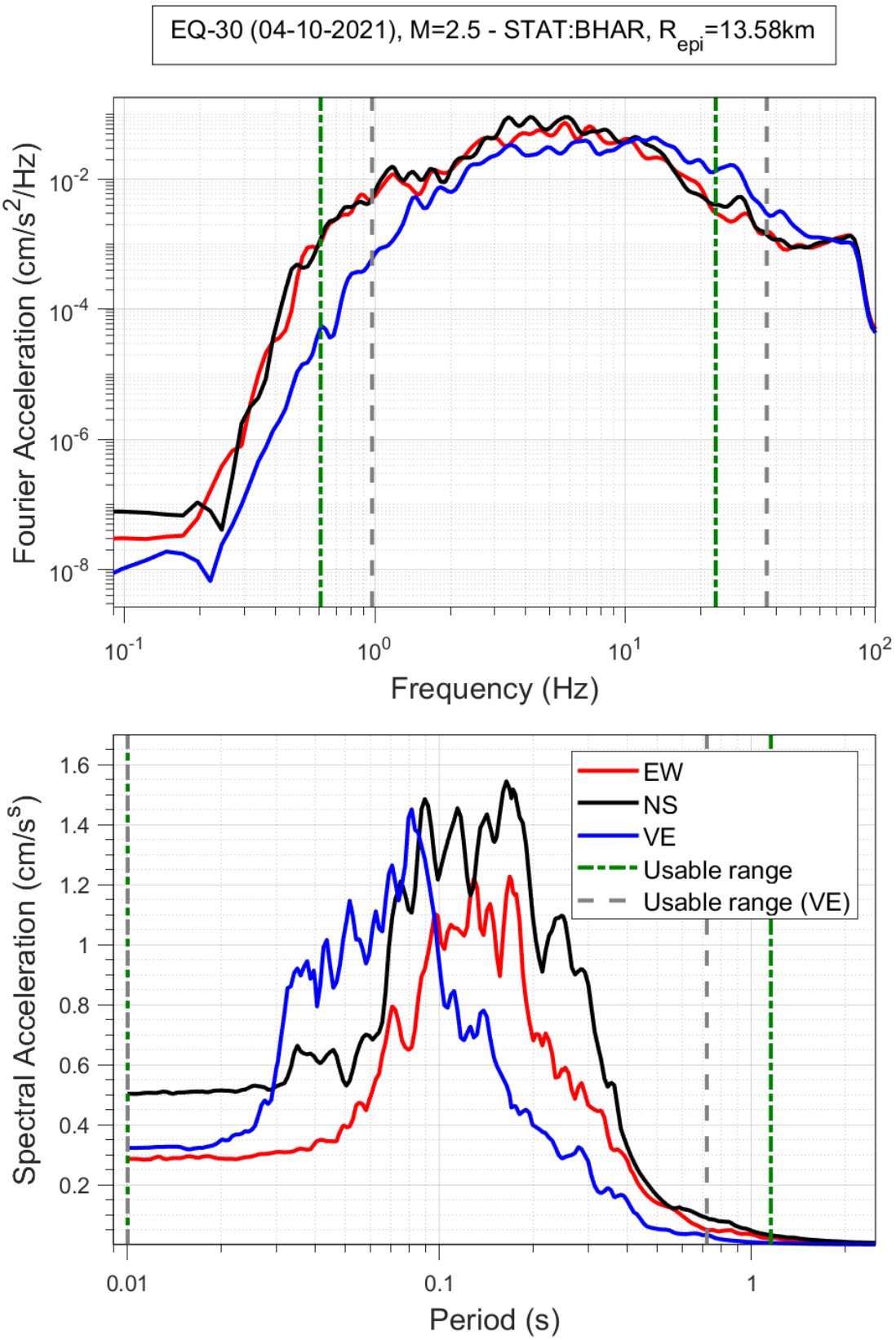
EQ-30 (04-10-2021), M=2.5 - STAT:BHAR, R_epi=13.58km
Fourier Acceleration (cm/s²/Hz)
10^-2
10^-4
10^-6
10^-8
10^-1
10^0
10^1
10^2
Frequency (Hz)
Spectral Acceleration (cm/s^s)
1.6
1.4
1.2
1
0.8
0.6
0.4
0.2
0.01
0.1
1
Period (s)
EW
NS
VE
Usable range
Usable range (VE)

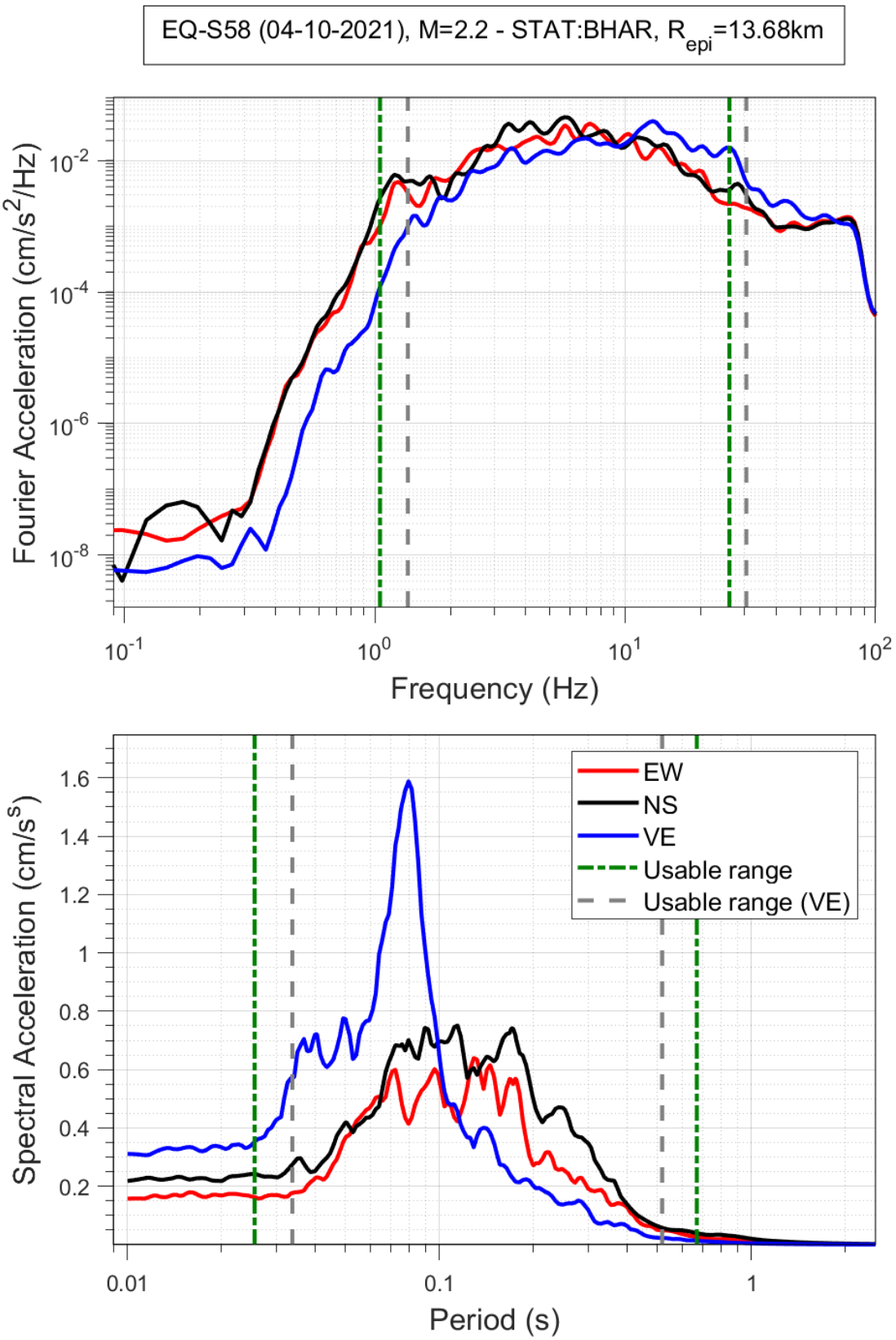
EQ-S58 (04-10-2021), M=2.2 - STAT:BHAR, R_epi=13.68km
Fourier Acceleration (cm/s²/Hz)
10^-2
10^-4
10^-6
10^-8
10^-1
10^0
10^1
10^2
Frequency (Hz)
Spectral Acceleration (cm/s²)
1.6
1.4
1.2
1
0.8
0.6
0.4
0.2
0.01
0.1
1
Period (s)
EW
NS
VE
Usable range
Usable range (VE)

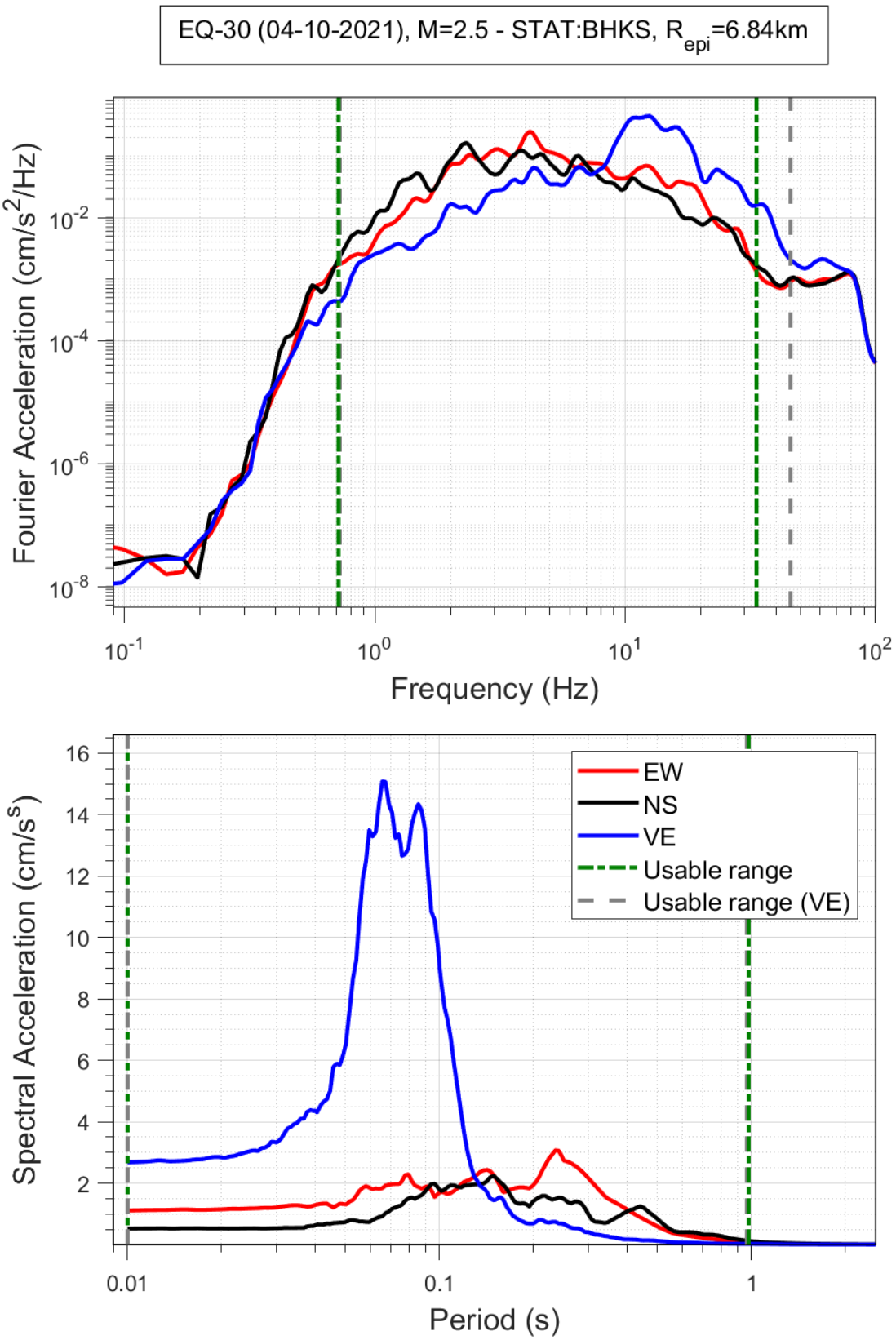
EQ-30 (04-10-2021), M=2.5 - STAT:BHKS, R_epi=6.84km
Fourier Acceleration (cm/s²/Hz)
10^-2
10^-4
10^-6
10^-8
10^-1
10^0
10^1
10^2
Frequency (Hz)
Spectral Acceleration (cm/s^s)
16
14
12
10
8
6
4
2
0.01
0.1
1
Period (s)
EW
NS
VE
Usable range
Usable range (VE)

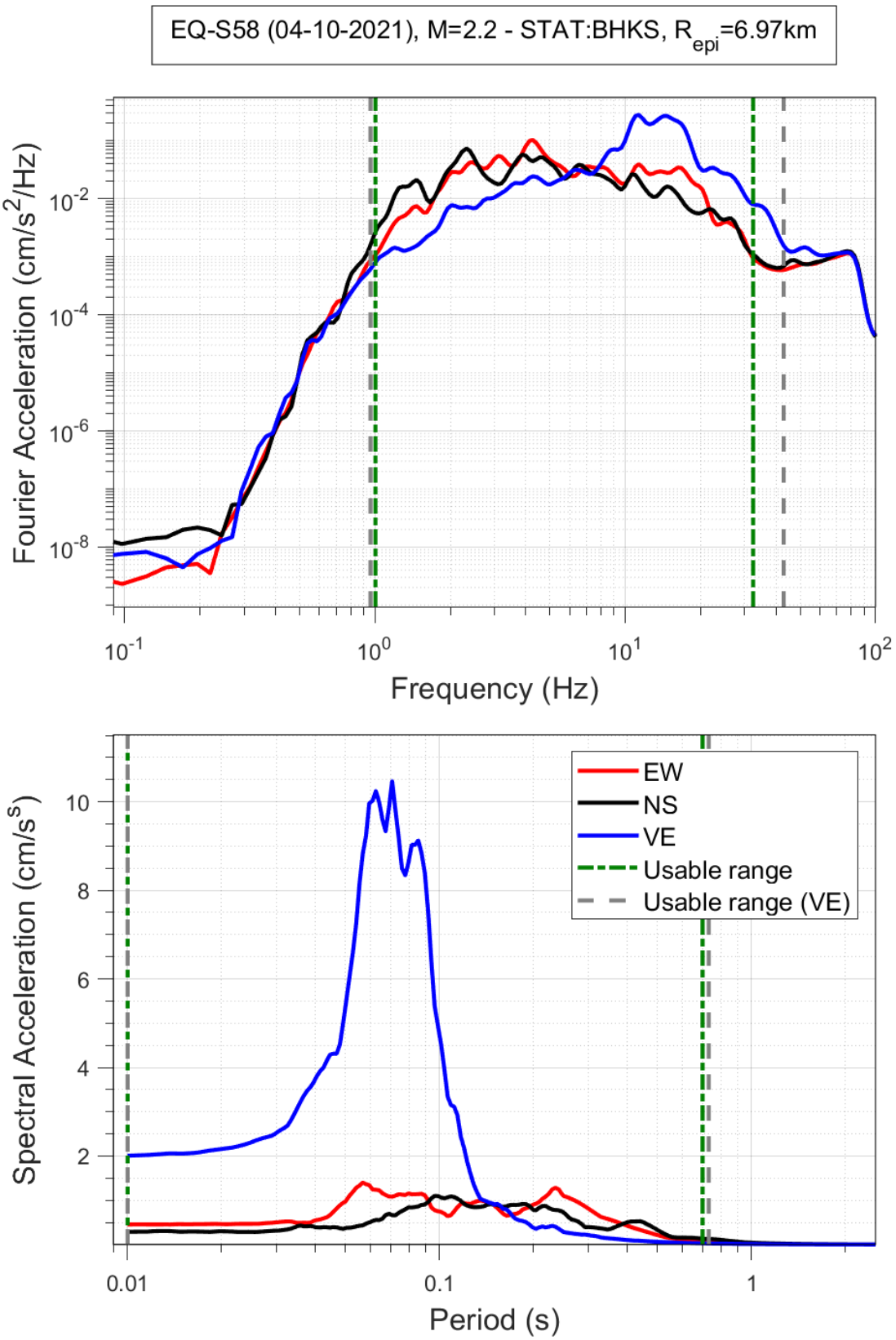
EQ-S58 (04-10-2021), M=2.2 - STAT:BHKS, R_epi=6.97km
Fourier Acceleration (cm/s²/Hz)
10^-2
10^-4
10^-6
10^-8
10^-1
10^0
10^1
10^2
Frequency (Hz)
Spectral Acceleration (cm/s²)
10
8
6
4
2
0.01
0.1
1
Period (s)
EW
NS
VE
Usable range
Usable range (VE)

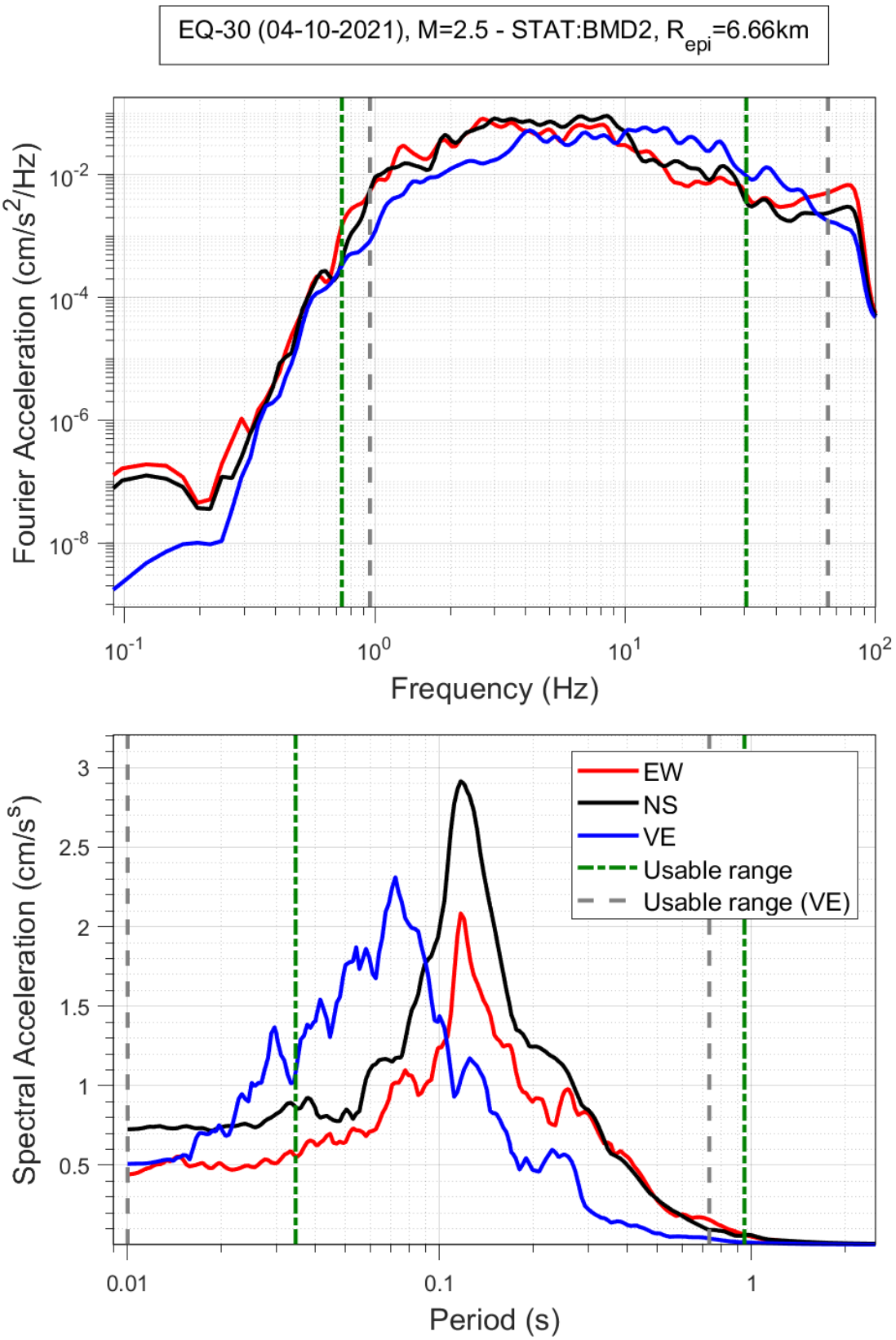
EQ-30 (04-10-2021), M=2.5 - STAT:BMD2, R_epi=6.66km
Fourier Acceleration (cm/s²/Hz)
10^-2
10^-4
10^-6
10^-8
10^-1
10^0
10^1
10^2
Frequency (Hz)
Spectral Acceleration (cm/s^s)
3
2.5
2
1.5
1
0.5
0.01
0.1
1
Period (s)
EW
NS
VE
Usable range
Usable range (VE)

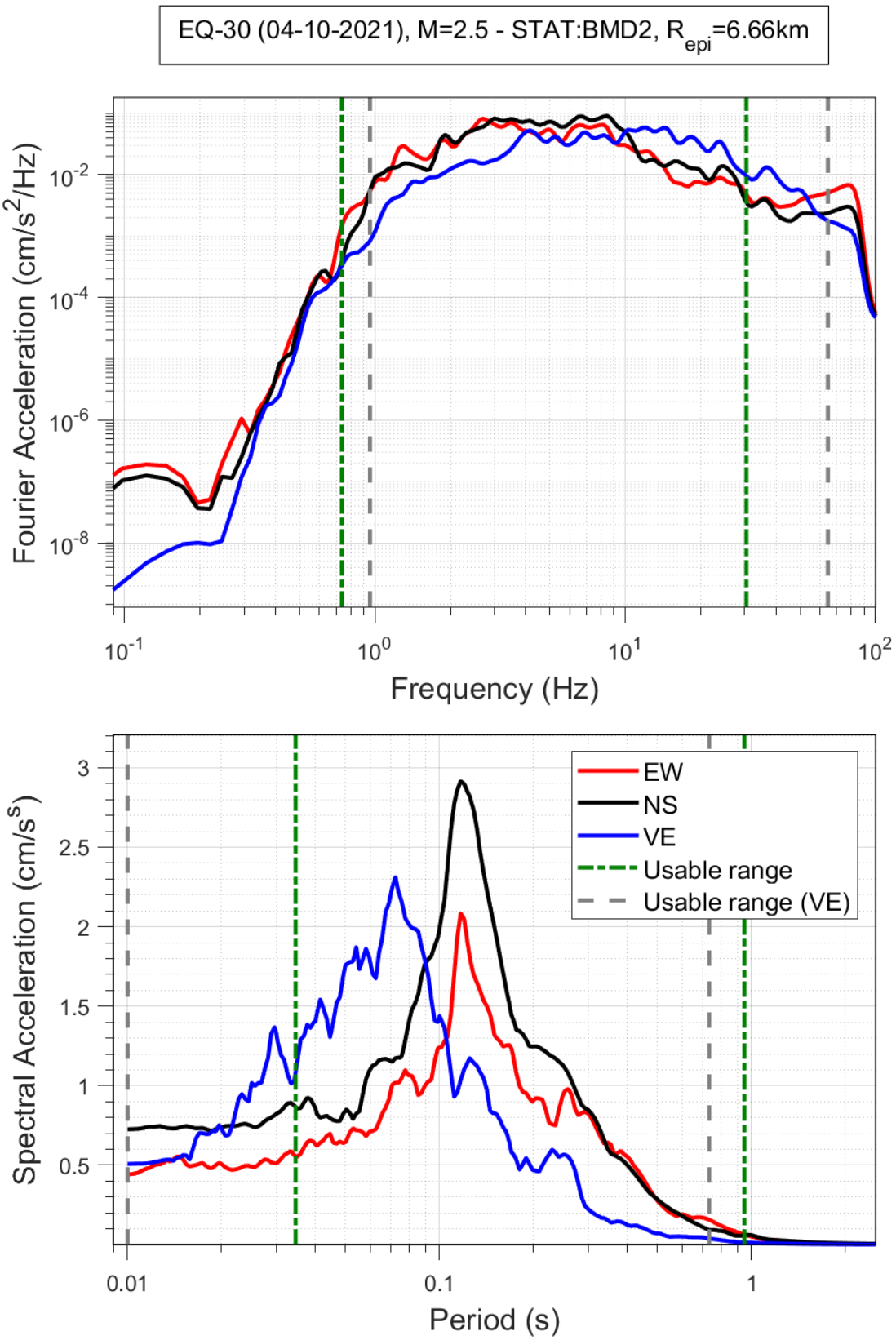
EQ-30 (04-10-2021), M=2.5 - STAT:BMD2, R_epi=6.66km
Fourier Acceleration (cm/s²/Hz)
10^-2
10^-4
10^-6
10^-8
10^-1
10^0
10^1
10^2
Frequency (Hz)
Spectral Acceleration (cm/s²)
3
2.5
2
1.5
1
0.5
0.01
0.1
1
Period (s)
EW
NS
VE
Usable range
Usable range (VE)

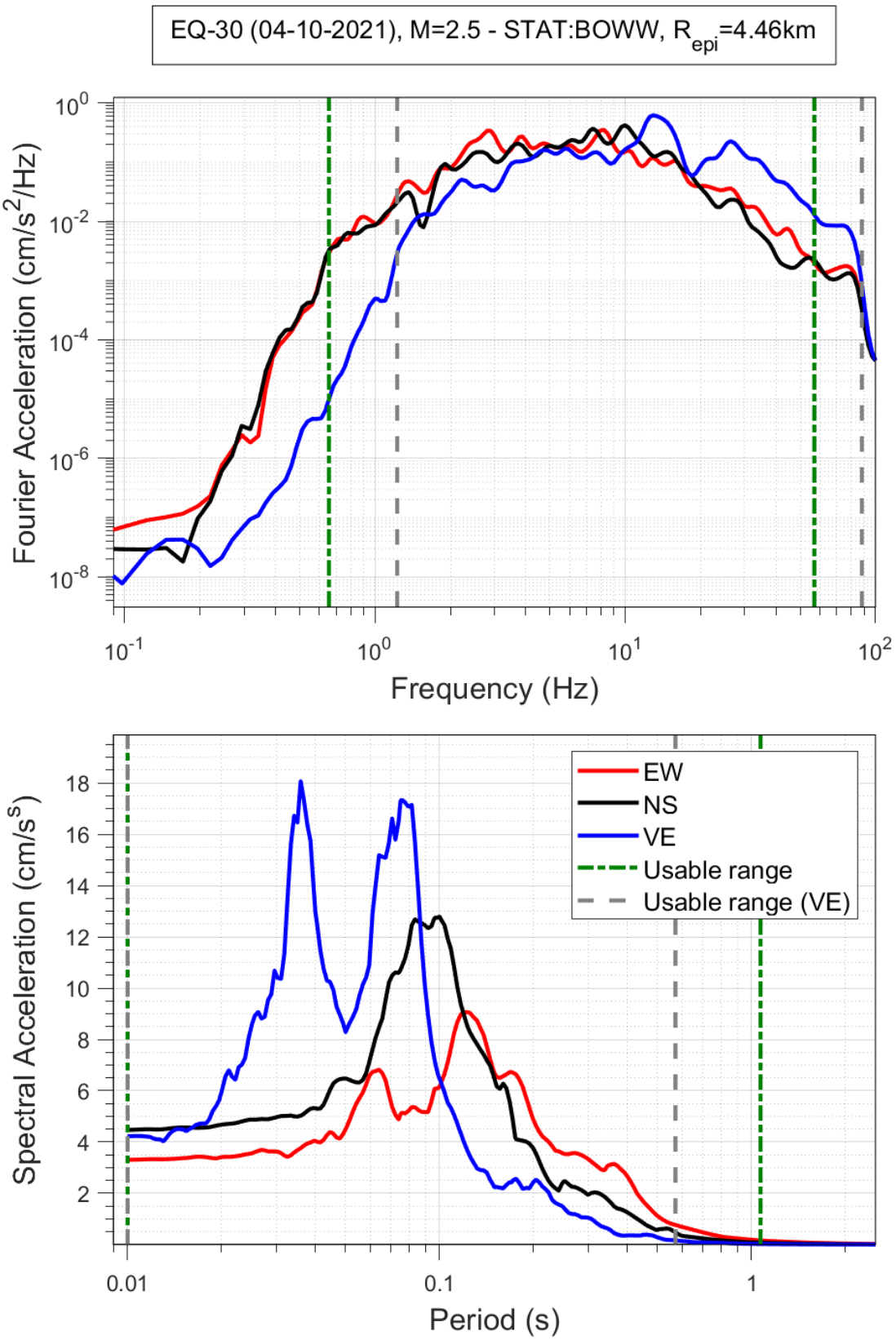
EQ-30 (04-10-2021), M=2.5 - STAT:BOWW, R_epi=4.46km
Fourier Acceleration (cm/s²/Hz)
Frequency (Hz)
Spectral Acceleration (cm/s²)
Period (s)
EW
NS
VE
Usable range
Usable range (VE)

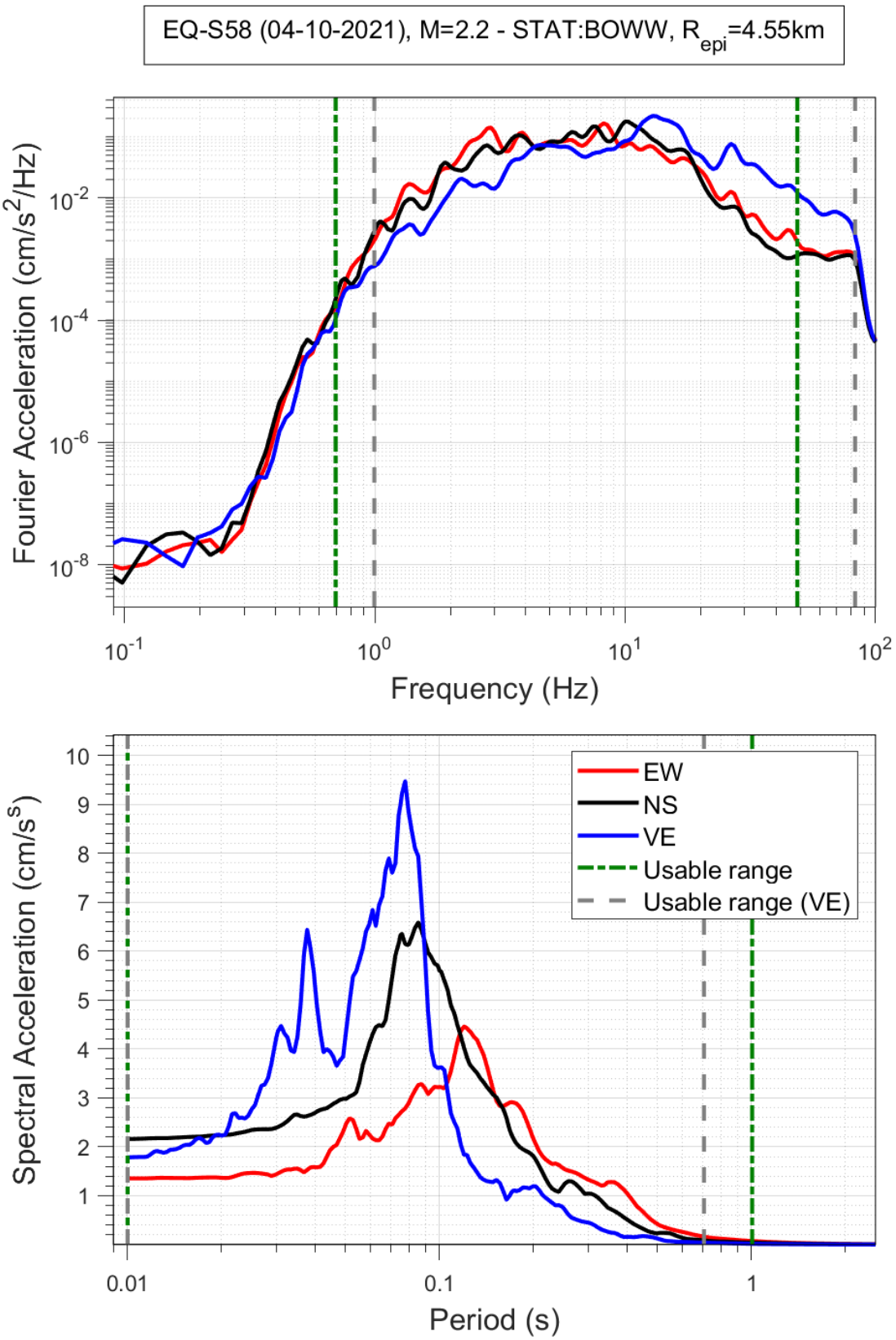
EQ-S58 (04-10-2021), M=2.2 - STAT:BOWW, R$_{epi}$=4.55km
Fourier Acceleration (cm/s^2/Hz)
10^{-2}
10^{-4}
10^{-6}
10^{-8}
10^{-1}
10^{0}
10^{1}
10^{2}
Frequency (Hz)
Spectral Acceleration (cm/s^s)
10
9
8
7
6
5
4
3
2
1
0.01
0.1
1
Period (s)
EW
NS
VE
Usable range
Usable range (VE)

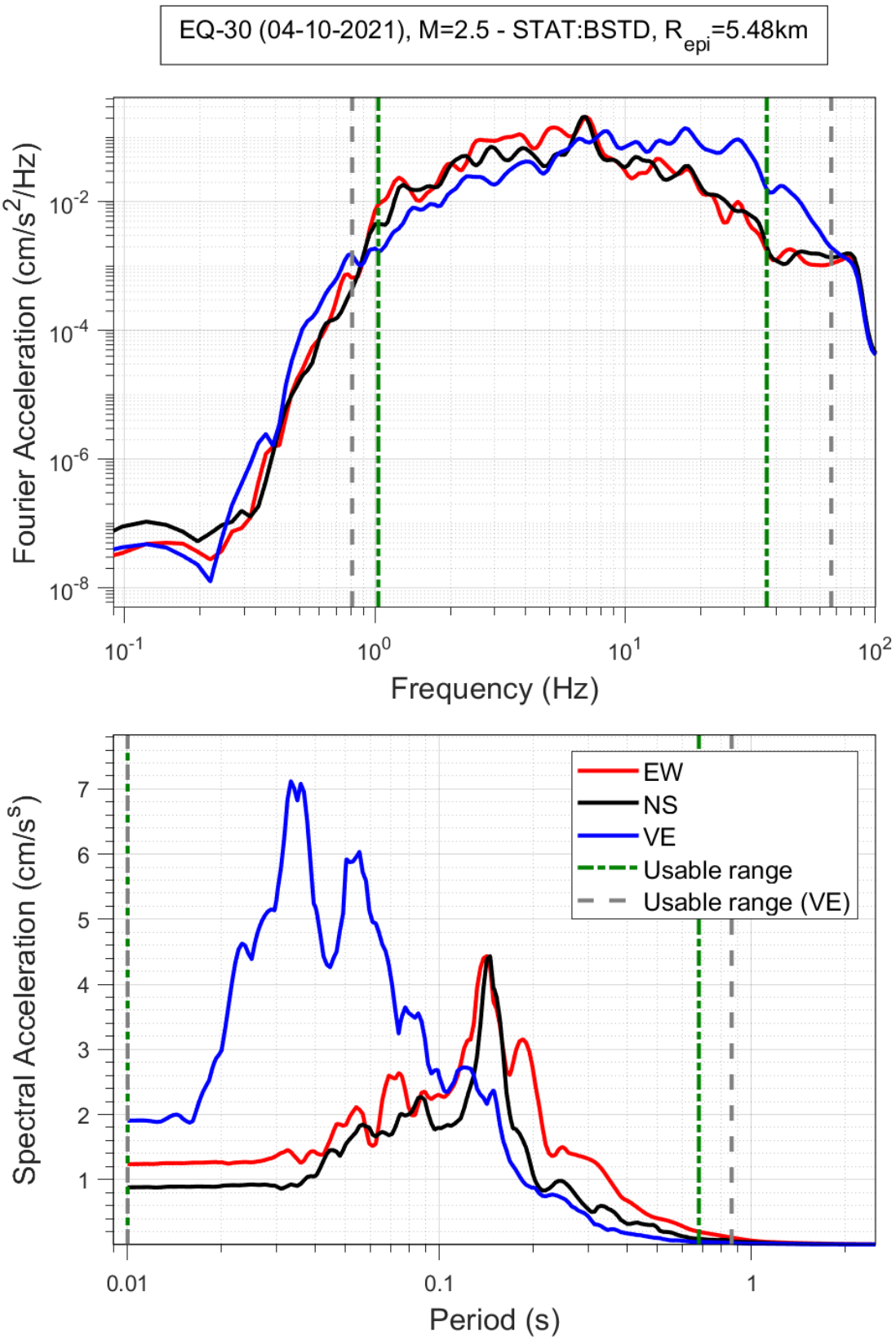
EQ-30 (04-10-2021), M=2.5 - STAT:BSTD, R epi =5.48km
Fourier Acceleration (cm/s2/Hz)
10-2
10-4
10-6
10-8
10-1
100
101
102
Frequency (Hz)
Spectral Acceleration (cm/s2)
7
6
5
4
3
2
1
0.01
0.1
1
Period (s)
EW
NS
VE
Usable range
Usable range (VE)

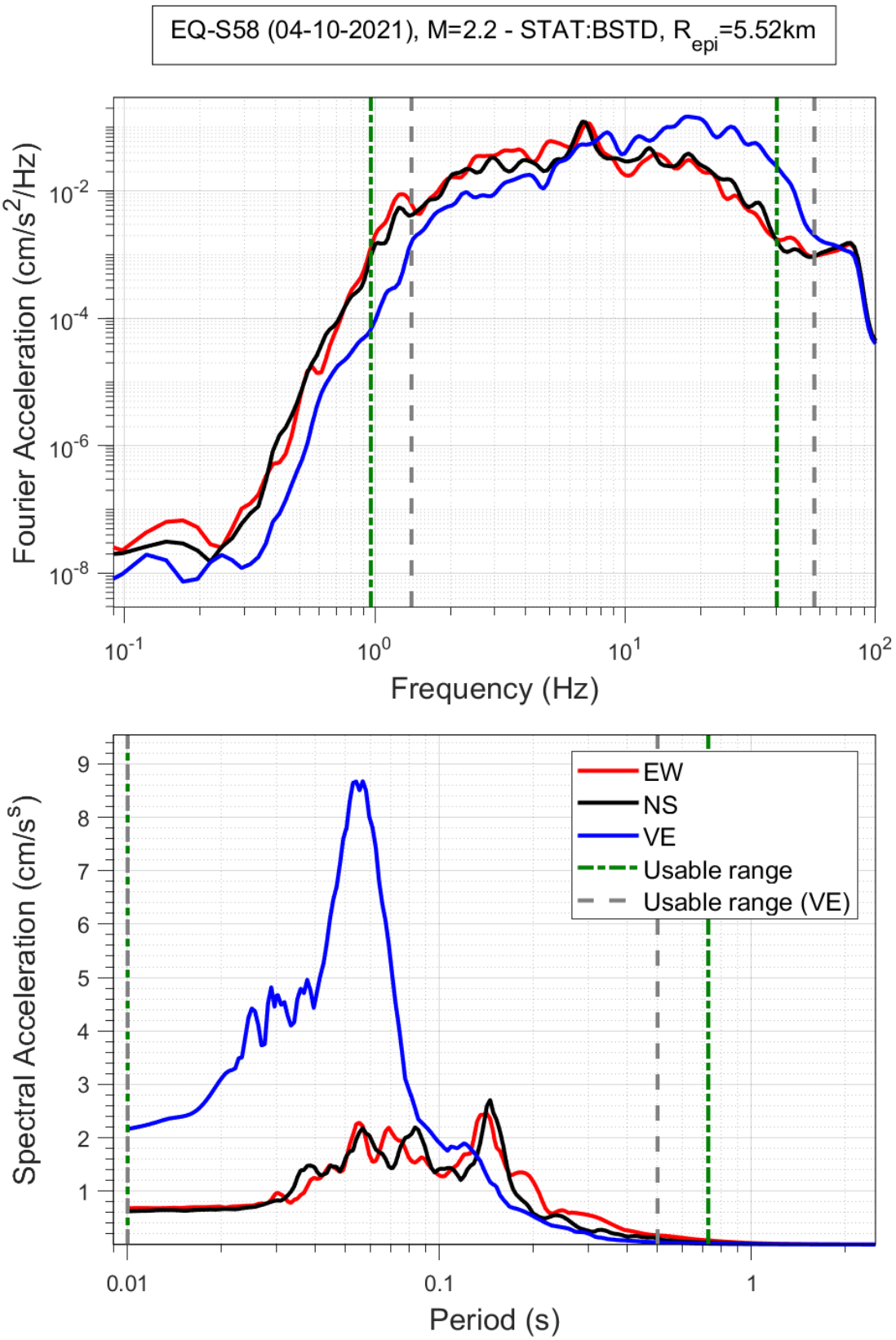
EQ-S58 (04-10-2021), M=2.2 - STAT:BSTD, R_epi=5.52km
Fourier Acceleration (cm/s²/Hz)
10^-2
10^-4
10^-6
10^-8
10^-1
10^0
10^1
10^2
Frequency (Hz)
Spectral Acceleration (cm/s²)
9
8
7
6
5
4
3
2
1
0.01
0.1
1
Period (s)
EW
NS
VE
Usable range
Usable range (VE)

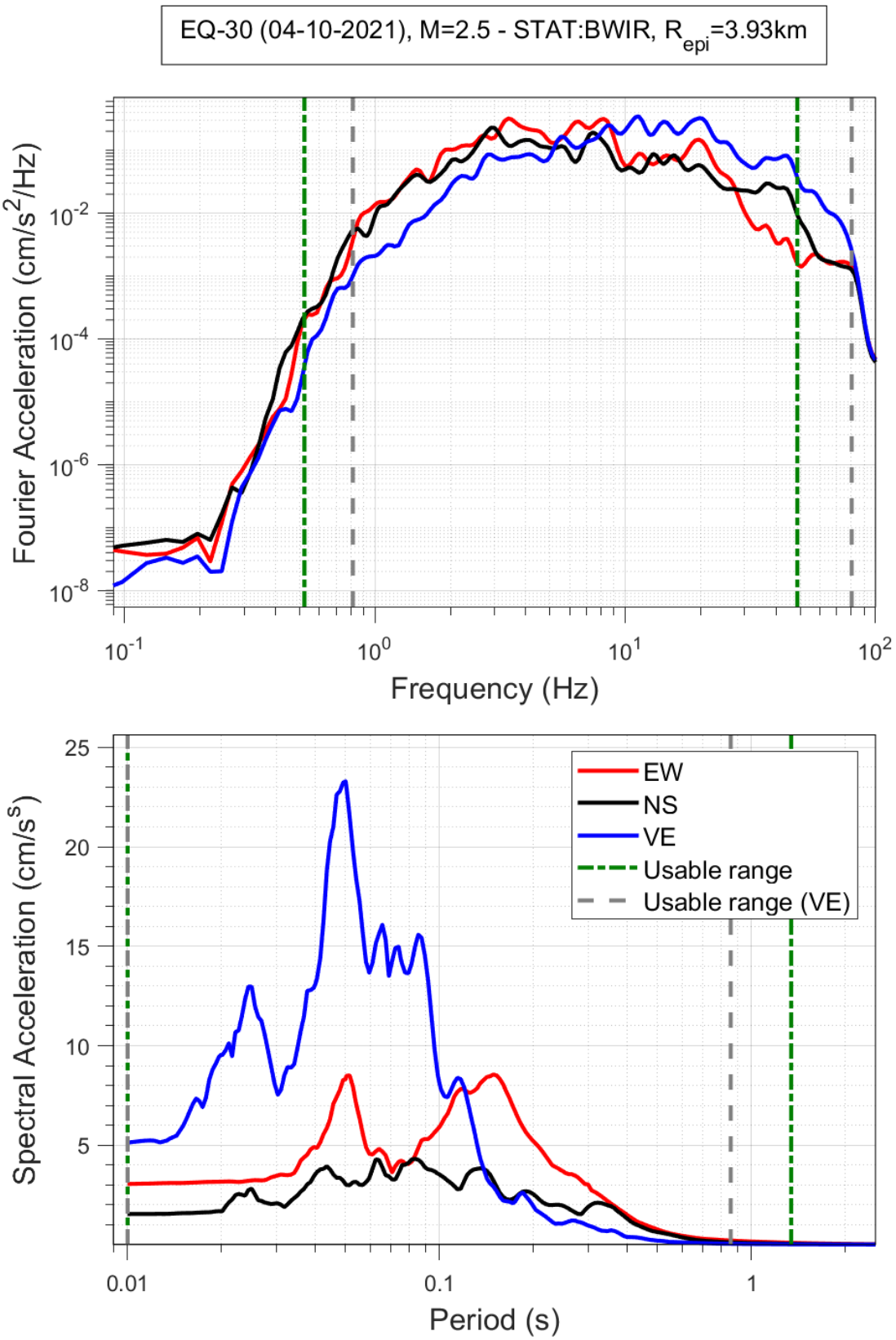
EQ-30 (04-10-2021), M=2.5 - STAT:BWIR, R_epi=3.93km
Fourier Acceleration (cm/s²/Hz)
10^-2
10^-4
10^-6
10^-8
10^-1
10^0
10^1
10^2
Frequency (Hz)
Spectral Acceleration (cm/s^s)
25
20
15
10
5
0.01
0.1
1
Period (s)
EW
NS
VE
Usable range
Usable range (VE)

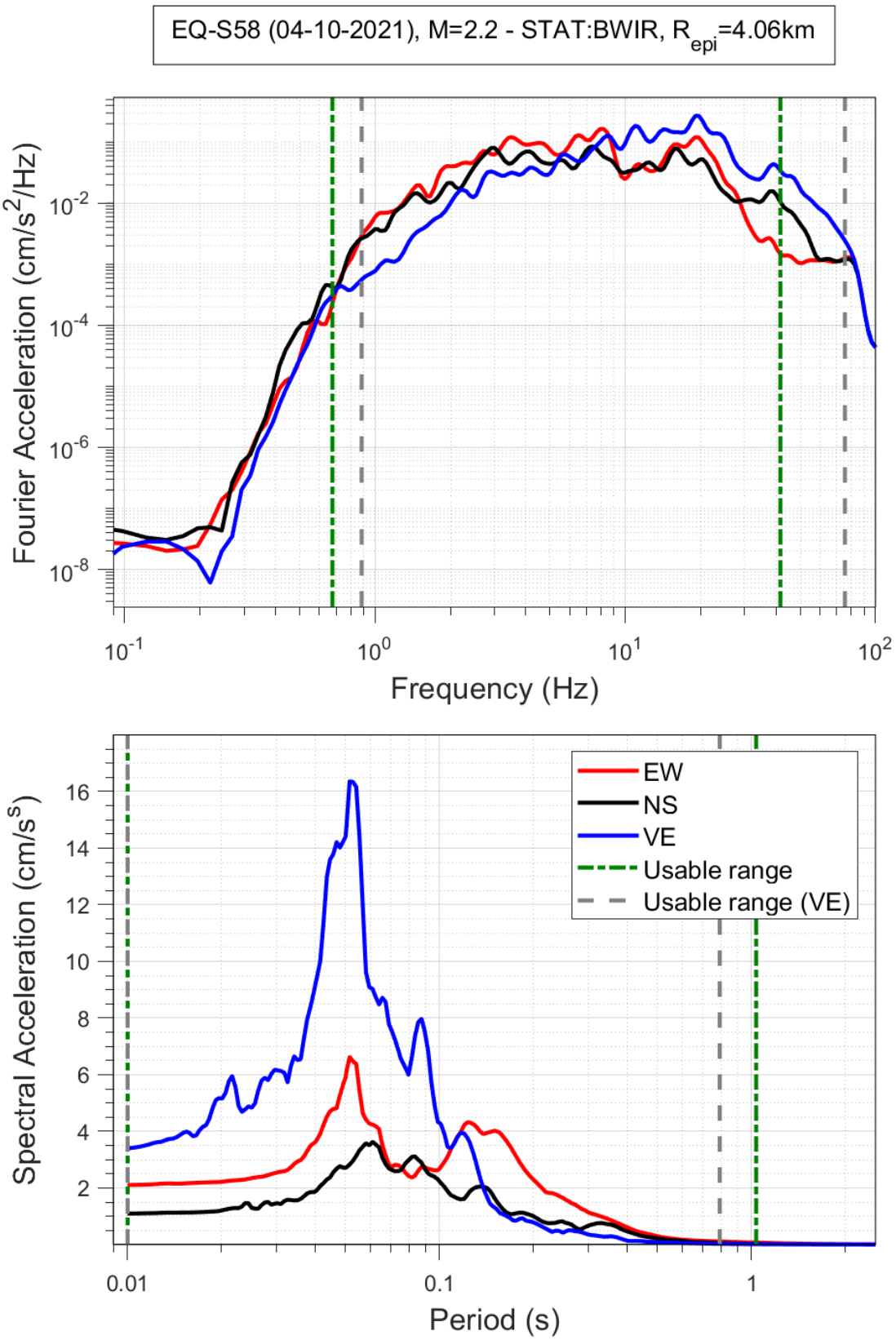
EQ-S58 (04-10-2021), M=2.2 - STAT:BWIR, R_epi=4.06km
Fourier Acceleration (cm/s²/Hz)
10^-2
10^-4
10^-6
10^-8
10^-1
10^0
10^1
10^2
Frequency (Hz)
Spectral Acceleration (cm/s²)
16
14
12
10
8
6
4
2
0.01
0.1
1
Period (s)
EW
NS
VE
Usable range
Usable range (VE)

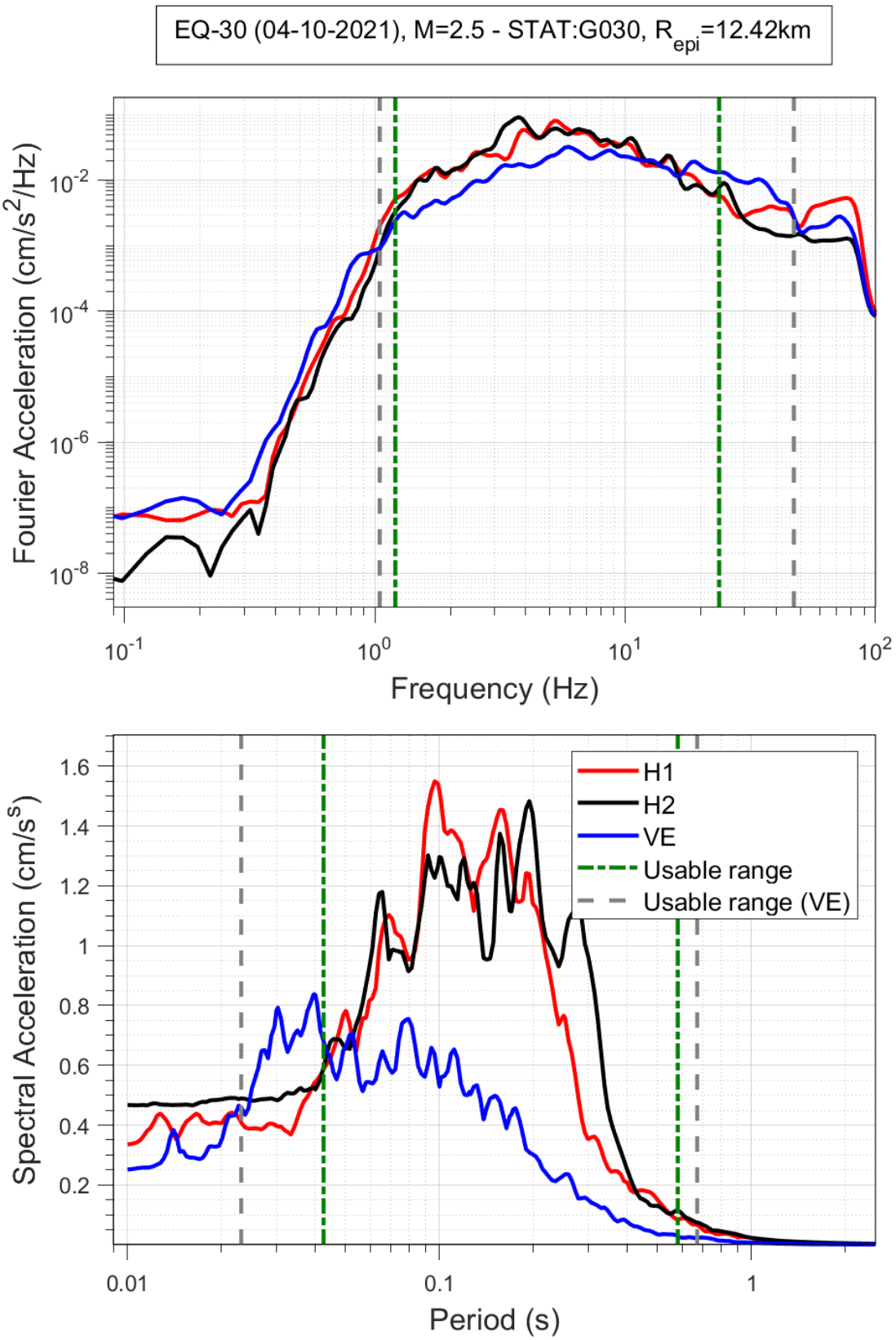
EQ-30 (04-10-2021), M=2.5 - STAT:G030, R_epi=12.42km
Fourier Acceleration (cm/s²/Hz)
10^-2
10^-4
10^-6
10^-8
10^-1
10^0
10^1
10^2
Frequency (Hz)
Spectral Acceleration (cm/s^s)
1.6
1.4
1.2
1
0.8
0.6
0.4
0.2
0.01
0.1
1
Period (s)
H1
H2
VE
Usable range
Usable range (VE)

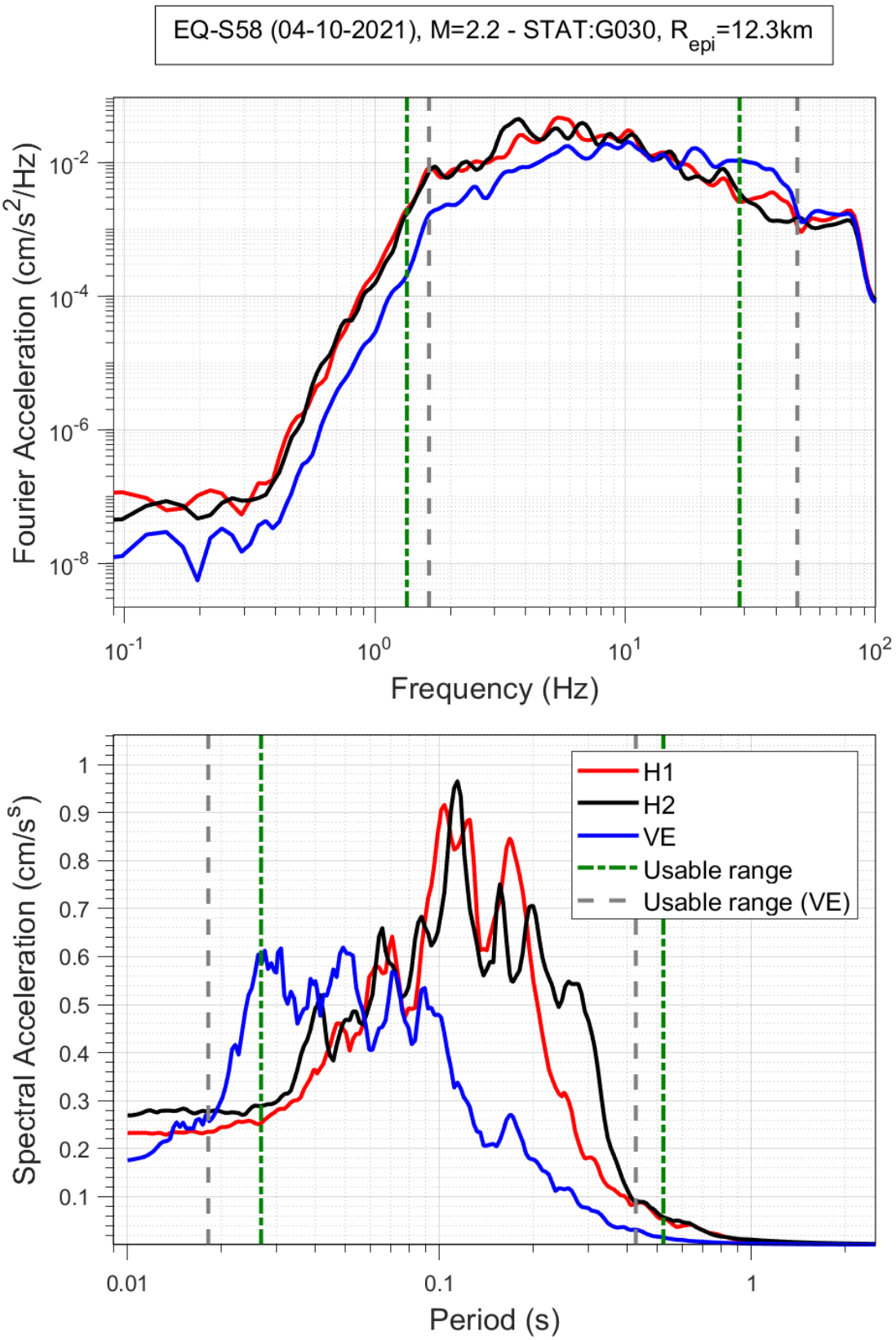
EQ-S58 (04-10-2021), M=2.2 - STAT:G030, R_epi=12.3km
Fourier Acceleration (cm/s²/Hz)
10^-2
10^-4
10^-6
10^-8
10^-1
10^0
10^1
10^2
Frequency (Hz)
Spectral Acceleration (cm/s²)
1
0.9
0.8
0.7
0.6
0.5
0.4
0.3
0.2
0.1
0.01
0.1
1
Period (s)
H1
H2
VE
Usable range
Usable range (VE)

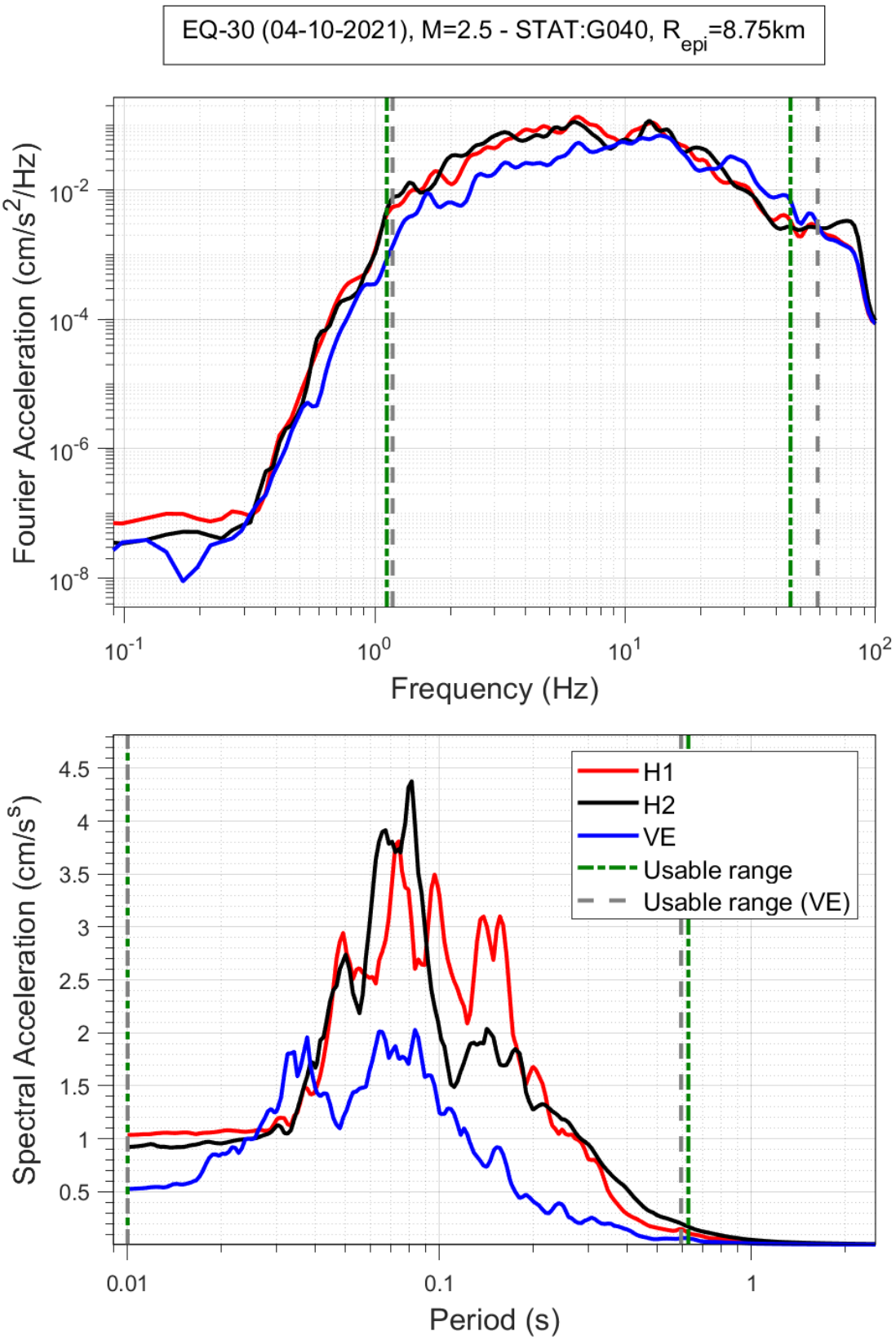
EQ-30 (04-10-2021), M=2.5 - STAT:G040, R epi =8.75km
Fourier Acceleration (cm/s2/Hz)
10-2
10-4
10-6
10-8
10-1
100
101
102
Frequency (Hz)
Spectral Acceleration (cm/s2)
4.5
4
3.5
3
2.5
2
1.5
1
0.5
0.01
0.1
1
Period (s)
H1
H2
VE
Usable range
Usable range (VE)

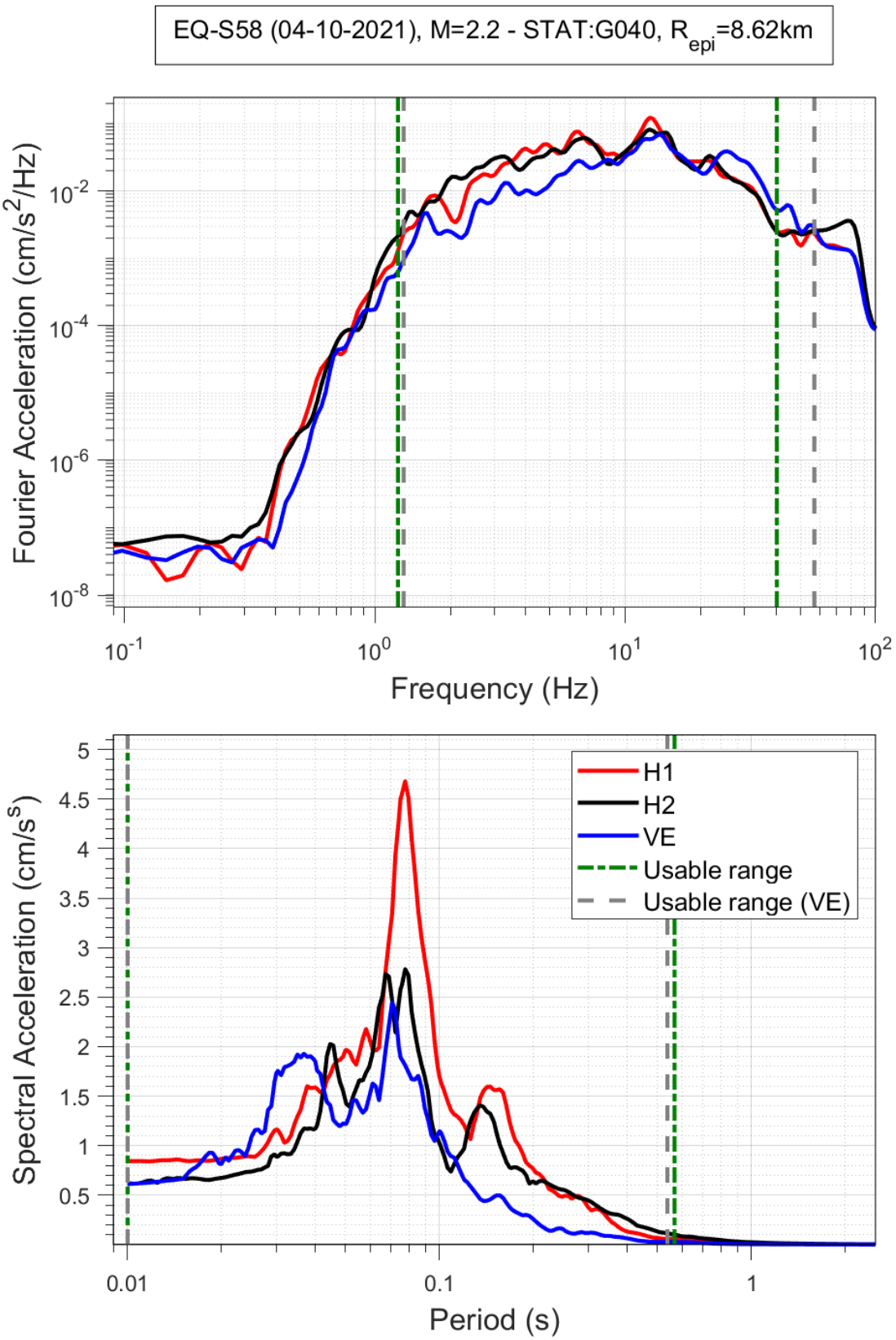
EQ-S58 (04-10-2021), M=2.2 - STAT:G040, R_epi=8.62km
Fourier Acceleration (cm/s²/Hz)
10^-2
10^-4
10^-6
10^-8
10^-1
10^0
10^1
10^2
Frequency (Hz)
Spectral Acceleration (cm/s^s)
5
4.5
4
3.5
3
2.5
2
1.5
1
0.5
0.01
0.1
1
Period (s)
H1
H2
VE
Usable range
Usable range (VE)

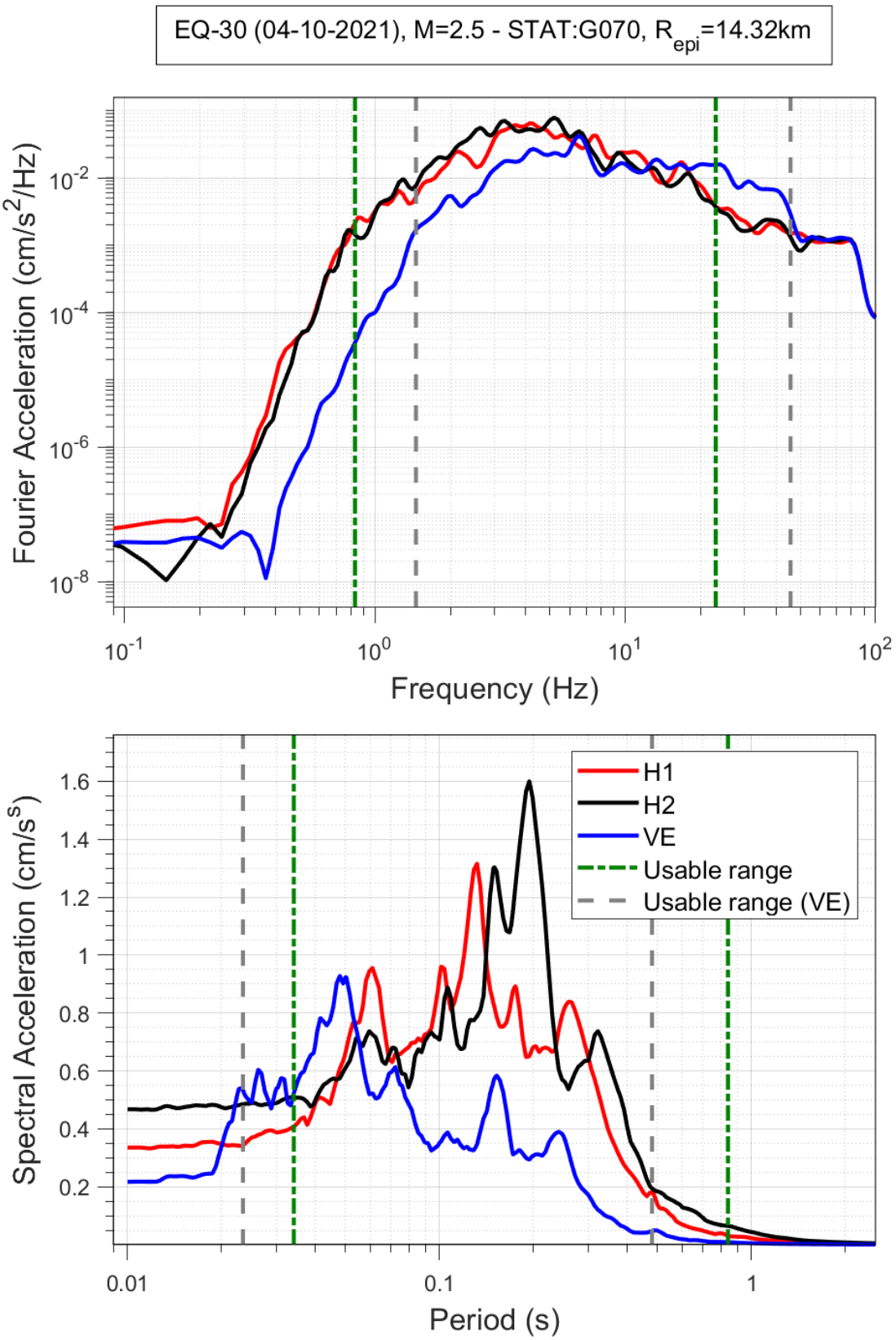
EQ-30 (04-10-2021), M=2.5 - STAT:G070, R_epi=14.32km
Fourier Acceleration (cm/s²/Hz)
10^-2
10^-4
10^-6
10^-8
10^-1
10^0
10^1
10^2
Frequency (Hz)
Spectral Acceleration (cm/s^s)
1.6
1.4
1.2
1
0.8
0.6
0.4
0.2
0.01
0.1
1
Period (s)
H1
H2
VE
Usable range
Usable range (VE)

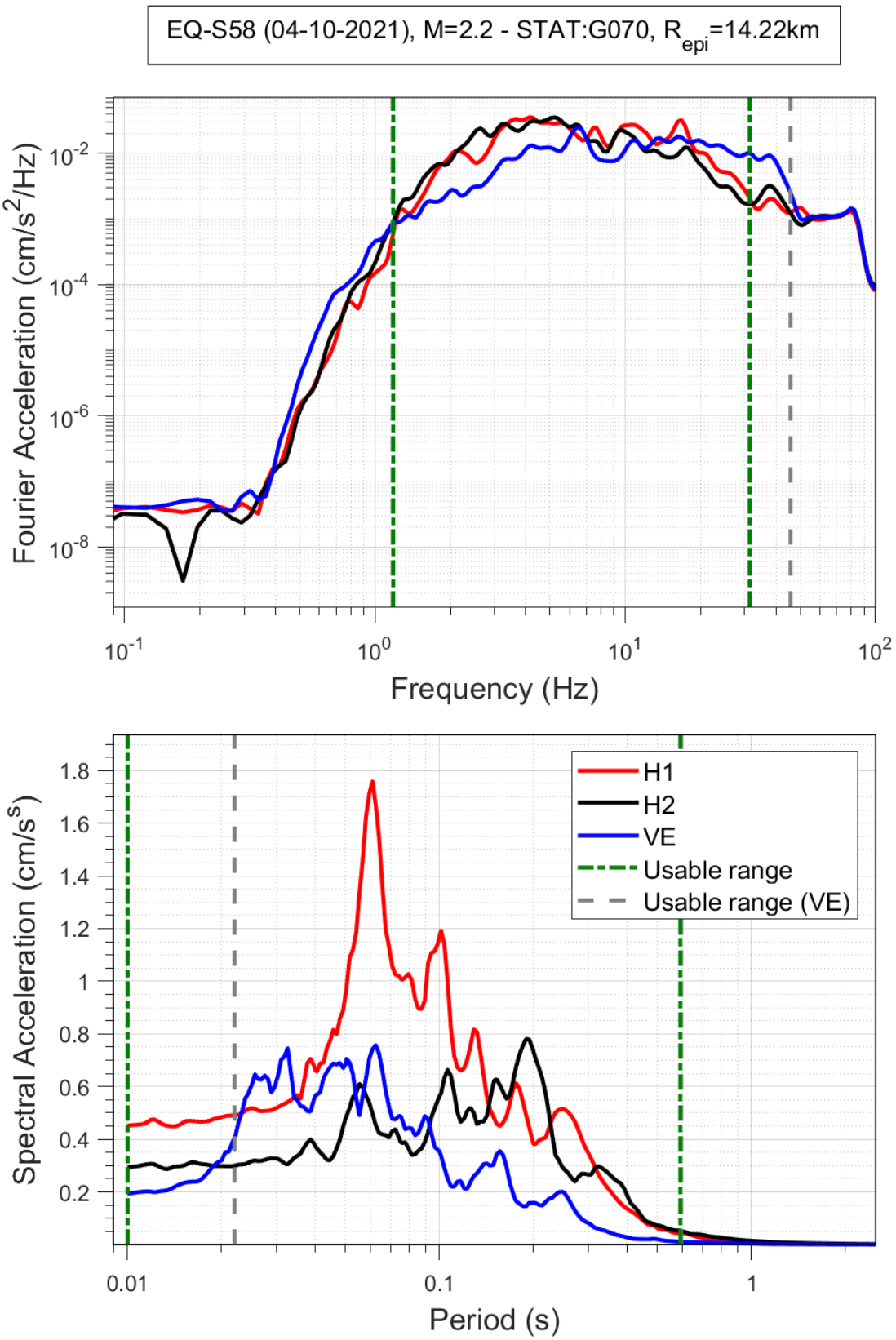
EQ-S58 (04-10-2021), M=2.2 - STAT:G070, R_epi=14.22km
Fourier Acceleration (cm/s²/Hz)
10^-2
10^-4
10^-6
10^-8
10^-1
10^0
10^1
10^2
Frequency (Hz)
Spectral Acceleration (cm/s^s)
1.8
1.6
1.4
1.2
1
0.8
0.6
0.4
0.2
0.01
0.1
1
Period (s)
H1
H2
VE
Usable range
Usable range (VE)

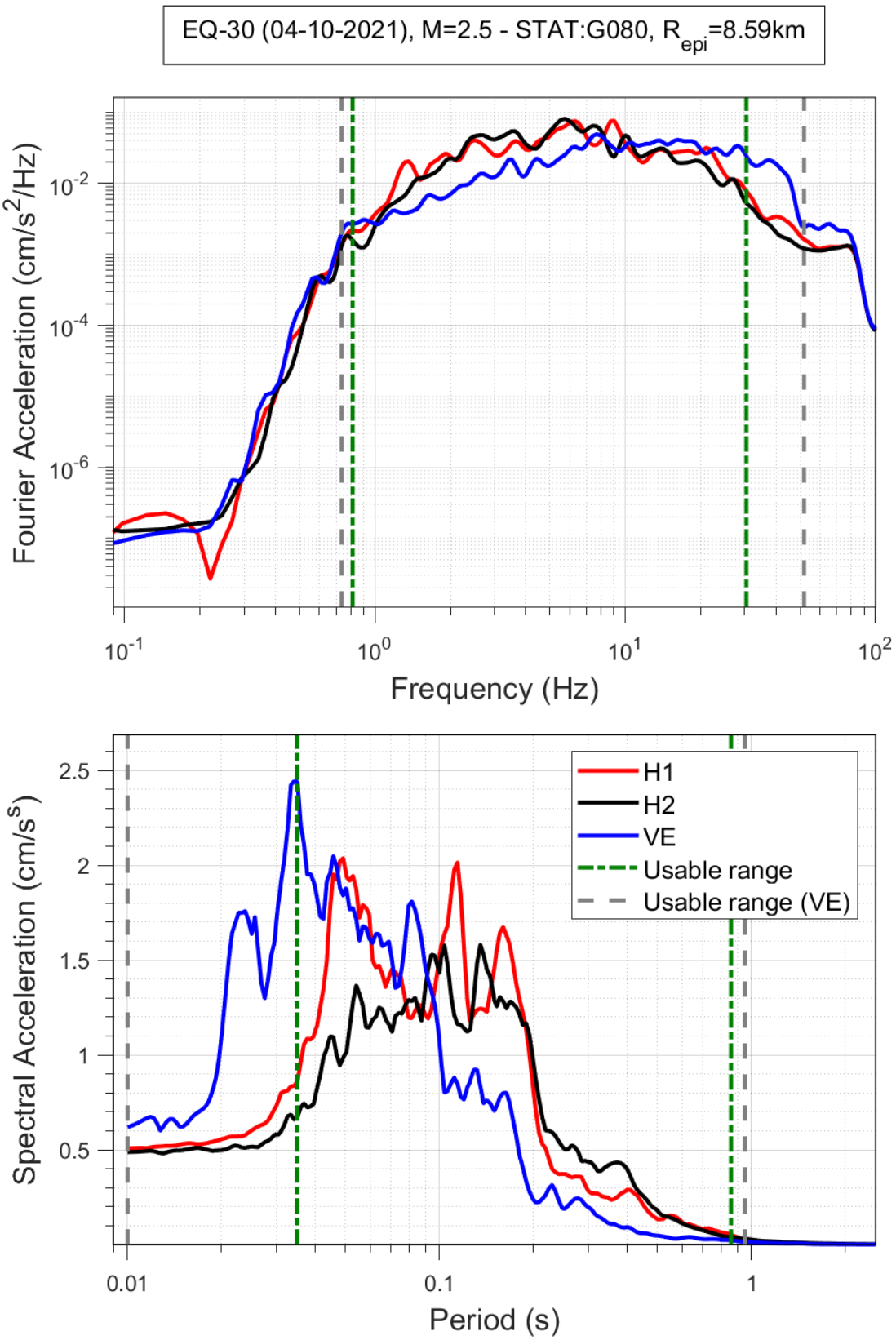
EQ-30 (04-10-2021), M=2.5 - STAT:G080, R_epi=8.59km
Fourier Acceleration (cm/s²/Hz)
10^-2
10^-4
10^-6
10^-1
10^0
10^1
10^2
Frequency (Hz)
Spectral Acceleration (cm/s²)
2.5
2
1.5
1
0.5
0.01
0.1
1
Period (s)
H1
H2
VE
Usable range
Usable range (VE)

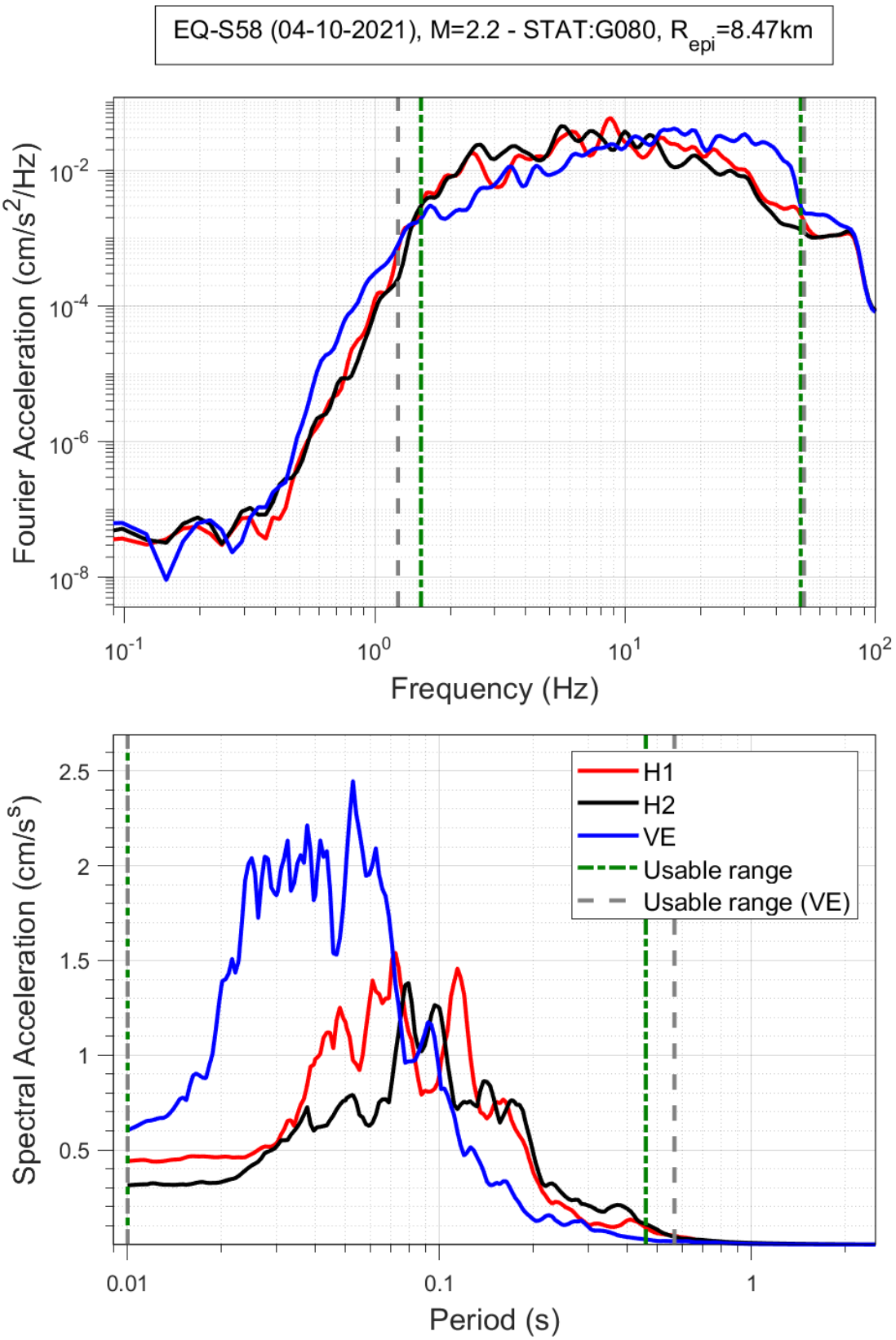
EQ-S58 (04-10-2021), M=2.2 - STAT:G080, R_epi=8.47km
Fourier Acceleration (cm/s²/Hz)
10^-2
10^-4
10^-6
10^-8
10^-1
10^0
10^1
10^2
Frequency (Hz)
Spectral Acceleration (cm/s²)
2.5
2
1.5
1
0.5
0.01
0.1
1
Period (s)
H1
H2
VE
Usable range
Usable range (VE)

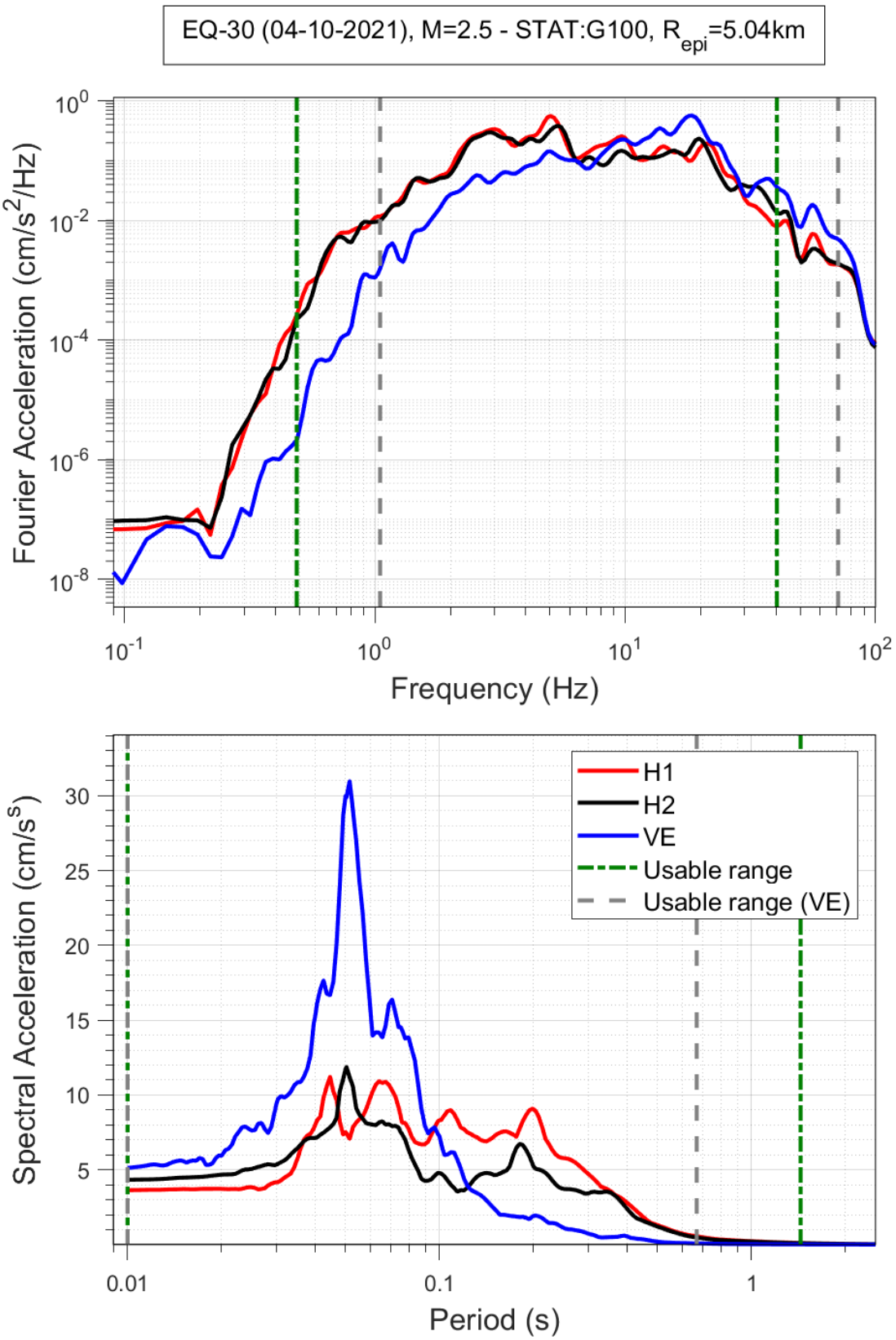
EQ-30 (04-10-2021), M=2.5 - STAT:G100, R epi=5.04km
Fourier Acceleration (cm/s2/Hz)
Frequency (Hz)
Spectral Acceleration (cm/s2)
Period (s)
H1
H2
VE
Usable range
Usable range (VE)

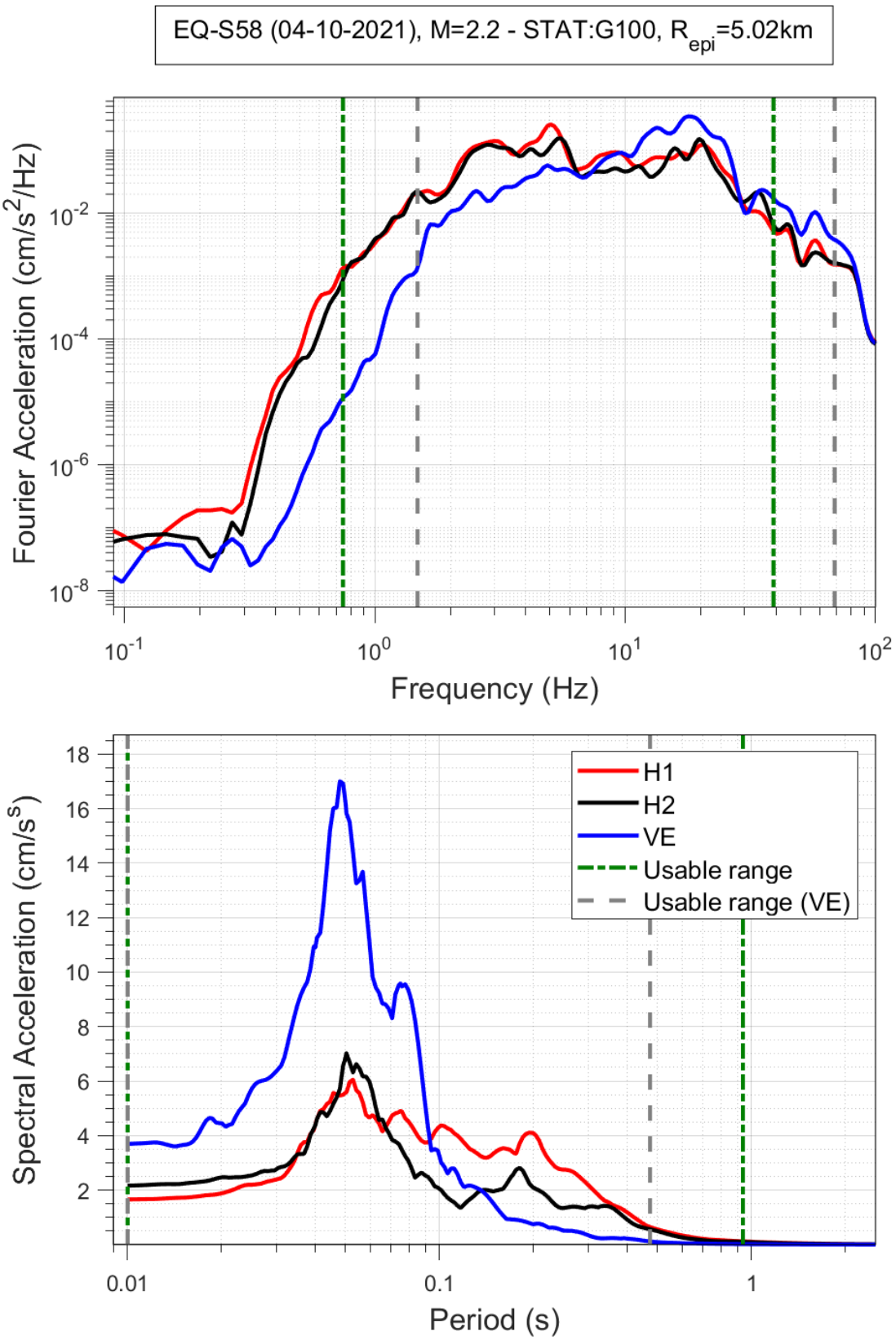
EQ-S58 (04-10-2021), M=2.2 - STAT:G100, R_epi=5.02km
Fourier Acceleration (cm/s²/Hz)
10^-2
10^-4
10^-6
10^-8
10^-1
10^0
10^1
10^2
Frequency (Hz)
Spectral Acceleration (cm/s²)
18
16
14
12
10
8
6
4
2
0.01
0.1
1
Period (s)
H1
H2
VE
Usable range
Usable range (VE)

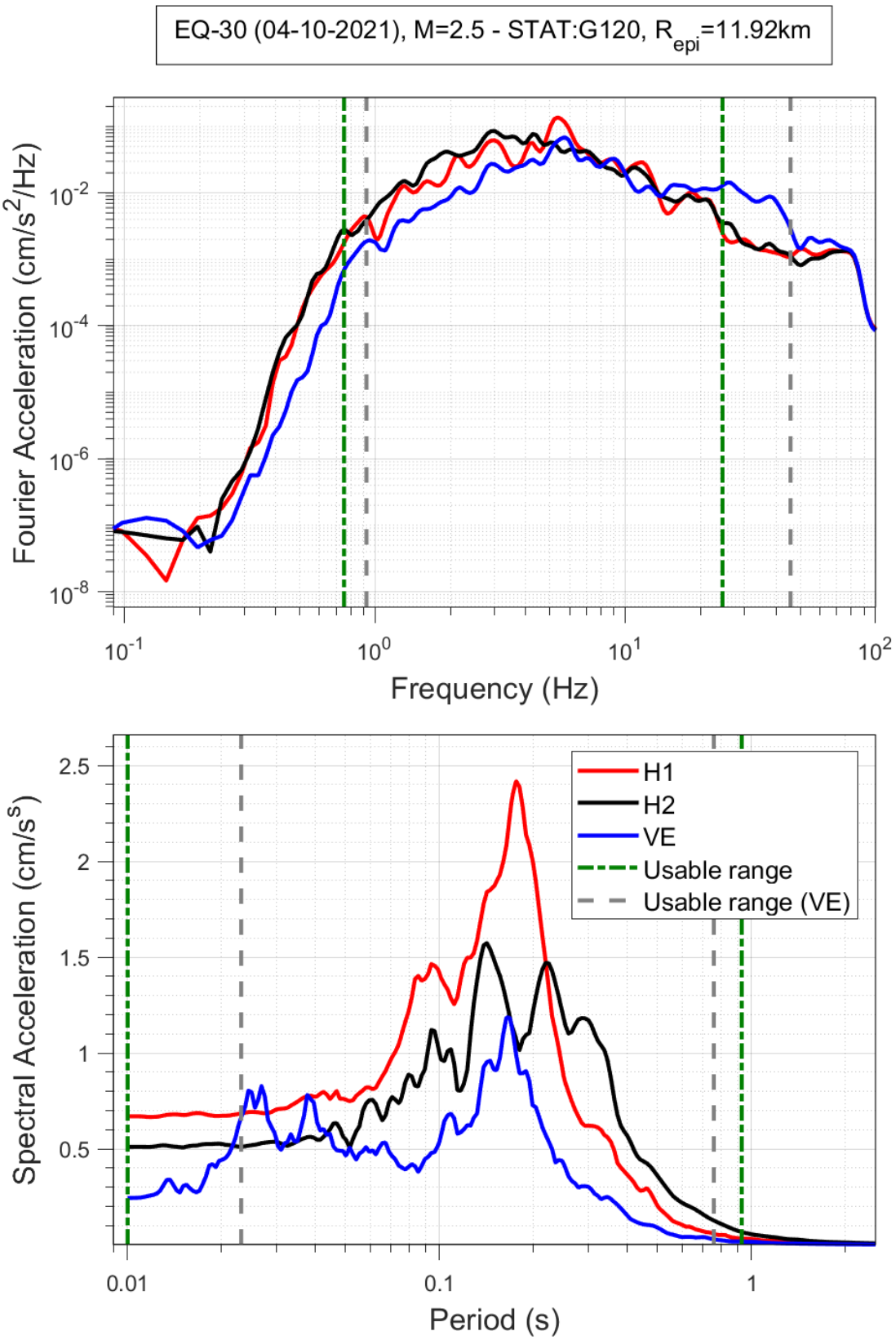
EQ-30 (04-10-2021), M=2.5 - STAT:G120, R_epi=11.92km
Fourier Acceleration (cm/s²/Hz)
10^-2
10^-4
10^-6
10^-8
10^-1
10^0
10^1
10^2
Frequency (Hz)
Spectral Acceleration (cm/s^s)
2.5
2
1.5
1
0.5
0.01
0.1
1
Period (s)
H1
H2
VE
Usable range
Usable range (VE)

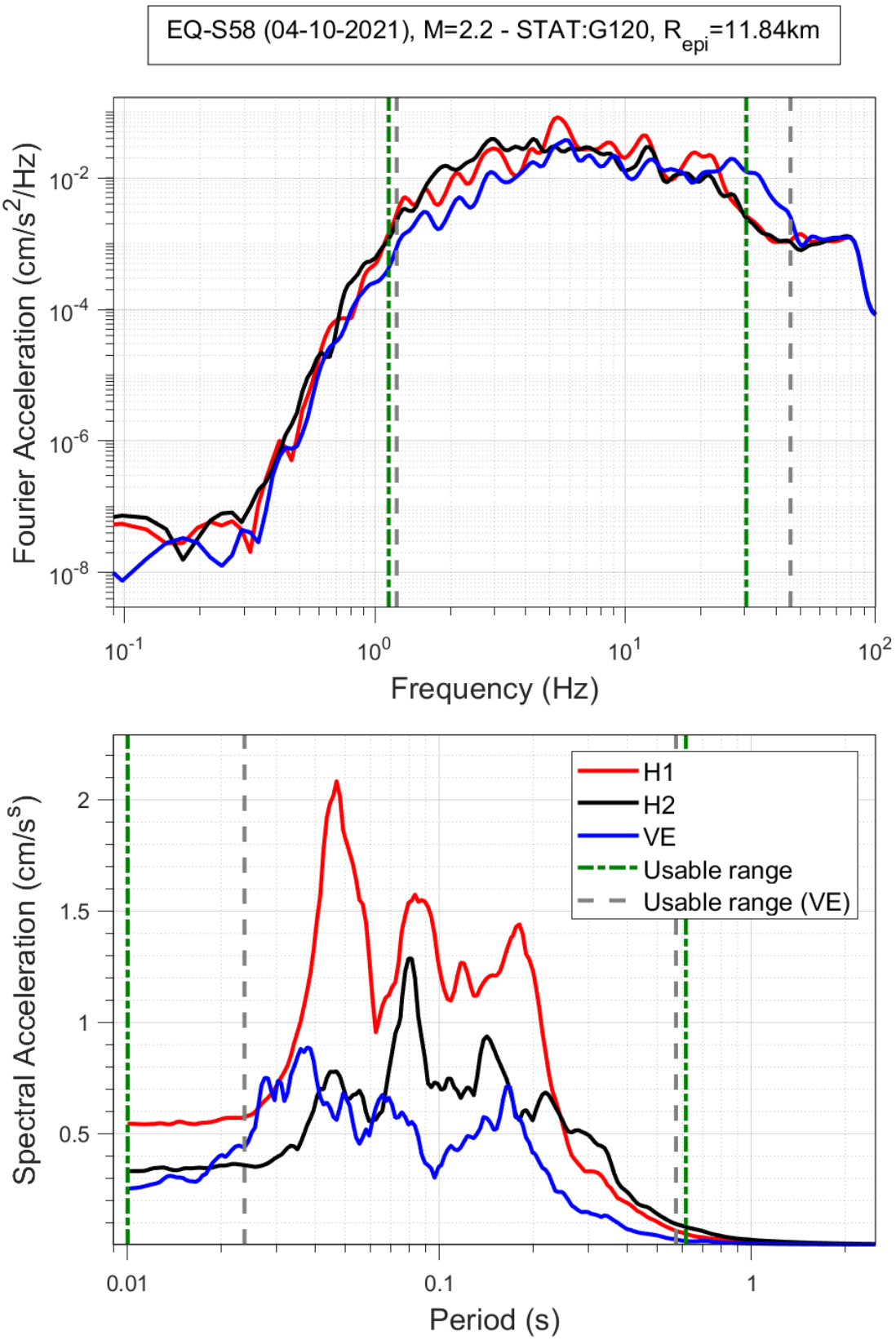
EQ-S58 (04-10-2021), M=2.2 - STAT:G120, R epi=11.84km
Fourier Acceleration (cm/s2/Hz)
10-2
10-4
10-6
10-8
10-1
100
101
102
Frequency (Hz)
Spectral Acceleration (cm/s2)
2
1.5
1
0.5
0.01
0.1
1
Period (s)
H1
H2
VE
Usable range
Usable range (VE)

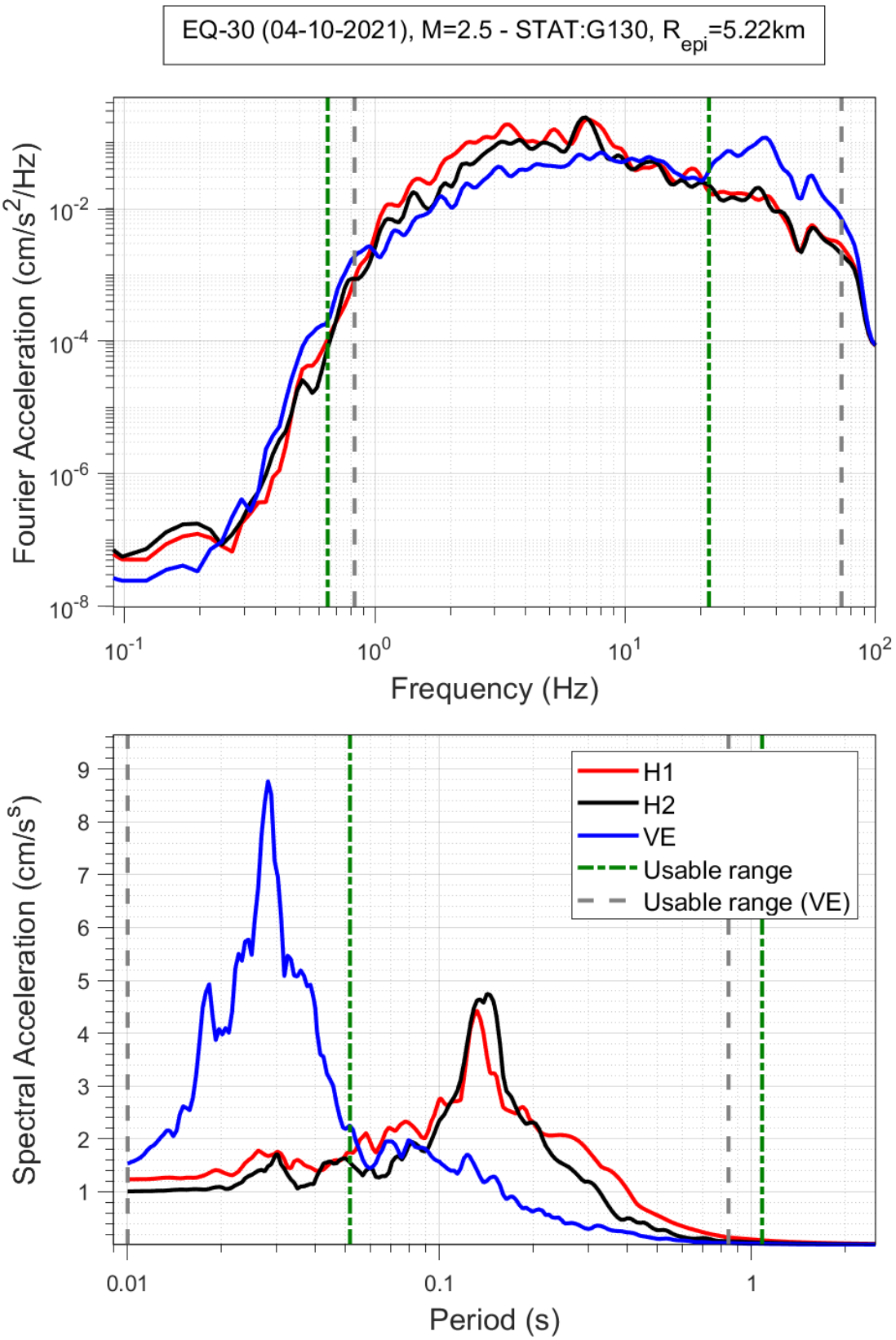
EQ-30 (04-10-2021), M=2.5 - STAT:G130, R_epi=5.22km
Fourier Acceleration (cm/s²/Hz)
10^-2
10^-4
10^-6
10^-8
10^-1
10^0
10^1
10^2
Frequency (Hz)
Spectral Acceleration (cm/s^s)
9
8
7
6
5
4
3
2
1
0.01
0.1
1
Period (s)
H1
H2
VE
Usable range
Usable range (VE)

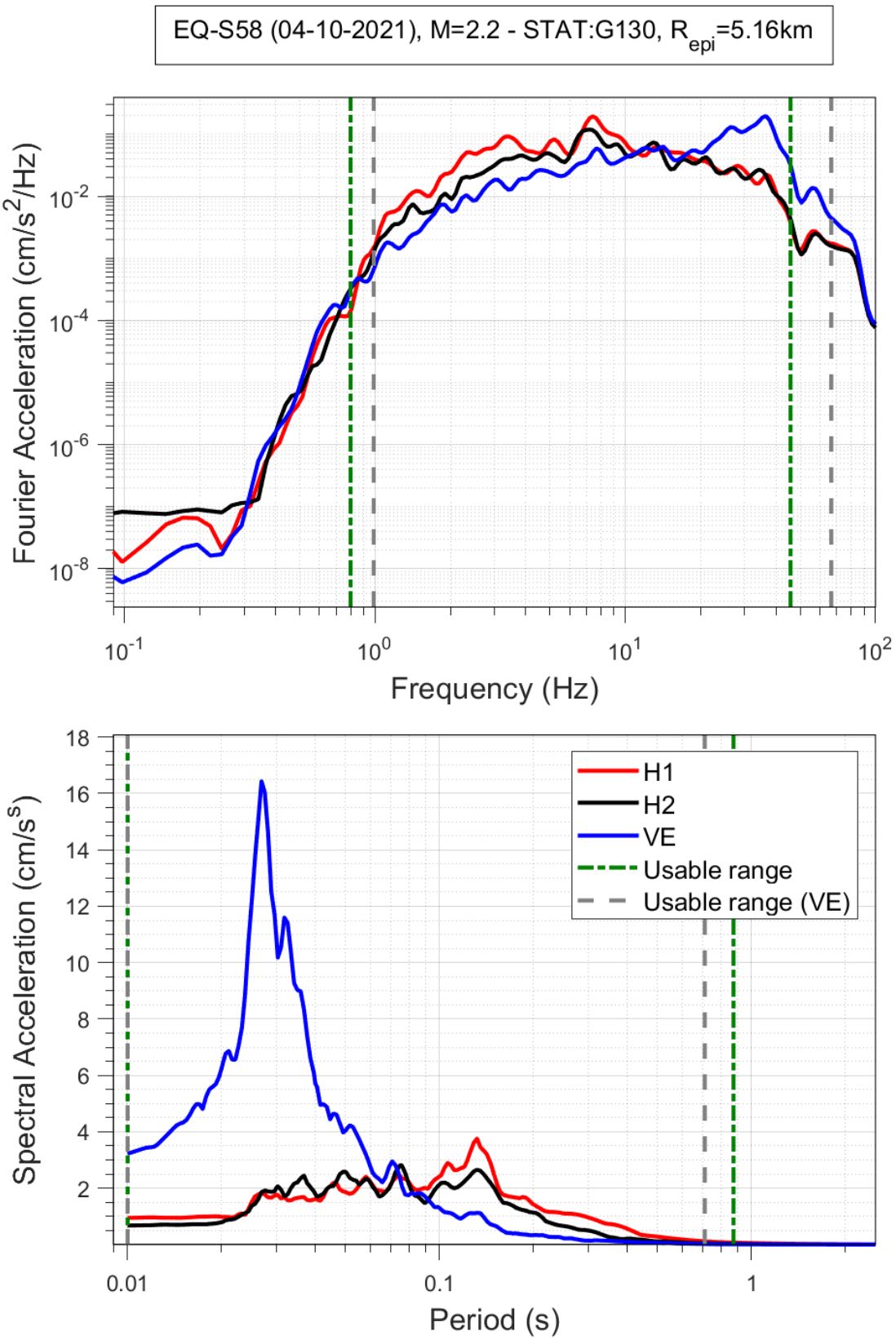
EQ-S58 (04-10-2021), M=2.2 - STAT:G130, R_epi=5.16km
Fourier Acceleration (cm/s²/Hz)
10^-2
10^-4
10^-6
10^-8
10^-1
10^0
10^1
10^2
Frequency (Hz)
Spectral Acceleration (cm/s²)
18
16
14
12
10
8
6
4
2
0.01
0.1
1
Period (s)
H1
H2
VE
Usable range
Usable range (VE)

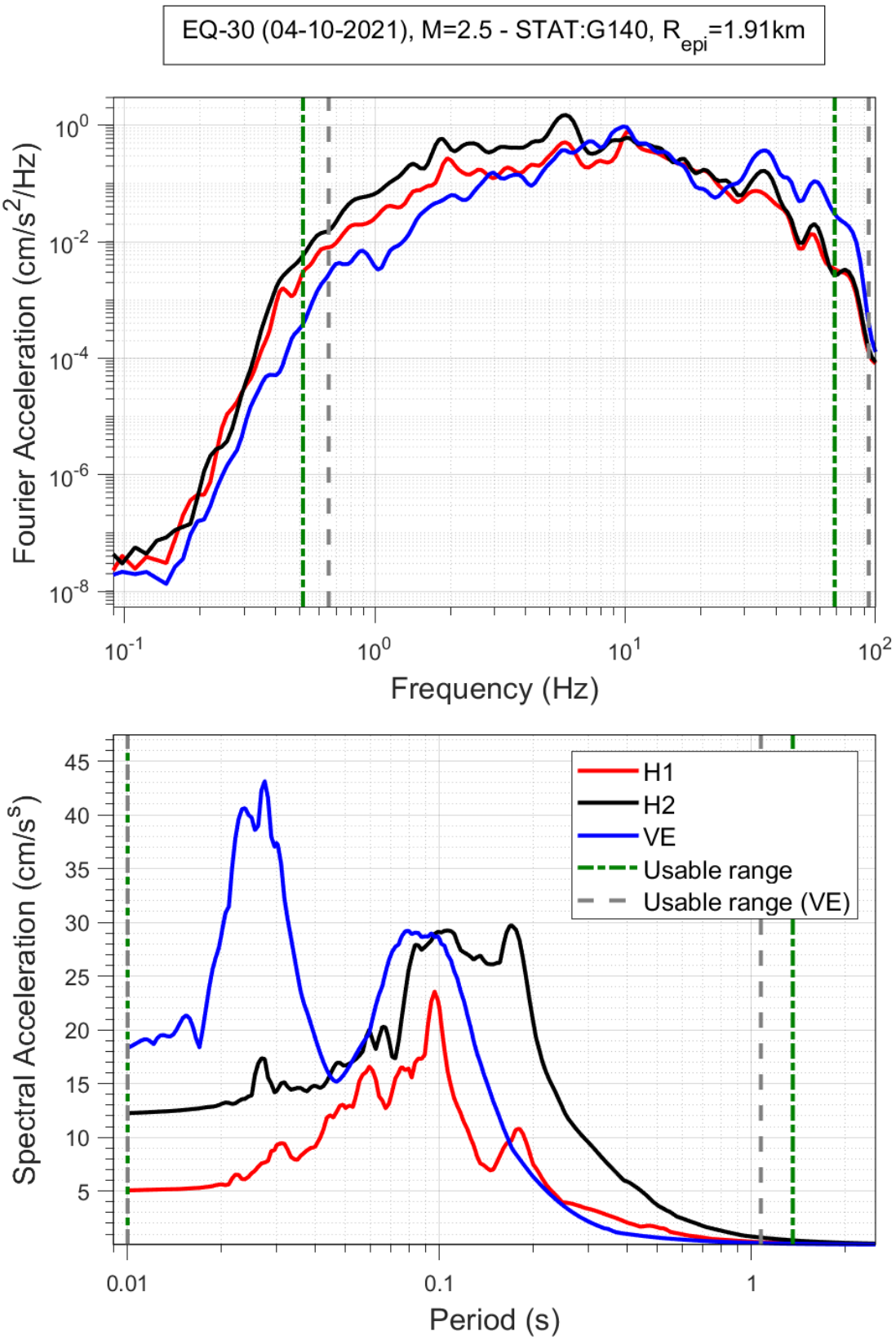
EQ-30 (04-10-2021), M=2.5 - STAT:G140, R_epi=1.91km
Fourier Acceleration (cm/s²/Hz)
Frequency (Hz)
Spectral Acceleration (cm/s²)
Period (s)
H1
H2
VE
Usable range
Usable range (VE)

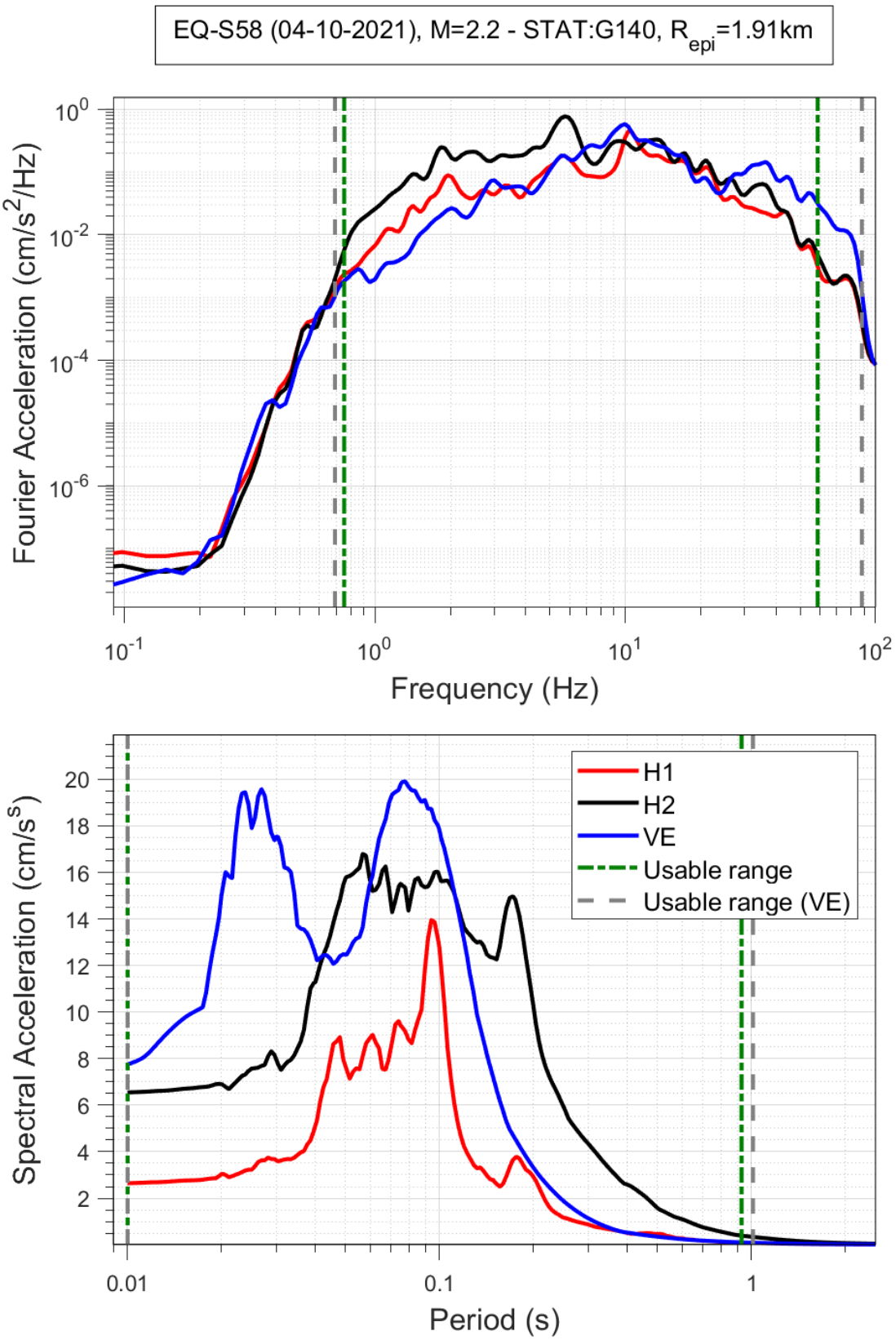
EQ-S58 (04-10-2021), M=2.2 - STAT:G140, R_epi=1.91km
Fourier Acceleration (cm/s²/Hz)
Frequency (Hz)
Spectral Acceleration (cm/s²)
Period (s)
H1
H2
VE
Usable range
Usable range (VE)

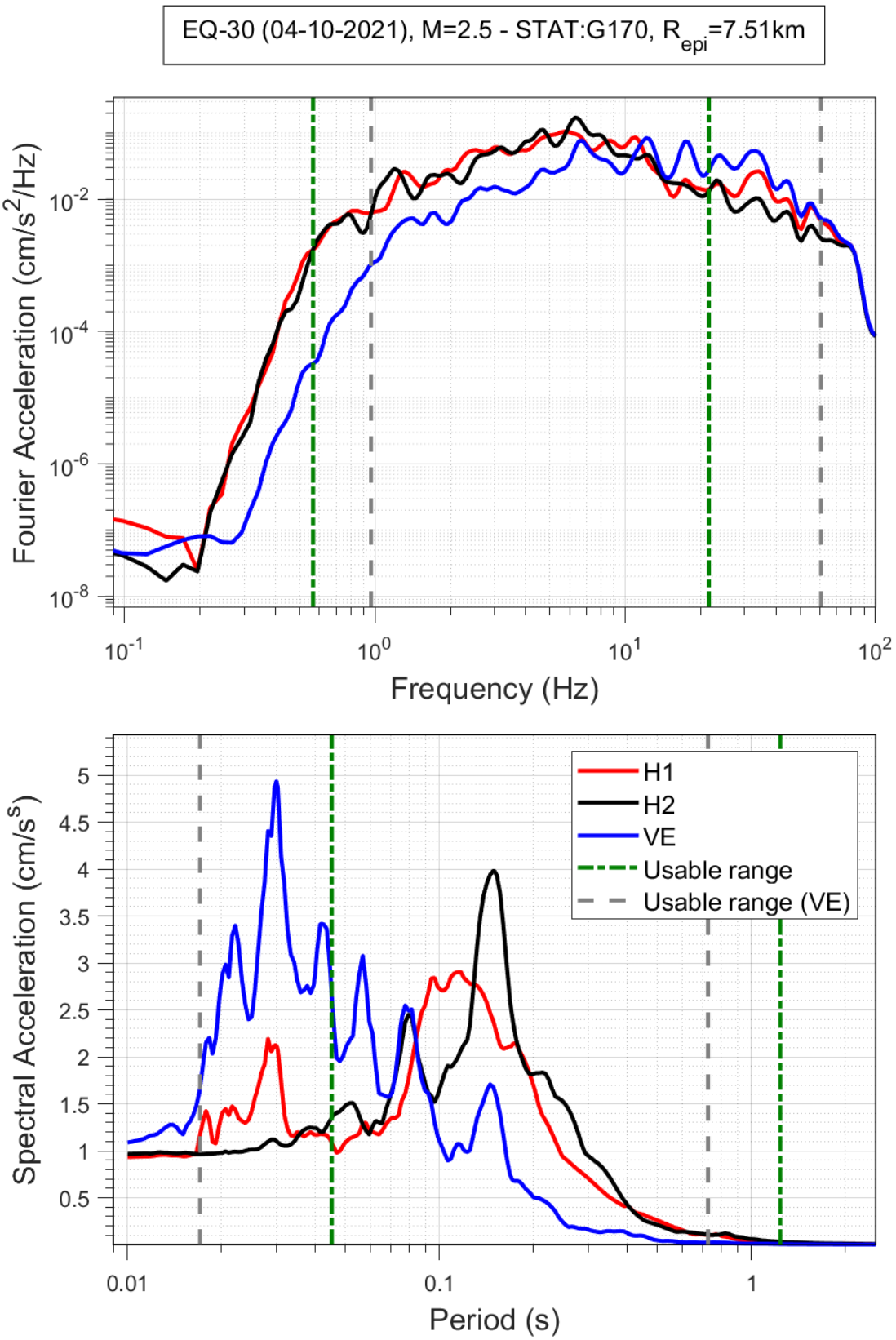
EQ-30 (04-10-2021), M=2.5 - STAT:G170, R_epi=7.51km
Fourier Acceleration (cm/s²/Hz)
10^-2
10^-4
10^-6
10^-8
10^-1
10^0
10^1
10^2
Frequency (Hz)
Spectral Acceleration (cm/s^s)
5
4.5
4
3.5
3
2.5
2
1.5
1
0.5
0.01
0.1
1
Period (s)
H1
H2
VE
Usable range
Usable range (VE)

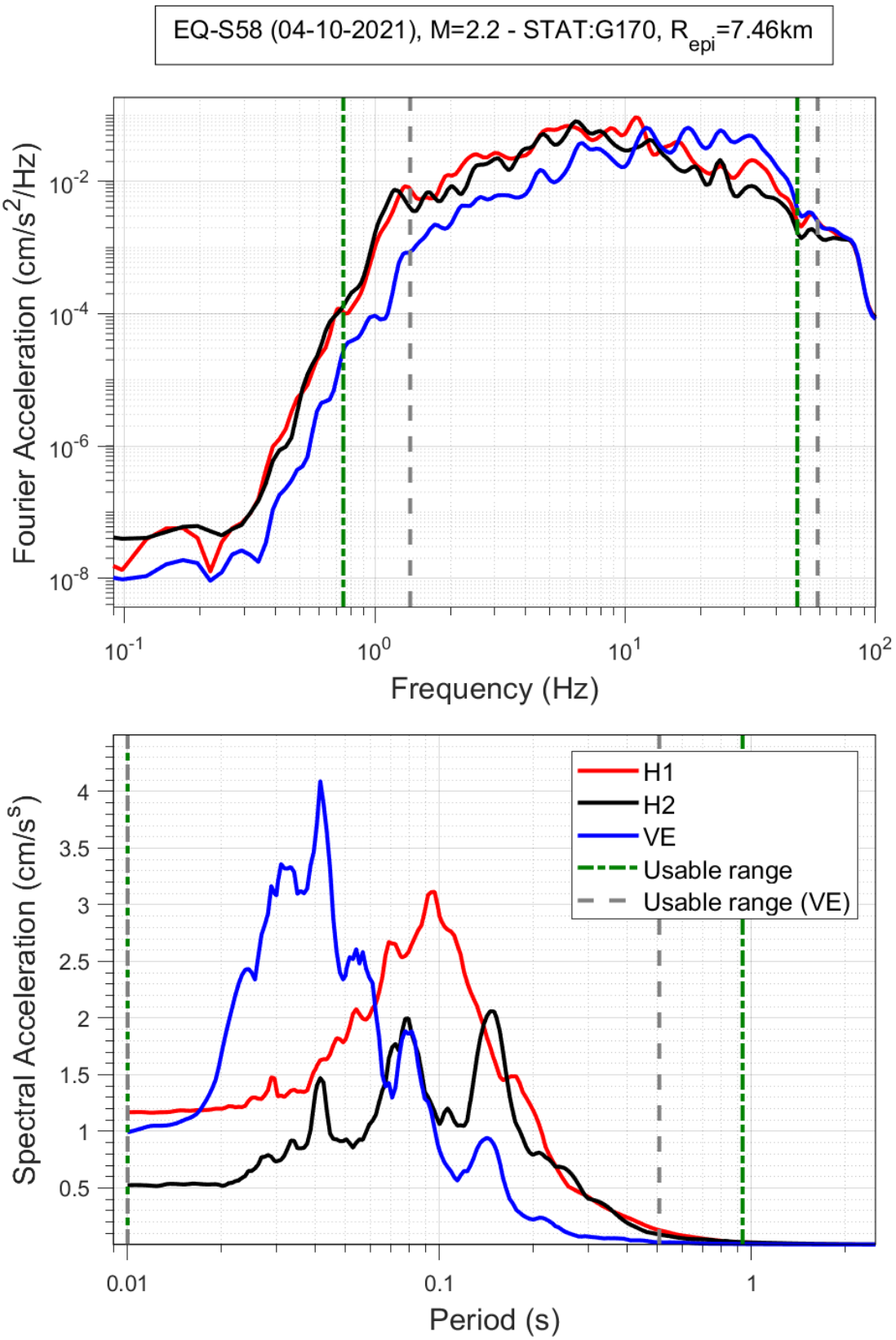
EQ-S58 (04-10-2021), M=2.2 - STAT:G170, R_epi=7.46km
Fourier Acceleration (cm/s²/Hz)
10^-2
10^-4
10^-6
10^-8
10^-1
10^0
10^1
10^2
Frequency (Hz)
Spectral Acceleration (cm/s^s)
4
3.5
3
2.5
2
1.5
1
0.5
0.01
0.1
1
Period (s)
H1
H2
VE
Usable range
Usable range (VE)

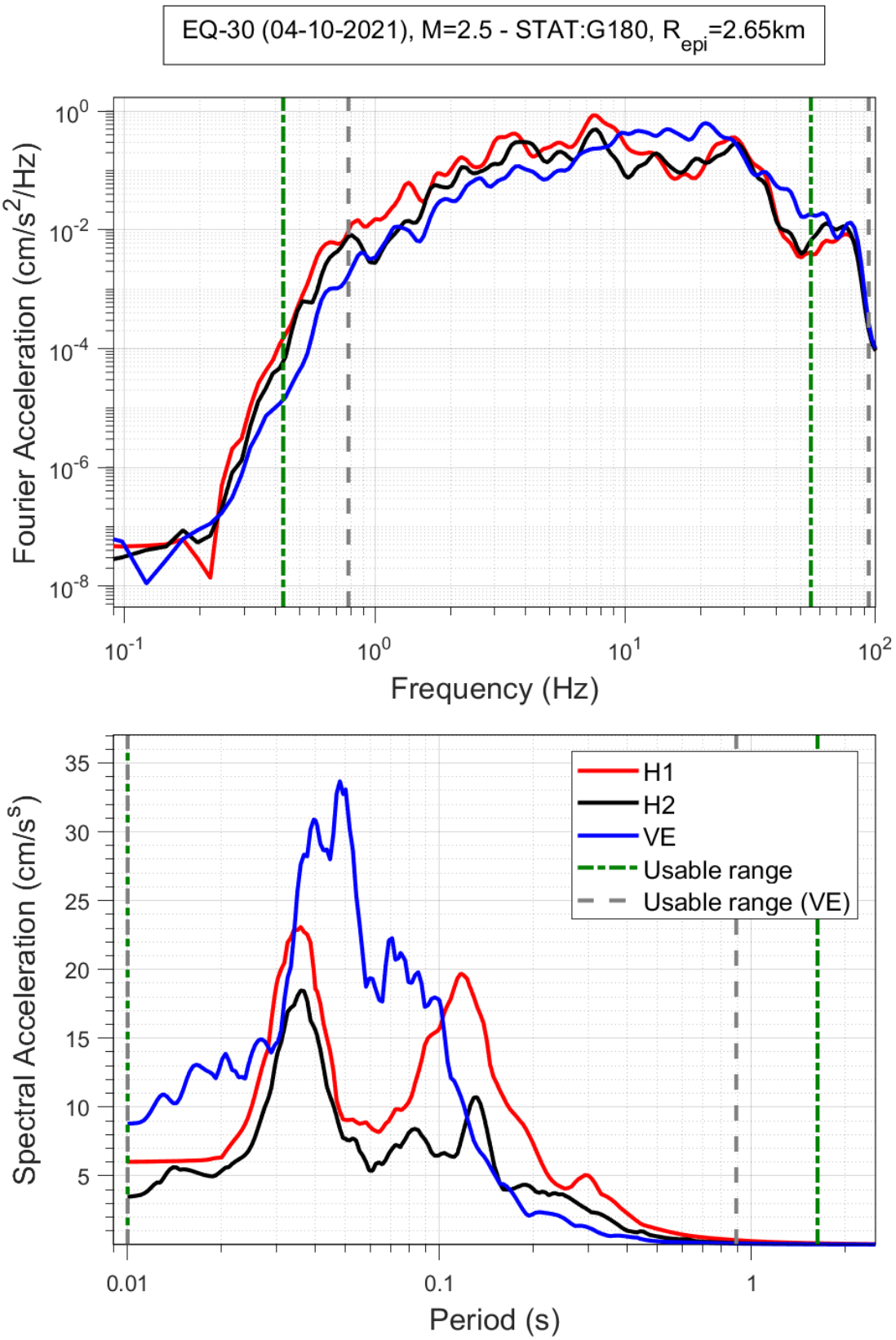
EQ-30 (04-10-2021), M=2.5 - STAT:G180, R_epi=2.65km
Fourier Acceleration (cm/s²/Hz)
Frequency (Hz)
Spectral Acceleration (cm/s²)
Period (s)
H1
H2
VE
Usable range
Usable range (VE)

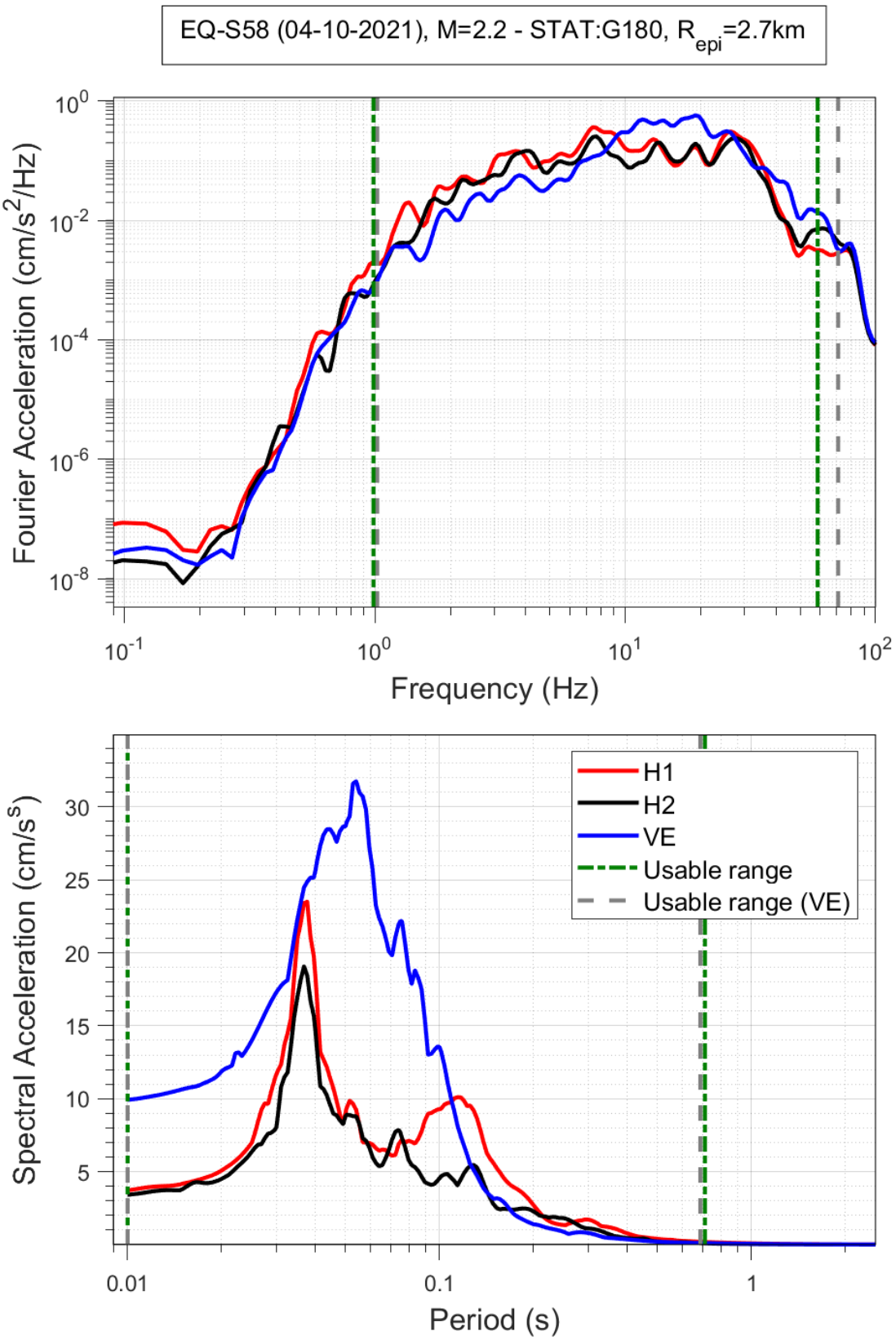
EQ-S58 (04-10-2021), M=2.2 - STAT:G180, R_epi=2.7km
Fourier Acceleration (cm/s²/Hz)
Frequency (Hz)
Spectral Acceleration (cm/s²)
Period (s)
H1
H2
VE
Usable range
Usable range (VE)

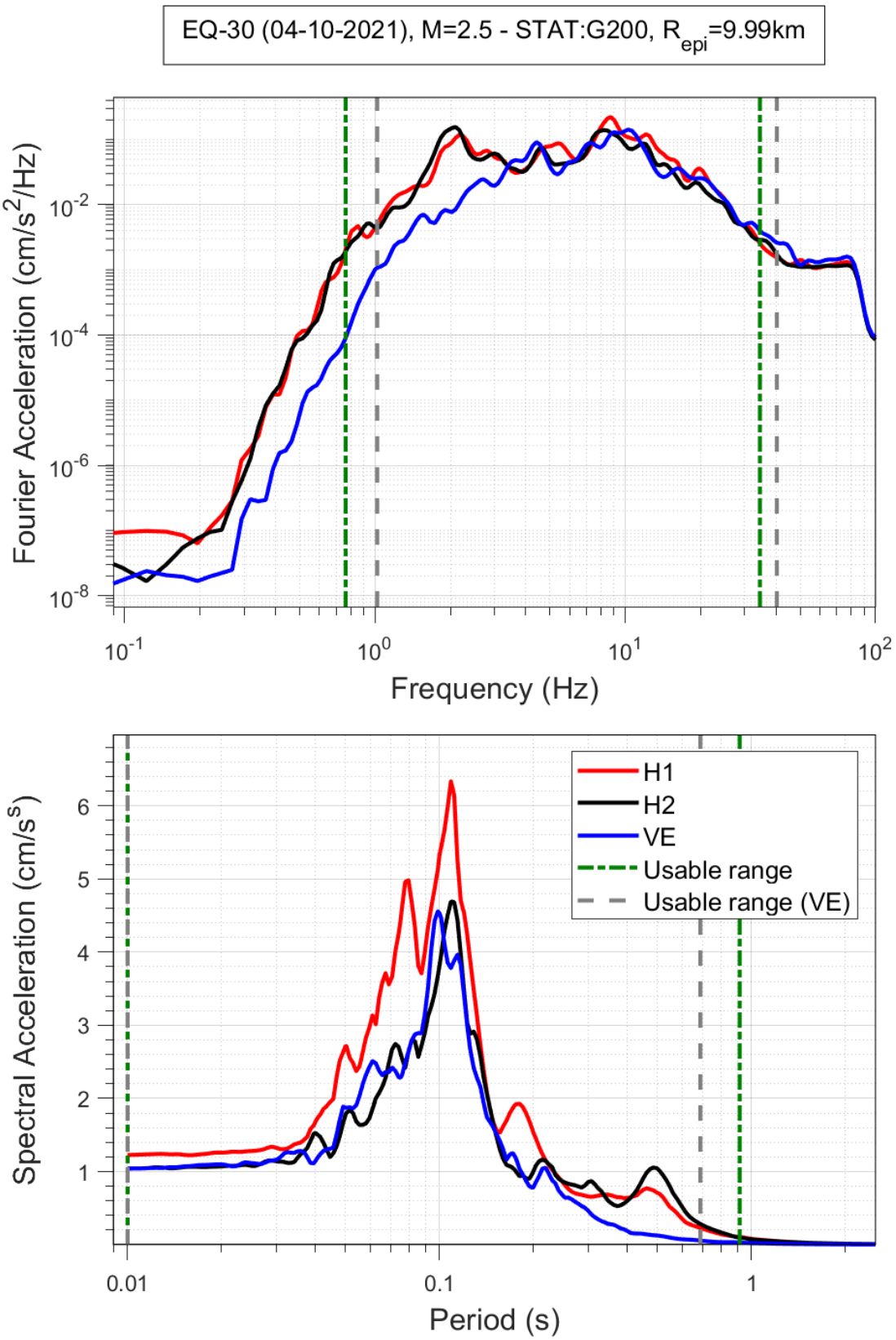
EQ-30 (04-10-2021), M=2.5 - STAT:G200, R_epi=9.99km
Fourier Acceleration (cm/s²/Hz)
10^-2
10^-4
10^-6
10^-8
10^-1
10^0
10^1
10^2
Frequency (Hz)
Spectral Acceleration (cm/s²)
6
5
4
3
2
1
0.01
0.1
1
Period (s)
H1
H2
VE
Usable range
Usable range (VE)

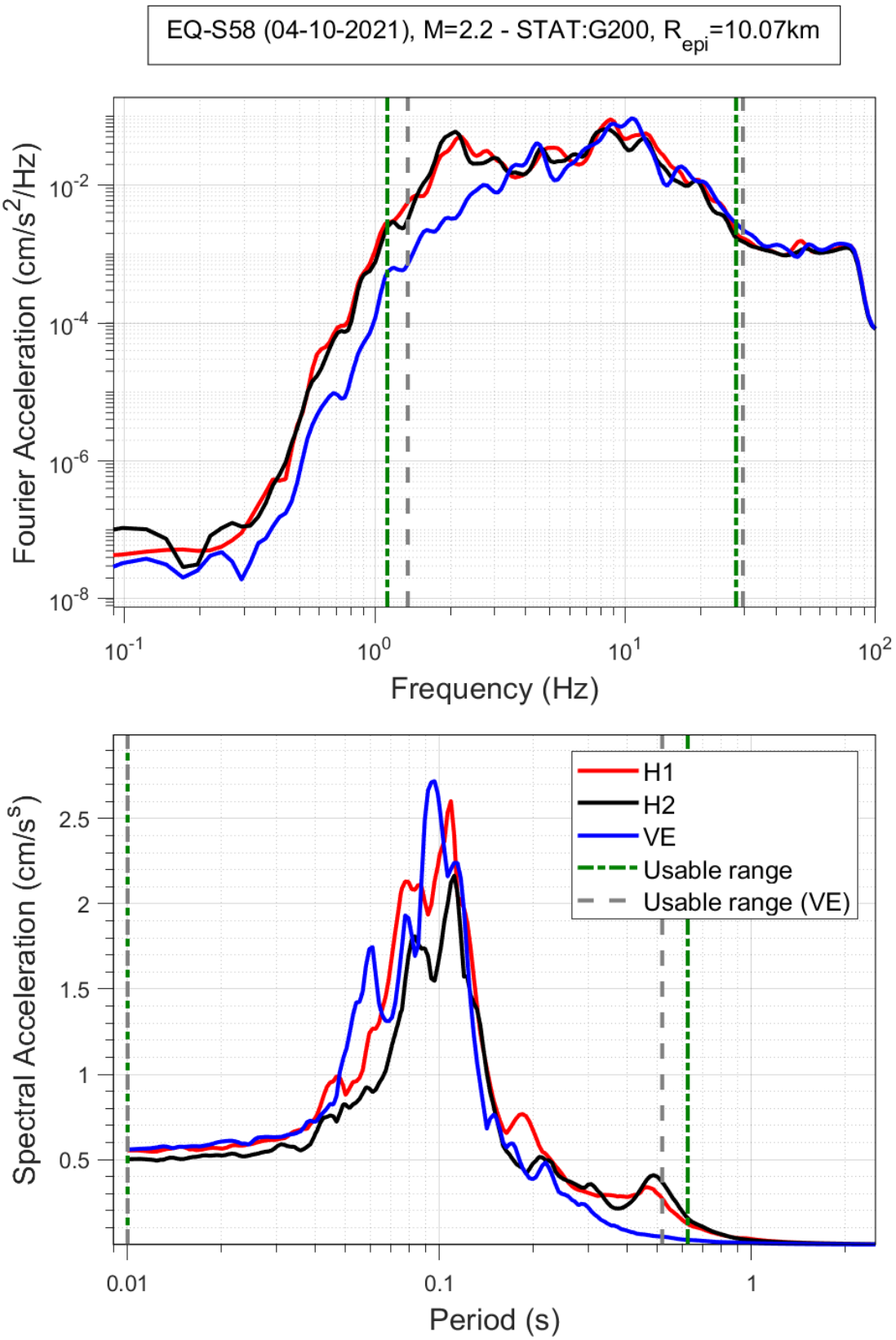
EQ-S58 (04-10-2021), M=2.2 - STAT:G200, R_epi=10.07km
Fourier Acceleration (cm/s²/Hz)
10^-2
10^-4
10^-6
10^-8
10^-1
10^0
10^1
10^2
Frequency (Hz)
Spectral Acceleration (cm/s^s)
2.5
2
1.5
1
0.5
0.01
0.1
1
Period (s)
H1
H2
VE
Usable range
Usable range (VE)

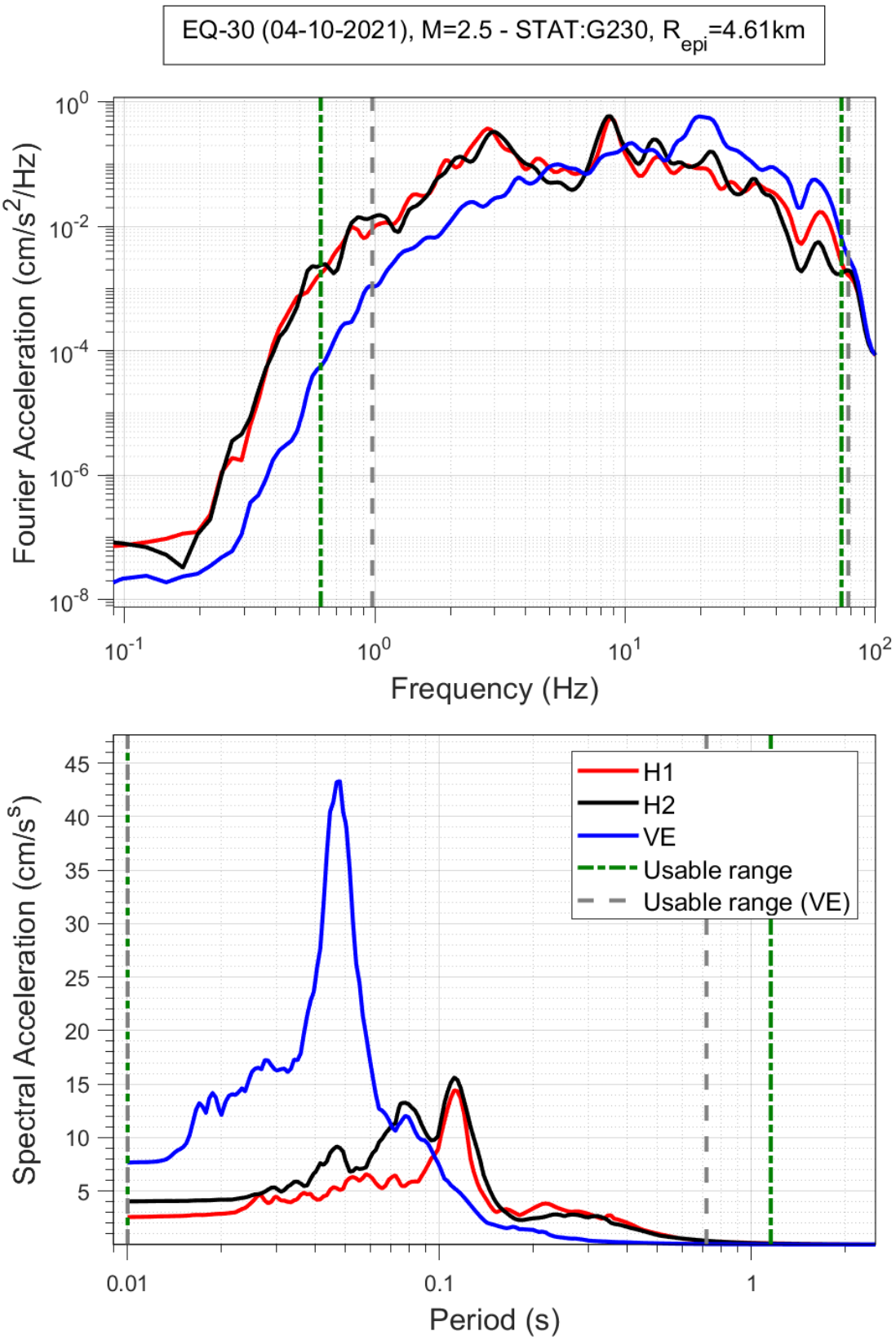
EQ-30 (04-10-2021), M=2.5 - STAT:G230, R_epi=4.61km
Fourier Acceleration (cm/s²/Hz)
Frequency (Hz)
Spectral Acceleration (cm/s²)
Period (s)
H1
H2
VE
Usable range
Usable range (VE)

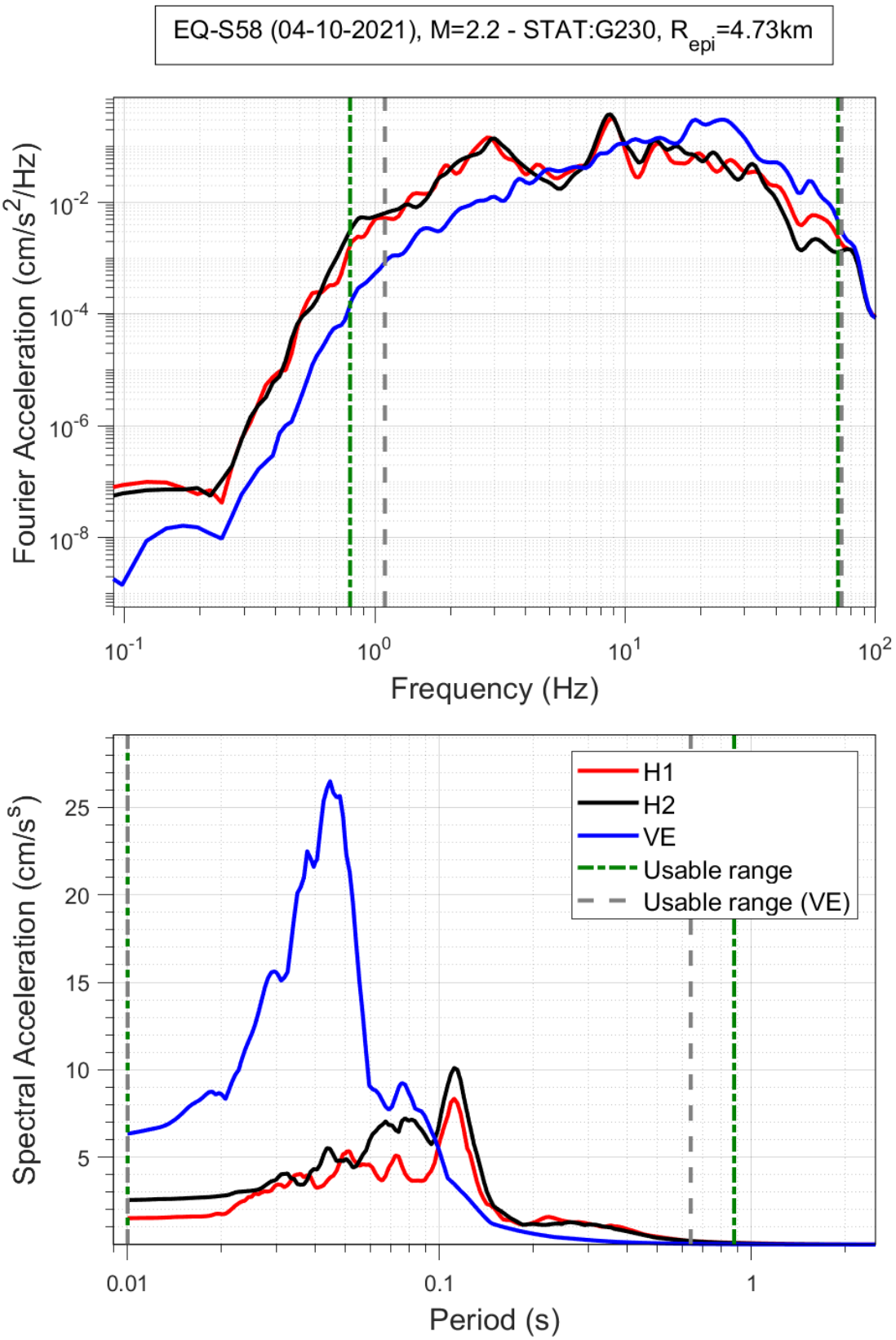
EQ-S58 (04-10-2021), M=2.2 - STAT:G230, R_epi=4.73km
Fourier Acceleration (cm/s²/Hz)
10^-2
10^-4
10^-6
10^-8
10^-1
10^0
10^1
10^2
Frequency (Hz)
Spectral Acceleration (cm/s²)
25
20
15
10
5
0.01
0.1
1
Period (s)
H1
H2
VE
Usable range
Usable range (VE)

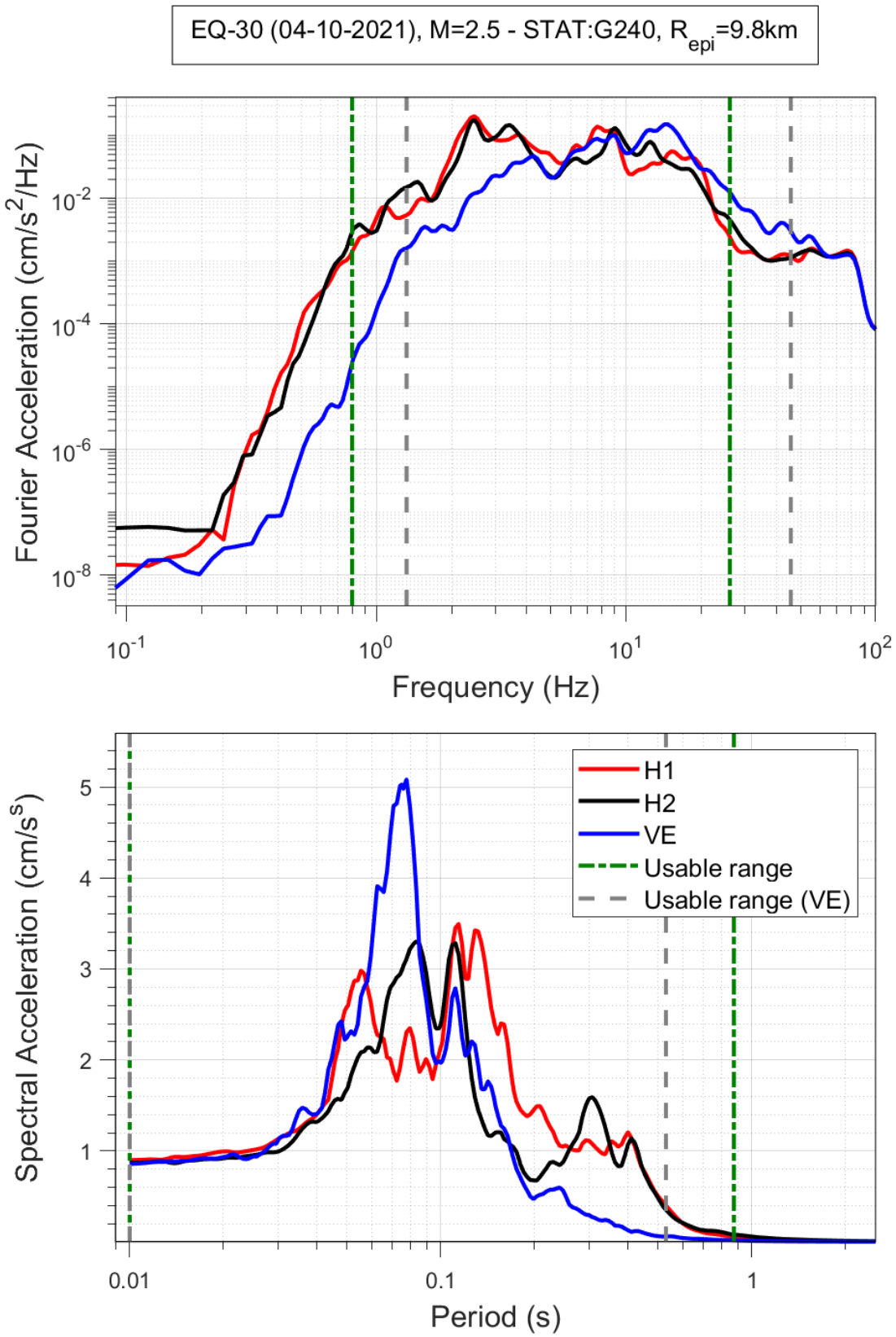
EQ-30 (04-10-2021), M=2.5 - STAT:G240, R_epi=9.8km
Fourier Acceleration (cm/s²/Hz)
10^-2
10^-4
10^-6
10^-8
10^-1
10^0
10^1
10^2
Frequency (Hz)
Spectral Acceleration (cm/s^s)
5
4
3
2
1
0.01
0.1
1
Period (s)
H1
H2
VE
Usable range
Usable range (VE)

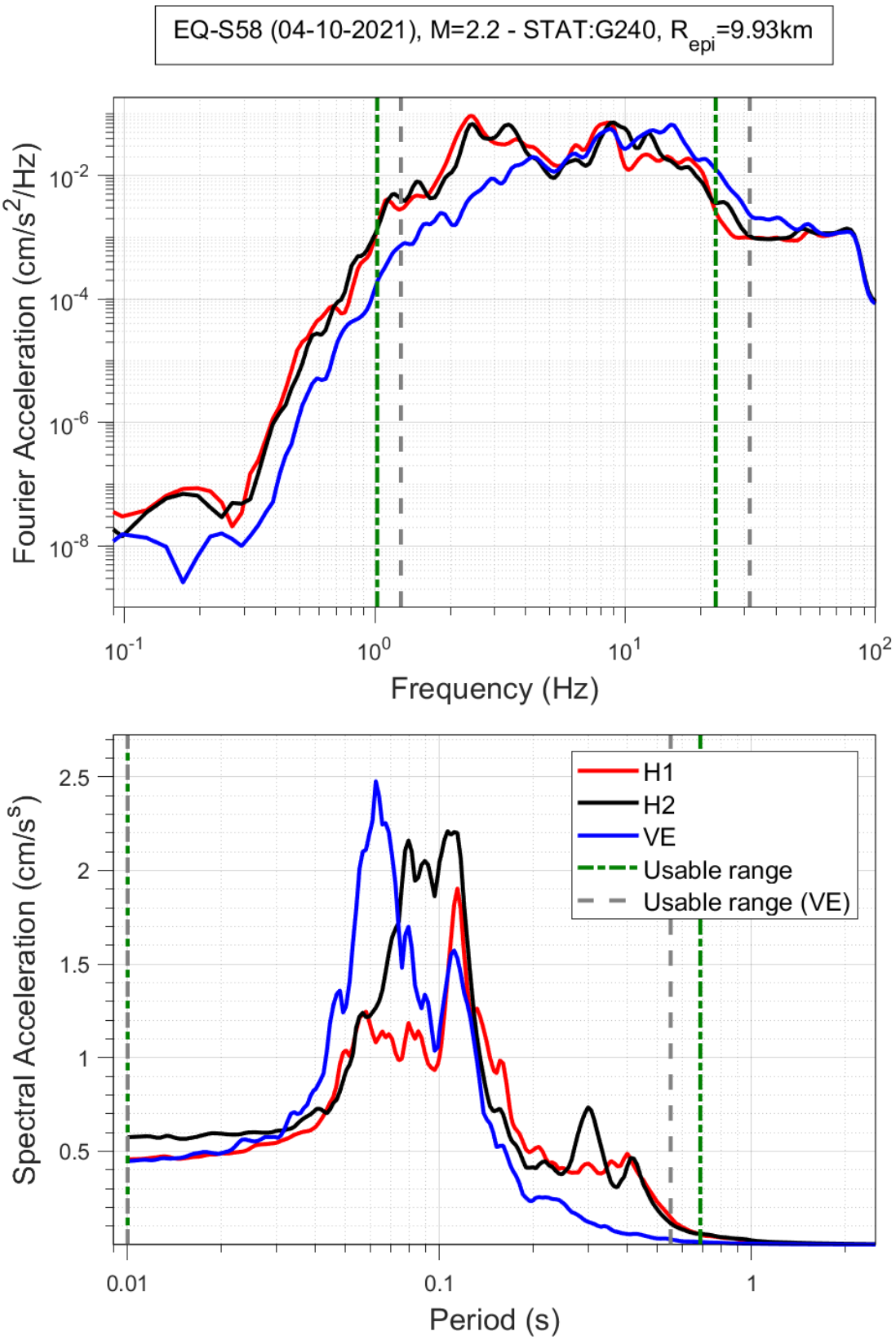
EQ-S58 (04-10-2021), M=2.2 - STAT:G240, R_epi=9.93km
Fourier Acceleration (cm/s²/Hz)
10^-2
10^-4
10^-6
10^-8
10^-1
10^0
10^1
10^2
Frequency (Hz)
Spectral Acceleration (cm/s^s)
2.5
2
1.5
1
0.5
0.01
0.1
1
Period (s)
H1
H2
VE
Usable range
Usable range (VE)

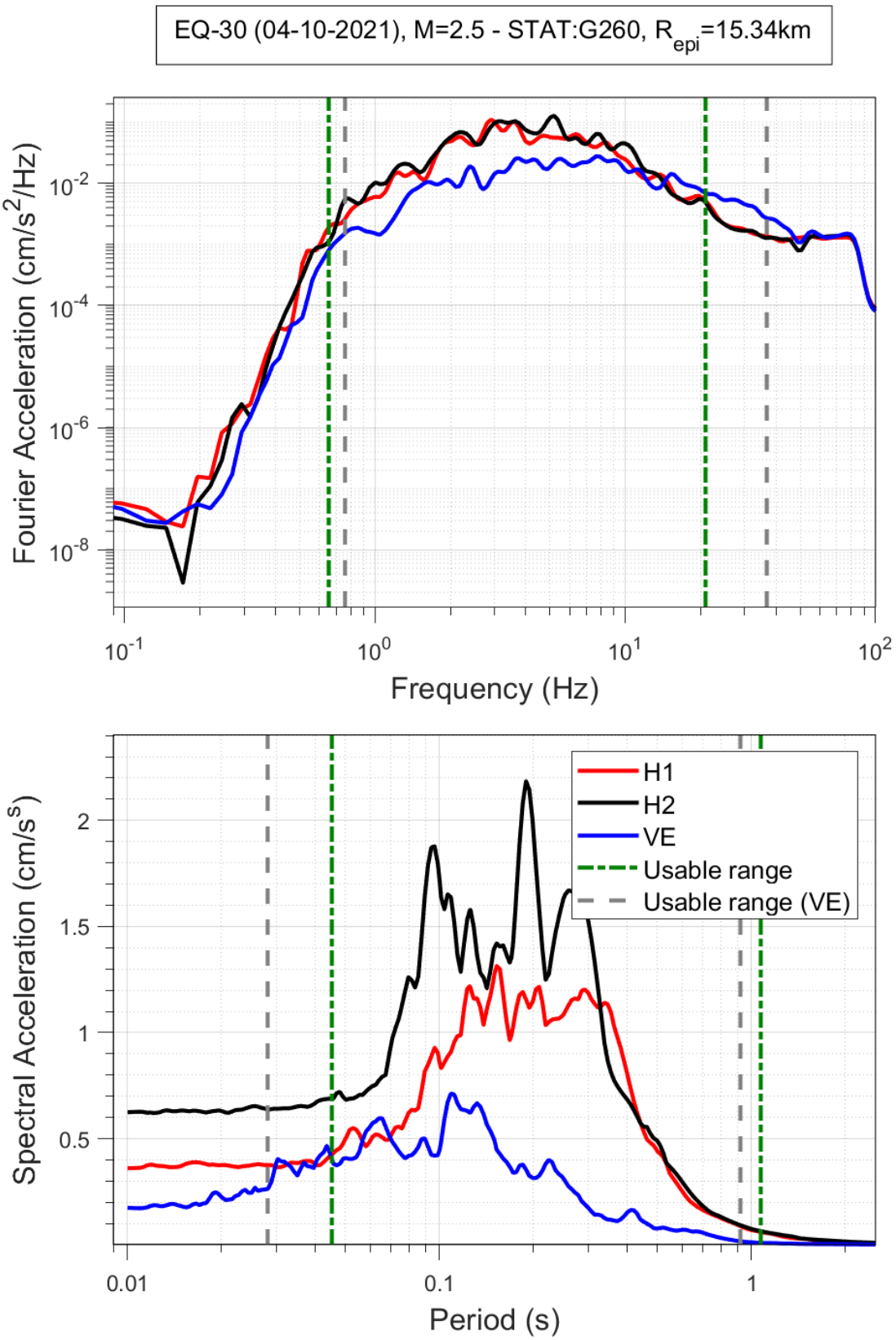
EQ-30 (04-10-2021), M=2.5 - STAT:G260, R_epi=15.34km
Fourier Acceleration (cm/s²/Hz)
10^-2
10^-4
10^-6
10^-8
10^-1
10^0
10^1
10^2
Frequency (Hz)
Spectral Acceleration (cm/s^s)
2
1.5
1
0.5
0.01
0.1
1
Period (s)
H1
H2
VE
Usable range
Usable range (VE)

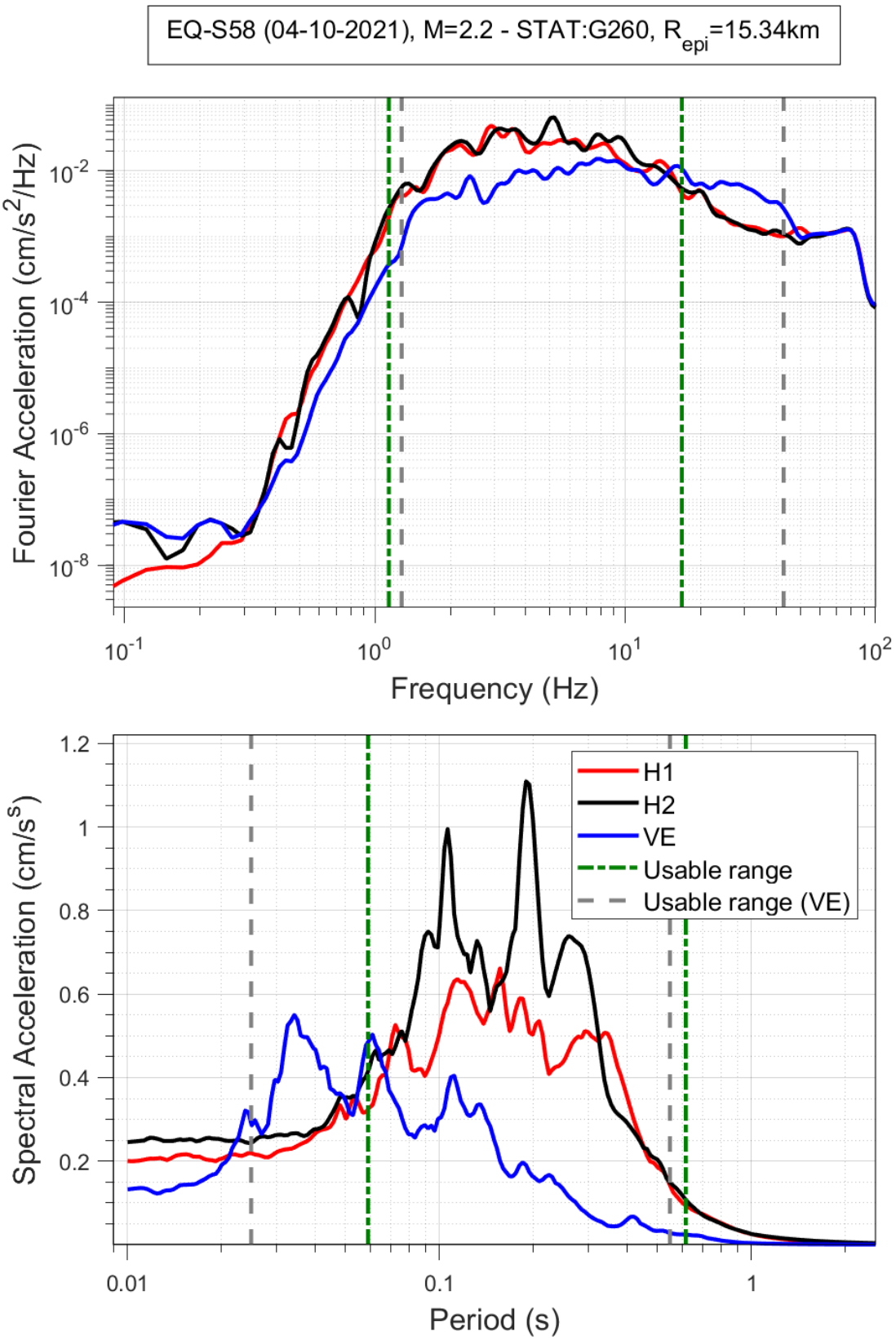
EQ-S58 (04-10-2021), M=2.2 - STAT:G260, R_epi=15.34km
Fourier Acceleration (cm/s²/Hz)
10^-2
10^-4
10^-6
10^-8
10^-1
10^0
10^1
10^2
Frequency (Hz)
Spectral Acceleration (cm/s^s)
1.2
1
0.8
0.6
0.4
0.2
0.01
0.1
1
Period (s)
H1
H2
VE
Usable range
Usable range (VE)

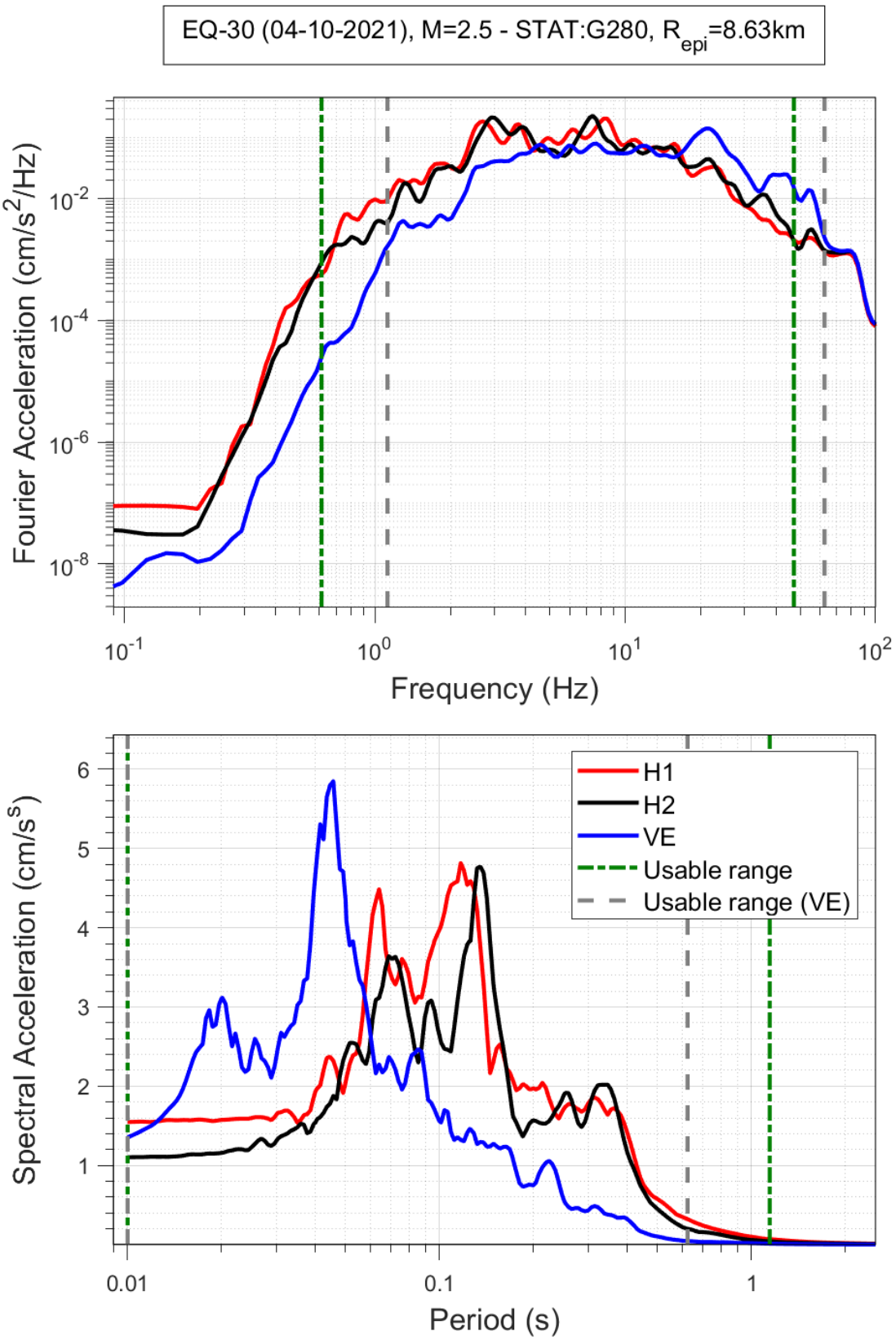
EQ-30 (04-10-2021), M=2.5 - STAT:G280, R_epi=8.63km
Fourier Acceleration (cm/s²/Hz)
10^-2
10^-4
10^-6
10^-8
10^-1
10^0
10^1
10^2
Frequency (Hz)
Spectral Acceleration (cm/s²)
6
5
4
3
2
1
0.01
0.1
1
Period (s)
H1
H2
VE
Usable range
Usable range (VE)

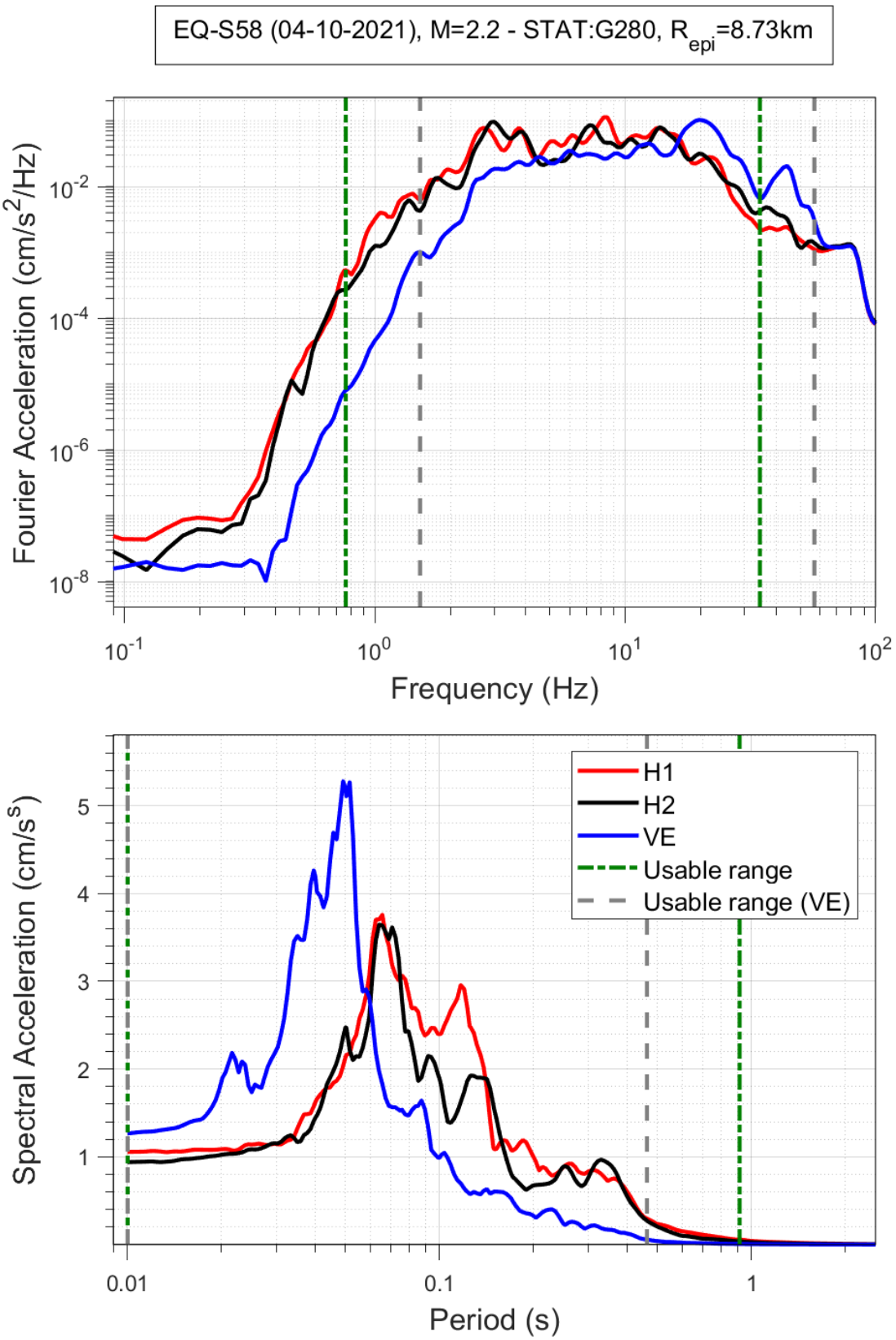
EQ-S58 (04-10-2021), M=2.2 - STAT:G280, R_epi=8.73km
Fourier Acceleration (cm/s²/Hz)
10^-2
10^-4
10^-6
10^-8
10^-1
10^0
10^1
10^2
Frequency (Hz)
Spectral Acceleration (cm/s²)
5
4
3
2
1
0.01
0.1
1
Period (s)
H1
H2
VE
Usable range
Usable range (VE)

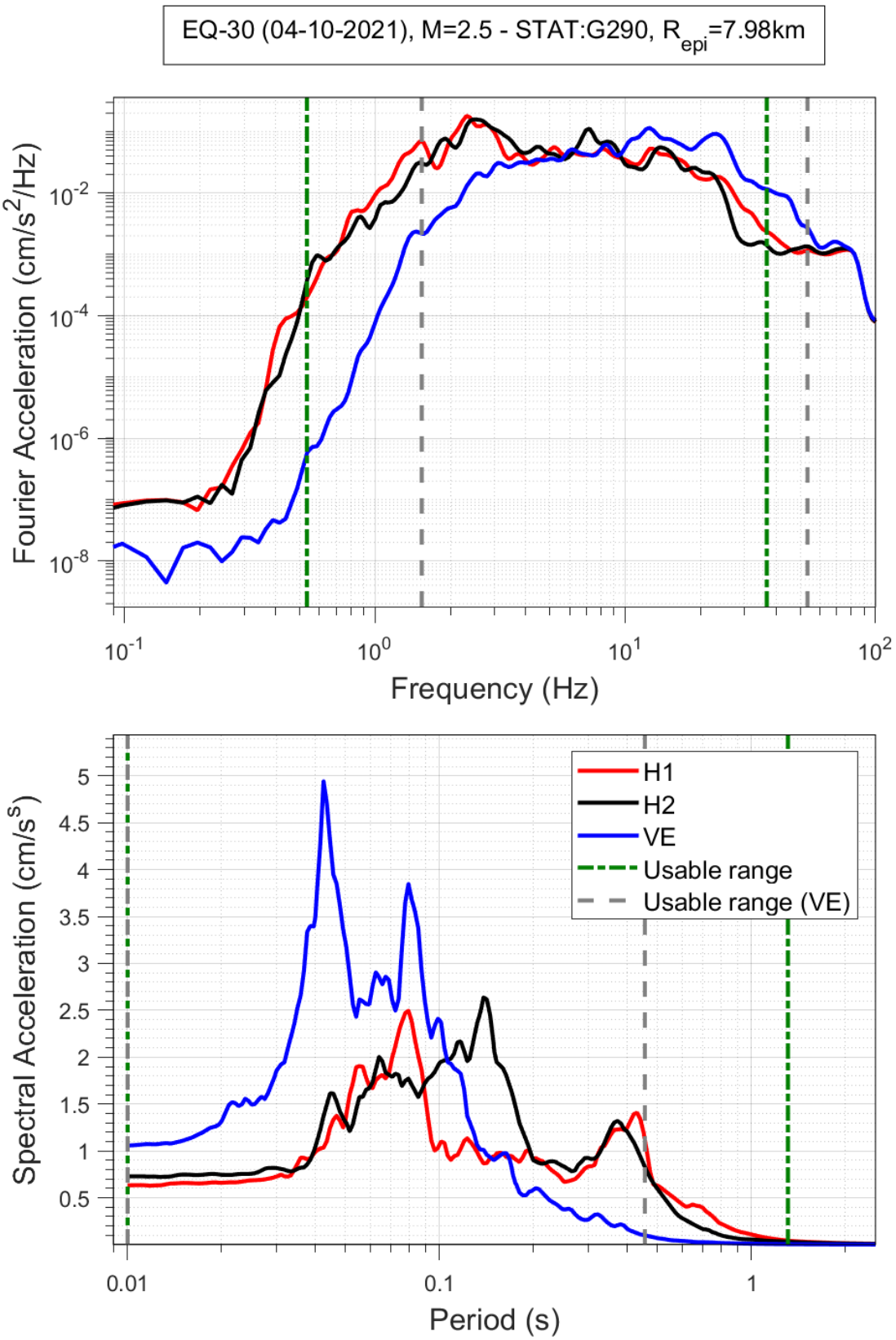
EQ-30 (04-10-2021), M=2.5 - STAT:G290, R_epi=7.98km
Fourier Acceleration (cm/s²/Hz)
10^-2
10^-4
10^-6
10^-8
10^-1
10^0
10^1
10^2
Frequency (Hz)
Spectral Acceleration (cm/s^s)
5
4.5
4
3.5
3
2.5
2
1.5
1
0.5
0.01
0.1
1
Period (s)
H1
H2
VE
Usable range
Usable range (VE)

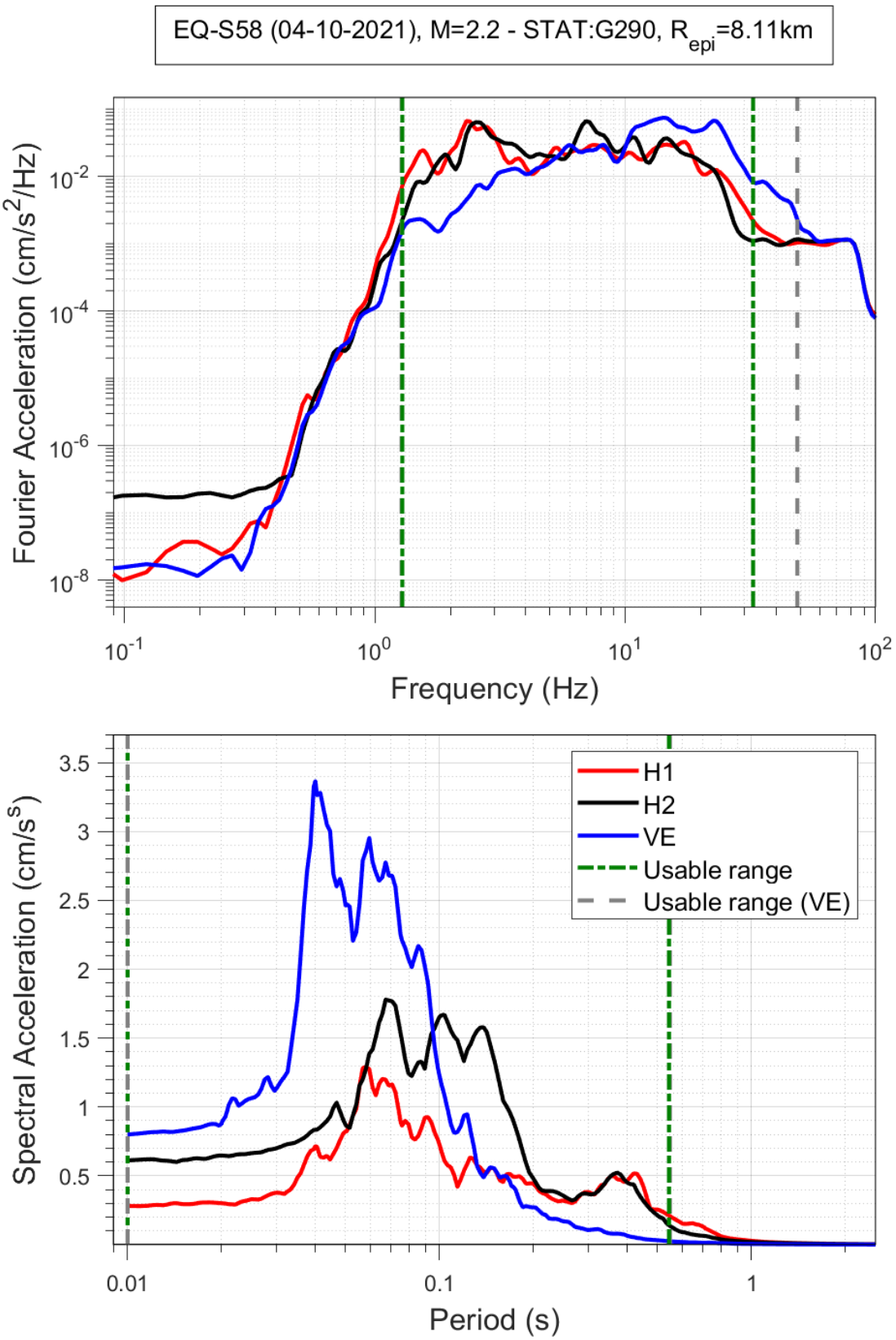
EQ-S58 (04-10-2021), M=2.2 - STAT:G290, R_epi=8.11km
Fourier Acceleration (cm/s²/Hz)
10^-2
10^-4
10^-6
10^-8
10^-1
10^0
10^1
10^2
Frequency (Hz)
Spectral Acceleration (cm/s^s)
3.5
3
2.5
2
1.5
1
0.5
0.01
0.1
1
Period (s)
H1
H2
VE
Usable range
Usable range (VE)

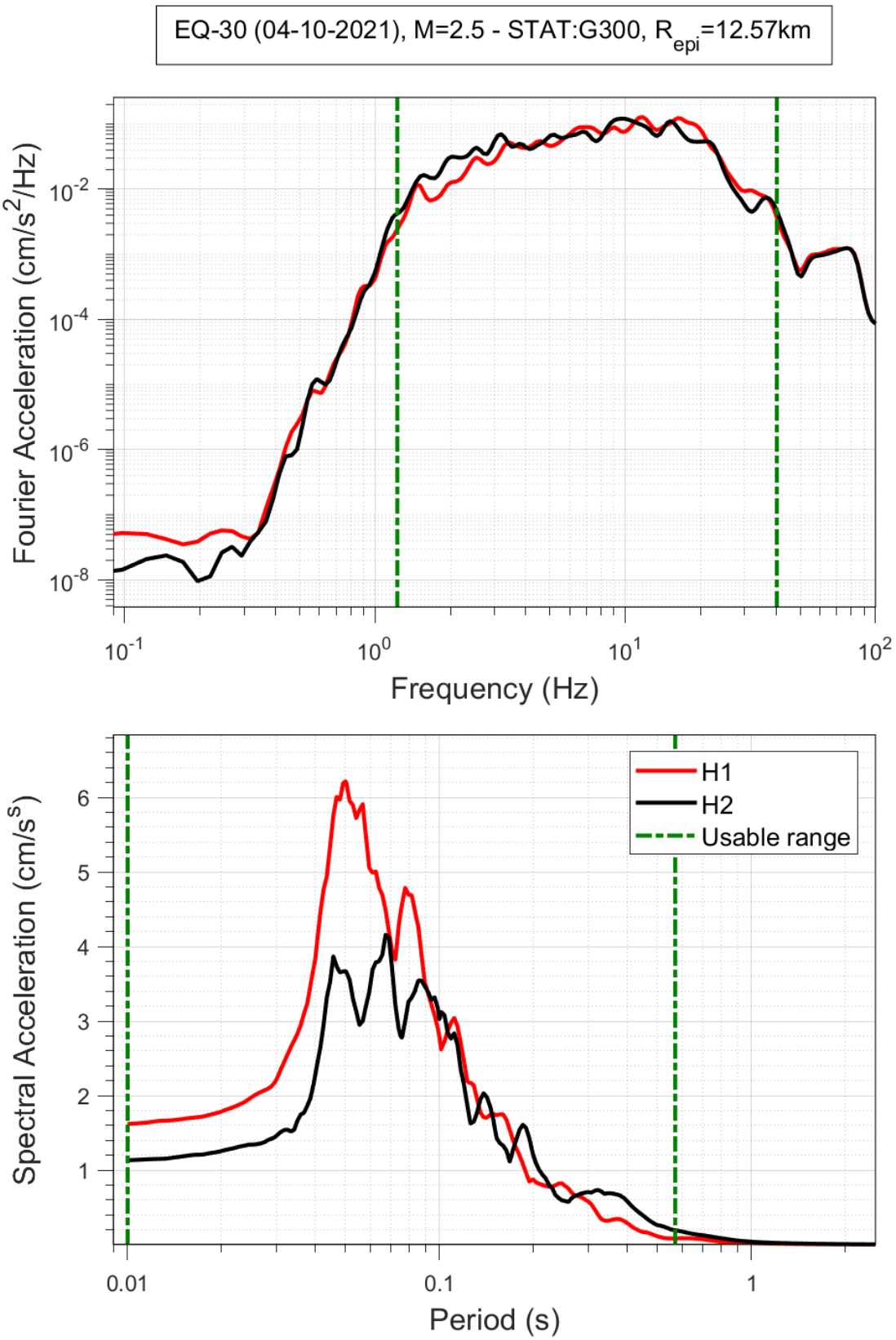
EQ-30 (04-10-2021), M=2.5 - STAT:G300, R_epi=12.57km
Fourier Acceleration (cm/s²/Hz)
10^-2
10^-4
10^-6
10^-8
10^-1
10^0
10^1
10^2
Frequency (Hz)
Spectral Acceleration (cm/s²)
6
5
4
3
2
1
0.01
0.1
1
Period (s)
H1
H2
Usable range

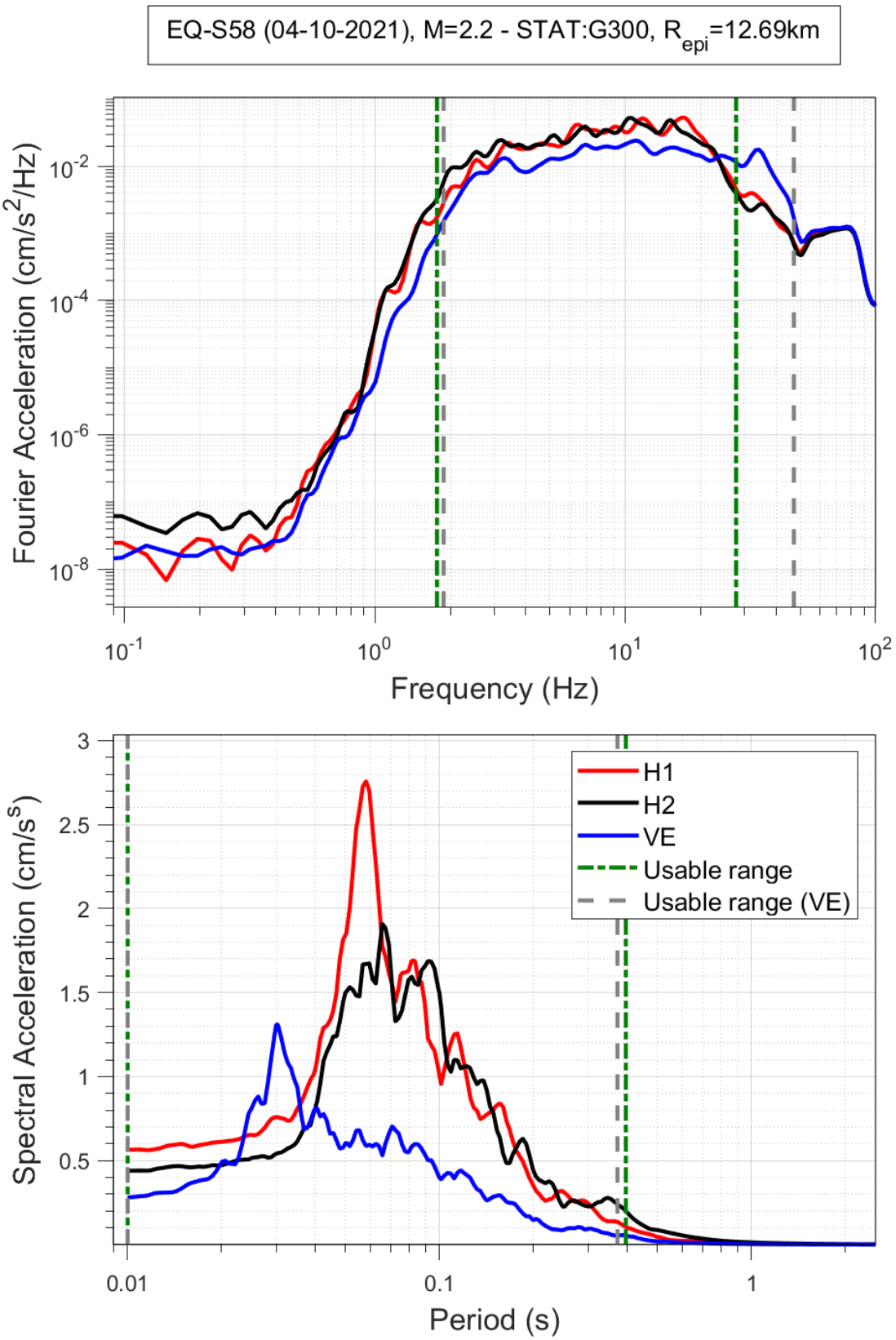
EQ-S58 (04-10-2021), M=2.2 - STAT:G300, R_epi=12.69km
Fourier Acceleration (cm/s²/Hz)
10^-2
10^-4
10^-6
10^-8
10^-1
10^0
10^1
10^2
Frequency (Hz)
Spectral Acceleration (cm/s^s)
3
2.5
2
1.5
1
0.5
0.01
0.1
1
Period (s)
H1
H2
VE
Usable range
Usable range (VE)

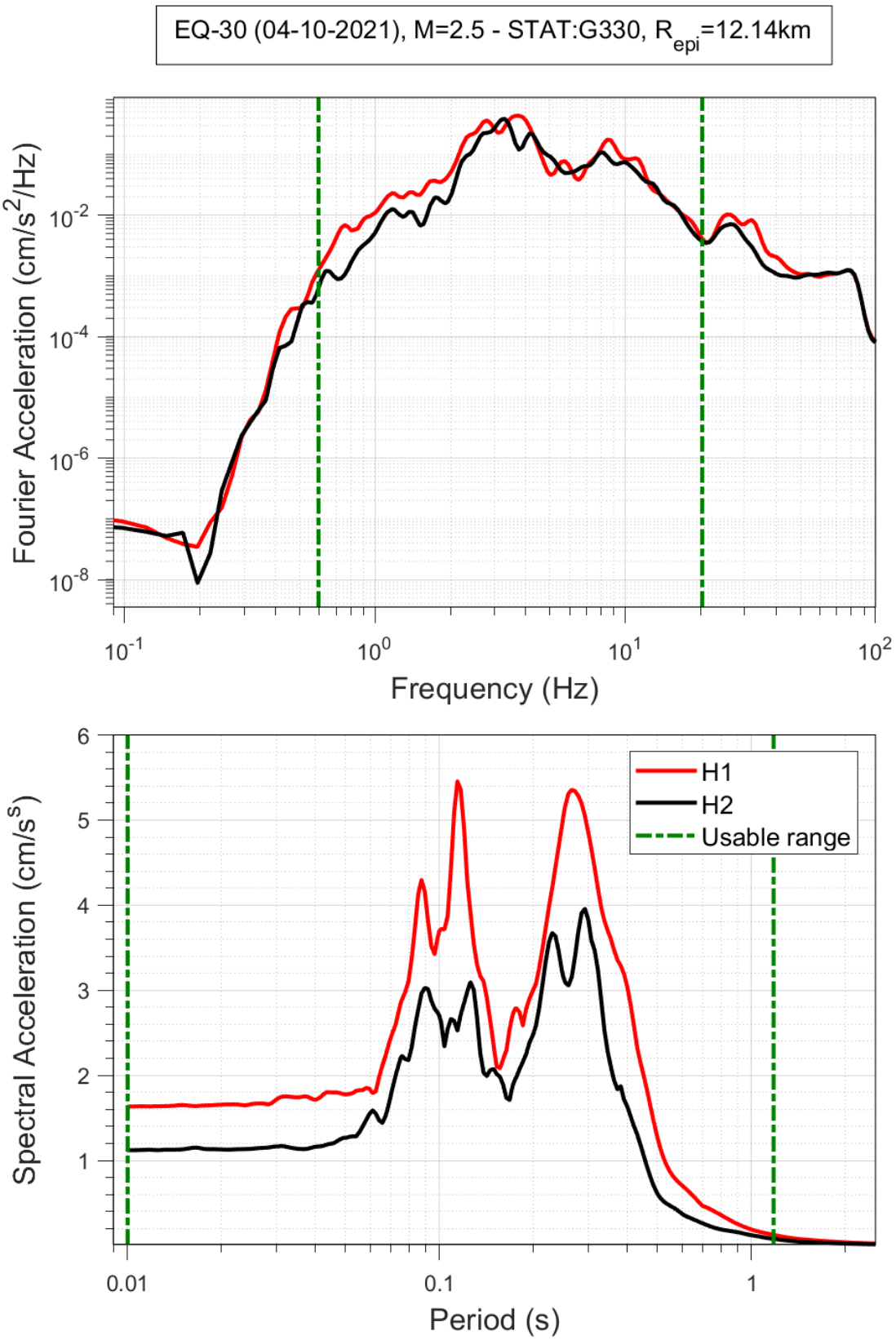
EQ-30 (04-10-2021), M=2.5 - STAT:G330, R_epi=12.14km
Fourier Acceleration (cm/s²/Hz)
10^-2
10^-4
10^-6
10^-8
10^-1
10^0
10^1
10^2
Frequency (Hz)
Spectral Acceleration (cm/s²)
6
5
4
3
2
1
H1
H2
Usable range
0.01
0.1
1
Period (s)

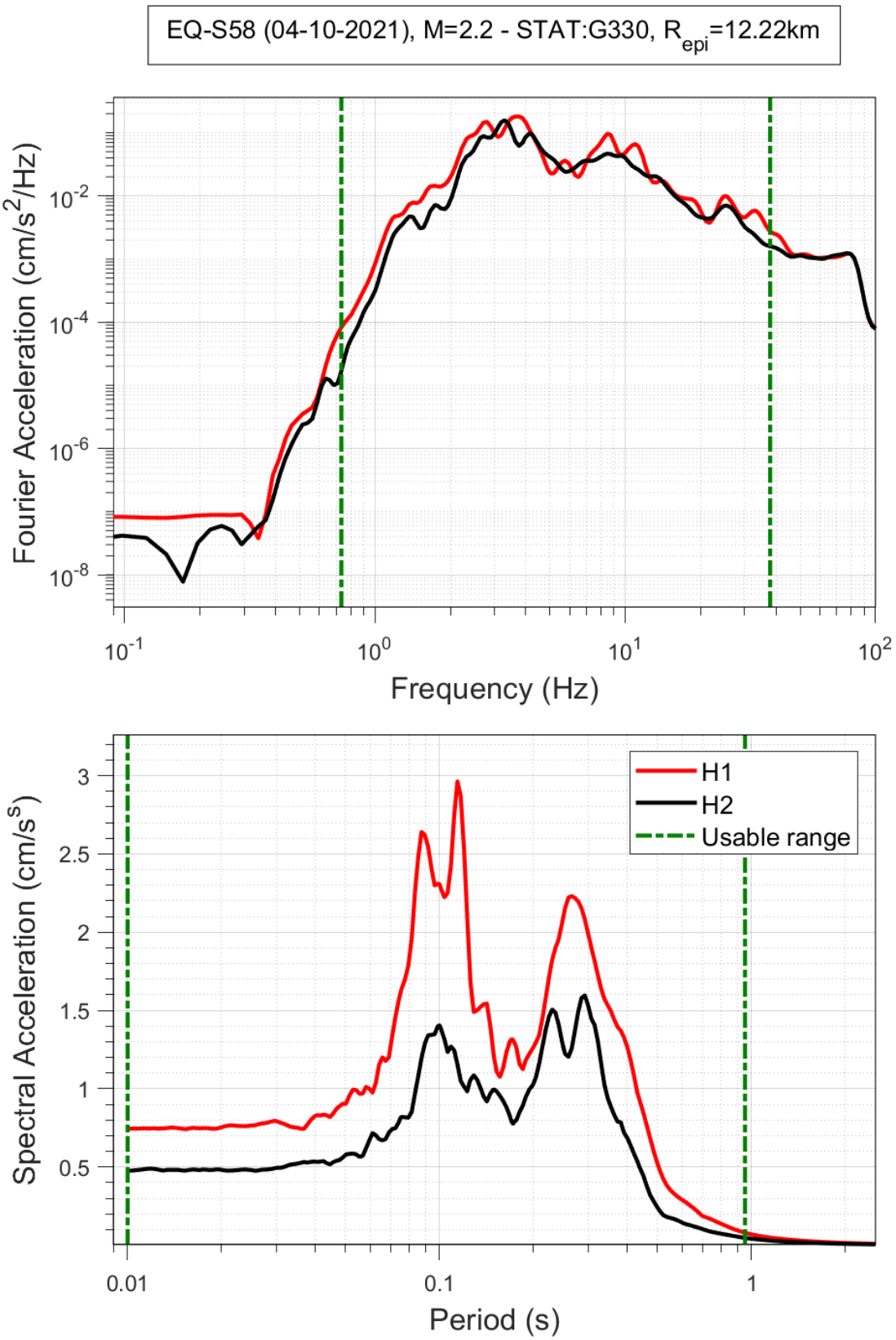
EQ-S58 (04-10-2021), M=2.2 - STAT:G330, R_epi=12.22km
Fourier Acceleration (cm/s²/Hz)
10^-2
10^-4
10^-6
10^-8
10^-1
10^0
10^1
10^2
Frequency (Hz)
Spectral Acceleration (cm/s²)
3
2.5
2
1.5
1
0.5
0.01
0.1
1
Period (s)
H1
H2
Usable range

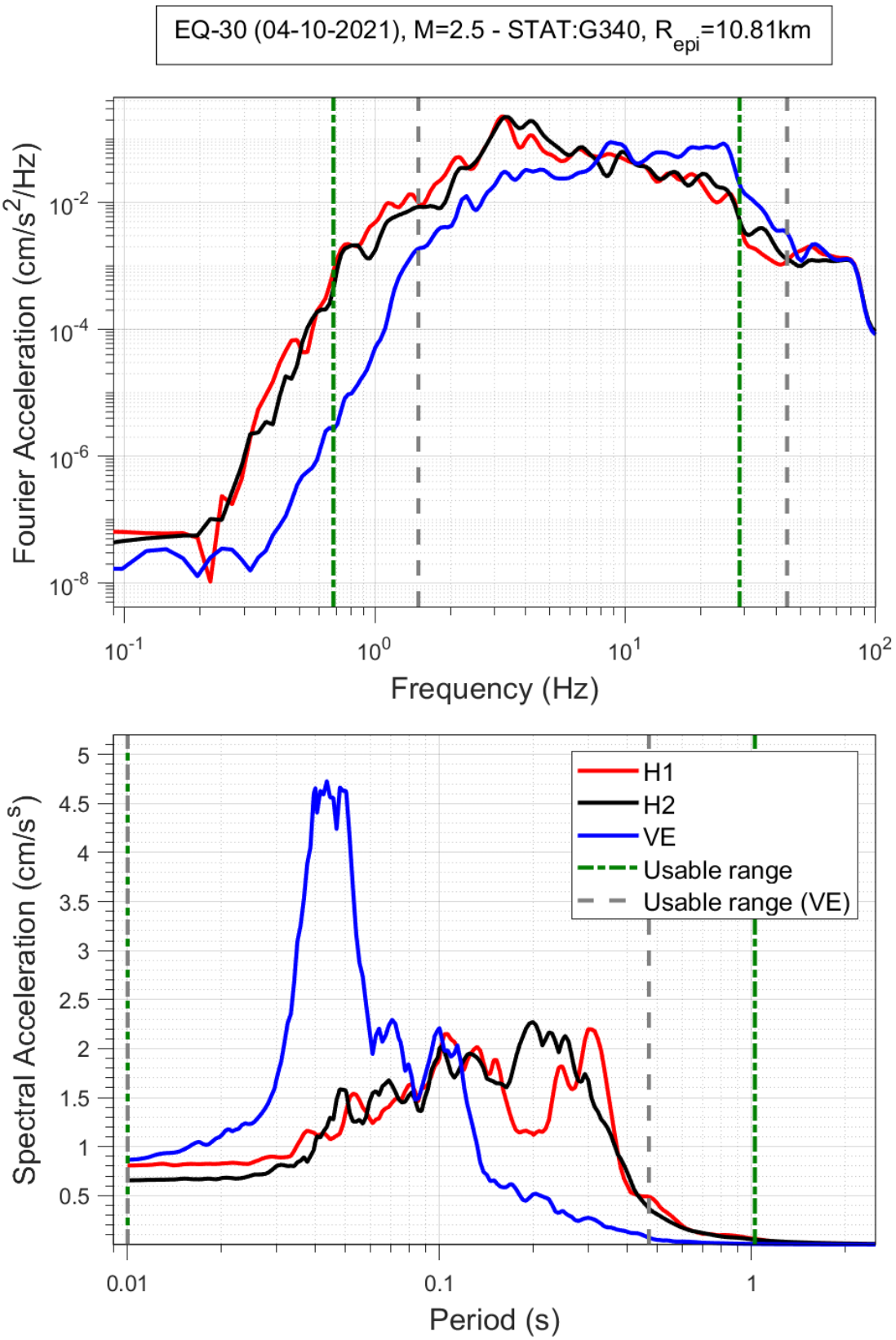
EQ-30 (04-10-2021), M=2.5 - STAT:G340, R_epi=10.81km
Fourier Acceleration (cm/s²/Hz)
10^-2
10^-4
10^-6
10^-8
10^-1
10^0
10^1
10^2
Frequency (Hz)
Spectral Acceleration (cm/s²)
5
4.5
4
3.5
3
2.5
2
1.5
1
0.5
0.01
0.1
1
Period (s)
H1
H2
VE
Usable range
Usable range (VE)

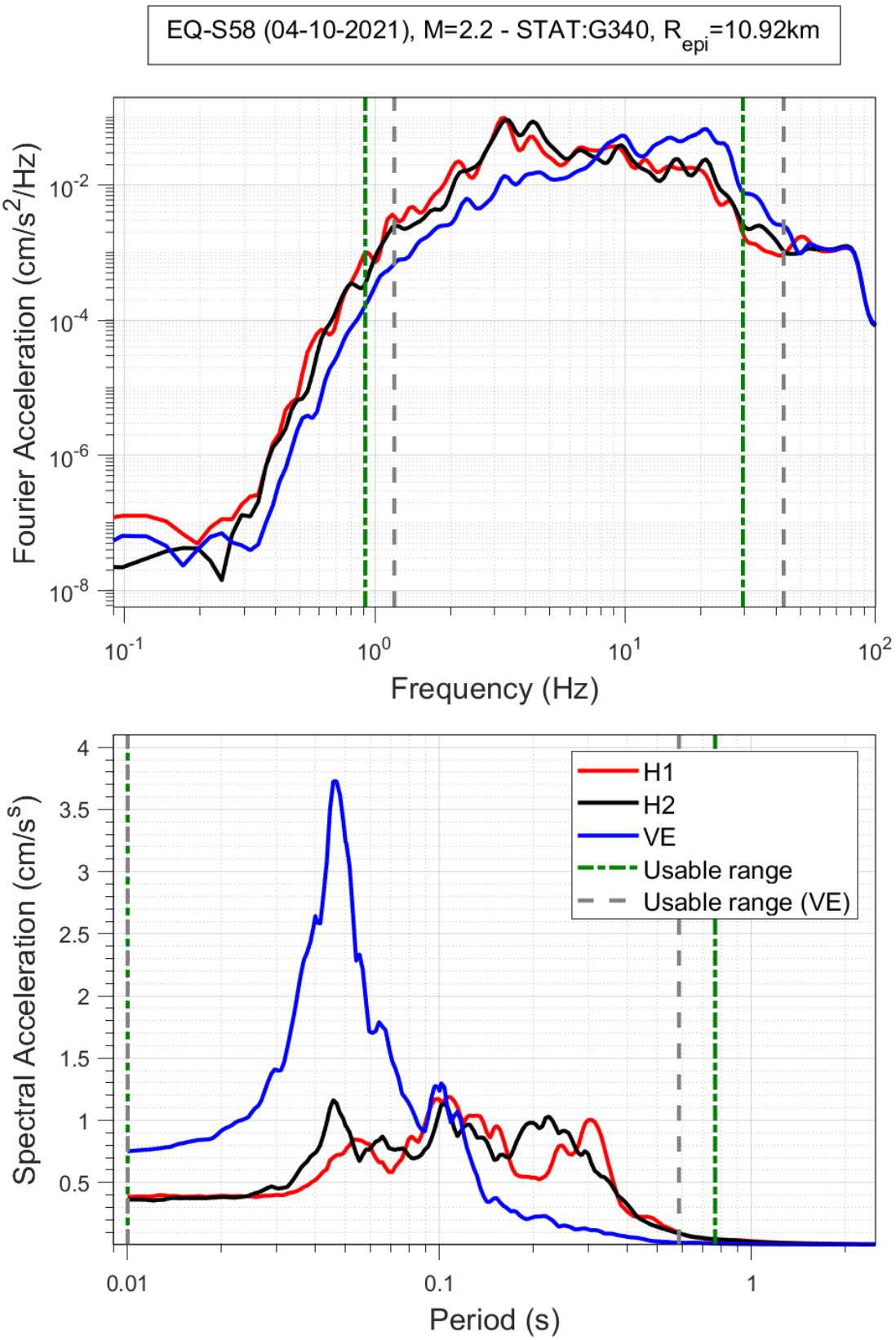
EQ-S58 (04-10-2021), M=2.2 - STAT:G340, R_epi=10.92km
Fourier Acceleration (cm/s²/Hz)
10^-2
10^-4
10^-6
10^-8
10^-1
10^0
10^1
10^2
Frequency (Hz)
Spectral Acceleration (cm/s²)
4
3.5
3
2.5
2
1.5
1
0.5
0.01
0.1
1
Period (s)
H1
H2
VE
Usable range
Usable range (VE)

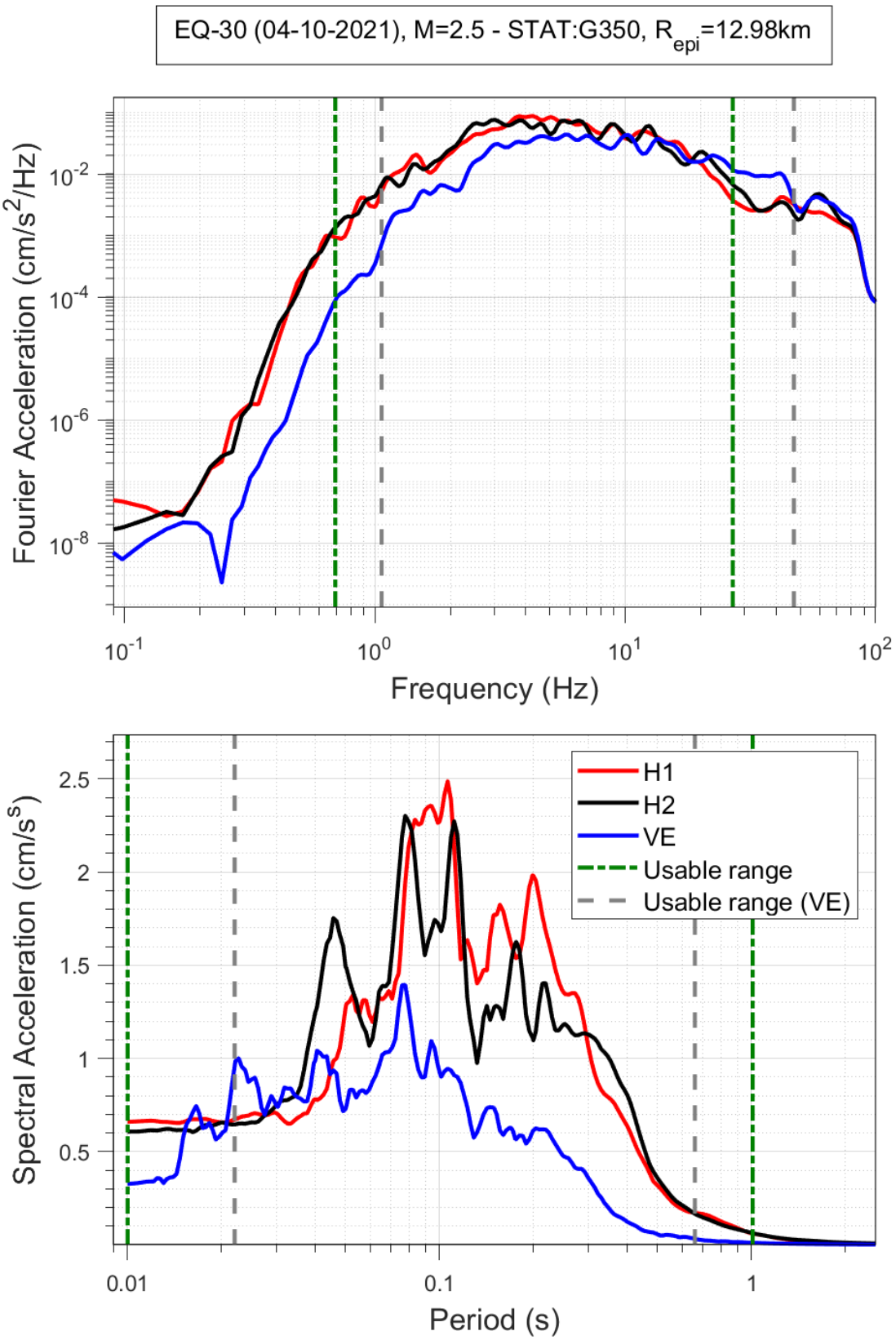
EQ-30 (04-10-2021), M=2.5 - STAT:G350, R_epi=12.98km
Fourier Acceleration (cm/s²/Hz)
10^-2
10^-4
10^-6
10^-8
10^-1
10^0
10^1
10^2
Frequency (Hz)
Spectral Acceleration (cm/s^s)
2.5
2
1.5
1
0.5
0.01
0.1
1
Period (s)
H1
H2
VE
Usable range
Usable range (VE)

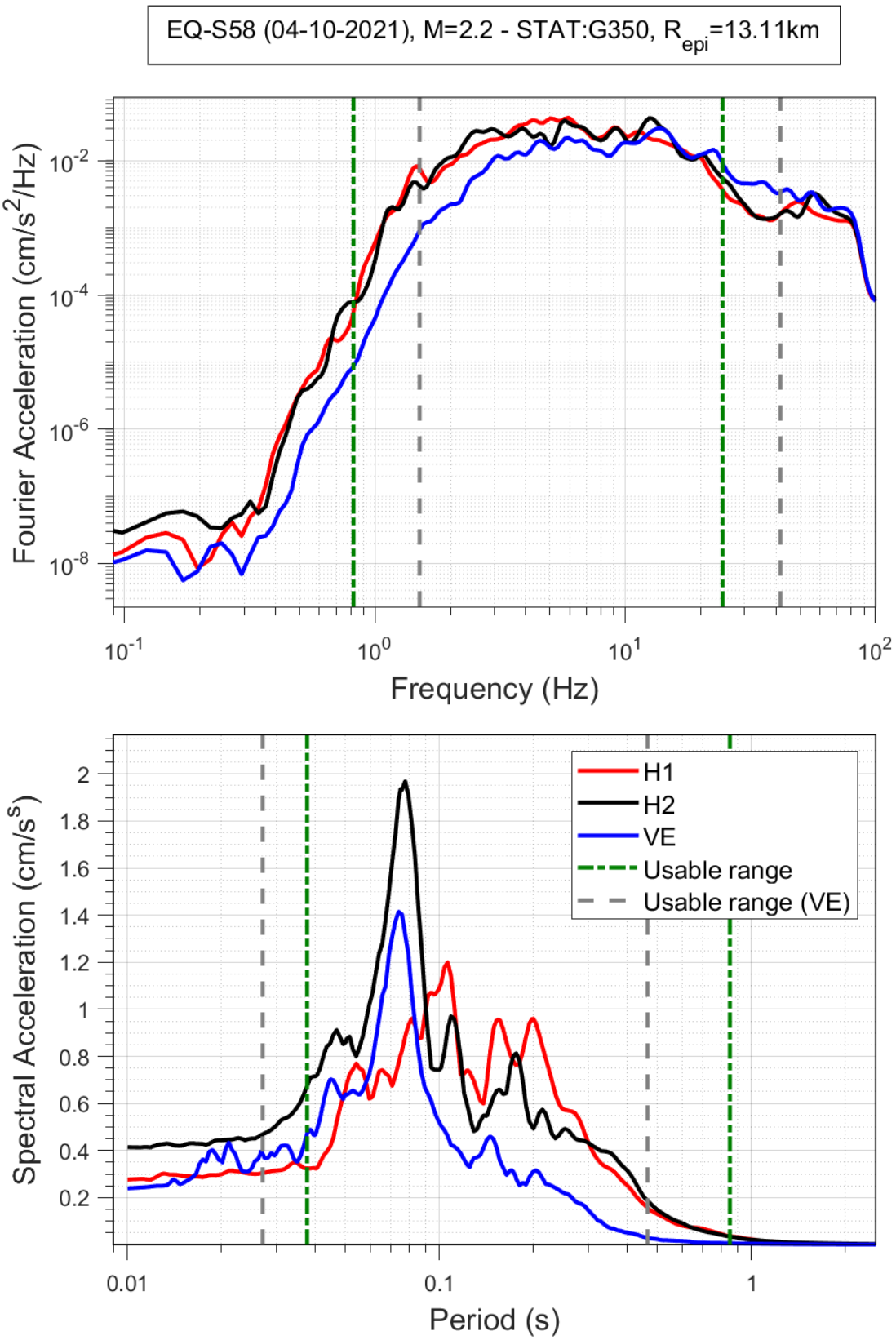
EQ-S58 (04-10-2021), M=2.2 - STAT:G350, R epi =13.11km
Fourier Acceleration (cm/s2/Hz)
10-2
10-4
10-6
10-8
10-1
100
101
102
Frequency (Hz)
Spectral Acceleration (cm/s)
2
1.8
1.6
1.4
1.2
1
0.8
0.6
0.4
0.2
0.01
0.1
1
Period (s)
H1
H2
VE
Usable range
Usable range (VE)

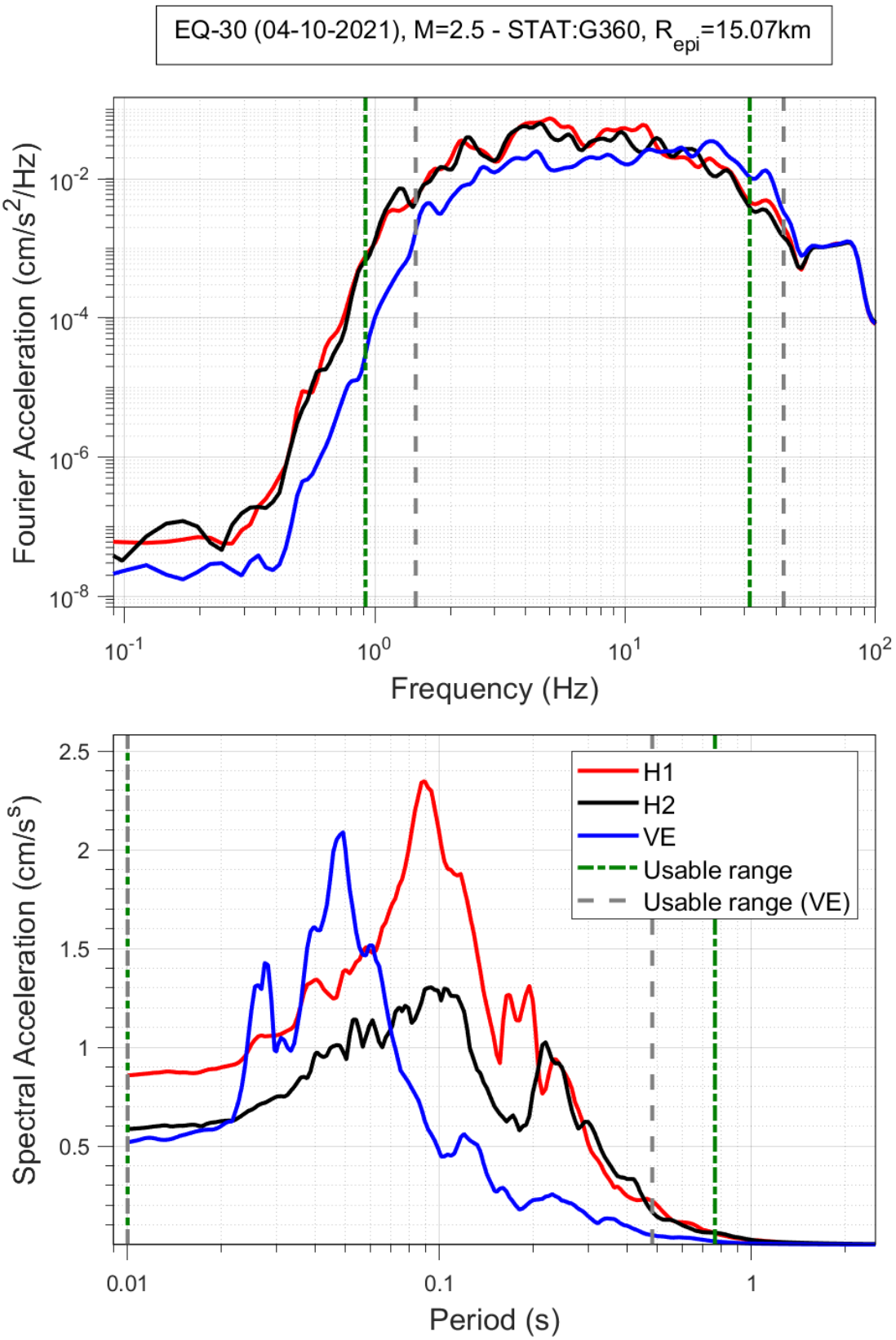
EQ-30 (04-10-2021), M=2.5 - STAT:G360, R_epi=15.07km
Fourier Acceleration (cm/s²/Hz)
10^-2
10^-4
10^-6
10^-8
10^-1
10^0
10^1
10^2
Frequency (Hz)
Spectral Acceleration (cm/s²)
2.5
2
1.5
1
0.5
0.01
0.1
1
Period (s)
H1
H2
VE
Usable range
Usable range (VE)

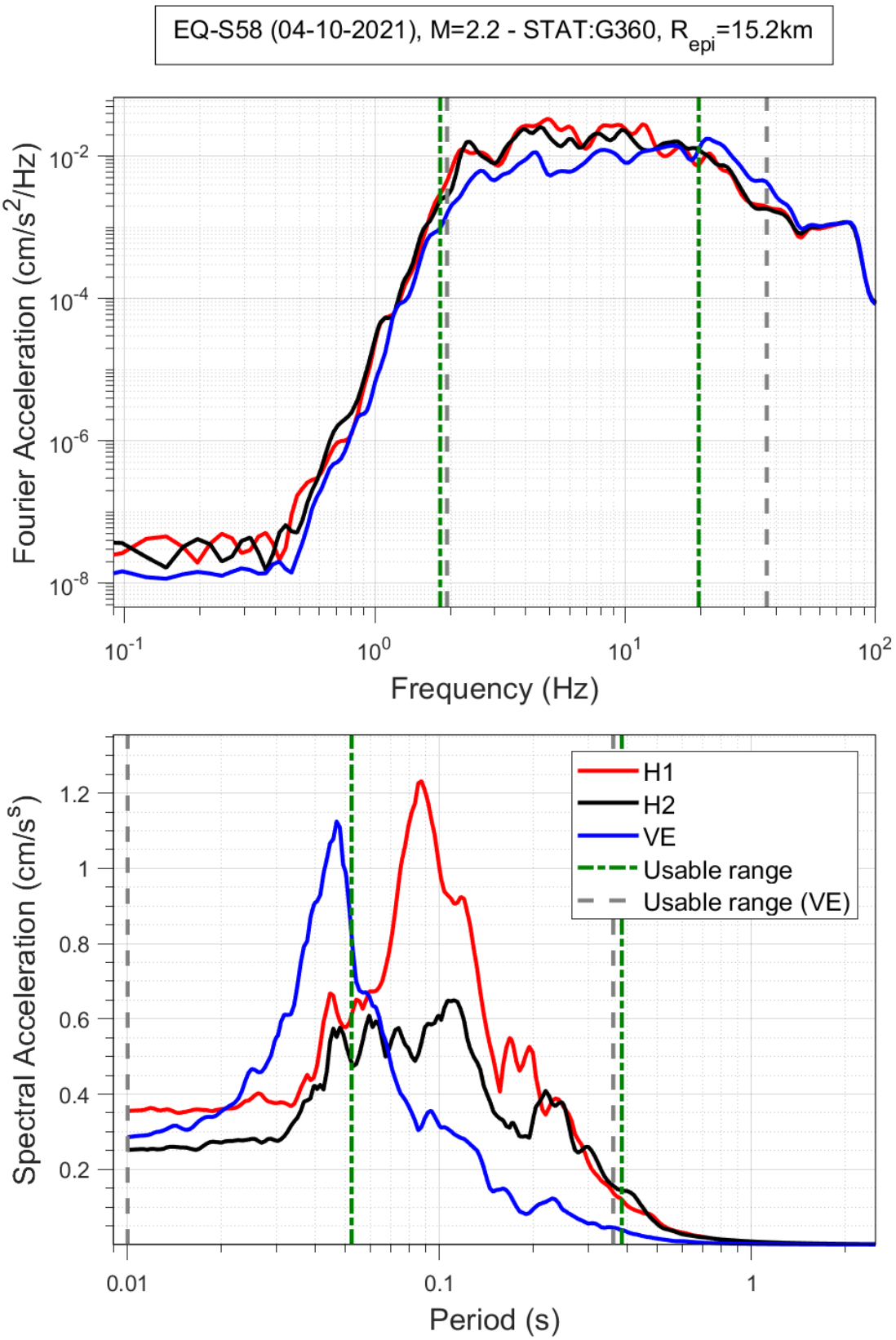
EQ-S58 (04-10-2021), M=2.2 - STAT:G360, R_epi=15.2km
Fourier Acceleration (cm/s²/Hz)
10^-2
10^-4
10^-6
10^-8
10^-1
10^0
10^1
10^2
Frequency (Hz)
Spectral Acceleration (cm/s^s)
1.2
1
0.8
0.6
0.4
0.2
0.01
0.1
1
Period (s)
H1
H2
VE
Usable range
Usable range (VE)

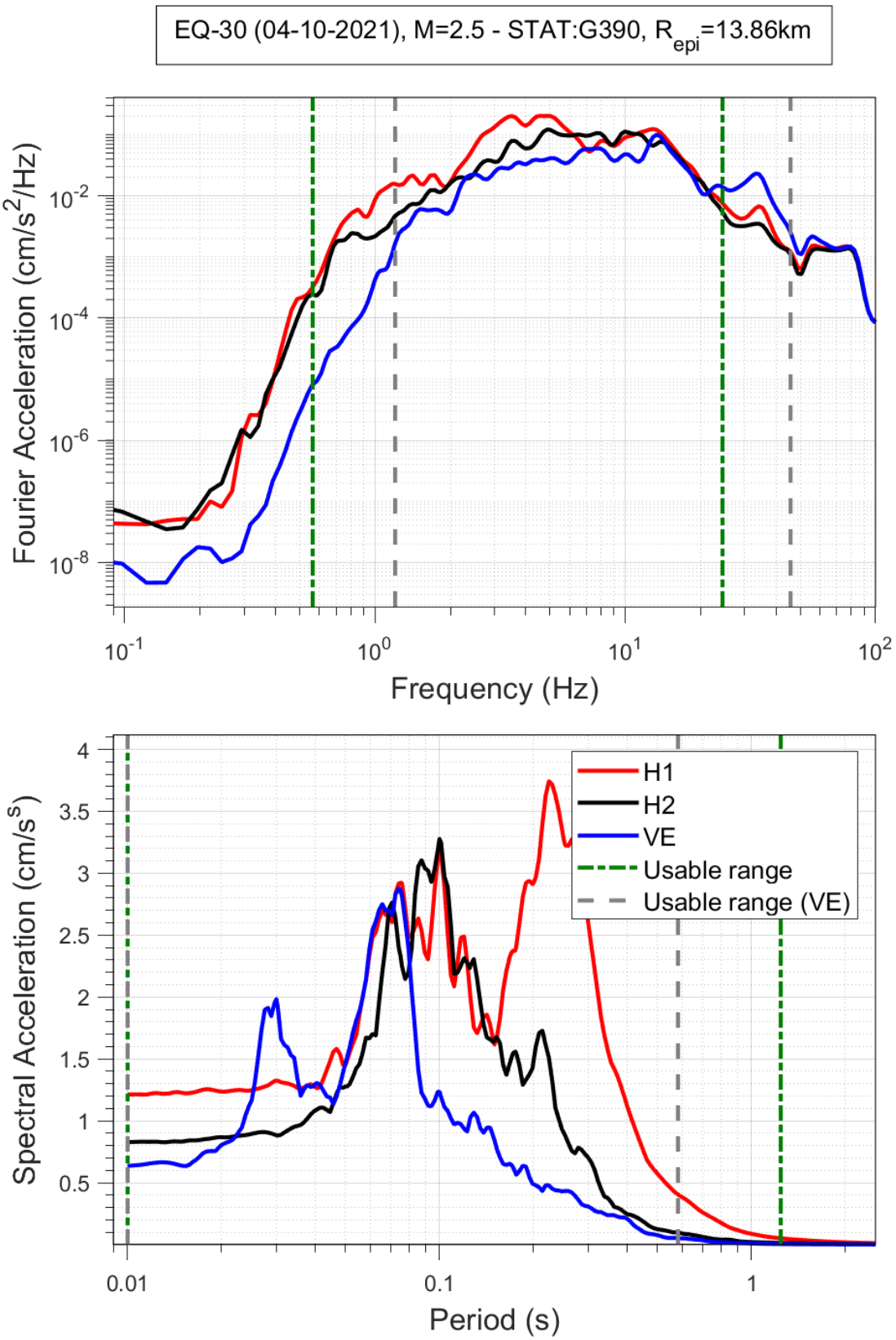
EQ-30 (04-10-2021), M=2.5 - STAT:G390, R_epi=13.86km
Fourier Acceleration (cm/s²/Hz)
10^-2
10^-4
10^-6
10^-8
10^-1
10^0
10^1
10^2
Frequency (Hz)
Spectral Acceleration (cm/s^s)
4
3.5
3
2.5
2
1.5
1
0.5
0.01
0.1
1
Period (s)
H1
H2
VE
Usable range
Usable range (VE)

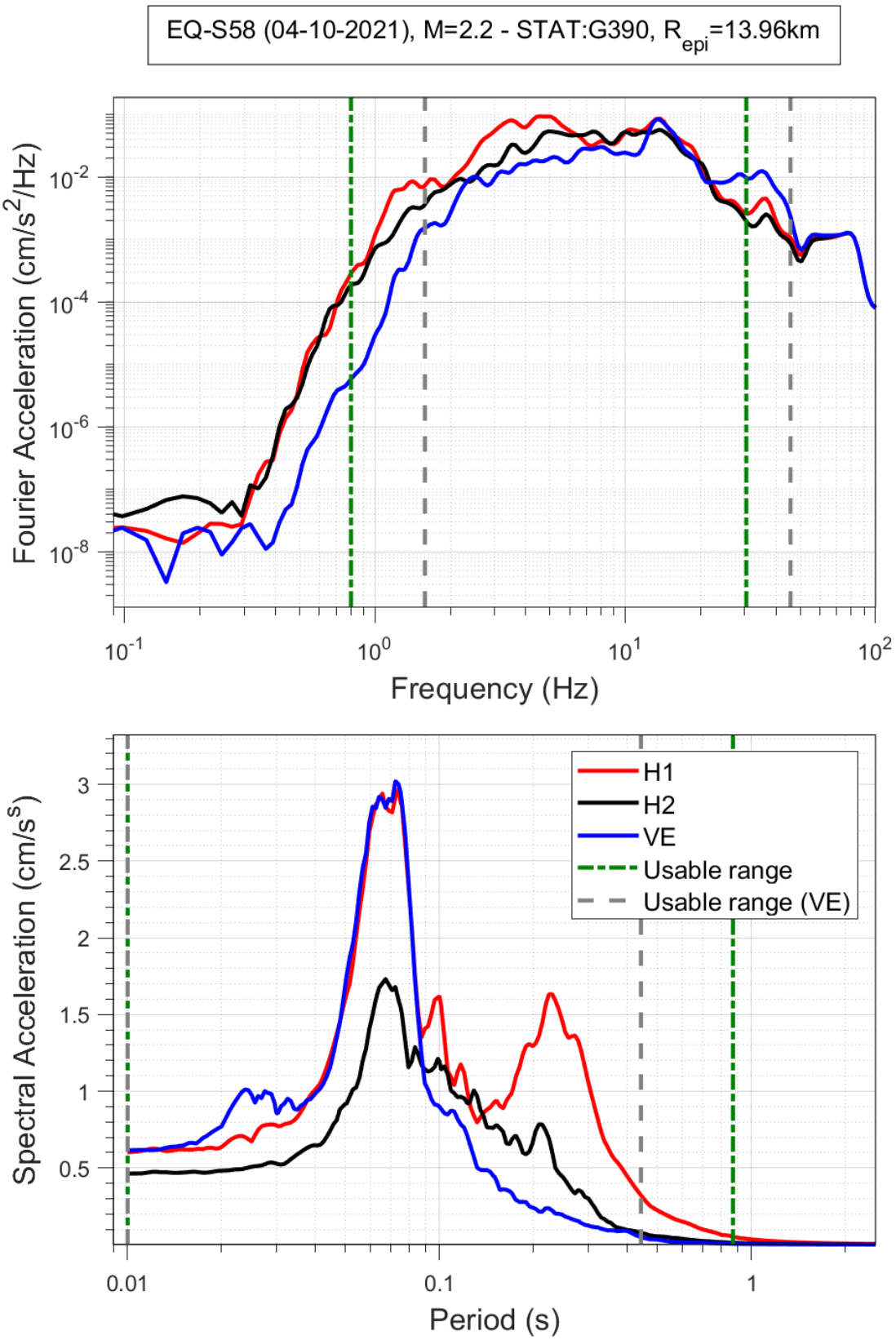
EQ-S58 (04-10-2021), M=2.2 - STAT:G390, R epi =13.96km
Fourier Acceleration (cm/s2/Hz)
10-2
10-4
10-6
10-8
10-1
100
101
102
Frequency (Hz)
Spectral Acceleration (cm/s)
3
2.5
2
1.5
1
0.5
0.01
0.1
1
Period (s)
H1
H2
VE
Usable range
Usable range (VE)

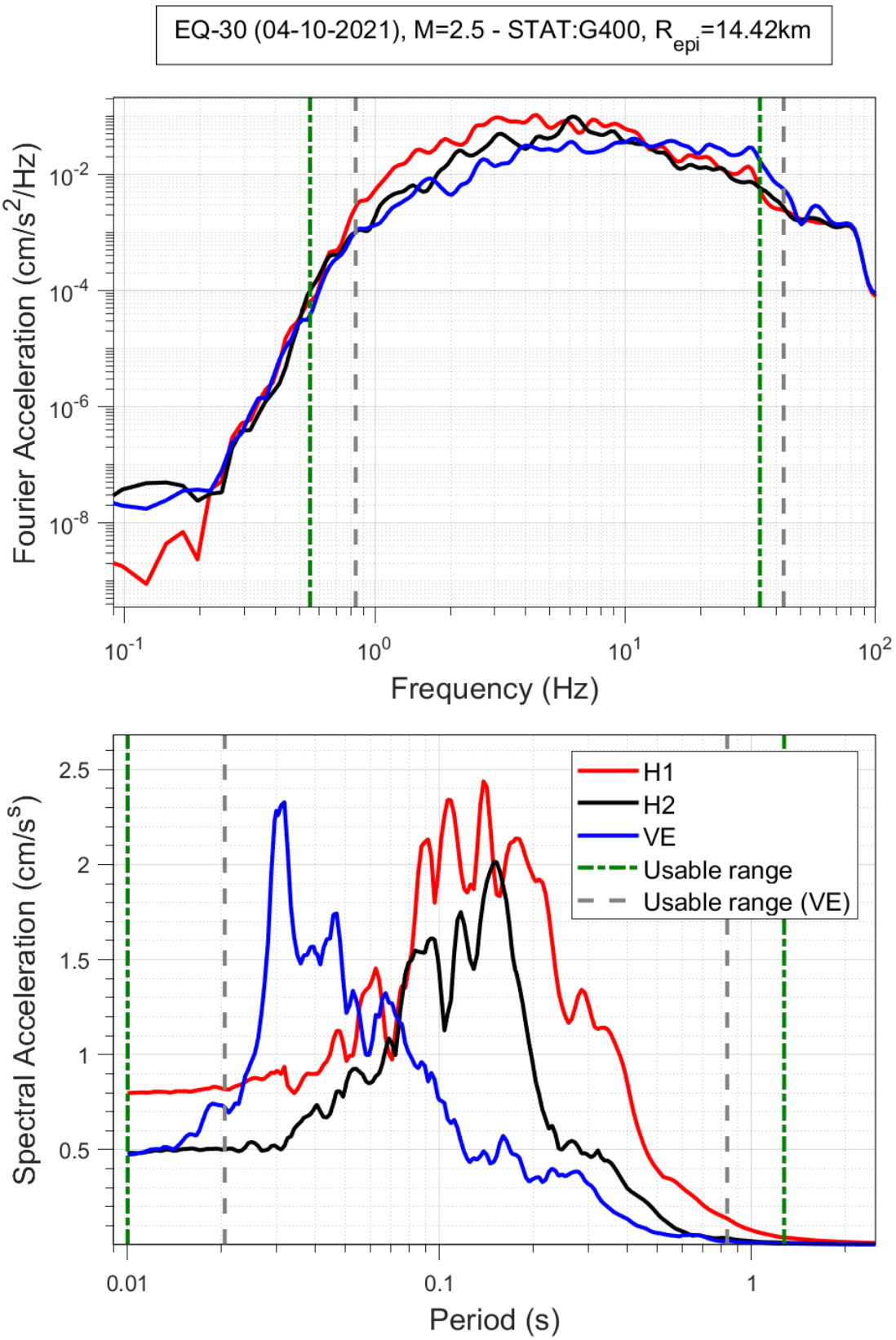
EQ-30 (04-10-2021), M=2.5 - STAT:G400, R_epi=14.42km
Fourier Acceleration (cm/s²/Hz)
10^-2
10^-4
10^-6
10^-8
10^-1
10^0
10^1
10^2
Frequency (Hz)
Spectral Acceleration (cm/s^s)
2.5
2
1.5
1
0.5
0.01
0.1
1
Period (s)
H1
H2
VE
Usable range
Usable range (VE)

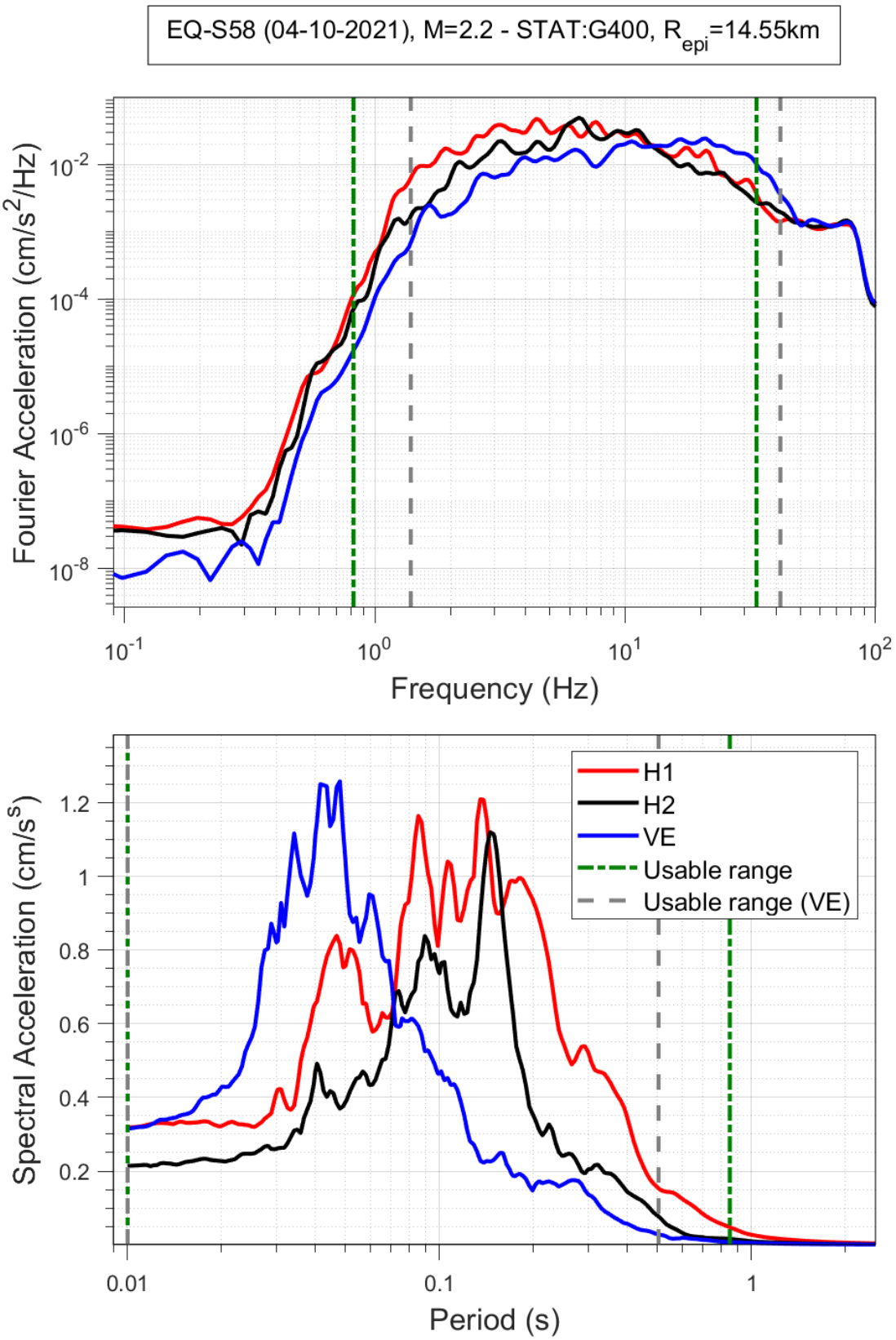
EQ-S58 (04-10-2021), M=2.2 - STAT:G400, R_epi=14.55km
Fourier Acceleration (cm/s²/Hz)
10^-2
10^-4
10^-6
10^-8
10^-1
10^0
10^1
10^2
Frequency (Hz)
Spectral Acceleration (cm/s^s)
1.2
1
0.8
0.6
0.4
0.2
0.01
0.1
1
Period (s)
H1
H2
VE
Usable range
Usable range (VE)

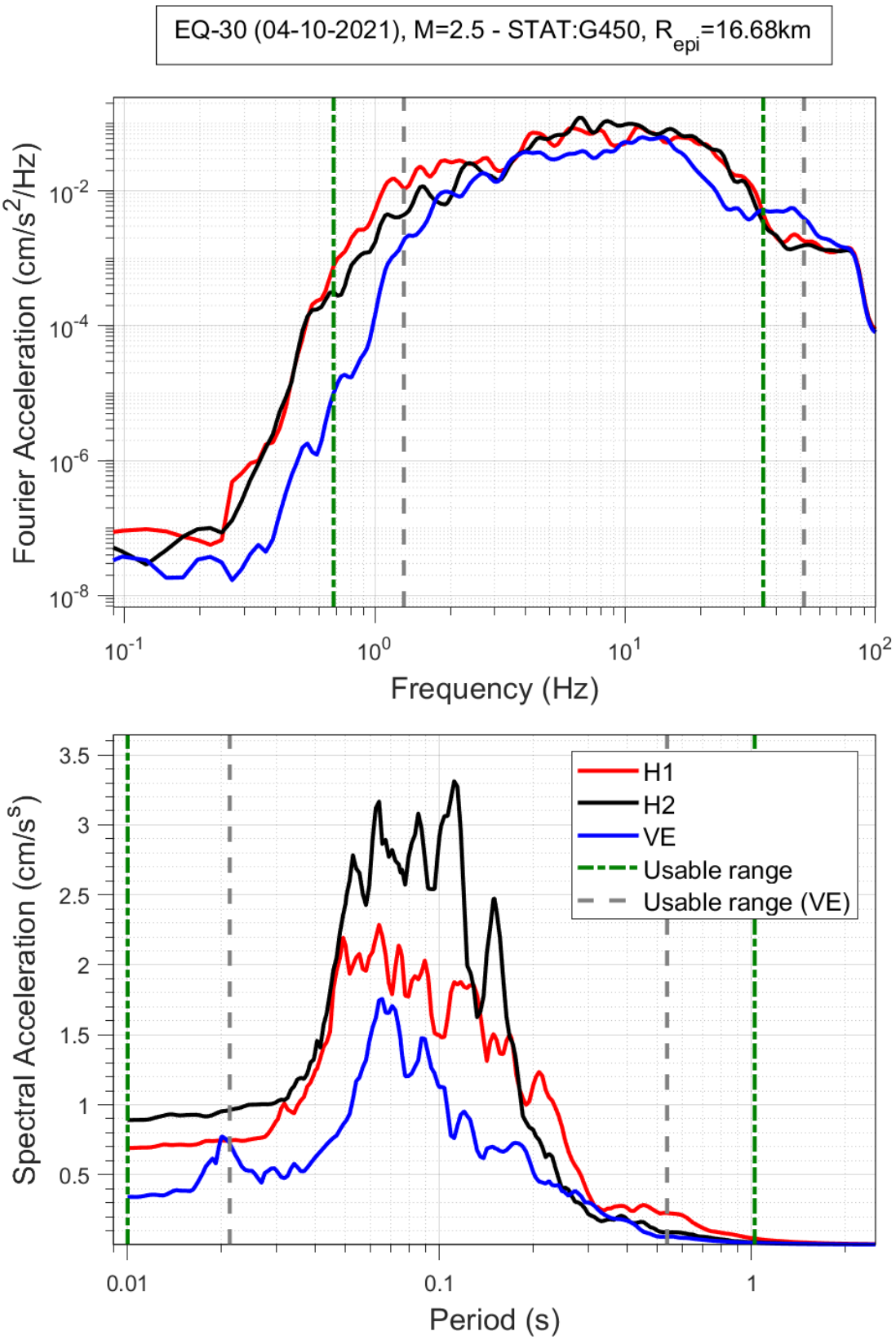
EQ-30 (04-10-2021), M=2.5 - STAT:G450, R_epi=16.68km
Fourier Acceleration (cm/s²/Hz)
10^-2
10^-4
10^-6
10^-8
10^-1
10^0
10^1
10^2
Frequency (Hz)
Spectral Acceleration (cm/s^s)
3.5
3
2.5
2
1.5
1
0.5
0.01
0.1
1
Period (s)
H1
H2
VE
Usable range
Usable range (VE)

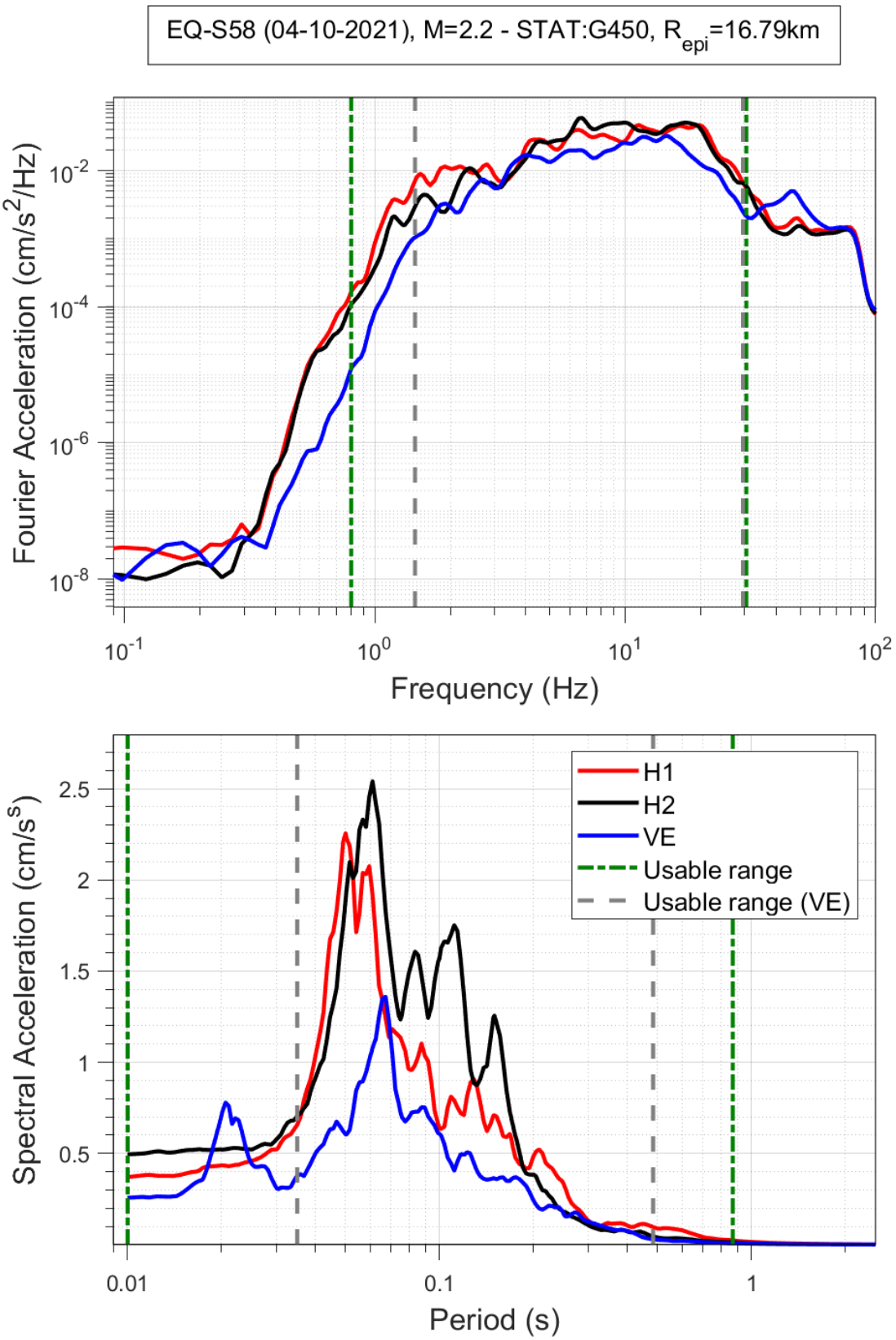
EQ-S58 (04-10-2021), M=2.2 - STAT:G450, R epi =16.79km
Fourier Acceleration (cm/s2/Hz)
10-2
10-4
10-6
10-8
10-1
100
101
102
Frequency (Hz)
Spectral Acceleration (cm/s2)
2.5
2
1.5
1
0.5
0.01
0.1
1
Period (s)
H1
H2
VE
Usable range
Usable range (VE)

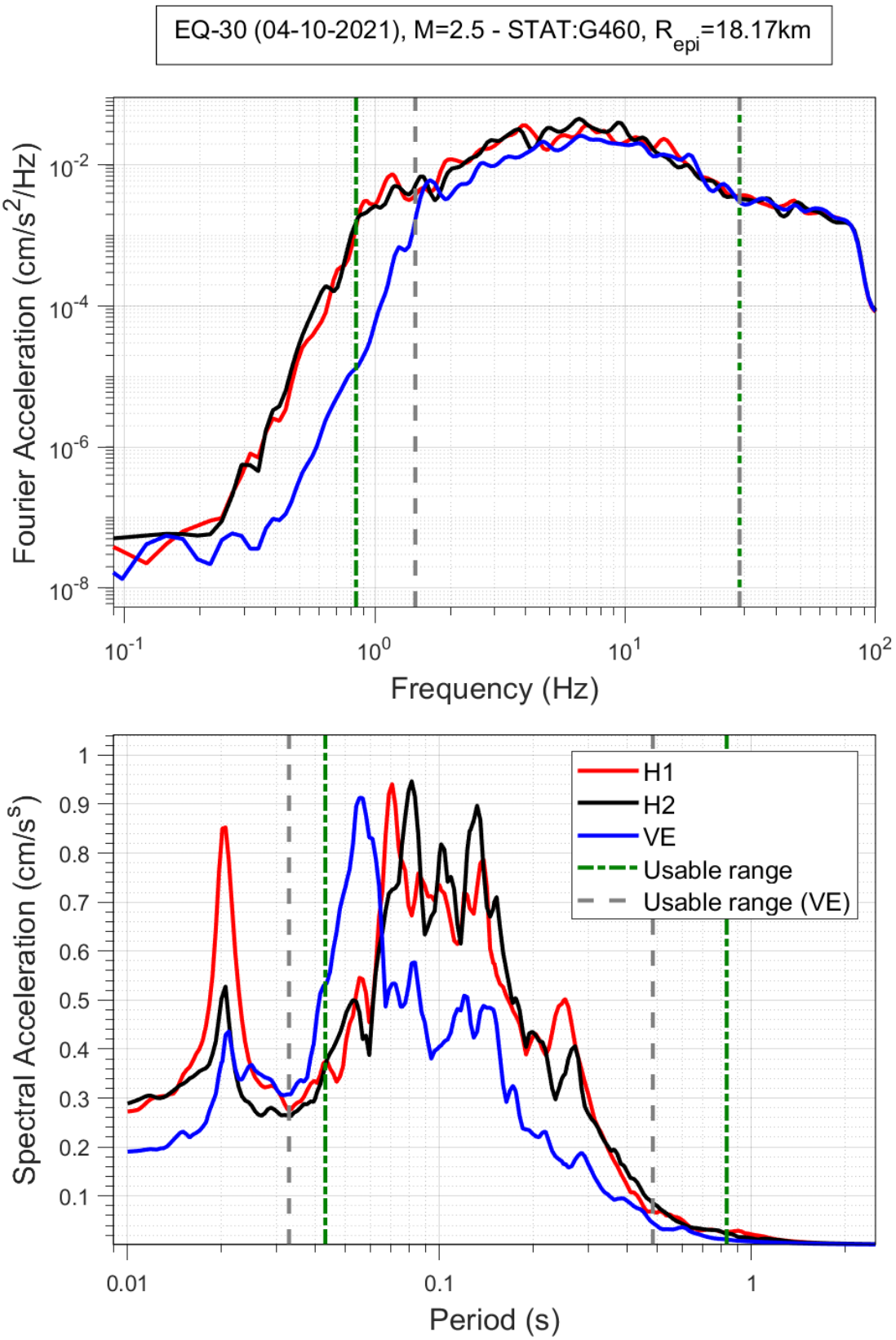
EQ-30 (04-10-2021), M=2.5 - STAT:G460, R_epi=18.17km
Fourier Acceleration (cm/s²/Hz)
10^-2
10^-4
10^-6
10^-8
10^-1
10^0
10^1
10^2
Frequency (Hz)
Spectral Acceleration (cm/s^s)
1
0.9
0.8
0.7
0.6
0.5
0.4
0.3
0.2
0.1
0.01
0.1
1
Period (s)
H1
H2
VE
Usable range
Usable range (VE)

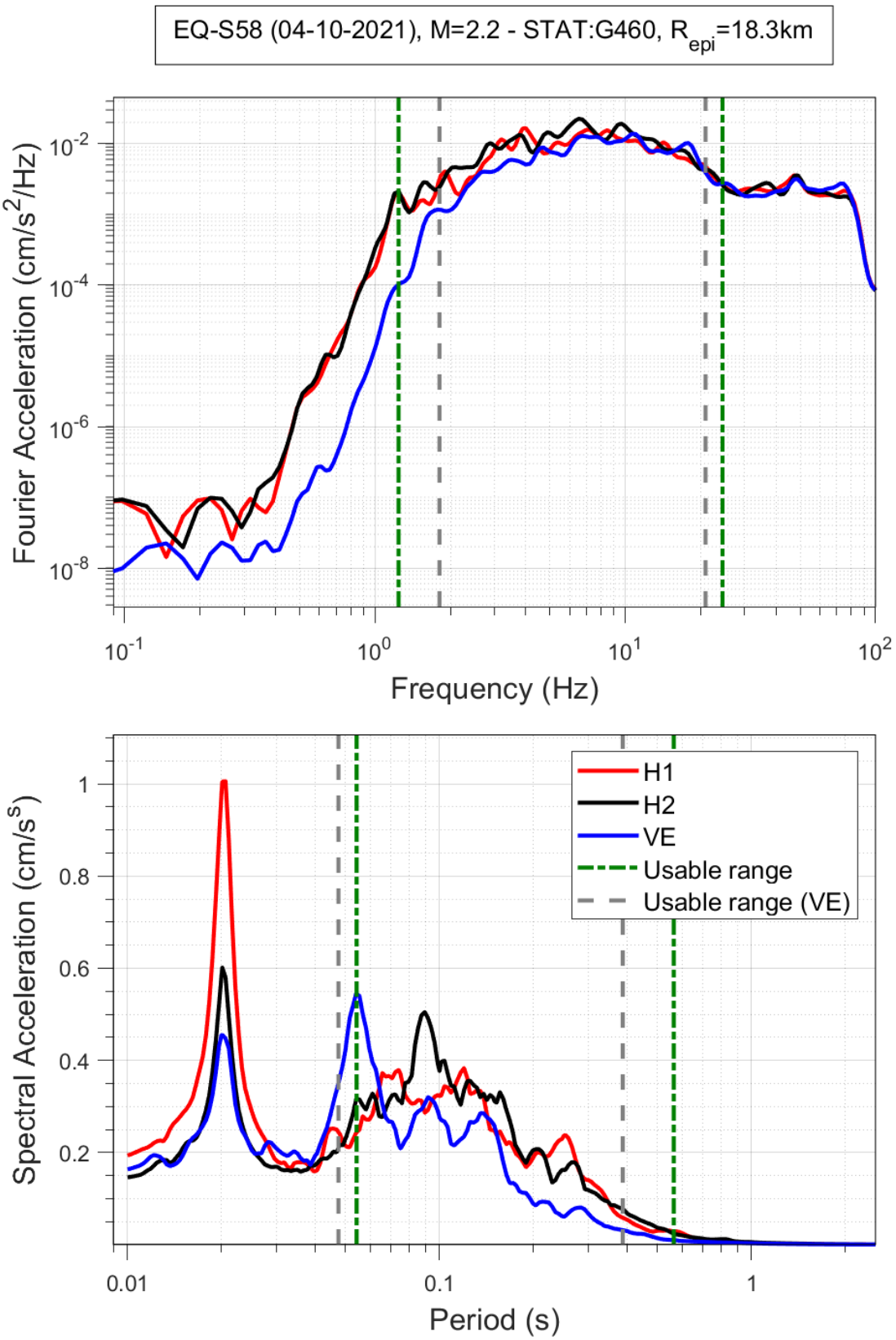
EQ-S58 (04-10-2021), M=2.2 - STAT:G460, R_epi=18.3km
Fourier Acceleration (cm/s²/Hz)
10^-2
10^-4
10^-6
10^-8
10^-1
10^0
10^1
10^2
Frequency (Hz)
Spectral Acceleration (cm/s^s)
1
0.8
0.6
0.4
0.2
0.01
0.1
1
Period (s)
H1
H2
VE
Usable range
Usable range (VE)

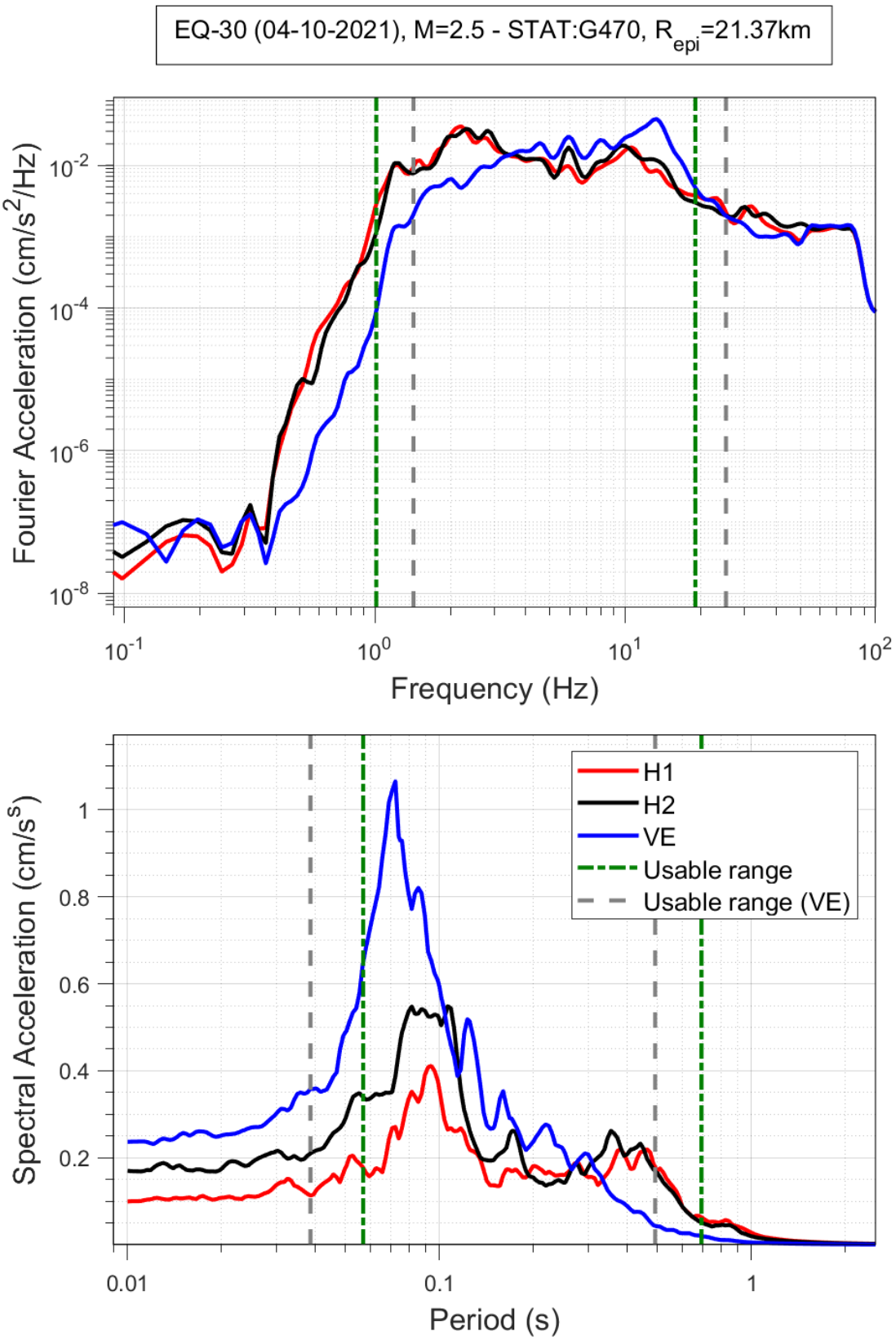
EQ-30 (04-10-2021), M=2.5 - STAT:G470, R_epi=21.37km
Fourier Acceleration (cm/s²/Hz)
10^-2
10^-4
10^-6
10^-8
10^-1
10^0
10^1
10^2
Frequency (Hz)
Spectral Acceleration (cm/s^s)
1
0.8
0.6
0.4
0.2
0.01
0.1
1
Period (s)
H1
H2
VE
Usable range
Usable range (VE)

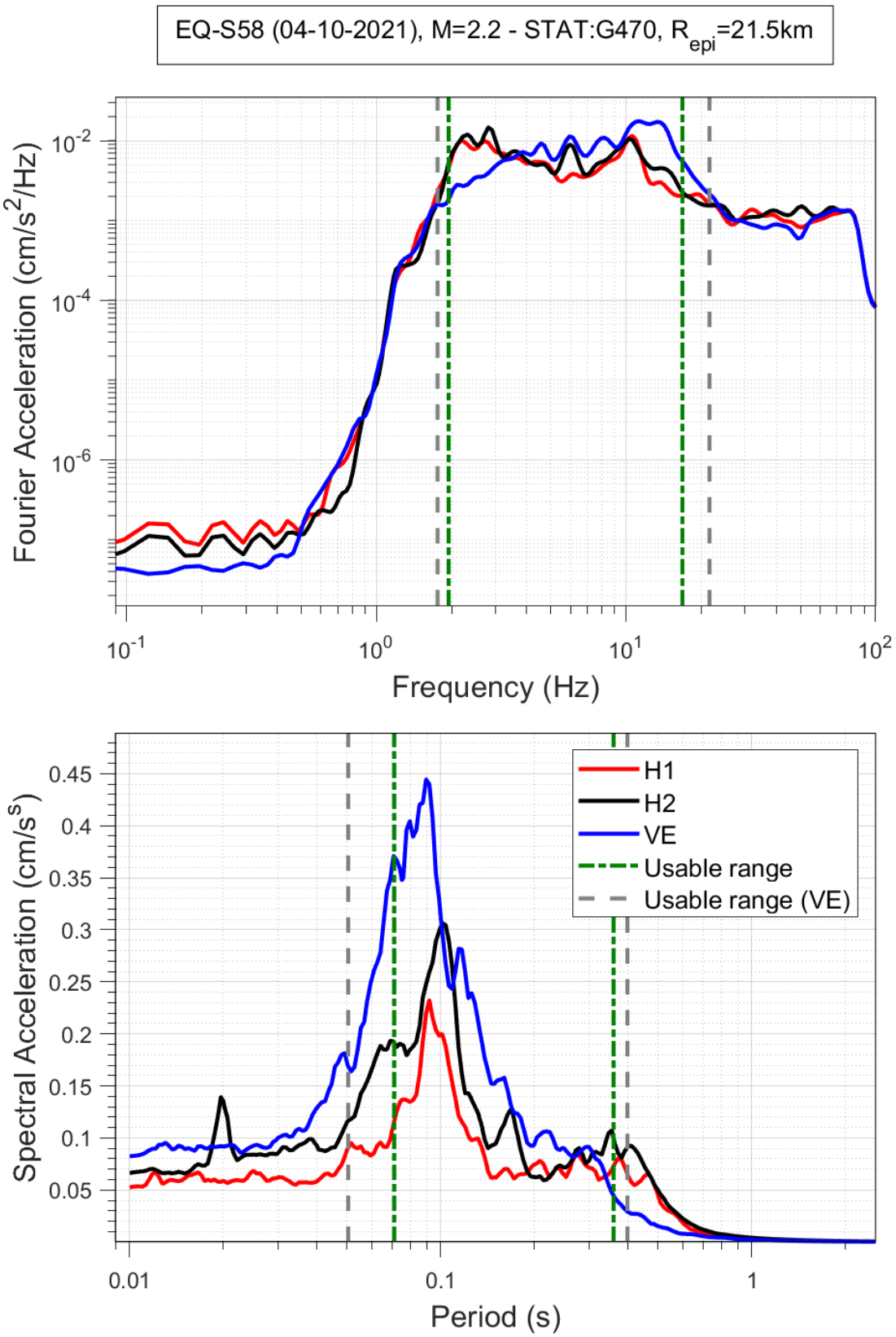
EQ-S58 (04-10-2021), M=2.2 - STAT:G470, R_epi=21.5km
Fourier Acceleration (cm/s²/Hz)
10^-2
10^-4
10^-6
10^-1
10^0
10^1
10^2
Frequency (Hz)
Spectral Acceleration (cm/s^s)
0.45
0.4
0.35
0.3
0.25
0.2
0.15
0.1
0.05
0.01
0.1
1
Period (s)
H1
H2
VE
Usable range
Usable range (VE)

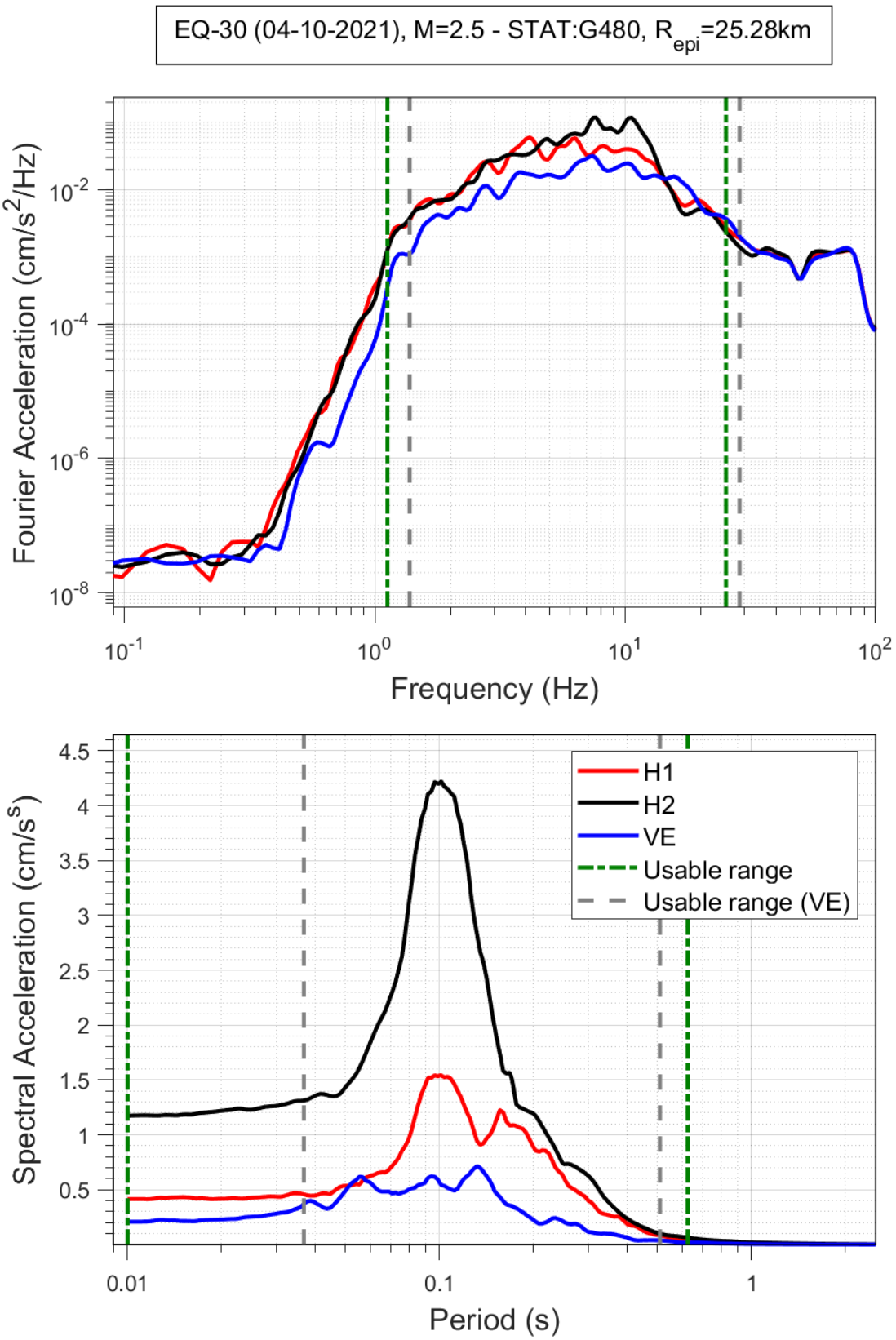
EQ-30 (04-10-2021), M=2.5 - STAT:G480, R_epi=25.28km
Fourier Acceleration (cm/s²/Hz)
10^-2
10^-4
10^-6
10^-8
10^-1
10^0
10^1
10^2
Frequency (Hz)
Spectral Acceleration (cm/s²)
4.5
4
3.5
3
2.5
2
1.5
1
0.5
0.01
0.1
1
Period (s)
H1
H2
VE
Usable range
Usable range (VE)

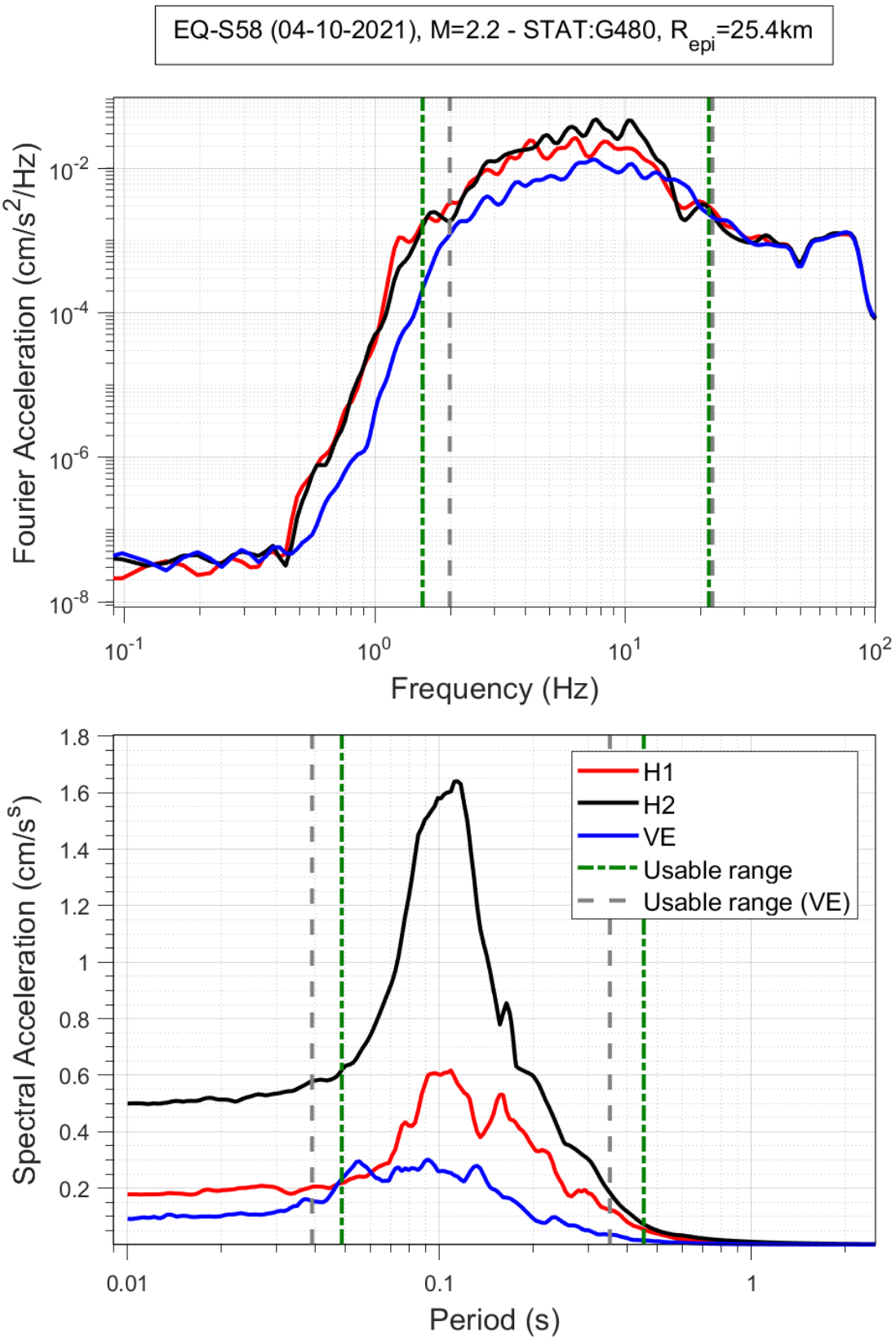
EQ-S58 (04-10-2021), M=2.2 - STAT:G480, R_epi=25.4km
Fourier Acceleration (cm/s²/Hz)
10^-2
10^-4
10^-6
10^-8
10^-1
10^0
10^1
10^2
Frequency (Hz)
Spectral Acceleration (cm/s^s)
1.8
1.6
1.4
1.2
1
0.8
0.6
0.4
0.2
0.01
0.1
1
Period (s)
H1
H2
VE
Usable range
Usable range (VE)

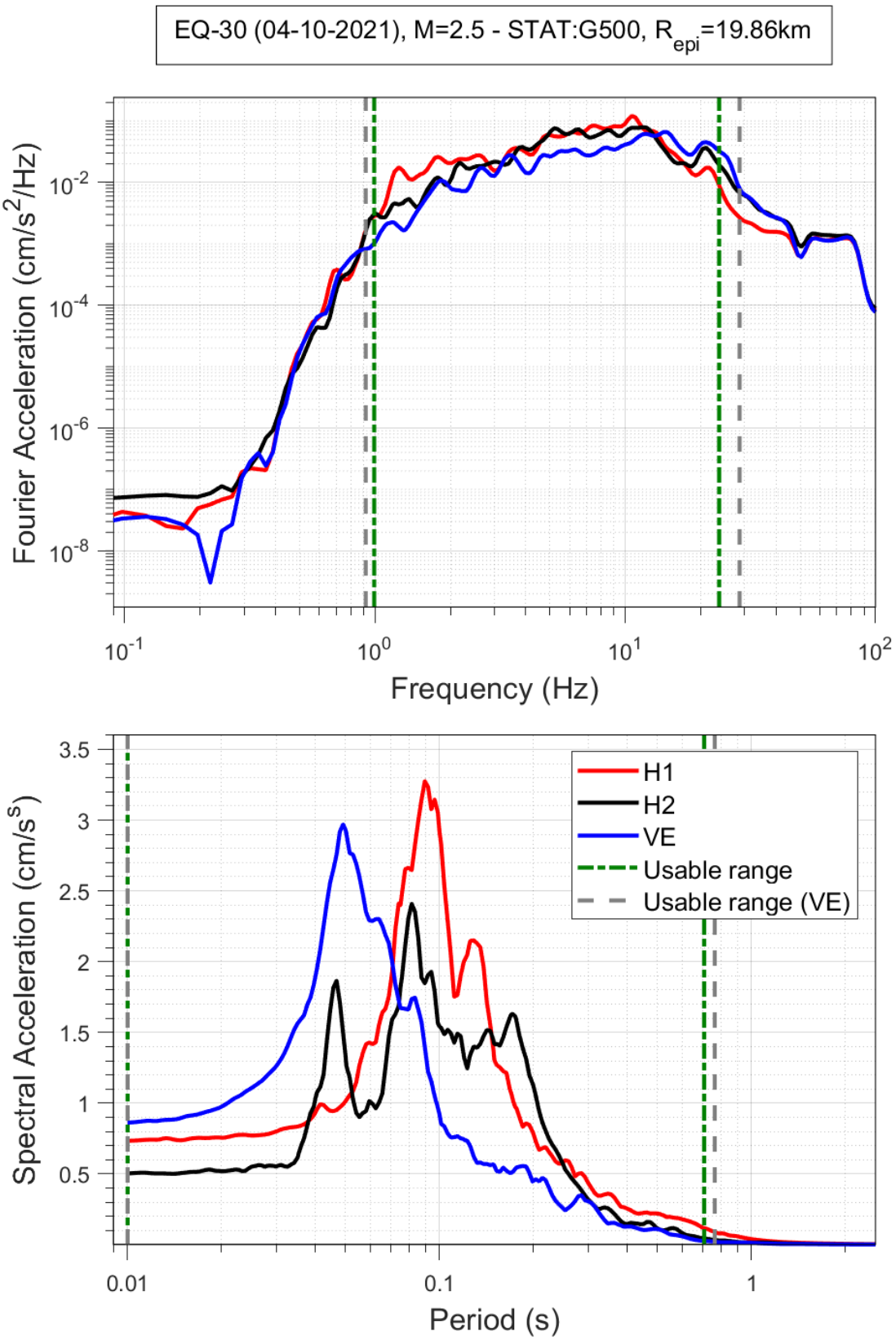
EQ-30 (04-10-2021), M=2.5 - STAT:G500, R_epi=19.86km
Fourier Acceleration (cm/s²/Hz)
10^-2
10^-4
10^-6
10^-8
10^-1
10^0
10^1
10^2
Frequency (Hz)
Spectral Acceleration (cm/s^s)
3.5
3
2.5
2
1.5
1
0.5
0.01
0.1
1
Period (s)
H1
H2
VE
Usable range
Usable range (VE)

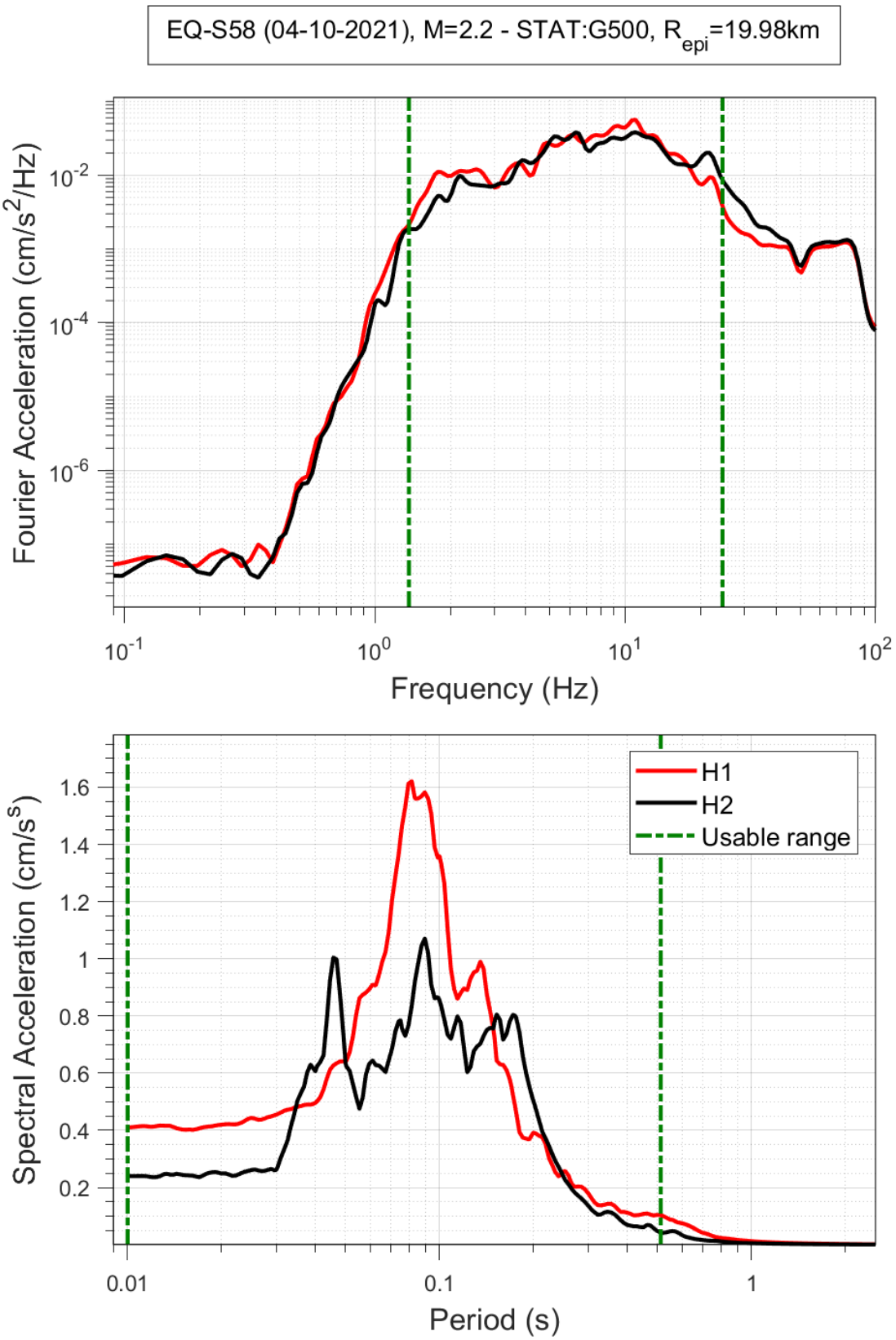
EQ-S58 (04-10-2021), M=2.2 - STAT:G500, R epi =19.98km
Fourier Acceleration (cm/s2/Hz)
10-2
10-4
10-6
10-1
100
101
102
Frequency (Hz)
Spectral Acceleration (cm/s)
1.6
1.4
1.2
1
0.8
0.6
0.4
0.2
0.01
0.1
1
Period (s)
H1
H2
Usable range

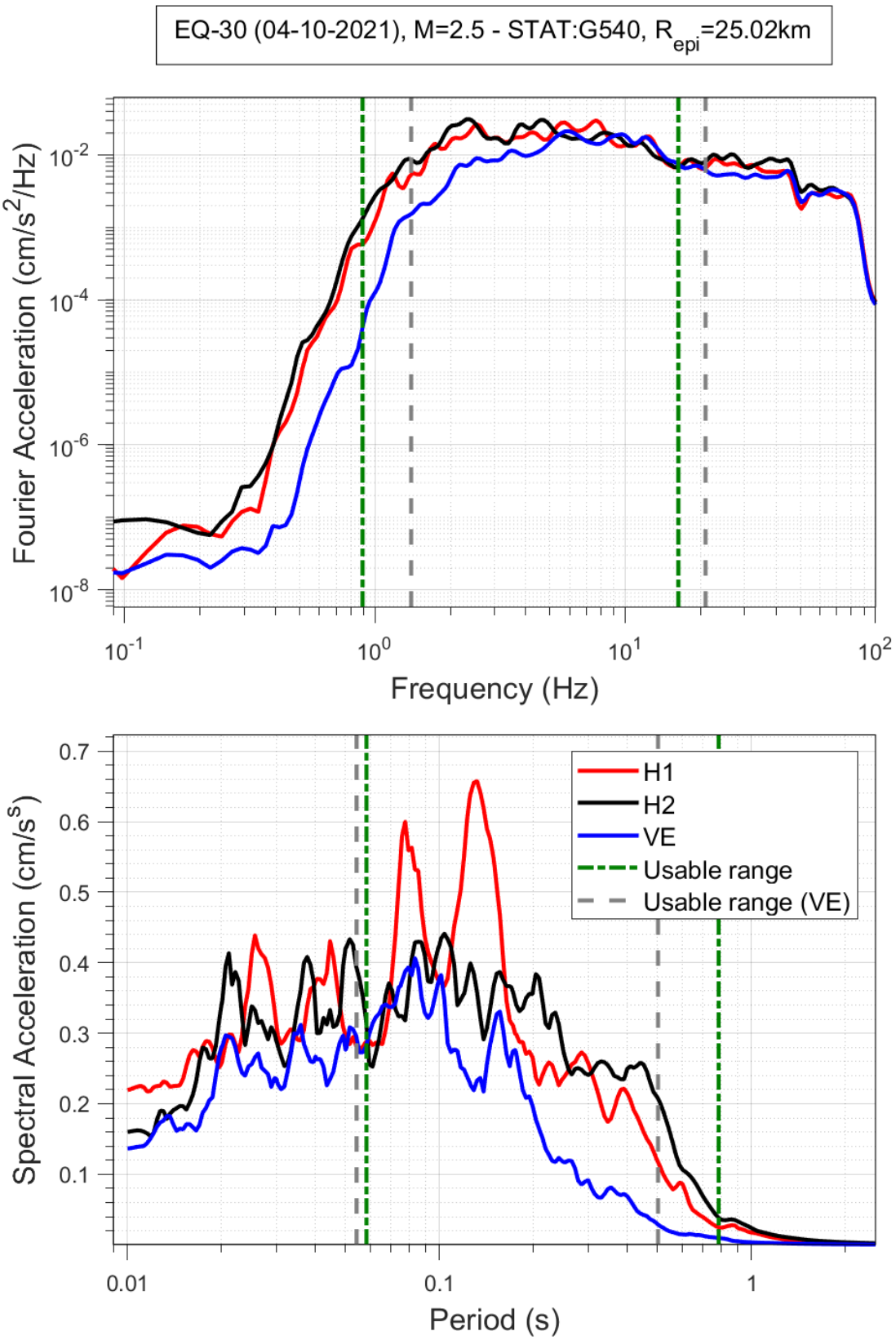
EQ-30 (04-10-2021), M=2.5 - STAT:G540, R_epi=25.02km
Fourier Acceleration (cm/s²/Hz)
10^-2
10^-4
10^-6
10^-8
10^-1
10^0
10^1
10^2
Frequency (Hz)
Spectral Acceleration (cm/s^s)
0.7
0.6
0.5
0.4
0.3
0.2
0.1
0.01
0.1
1
Period (s)
H1
H2
VE
Usable range
Usable range (VE)

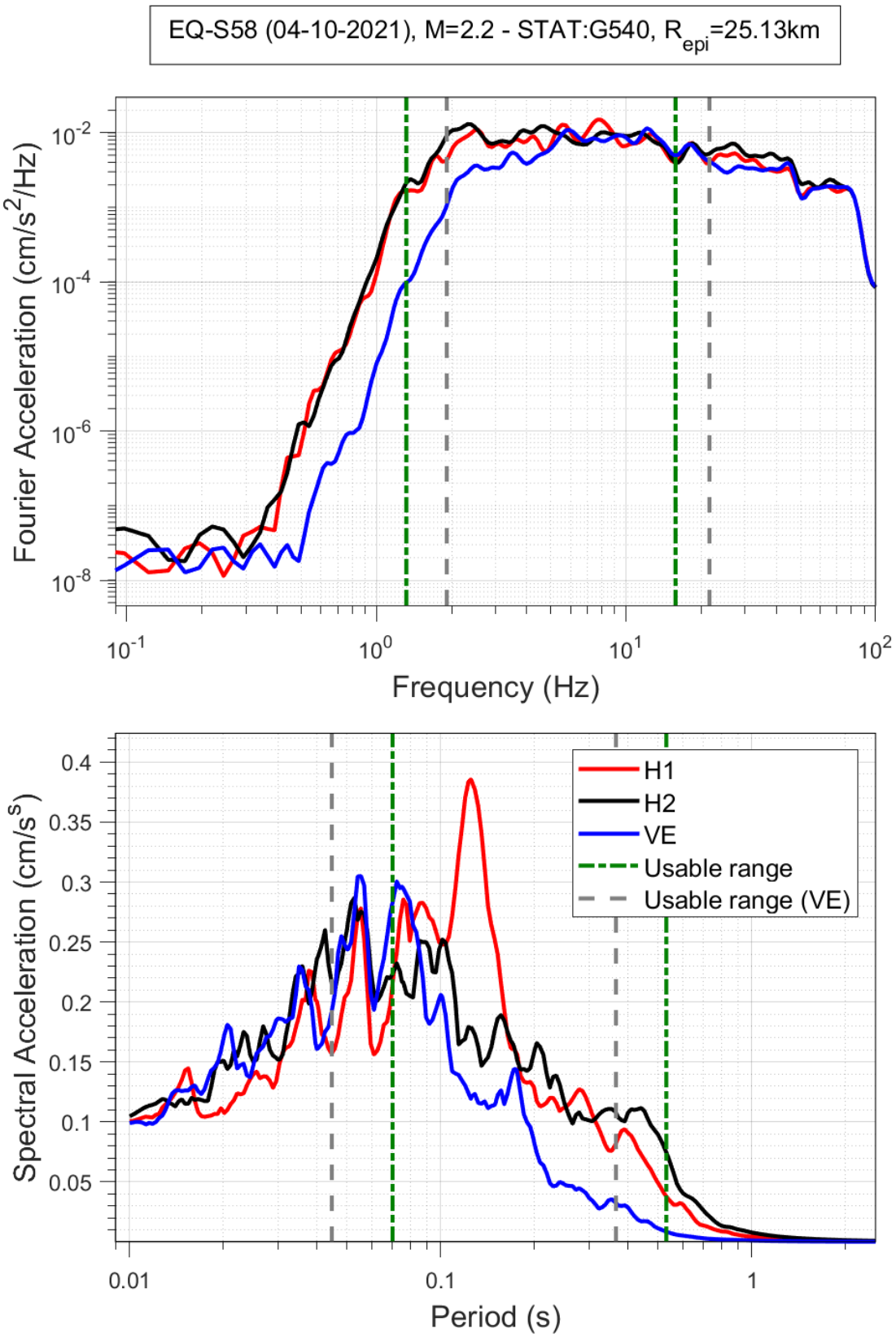
EQ-S58 (04-10-2021), M=2.2 - STAT:G540, R_epi=25.13km
Fourier Acceleration (cm/s²/Hz)
10^-2
10^-4
10^-6
10^-8
10^-1
10^0
10^1
10^2
Frequency (Hz)
Spectral Acceleration (cm/s^s)
0.4
0.35
0.3
0.25
0.2
0.15
0.1
0.05
0.01
0.1
1
Period (s)
H1
H2
VE
Usable range
Usable range (VE)

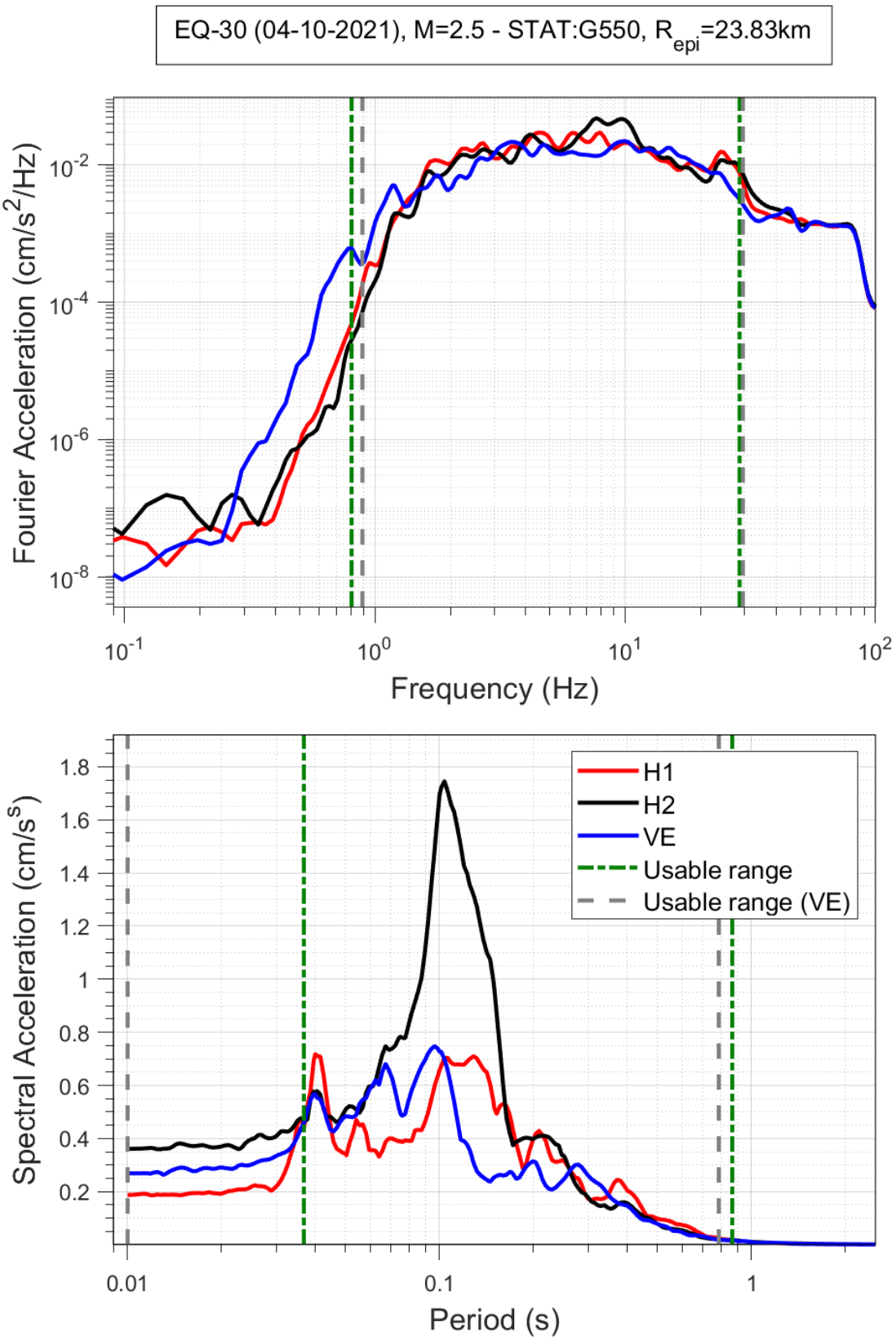
EQ-30 (04-10-2021), M=2.5 - STAT:G550, R_epi=23.83km
Fourier Acceleration (cm/s²/Hz)
10^-2
10^-4
10^-6
10^-8
10^-1
10^0
10^1
10^2
Frequency (Hz)
Spectral Acceleration (cm/s^s)
1.8
1.6
1.4
1.2
1
0.8
0.6
0.4
0.2
0.01
0.1
1
Period (s)
H1
H2
VE
Usable range
Usable range (VE)

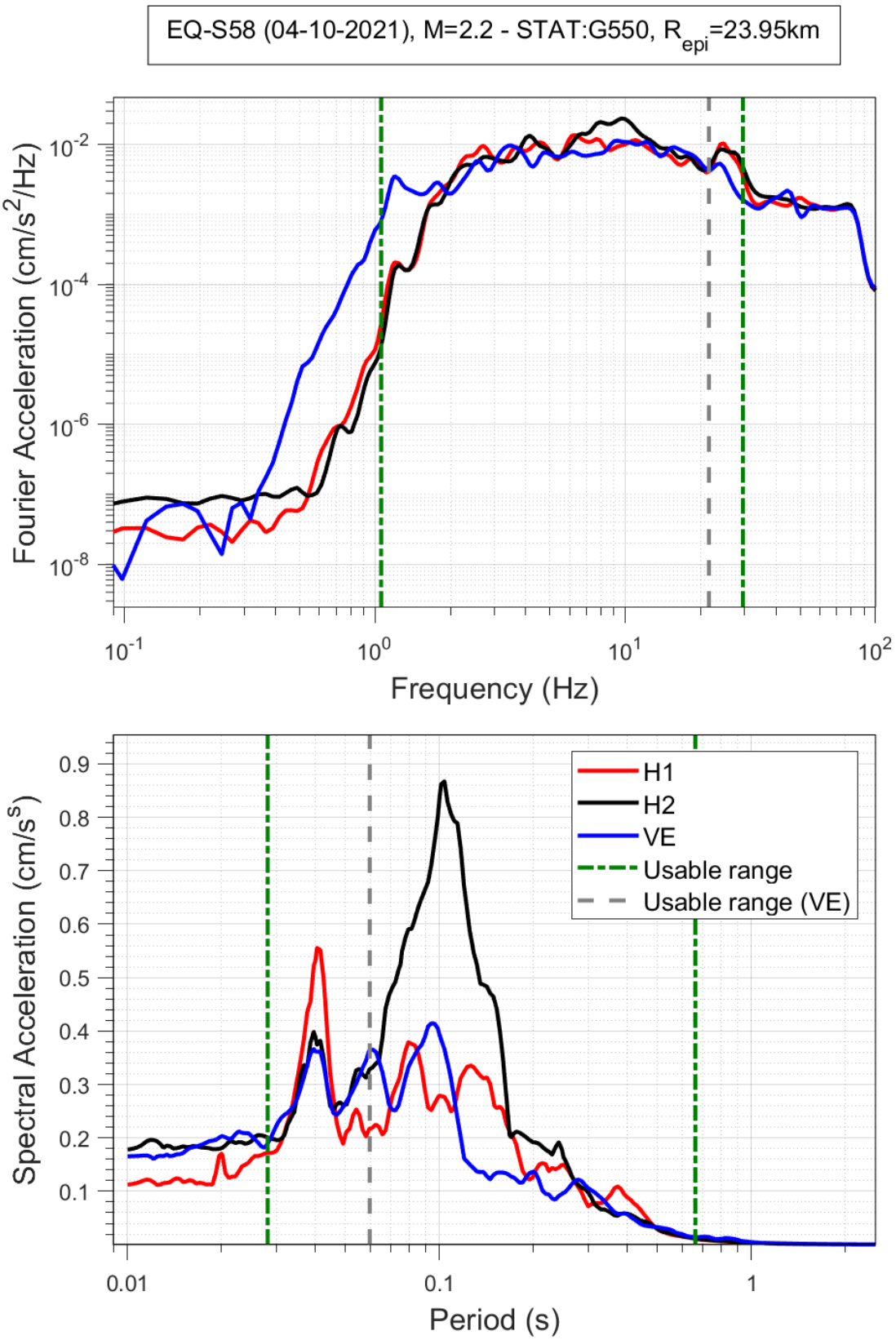
EQ-S58 (04-10-2021), M=2.2 - STAT:G550, R epi =23.95km
Fourier Acceleration (cm/s2/Hz)
10-2
10-4
10-6
10-8
10-1
100
101
102
Frequency (Hz)
Spectral Acceleration (cm/s2)
0.9
0.8
0.7
0.6
0.5
0.4
0.3
0.2
0.1
0.01
0.1
1
Period (s)
H1
H2
VE
Usable range
Usable range (VE)

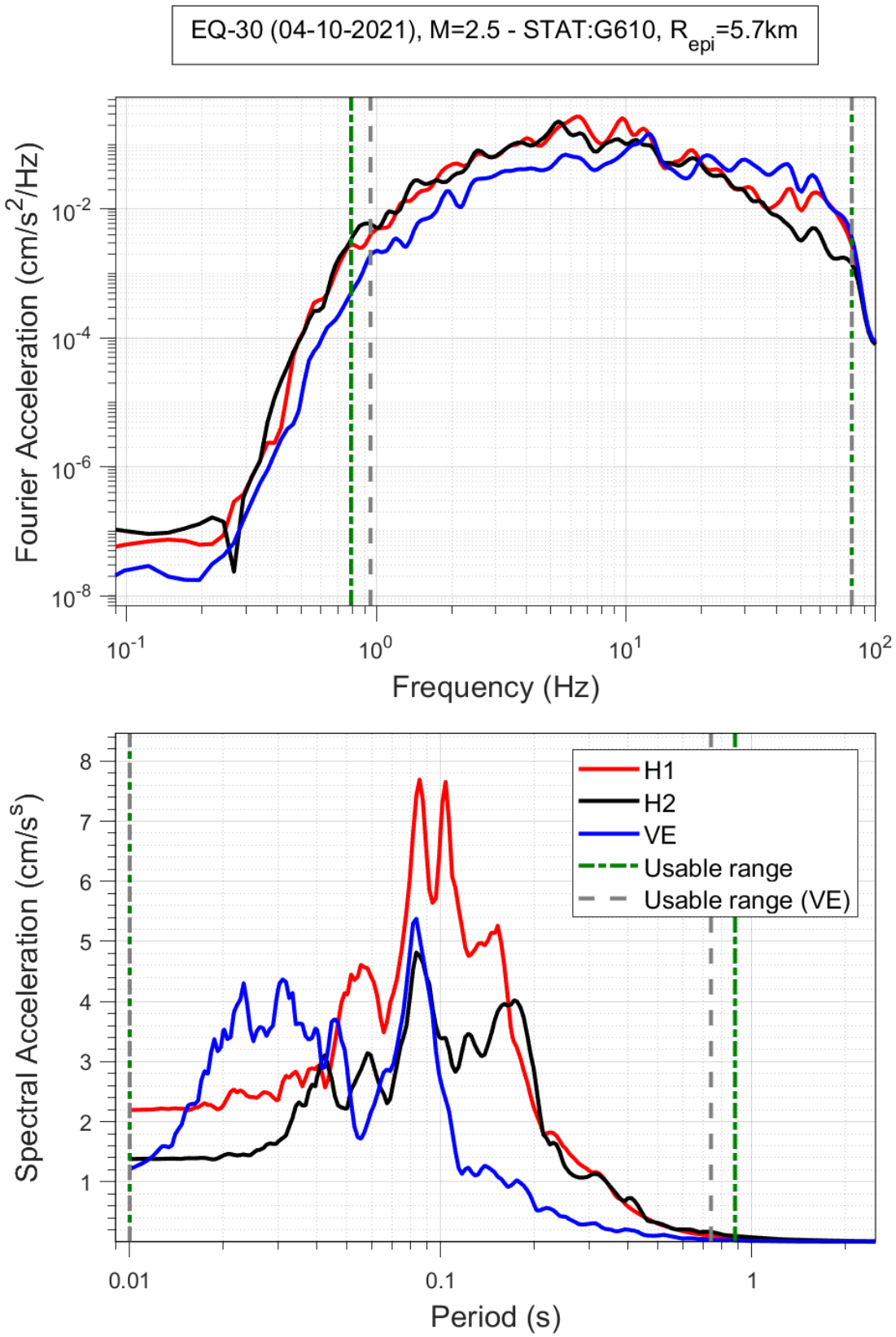
EQ-30 (04-10-2021), M=2.5 - STAT:G610, R_epi=5.7km
Fourier Acceleration (cm/s²/Hz)
10^-2
10^-4
10^-6
10^-8
10^-1
10^0
10^1
10^2
Frequency (Hz)
Spectral Acceleration (cm/s^s)
8
7
6
5
4
3
2
1
0.01
0.1
1
Period (s)
H1
H2
VE
Usable range
Usable range (VE)

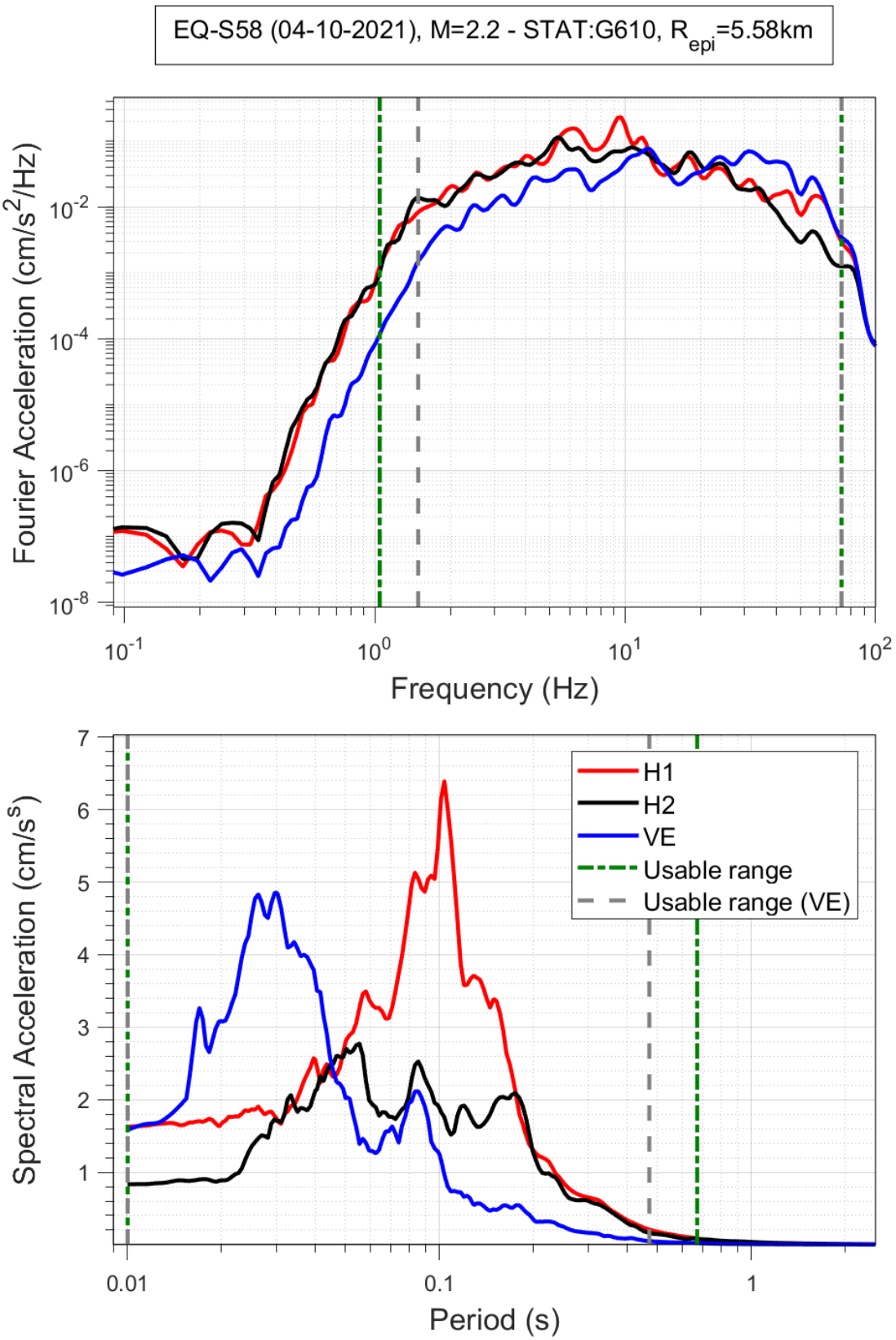
EQ-S58 (04-10-2021), M=2.2 - STAT:G610, R_epi=5.58km
Fourier Acceleration (cm/s²/Hz)
10^-2
10^-4
10^-6
10^-8
10^-1
10^0
10^1
10^2
Frequency (Hz)
Spectral Acceleration (cm/s^s)
7
6
5
4
3
2
1
0.01
0.1
1
Period (s)
H1
H2
VE
Usable range
Usable range (VE)

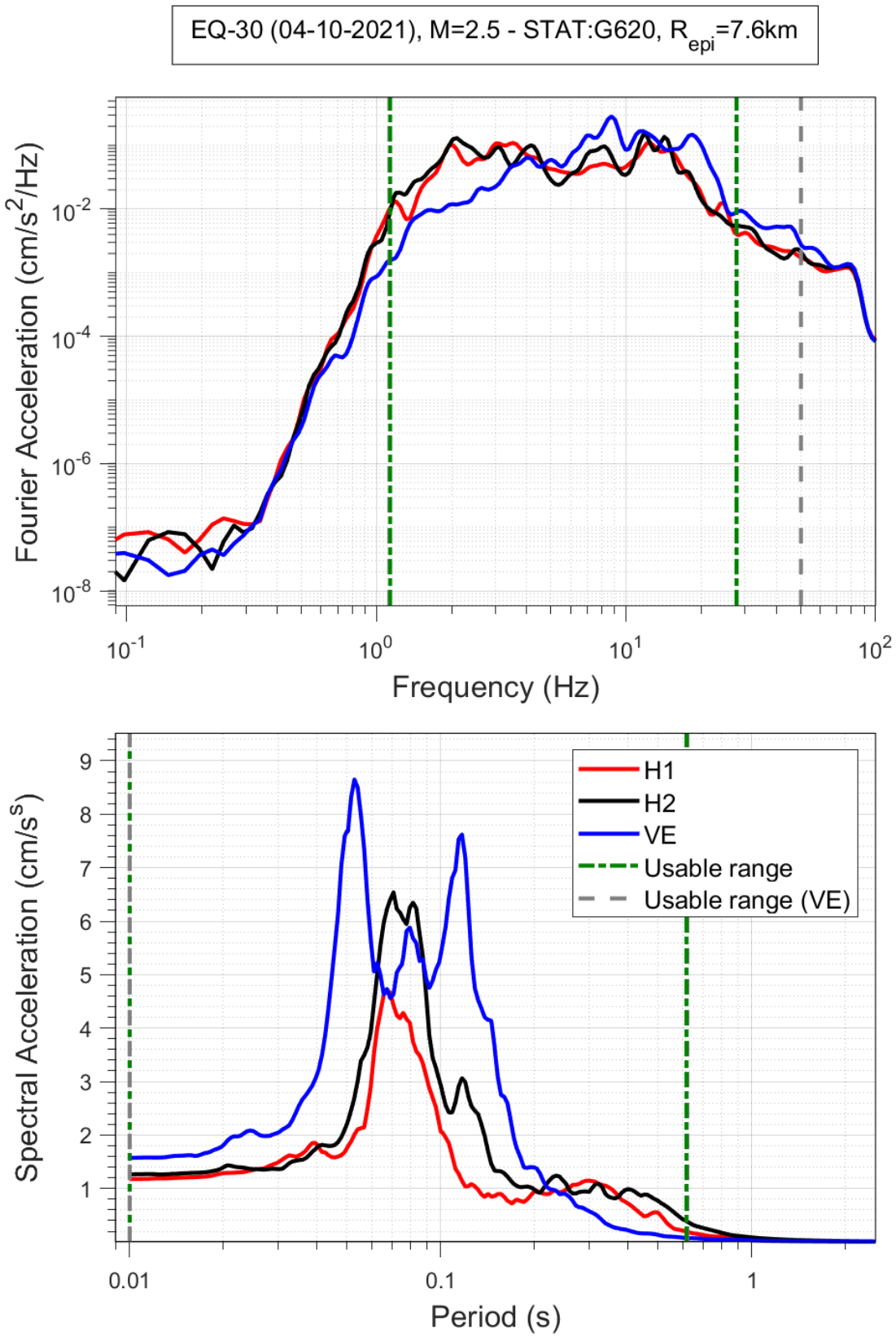
EQ-30 (04-10-2021), M=2.5 - STAT:G620, R_epi=7.6km
Fourier Acceleration (cm/s²/Hz)
10^-2
10^-4
10^-6
10^-8
10^-1
10^0
10^1
10^2
Frequency (Hz)
Spectral Acceleration (cm/s²)
9
8
7
6
5
4
3
2
1
0.01
0.1
1
Period (s)
H1
H2
VE
Usable range
Usable range (VE)

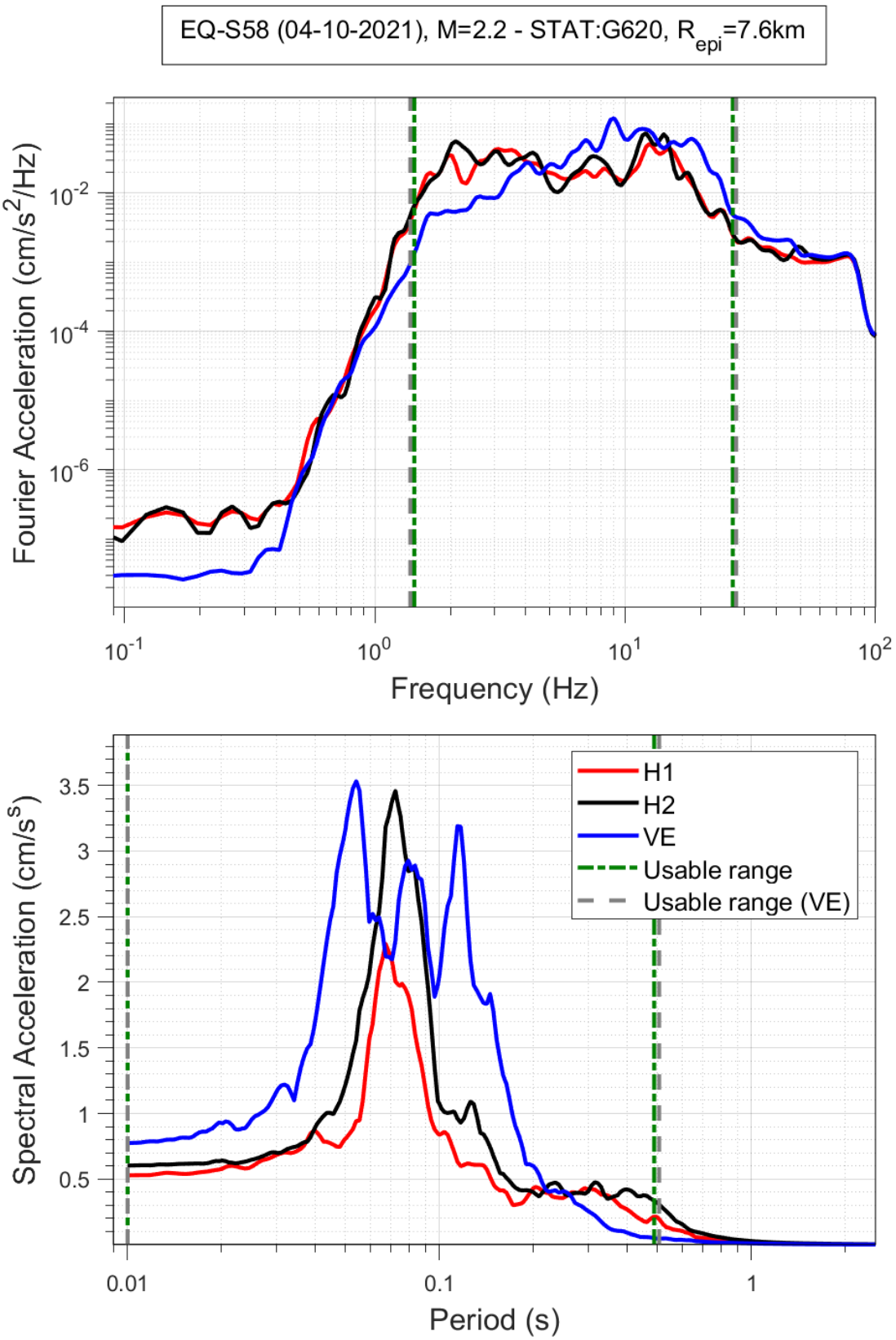
EQ-S58 (04-10-2021), M=2.2 - STAT:G620, R_epi=7.6km
Fourier Acceleration (cm/s²/Hz)
10^-2
10^-4
10^-6
10^-1
10^0
10^1
10^2
Frequency (Hz)
Spectral Acceleration (cm/s²)
3.5
3
2.5
2
1.5
1
0.5
0.01
0.1
1
Period (s)
H1
H2
VE
Usable range
Usable range (VE)

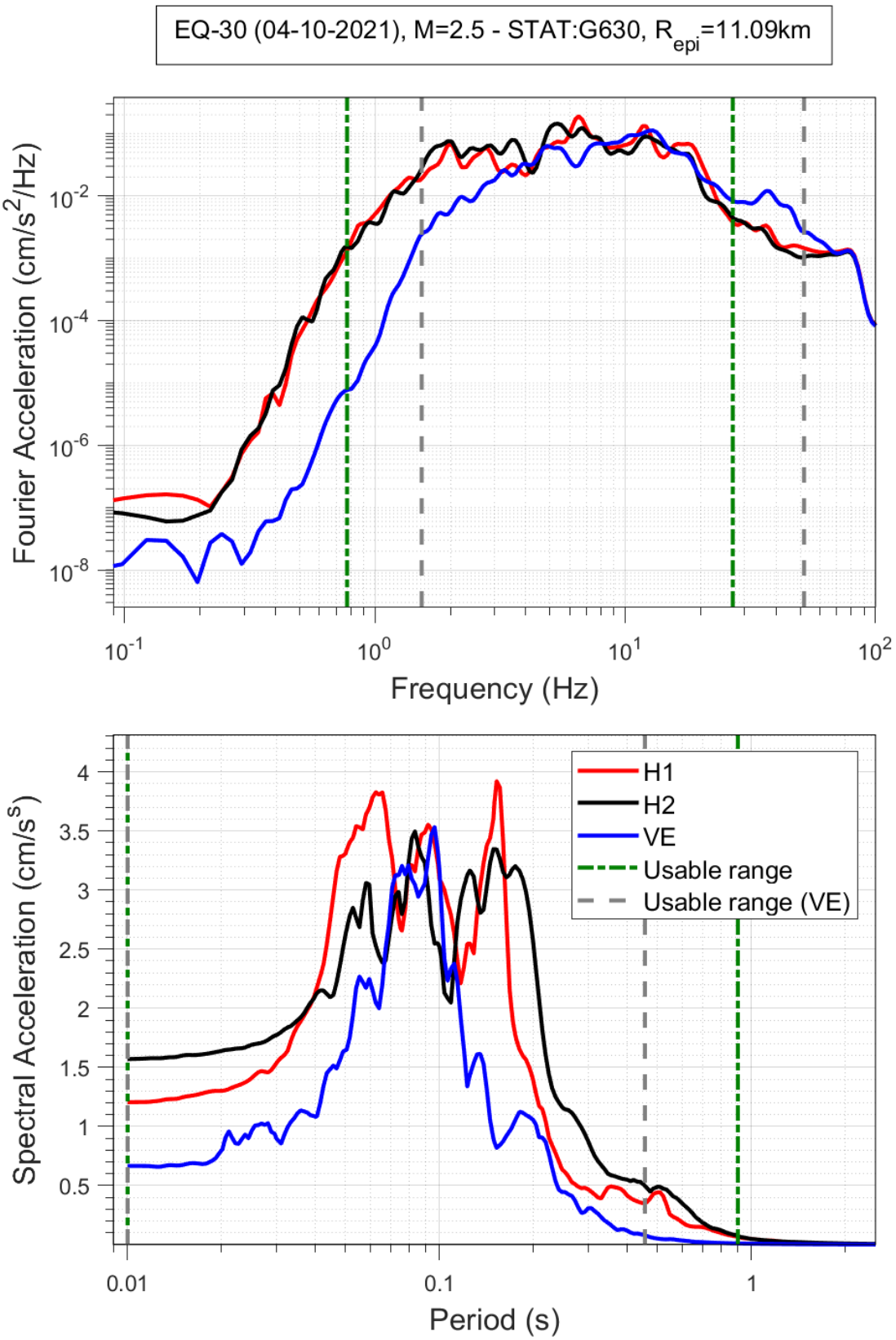
EQ-30 (04-10-2021), M=2.5 - STAT:G630, R_epi=11.09km
Fourier Acceleration (cm/s²/Hz)
10^-2
10^-4
10^-6
10^-8
10^-1
10^0
10^1
10^2
Frequency (Hz)
Spectral Acceleration (cm/s^s)
4
3.5
3
2.5
2
1.5
1
0.5
0.01
0.1
1
Period (s)
H1
H2
VE
Usable range
Usable range (VE)

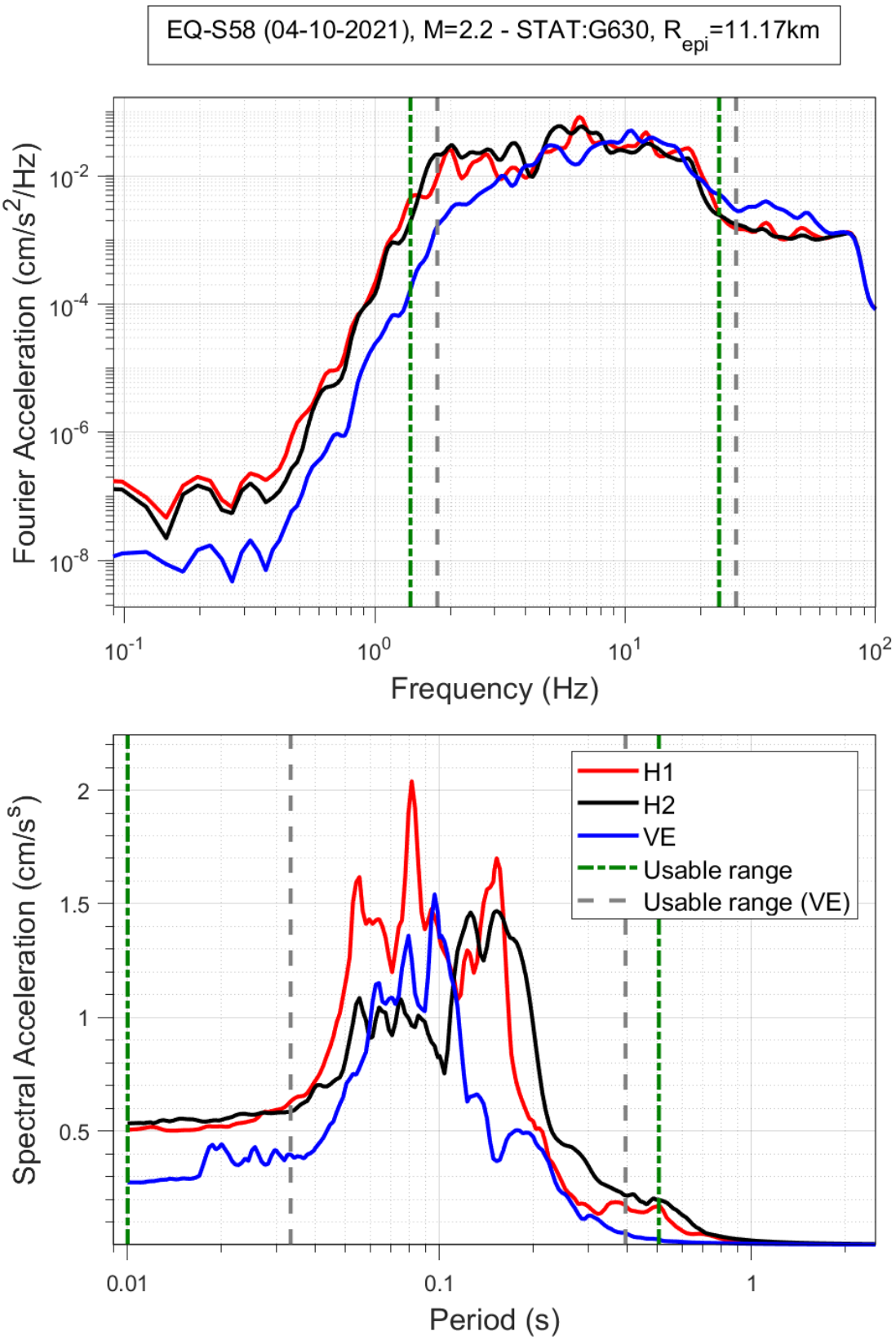
EQ-S58 (04-10-2021), M=2.2 - STAT:G630, R_epi=11.17km
Fourier Acceleration (cm/s²/Hz)
10^-2
10^-4
10^-6
10^-8
10^-1
10^0
10^1
10^2
Frequency (Hz)
Spectral Acceleration (cm/s²)
2
1.5
1
0.5
0.01
0.1
1
Period (s)
H1
H2
VE
Usable range
Usable range (VE)

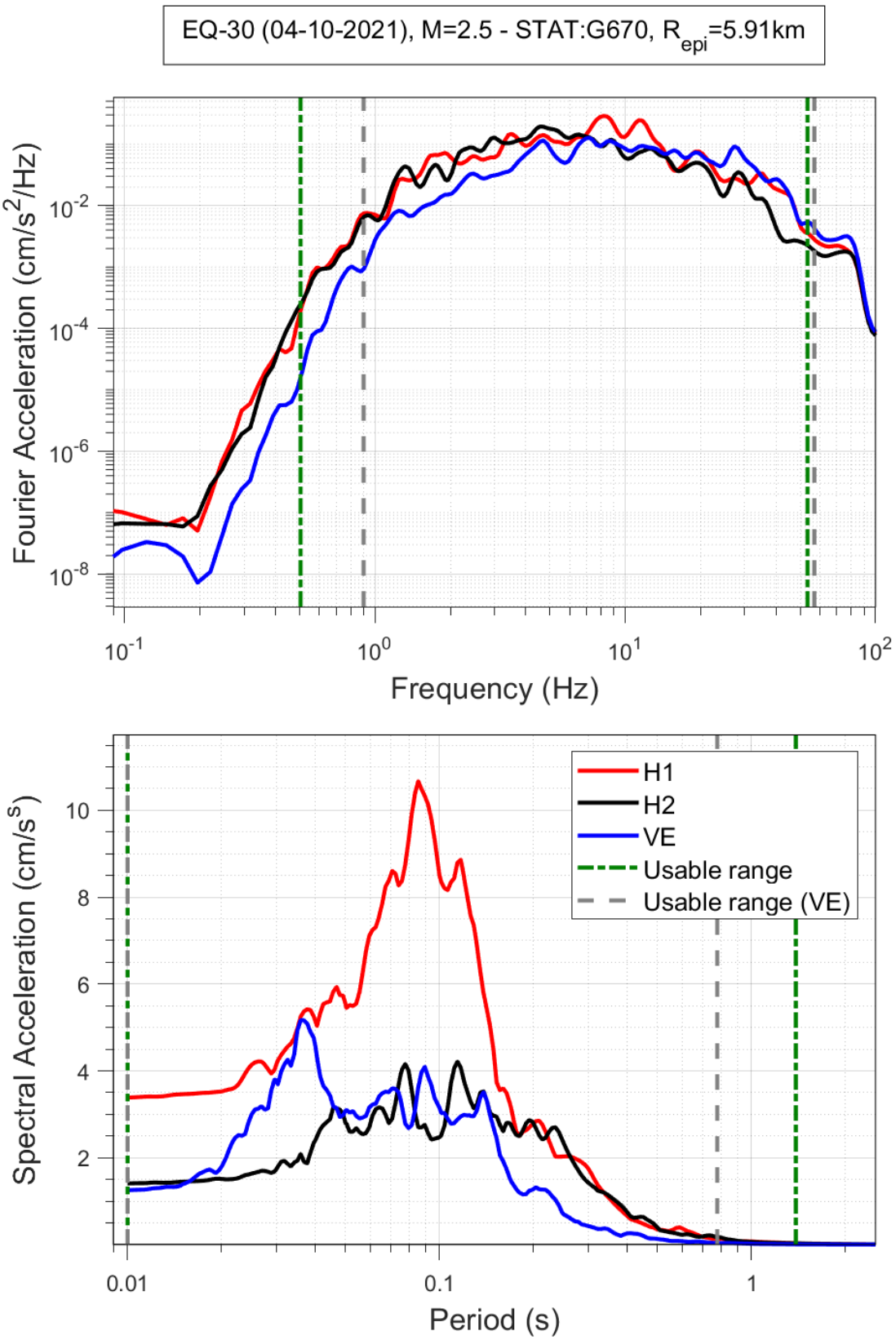
EQ-30 (04-10-2021), M=2.5 - STAT:G670, R_epi=5.91km
Fourier Acceleration (cm/s²/Hz)
10^-2
10^-4
10^-6
10^-8
10^-1
10^0
10^1
10^2
Frequency (Hz)
Spectral Acceleration (cm/s²)
10
8
6
4
2
0.01
0.1
1
Period (s)
H1
H2
VE
Usable range
Usable range (VE)

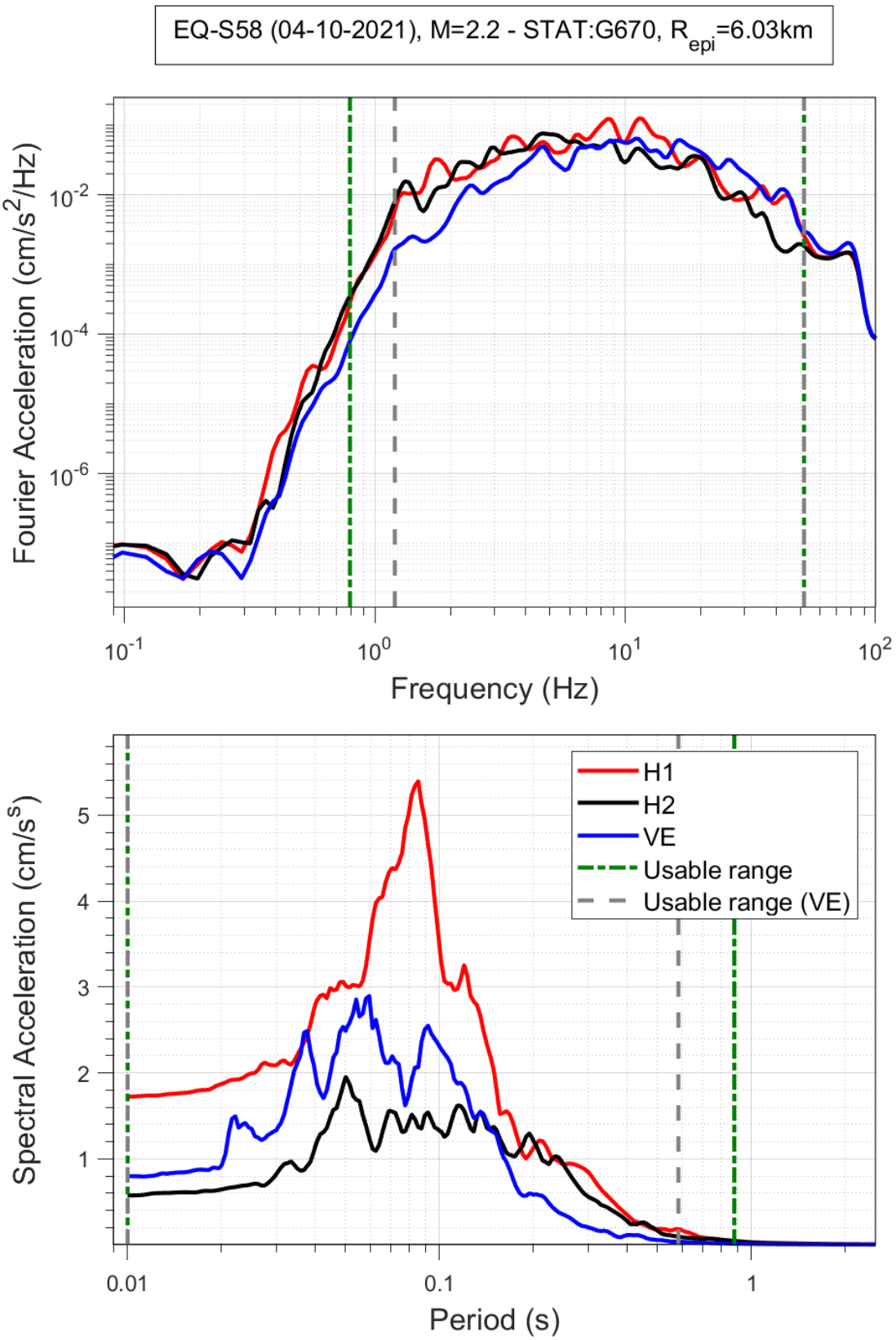
EQ-S58 (04-10-2021), M=2.2 - STAT:G670, R_epi=6.03km
Fourier Acceleration (cm/s²/Hz)
10^-2
10^-4
10^-6
10^-1
10^0
10^1
10^2
Frequency (Hz)
Spectral Acceleration (cm/s^s)
5
4
3
2
1
0.01
0.1
1
Period (s)
H1
H2
VE
Usable range
Usable range (VE)

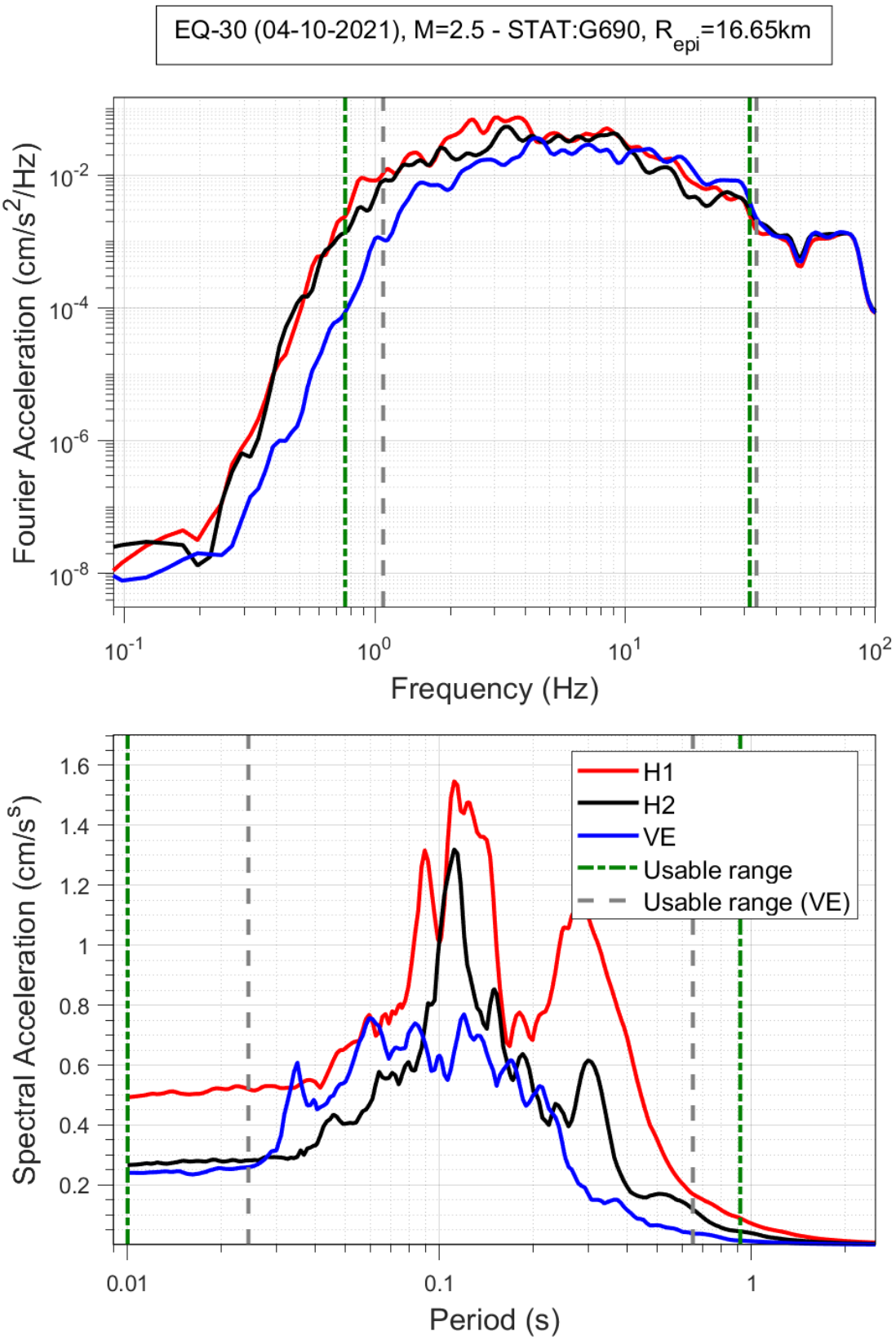
EQ-30 (04-10-2021), M=2.5 - STAT:G690, R_epi=16.65km
Fourier Acceleration (cm/s²/Hz)
10^-2
10^-4
10^-6
10^-8
10^-1
10^0
10^1
10^2
Frequency (Hz)
Spectral Acceleration (cm/s^s)
1.6
1.4
1.2
1
0.8
0.6
0.4
0.2
0.01
0.1
1
Period (s)
H1
H2
VE
Usable range
Usable range (VE)

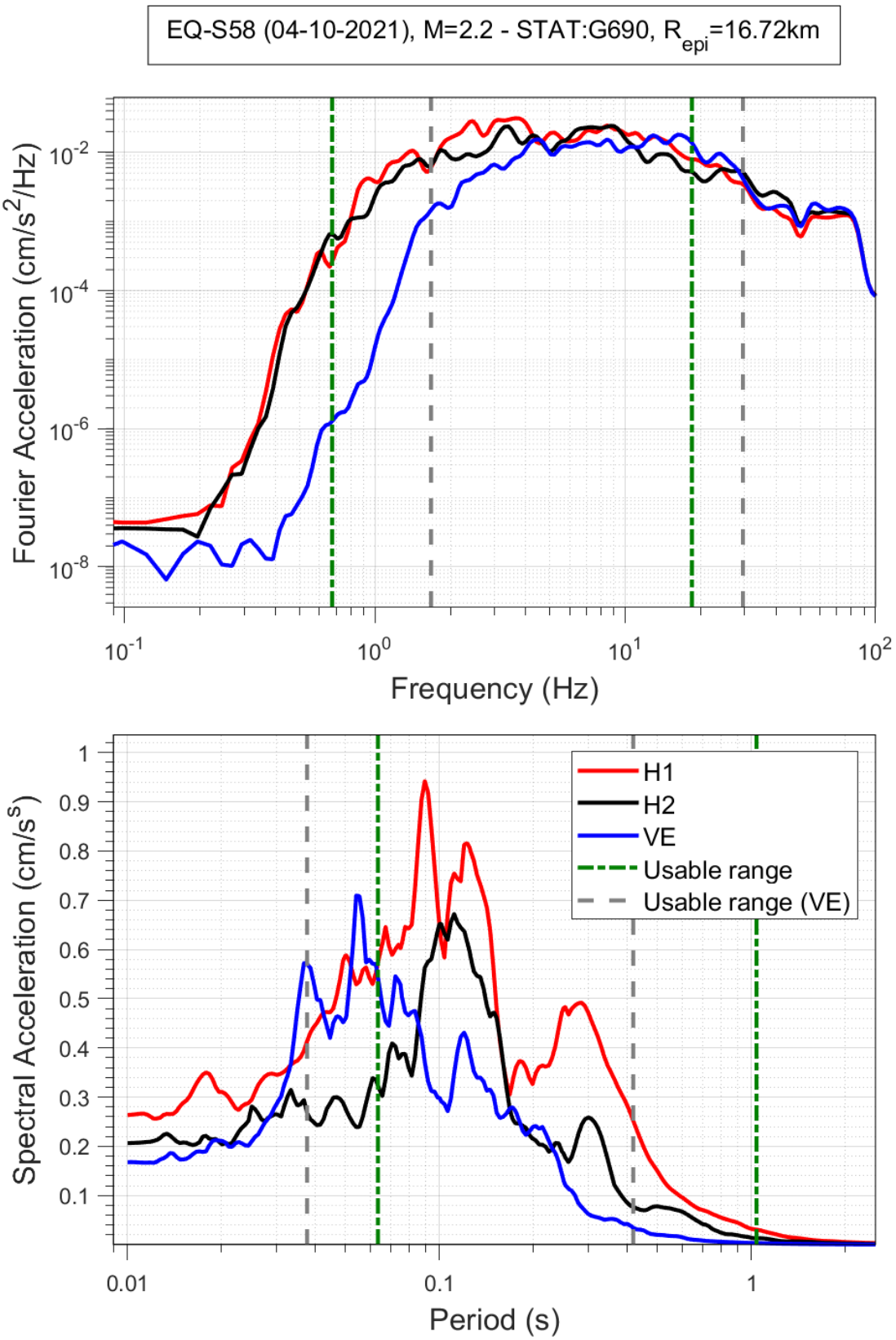
EQ-S58 (04-10-2021), M=2.2 - STAT:G690, R_epi=16.72km
Fourier Acceleration (cm/s²/Hz)
Frequency (Hz)
Spectral Acceleration (cm/s)
Period (s)
H1
H2
VE
Usable range
Usable range (VE)

Appendix D – Evaluation of the hypocentre and source mechanism of the earthquake with a magnitude of 1.7 near Westeremden on 8th November 2021

Here follows the evaluation of the recordings obtained from the seismic moniting network operated by KNMI of Westeremden earthquake on 8th November. This evaluation was prepared at rhe Shell laboratory in Amsterdam using automated Full-Wave-Form inversion.

This earthquake was assigned number 52.

Event 52 - Westeremden
08 November 2021 01:52:16

8 November 2021

Induced Seismicity Taskforce

Disclaimer

- The results presented in this report have been automatically generated using an unconstrained full waveform, event location and moment tensor inversion workflow, developed by the Induced Seismicity Taskforce at Shell.
- These results have not been previously reviewed.
- For questions related to the results then you should contact:
  - Chris Willacy (Christopher.Willacy@Shell.com) or
  - Jan-Willem Blokland (Jan-Willem.Blokland@Shell.com)

Event summary

The event happened at:

Date	08 November 2021
Time	01:52:16.370000

The event is located at:

Location	Westeremden
Northing (m)	594850
Easting (m)	242850
Depth (m)	2850

The source characteristics are:

	Solution 1	Solution 2
Strike angle (degree)	130.45	351.10
Dip angle (degree)	26.85	63.02
Rake angle (degree)	-125.69	-72.80
Isotropic (percentage)	-7.05	-7.05
CLVD (percentage)	-11.93	-11.93
Magnitude M_{L}	1.70	1.70

Magnitude summary

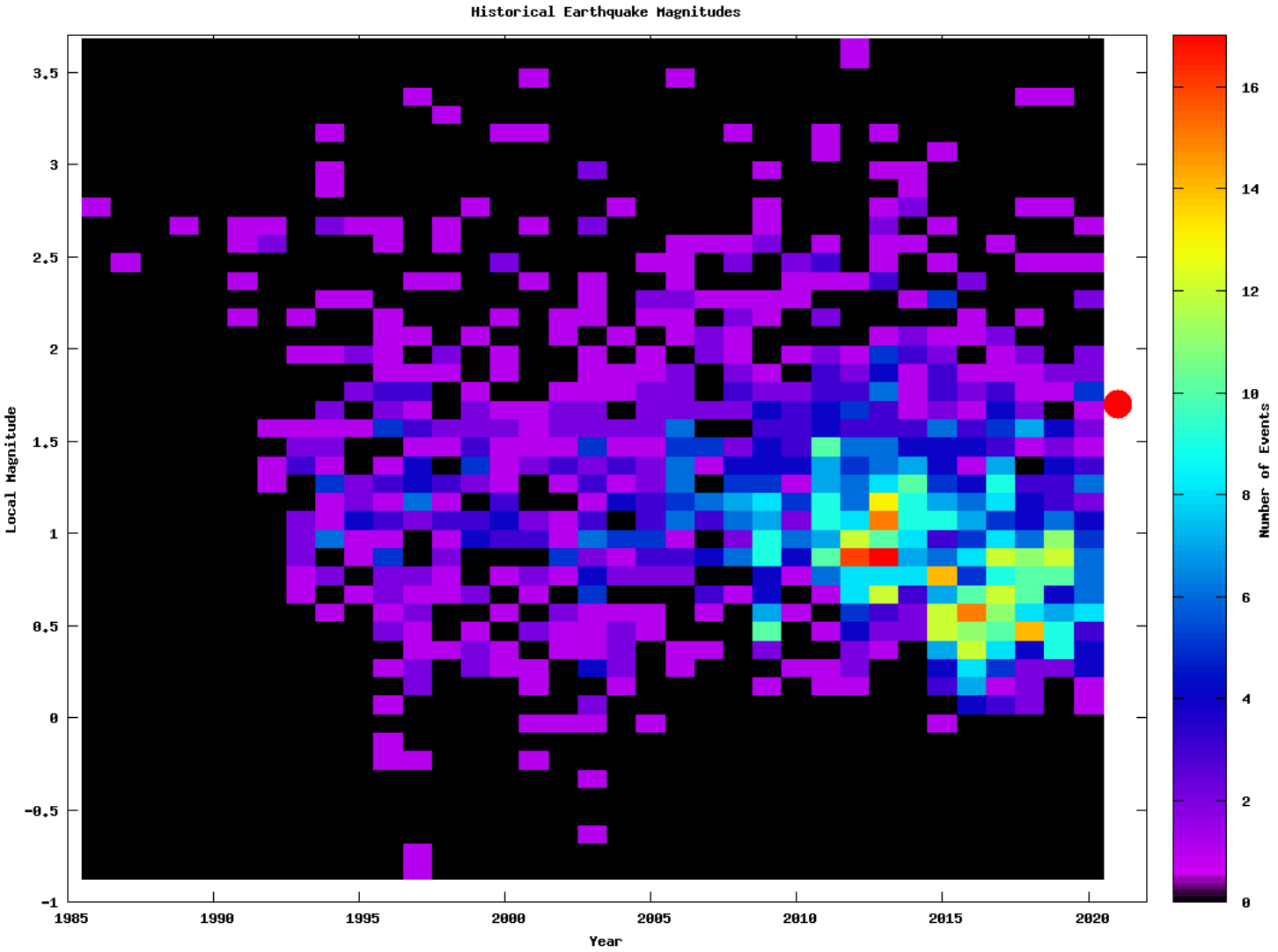

Regional and historical map

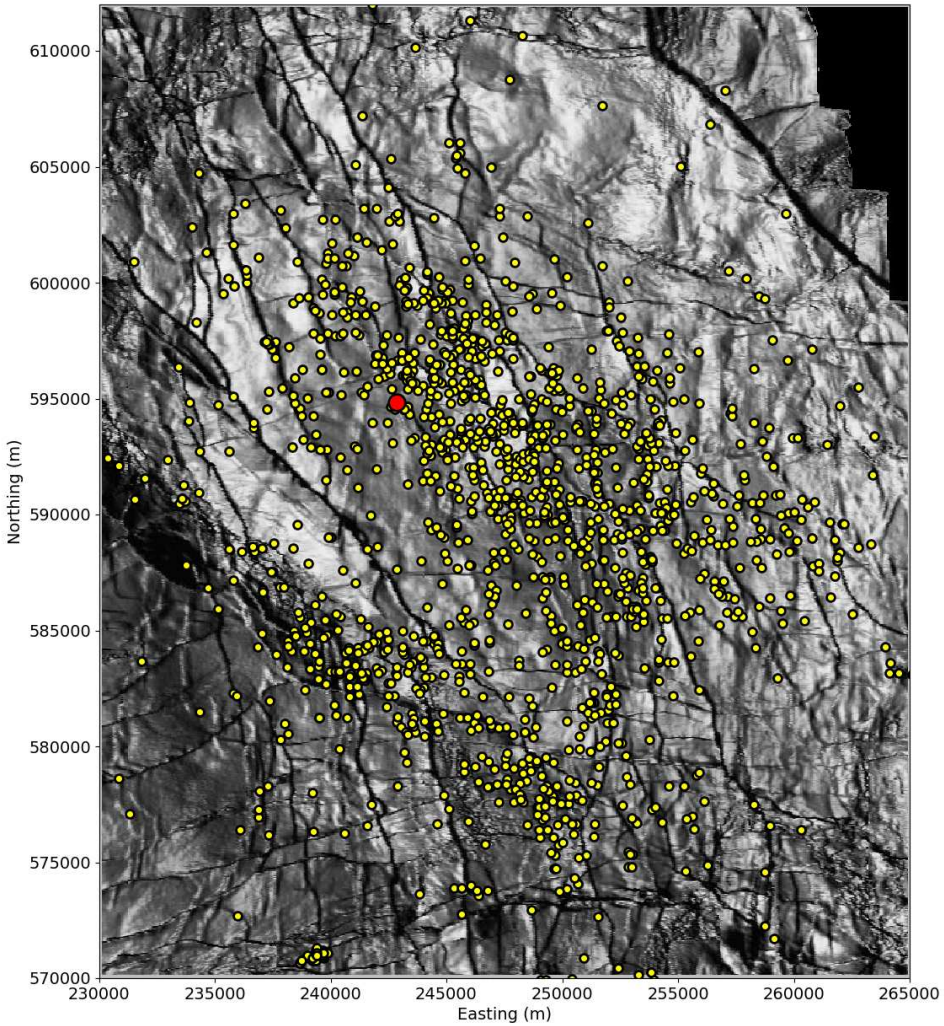

Event depth summary

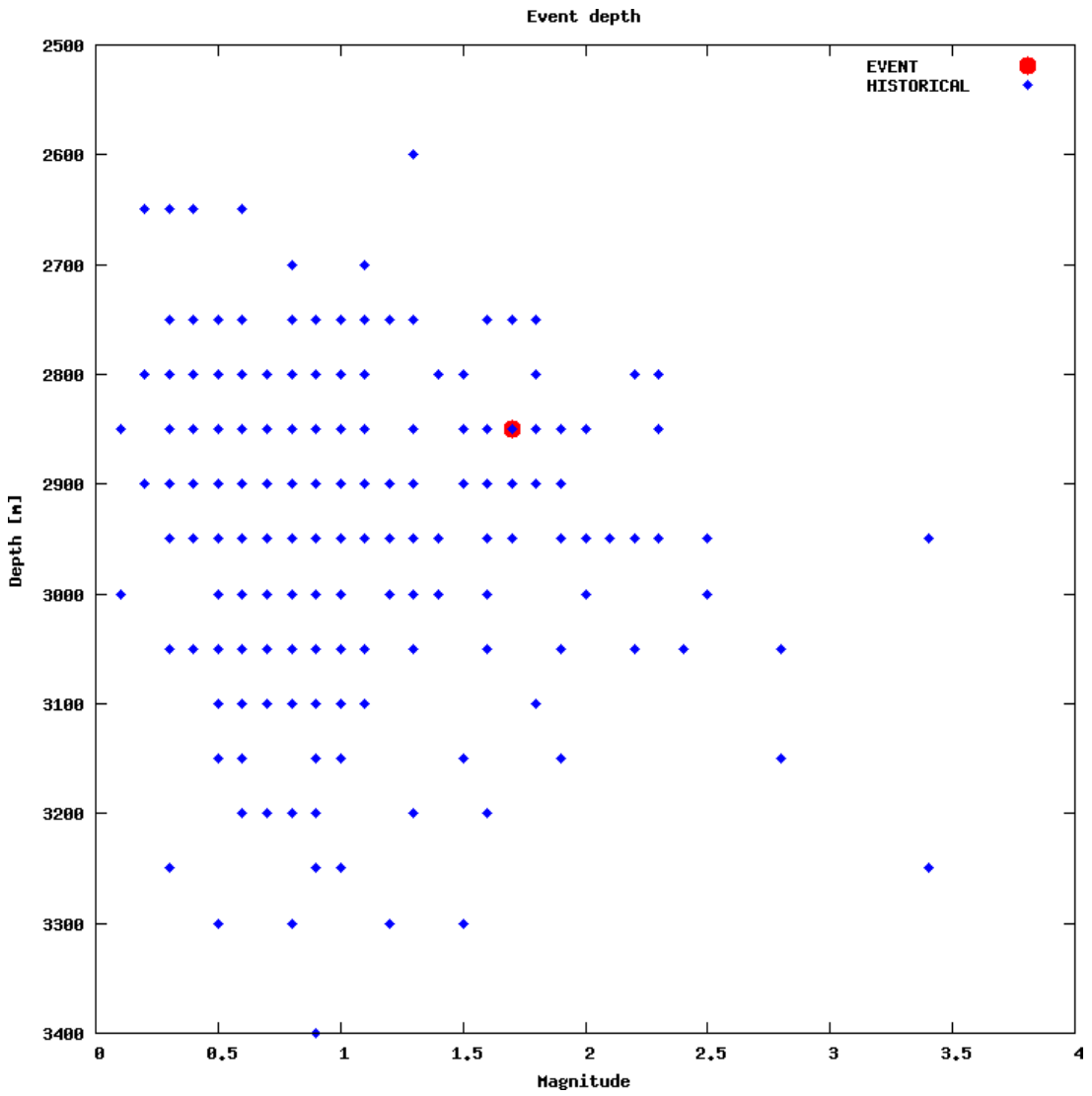

Event location - Map

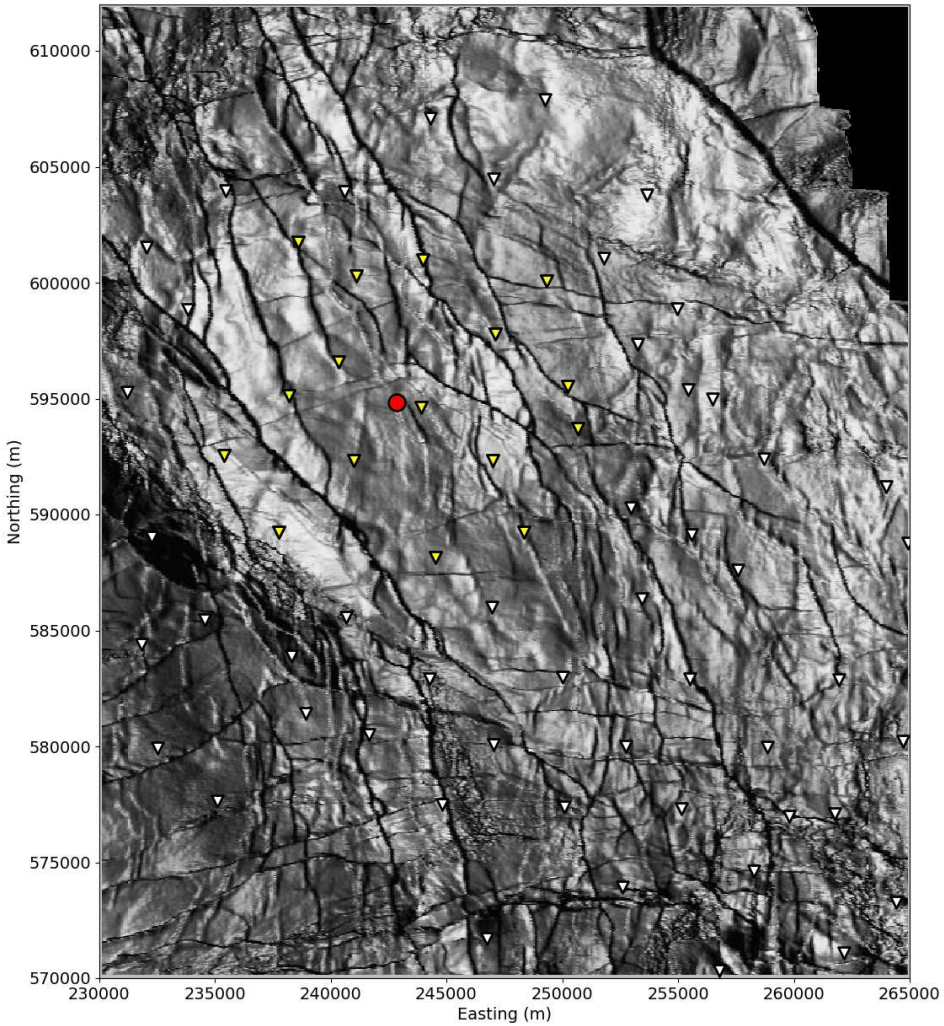

Event location and depth

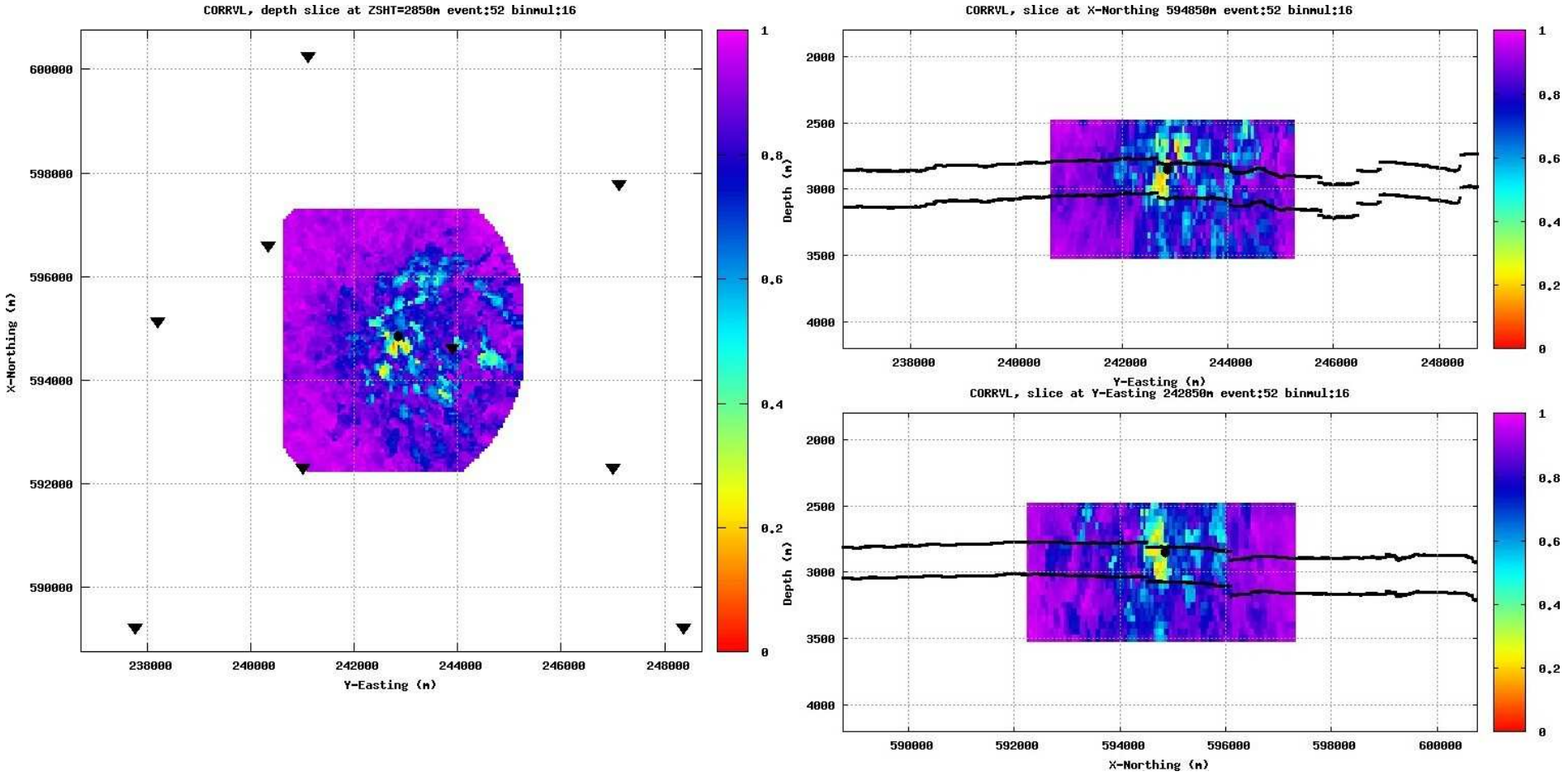

Moment tensor

Double-coupled part

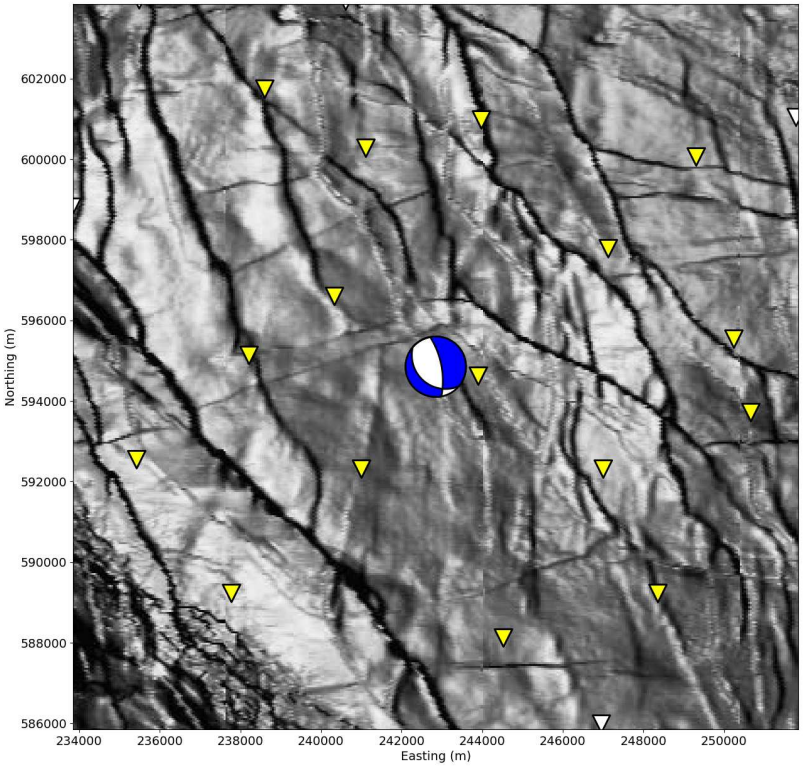

Full

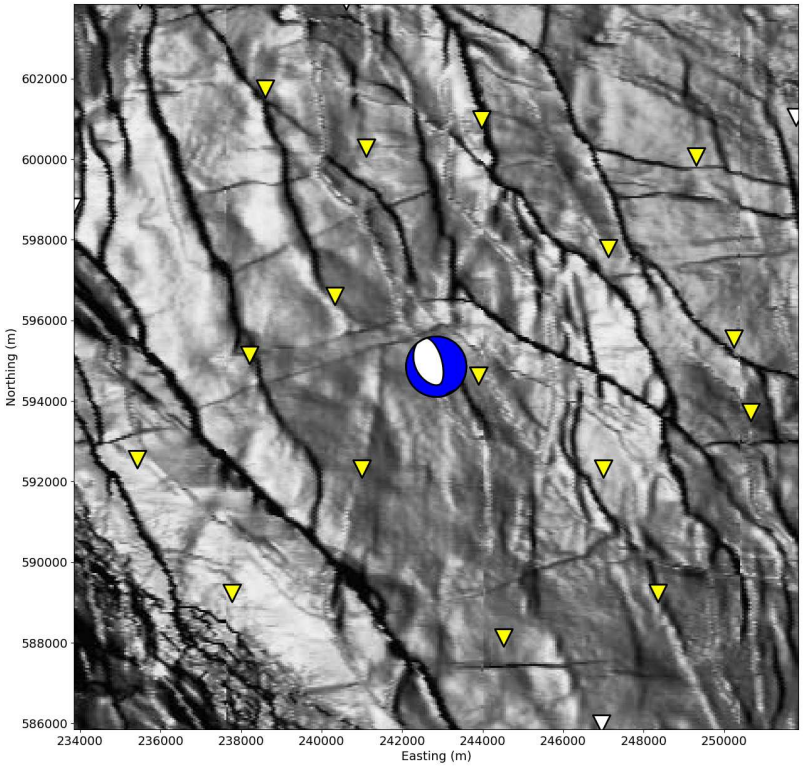

Moment Tensor: Decomposition

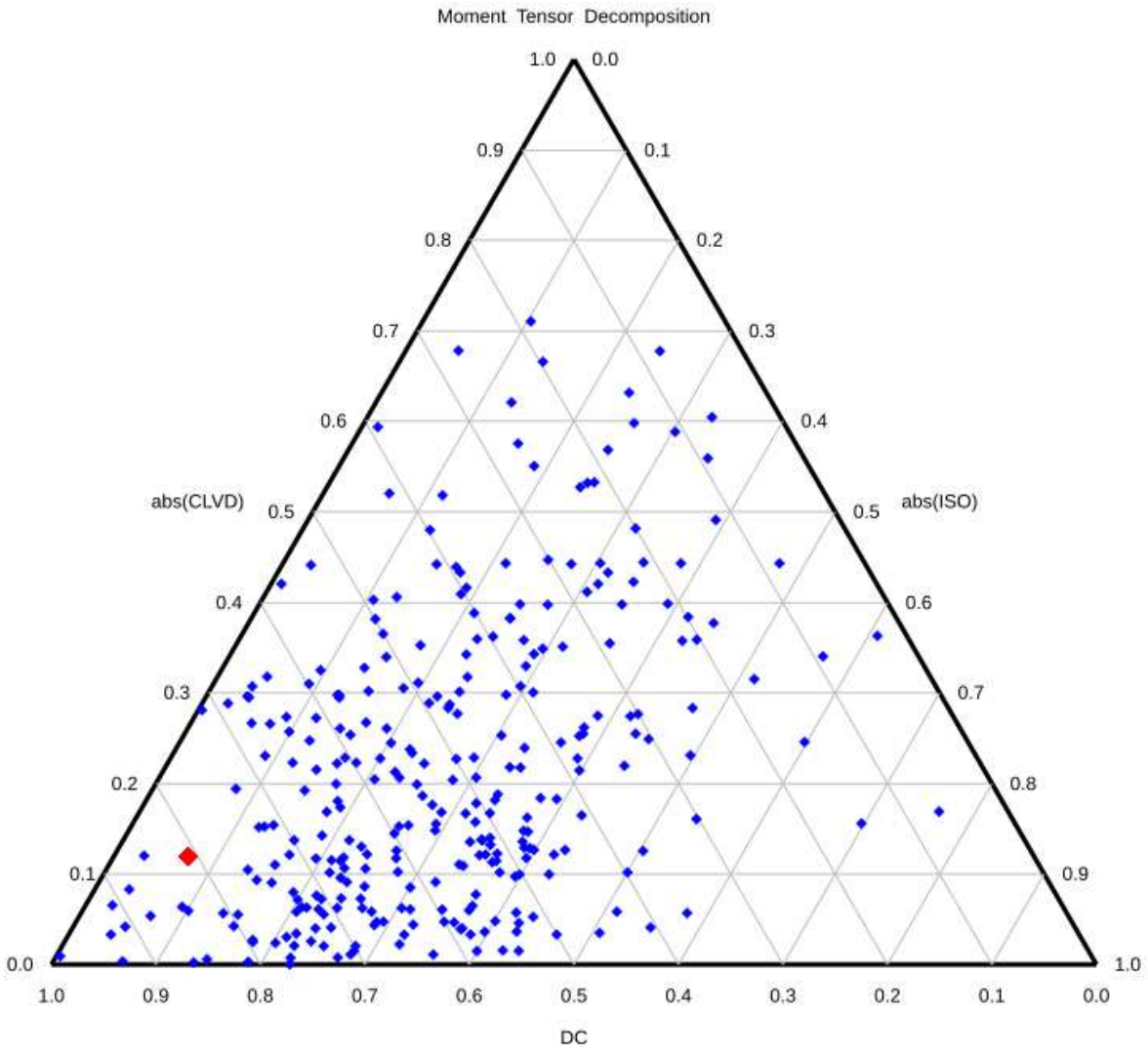

Field data traces

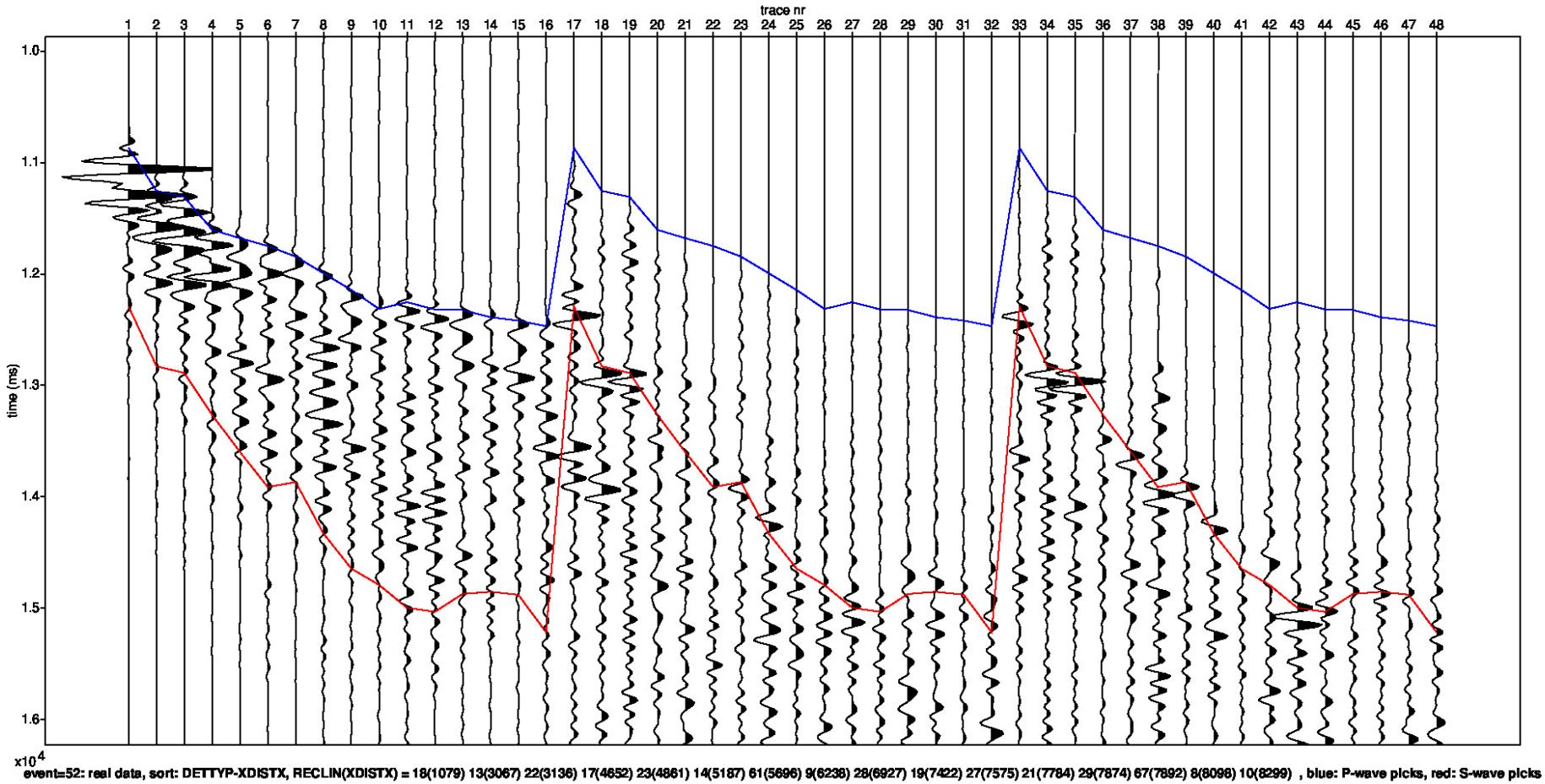

Modelled data traces

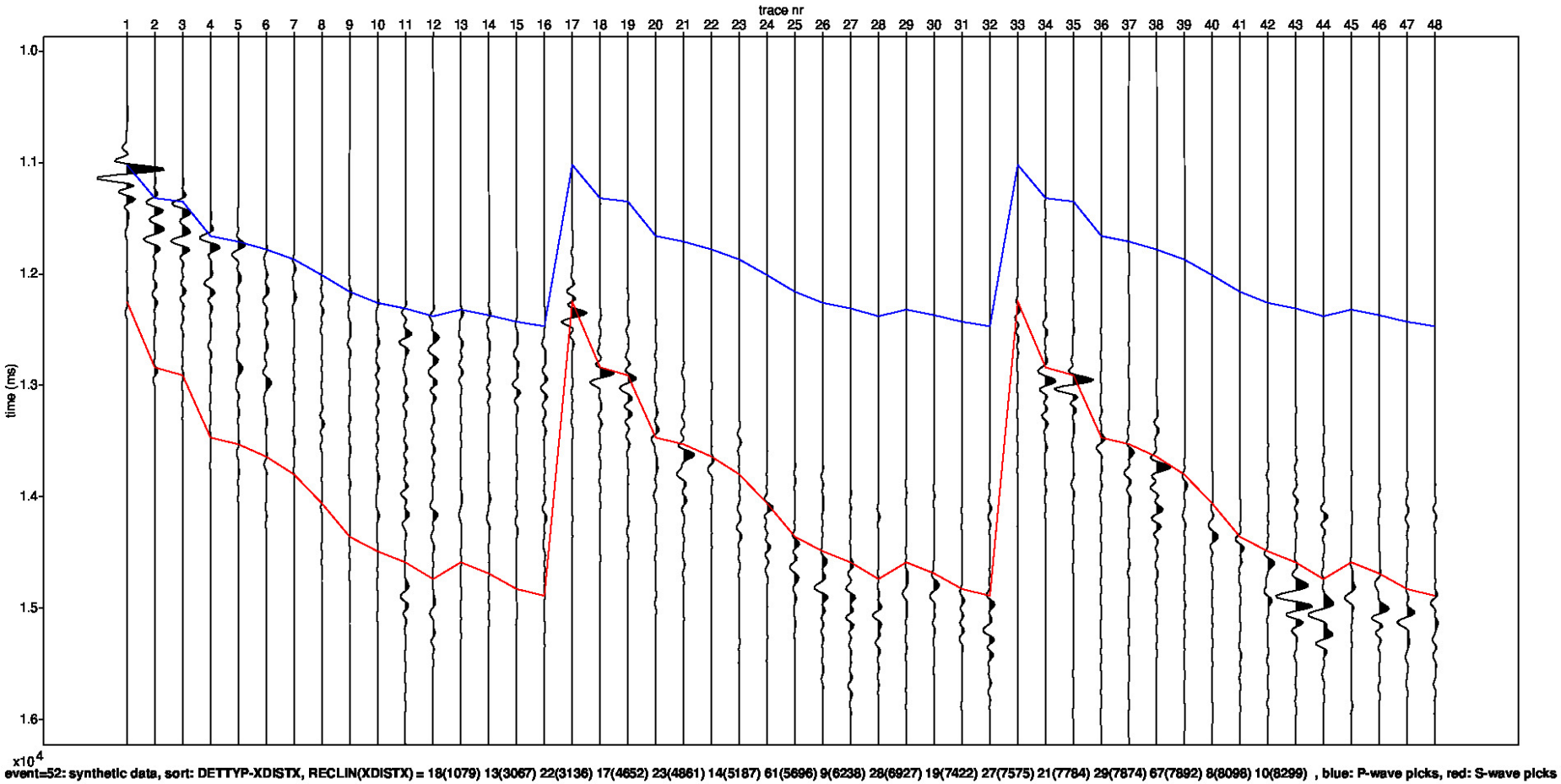

Appendix - Figure Captions

Page

3 Detailed parameter summary for the event. Both primary and secondary focal plane solutions are provided from the moment tensor inversion.

4 Magnitude summary. Prior years are displayed as a “heat map” where the number of events for a given magnitude is displayed per grid cell. The current event is displayed in red.

5 Regional map showing the historical events from KNMI (1986-2019) in blue and the location of the current event in red.

6 Event depth summary. Depths from our automatic workflow (2018-2020) are shown in blue and the current event depth is shown in red. The resolution of the vertical grid is 50m.

7 Event location details for the current event, superimposed on the top Rotliegend depth horizon. Station locations as shown as inverted triangles. Blue triangles are the actual stations used to locate the event whose epicentre is shown by the red dot.

8 QC displays extracted from the objective function for the current event location. The colour attribute displayed is 1 minus the normalized cross correlation between observed and synthetic waveforms. Station locations are shown as black inverted triangles on the map and the event location is shown by the black dot (left plot). The west to east and north to south vertical profiles are shown on the right. The top and base reservoir are shown for reference as black lines.

Appendix - Figure Captions (continued)

Page

9 Moment tensor inversion results for the event. The double couple portion of the moment tensor is shown on the left and the full moment tensor is displayed on the right. Station locations used in the inversion are shown as inverted triangles.

10 Ternary diagram showing the moment tensor decompositions into relative double-couple(DC), isotropic (ISO) and compensated linear vector dipole (CLVD) contributions. The automatic Shell events (2018-2020) are shown in blue and the current event is highlighted in red.

11 Observed traces for each station and each component. The automatic picks for the P- and S-waves are indicated by the blue and red lines respectively.

12 Modelled waveform data for each station and each component. The automatic picks for the P- and S-waves are indicated by the blue and red lines respectively.